Mechanical Properties of Blended Steel Fibre Reinforced Concrete Using Manufactured and Recycled Fibres from Tyres

A thesis submitted for the degree of Doctor of Philosophy

By Hang Hu

(BSc, MSc)

Department of Civil and Structural Engineering

The University of Sheffield

July 2018

感恩我的父亲母亲！

To my wife,

Thank you for raising me up to walk on stormy seas,

I promise to love you forever.

愿自己永远沐浴梦想之光，感受晨曦之美。

Acknowledgements

I would like to express my deepest gratitude and appreciation to my main doctoral supervisor, Professor Kypros Pilakoutas, for his great supervision, continuous help, encouragement, patience and brilliant advice during these difficult years.

I am very grateful to my second supervisor Dr Maurizio Guadagnini for his patience, precious time, great support and guidance.

Special thanks to Dr Panos Papastergiou for his kind assistance in experimental work, reviewing my poor English writing and very warm encouragement.

I also would like to thank Dr Harris Angelakopoulos and Dr Fabio Figueiredo for their continuous help and the joint publications.

Great thanks to all former and current researchers of the Concrete and Earthquake Engineering (CEE) research group for creating a dynamic research environment, in particular Dr Reyes Garcia, Dr Van Hien, Dr Jun Ye, Dr Hamed Fergani, Dr Samar Raffoul, Dr Asif Hussain Shah, Mr Ruizhi Zuo, Mr Zahran Al-Kamyani, Mr Abdulaziz Alsaif, Miss Neda Nabid, Mr Zhao Wang, Mr Imad El Khouri, Mr Hao Wen and Mr Zhijian Chen.

Great thanks to the technical staff of the Heavy Structures Lab, in particular Mr Kieran Nash, Mr Markwell and Mr Shaun Waters, for their patience and great technical support.

I acknowledge the financial support of China Scholarship Council (CSC number: 201508060086) throughout these years of study.

This research has been funded by the European Union Seventh Framework Programme [FP7/2007-2013] under grant agreement n° 603722 (www.anagennisi.org) and the UK Technology Strategy Board (TSB) project “Re-use of steel cord from tyres as reinforcement in sustainable construction” under the grant agreement n° 101691.

I am deeply indebted to my family, especially my wife for her unconditional and true love, continuous support and care during these years of absence.

Abstract

The construction industry is capable of mitigating the global environmental problems through the utilisation of waste materials in concrete. The use of sorted steel fibres recycled from end-of-life tyres (RTSF) and steel cords recycled from un-vulcanised rubber belt off-cuts (RTSC), as a viable alternative to manufactured steel fibres (MSF) in concrete applications, may lead to significant environmental benefits and enhanced structural performance. This study aims to understand the mechanical (compressive and flexural) behaviour of steel fibre reinforced concrete (SFRC) using blended MSF and RTSF, as well as recycled-fibre blends (RTSC and RTSF), leading to design-oriented models for blended SFRC at total dosages ($\leq$45 kgm^3) typical for concrete slab applications such as slabs-on-grade and suspended slabs. An extensive experimental programme including compressive, 3-point bending and round panel tests on SFRC specimens was undertaken as part of this study, along with direct tensile and pull-out tests on RTSC. About 500 tests were conducted and 18 SFRC mixes examined.

For SFRC using MSF and RTSF, a strong correlation is found in the flexural behaviour of the SFRC prism and round panel specimens, and conversion equations are proposed. It is found that the mechanical properties of blended mixes using RTSF vary depending on dosages, but are comparable with those of MSF-only mixes at the same fibre dosage. For blended mixes containing 10 kg/m^3 of RTSF, a positive synergetic effect is obtained, with RTSF making a positive contribution at the early stages of cracking.

RTSC possess a high tensile strength (>2600 MPa) and exhibit a good bond to concrete matrix. Through pull-out tests, the critical embedded length of RTSC is found to be in the range of 25-40 mm. RTSC are found to be extremely well mobilised at larger crack widths and the post-cracking strength of recycled-fibre mixes (RTSC on their own or blended with RTSF) is significantly higher (more than double) than MSF-only mixes at the same total fibre dosage. In addition, the flexural performance of concrete reinforced with recycled fibre blends improves with increasing amounts of RTSC.

Utilising the extensive experimental work, the accuracy of the $\sigma - \varepsilon$ relations proposed by current design guidelines (RILEM TC 162-TDF and Model Code 2010) for SFRC is assessed. These are found to have significant inaccuracies and a simplified trilinear relation is proposed for blended SFRC at low dosages. It is found that the tensile strength of SFRC with RTSF at a low total fibre dosage is only marginally improved by fibre addition, and the post-cracking tensile strengths at different strains can be determined directly from residual flexural tensile strengths (f_{Ri}) of prisms. The proposed $\sigma - \varepsilon$ relations can be used directly for the design of slabs-on-grade and other SFRC applications.

Table of contents

List of Figures

List of Tables

List of Abbreviations and Symbols

Abbreviations

ACI	American Concrete Institute
ASTM	American Society for Testing and Materials
BC	Brittle Cracking
CDP	Concrete Damage Plasticity
CMOD	Crack Mouth Opening Displacement
COV	Coefficient of Variation
CSC	Concrete Smeared Cracking
FE	Finite Element
FIB	International Federation for Structural Concrete
FRC	Fibre Reinforced Concrete
GGBS	Ground Granulated Blastfurnace Slag
ITZ	Interface Transition Zone
LCA	Life Cycle Assessment
LOP	Limit of Proportionality
LVDT	Linear Variable Differential Transducers
MSF	Manufactured Steel Fibres
RILEM	International Union of Laboratories and Experts in Construction Materials, Systems and Structures
RTSC	Recycled Tyre Steel Cords
RTSF	Recycled Tyre Steel Fibres
SFRC	Steel Fibre Reinforced Concrete
SLS	Serviceability Limit State
ULS	Ultimate Limit State
w/c	Water cement ratio

Symbols

A	Cross sectional area of RTSC
A_1	Actual cross sectional area of RTSC
A_2	Cross sectional area of RTSC estimated based on the nominal cross-sectional area of each filament and the number of filaments contained in each cord

b	Unit width of the round panel
c	Distance between the edge of the panel and the central line of the support
d	Measured round panel thickness (Chapter 2), or effective specimen depth (Chapter 4)
d_0	Nominal round panel thickness
d_1	Actual diameter of RTSC
d_2'	Diameter of each filament contained in RTSC
d_c	Damage factor for concrete under compression
d_t	Damage factor for concrete under tension
δ	The specified central deflection up to which the energy absorption capacity is calculated
δ_0	Unit vertical displacement induced by the concentrated load
E	Energy absorption capacity
E_5	Energy absorption capacity up to central deflection of 5 mm
E_{10}	Energy absorption capacity up to central deflection of 10 mm
E_{20}	Energy absorption capacity up to central deflection of 20 mm
E_{40}	Energy absorption capacity up to central deflection of 40 mm
E_c	Compressive modulus of elasticity
E_{cm}	Mean compressive modulus of elasticity
E_{fm}	Mean flexural modulus of elasticity
E'	Measured energy absorption capacity
ϵ	Flow potential eccentricity
$\varepsilon_{A,A',B}$	Tensile strains corresponding to $\sigma_{A,A',B}$ proposed by Model Code 2010
ε_{Fu}	Ultimate tensile strain of SFRC proposed by Model Code 2010
ε_{SLS}	Tensile strain of SFRC at the Serviceability Limit State (SLS)
ε_{ULS}	Tensile strain of SFRC at the Ultimate Limit State (ULS)
ε_1'	Tensile strain of SFRC that is used to define the elastic portion of the load-deflection curve and the tensile contribution of the concrete
ε_2'	Tensile strain of SFRC that is associated with the peak load and the behaviour of SFRC with only microcracks (SLS)
ε_3'	Tensile strain of SFRC that is used to define the tail of the curve and represent the behaviour of SFRC at large cracks (ULS)
ε_u'	Ultimate limit tensile strain of SFRC proposed by the author
$\tilde{\varepsilon}_c^{pl}$	Plastic strain of concrete (compression)
$\tilde{\varepsilon}_t^{pl}$	Plastic strain of concrete (tension)
f_{cc}	Compressive cylinder strength of concrete

$F_{ctm,fl}$	Applied flexural load corresponding to LOP
$f_{ctm,fl}$	LOP, the flexural stress corresponding to the maximum load recorded up to a CMOD of 0.05 mm
f_{cu}	Compressive cube strength of concrete
$f_{eq,3}$	An equivalent flexural tensile strength proposed by RILEM
f_{Ftu}	Tensile strength of cracked SFRC at the ultimate limit state proposed by Model Code 2010
F_L	Applied flexural load corresponding to LOP
f_L	LOP, the flexural stress corresponding to the maximum load recorded up to a CMOD of 0.05 mm.
f_{Lk}	Characteristic value of f_L
F_R	Applied flexural load
f_R	Residual flexural tensile strengths
F_{R1}	Applied flexural load at CMOD of 0.5 mm
f_{R1}	Residual flexural tensile strength at CMOD of 0.5 mm
f_{R1k}	Characteristic value of f_{R1}
F_{R2}	Applied flexural load at CMOD of 1.5 mm
f_{R2}	Residual flexural tensile strength at CMOD of 1.5 mm
F_{R3}	Applied flexural load at CMOD of 2.5 mm
f_{R3}	Residual flexural tensile strength at CMOD of 2.5 mm
f_{R3k}	Characteristic value of f_{R3}
F_{R4}	Applied flexural load at CMOD of 3.5 mm
f_{R4}	Residual flexural tensile strength at CMOD of 3.5 mm
f_t	Tensile strength of plain concrete or SFRC
f_{u-1}	Flexural strength of SFRC prisms
f_{u-3}	Flexural strength of SFRC round panels
f_{u-pc}	Flexural strength of plain concrete prisms
h	Required SFRC slab thickness
h_{sp}	Distance between the notch tip to the top of the cross-section
I	The second moment of area of the middle cross-section
I_{f_R}	Improvement ratio, which is a function of the normalised residual flexural tensile strength of the recycled-fibre mixes with respect to the control mixes at the same total fibre dosage
K_c	Ratio of the second stress invariant on the tensile meridian to that on the compressive meridian
k_h	Size factor to accommodate the size effect of various SFRC structural elements

l	Span of the prism
m	Moment of resistance of the round panel per unit length
ν	Poisson's ratio
$\frac{P}{\delta}$	Slope of the initial part of the load-deflection curve
ψ	Dilation angle
P_u	Ultimate load for round panels
R	Measured round panel radius
r	Radius of the circular loading plate
R_0	Nominal round panel radius
R^2	Coefficient of determination
S_i	Synergy ratio, where i represents the f_R values obtained from prism tests or E values derived from round panel tests
$\sigma_{1,2,3}$	Tensile strength of SFRC proposed by RILEM TC 162-TDF
σ_{m1}	Average tensile strength of RTSC based on A_1
σ_{m2}	Average tensile strength of RTSC based on A_2
σ_{max}	Nominal maximum flexural stress of sections on yield lines
σ_{SLS}	Tensile strength of SFRC at the Serviceability Limit State (SLS)
σ_{ULS}	Tensile strength of SFRC at the Ultimate Limit State (ULS)
$\sigma_{A,A',B,C,D,Q,E}$	Tensile strength values used in the stress-strain models proposed by Model Code 2010
σ_1'	Tensile strength of SFRC corresponding to ε_1'
σ_2'	Tensile strength of SFRC corresponding to ε_2'
σ_3'	Tensile strength of SFRC corresponding to ε_3'
$\frac{\sigma_{bo}}{\sigma_{co}}$	Ratio of biaxial to uniaxial compressive strength
$\sigma - \varepsilon$	Stress-strain relationship
$\sigma' - \varepsilon'$	Simplified trilinear stress-strain relationship proposed by the author
$\sigma - w$	Stress-crack width relationship
s_{rm}	Mean distance between cracks
V_f	Volume fraction of fibres
w_u	Maximum crack opening accepted in structural design
y	Neutral axis depth

Chapter 1 Introduction

This chapter presents motivation and background of this research, followed by the aims and objectives, methodology and the layout of this thesis.

1.1 Motivation

With population growth, industrialisation and rapid urbanisation, natural resources for construction materials are rapidly being depleted and a significant amount of unusable or unwanted materials is discarded, resulting in serious environmental problems worldwide [1]. According to The EC Waste Framework Directive 2008/98/EC [2], disposal and energy recovery are in the lowest levels of the waste hierarchy, whilst recycling and reuse are the most preferable. Since concrete is still one of the most popular construction materials worldwide, the construction industry is capable of mitigating the global environmental problems through the utilisation of waste materials in concrete. Whilst much research has been done on recycling aggregates and other fillers in concrete, little work has been done on reusing (or recycling) materials for their tensile properties.

Approximately 1 billion tyres (17 million tonnes) [1] reach the end of their useful lives worldwide every year [3]. From the end-of-life tyres, the tyre recycling industry has developed various processes to extract rubber, steel and polymer. Though rubber is the most abundant and visible material in a tyre, steel and polymer cords are needed to reinforce the rubber to resist the high pressures expected during the working life of tyres and provide stiffness. The high quality, tensile strength and flexibility make those cords attractive as potential reinforcement in concrete. The most commonly used and financially viable tyre recycling techniques adopt a combination of mechanical shredding and granulation, during which steel fibres of irregular shape, length and diameter are extracted magnetically. However, these fibres are heavily contaminated with rubber (up to 20% by mass) and (if used as they are) are prone to agglomeration (balling of fibres which creates weak areas in concrete) due to significant geometrical irregularities and excessive aspect ratios. Further processing is thus required to: (1) minimise rubber contamination (to less than 0.5% by mass); (2) limit the fibre length and diameter distribution to those that are effective in concrete; (3) and avoid agglomeration before and during concrete mixing. Only after the tyre wire has been cleaned, sorted and classified, the product (“Recycled Tyre Steel Fibres” (RTSF)) can satisfy the Quality Assessment requirements for construction materials and thus can be used in concrete as structural reinforcement. Typically, RTSF have variable geometrical properties with individual fibres being curved. The diameters of the majority of RTSF are in the range of 0.1-0.4 mm and their lengths are between 10 and 40 mm, with average lengths ranging from 20 to 26 mm. Since 1999, extensive experimental work has been undertaken at the University of Sheffield [4–15] to investigate the mechanical properties of RTSF and their potential in structural

applications, and this has led to patents being awarded worldwide [16] for the use of tyre wire in concrete

About 1.5 billion tyres are produced per annum worldwide [3]. During the tyre manufacturing process, roughly 5% (by weight) of un-vulcanised rubber belt off-cuts is generated, which still contains a large amount of high-specification steel cords used to reinforce the treads and sidewalls of car and truck tyres. However, most of those steel cords are still disposed of as waste or used for energy recovery (incineration) together with rubber. Recently, the tyre recycling industry has developed a novel cryogenic process to extract the steel cords undisturbed (i.e. they do not unravel as during shredding) from un-vulcanised off-cuts, and these "Recycled Tyre Steel Cords (RTSC)"cut to predetermined lengths are also suitable as concrete reinforcement, since they are very similar to Manufactured Steel Fibres (MSF).

The use of RTSF and RTSC as a viable alternative to MSF in concrete applications may lead to significant environmental benefits and enhanced structural performance.

1.2 Research background

1.2.1 Manufactured Steel Fibres (MSF)

Since ancient times, fibres in the form of hay or horsehair were used to reinforce brittle construction materials (e.g. clay) [17]. From 1900's, asbestos fibres were used in concrete as reinforcement [17,18]. Such fibres were then found to be carcinogenic, leading to a demand for safer reinforcing solutions [18,19]. In the early 1960s, the potential of MSF as randomly dispersed reinforcement in concrete was first investigated in the United States [20].

When Steel Fibre Reinforced Concrete (SFRC) is subjected to flexural loading or other environmental actions (e.g. temperature gradient), multiple distributed cracks with relatively small widths tend to occur instead of large throughout cracks as developed in plain concrete, leading to significant enhancement of flexural toughness, permeability, serviceability performance and durability [17,21–25]. Other benefits gained from adding MSF in concrete include fatigue resistance, impact and shrinkage resistance [7,12,14,20,26,27]. However, in the majority of SFRC applications, only single-type-MSF reinforced concrete is used [28]. Since the production of MSF requires a large amount of natural resources and energy input, more

sustainable solutions (i.e. RTSF and RTSC) are being considered as potential candidates to reinforce concrete.

1.2.2 Steel fibres recycled from tyres (RTSF or RTSC)

Previous research on RTSF showed that these fibres can be used in various construction applications such as industrial flooring (conventionally-placed or pumped concrete) [4,7–9,11,12,14,24,29–34], slope stabilisation (sprayed concrete) [15], precast elements (self-compacting concrete) [12,35,36] and concrete pavements (roller-compacted concrete) [13,15,37]. For sustainability, Life Cycle Assessment (LCA) studies [38,39] have shown that very low (less than 5%) energy input is required for the production of RTSF, compared to that of conventional MSF, which highlights the significant environmental benefits of using RTSF in concrete.

RTSC are extracted from un-vulcanised off-cuts as a whole (0.5 to 2m long) with almost no impurities. Each cord consists of a number of steel filaments twisted together and often a filament wound helically around them. The inclusion of the outer filament is intended to prevent unravelling of RTSC and enhance bond with the rubber. The filament may also improve the cord surface characteristics in concrete, contributing to improved interfacial bond, and enhanced pull-out resistance. As the mechanical properties of composites are dependent on the properties of the constituent materials and their interfacial bond characteristics [11,24], there is a need to investigate the mechanical properties (tensile strength) of RTSC and the interfacial bond behaviour between RTSC and concrete matrix.

One disadvantage of using RTSF on their own in concrete is that, as a large portion of the RTSF lengths is smaller than the diameter of the typical coarse aggregates, the flexural performance of RTSF-only mixes is usually inferior to MSF-only mixes at the same fibre dosage, especially when large cracks are developed [5,15,24,31]. Hence, to achieve equivalent or even better mechanical properties compared to MSF-only mixes at a certain dosage, a likely use of RTSF, is to blend RTSF with longer and larger-diameter fibres (e.g. MSF or RTSC).

1.2.3 Blended steel fibres

The fracture process of concrete matrix is multi-scale and progressive [28]. When blended fibres of different aspect ratios (length/diameter) and physical properties are added in concrete (“fibre

hybridisation [22]"), they can provide better crack control over a broader range of crack widths, whilst single-type fibres are effective in arresting or bridging cracks of specified widths.

Several studies [22,28,30,34,40–45] on hybrid FRC (or mortar) have demonstrated that fibre hybridisation can lead to better performance than that of single-type fibres. Younis et al. [46] reported that hybrid SFRC using 1% (by mass) of cleaned and sorted RTSF blended with 1% of undulated MSF exhibited higher flexural strength and toughness, compared to SFRC mixes containing 2% of undulated MSF. Nevertheless, this positive synergetic effect has not always been observed in previous studies using recycled tyre wire due to fibre agglomeration or unsuitable fibre combinations [30,47], in particular when unclassified and unsorted fibres were used. Since RTSF have a wide range of fibre length distribution and a higher nominal tensile strength than typical MSF, blended mixes using MSF and RTSF need to be investigated. Furthermore, as RTSC are made of high-specification steel, SFRC using RTSC on their own or blended with RTSF could potentially provide better mechanical performance, leading to 100% replacement of MSF with more sustainable steel fibres in concrete constructions. Steel fibre dosages ranging between 30 and 45 kg/m^3 are commonly used in structural applications such as slabs-on-grade and suspended slabs on piles, to resist flexural and punching shear failure modes. Hence, the investigations on the properties of blended SFRC need to focus on low total fibre dosages (up to 45 kg/m^3).

Current design guidelines (i.e. RILEM TC 162-TDF [48] and Model Code 2010 [49]) rely on test results from SFRC using single-type fibres (i.e. MSF) and it is not certain if the uniaxial tensile stress-strain ($\sigma - \varepsilon$) relationship adopted by these guidelines is also suitable for blended SFRC mixes using recycled fibres. This could potentially become a barrier to the wider use of recycled fibres in construction applications. Hence, for blended SFRC at low dosages, it is vital to examine the accuracy of the $\sigma - \varepsilon$ relationship adopted by the guidelines and, if necessary, to make necessary changes.

1.2.4 Anagennisi & Clean Steel projects

The work presented in this study is part of the FP7 EU-funded project ''Anagennisi - Innovative Use of all Tyre Components in Concrete" [50] and the UK Technology Strategy Board (currently called Innovate UK) funded project "Clean Steel - Re-use of steel cord from tyres as reinforcement in sustainable construction". Both projects were successfully completed and managed by the Concrete and Earthquake research group at The University of Sheffield.

The aim of Anagennisi project was to develop innovative solutions to reuse all end-of-life tyre components in high-value concrete applications with reduced environmental impact, whilst the Clean Steel project aimed to reuse RTSC as randomly distributed reinforcement in different construction applications, such as industrial flooring or slope stabilisation. Anagennisi also investigated the behaviour of FRP-confined rubberised concrete and standardised LCA/LCCA (life cycle analysis/life cycle cost analysis) protocols as well as shrinkage-cracking control using recycled polymer fibres.

1.3 Aims and objectives

This research aims to investigate the mechanical behaviour of blended SFRC using manufactured and recycled fibres from tyres at low total dosages (up to 45 kg/m^3), leading to design-oriented models for blended SFRC.

The objectives of this study are listed below:

1. Investigate the mechanical (compressive and flexural) properties of SFRC using blended MSF or RTSC and RTSF at low total fibre dosages.
2. Evaluate the tensile strength of RTSC and investigate interfacial bond behaviour.
3. Investigate different test methods and identify correlations in the flexural behaviour of notched SFRC prism and round panel specimens.
4. Quantify synergies in blended SFRC mixes.
5. Assess the accuracy of uniaxial tensile stress-strain ($\sigma - \varepsilon$) relations proposed by RILEM TC 162-TDF and Model Code 2010.
6. Propose uniaxial tensile stress-strain ($\sigma - \varepsilon$) relationships for blended SFRC at low total fibre dosages (up to 45 kg/m^3).

1.4 Thesis layout & methodology

This thesis adopts an alternative format and comprises three papers published or submitted to peer-reviewed journals.

Chapter 2 is based on Hu et al. [51] and addresses objectives 1, 3, and 4. It investigates the mechanical properties of 10 SFRC mixes comprising MSF only or blended with RTSF at total fibre dosages of 30, 35 and 45 kg/m^3. To characterise the flexural behaviour of the mixes, two flexural

test methods (EN 14651:2005 3-point notched prism tests and ASTM C1550-05 centrally loaded round panel tests) are employed. Correlations between the flexural behaviour of the SFRC prism and round panel specimens are investigated. The effect of fibre and flexural test types on the synergy in blended mixes is discussed.

Chapter 3 is based on Hu et al. [52] and addresses objectives 1 and 2. It evaluates the potential of two types of recycled fibres (RTSC and RTSF) to substitute MSF in concrete. Direct tensile and single-fibre pull-out tests are carried out to examine the tensile strength of RTSC and the interfacial bond behaviour between RTSC and concrete matrix, respectively. The flexural characteristics of 8 SFRC mixes at fibre dosages of 30 and 45 kg/m^3 are examined by using the EN 14651:2005 3-point notched prism tests. RTSC with lengths of 60 mm are used on their own, or blended with RTSF at varying dosages. The performance of two MSF-only mixes and one RTSF-only mix is also examined. Comparisons in terms of flexural performance are made between MSF-only mixes versus recycled-fibre (RTSC on their own or blended with RTSF) mixes at the same total dosage.

Chapter 4 is based on Hu et al. [53] and addresses objectives 5 and 6. It investigates the uniaxial tensile stress-strain ($\sigma - \varepsilon$) relationship of blended SFRC at low total fibre dosages (up to 45 kg/m^3). The accuracy of two $\sigma - \varepsilon$ relations proposed by RILEM TC 162-TDF and Model Code 2010 is assessed using the experimental results from SFRC prisms reinforced with MSF on their own or blended with RTSF. Nonlinear finite element (FE) analysis is used to determine the uniaxial tensile $\sigma - \varepsilon$ relations of the examined mixes, and a simplified trilinear relation for blended SFRC at low dosages is proposed.

Chapter 5 includes general discussion, conclusions and recommendations for future work.

References

[1] WBCSD, End-of-life tires: a framework for effective management systems, http://www.wbcsd.org/DocRoot/lBTHZFGcpBK5OxTDXlpS/EndOfLifeTires_171208.pdf. 2010, (accessed 17. 07 .21).

[2] European Parliament and Council, Directive 2008/98/EC of the European Parliament and of the Council of 19 November 2008 on waste and repealing certain directives, Off. J. Eur. Union. 13 (2008) 3–30.

[3] ETRA, Introduction to tyre recycling: 2013, The European Tyre Recycling Association, Brussels, Belgium, 2013.

[4] H. Tlemat, K. Pilakoutas, K. Neocleous, Stress-strain characteristic of SFRC using recycled fibres, Mater. Struct. 39 (2006) 365–377. doi:10.1617/s11527-005-9009-4.

[5] H. Tlemat, K. Pilakoutas, K. Neocleous, Modelling of SFRC using inverse finite element analysis, Mater. Struct. 39 (2006) 221–233. doi:10.1617/s11527-005-9010-y.

[6] K. Neocleous, H. Tlemat, K. Pilakoutas, Design issues for concrete reinforced with steel fibers, including fibers recovered from used tires, J. Mater. Civ. Eng. 18 (2006) 677–685. doi:10.1061/(ASCE)0899-1561(2006)18:5(677).

[7] A.G. Graeff, K. Pilakoutas, K. Neocleous, M.V.N.N. Peres, Fatigue resistance and cracking mechanism of concrete pavements reinforced with recycled steel fibres recovered from post-consumer tyres, Eng. Struct. 45 (2012) 385–395. doi:10.1016/j.engstruct.2012.06.030.

[8] N. Jafarifar, K. Pilakoutas, T. Bennett, Moisture transport and drying shrinkage properties of steel-fibre-reinforced-concrete, Constr. Build. Mater. 73 (2014) 41–50. doi:10.1016/j.conbuildmat.2014.09.039.

[9] K.H. Younis, K. Pilakoutas, Strength prediction model and methods for improving recycled aggregate concrete, Constr. Build. Mater. 49 (2013) 688–701. doi:10.1016/j.conbuildmat.2013.09.003.

[10] K.H. Younis, K. Pilakoutas, Assessment of post-restrained shrinkage mechanical properties of concrete, ACI Mater. J. 113 (2016) 267–276. doi:10.14359/51688699.

[11] H. Tlemat, Steel fibres from waste tyres to concrete, testing, modelling and design, The University of Sheffield, Sheffield, UK, 2004.

[12] A.G. Graeff, Long-term performance of recycled steel fibre reinforced concrete for pavement applications, The University of Sheffield, UK, 2011.

[13] K. Neocleous, H. Angelakopoulos, K. Pilakoutas, M. Guadagnini, Fibre-reinforced roller-compacted concrete transport pavements, Proc. Inst. Civ. Eng. - Transp. 164 (2011) 97–109. doi:10.1680/tran.9.00043.

[14] N. Jafarifar, Shrinkage behaviour of steel fibre reinfoced concrete pavements, The University of Sheffield, Sheffield, UK, 2012.

[15] H. Angelakopoulos, Reused post-consumer tyre steel fibres in roller compacted concrete, The University of Sheffield, Sheffield, UK, 2016.

[16] UFSD, Thin wire reinforcement for concrete. British Patent Application No 0130852.7 and 0511012.7, filed by The University of Sheffield on 24/12/01 and published on 9/11/2005, Sheffield, UK, 2001.

[17] A.M. Brandt, Fibre reinforced cement-based (FRC) composites after over 40 years of development in building and civil engineering, Compos. Struct. 86 (2008) 3–9. doi:10.1016/j.compstruct.2008.03.006.

[18] W. Labib, An Experimental Study and Finite Element Analysis of Punching Shear Failure in Steel Fibre-Reinforced Concrete Ground-Suspended Floor Slabs, Liverpool John Moores University, Liverpool, UK, 2008.

[19] ACI 544.1R-96 (Reapproved 2002), State-of-the-art report on fiber reinforced concrete. American Concrete Institute, Michigan, US, 2002.

[20] J.J.P. Romualdi, J. a Mandel, Tensile Strength of concrete Affected by Uniformly Distributed and Closely Spaced Short Lengths of wire Reinforcement, ACI J. Proc. 61 (1964) 657–672. doi:10.14359/7801.

[21] F. Minelli, G.A. Plizzari, Fiber reinforced concrete characterization through round panel test - Part I: experimental study, in: Proceedings of the 7th international conference on fracture mechanics of concrete and concrete structures (FRAMCOS), 2010: pp. 1451–1460.

[22] N. Banthia, M. Sappakittipakorn, Toughness enhancement in steel fiber reinforced

concrete through fiber hybridization, Cem. Concr. Res. 37 (2007) 1366–1372. doi:10.1016/j.cemconres.2007.05.005.

[23] N. Banthia, J. Sheng, Fracture toughness of micro-fiber reinforced cement composites, Cem. Concr. Compos. 18 (1996) 251–269. doi:10.1016/0958-9465(95)00030-5.

[24] M.A. Aiello, F. Leuzzi, G. Centonze, A. Maffezzoli, Use of steel fibres recovered from waste tyres as reinforcement in concrete: Pull-out behaviour, compressive and flexural strength, Waste Manag. 29 (2009) 1960–1970. doi:10.1016/j.wasman.2008.12.002.

[25] H. Salehian, J.A.O. Barros, M. Taheri, Evaluation of the influence of post-cracking response of steel fibre reinforced concrete (SFRC) on load carrying capacity of SFRC panels, Constr. Build. Mater. 73 (2014) 289–304. doi:10.1016/j.conbuildmat.2014.09.043.

[26] B. Mobasher, Mechanics of fiber and textile reinforced cement, CRC Press, Florida, US, 2012.

[27] Ş. Yazıcı, G. İnan, V. Tabak, Effect of aspect ratio and volume fraction of steel fiber on the mechanical properties of SFRC, Constr. Build. Mater. 21 (2007) 1250–1253. doi:10.1016/j.conbuildmat.2006.05.025.

[28] N. Banthia, S.M. Soleimani, Flexural response of hybrid fiber-reinforced cementitious composites, ACI Mater. J. 102 (2005) 382–389.

[29] G. Groli, Crack width control in RC elements with recycled steel fibres and applications to integral structures: theoretical and experimental study, Polytechnical University of Madrid, Madrid, Spain, 2014.

[30] E. Martinelli, A. Caggiano, H. Xargay, An experimental study on the post-cracking behaviour of Hybrid Industrial/Recycled Steel Fibre-Reinforced Concrete, Constr. Build. Mater. 94 (2015) 290–298. doi:10.1016/j.conbuildmat.2015.07.007.

[31] G. Centonze, M. Leone, M.A. Aiello, Steel fibers from waste tires as reinforcement in concrete: A mechanical characterization, Constr. Build. Mater. 36 (2012) 46–57. doi:10.1016/j.conbuildmat.2012.04.088.

[32] M. Leone, G. Centonze, D. Colonna, F. Micelli, M.A. Aiello, Fiber-reinforced concrete with low content of recycled steel fiber: Shear behaviour, Constr. Build. Mater. 161 (2018) 141–155. doi:10.1016/j.conbuildmat.2017.11.101.

[33] Z. Zamanzadeh, L. Lourenço, J. Barros, Recycled steel fibre reinforced concrete failing in bending and in shear, Constr. Build. Mater. 85 (2015) 195–207. doi:10.1016/j.conbuildmat.2015.03.070.

[34] D. Bjegovic, A. Baricevic, S. Lakusic, D. Damjanovic, I. Duvnjak, Positive interaction of industrial and recycled steel fibres in fibre reinforced concrete, J. Civ. Eng. Manag. 19 (2013) S50–S60. doi:10.3846/13923730.2013.802710.

[35] M. Skazlić, A. Baričević, D. Bjegović, Fibre reinforced SCC concrete with recycled fibres, Newsletter. (2017) 1–7.

[36] G. Groli, A.P. Caldentey, A.G. Soto, Cracking performance of SCC reinforced with recycled fibres - an experimental study, Struct. Concr. 15 (2014) 136–153. doi:10.1002/suco.201300008.

[37] H. Angelakopoulos, P. Papastergiou, K. Pilakoutas, Fibrous roller-compacted concrete with recycled materials - Feasibility study, Mag. Concr. Res. 67 (2015). doi:10.1680/macr.14.00246.

[38] H. Angelakopoulos, P Waldron, Tyre wire in Concrete Leading to Environmental sustainability. CIP Eco-innovation project, Twincletoes project - Layman's report, Twincon Ltd, Sheffield, UK, 2015.

[39] K. Neocleous, S.G. Maxineasa, L. Dumitrescu, K. Themistocleous, N. Taranu and D. Hadjimitsis, D1.6 Preliminary LCA. Anagennisi Project, Anagennisi: innovative use of all tyre components in concrete, 2014.

[40] N. Banthia, N. Nandakumar, Crack growth resistance of hybrid fiber reinforced cement composites, Cem. Concr. Compos. 25 (2003) 3–9.

[41] L.G. Sorelli, A. Meda, G.A. Plizzari, Bending and uniaxial tensile tests on concrete reinforced with hybrid steel fibers, J. Mater. Civ. Eng. 17 (2005) 519–527. doi:10.1061/(ASCE)0899-1561(2005)17:5(519).

[42] J.S. Lawler, T. Wilhelm, D. Zampini, S.P. Shah, Fracture processes of hybrid fiber-reinforced mortar, Mater. Struct. 36 (2003) 197–208. doi:10.1007/BF02479558.

[43] C.X. Qian, P. Stroeven, Development of hybrid polypropylene-steel fibre-reinforced concrete, Cem. Concr. Res. 30 (2000) 63–69. doi:10.1016/S0008-8846(99)00202-1.

[44] P. Rashiddadash, A.A. Ramezanianpour, M. Mahdikhani, Experimental investigation on

flexural toughness of hybrid fiber reinforced concrete (HFRC) containing metakaolin and pumice, Constr. Build. Mater. 51 (2014) 313–320. doi:10.1016/j.conbuildmat.2013.10.087.

[45] Y. Mohammadi, S.P. Singh, S.K. Kaushik, Properties of steel fibrous concrete containing mixed fibres in fresh and hardened state, Constr. Build. Mater. 22 (2008) 956–965. doi:10.1016/j.conbuildmat.2006.12.004.

[46] K.H. Younis, K. Pilakoutas, M. Guadagnini, H. Angelakopoulos, Feasibility of Using Recycled Steel Fibres To Enhance the Behaviour of Recycled Aggregate Concrete, FRC 2014 Jt. ACI-Fib Int. Work. - Fibre Reinf. Concr. from Des. to Struct. Appl. (2014) 598–608.

[47] A. Baricevic, D. Bjegovic, M. Skazlic, Hybrid fiber-reinforced concrete with unsorted recycled-tire steel Fibers, J. Mater. Civ. Eng. 29 (2017) 6017005. doi:10.1061/(ASCE)MT.1943-5533.0001906.

[48] Rilem TC 162-TDF, σ-ε-Design Method, Mater. Struct. 36 (2003) 560–567. doi:10.1007/BF02480834.

[49] F.I. du Béton, Fib Model Code for Concrete Structures 2010, Wilhelm Ernst & Sohn, Berlin, Germany, 2013.

[50] Anagennisi Project, Anagennisi: innovative use of all tyre components in concrete. http://anagennisi.org/wordpress/, 2014 (accessed 2018.03.20).

[51] H. Hu, P. Papastergiou, H. Angelakopoulos, M. Guadagnini, K. Pilakoutas, Mechanical properties of SFRC using blended manufactured and recycled tyre steel fibres, Constr. Build. Mater. 163 (2018) 376–389. doi:10.1016/j.conbuildmat.2017.12.116.

[52] H. Hu, P. Papastergiou, H. Angelakopoulos, M. Guadagnini, K. Pilakoutas, Mechanical properties of SFRC using blended recycled tyre steel cords and recycled tyre steel fibres, Construction and Building Materials, 2018. **Submitted for publication.**

[53] H. Hu, Z. Wang, F.P. Figueiredo, P. Papastergiou, M. Guadagnini, K. Pilakoutas, Post-cracking tensile behaviour of blended steel fibre reinforced concrete, Structural Concrete, 2018. **Submitted for publication.**

Chapter 2 Mechanical Properties of SFRC Using Blended Manufactured and Recycled Tyre Steel Fibres

H. Hu, P. Papastergiou, H. Angelakopoulos, M. Guadagnini, K. Pilakoutas, Mechanical properties of SFRC using blended manufactured and recycled tyre steel fibres, Construction and Building Materials. 163 (2018) 376–389. doi:10.1016/j.conbuildmat.2017.12.116.

Author contribution statement

Dr Papastergiou, Dr Guadagnini and Prof. Pilakoutas coordinated the Anagennisi project. Dr Angelakopoulos supplied the fibres used and provided practical information on mix design and fibre characteristics. All authors discussed the results and commented on the manuscript.

ABSTRACT

This chapter investigates the mechanical properties of 10 steel fibre reinforced concrete (SFRC) mixes at fibre dosages of 30, 35 and 45 kg/m^3. Manufactured Steel Fibres (MSF) are used on their own, or blended with sorted steel fibres recycled from end-of-life tyres (RTSF). To characterise the flexural behaviour of the mixes, two flexural test methods, EN 14651:2005 3-point notched prism tests and ASTM C1550-05 centrally loaded round panel tests are employed. A strong correlation is found in the flexural behaviour of the SFRC prism and round panel specimens, with corresponding conversion equations proposed. The mechanical properties of hybrid mixes using RTSF vary depending on dosages, but are comparable with those of MSF-only mixes at the same fibre dosage. A positive synergetic effect is derived from hybrid mixes containing 10 kg/m^3 of RTSF.

This chapter consists of a “stand-alone” journal paper and includes a relevant bibliography at the end of the chapter. Additional information and further test results are presented in Appendix A. This includes concrete mix design, compressive cube strength from cubes, residual flexural tensile strength from prisms, load-deflection (or –CMOD) curves for each prism, energy absorption capacity of round panels and flexural test results for each panel.

2.1 Introduction

Annually about 1.5 billion tyres are produced and around 1 billion tyres (17 million tonnes) [1] reach their end of life worldwide [2]. To minimise the environmental impact of end-of-life tyres and generate value, the tyre recycling industry has developed various processes to extract the main tyre constituents (rubber, steel and polymer) [3]. The most commonly used and financially viable tyre recycling techniques adopt a combination of mechanical shredding and granulation, which produces steel fibres of irregular shapes, lengths and diameters. However, these fibres are often heavily contaminated with rubber (up to 20% by mass) and are prone to agglomeration due to significant geometrical irregularities and excessive aspect ratios. Further processing is thus required to: (1) minimise rubber contamination to less than 0.5% by mass, (2) limit the fibre length and diameter distribution to those that are effective in concrete (3) and avoid agglomeration before and during concrete mixing. Only after the tyre wire has been cleaned, sorted and classified, the product ("Recycled Tyre Steel Fibres" (RTSF)) can satisfy the Quality Assessment requirements for construction materials and thus can be used in concrete as structural reinforcement. Since 1999, numerous studies have been conducted at The University of Sheffield to investigate the mechanical properties of RTSF [4–10] and their potential in structural applications [11–15], and a patent application was filed in 2001 [16]. A spin-out company now produces classified RTSF. Comparative LCA studies [17,18] have shown that the RTSF production consumes only up to 5% of the energy required for the production of typical Manufactured Steel Fibres (MSF), highlighting the significant environmental benefits of RTSF.

MSF are commonly used as reinforcement in concrete applications such as industrial flooring [3,19,20] and tunnel linings [21]. Previous research [20,22–29] showed that the incorporation of steel fibres can significantly enhance the post-cracking residual strength and flexural toughness of a cementitious matrix, whilst their influence on compressive strength and modulus of elasticity is relatively small, unless a high fibre dosage is used [30]. However, in the majority of SFRC applications [26], only single-type fibre (i.e. MSF) reinforced concrete is used. The use of single-type fibres can be effective in arresting or bridging cracks of specified widths, but the fracture process of concrete matrix is more multi-scale and gradual [26]. The use of blended fibres with different aspect ratios (length/diameter) and physical properties ("fibre hybridisation [23]" in concrete), may provide better crack control over a broader range of crack widths. Several studies [23,25–27,29,31–35] on hybrid FRC (or mortar) have demonstrated that fibre hybridisation can lead to a better performance than that of single-type fibres. Younis et al. [36]

reported that hybrid SFRC using 1% (by mass) of cleaned and sorted RTSF blended with 1% of undulated MSF exhibited higher flexural strength and toughness, compared to SFRC mixes containing 2% of undulated MSF. Nevertheless, this positive synergetic effect has not always been observed in previous studies using recycled tyre wire due to fibre agglomeration or unsuitable fibre combinations [33,37], in particular when unclassified and unsorted fibres were used. Since RTSF have a wide fibre length distribution and a higher nominal tensile strength than typical MSF, the mechanical properties of hybrid SFRC containing both MSF and classified RTSF, at different dosages, needs to be investigated. The results presented in this study are part of the FP7 EU-funded project "Anagennisi" [38] which aimed to develop uses for all tyre components in concrete.

Uniaxial tension tests for SFRC are difficult to conduct and interpret [11,12,30,39] and as a consequence flexural tests have become the preferred method to characterise the post-cracking residual flexural tensile strength and flexural toughness of SFRC. Nonetheless, various testing methodologies are available in different design codes of practice (Europe: [30,40–45], US: [46–48], Japan: [49]) and several researchers have developed their own test methods [50–52], including 3 or 4-point prism and single-point loaded, square slab and round panel tests. Compared with 4-point un-notched prism and square slab tests, EN 14651:2005 3-point (or even 4-point) notched prism [41] and ASTM C1550-05 round panel tests [48] have the advantage of generating consistent and predictable modes of failure [52], leading to a better comparison between different materials tested. Hence, these two tests are more universally adopted than others.

FRC test results are characterised by high variability due to non-uniformity in fibre distribution. Furthermore, test results from prisms are often associated with a larger scatter when compared to those from round panels, mainly due to significant differences in the fracture zone (roughly 187 cm^2 for prisms whilst 900 cm^2 for round panels). As a consequence of this, a minimum number of 12 tests for prisms [53] and 3 tests [48] for round panels are required per mix. It should be noted that prisms come with the extra requirement of saw cutting for notching, but the actual test is simpler and only requires a small-capacity testing machine.

Owing to the extensive experimental workload required, only one of the two testing methods is adopted in most research studies [14,20,51,52,54–58], which makes comparisons difficult. For the design of SFRC structures, the post-cracking residual flexural tensile strength f_R of SFRC prisms is commonly adopted in RILEM TC 162-TDF [40], FIB Model Code 2010 [30], and Concrete

Society TR 34 [45]. This underscores the need to determine this quantity accurately and to correlate the results from the standard 3-point notched prism tests and the round panel tests used in the American practice. One problem associated with such a correlation is that different fracture parameters are adopted in these two tests. f_R values at specified crack mouth openings (CMODs) are used for prism tests, while energy absorption capacity (E values) up to selected deflections are adopted for round panel tests. Furthermore, flexural strength f_u of the prisms can be calculated from the peak load of the load-deflection curves, but its counterpart from round panels is not included in ASTM C-1550. Bernard [20] proposed a calculation for the flexural strength based on the yield line theory for ASTM round panels, but the size of the loading plate (area of load) was not considered. Limited studies [20,51,52,59,60] have investigated the correlation between SFRC prisms with different geometric characteristics and round panel tests with regard to fracture parameters, but only MSF or some synthetic fibres (e.g. polypropylene fibres) were examined. The correlations between 3-point notched prism and round panel tests for steel fibre hybrids are rare and inconclusive, especially when RTSF is incorporated.

To address several of the above issues, the flexural performance of 10 SFRC mixes, using MSF on their own or blended together, is examined in this study employing both prism and round panels. This paper is structured as follows; section 2.2 introduces the experimental details of this study, including the geometrical and mechanical characterisation of both MSF and RTSF, the experimental campaign and concrete mix design. Section 2.3 presents the experimental results of SFRC under uniaxial compression and flexure (using two types of tests). Thereafter, correlations between the two flexural tests and the synergetic effect in hybrid mixes are discussed. Section 2.4 presents the design considerations of using hybrid SFRC reinforced with RTSF in structural applications and section 2.5 summarises key research findings.

2.2 Experimental details

2.2.1 Fibre characterisation

RTSF (Figure 2-1 (a)) and two types of manufactured undulated (crimped) steel fibres, MSF1 (Figure 2-1 (b)) and MSF 2 (Figure 2-1 (c)) were used in the study. Previous studies conducted by Neocleous et al. [13] suggests that RTSF with an aspect ratio greater than 200, can induce fibre balling even at low fibre dosages. A photography system was developed to determine the length and aspect ratio distribution of RTSF [15]. The system captures images of fibres passing in front

of a screen with a high-speed camera and analyses the geometry of each fibre. The length distribution of a representative sample of approximately 60,000 fibres was found to be 68% (by mass) between 15-40 mm (Figure 2-2 (a)) with a mean length of 23 mm. Figure 2-2 (b) shows a histogram of the RTSF aspect ratio distribution, where a mean value of around 100 has been obtained. MSF1 had greater length, diameter and tensile strength than MSF2. Table 2-1 summarises the geometrical and mechanical characteristics of the three fibre types.

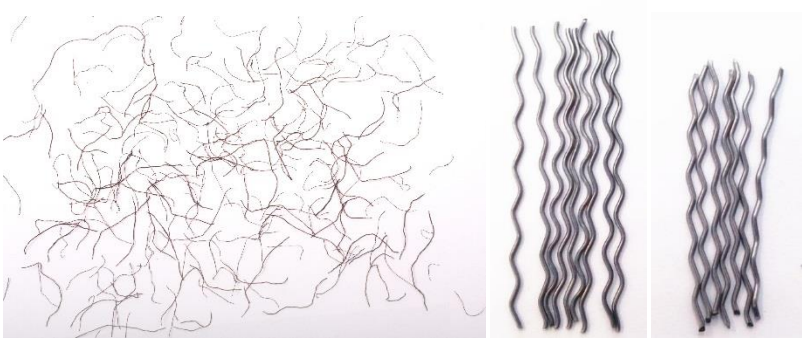

(a) (b) (c)

Figure 2-1: (a) RTSF, (b) MSF1 and (c) MSF2

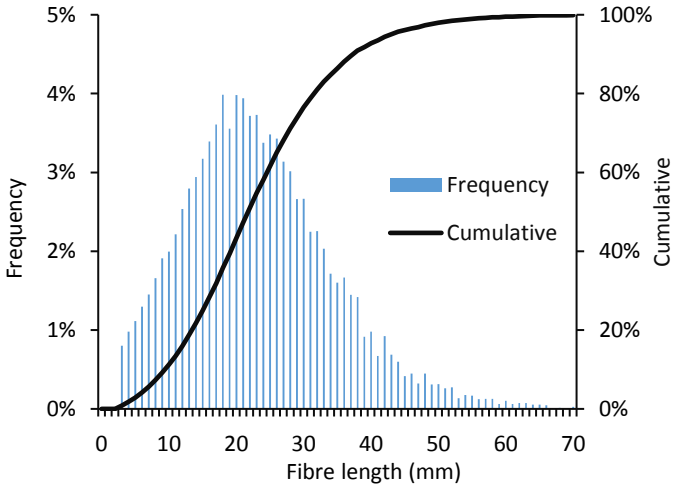

(a)

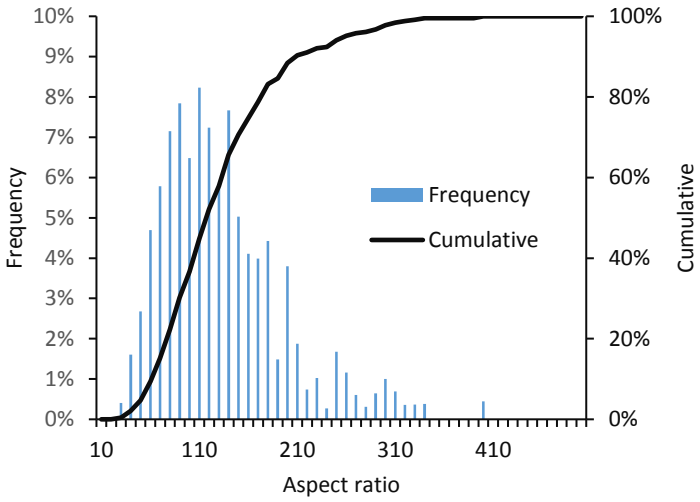

(b)

Figure 2-2: RTSF histograms: (a) fibre length distribution; (b) aspect ratio distribution

Table 2-1: Geometrical and mechanical specifications of RTSF, MSF1 and MSF2

Fibre type	Length (mm)	Diameter (mm)	Aspect ratio	Tensile strength (MPa)	Elastic modulus (GPa)
a - RTSF	23*	0.22*	100*	2570*	200
b - MSF1	60±2	1.0±0.04	60.0	1450	200
c - MSF2	55±2	0.8±0.04	68.8	1050	200

* The nominal (mean) values for RTSF

2.2.2 SFRC mixes tested and mix design

Steel fibre dosages ranging between 30-45 kg/m^3 are commonly used in structural applications such as slabs-on-grade and suspended slabs on piles, to resist flexural and punching shear failure modes. Hence, two fibre dosages, were mainly investigated in this study: 30 kg/m^3 (volume fraction $V_f = 0.38\%$) and 45 kg/m^3 ($V_f = 0.57\%$). An additional mix of 35 kg/m^3 ($V_f = 0.45\%$) (mix F) was also tested to evaluate the performance of the higher strength MSF1 fibre at a lower dosage than the typical dosage of 45 kg/m^3 used in suspended slabs. A RTSF-only mix at 45 kg/m^3 was also tried but discarded due to balling issues, indicating the critical fibre dosage of RTSF using a conventional mixer is about 30 kg/m^3. A higher dosage of RTSF up to 36 kg/m^3 was reported by Centonze et al. [61] when a planetary mixer was employed. Table 2-2 shows details of the mixes including fibre type examined and their dosage.

To characterise the flexural and compressive properties of SFRC, 12 (or 6) prisms, 3 round panels and 3 cubes were cast per mix. Only 6 prisms were cast for mixes C, D, E, I and J to have a more comprehensive parametric investigation with less experimental workload. Due to the large volume of concrete required, the SFRC mixes were cast in 5 separate batches of ready-mixed concrete. For each batch, 6 plain concrete prisms and 3 cubes were also cast and then tested as control specimens.

Table 2-2: Experimental campaign

Total fibre dosage (kg/m^3)	Mix	Bat. no.	Plast. (L/m^3)	Additional Water (L/m^3)	Slump (mm) before/after	MSF1 dosage (kg/m^3)	MSF2 dosage (kg/m^3)	RTSF dosage (kg/m^3)	Avg. f_{cu} (MPa) SFRC/Plain	Stdev. (MPa) SFRC/Plain
30	A	3	1.8	6.6	20/70	-	30	-	43.9/42.0	1.8/0.9
	B	4	1.5	3.3	60/120	-	20	10	42.6/46.1	2.2/2.0
	C	1	1.5	0	100/100	-	15	15	44.3/47.5	1.9/1.1
	D	1	1.5	0	100/100	-	10	20	44.6/47.5	1.9/1.1
	E	5	1.5	3.3	50/150	-	-	30	41.8/37.6	1.9/3.7
35	F	3	1.8	6.6	20/70	35	-	-	42.9/42.0	1.9/0.9
45	G	3	1.8	6.6	20/70	45	-	-	41.9/42.0	1.0/0.9
	H	4	1.5	3.3	60/120	35	-	10	42.8/46.1	0.2/2.0
	I	1	1.5	0	100/100	22.5	-	22.5	50.3/47.5	2.4/1.1
	J	2	1.5	3.3	30/80	10	-	35	44.5/39.9	0.7/1.0

The fibres were added manually during mixing, and vibration was applied after the moulds were filled with concrete. The specimens were cured in the moulds for 48 hours. After demoulding, all specimens were covered with wetted hessian fabric and plastic sheet was placed on top to retain moisture for the duration of curing, at a temperature of 22 ± 3 °C. After 28 days of curing, all hessian and plastic sheets were removed and specimens were left to dry. All specimens were tested at the age of 35-60 days.

The workability of concrete can be affected adversely by fibre inclusion [62,63]. Though the slump test is not the best indicator of workability for SFRC materials (ACI 544.2R-89 [64]), it is still used as a qualitative measure to maintain a consistent workability of concrete from batch to batch and it is still extensively used by the flooring industry. The common procedure adopted by the flooring industry for adding fibres in concrete was followed: The initial slump of the delivered ready-mix concrete was taken which ranged from 20 to 100 mm (see Table 2-2) and

additional water was added to the concrete mix if the measured slump was lower than 100 mm. After the addition of the water, the slump was checked again to reach at least 70 mm. Superplasticiser was then added which caused a collapse slump (beyond 260 mm). After the addition of fibres, the slump reduced to roughly the same levels as after the addition of the water (70-150 mm). No major fibre agglomeration has been observed during all 5 concrete castings; the target concrete compressive strength, f_{cu}, was 40 MPa. The concrete mix design was 150 kg/m^3 of cement, 150 kg/m^3 of GGBS, 1097 kg/m^3 of coarse aggregates (4-20 mm), 804 kg/m^3 of coarse gravel aggregates (0-4 mm). The initial water cement ratio (w/c) was 0.55.

2.2.3 Compressive cube tests: specimens preparation and testing procedure

The concrete cubes (150 mm) were tested under uniaxial compressive loading according to EN 12390-3: 2009 [65]. The dimensions of each cube were recorded before testing.

2.2.4 Flexural tests on prisms: specimens preparation and testing procedure

According to EN 14651:2005 [41], a notch (5 mm thick and 25 mm deep) was sawn at mid-span of each prism (150 mm x 150 mm x 550 mm) a day before testing. All prisms were tested under 3-point bending (Figure 2-3), using a 300 kN universal electromechanical testing machine. Two central deflections were recorded on either side of the specimens using two Linear Variable Differential Transformers (LVDTs), placed on an aluminium yoke. The Crack Mouth Opening Displacement (CMOD) was also measured at mid-span with a 12.5 mm clip gauge (mounted under the notch of the prism). The loading point was free to rotate both in-plane and out-of-plane and the appropriate horizontal degrees of freedom were enabled at the supports. The tests were CMOD-controlled at a constant rate of 0.05 mm/min for CMOD from 0 to 0.1 mm and 0.2 mm/min for CMOD from 0.1mm until 4 mm. The dimensions of each specimen, including the distance between the tip of the notch to the top of each specimen were recorded before testing. All cracks initiated from the notch tip and then propagated to the top of the prism.

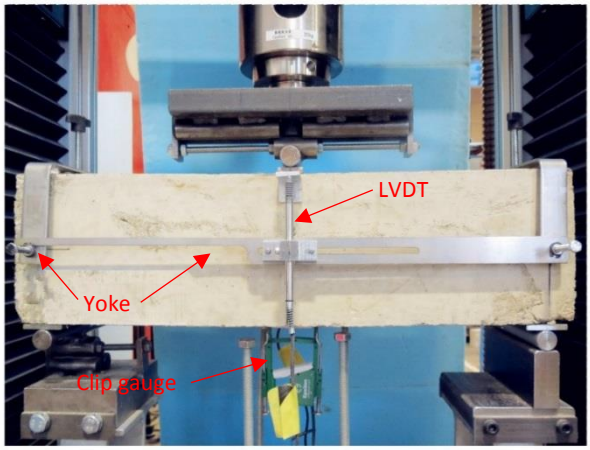

Figure 2-3: Flexural prism testing setup

2.2.5 Flexural tests on round panels: specimens preparation and testing procedure

The SFRC round panels were tested using a 250 kN hydraulic actuator, following the testing arrangement and procedure of ASTM C1550-05 [48]. Each round panel was centrally loaded and supported on three symmetrically (120°) arranged pivots on a pitch circle diameter of 750 mm (Figure 2-4). The test was under displacement control at a constant central deflection rate of 4 mm/min up to a maximum central deflection of 45 mm. Cracks initiated from the bottom central point of the panel and gradually propagated to the edges between the supports, forming three radial cracks at angles of 120°. Due to the random distribution of aggregates and fibres, the principal cracks do not propagate in a straight line (Figure 2-5). Furthermore, a large number of secondary cracks developed from the macrocracks.

Figure 2-4: Flexural round panel test setup

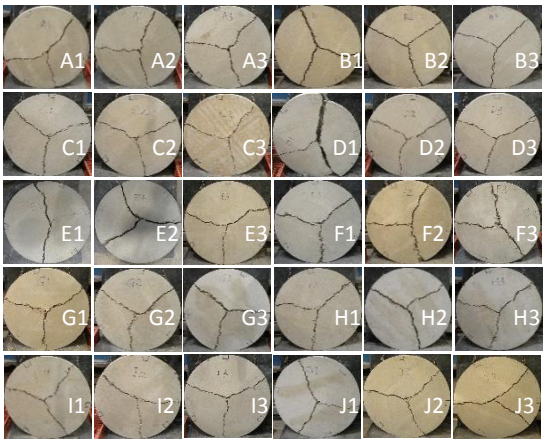

Figure 2-5: All SFRC round panels (after testing)

2.3 Experimental studies and results

2.3.1 Compressive tests

The SFRC cube compressive strength f_{cu} ranged from 41.8 to 50.3 MPa, whilst the plain concrete compressive strength ranged from 37.6 to 47.5 MPa (see Table 2-2). The variability found is considered typical for ready mixed concrete. Compared to plain concrete, the compressive strength marginally increased up to approximately 5% due to the addition of MSF only, while an increase of around 10% was observed for mix E [RTSF (30)]. For hybrid mixes, there was a small loss of strength (roughly 7%) at total fibre dosage of 30 kg/m^3, while at 45 kg/m^3, the strength

change ranged from -7% to 11 %. Overall, the compressive strength of the hybrids was slightly better when using a higher dosage of RTSF.

In literature, the influence of steel fibres on the compressive strength of concrete is still inconclusive. For MSF, up to around 20% increase of compressive strength is reported by [29,62,66] when up to 78kg/m^3 of fibres was added, whilst a marginal effect or even a reduction up to 10% of compressive strength can be found in [67,68]. Very few studies investigated the effect of RTSF on the compressive strength of concrete. Up to 20% of enhancement was reported in [9,61,63] when adding no more than 48 kg/m^3 of RTSF, whilst a marginal effect was also reported in [33,35]. The variability in compressive strength can be explained by the fact that air trapped around fibres can decrease the strength [3], whilst fibres can arrest lateral microcracks and delay their coalescence in macrocracks, leading to marginal increases in strength. A significant reduction up to 20% was reported in [69] for concrete with unclassified and unsorted steel beads from waste tyres. This reduction in strength may be due to rubber (in free form or attached to the steel), and the highly variable geometrical characteristics of the beads that are prone to agglomeration. This highlights the importance of using clean and classified RTSF to limit variability.

2.3.2 Flexural prism tests

2.3.2.1 Relationship between measured deflection and CMOD values

The mid-span deflection of a prism was taken as the mean of the deflection values measured from the 2 vertical LVDTs. It is noted that both vertical displacement measurements were in good agreement (see Figure 2-6) indicating little torsional effects, as also found by Soutsos et al. [66].

A linear relation between CMOD and average deflection is proposed by EN 14651:2005 [41], as given below,

$$Averaged\ \ deflection\ (mm) = k * CMOD\ (mm) + 0.04\ mm, k = 0.85 \quad (2\text{-}1)$$

This has been also confirmed by this study, where a very strong correlation was found between CMOD and averaged deflection values for all SFRC prisms tested. k ranged from 0.77 to 0.82, with coefficients of determination $R^2 > 0.99$.

Slightly higher values of k than those proposed by EN 14651 was reported in [51] when adding 45 kg/m^3 of hooked-end MSF with an aspect ratio of 66.7 in concrete. A linear relation between

CMOD and average deflection employing 4-point notched SFRC prism tests was reported in [37], when both MSF and unsorted RTSF were used. The linear relationship between CMOD and deflection values allows for the possibility of measuring just one of them in the prism test.

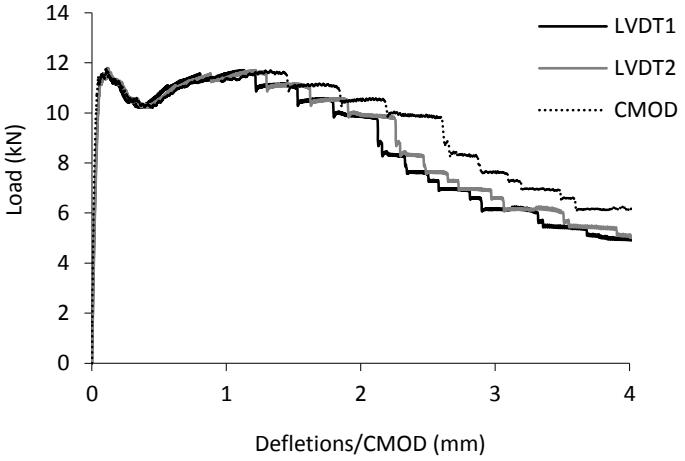

Figure 2-6: Typical deflection values obtained from 2 LVDTs and CMOD

2.3.2.2 Load-deflection curves

Since load-CMOD curves showed very similar behaviour to load-deflection curves, only the load-deflection curves are presented and discussed in this section. Figures 2-7 and 2-8 show the load-deflection curves for SFRC mixes at 30 kg/m^3, and 45 kg/m^3 (and also 35 kg/m^3), respectively. Load-deflection curves for single-fibre-type reinforced concrete and plain concrete prisms are shown in solid lines, while hybrid SFRC prisms are shown in dashed lines.

The solid red curves indicate the typical brittle behaviour of plain concrete, which highlights the weakness of concrete in tension. Generally, improved flexural performance can be obtained from concrete with higher total fibre dosage, from 30 kg/m^3 to 45 kg/m^3. The 35 and all 45 kg/m^3 mixes exhibited deflection hardening behaviour, which was only found from hybrid mix B [MSF2 (20) + RTSF (10)] at the total fibre dosage of 30 kg/m^3.

The best flexural performance was found from hybrid mixes B [MSF2 (20) + RTSF (10)] and H [MSF1 (35) + RTSF (10)] in the two groups of mixes, indicating that hybrid SFRC mixes containing 10 kg/m^3 of RTSF can show better flexural performance than MSF-only mixes at the same fibre dosage. Compared to other SFRC mixes, a sharper descending gradient occurs for mixes

containing more than 22.5 kg/m^3 of RTSF (RTSF-only mix E and hybrid mixes I and J) starting at a deflection of approximately 1.5 mm. This may be due to the fact that shorter RTSF can debond or even pull out at large crack widths, leading to progressive damage. This also suggests that RTSF, due to their geometrical characteristics, are less effective at controlling macrocracks than MSF, as also reported by Graeff et al. [7] for fatigue tests and Zamanzadeh et al. [54].

FIB Model Code 2010 [30] relates the constitutive laws of FRC at the SLS and ULS to the CMODs of 0.5 mm and 2.5 mm for the prism tests, respectively. This implies that the contribution of RTSF can be more beneficial at service conditions, but less helpful at large displacements or crack widths.

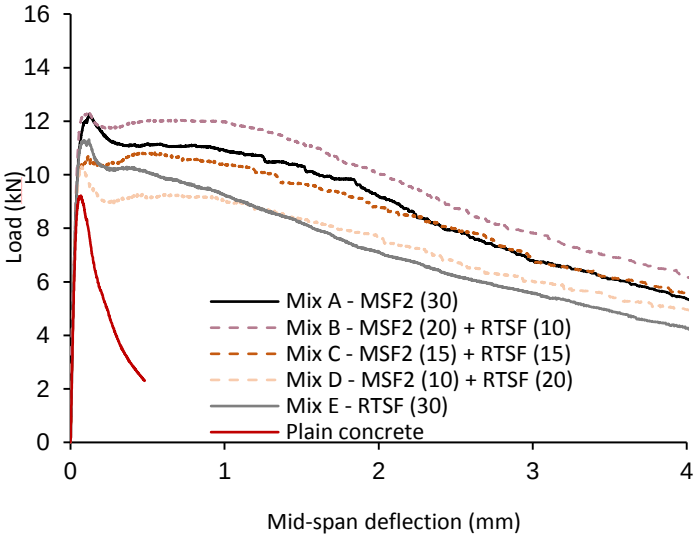

Figure 2-7: Load-deflection curves for SFRC mixes at 30 kg/m^3

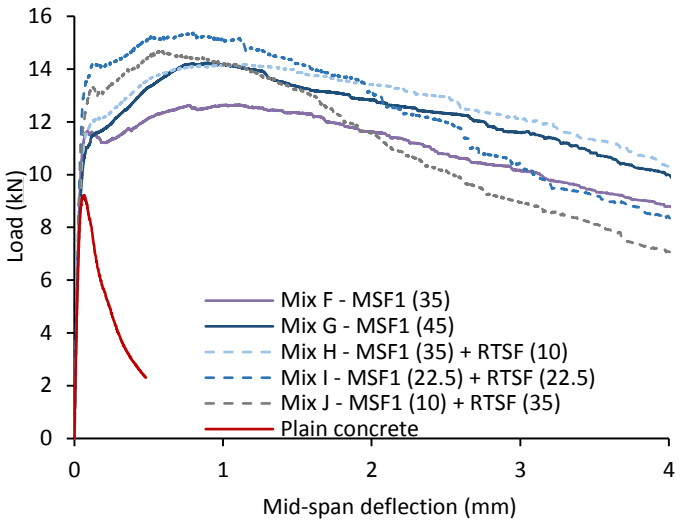

Figure 2-8: Load-deflection curves for mixes at 35 and 45 kg/m³

2.3.2.3 Flexural modulus of elasticity (E_{fm}), residual flexural tensile strength (f_R) and flexural strength (f_{u-1})

Flexural modulus of elasticity (E_{fm})

The modulus of elasticity of concrete can be measured directly via compressive tests or indirectly via flexural tests. Elastic analysis was used to determine the flexural modulus (by matching results up to 40% of the peak flexural load) from flexural tests (Figure 2-9). Since the load spreading effect was found to be negligible [12], the dimensions of the loading and supporting rollers were not considered. Ignoring shear deformation in the prism, the linear equation relating the load-deflection stiffness to E_{fm} is given below,

$$E_{fm} = \frac{Pl^3}{48I\delta} \quad (2\text{-}2)$$

Where $\frac{P}{\delta}$ (kN/mm) is the slope of the initial part of the load-deflection curve, l (mm) is the span of the prism, I (mm⁴) is the second moment of area of the middle cross-section.

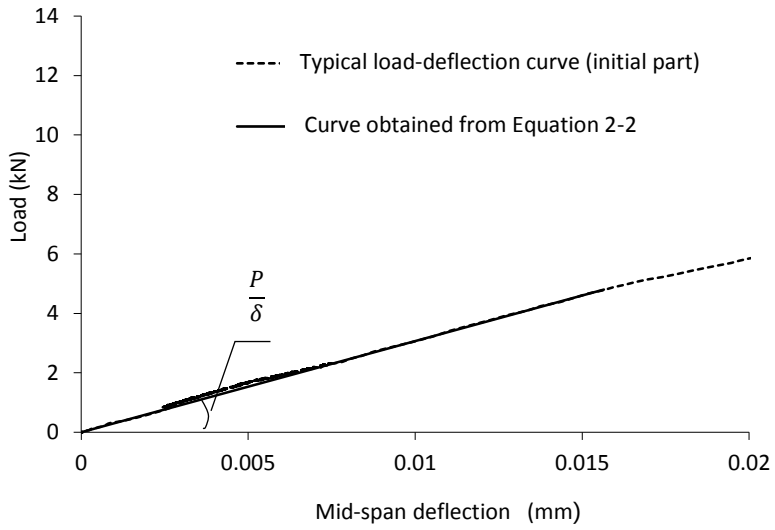

Figure 2-9: The determination of flexural modulus E_{fm}

Figure 2-10 shows the flexural modulus E_{fm} and related standard deviations of all SFRC mixes tested. The counterparts for plain concrete are shown in grey columns.

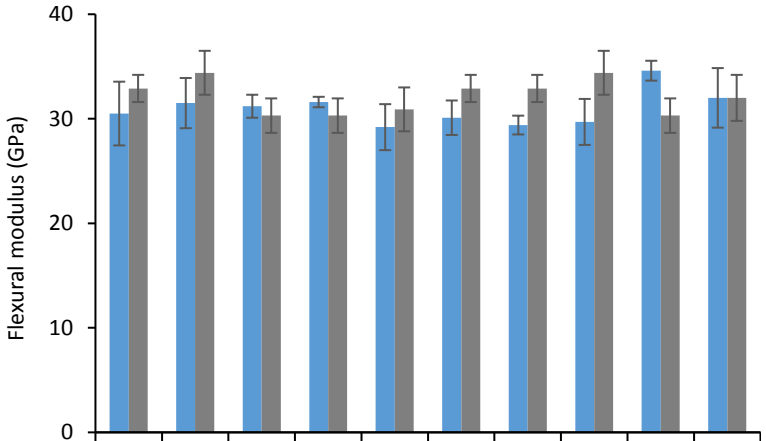

	A	B	C	D	E	F	G	H	I	J
SFRC mixes	30.5	31.5	31.2	31.6	29.2	30.1	29.4	29.7	34.6	32.0
Plain concrete	32.9	34.4	30.3	30.3	30.9	32.9	32.9	34.4	30.3	32.0

Figure 2-10: E_{fm} of SFRC and plain concrete prisms

All SFRC prisms showed similar E_{fm} to the plain concrete. A similar conclusion was also arrived by Jafarifar [14], when 60 kg/m^3 of RTSF (of slightly shorter lengths) was added to conventional concrete or roller compacted concrete. RTSF-reinforced mixes showed comparable moduli and

standard deviations to MSF-only mixes. Air entrapped around the fibres could have a negative effect on the elastic modulus, while the steel fibres can contribute in a positive manner. Since both effects are small in low fibre dosages, no significant change in the elastic properties is expected.

Residual flexural tensile strength (f_R)

EN 14651:2005 [41] follows a methodology first adopted by RILEM TC 162-TDF [40], to characterise the residual flexural tensile behaviour of SFRC prisms, where flexural stresses (f_{R1}, f_{R2}, f_{R3} and f_{R4}) are calculated from the load-CMOD curves at 0.5, 1.5, 2.5 and 3.5 mm of CMOD, respectively. The calculation of f_R [41] for 3-point bending test is given below,

$$f_{Ri} = \frac{3F_{Ri}l}{2bh_{sp}^2} \tag{2-3}$$

Where F_{Ri} (N) is the applied load at CMODs of 0.5, 1.5, 2.5 and 3.5 mm ($i = 1,2,3,4$). $b = 150\ mm$ is the width of prism and h_{sp} is the distance between the tip of the notch to the top of the specimen.

Figure 2-11 shows the f_{Ri} values (in MPa) of all SFRC mixes. Coefficients of variation (COV) for those values are listed in brackets.

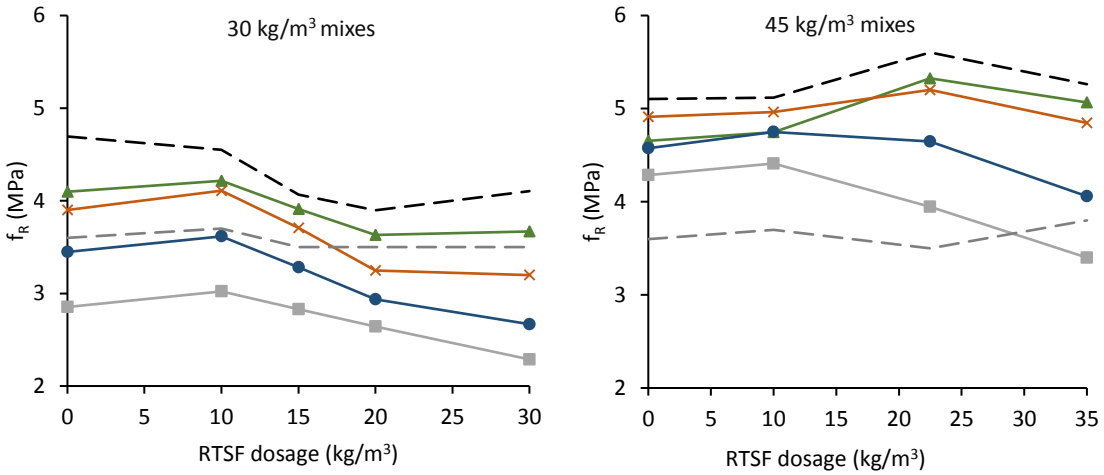

	A	B	C	D	E	F	G	H	I	J
$f_{u\text{-}pc}$	3.1 (10%)	3.2 (9%)	3.0 (7%)	3.0 (7%)	3.0 (13%)	3.1 (10%)	3.1 (10%)	3.2 (9%)	3.0 (7%)	3.3 (9%)
$f_{u\text{-}1}$	4.2 (17%)	4.0 (13%)	3.6 (6%)	3.4 (2%)	3.6 (7%)	4.3 (17%)	4.6 (18%)	4.6 (20%)	5.1 (14%)	4.8 (12%)
f_{R1}	3.6 (25%)	3.7 (16%)	3.4 (6%)	3.1 (16%)	3.2 (10%)	3.8 (19%)	4.2 (19%)	4.2 (21%)	4.8 (15%)	4.6 (14%)
f_{R2}	3.4 (27%)	3.6 (18%)	3.2 (7%)	2.7 (20%)	2.7 (12%)	4.0 (18%)	4.4 17%)	4.5 (21%)	4.7 (10%)	4.3 (10%)
f_{R3}	2.9 (32%)	3.1 (19%)	2.8 (8%)	2.4 (21%)	2.2 (16%)	3.7 (16%)	4.1 (14%)	4.2 (21%)	4.1 (11%)	3.6 (12%)
f_{R4}	2.4 (34%)	2.5 (25%)	2.3 (10%)	2.1 (26%)	1.8 (18%)	3.3 (17%)	3.8 (17%)	3.9 (24%)	3.4 (11%)	2.9 (13%)

Figure 2-11: f_{u-1} and f_R values of prisms (in MPa), and COV (in %)

Since plain concrete always fails in flexure before CMOD reaches 0.5 mm, f_R values and correspondant variability values for plain concrete mixes are not applicable. Figure 2-11 shows that f_{R4} values for 30 kg/m^3 SFRC mixes are lower than the flexural strength of the correspondent plain concrete, however, f_{R4} values for 35 kg/m^3 and 45 kg/m^3 mixes (apart from hybrid mix J containing 35 kg/m^3 of RTSF) are higher, indicating that MSF are more effective at "bridging" macrocracks due to their longer length, larger diameter and deformed shape. The COV for the residual flexural tensile strengths for all mixes are within the range of 40%, which is in agreement with literature [51,54,70].

In this study, f_{R1} and f_{R2}, f_{R3} and f_{R4} are shown to correlate to each other very well (Figure 2-12). In literature, a strong correlation between f_{R1} and f_{R4} was also reported in [67] for two

types of hooked-ends MSF and linear relations between f_{R1} and f_{R3}, f_{R1} and f_{R4} were found by Zamanzadeh et al. [54] for unclassified RTSF. However, a strong correlation between f_{R1} and f_{R3} or f_{R4} was not found in this study.

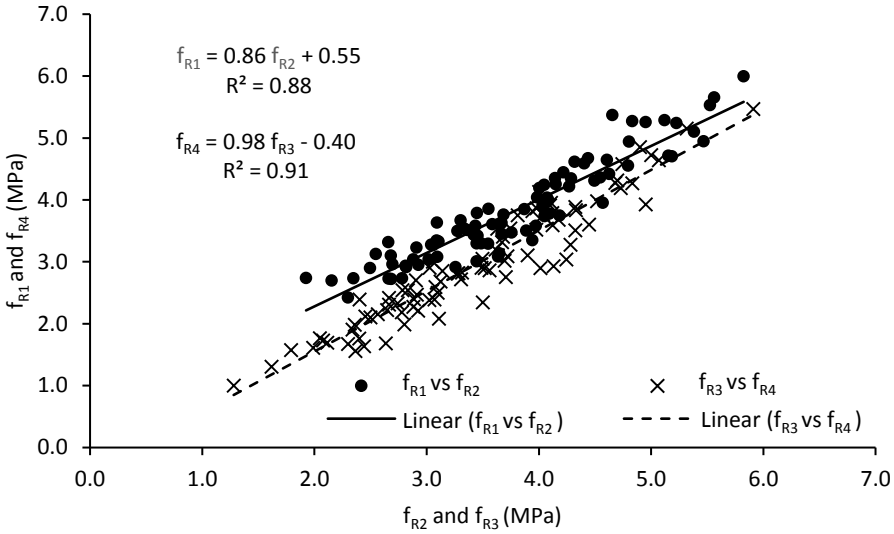

Figure 2-12: Correlation between f_{R1} and f_{R2}, f_{R3} and f_{R4} of all prisms

Flexural strength (f_{u-1})

The concept of Limit of Proportionality (LOP), as a representation of the flexural tensile strength or initiation of flexural cracking, is adopted by EN 14651:2005 [41]. In an attempt to determine LOP values, it was found that the standard procedure is susceptible to initial recording errors and irregularities in the load-deflection curves. A similar observation was made by Neocleous et al. [6]. On the other hand, flexural strength (f_u), adopted in EN 12390-5 [44], is the stress obtained from the peak load of the load-deflection curves for 4-point prism bending tests. The use of f_u was found to be less subjective and more convenient to compare prism tests to panel tests, as discussed later. The calculation of f_u is given below, where F_u (N) is the peak load of the load-deflection curves.

$$f_u = \frac{3F_u l}{2bh_{sp}^2} \quad (2\text{-}4)$$

In Figure 2-11, the subscript –pc for f_u values (in MPa) refers to plain concrete prisms, and -1 for SFRC prisms since 1 principal crack is always developed in the prism. Coefficients of variation

(COV) for those values are listed in brackets, and the small COV for f_{u-pc} suggests that the set-up for prism tests is stable and reliable. It is noted that for SFRC mixes, the COV increases from f_{u-1}, f_{R1} to f_{R4}. This can be explained by the fact that the post-cracking behaviour of SFRC depends increasingly more on fibre-matrix interaction, fibre distribution and orientation as cracks open, than the resistance provided by the matrix itself such as through aggregate interlock.

Compared to plain concrete of the same batch, f_{u-1} increased by approximately 15% to 40% and 45% to 70% at total fibre dosages of 30 kg/m^3, 45 (and 35) kg/m^3, respectively. This confirms the positive effect of steel fibres in arresting microcracks and delaying their coalescence to form macrocracks, and it is evident that higher total fibre dosages can lead to higherf_{u-1} values. At 30 kg/m^3, the use of blended fibres did not enhance the f_{u-1} values, whilst at 45 kg/m^3, hybrid mixes showed similar or higher flexural strength than mix G (45 kg/m^3 of MSF).

2.3.3 Flexural round panel tests

2.3.3.1 Deflection values measured by external and internal LVDTs

The flexural toughness is evaluated based on the energy absorption capacity at specific central deflections. A transducer was mounted centrally beneath the panel to measure central deflection. The deflection from this and the internal transducer of the actuator are compared in Figure 2-13. As expected, the initial part of the deflection behaviour is better represented by the external LVDT, since extraneous deflections (arising from deformation of the load frame and concrete crushing at the supports) are included in the actuator (internal) displacement record. However, there is only a marginal difference in the post-cracking behaviour between the two sets of measurements.

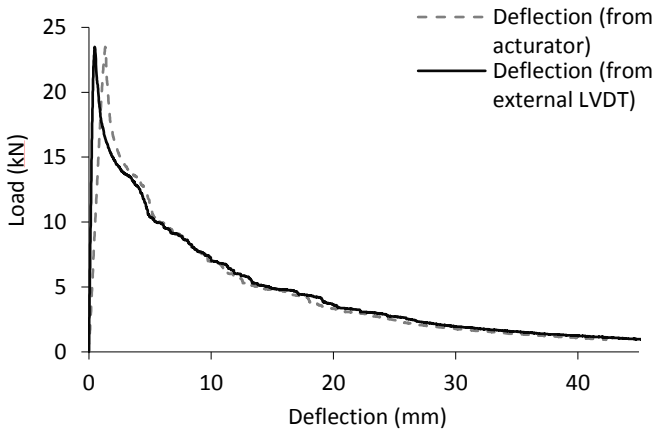

(a)

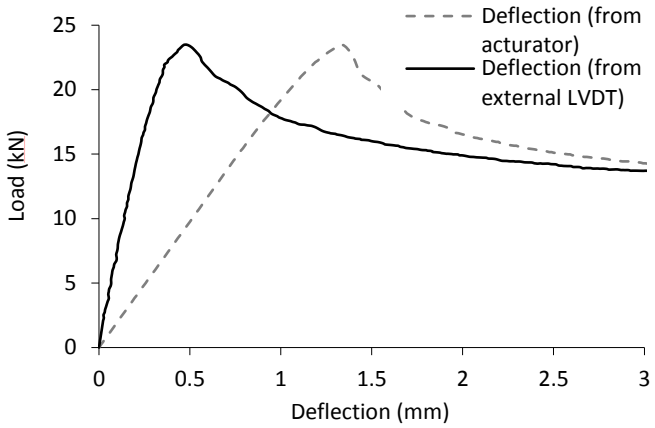

(b)

Figure 2-13: Deflection measurements from the actuator and external LVDTs (a) a typical load-deflection curve, (b) initial part of the curve

The diameter of each panel was measured prior to testing, using the average value of three measurements coincident with the support locations. After testing, the thicknesses of the panels were measured along the three principal cracks to estimate the average thickness; three measurements were taken along each crack and one in the centre (10 measurements in total). Both diameter and thickness measurements confirm that the panels tested were within the limits of the standard.

2.3.3.2 Load-deflection curves

Figures 2-14 and 2-15 show the load-deflection curves for SFRC round panels at the total fibre dosages of 30 kg/m^3 and 45 kg/m^3 (also 35 kg/m^3), respectively. As opposed to the prism tests, only deflection softening behaviour is observed. The beneficial effect of increasing the total fibre dosage on the flexural behaviour of SFRC round panels can be seen, with mixes at 45 (and 35) kg/m^3 demonstrating an enhanced peak load and flexural toughness, when compared to mixes at 30 kg/m^3.

At 30 kg/m^3, the best overall flexural performance was observed from hybrid mix B containing 10 kg/m^3 of RTSF, whilst the lowest was found from RTSF-only mix E [RTSF (30)]. Blending RTSF

with MSF results in a synergy that is able to combine the benefits of the individual fibre types at controlling cracks at different stages.

At 45 kg/m^3, the best flexural behaviour was seen for the hybrid mix I [MSF1 (35) + RTSF (10)]. Surprisingly, the increase of MSF1 dosage (comparing mix G to F) in concrete showed little change in the post-cracking behaviour of SFRC, which might be an indication that the 45 kg/m^3 exceeds the optimum fibre content for this fibre type, as it can cause more balling and air trapped in the mix. In hybrid mixes, the replacement of MSF with more than 22.5 kg/m^3 of RTSF (mixes I and J) showed the lowest post-cracking capacity at large cracks, confirming the limitations of RTSF in controlling large cracks due to a combination of fibre breakage and fibre pull-out.

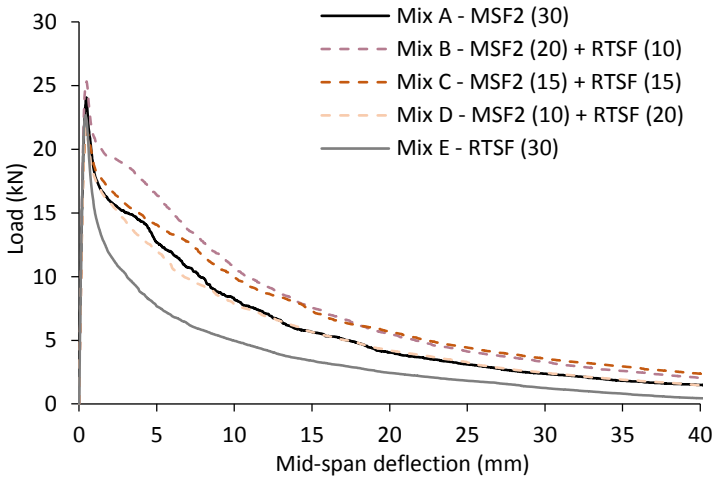

Figure 2-14: Load-deflection curves for SFRC mixes at 30 kg/m^3

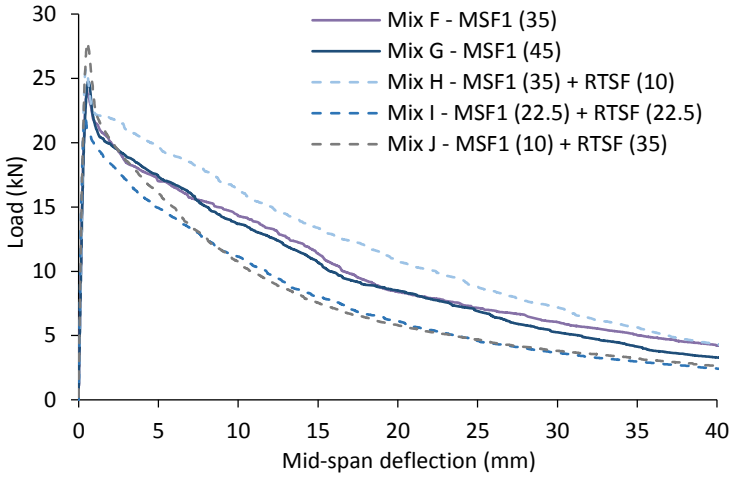

Figure 2-15: Load-deflection curves for SFRC mixes at 35 and 45 kg/m³

2.3.3.3 Energy absorption (E) and flexural strength (f_{u-3})

Energy absorption capacity

To assess the flexural toughness of the round panels, the energy absorption capacity E' up to central deflections of 5, 10, 20 and 40 mm were obtained from the load-deflection curves according to ASTM C1550-05 [48]. As seen in Equation 2-5, a correction factor $\beta = 2 - (\delta - 0.5)/80$ is used to accommodate for the variability in thickness, since thickness has a more pronounced influence on the post-cracking behaviour of panels than diameter [20].

$$E = E' \left(\frac{d_0}{d}\right)^{\beta} \left(\frac{R_0}{R}\right) \tag{2-5}$$

Where δ (in mm) is the specified central deflection up to which the energy absorption capacity is calculated; $R_0 = 400\,mm$ and $d_0 = 75\,mm$ are the nominal round panel radius and thickness, respectively; R and d are the measured radius and thickness values.

Figure 2-16 shows the energy absorption capacity (E, in J) for all SFRC mixes and their corresponding COV (shown in brackets). In general, the 35 and all 45 kg/m³ mixes showed higher energy absorption capacity than the 30 kg/m³ mixes, confirming the positive effect of fibre dosage on flexural toughness.

Interestingly, the replacement of MSF with varying dosages of RTSF did not affect the variability of flexural toughness. The flexural strength (f_{u-3}, in MPa) and the corresponding COV are also presented in Figure 2-16, as discussed later.

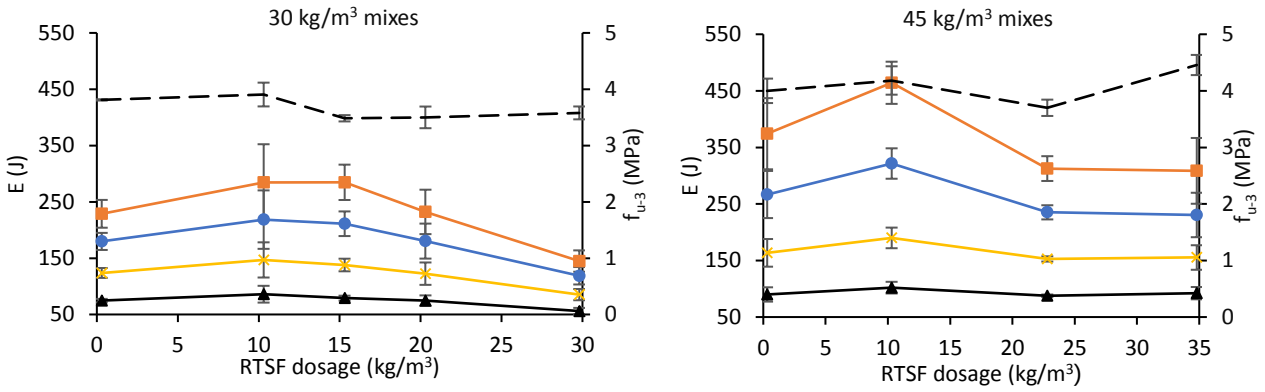

	A	B	C	D	E	F	G	H	I	J
f_{u-3}	3.7 (0%)	3.8 (5%)	3.4 (2%)	3.5 (6%)	3.5 (3%)	3.6 (4%)	3.8 (5%)	4.1 (6%)	3.7 (4%)	4.3 (4%)
E_5	74 (4%)	86 (14%)	79 (5%)	75 (10%)	56 (8%)	86 (5%)	90 (12%)	102 (8%)	88 (2%)	92 (10%)
E_{10}	124 (6%)	147 (17%)	138 (7%)	122 (13%)	85 (10%)	157 (5%)	164 (12%)	190 (8%)	153 (3%)	155 (11%)
E_{20}	180 (7%)	218 (19%)	211 (9%)	180 (14%)	119 (11%)	262 (6%)	267 (13%)	321 (7%)	235 (4%)	230 (14%)
E_{40}	229 (9%)	285 (19%)	285 (9%)	232 (14%)	145 (11%)	379 (8%)	374 (14%)	464 (7%)	313 (6%)	309 (15%)

Figure 2-16: f_{u-3}, E_5, E_{10}, E_{20} and E_{40} of SFRC round panels

Strong correlations are found between E_5 and E_{10}, E_{20} and E_{40} (Figure 2-17), possibly because the larger fracture zone activated can lead to a more consistent post-cracking behaviour than that of the notched prisms.

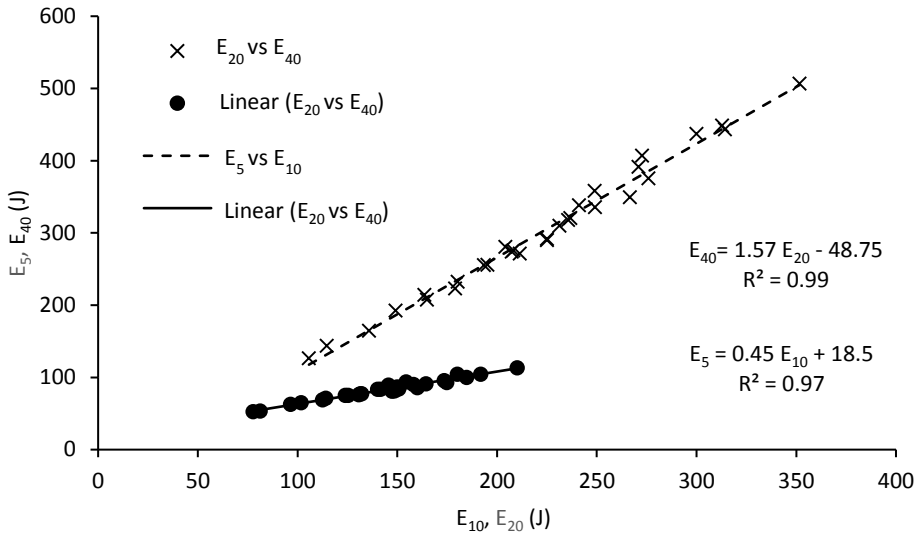

Figure 2-17: Correlations between E_5 and E_{10}, E_{20} and E_{40} of SFRC panels

Flexural strength (f_{u-3})

As there is no direct correlation between the residual flexural tensile strength f_R and the energy absorption capacity E used by the two standards, a common parameter is needed to compare the results from the two tests.

The yield line theory developed by Johansen in 1972, is a practical method to provide an upper bound solution for the collapse load of a structure and can help obtain the flexural strength from panels [20]. Although the yield line method was originally developed for plastic materials, this approach has been found useful even for lightly reinforced SFRC. The Concrete Society TR 34 [45] adopts this method to determine the ultimate (peak) load capacity of FRC ground-supported slabs under different load combinations. Bernard [20] proposed an analytical relationship between the ultimate load and the moment of resistance per unit length at yield lines for the ASTM round panels. However, the loading actuator was taken as a point load, which underestimates the effect of the real load being applied through a circular plate, hence overestimates flexural strength. By considering the actual geometry of the loading plate (see Figure 2-18), the ultimate load can be determined as,

$$P_u = \frac{m[3\sqrt{3}(R-r)+2\pi r]}{R-r-c} \quad (2\text{-}6)$$

As for the prisms, the moment of resistance of the panel per unit length can be calculated by considering a linear elastic distribution of stress across the section,

$$m = \frac{1}{6} b d^2 \sigma_{max} \quad (2\text{-}7)$$

Hence, the flexural strength f_{u-3} (since 3 principal cracks are always developed) of a SFRC round panel can be expressed as,

$$f_{u-3} = \sigma_{max} = \frac{6P_u(R-c-r)}{bd^2[3\sqrt{3}(R-r)+2\pi r]} \quad (2\text{-}8)$$

Equation 2-8 shows that if the radius of the loading plate is ignored, the flexural strength f_{u-3} can be overestimated by 18%.

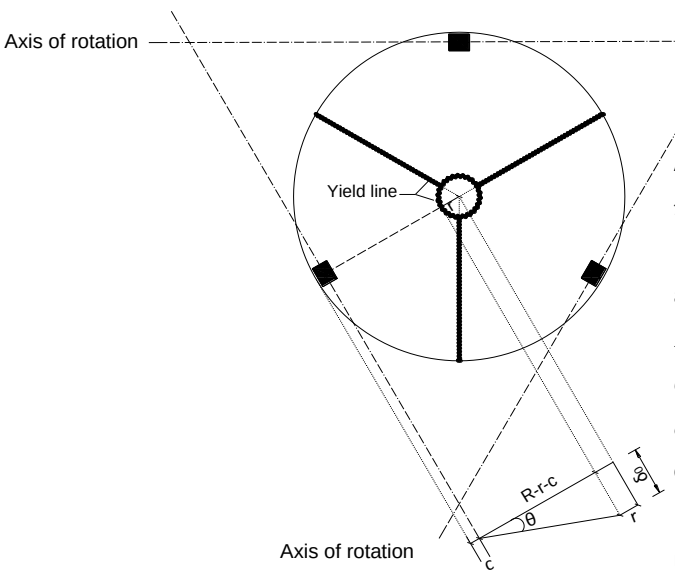

ASTM C1550-05:

$r = 0.05\ m$, the radius of the circular loading plate;

$c = 0.025\ m$, the distance between the edge of the panel and the central line of the support.

R (in m) is the radius (measured) of the round panel;

d (in m) is the thickness (measured) of the panel;

δ_0 is the unit vertical displacement induced by the concentrated load;

$b = 1\ m$ is the unit width of the panel; σ_{max} is the nominal maximum flexural stress of sections on yield lines.

Figure 2-18: Yield line analysis of an ASTM C1550-05 round panel

The circular yield line in the centre of the specimen (Figure 2-18), does not appear in the failure photos of the tested round panels at the bottom (Figure 2-5), as the potential failure (yield line) pattern is based on an assumption of perfectly plastic behaviour of a round panel. In fact, after loading, concentrated microcracking develops in a small region on the soffit of a lightly reinforced panel where the flexural capacity of SFRC has been exceeded. Furthermore, three main cracks starting from a point of maximum deflection will migrate to the edges between each pair of supports.

Figure 2-16 compares the values of f_{u-3} for all SFRC round panels. The largest f_{u-3} values are obtained from hybrid mixes B [MSF2 (20) + RTSF (10)] and J [MSF2 (10) + RTSF (35)] at 30 and 45 kg/m^3, respectively. COV for f_{u-3} for all mixes, are in the range of 0 - 6% (shown in brackets in

Figure 2-16). For all mixes, the variability in the energy absorption capacity calculated at different deflection values increases with the increase in deflection and corresponding crack opening. This indicates the fibre-matrix interaction, fibre distribution and orientation became more predominant as cracks open.

2.3.4 Correlation in the behaviour of SFRC prisms and round panels

Since the fracture parameters (prisms: f_{u-1} and f_R values; panels: f_{u-3} and E values) represent the fracture properties of the same material, the flexural behaviour of the SFRC prisms and round panels is expected to be related.

The relation between f_{u-1} and f_{u-3} is shown in Figure 2-19. In general, the values from prisms f_{u-1} are up to 13% higher than those from round panels for 30 kg/m^3 mixes and 11 -18% (except for mix I) for 45 (and the 35) kg/m^3 mixes. This can be partly attributed to the different methodology used in each test. For example, in the prism tests the specimens are notched to force the crack to occur at a given location, hence the crack does not necessarily open at the section exhibiting the lowest material strength. In the round panels, however, the yield lines form naturally and follow the weakest sections. It is noted that the round panels have a much larger crack length (yield line equivalent) than the prisms and, hence, they are expected to show a lower COV as confirmed by the results in Figures 2-9 and 2-16.

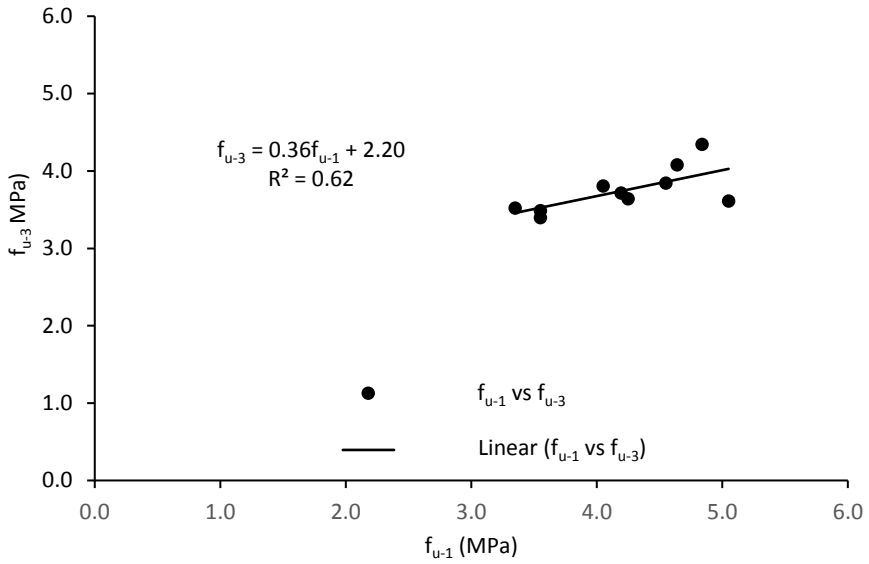

Figure 2-19: Correlations between f_{u-1} (prisms) and f_{u-3} (round panels)

Figure 2-20 shows the correlations between f_{R1} and E_5, f_{R4} and E_{40}. The weaker correlation between f_{R4} and E_{40} highlights the more variable behaviour of SFRC at large cracks, which can be influenced by the effectiveness of just a few fibres in the case of the prism tests. There is a reasonable correlation between f_{R1} and E_5, which indicates that the two tests, though dissimilar, they more or less provide the same information. These three mathematical correlations can help engineers to convert the fracture parameter, from one test to the other, at peak stress (f_{u-1} and f_{u-3}), the SLS (f_{R1} and E_5) and ULS (f_{R4} and E_{40}). It is noted that the proposed equations are only valid for the conversion from ASTM C1550-05 round panel tests to EN 14651:2005 prism tests. In order to better compare and exchange results obtained from different test methods, a broad database of specimens with varying geometry, loading scheme, concrete strength, fibre dosage and volume, is still needed.

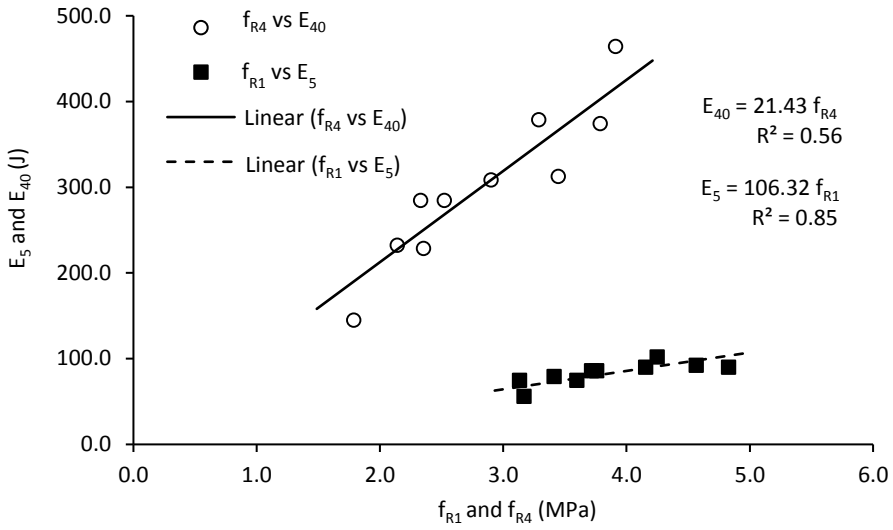

Figure 2-20: Correlations between f_{R1} (prisms) and E_5 (round panels), f_{R4} (prisms) and E_{40} (panels)

2.3.5 Synergetic effect in hybrid mixes

To quantify the synergetic effect in hybrid SFRC mixes, a synergy ratio S_i, which is a function of the normalised fracture parameters i of the hybrid mixes with those of the control mixes (MSF-only mixes A and G), is adopted:

$$S_i = (\frac{i_{hybrid}}{i_{MSF}} - 1) \times 100, \text{ in \%} \quad (2\text{-}9)$$

Where i represents the f_R values obtained from prism tests or E values derived from round panel tests. Figure 2-21 shows the S_{f_R} values (dashed lines) and the S_E values (solid lines) for all hybrid mixes.

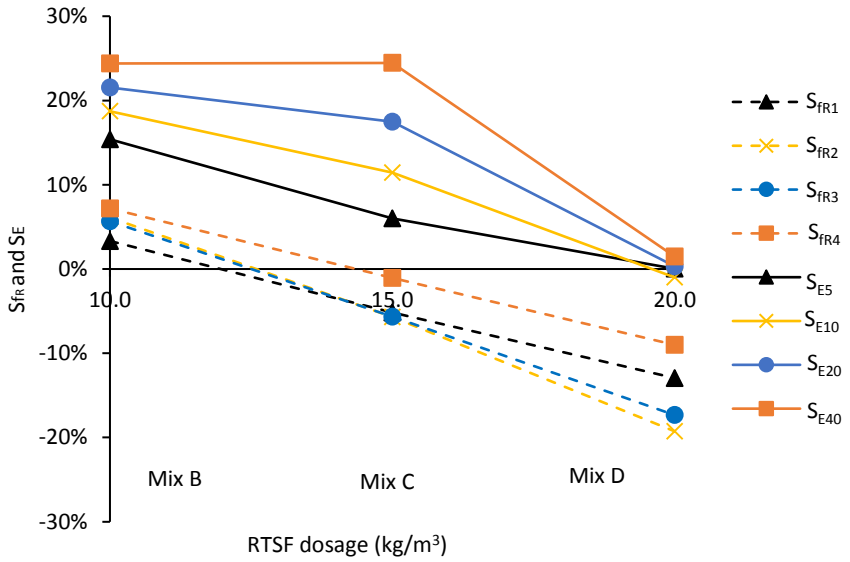

(a)

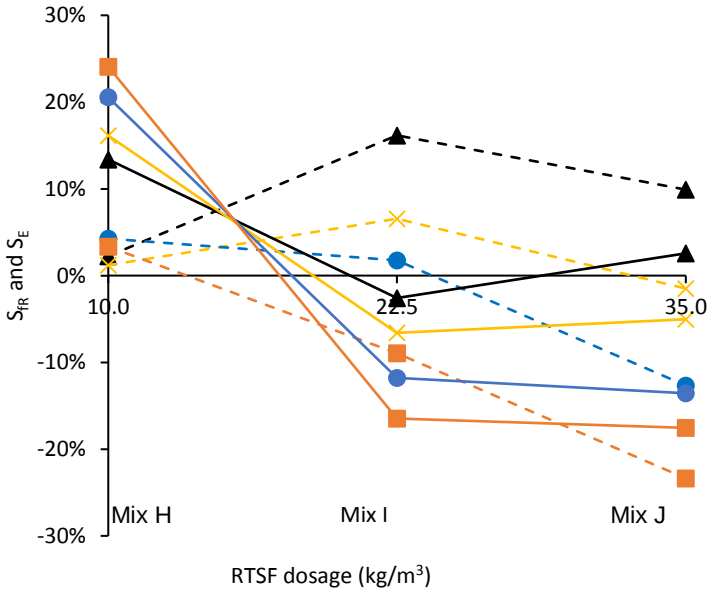

(b)

Figure 2-21: Synergetic ratios S_i for hybrid mixes at (a) 30 kg/m³ (b) 45 kg/m³

2.3.5.1 Effect of test type

For the same mix, different and contradictory S_i values are observed for each type of test. For example, for hybrid mix C [MSF2 (10) + RTSF (20)], negative S_i values (-1% to -6%) are determined from the prism tests, whilst positive values (6 - 24%) are shown for the round panel tests. These differences can be explained by the: (1) nature of the parameter measured by f_R and E values - f_R is a local value of residual stress whist E quantifies all the energy under the curve; (2) magnitude of crack width - the crack widths in the round panels are much wider at the corresponding E values than at the f_R values of the prism tests; (3) length and nature of the fracture zone - in the prism tests the fracture zone is forced to occur at the notched section with a length of 150 mm, whilst in the panel tests the 3 fracture zones (each around 400 mm long) follow the weakest section in the region of maximum stress; (4) fibre orientation - as fibres are prone to orientating along boundaries, the fibres in the beams are more favourably oriented. Further research is thus needed to investigate the effect of fibre orientation and distribution (in particular for hybrid mixes) on the mechanical properties of multi-scale SFRC specimens.

2.3.5.2 Effect of fibre dosage

The overall trend (see Figure 2-21) in both tests shows that small amounts of RTSF (up to 10 kg/m^3) offer a significant synergetic effect, but as their quantity increases that effect diminishes and eventually reverses. As previously discussed, RTSF tend to be more effective than MSF in controlling microcracks, such that the hybrid mixes containing RTSF can perform better than MSF-only mixes at the initial microcracking stage. However, even at larger cracks the hybrid mixes containing a low RTSF dosage (i.e. 10 kg/m^3) also exhibit better performance than MSF-only mixes, despite RTSF being less effective in controlling macrocracks. A likely cause is that the better distribution of RTSF (due to higher fibre count as a result of their “fineness”) increases the strength of the concrete matrix (see f_{u-1} for mix E [RTSF (30)], Figure 2-9, compared to plain concrete), which can lead to an improved fibre-matrix interfacial bond performance and thus increased pull-out resistance of MSF. A positive fibre interlock effect may also be provided by the closely spaced RTSF, even though fibre interlock usually occurs at a high fibre percentage [11]. In the case of round panel tests, where new microcracks develop at different stages of loading, more RTSF are continuously engaged in controlling microcracking and dissipating energy. In contrast, for hybrid mixes containing a high dosage of RTSF (and less MSF), fewer MSF bridge macrocracks and this can lead to a significant degradation of the flexural performance at

larger cracks, and potentially increase variability, as the behaviour of SFRC depends more strongly upon the location and orientation of fewer MSF.

2.4 Design considerations of SFRC with RTSF under flexure

The positive synergetic effect between MSF and RTSF could lead to the reduction of slab thickness, less joints and less conventional reinforcement, as well as significant savings in construction time and labour cost. Hence, this synergy should be exploited during the design stage of concrete slab applications such as slabs-on-grade and suspended slabs.

2.4.1 Flexural strength and uniaxial tensile strength of SFRC

For the SFRC mixes tested in this study, an increase of 13 - 70% in f_{u-1} was obtained when compared to the strength of plain concrete. As reported by ACI 544.1R-96 [19], the increase in the direct tensile strength of SFRC is much lower than that in the flexural strength, since the stress-strain distribution in the tension zone of a specimen alters from elastic to nearly plastic after cracking. However, the uniaxial tensile stress-strain relationship proposed by RILEM TC 162-TDF [40] (Figure 2-22) suggests that the tensile strength (f_t) of SFRC is proportional to the LOP derived from the prism tests, whilst in Model code 2010 [30] an identical tensile strength as plain concrete is assumed when FRC shows softening or slight hardening behaviour. These two models can lead to significantly different predictions of the tensile strength f_t of SFRC, although none of them may be intended to accurately predict the tensile behaviour of SFRC. For example, the tensile strength of mix H [MSF1 (35) + RTSF (10)] is predicted to be 3.41 MPa based on the RILEM approach, whist the strength is 2.05 MPa according to Model Code 2010. Since several studies [4,67] have reported overestimates of flexural behaviour of SFRC using the RILEM approach, it is proposed that for design purposes the same tensile strength as plain concrete is assumed for hybrid SFRC containing RTSF at a low total fibre dosage.

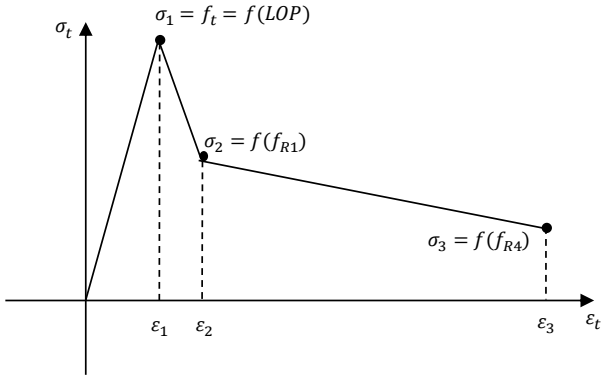

(a)

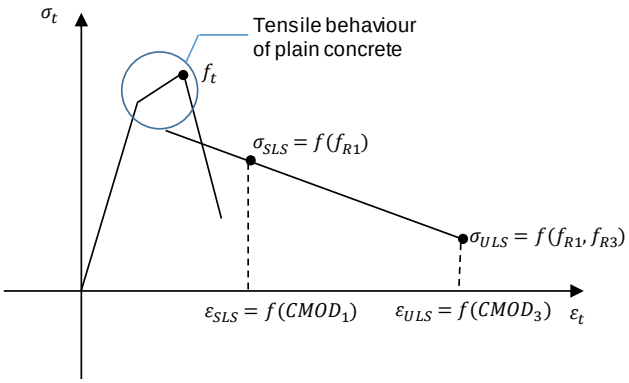

(b)

Figure 2-22: Uniaxial tensile stress-strain diagrams for SFRC proposed by (a) RILEM TC 162-TDF (b) Model Code 2010

2.4.2 Residual flexural tensile strength and energy absorption capacity

The f_{R1} and f_{R2}, f_{R3} and f_{R4} values for SFRC prisms obtained in this study are strongly correlated. This implies that just two independent fracture parameters, e.g. f_{R1} and f_{R4}, are sufficient to represent the post-cracking behaviour of SFRC at small (i.e. the SLS) and large cracks (i.e. the ULS), respectively. Likewise, for the round panel tests, E_5 and E_{40} seem to be sufficient to quantify the flexural toughness of SFRC.

In current design guidelines for SFRC applications, two representative values of f_R out of four, are usually used: f_{R1}, along with f_{R3} or f_{R4}. For the design of SFRC ground-supported slabs at the Ultimate Limit state (ULS), the Concrete Society TR 34 [45] suggests that f_{R1} refers to the axial tensile strength at the crack tip, while the strength at the bottom crack opening is proportional to f_{R4} (Figure 2-23). For the determination of uniaxial tensile stress-strain diagrams

of SFRC (see Figure 2-22), only f_{R1} and f_{R4} are used by RILEM TC 162-TDF [40], whilst only f_{R1} and f_{R3} are employed in Model Code 2010 [30].

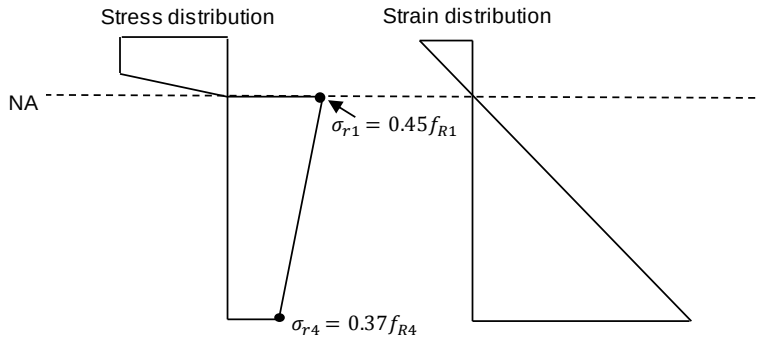

Figure 2-23: Stress block of a FRC floor section at the ULS (adopted by the Concrete Society TR 34)

2.4.3 Ground-supported slab thickness analysis

This section aims to quantify the effect of fibre type and dosage on the design of slab thickness, using the experimental results of the SFRC prisms examined in this study. As an example, a critical case for ground-supported slabs under flexure is considered, with two adjacent point loads (e.g. induced by back-to-back racking legs) applied near an edge of the slab. The design assumptions include a maximum leg load of 78 kN, a typical contact area of 100 mm×100 mm per leg, spacing between two racking legs of 300 mm, and radius of relative stiffness (the stiffness of concrete slab relative to that of sub-grade material) of 650 mm. The design flexural strength of all SFRC mixes, is taken as 2 MPa, which is proposed to be the same as the design flexural tensile strength of plain concrete, according to the Concrete Society TR 34 [45].

Following the Concrete Society TR 34 design method for FRC ground-supported slabs, the relationship between required SFRC slab thickness (h) and the residual flexural tensile strengths f_{R1} and f_{R4} is given by Equation (2-10):

$$h \geq \sqrt{\frac{72655}{0.072f_{R1}+0.107f_{R4}+1.72}} \tag{2-10}$$

Figure 2-24 shows the relation between RTSF dosage for each of the SFRC mixes examined in this study and required slab thickness. As the total fibre dosage increased from 30 kg/m^3 to 45 (and 35) kg/m^3, the required slab thicknesses decreased, as expected. However, the required

slab thicknesses did not vary considerably at the same total fibre dosage. Hybrid mixes B and H, both with 10 kg/m^3 of RTSF, exhibited the smallest slab thickness requirements.

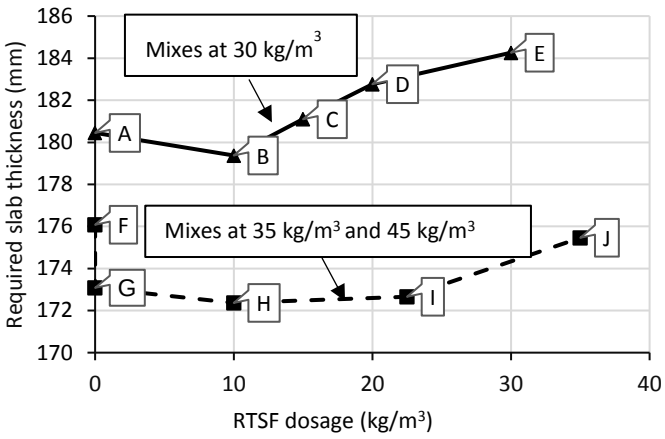

Figure 2-24: Relationship between RTSF dosage and required SFRC slab thickness for the examined SFRC mixes

The results demonstrate that hybrid mixes with RTSF can be competitive substitutes to MSF-only solutions for industrial concrete flooring applications. Such mixes could enable designs with less volume of concrete required, as well as up to 35 kg/m^3 MSF replacement with lower embodied energy fibres (i.e. RTSF).

2.5 Conclusions

The mechanical properties of 10 SFRC mixes using MSF and RTSF hybrids have been investigated by means of compressive cube, 3-point notched prism and round panel tests. The main research findings are:

- MSF and RTSF hybrids do not significantly affect f_{cu} and E_{fm}.
- RTSF are more effective in controlling microcracks. As cracks open, the flexural behaviour of SFRC depends increasingly more on fibre-matrix interaction, fibre orientation and distribution.
- Owing to the nonhomogeneous fibre distribution of SFRC, the variability of the fracture parameters obtained from prism tests was up to 35%, and up to 20% for round panels.

The MSF and RTSF hybridisation has little effect on the scatter of the fracture parameters.

- Strong correlations exist between f_{R1} and f_{R2}, f_{R3} and f_{R4} (for prisms), as well as E_5 and E_{10}, E_{20} and E_{40} (for round panels). Correlations in the flexural behaviour of the SFRC prisms and round panels are reported. Proposed equations could be used by engineers to convert fracture parameters from one test to the other, but a wide testing database is still required.
- Hybrid mixes containing 10 kg/m^3 of RTSF at the total fibre dosage of 30 and 45 kg/m^3 offer significant synergetic effect. However, as the RTSF content increases, the performance drops below that of MSF-only mixes.
- It is noted that these research findings are based on limited experimental data, further research on various aspects (fibre dosage, fibre type and loading configuration, etc.) is still needed to increase the range of validity and expand the conclusions.

References

[1] ETRA, Introduction to tyre recycling: 2013, The European Tyre Recycling Association, Brussels, Belgium, 2013.

[2] WBCSD, End-of-life tires: a framework for effective management systems, http://www.wbcsd.org/DocRoot/lBTHZFGcpBK5OxTDXlpS/EndOfLifeTires_171208.pdf. 2010, (accessed 17. 07 .21).

[3] K. Pilakoutas, K. Neocleous, H. Tlemat, Reuse of tyre steel fibres as concrete reinforcement, Eng. Sustain. 157 (2004) 131–138.

[4] H. Tlemat, K. Pilakoutas, K. Neocleous, Stress-strain characteristic of SFRC using recycled fibres, Mater. Struct. 39 (2006) 365–377. doi:10.1617/s11527-005-9009-4.

[5] H. Tlemat, K. Pilakoutas, K. Neocleous, Modelling of SFRC using inverse finite element analysis, Mater. Struct. 39 (2006) 221–233. doi:10.1617/s11527-005-9010-y.

[6] K. Neocleous, H. Tlemat, K. Pilakoutas, Design issues for concrete reinforced with steel fibers, including fibers recovered from used tires, J. Mater. Civ. Eng. 18 (2006) 677–685. doi:10.1061/(ASCE)0899-1561(2006)18:5(677).

[7] A.G. Graeff, K. Pilakoutas, K. Neocleous, M.V.N.N. Peres, Fatigue resistance and cracking mechanism of concrete pavements reinforced with recycled steel fibres recovered from post-consumer tyres, Eng. Struct. 45 (2012) 385–395. doi:10.1016/j.engstruct.2012.06.030.

[8] N. Jafarifar, K. Pilakoutas, T. Bennett, Moisture transport and drying shrinkage properties of steel-fibre-reinforced-concrete, Constr. Build. Mater. 73 (2014) 41–50. doi:10.1016/j.conbuildmat.2014.09.039.

[9] K.H. Younis, K. Pilakoutas, Strength prediction model and methods for improving recycled aggregate concrete, Constr. Build. Mater. 49 (2013) 688–701. doi:10.1016/j.conbuildmat.2013.09.003.

[10] K.H. Younis, K. Pilakoutas, Assessment of post-restrained shrinkage mechanical properties of concrete, ACI Mater. J. 113 (2016) 267–276. doi:10.14359/51688699.

[11] H. Tlemat, Steel fibres from waste tyres to concrete, testing, modelling and design, The University of Sheffield, Sheffield, UK, 2004.

[12] A.G. Graeff, Long-term performance of recycled steel fibre reinforced concrete for pavement applications, The University of Sheffield, UK, 2011.

[13] K. Neocleous, H. Angelakopoulos, K. Pilakoutas, M. Guadagnini, Fibre-reinforced roller-compacted concrete transport pavements, in: Proceedings of the institution of civil engineers - transport, 2011: pp. 97–109. doi:10.1680/tran.9.00043.

[14] N. Jafarifar, Shrinkage behaviour of steel fibre reinfoced concrete pavements, The University of Sheffield, Sheffield, UK, 2012.

[15] H. Angelakopoulos, Reused post-consumer tyre steel fibres in roller compacted concrete, The University of Sheffield, Sheffield, UK, 2016.

[16] UFSD, Thin wire reinforcement for concrete. British Patent Application No 0130852.7 and 0511012.7, filed by The University of Sheffield on 24/12/01 and published on 9/11/2005, Sheffield, UK, 2001.

[17] H. Angelakopoulos, P Waldron, Tyre wire in Concrete Leading to Environmental sustainability. CIP Eco-innovation project Twincletoes project - Layman's report, Twincon Ltd, Sheffield, UK, 2015.

[18] K. Neocleous, S.G. Maxineasa, L. Dumitrescu, K. Themistocleous, N. Taranu and D. Hadjimitsis, D1.6 Preliminary LCA. Anagennisi Project, Anagennisi: innovative use of all tyre components in concrete, 2014.

[19] ACI 544.8R-16, Report on indirect method to obtain stress-strain response of fiber-reinforced concrete (FRC). American Concrete Institute, Michigan, US, 2016.

[20] E.S. Bernard, Influence of toughness on the apparent cracking load of fiber-reinforced concrete slabs, J. Struct. Eng. 132 (2006) 1976–1983. doi:10.1061/(ASCE)0733-9445(2006)132:12(1976).

[21] M. Colombo, M. di Prisco, L. Mazzoleni, Sprayed tunnel linings: a comparison between several reinforcement solutions, Mater. Struct. 42 (2009) 1295–1311. doi:10.1617/s11527-009-9528-5.

[22] V.S. Gopalaratnam, R. Gettu, On the characterization of flexural toughness in fiber reinforced concretes, Cem. Concr. Compos. 17 (1995) 239–254. doi:10.1016/0958-9465(95)99506-O.

[23] N. Banthia, M. Sappakittipakorn, Toughness enhancement in steel fiber reinforced concrete through fiber hybridization, Cem. Concr. Res. 37 (2007) 1366–1372. doi:10.1016/j.cemconres.2007.05.005.

[24] N. Banthia, J. Sheng, Fracture toughness of micro-fiber reinforced cement composites, Cem. Concr. Compos. 18 (1996) 251–269. doi:10.1016/0958-9465(95)00030-5.

[25] P. Rashiddadash, A.A. Ramezanianpour, M. Mahdikhani, Experimental investigation on flexural toughness of hybrid fiber reinforced concrete (HFRC) containing metakaolin and pumice, Constr. Build. Mater. 51 (2014) 313–320. doi:10.1016/j.conbuildmat.2013.10.087.

[26] N. Banthia, S.M. Soleimani, Flexural response of hybrid fiber-reinforced cementitious composites, ACI Mater. J. 102 (2005) 382–389.

[27] J.S. Lawler, T. Wilhelm, D. Zampini, S.P. Shah, Fracture processes of hybrid fiber-reinforced mortar, Mater. Struct. 36 (2003) 197–208. doi:10.1007/BF02479558.

[28] G. Tiberti, F. Minelli, G. Plizzari, Reinforcement optimization of fiber reinforced concrete linings for conventional tunnels, Compos. Part B. 58 (2014) 199–207. doi:10.1016/j.compositesb.2013.10.012.

[29] Y. Mohammadi, S.P. Singh, S.K. Kaushik, Properties of steel fibrous concrete containing mixed fibres in fresh and hardened state, Constr. Build. Mater. 22 (2008) 956–965. doi:10.1016/j.conbuildmat.2006.12.004.

[30] F.I. du Béton, Fib Model Code for Concrete Structures 2010, Wilhelm Ernst & Sohn, Berlin, Germany, 2013.

[31] N. Banthia, N. Nandakumar, Crack growth resistance of hybrid fiber reinforced cement composites, Cem. Concr. Compos. 25 (2003) 3–9.

[32] L.G. Sorelli, A. Meda, G.A. Plizzari, Bending and uniaxial tensile tests on concrete reinforced with hybrid Steel Fibers, J. Mater. Civ. Eng. 17 (2005) 519–527. doi:10.1061/(ASCE)0899-1561(2005)17:5(519).

[33] E. Martinelli, A. Caggiano, H. Xargay, An experimental study on the post-cracking behaviour of Hybrid Industrial/Recycled Steel Fibre-Reinforced Concrete, Constr. Build. Mater. 94 (2015) 290–298. doi:10.1016/j.conbuildmat.2015.07.007.

[34] C.X. Qian, P. Stroeven, Development of hybrid polypropylene-steel fibre-reinforced concrete, Cem. Concr. Res. 30 (2000) 63–69. doi:10.1016/S0008-8846(99)00202-1.

[35] D. Bjegovic, A. Baricevic, S. Lakusic, D. Damjanovic, I. Duvnjak, Positive interaction of industrial and recycled steel fibres in fibre reinforced concrete, J. Civ. Eng. Manag. 19 (2013) S50–S60. doi:10.3846/13923730.2013.802710.

[36] K.H. Younis, K. Pilakoutas, M. Guadagnini, H. Angelakopoulos, Feasibility of Using Recycled Steel Fibres To Enhance the Behaviour of Recycled Aggregate Concrete, FRC 2014 Jt. ACI-Fib Int. Work. - Fibre Reinf. Concr. from Des. to Struct. Appl. (2014) 598–608.

[37] A. Baricevic, D. Bjegovic, M. Skazlic, Hybrid fiber-reinforced concrete with unsorted recycled-tire steel Fibers, J. Mater. Civ. Eng. 29 (2017) 6017005. doi:10.1061/(ASCE)MT.1943-5533.0001906.

[38] Anagennisi Project, Anagennisi: innovative use of all tyre components in concrete. http://anagennisi.org/wordpress/, 2014 (accessed 2017.07.20).

[39] ACI 544.1R-96 (Reapproved 2002), State-of-the-art report on fiber reinforced concrete. American Concrete Institute, Michigan, US, 2002.

[40] Rilem Tc 162-Tdf, σ-ε-Design method, Mater. Struct. 36 (2003) 560–567. doi:10.1007/BF02480834.

[41] BS EN 14651:2005, Test method for metallic fibre concrete - Measuring the flexural tensile strength (limit of proportionality (LOP), residual). British Standards Institution, London, UK, 2005.

[42] BS EN 14488-3:2006, Testing sprayed concrete - Part 3: Flexural strengths (first peak, ultimate and residual) of fibre reinforced beam specimens. British Standards Institution, London, UK, 2006.

[43] BS EN 14488-5:2006, Testing sprayed concrete - Part 5: Determination of energy absorption capacity of fibre reinforced slab specimens, British Standards Institution, London, UK, 2006.

[44] BS EN 12390-5:2009, Testing hardened concrete - Part 5: Flexural strength of test specimens. British Standards Institution, London, UK, 2009.

[45] Technical report 34, Concrete industrial ground floors: a guide to their design and construction, The Concrete Society, Surrey, UK, 2013.

[46] ASTM C1018-97, Standard test method for flexural toughness and first-crack strength of riber-reinforced concrete (using beam with third-point loading), ASTM International, Pennsylvania, US, 1997.

[47] ASTM C1609/C1609M-05, Standard test method for flexural performance of fiber-reinforced concrete (using beam with third-point loading), ASTM International, Pennsylvania, US, 2005.

[48] ASTM C1550-05, Standard test method for flexural toughness of fiber reinforced concrete (using centrally loaded round panel), ASTM International, Pennsylvania, US, 2005.

[49] JSCE-SF4, Standard for flexural strength and flexural toughness, method of tests for steel fiber reinforced concrete, Concrete library of JSCE, Japan Concrete Institute (JCI), Japan,1984.

[50] B. Mobasher, Mechanics of fiber and textile reinforced cement, CRC Press, Florida, US, 2012.

[51] S. Oikonomou-mpegetis, Behaviour and design of steel fibre reinforced concrete slabs, Imperial College London, London, UK, 2012.

[52] F. Minelli, G.A. Plizzari, Fiber reinforced concrete characterization through round panel test - Part I: experimental study, in: Proceedings of the 7th international conference on fracture mechanics of concrete and concrete structures (FRAMCOS), 2010: pp. 1451–1460.

[53] BS EN 14889-1:2006, Fibres for concrete-Part 1: Steel fibres-definitions, specifications and conformity. British Standards Institution, London, UK, 2006.

[54] Z. Zamanzadeh, L. Lourenço, J. Barros, Recycled steel fibre reinforced concrete failing in bending and in shear, Constr. Build. Mater. 85 (2015) 195–207. doi:10.1016/j.conbuildmat.2015.03.070.

[55] A. Caratelli, A. Meda, Z. Rinaldi, Design according to MC2010 of a fibre-reinforced concrete tunnel in Monte Lirio, Panama, Struct. Concr. 13 (2012) 166–173. doi:10.1002/suco.201100034.

[56] G. Groli, A.P. Caldentey, A.G. Soto, Cracking performance of SCC reinforced with recycled fibres - an experimental study, Struct. Concr. 15 (2014) 136–153. doi:10.1002/suco.201300008.

[57] G. Groli, Crack width control in RC elements with recycled steel fibres and applications to integral structures: theoretical and experimental study, Polytechnical University of Madrid, Madrid, Spain, 2014.

[58] Q. Gu, H. Xu, S. Mindess, An improved test method and numerical analysis for crack opening resistance of FRC round determinate panels, Wuhan Univ. J. Nat. Sci. 14 (2009) 47–52. doi:10.1007/s11859-009-0111-2.

[59] E.S. Bernard, Correlations in the behaviour of fibre reinforced shotcrete beam and panel specimens, Mater. Struct. 35 (2002) 156–164. doi:10.1007/BF02533584.

[60] B.W. Xu, H.S. Shi, Correlations among mechanical properties of steel fiber reinforced concrete, Constr. Build. Mater. 23 (2009) 3468–3474. doi:10.1016/j.conbuildmat.2009.08.017.

[61] G. Centonze, M. Leone, M.A. Aiello, Steel fibers from waste tires as reinforcement in concrete: A mechanical characterization, Constr. Build. Mater. 36 (2012) 46–57. doi:10.1016/j.conbuildmat.2012.04.088.

[62] Ş. Yazıcı, G. İnan, V. Tabak, Effect of aspect ratio and volume fraction of steel fiber on the mechanical properties of SFRC, Constr. Build. Mater. 21 (2007) 1250–1253. doi:10.1016/j.conbuildmat.2006.05.025.

[63] M.A. Aiello, F. Leuzzi, G. Centonze, A. Maffezzoli, Use of steel fibres recovered from waste tyres as reinforcement in concrete: Pull-out behaviour, compressive and flexural strength, Waste Manag. 29 (2009) 1960–1970. doi:10.1016/j.wasman.2008.12.002.

[64] ACI 544.2R-89 (Reapproved 1999), Measurement of properties of fiber reinforced concrete. American Concrete Institute, Michigan, US, 1999.

[65] BS EN 12390-3:2009, Testing hardened concrete - Part 3: Compressive strength of test specimens. British Standards Institution, London, UK, 2009.

[66] M.N. Soutsos, T.T. Le, A.P. Lampropoulos, Flexural performance of fibre reinforced concrete made with steel and synthetic fibres, Constr. Build. Mater. 36 (2012) 704–710. doi:10.1016/j.conbuildmat.2012.06.042.

[67] J. a. O. Barros, V.M.C.F. Cunha, A.F. Ribeiro, J.A.B. Antunes, Post-cracking behaviour of steel fibre reinforced concrete, Mater. Struct. 38 (2004) 47–56. doi:10.1617/14058.

[68] R.D. Neves, J.C.O. Fernandes de Almeida, Compressive behaviour of steel fibre reinforced concrete, Struct. Concr. 6 (2005) 1–8. doi:10.1680/stco.6.1.1.62458.

[69] C.G. Papakonstantinou, M.J. Tobolski, Use of waste tire steel beads in Portland cement concrete, Cem. Concr. Res. 36 (2006) 1686–1691. doi:10.1016/j.cemconres.2006.05.015.

[70] B.I.G. Barr, M.K. Lee, E.J. de Place Hansen, D. Dupont, E. Erdem, S. Schaerlaekens, B. Schnütgen, H. Stang, L. Vandewalle, Round-robin analysis of the RILEM TC 162-TDF beam-bending test: Part 1-Test method evaluation, Mater. Struct. 36 (2003) 609–620. doi:10.1007/BF02483281.

Chapter 3 Mechanical Properties of SFRC Using Blended Recycled Tyre Steel Cords and Recycled Tyre Steel Fibres

H. Hu, P. Papastergiou, H. Angelakopoulos, M. Guadagnini, K. Pilakoutas, Mechanical properties of SFRC using blended recycled tyre steel cords and recycled tyre steel fibres, Construction and Building Materials, 2018. **Submitted.**

Author contribution statement

Dr Papastergiou, Dr Guadagnini and Prof. Pilakoutas coordinated the Anagennisi and Clean Steel projects. Dr Angelakopoulos supplied the fibres used and provided practical information on mix design and fibre characteristics. All authors discussed the results and commented on the manuscript.

ABSTRACT

Processed high-specification steel cords (RTSC) extracted from un-vulcanised rubber belt off-cuts have the potential to substitute (manufactured steel fibres) MSF in concrete, leading to enhanced structural performance and significant environmental benefits. The target of this research is to demonstrate that recycled-only fibre mixes could meet or exceed the performance of MSF-only mixes, at the same total fibre dosage. Direct tensile and single-fibre pull-out tests are carried out, to evaluate the tensile strength of RTSC and the interfacial bond behaviour between RTSC and concrete matrix, respectively. It is found that RTSC have a tensile strength greater than 2600 MPa and their critical embedded length is in the range of 25-40 mm. The flexural characteristics of 8 steel fibre reinforced concrete (SFRC) mixes at fibre dosages of 30 and 45 kg/m^3 are examined by using EN 14651:2005 3-point notched prism tests. RTSC with lengths of 60 mm are used on their own, or blended with post-processed steel fibres recovered from end-of-life tyres (RTSF) at varying dosages. The performance of two manufactured steel fibres (MSF)-only mixes and a RTSF-only mix is also examined. Comparisons in terms of flexural performance are made between MSF-only mixes versus recycled-fibre (RTSC on their own or blended with RTSF) mixes at the same total dosage. RTSC are found to be extremely well mobilised at larger crack widths and the post-cracking strength of recycled-fibre mixes is significantly higher (up to 103%) than MSF-only mixes at the same total fibre dosage. In addition, the flexural performance of concrete with recycled-fibre blends improves with increasing amounts of RTSC.

This chapter consists of a “stand-alone” journal paper and includes a relevant bibliography at the end of the chapter. Additional information and further test results are presented in Appendix B. This includes tensile test results for RTSC, concrete mix design for RTSC pull-out tests, compressive and splitting tensile strength from cylinders, failure load for each pull-out test, compressive strength from cubes, residual flexural tensile strength from prisms and load-deflection (or –CMOD) curves for each prism examined.

3.1 Introduction

About 1.5 billion tyres are produced annually worldwide and a large amount (5-10% by weight) of un-vulcanised rubber belt off-cuts (containing rubber and steel cords used to reinforce the treads and sidewalls of car and truck tyres), are generated during the process of tyre manufacture. Un-vulcanised rubber can be easily recycled or reused in tyre production. However, most of the steel cords are still disposed of as waste or used for energy recovery (incineration) together with rubber. This is the lowest level in the hierarchy of preferred waste disposal routes for all waste products, as proposed by The EC Waste Framework Directive 2008/98/EC [1]. Recently, the tyre recycling industry has developed a novel cryogenic process to extract steel from un-vulcanised off-cuts, which can yield clean and high-specification steel cords in a variety of lengths typically ranging from 0.5-2.0 m. After cutting them into predetermined lengths suitable for concrete mixing, these cords, called "Recycled Tyre Steel Cord (RTSC)", have the potential to be used as randomly distributed reinforcement in concrete, hence meeting the highest level of the Waste Framework Directive hierarchy, re-use [1].

On the other hand, approximately 1 billion tyres (17 million tonnes) [2] reach the end of their useful lives worldwide every year [3]. A combination of mechanical shredding and granulation is widely used by the tyre recycling industry to extract steel of irregular shapes, lengths and diameters as well as rubber crumb from post-consumer tyres [4]. Rubber crumb can be partially reused in rubber products and other products using polymer binders. Recently, rubber has also been used as aggregate in concrete structural elements [5,6]. However, after further processing, steel fibres can be cleaned (rubber contamination below 0.5% by mass), sorted and classified (Figure 1). Since 1999, extensive experimental work has been undertaken at the University of Sheffield [7–19] to investigate the mechanical properties of recycled tyre steel fibres (RTSF) and their potential in structural applications. It was found that RTSF can be a promising candidate to partially or even entirely substitute manufactured steel fibres (MSF) in a variety of structural concrete applications including conventionally-placed concrete [7,10–12,14,15,17,19–26], sprayed concrete [18], self-compacted concrete [15,27,28] and roller-compacted concrete [16,18,29]. For sustainability, Life Cycle Assessment (LCA) studies [30,31] have shown that very low (less than 5%) energy input is required for the production of RTSF, compared to that of typical MSF, which highlights the significant environmental benefits of using RTSF in concrete.

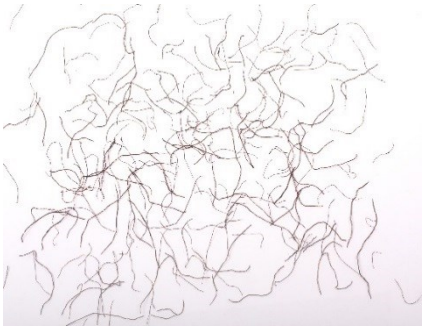

Figure 3-1: Recycled Tyre Steel Fibres (RTSF) [19]

One disadvantage of using RTSF alone in concrete is that, as a large portion of RTSF lengths is smaller than the nominal size of typical coarse aggregates, the flexural performance of RTSF-only mixes is inferior to MSF-only mixes at the same fibre dosage, especially when large cracks are developed [8,18,19,22,23]. Hence, to achieve an equivalent post-cracking capacity of MSF-only mixes at a certain fibre dosage, a higher dosage of RTSF is usually required. For conventional mixing, the critical dosage of clean and sorted RTSF was found to be about 30 kg/m^3 in concrete [19]. Beyond this dosage, the workability of concrete can be adversely affected and even fibre balling can occur, leading to degradation in the mechanical characteristics of SFRC. To achieve equivalent or even better mechanical properties to MSF-only mixes at the same dosage, a more likely use of RTSF, is to blend MSF and small amounts of RTSF together in concrete. Compared to MSF-only mixes at the total fibre dosages of 30-45 kg/m^3, a previous study conducted by the authors [19] found that better flexural performance of SFRC can be obtained from blended mixes containing both MSF and 10 kg/m^3 of RTSF. The target of this research is to achieve recycled-fibre-only mixes that meet or exceed the performance of MSF-only mixes, at the same total fibre dosage. Hence, the present study investigates the mechanical properties of SFRC using RTSC on their own or blended with sorted and classified RTSF, at varying dosages. The results presented in this study are part of the FP7 EU-funded project ‘‘Anagennisi” [32] and the UK Technology Strategy Board (currently called Innovate UK) funded project “Re-use of steel cord from tyres as reinforcement in sustainable construction” which aimed to re-use steel cord from tyres as randomly distributed reinforcement in different construction applications.

Uniaxial tension tests for SFRC are difficult to perform and interpret [14,15,33,34] and as a consequence flexural tests are the preferred method to characterise the nominal tensile characteristics of SFRC. Compared to other test methods such as, 4-point un-notched prism and square slab tests, the EN 14651: 2005 3-point notched prism (or circular slab) tests [35] have the

advantage of generating consistent and predictable crack patterns, leading to better comparisons between SFRC mixes. Hence, the EN 14651: 2005 notched prism tests are adopted to quantify the flexural performance of SFRC using RTSC alone or blended with RTSF at varying dosages.

Section 3.2 of this paper presents the geometrical and mechanical characteristics of RTSC, RTSF and two types of MSF used. As the mechanical properties of composites are dependent on the properties of the constituent materials and their interfacial bond characteristics [14,23], section 3.3 investigates the bond behaviour between RTSC and concrete matrix by employing RTSC pull-out tests. Section 3.4 reports the concrete mix design and SFRC mixes examined, as well as test set-ups and procedures adopted for the compressive cube and flexural prism tests. Section 3.5 discusses and compares the experimental results. Section 3.6 summarises key research findings.

3.2 Fibre characterisation

3.2.1 Geometrical characterisation

RTSC (Figure 3-2 (a)) and RTSF (see Figure 3-1), as well as two types of manufactured undulated (crimped) steel fibres, MSF1 (Figure 3-2 (b)) and MSF2 (Figure 3-2 (c)) were used in this study. RTSC were cut into lengths of 60 mm (the typical length of MSF used in industrial concrete flooring applications), to ensure an effective bond performance between RTSC and surrounding concrete matrix, as discussed in section 3.3.

The nominal cord diameter was 0.75 mm. Each cord consisted of 11 steel filaments twisted together and a filament helically wound around them. The inclusion of the outer filament is intended to prevent unravelling of RTSC and enhance bond to rubber. Hence, this outer filament can potentially also contribute to improved interfacial bond to concrete and enhanced pull-out resistance of RTSC.

The cleaned and sorted RTSF used in this study are from the same source as reported in [19]. Based on a representative sample of approximately 15,000 fibres, Figures 3-3(a) and (b) [19] show the RTSF length and aspect ratio distributions determined through the use of specially developed optical system [18]. The RTSF length distribution histogram showed that 68% (by mass) was in the range of 15-40 mm, with an average length of 23 mm. The aspect ratio distribution analysis suggested that the average aspect ratio of RTSF was around 100. For the two types of undulated MSF used, MSF1 had greater length, diameter and tensile strength than

MSF2. Table 3-1 summarises the geometrical characteristics of RTSC, RTSF and the two types of MSF used.

(a) (b) (c)

Figure 3-2: (a) RTSC, (b) MSF1 and (c) MSF2 [19]

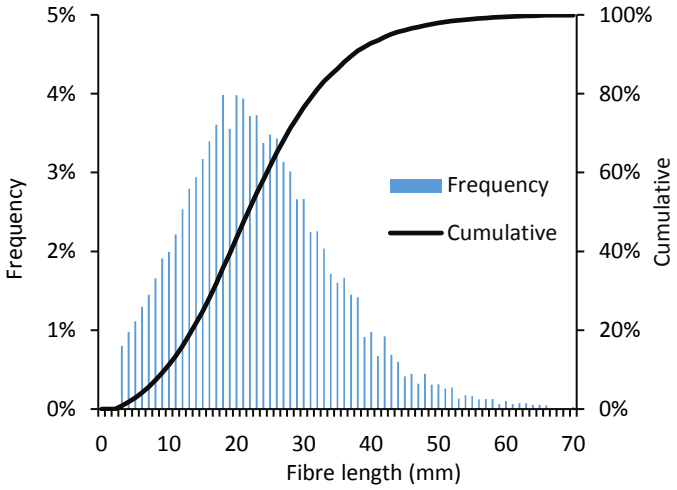

(a)

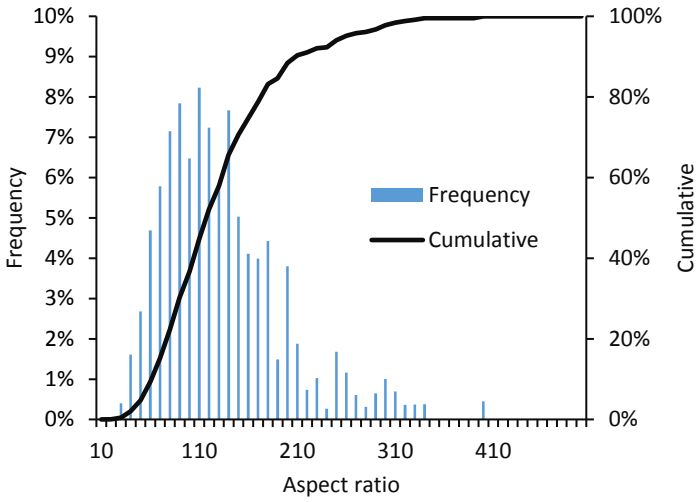

(b)

Figure 3-3: RTSF histograms: (a) fibre length distribution, (b) aspect ratio distribution [19]

Table 3-1: Geometrical and mechanical specifications of RTSC, RTSF, MSF1 and MSF2

Fibre type	Length	Diameter	Aspect ratio	Tensile strength (MPa)
RTSC	60±2	0.75±0.04	75	2612
RTSF	23*	0.22*	100*	2570*
MSF1	60±2	1.00±0.04	60	1450
MSF2	55±2	0.80±0.04	69	1050

*The nominal (mean) values for RTSF

3.2.2 Mechanical characterisation

Thirty RTSC were tested under direct tension to examine their tensile properties. According to BS EN 10002-1: 2001 [36], steel cords were subjected to direct tension using a 5 kN tensometer under load control, at a constant stress rate of 20 $MPa * s^{-1}$. Screwed jaws were initially used to secure the cords; however, premature failures occurred at locations adjacent to the jaws. Hence, the ends of RTSC were wrapped on small high-strength aluminium cylinders that were fixed within the screwed jaws (see Figure 3-4). This arrangement ensured that the tensile force could be applied axially, minimising any bending and preventing failure at the ends.

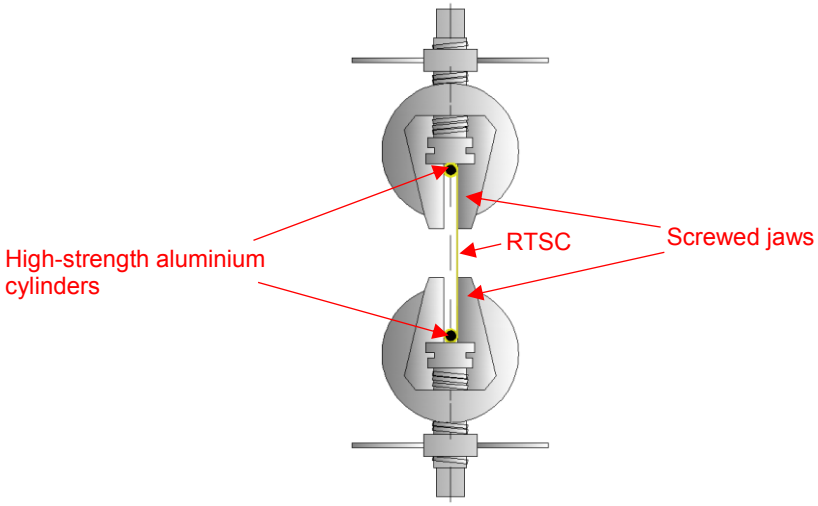

Figure 3-4: RTSC tensile testing setup

Two methods were used to estimate the cord area, A: the actual cord diameter d_1 was measured by a digital calliper after each cord was fully tightened, leading to an actual cord area A_1 insignificantly affected by the space among the filaments. The cord area A_2 was estimated based on the nominal cross-sectional area of each filament (about 0.03 mm^2) and the number of filaments (i.e. 12) contained in each cord. Table 3-2 reports the average tensile strength σ_{m1} and σ_{m2} based on A_1 and A_2 values, respectively.

Table 3-2: Tensile strength of RTSC

Cord diameter d_1 (mm)	Cord area A_1 (mm²)	Average tensile strength σ_{m1} (MPa)	Number of filaments	Diameter of each filament d_2' (mm²)	Nominal cord area A_2 (mm²)	Average tensile strength σ_{m2} (MPa)
0.75±0.04	0.44±0.05	2612±110	12	0.20±0.01	0.38±0.04	3061±129

Based on the actual cord area A_1, the mean tensile strength of RTSC is conservatively found to be 2612 MPa, which is similar to the strength of RTSF [18] (see Table 3-1) and still about twice the strength of MSF1 and MSF2.

3.3 Pull-out behaviour of RTSC

3.3.1 Experimental details

Bond between steel fibres and concrete matrix is normally expected to be the weak link that governs the mechanical characteristics of SFRC [14,37]. Pull-out tests of fibres in various concrete types can be performed to examine fibre efficiency at different embedment lengths, so as to provide an understanding of the post-cracking behaviour of SFRC [23,38,39]. As there is no universally accepted fibre pull-out test [14], various testing and loading arrangements have been adopted in different experimental studies for MSF or RTSF [14,37,40,41]. In general, the available pull-out tests can be categorised in single and multiple fibre pull-out tests. Single fibre tests are more common due to their simplicity. Single fibre pull-out test results for RTSF reported in literature [14,23] suggest that the pull-out resistance of RTSF is comparable to that of typical MSF. To the best knowledge of the authors, no studies have investigated the pull-out behaviour of steel cords or RTSC.

To examine the pull-out behaviour of RTSC, 18 RTSC pull-out tests were performed by examining three different RTSC embedment lengths: 10, 25 and 40 mm (6 tests per length) (Table 3-3). To keep RTSC vertical during casting, the cords were passed through rectangular polystyrene plates and then glued on the plates prior to casting (Figure 3-5 (a)). In each steel mould, two small polystyrene plates were placed to create three cubical (75 mm) compartments. During casting, these compartments were filled with fresh concrete, with the cords centrally embedded. After vibration, the moulds and the plates were kept together with adhesive tape (Figure 3-5 (b)). The specimens were demoulded the next day and then cured under standard laboratory conditions.

Since bond strength is related to the compressive and tensile properties of the surrounding matrix [40], six cylinders (diameter: 100 mm, length: 200 mm) were tested in compression (BS EN 12390-3:2009 [42]) and six in splitting tension (BS EN 12390-6:2009 [43]). At 28 days, the average compressive strength was 25.6 MPa (COV=13.3%) whilst the average tensile splitting strength was 3.2 MPa (COV=12.5%).

Figure 3-6 shows a typical single-fibre pull-out test setup for RTSC. Each 75 mm concrete cube was placed in a steel reaction frame that was specifically manufactured for the test. The free end of each RTSC was sandwiched in two thin aluminium plates to avoid any premature cord failure at the jaws of the testing machine. All tests were performed under displacement control,

at a constant rate of 0.2 mm/min for displacements up to 2 mm and 0.5 mm/min for displacements from 2 mm to 10 mm and 2mm/min beyond 10 mm until failure occurred. During testing, the pull-out load–slip curve for each specimen was recorded.

(a) (b)

Figure 3-5: (a) Before casting, (b) after vibration

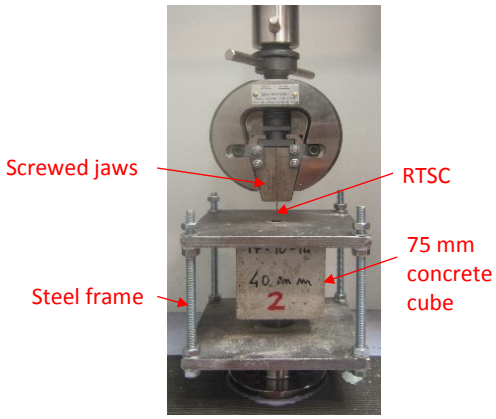

Figure 3-6: RTSC pull-out testing setup

3.3.2 Results and discussion

Two typical failure modes were observed in the tests: cord pull-out (Figure 3-7 (a)) and cord rupture (Figure 3-7 (b)). Figure 3-8 shows a sketch of typical pull-out load-slip curves (indicated in black and blue lines) representing both failure modes of RTSC. These curves were extracted from tests on specimens with an embedment length of 40 mm.

(a) (b)

Figure 3-7: Typical failure modes for RTSC: (a) cord pull-out; (b) cord rupture

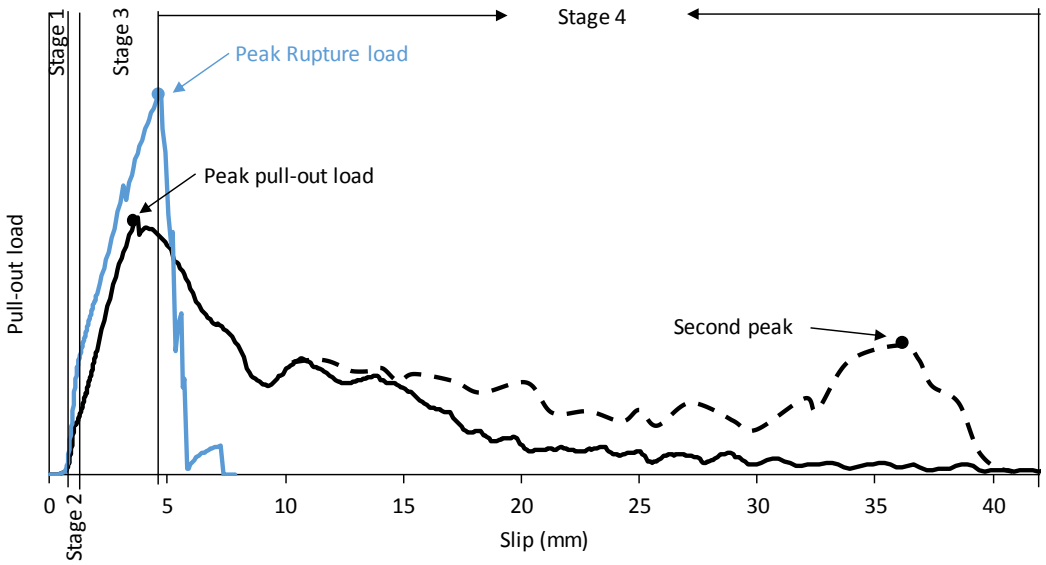

Figure 3-8: Typical pull-out load-slip curves for RTSC failed by pull-out and rupture

Four stages of pull-out response of RTSC can be identified. In stage 1 the softer initial part of the curve corresponds to the cord (exposed part) straightening at very low stresses, until all filaments are tightened and their wrinkles removed. In stage 2, the curve is more or less linear, corresponding to the elastic or adhesive bond [44] between the cord and matrix. At this stage, shear stresses induced along the cords are smaller than the bond strength between the cords and surrounding matrix. During stage 3, the nonlinearity of the curve starts with damage (microcracking) at the Interfacial Transition Zone (ITZ) in concrete [44], which results in the gradual loss of RTSC adhesive and mechanical bond. Loss of adhesive and mechanical bond then

spreads from the top end of RTSC. In stage 4, when the entire length debonds, the pull-out load starts decreasing with increasing slip, which indicates a progressive loss of frictional stress. For RTSC with larger embedment lengths (i.e. 25 and 40 mm), sometimes a second peak (indicated by a dashed line in Figure 3-8) can be observed in the curve due to wedging of RTSC (potentially induced by the outer spiral filament). However, cord rupture can also occur at long embedment lengths when the adhesive bond is sufficient to develop the fibre strength. In this case, some of the most highly stressed filaments fracture first, followed by a progressive damage of the other filaments due to the reduction of the effective cord area, along with a sharp drop in load.

Figures 3-9 (a)-(c) show the pull-out load-slip curves for RTSC with embedment lengths of 10, 25 and 40 mm, respectively. In these figures, the initial part of the curves (stage 1 in Figure 3-8) is omitted for comparison purposes. For embedment lengths of 10 and 25 mm (Figure 3-9 (a) and (b)), although high variability is observed, all specimens exhibited a similar interfacial bond behaviour and failed by cord pull-out. The variability can be largely due to the voids and flaws unevenly distributed in the concrete matrix (in particular in the area near the concrete surface), leading to uneven bond strength between RTSC and the matrix along the embedment length. For the embedment length of 40 mm (Figure 3-9 (c)), four samples ruptured, whilst the other two failed by cord pull-out.

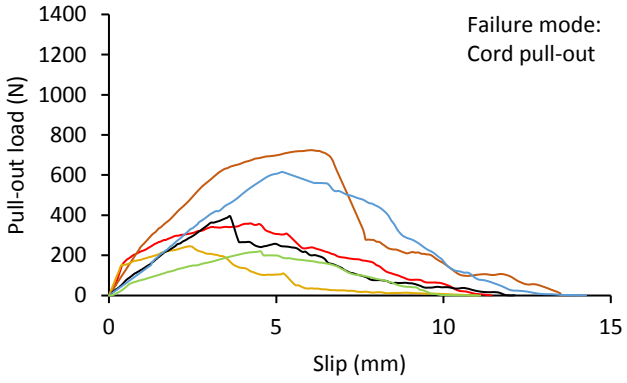

(a) Embedment length =10 mm

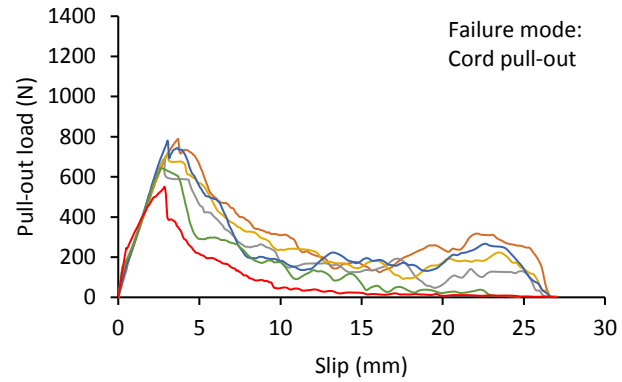

(b) Embedment length =25 mm

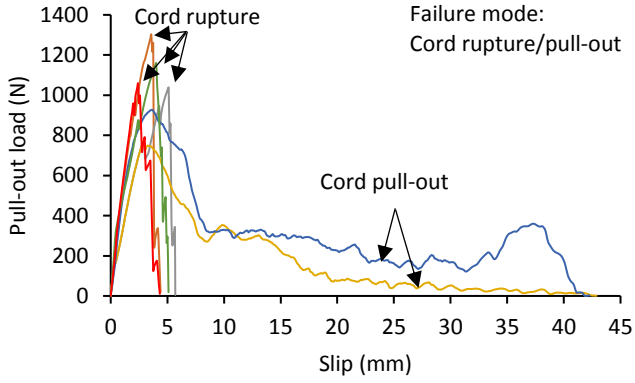

(c) Embedment length =40 mm

Figure 3-9: Pull-out load-slip curves for RTSC with different embedment lengths: (a) 10mm; (b) 25 mm; (c) 40 mm

Table 3-3 presents the average failure load and corresponding energy dissipation for the three different embedment lengths, along with their coefficients of variation (COV). "P" indicates pull-out and "R" represents rupture.

Table 3-3: Average failure load and energy for RTSC with different embedment lengths

Embedment length (mm)	No. of specimens tested	Failure mode	Failure load (N)	Energy (Joule)
10	6	P	426 (48)	2.5 (61)
25	6	P	695 (13)	5.9 (35)
40	6	P/R*	853 (12)/1139 (11)*	11 (36)/3 (16)*

*Results for specimens failed due to cord rupture

As expected, for specimens that failed by pull-out, the failure load and the dissipated energy increased with the embedment length. In comparison to the results reported in literature [14,37,40], the peak pull-out load and dissipated energy of RTSC are significantly better than those of straight or deformed MSF. For flattened-end MSF (diameter: 1mm) embedded in conventionally-placed concrete, Tlemat [14] reported peak load of approximately 380 N, 500 N and 700 N for embedment lengths of 10, 20 and 30 mm respectively. When hooked-end MSF were embedded in self-compacting concrete, Cunha et al. [37] reported peak pull-out load of 321 N, 348 N and 388 N for embedment lengths of 10, 20 and 30 mm, respectively. Banthia [40] investigated the effect of fibre and matrix type, curing and test temperature on the pull-out properties of different MSF types. In all cases, the largest peak load (551 N) and dissipated energy (7.4 Joule) were observed for crimped MSF (length: 58 mm, diameter: 1 mm) under double sided pull-out load. Moreover, the COV (in failure load and energy dissipation) was about 21% for straight MSF and 5-11% for deformed MSF in literature [40], which is similar to that for RTSC at embedment lengths of 25 and 40 mm in the present study. This indicates that RTSC can exhibit consistent pull-out behaviour and hence, can provide a reliable way to enhance the post-cracking resistance of concrete.

For specimens with an embedment length of 40 mm, it was observed that the average failure load for cord pull-out was roughly 33% lower than that for cord rupture. However, as cord rupture is undesirable [14,37,40], the critical embedded length of RTSC should be in the range of 25-40 mm (more likely 25-30 mm). Considering the potential difficulties in mixing high aspect ratio fibres (or cords) in concrete, the length of RTSC used in conventionally-placed concrete is recommended to be in the range of 50-60 mm. This recommended length is considered twice the critical embedded cord length (25-30 mm) by assuming the same fibre length is embedded into both sides of a given crack. However, further research is still required to confirm the exact length range.

3.4 Flexural tests

3.4.1 SFRC mixes and concrete mix design

Two fibre dosages commonly used by the industrial flooring industry were assessed in this study: 30 kg/m^3 (volume fraction $V_f = 0.38\%$) and 45 ($V_f = 0.57\%$) kg/m^3. Concrete reinforced with 30 kg/m^3 of MSF is commonly used for slabs-on-grade, whilst 45 kg/m^3 is usually used for suspended slabs (on piles).

The objective of this test programme was to determine the mechanical (compressive and flexural) characteristics of five SFRC mixes using RTSC on their own or blended with sorted RTSF. Two MSF-only mixes and one RTSF-only mix were also cast and used as control mixes. MSF1 (high strength) were used at the higher dosage of 45 kg/m^3, whilst MSF2 were used at 30 kg/m^3. Using a conventional tilting mixer, the critical (in terms of balling) dosage of RTSF in concrete was found to be about 30 kg/m^3 [19] and hence no 45 kg/m^3 RTSF was cast. For each mix, six cubes (150 mm) and twelve prisms (150 mm × 150 mm × 550 mm) were cast to characterise the compressive and flexural properties. Due to the large volume of concrete used, the SFRC mixes were cast in 2 separate batches using ready-mixed concrete (1st batch: mixes A–D at 30 kg/m^3 and 2nd batch: mixes E–H at 45 kg/m^3). Six plain concrete cubes and twelve prisms were also cast for each batch. Table 3-4 shows the details of the SFRC mixes including fibre type and dosage.

Table 3-4: Experimental programme

Total fibre dosage (kg/m^3)	Mix	MSF dosage (kg/m^3)	RTSC dosage (kg/m^3)	RTSF Dosage (kg/m^3)	Cement (kg/m^3)	Coarse aggregate (4-20 mm) (kg/m^3)	Fine aggregate (0-4 mm) (kg/m^3)	GGBS (kg/m^3)	Plast. (L/m^3)	Add. water	Slump (mm)	
											Initial	Final
30	A	30 (MSF2)	-	-	150	1097	804	150	3.0	6.7	35	90
	B	-	20	10	150	1097	804	150	3.0	6.7	35	90
	C	-	30	-	150	1097	804	150	3.0	6.7	35	90
	D	-	-	30	150	1097	804	150	3.0	6.7	35	90
45	E	45 (MSF1)	-	-	150	1097	804	150	1.3	6.7	45	75
	F	-	22.5	22.5	150	1097	804	150	1.3	6.7	45	75
	G	-	35	10	150	1097	804	150	1.3	6.7	45	75
	H	-	45	-	150	1097	804	150	1.3	6.7	45	75

The mix proportions (w/c ratio=0.55) used in this study (shown in Table 3-4) are the same as used in a previous study by the authors [19] to allow direct comparisons and to help to establish a robust SFRC experimental database. The target concrete compressive strength, f_{cu}, was 40 MPa. The casting procedure followed EN 14651: 2005 [35]; all prismatic (and also cubic) moulds were filled in two layers (centre first), and were vibrated 10 to 20 seconds for each layer, depending on concrete consistency.

The common procedure adopted by the flooring industry for adding fibres in concrete was followed in this study [19]. As fibre addition can adversely affect the workability of concrete [23,45,46], the slump was monitored before and after fibre addition. Although the slump test is not the best indicator of workability for SFRC (ACI 544.2R-89 [39]), it is still extensively used by the flooring industry as a qualitative measure to monitor the workability of concrete from batch to batch. The slump of the ready-mix concrete was increased by adding water (6.7 L/m^3) and the

necessary amount of plasticiser until collapse (slump> 260 mm). After the fibre addition, the final slump for both batches reduced significantly but stayed within the target limits of 70-150 mm. For both batches, no major balling issues were observed, indicating that the casting procedure originally developed for MSF is applicable to both RTSC and RTSF. The specimens were demoulded two days after casting and then covered with wetted hessian fabric and plastic sheets to retain moisture for the duration of curing, at laboratory conditions (22 ± 3 °C). After 28 days of curing, all hessian and plastic sheets were removed and specimens were left to dry. All specimens were 69-90 days old when tested.

3.4.2 Compressive cube tests: Testing procedure

According to BS EN 12390-3: 2009 [42], the SFRC and plain concrete cubes (150 mm) were tested under uniaxial compressive loading, at a constant loading rate of 0.4 $N/mm^2/s$. The dimensions of each specimen were measured and recorded before testing.

3.4.3 Flexural tests on prisms: Testing setup and procedure

According to EN 14651:2005 [35], a notch (5 mm wide and 25 mm deep) was sawn at mid-span of each prism (150 x 150 x 550 mm) a day before testing. All specimens were tested under a 3-point bending arrangement (Figure 3-10), employing a 300 kN universal electromechanical testing machine. To eliminate deformations induced by torsional moments [47], a yoke was used as first adopted by Japanese Society of Civil Engineers standard [48]. The applied load, central deflection and Crack Mouth Opening Displacement (CMOD) of all prisms were recorded. Central deflections were measured by two Linear Variable Differential Transducers (LVDTs) fixed on either side of the yoke, and a clip gauge (gauge length of 12.5 mm) was mounted at the bottom in glued blocks across the notch to monitor CMOD. The tests were CMOD-controlled, as CMOD-control provides more stable results compared to deflection-control [49]. The distance between the bottom of the specimen and the CMOD measurement level (knife edge thickness) was 5 mm. This is expected to result in only a small error in CMOD measurement which is generally neglected [49]. The machine was initially operated at a constant CMOD rate of 0.05 mm/min for CMOD from 0 to 0.1 mm and then increased to 0.2 mm/min for CMOD between 0.1mm and 4 mm. The geometrical dimensions of each specimen were registered before testing, including the distance between the notch tip to the top of the cross-section. As expected, the notch acted as a “crack inducer” during testing [7] and all cracks initiated from the notch tip and then propagated towards the top of the specimen.

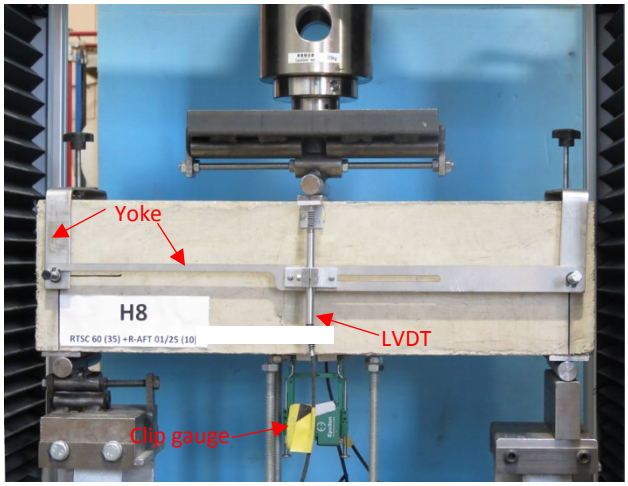

Figure 3-10: Experimental arrangement for prism test

3.5 Test results and discussion

3.5.1 Compressive strength

Table 3-5 reports the mean compressive cube strength (and variability) for plain concrete and SFRC. The plain concrete compressive strength for both batches was about 46 MPa, whilst the strength for SFRC varied from 47.2 to 55.7 MPa.

Table 3-5: Results of compressive tests

Mix	Compressive strength (MPa)	Standard deviation (MPa)	COV (%)
A [MSF2 (30)]	49.1	3.1	6
B [RTSC (20) + RTSF (10)]	48.9	1.7	3
C [RTSC (30)]	49.8	3.9	8
D RTSF [30]	48.1	2.0	4
Plain concrete 1*	46.2	2.4	5
E [MSF1 (45)]	48.3	1.9	4
F [RTSC (22.5) +RTSF (22.5)]	55.7	1.6	3
G [RTSC (35) + RTSF (10)]	48.4	0.8	2
H [RTSC (45)]	47.2	1.0	2
Plain concrete 2*	45.8	2.7	6

*Batch number

Overall, the compressive strength of the examined SFRC mixes was not significantly affected by the addition of steel fibres. Up to 6% increase in strength was seen from concrete reinforced with single-type fibres at 30 (mixes A [MSF2 (30)], C [RTSC (30)] and D [RTSF (30)]) and 45 kg/m^3 (mixes E [MSF1 (45)] and H [RTSC (45)]). Similar enhancement was obtained from concrete with recycled-fibre blends containing 10 kg/m^3 of RTSF, at the total dosages of 30 (mix B) and 45 kg/m^3 (mix G), whilst blended mix F (22.5 kg/m^3 of RTSC and 22.5 kg/m^3 of RTSF) exhibited the highest improvement (20%). In general, the compressive strength of concrete was only slightly higher when recycled fibres (RTSC and (or) RTSF) were used.

Studies on the effect of steel fibres on the compressive strength of concrete are still inconclusive. For MSF, when a low dosage (less than about 40 kg/m^3 [50]) of fibres was added in concrete, the change in strength varied from -10% to 21% [19,22,23,51]. A Similar range of variation in strength for adding up to 48 kg/m^3 of classified and cleaned RTSF in concrete was reported in literature [7,19,22,23,52]. Several studies also investigated the influence of blended steel fibres on the strength of concrete. An increase of up to 16% in strength was reported in [53,54] for the hybridisation of two different types of MSF at total dosages up to 60 kg/m^3, whilst a range between -7% and 11% was found by the authors when RTSF were blended with MSF at a total dosage up to 45 kg/m^3 [19]. The different effects of fibres on the strength of concrete can be explained by the fact that fibre incorporation can trap air and degrade the compaction of concrete which reduces the strength, whilst fibres can delay the formation and propagation of lateral cracks in concrete, thus increasing the strength [53]. Hence, the strength enhancement of the reinforcement is reduced by air introduced during mixing, and as the workability of SFRC is not so easily controlled when specific w/c ratios are required, significant variations can occur.

As evidenced by the low COV values obtained for RTSC-reinforced mixes (B, C, F, G and H) and mix D [RTSF (30)], the addition of low total dosages of the recycled fibres used in this study was found to have a negligible effect on the variability in compressive strength.

3.5.2 Flexural behaviour of SFRC prisms

3.5.2.1 Load-deflection curves

The mid-span deflection of each prism was derived by averaging the deflection values measured by two vertical LVDTs. As CMOD is in general proportional to central deflection [19,35], only load-deflection curves are presented and discussed in this section. Figures 3-11 (a) and (b) show the average (displacement based) load-deflection curves for the SFRC mixes at total fibre

dosages of 30 and 45 kg/m^3, respectively. The curves for blended SFRC mixes using both RTSC and RTSF are indicated by dashed lines, while single-type-fibre mixes and plain concrete are shown in solid lines.

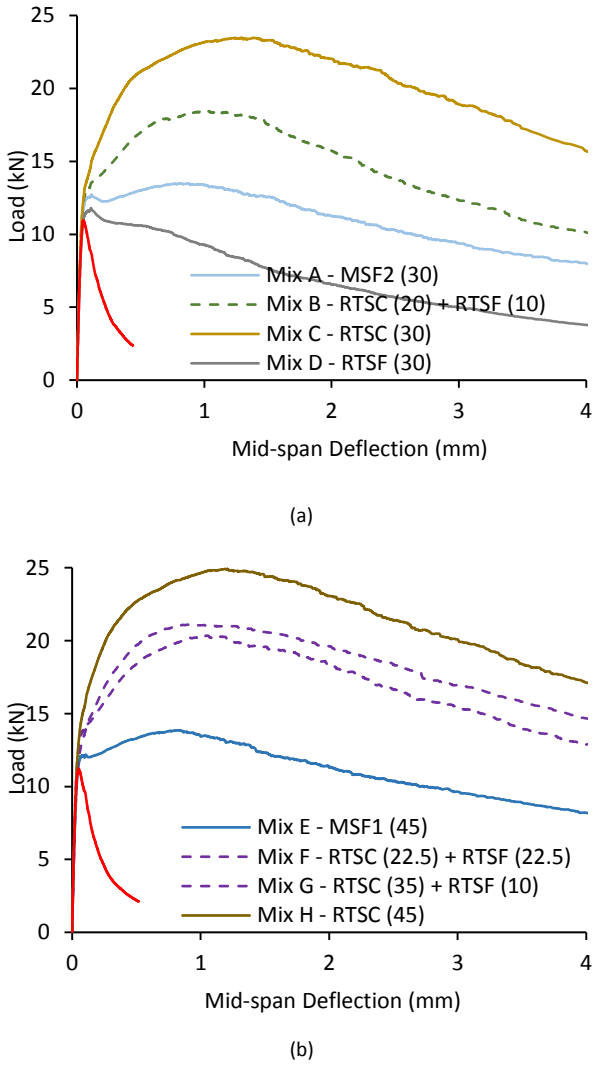

Figure 3-11: Load-deflection curves for SFRC prisms at: (a) 30 and (b) 45 kg/m^3

Comparing the performance of SFRC mixes to those of plain concrete 1 and 2 (indicated in solid red lines), it is possible to note a significant enhancement in flexural toughness. Furthermore, the increase in the total fibre dosage, from 30 to 45 kg/m^3, leads to an improved flexural performance. Similar to MSF-only mixes (A and E), all RTSC reinforced mixes (B, C, F, G and H) exhibited deflection hardening behaviour [55], which highlights the excellent performance of

RTSC. Softening behaviour was only seen in mix D with 30 kg/m^3 of RTSF, which is in accordance with the test results previously reported by the authors [19].

For both groups of mixes (30 and 45 kg/m^3), concrete reinforced with RTSC-only (i.e. mix C; RTSC (30) and H; RTSC (45)) exhibited the best flexural performance, followed by SFRC using blended RTSC and RTSF at varying dosages. All hybrid mixes exhibited better flexural performance than MSF-only mixes at the same total dosages. A slight drop after the peak load was observed for MSF-only mixes and this can be attributed to the straightening of the undulation in MSF as the crack initially develops. This is followed by an ascending branch, however, once the fibres are mobilised [56]. Mix D containing 30 kg/m^3 of RTSF exhibited a typical deflection softening behaviour with a steep load drop at a deflection of about 0.5 mm. This behaviour was possibly caused by pull-out or even fracturing of the fibres due to their specific geometrical (short and thin) and mechanical (not straight and no hooks [21]) characteristics, leading to progressive damage of the specimen.

Fib Model Code 2010 [33] relates the uniaxial tensile stress-strain relations of SFRC at SLS and ULS to CMODs of 0.5 mm (mid-span deflection of about 0.44 mm) and 2.5 mm (mid-span deflection of about 2 mm) for prism tests, respectively. At these deformations, RTSC are shown to be extremely effective at both service and ultimate conditions, whilst RTSF on their own are less effective, in particular at large displacements or crack widths due to their shorter lengths.

3.5.2.2 Test results and characterisation of SFRC mixes

LOP (f_L), residual flexural tensile strength (f_R)

According to EN 12390-5:2005 [35], the limit of proportionality (LOP) and the residual flexural tensile strength parameters (f_R) can be determined from the load-deflection (or CMOD) curves. The LOP (f_L) is defined as the flexural stress corresponding to the maximum load recorded up to a CMOD of 0.05 mm, whilst four residual flexural tensile strength parameters (f_{R1}, f_{R2}, f_{R3} and f_{R4}) are calculated from the post-cracking stage of the load-CMOD curves at 0.5, 1.5, 2.5 and 3.5 mm of CMOD, respectively. The calculation of these parameters are given below [35]:

$$f_L = \frac{3F_L l}{2bh_{sp}^2}, f_{Ri} = \frac{3F_{Ri} l}{2bh_{sp}^2} \quad (3\text{-}1)$$

Where F_L (N) is the load corresponding to LOP, and F_{Ri} (N) is the load at CMODs of 0.5, 1.5, 2.5 and 3.5 mm ($i = 1,2,3,4$), respectively. $b = 150\ mm$ is the width of the specimen, $l = 500\ mm$ is the span length and h_{sp} is the distance between the notch tip to the top of the cross-section.

Figure 3-12 reports the average values of f_L and f_{Ri} from the prism tests, along with the corresponding COV shown in brackets. The relationship between RTSC dosage and the fracture parameters (f_L and f_{Ri}) is shown by line charts. f_{Ri} values cannot be calculated for plain concrete prisms due to lack of toughness , whilst the f_L=3.6 MPa for plain concrete 1 and 2 is shown in black dashed lines in the figure.

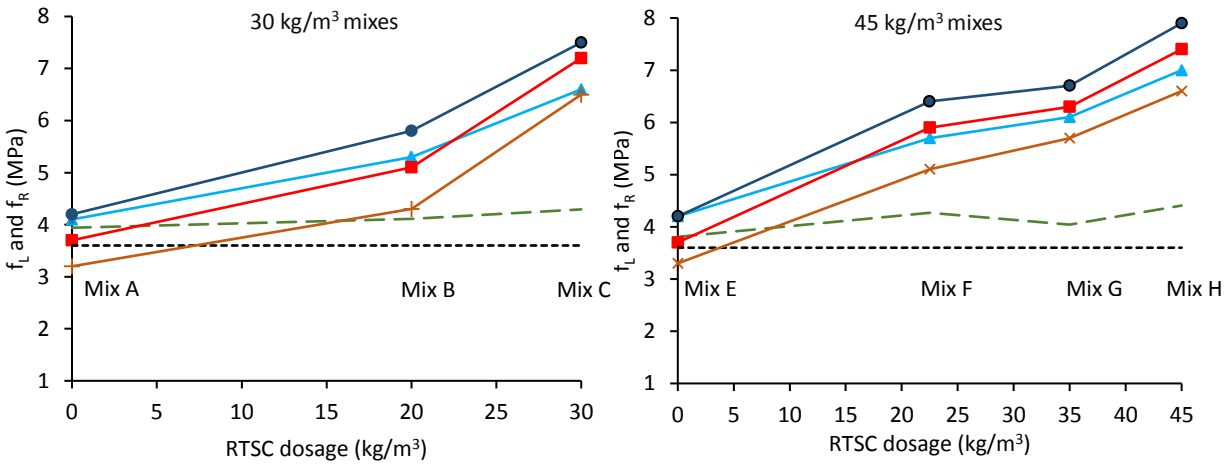

	A	B	C	D	E	F	G	H
f_L	3.9 (11%)	4.1 (8%)	4.3 (7%)	3.7 (11%)	3.8 (5%)	4.3 (10%)	4.0 (8%)	4.4 (9%)
f_{R1}	4.1 (15%)	5.3 (18%)	6.6 (11%)	3.4 (25%)	4.2 (12%)	5.7 (15%)	6.1 (18%)	7.0 (9%)
f_{R2}	4.2 (15%)	5.8 (17%)	7.5 (8%)	2.7 (32%)	4.2 (12%)	6.4 (15%)	6.7 (19%)	7.9 (9%)
f_{R3}	3.7 (14%)	5.1 (19%)	7.2 (9%)	2.1 (31%)	3.7 (12%)	5.9 (14%)	6.3 (21%)	7.4 (10%)
f_{R4}	3.2 (15%)	4.3 (21%)	6.5 (11%)	1.7 (32%)	3.3 (13%)	5.1 (17%)	5.7 (23%)	6.6 (10%)

Figure 3-12: f_L and f_R values of prisms (in MPa), and COV (in %)

RTSC-reinforced mixes exhibited slightly higher f_L values than MSF-only mixes at the same total fibre dosage, and the overall increase in f_L was in the range of 2-22%. As the LOP (f_L) represents the flexural strength of the concrete matrix, it can be concluded that the presence of fibres enhances the concrete matrix strength by delaying the formation of microcracks. Similar f_L values were derived from RTSF-only mix D and MSF-only mixes, indicating that RTSF-only mixes are comparable to MSF-only mixes at controlling microcracks, as reported also in literature [25] and [10] for fatigue tests.

For both total dosages, f_{Ri} values increase significantly with increasing amounts of RTSC. f_{R4} is higher than f_L for all RTSC-reinforced mixes (up to 50%), whilst it is 13-18% lower in the MSF-only mixes. This indicates that RTSC are more beneficial than MSF at bridging macrocracks at the same total dosage. For RTSC-reinforced mixes, f_{R1} values are smaller than f_{R2} values, and even

lower than f_{R3} values (for mixes containing high dosages of RTSC), indicating the higher mobilisation of RTSC with increasing CMOD. The lower f_{Ri} values of the RTSF-only mix D confirm that RTSF on their own are less effective at controlling large crack widths than MSF and RTSC.

The COV of the f_{Ri} values for all SFRC mixes are within the range of 40%, which is in agreement with values reported in literature [19,25,57,58]. The COV values for the recycled-fibre mixes are similar to MSF-only mixes at the same total fibre dosage, indicating that recycled steel fibres (RTSC alone or blended with a small amount of RTSF) had little effect on the variability of the post-cracking behaviour of SFRC. For all SFRC mixes, the COV values overall increase from f_L, f_{R1} to f_{R4}. This may be due to the fact that compared with the resistance provided by the matrix itself prior to cracking, the post-cracking behaviour of SFRC relies increasingly on more variable parameters, such as fibre-matrix interaction and fibre distribution [19]. This can also explain why the f_{R2}, f_{R3} and f_{R4} values for the RTSF-only mix D show more scatter than other SFRC mixes. Hence, although RTSF are better distributed throughout the volume of the concrete due to their "fineness" and were found in the previous work [19] to reduce variability at f_L and f_{R1}, the post-cracking behaviour of RTSF-only mixes at large cracks is more variable, as their behaviour at this stage is highly governed by the variable pull-out performance, which is significantly influenced by large slip and highly variable geometrical characteristics.

Flexural modulus of elasticity (E_{fm})

The modulus of elasticity of concrete can be measured directly via compressive tests or indirectly via flexural tests. Elastic analysis is normally used to determine the flexural modulus E_{fm} from central deflection in flexural tests, by using the linear portion of results up to 40% of the peak flexural load. Since the load spreading effect was found to be negligible [15], the dimensions of the loading and supporting rollers were not taken into consideration. Ignoring shear deformation developed in the prism, the linear equation relating the load-deflection stiffness to E_{fm} is given below,

$$E_{fm} = \frac{Pl^3}{48I\delta} \tag{3-2}$$

Where $\frac{P}{\delta}$ (kN/mm) is the slope of the initial part of the load-deflection curve and I (mm^4) is the second moment of area of the middle cross-section.

Table 3-6 reports the average E_{fm} values and their COV (listed in brackets) for all SFRC mixes. All SFRC mixes show slightly lower E_{fm} than plain concrete (36.9 (7%) GPa for the 1st batch and

35.5 (7%) GPa for the 2nd batch). A similar observation was made by Angelakopoulos [18] for roller compacted concrete reinforced with RTSF and MSF. Although steel fibres should increase the E_{fm} of a perfect concrete composite, they tend to trap air and that has an adverse effect on E_{fm}. The effect of increased air is better demonstrated by the linear relationship between density of SFRC and E_{fm} of prisms from the same mix, as reported in literature [18]. However, for the relatively low total fibre dosages (30 and 45 kg/m^3) examined in this study, as expected, the influence of the steel fibres on the elastic properties is found to be insignificant. Furthermore, the E_{fm} of the recycled-fibre mixes is similar to the MSF-only mixes.

Table 3-6: E_{fm} and characterisation of the tested SFRC mixes

Mix	E_{fm} (GPa)	f_{Lk} (MPa)	f_{R1k} (MPa)	f_{R3k} (MPa)	f_{R1k}/f_{Lk}	f_{R3k}/f_{R1k}	Strength class
A [MSF2 (30)]	31.4 (7%)	3.2	3.0	2.8	1.0	0.92	3.0 c
B [RTSC (20) + RTSF (10)]	32.4 (13%)	3.6	3.7	3.5	1.0	0.96	3.0 c
C [RTSC (30)]	30.3 (9%)	3.8	5.4	6.1	1.4	1.12	5.0 d
D RTSF [30]	32.0 (16%)	3.0	2.0	1.0	0.7	0.51	2.0 a
E [MSF1]	32.5 (8%)	3.5	3.4	3.2	1.0	0.94	3.0 c
F [RTSC (22.5) +RTSF (22.5)]	34.6 (9%)	3.6	4.3	4.5	1.2	1.06	4.0 c
G [RTSC (35) + RTSF (10)]	30.4 (10%)	3.5	4.3	4.0	1.2	0.93	4.0 c
H [RTSC (45)]	29.7 (7%)	3.7	5.9	6.2	1.6	1.06	5.0 c

Classification of SFRC mixes

To classify the post-cracking performance of FRC materials, two parameters using characteristic residual flexural tensile strengths, f_{Rik}, are adopted by Model Code 2010 [33]: f_{R1k} and f_{R3k} / f_{R1k}. f_{R1k} (using specific strength classes) is used to represent the post-cracking performance of FRC at serviceability conditions. The strength classes used are: 1.0, 1.5, 2.0, 2.5, 3.0, 4.0, 5.0, 6.0, 7.0, and 8.0 (MPa). The ratio f_{R3k}/f_{R1k} which reflects the cracked performance of the material at ultimate conditions is shown by a letter a, b, c, d or e, where a is for 0.5≤ f_{R3k} / f_{R1k} ≤0.7, b is for 0.7≤ f_{R3k} / f_{R1k} ≤0.9, c is for 0.9≤ f_{R3k} / f_{R1k} ≤1.1, d is for 1.1≤f_{R3k}/f_{R1k}≤1.3 and e is for 1.3≤f_{R3k}/f_{R1k}. Model code 2010 [33] suggests that if the minimum performance requirements in terms of ratios f_{R1k}/f_{Lk}>0.4 and f_{R3k}/f_{R1k}>0.5 are satisfied (f_{Lk} is the characteristic value of LOP), a SFRC mix can be used to partially (or even entirely) substitute conventional reinforcement in concrete at the ultimate limit state. The characteristic strength values (f_{Lk} and f_{Rik}) were determined from the mean values by assuming a Student's t-distribution, and the effect of the number of the tested specimens for

each mix was considered according to RILEM TC 162-TDF [59]. Table 3-6 presents the values of f_{Lk} and f_{Rik} for the tested mixes as well as their strength classes.

Overall, the two ratios (f_{R1k}/f_{Lk}>0.4 and f_{R3k}/f_{R1k}>0.5) adopted by Model Code 2010 are exceeded for all tested mixes, which indicates that recycled steel fibres can partially or even entirely replace conventional reinforcement in concrete at limit conditions. More importantly, the hybridisation of RTSC and RTSF at varying dosages exhibits different but comparable (or even better) strength classes to the MSF-only mixes.

3.5.3 Effectiveness of recycled-fibre mixes

3.5.3.1 Recycled fibres (RTSC and RTSF) vs MSF

To quantify the improvement in the post-cracking performance of SFRC using recycled fibres, an improvement ratio $I_{f_{Ri}}$, which is a function of the normalised residual flexural tensile strength f_{Ri} of the recycled-fibre mixes (B, C, D, F, G and H) with respect to the control mixes (MSF-only mixes A and E) at the same total fibre dosage, is adopted:

$$I_{f_{Ri}} = \left(\frac{f_{Ri_{(Recycled)}}}{f_{Ri_{(MSF)}}} - 1\right) \times 100, \text{ in \%} \quad (3\text{-}3)$$

where f_{Ri} represents the average residual flexural tensile strength (f_{R1}, f_{R2}, f_{R3}, f_{R4}) of the SFRC mixes. Figures 3-13 (a) and (b) show the I_{f_R} values of the recycled fibre mixes at 30 kg/m^3 (mixes B, C and D) and 45 kg/m^3 (mixes F, G and H), respectively.

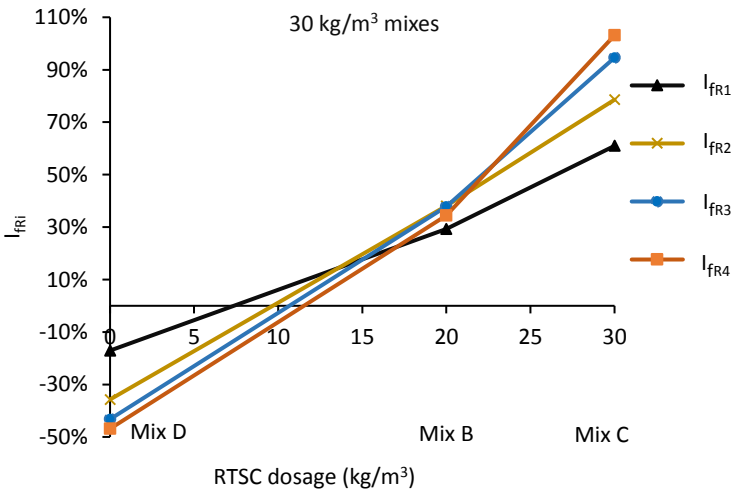

(a)

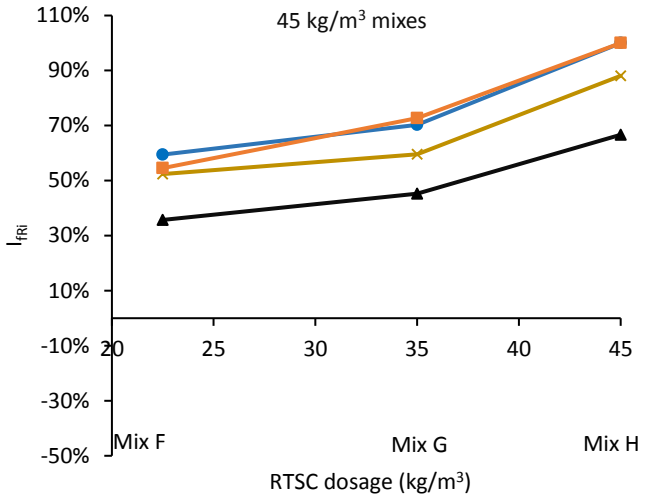

(b)

Figure 3-13: Improvement ratio $I_{f_{Ri}}$ for SFRC mixes at (a) 30 kg/m³ (b) 45 kg/m³

Compared to MSF-only mixes at the same total fibre dosage, negative $I_{f_{Ri}}$ values (between -17 and -47%) are obtained from mix D containing 30kg/m³ of RTSF, and the $I_{f_{Ri}}$ becomes increasingly smaller from f_{R1} to f_{R4}. This again confirms that the effectiveness of RTSF on their own at controlling cracks degrades gradually as cracks open, due to their smaller lengths and diameters.

On the other hand, highly enhanced post-cracking performance is observed for mixes reinforced with RTSC-only or blended with RTSF, and their performance improves with increasing amounts of RTSC. For the two total dosages (30 and 45 kg/m³), the highest $I_{f_{Ri}}$ values in the range of 61-103% are seen for RTSC-only mixes C and H, followed by the blended mixes B, F and G. At 30 kg/m³, the $I_{f_{Ri}}$ of the blended mix B [RTSC (20) + RTSF (10)] ranges from 30% to 40%, whilst 35-75% of $I_{f_{Ri}}$ are observed for the recycled-fibre blends (mixes F and G) containing up to 35 kg/m³ of RTSC at 45 kg/m³. At both total dosages, it is noted that the $I_{f_{Ri}}$ values increase with increasing amounts of RTSC and when using more than 20 kg/m³ of RTSC (mixes C, G and H), the $I_{f_{Ri}}$ values overall increase substantially from f_{R1} to f_{R4}. This again confirms that RTSC are better mobilised at larger crack widths.

3.5.3.2 SFRC slab thickness

This section aims to quantify the effectiveness of recycled fibres in concrete flooring applications, using the experimental results (compressive and flexural properties) of the examined SFRC

mixes. As a practical example, a critical case for ground-supported slabs under flexure is considered, with two closely spaced point loads (e.g. back-to-back racking legs) applied near an edge of the slab. The assumptions include a design leg load of 78 kN and a typical contact area of 100 × 100 mm per leg, the spacing between two racking legs of 300 mm, and radius of relative stiffness (the stiffness of concrete slab relative to that of sub-grade material) of 650 mm. The design flexural tensile strength of all SFRC mixes is considered to be 2 MPa, which is assumed to be the same as the design flexural tensile strength of plain concrete, according to the Concrete Society TR 34 [60]. Following the design procedures for FRC ground-supported slabs adopted by Concrete Society TR 34 [60], the relation between RTSC dosages and the required slab thicknesses for the tested SFRC mixes is shown in Figure 3-14.

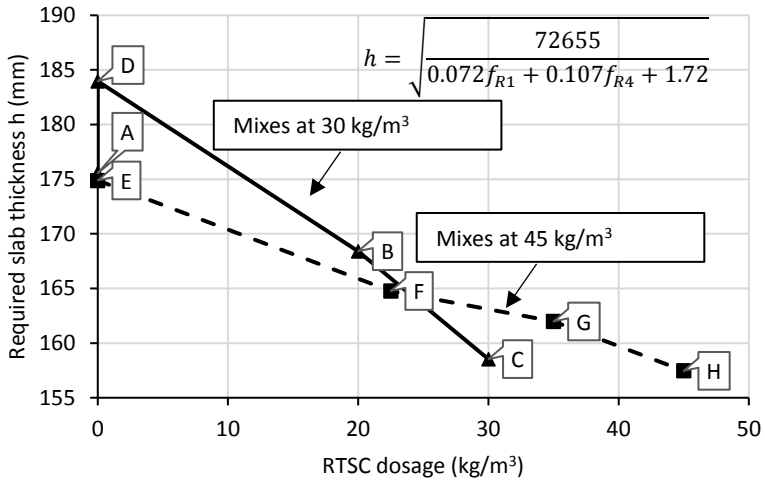

Figure 3-14: Relation between RTSC dosages and required slab thicknesses for the examined SFRC mixes

For both total dosages (30 and 45 kg/m^3), RTSC-only mixes C (159 mm) and H (157 mm) exhibit the lowest slab thickness requirements, whilst mix D (containing 30 kg/m^3 of RTSF) shows the highest requirement (184 mm). Compared to MSF-only mixes A and E with required thicknesses of about 175 mm, the smaller required thicknesses for the recycled-fibre mixes demonstrate that recycled fibres can be competitive (or even better) substitutes to MSF-only solutions for industrial concrete flooring applications. Such mixes can enable designs with significantly less volume of concrete required, as well as 100% replacement of MSF with more sustainable steel fibres (i.e. RTSC and RTSF).

3.6 Conclusions

The mechanical properties of concrete reinforced with RTSC and RTSF at varying dosages have been investigated by means of direct tensile, pull-out, compressive cube, and flexural prism tests. The following concluding remarks can be made:

- The tensile and pull-out properties of RTSC are similar to (or even better than) typical MSF.
- The critical embedded length of RTSC is in the range of 25-40 mm, and thus the recommended length of RTSC ranges from 50 to 60 mm.
- Similar to MSF, recycled-fibre mixes (at low total dosages of RTSC on their own or blended with RTSF) do not significantly affect f_{cu} and E_{fm}.
- RTSC and RTSF have a marginal effect on the variability of the residual flexural tensile strength of SFRC. Compared with the resistance provided by the matrix itself prior to cracking, the post-cracking behaviour of SFRC relies increasingly on more variable parameters, such as fibre-matrix interaction and fibre distribution.
- RTSF-only mixes are comparable to MSF-only mixes at serviceability conditions. However, due to the smaller lengths and diameters of RTSF, their effectiveness at controlling cracks degrades gradually as cracks open.
- RTSC are more effective than MSF at arresting microcracks and bridging macrocracks at the same total dosage and RTSC are better mobilised at larger crack widths.
- The post-cracking strength of recycled-fibre mixes is significantly higher (up to 103%) than MSF-only mixes at the same total fibre dosage. For the recycled-fibre blends, overall their flexural performance improves with increasing amounts of RTSC.
- It is noted that these research findings are based on limited experimental data, further research on various aspects (fibre dosage, fibre type and loading configuration, etc.) is still needed to increase the range of validity and expand the conclusions.

References

[1] European Parliament and Council, Directive 2008/98/EC of the European Parliament and of the Council of 19 November 2008 on waste and repealing certain directives, Off. J. Eur. Union. 13 (2008) 3–30.

[2] WBCSD, End-of-life tires: a framework for effective management systems, http://www.wbcsd.org/DocRoot/lBTHZFGcpBK5OxTDXlpS/EndOfLifeTires_171208.pdf. 2010, (accessed 18. 03 .21).

[3] ETRA, Introduction to tyre recycling: 2013, The European Tyre Recycling Association, Brussels, Belgium, 2013.

[4] K. Pilakoutas, K. Neocleous, H. Tlemat, Reuse of tyre steel fibres as concrete reinforcement, Eng. Sustain. 157 (2004) 131–138.

[5] S. Raffoul, R. Garcia, K. Pilakoutas, M. Guadagnini, N.F. Medina, Optimisation of rubberised concrete with high rubber content: An experimental investigation, Constr. Build. Mater. 124 (2016) 391–404. doi:10.1016/j.conbuildmat.2016.07.054.

[6] S. Raffoul, R. Garcia, D. Escolano-Margarit, M. Guadagnini, I. Hajirasouliha, K. Pilakoutas, Behaviour of unconfined and FRP-confined rubberised concrete in axial compression, Constr. Build. Mater. 147 (2017) 388–397. doi:10.1016/j.conbuildmat.2017.04.175.

[7] H. Tlemat, K. Pilakoutas, K. Neocleous, Stress-strain characteristic of SFRC using recycled fibres, Mater. Struct. 39 (2006) 365–377. doi:10.1617/s11527-005-9009-4.

[8] H. Tlemat, K. Pilakoutas, K. Neocleous, Modelling of SFRC using inverse finite element analysis, Mater. Struct. 39 (2006) 221–233. doi:10.1617/s11527-005-9010-y.

[9] K. Neocleous, H. Tlemat, K. Pilakoutas, Design issues for concrete reinforced with steel fibers, including fibers recovered from used tires, J. Mater. Civ. Eng. 18 (2006) 677–685. doi:10.1061/(ASCE)0899-1561(2006)18:5(677).

[10] A.G. Graeff, K. Pilakoutas, K. Neocleous, M.V.N.N. Peres, Fatigue resistance and cracking mechanism of concrete pavements reinforced with recycled steel fibres recovered from

post-consumer tyres, Eng. Struct. 45 (2012) 385–395. doi:10.1016/j.engstruct.2012.06.030.

[11] N. Jafarifar, K. Pilakoutas, T. Bennett, Moisture transport and drying shrinkage properties of steel-fibre-reinforced-concrete, Constr. Build. Mater. 73 (2014) 41–50. doi:10.1016/j.conbuildmat.2014.09.039.

[12] K.H. Younis, K. Pilakoutas, Strength prediction model and methods for improving recycled aggregate concrete, Constr. Build. Mater. 49 (2013) 688–701. doi:10.1016/j.conbuildmat.2013.09.003.

[13] K.H. Younis, K. Pilakoutas, Assessment of post-restrained shrinkage mechanical properties of concrete, ACI Mater. J. 113 (2016) 267–276. doi:10.14359/51688699.

[14] H. Tlemat, Steel fibres from waste tyres to concrete, testing, modelling and design, The University of Sheffield, Sheffield, UK, 2004.

[15] A.G. Graeff, Long-term performance of recycled steel fibre reinforced concrete for pavement applications, The University of Sheffield, UK, 2011.

[16] K. Neocleous, H. Angelakopoulos, K. Pilakoutas, M. Guadagnini, Fibre-reinforced roller-compacted concrete transport pavements, Proc. Inst. Civ. Eng. - Transp. 164 (2011) 97–109. doi:10.1680/tran.9.00043.

[17] N. Jafarifar, Shrinkage behaviour of steel fibre reinfoced concrete pavements, The University of Sheffield, Sheffield, UK, 2012.

[18] H. Angelakopoulos, Reused post-consumer tyre steel fibres in roller compacted concrete, The University of Sheffield, Sheffield, UK, 2016.

[19] H. Hu, P. Papastergiou, H. Angelakopoulos, M. Guadagnini, K. Pilakoutas, Mechanical properties of SFRC using blended manufactured and recycled tyre steel fibres, Constr. Build. Mater. 163 (2018) 376–389. doi:10.1016/j.conbuildmat.2017.12.116.

[20] G. Groli, Crack width control in RC elements with recycled steel fibres and applications to integral structures: theoretical and experimental study, Polytechnical University of

Madrid, Madrid, Spain, 2014.

[21] E. Martinelli, A. Caggiano, H. Xargay, An experimental study on the post-cracking behaviour of Hybrid Industrial/Recycled Steel Fibre-Reinforced Concrete, Constr. Build. Mater. 94 (2015) 290–298. doi:10.1016/j.conbuildmat.2015.07.007.

[22] G. Centonze, M. Leone, M.A. Aiello, Steel fibers from waste tires as reinforcement in concrete: A mechanical characterization, Constr. Build. Mater. 36 (2012) 46–57. doi:10.1016/j.conbuildmat.2012.04.088.

[23] M.A. Aiello, F. Leuzzi, G. Centonze, A. Maffezzoli, Use of steel fibres recovered from waste tyres as reinforcement in concrete: Pull-out behaviour, compressive and flexural strength, Waste Manag. 29 (2009) 1960–1970. doi:10.1016/j.wasman.2008.12.002.

[24] M. Leone, G. Centonze, D. Colonna, F. Micelli, M.A. Aiello, Fiber-reinforced concrete with low content of recycled steel fiber: Shear behaviour, Constr. Build. Mater. 161 (2018) 141–155. doi:10.1016/j.conbuildmat.2017.11.101.

[25] Z. Zamanzadeh, L. Lourenço, J. Barros, Recycled steel fibre reinforced concrete failing in bending and in shear, Constr. Build. Mater. 85 (2015) 195–207. doi:10.1016/j.conbuildmat.2015.03.070.

[26] D. Bjegovic, A. Baricevic, S. Lakusic, D. Damjanovic, I. Duvnjak, Positive interaction of industrial and recycled steel fibres in fibre reinforced concrete, J. Civ. Eng. Manag. 19 (2013) S50–S60. doi:10.3846/13923730.2013.802710.

[27] M. Skazlić, A. Baričević, D. Bjegović, Fibre reinforced SCC concrete with recycled fibres, Newsletter. (2017) 1–7.

[28] G. Groli, A.P. Caldentey, A.G. Soto, Cracking performance of SCC reinforced with recycled fibres - an experimental study, Struct. Concr. 15 (2014) 136–153. doi:10.1002/suco.201300008.

[29] H. Angelakopoulos, P. Papastergiou, K. Pilakoutas, Fibrous roller-compacted concrete with recycled materials - Feasibility study, Mag. Concr. Res. 67 (2015).

doi:10.1680/macr.14.00246.

[30] H. Angelakopoulos, P Waldron, Tyre wire in Concrete Leading to Environmental sustainability. CIP Eco-innovation project, Twincletoes project - Layman's report, Twincon Ltd, Sheffield, UK, 2015.

[31] K. Neocleous, S.G. Maxineasa, L. Dumitrescu, K. Themistocleous, N. Taranu and D. Hadjimitsis, D1.6 Preliminary LCA. Anagennisi Project, Anagennisi: innovative use of all tyre components in concrete, 2014.

[32] Anagennisi Project, Anagennisi: innovative use of all tyre components in concrete. http://anagennisi.org/wordpress/, 2014 (accessed 2018.03.20).

[33] F.I. du Béton, Fib Model Code for Concrete Structures 2010, Wilhelm Ernst & Sohn, Berlin, Germany, 2013.

[34] ACI 544.8R-16, Report on indirect method to obtain stress-strain response of fiber-reinforced concrete (FRC). American Concrete Institute, Michigan, US, 2016.

[35] BS EN 14651:2005, Test method for metallic fibre concrete - Measuring the flexural tensile strength (limit of proportionality (LOP), residual). British Standards Institution, London, UK, 2005.

[36] BS EN 10002-1:2001 Metallic materials - Tensile testing - Part 1: Method of test at ambient temperature. British Standards Institution, London, UK, 2001.

[37] V.M.C.F. Cunha, J.A.O. Barros, J.M. Sena-Cruz, Pullout Behavior of Steel Fibers in Self-Compacting Concrete, J. Mater. Civ. Eng. 22 (2010) 1–9. doi:10.1061/(ASCE)MT.1943-5533.0000001.

[38] ACI 544.4R-88 (Reapproved 1999), Design considerations for steel fiber reinforced concrete. American Concrete Institute, Michigan, US, 1999.

[39] ACI 544.2R-89 (Reapproved 1999), Measurement of properties of fiber reinforced concrete. American Concrete Institute, Michigan, US, 1999.

[40] N. Banthia, A study of some factors affecting the fiber–matrix bond in steel fiber

reinforced concrete, Can. J. Civ. Eng. 17 (1990) 610–620. doi:10.1139/l90-069.

[41] P. Robins, S. Austin, P. Jones, Pull-out behaviour of hooked steel fibres, Mater. Struct. 35 (2002) 434–442. doi:10.1007/BF02483148.

[42] BS EN 12390-3:2009, Testing hardened concrete - Part 3: Compressive strength of test specimens. British Standards Institution, London, UK, 2009.

[43] BS EN 12390-6:2009, Testing hardened concrete - Part 6: Tensile splitting strength of test specimens. British Standards Institution, London, UK, 2009.

[44] V.M.C.F. Cunha, J.A.O. Barros, J.M. Sena-Cruz, Pull-out behaviour of hooked-end steel fibres in self-compacting concrete. Technical Report 07-DEC/E06, University of Minho, Portugal, 2007.

[45] Ş. Yazıcı, G. İnan, V. Tabak, Effect of aspect ratio and volume fraction of steel fiber on the mechanical properties of SFRC, Constr. Build. Mater. 21 (2007) 1250–1253. doi:10.1016/j.conbuildmat.2006.05.025.

[46] Y. Mohammadi, S.P. Singh, S.K. Kaushik, Properties of steel fibrous concrete containing mixed fibres in fresh and hardened state, Constr. Build. Mater. 22 (2008) 956–965. doi:10.1016/j.conbuildmat.2006.12.004.

[47] N. Banthia, J.F. Trottier, Test methods for flexural toughness characterization of fiber reinforced concrete: some concerns and a proposition, ACI Mater. J. 92 (1995) 48–57.

[48] JSCE-SF4, Standard for flexural strength and flexural toughness, method of tests for steel fiber reinforced concrete, Concrete library of JSCE, Japan Concrete Institute (JCI), Japan,1984.

[49] B.I.G. Barr, M.K. Lee, E.J. de Place Hansen, D. Dupont, E. Erdem, S. Schaerlaekens, B. Schnütgen, H. Stang, L. Vandewalle, Round-robin analysis of the RILEM TC 162-TDF beam-bending test: Part 2 - Approximation of δ from the CMOD response, Mater. Struct. 36 (2003) 631–635. doi:10.1007/BF02483283.

[50] R.F. Zollo, Fiber-reinforced concrete: an overview after 30 years of development, Cem.

Concr. Compos. 19 (1997) 107–122. doi:10.1016/S0958-9465(96)00046-7.

[51] M.N. Soutsos, T.T. Le, A.P. Lampropoulos, Flexural performance of fibre reinforced concrete made with steel and synthetic fibres, Constr. Build. Mater. 36 (2012) 704–710. doi:10.1016/j.conbuildmat.2012.06.042.

[52] K.H. Younis, K. Pilakoutas, M. Guadagnini, H. Angelakopoulos, Feasibility of Using Recycled Steel Fibres To Enhance the Behaviour of Recycled Aggregate Concrete, FRC 2014 Jt. ACI-Fib Int. Work. - Fibre Reinf. Concr. from Des. to Struct. Appl. (2014) 598–608.

[53] N. Banthia, M. Sappakittipakorn, Toughness enhancement in steel fiber reinforced concrete through fiber hybridization, Cem. Concr. Res. 37 (2007) 1366–1372. doi:10.1016/j.cemconres.2007.05.005.

[54] L.G. Sorelli, A. Meda, G.A. Plizzari, Bending and uniaxial tensile tests on concrete reinforced with hybrid steel fibers, J. Mater. Civ. Eng. 17 (2005) 519–527. doi:10.1061/(ASCE)0899-1561(2005)17:5(519).

[55] A.E. Naaman, H.W. Reinhardt, Proposed classification of HPFRC composites based on their tensile response, Mater. Struct. 39 (2007) 547–555. doi:10.1617/s11527-006-9103-2.

[56] G. Chanvillard, P.C. Aitcin, Pull-out behavior of corrugated steel fibers qualitative and statistical analysis, Adv. Cem. Based Mater. 4 (1996) 28–41. doi:10.1016/1065-7355(96)00036-3.

[57] S. Oikonomou-mpegetis, Behaviour and Design of Steel Fibre Reinforced Concrete Slabs, Imperial College London, London, UK, 2012.

[58] B.I.G. Barr, M.K. Lee, E.J. de Place Hansen, D. Dupont, E. Erdem, S. Schaerlaekens, B. Schnütgen, H. Stang, L. Vandewalle, Round-robin analysis of the RILEM TC 162-TDF beam-bending test: Part 1—Test method evaluation, Mater. Struct. 36 (2003) 609–620. doi:10.1007/BF02483281.

[59] Rilem TC 162-TDF, σ-ε-Design Method, Mater. Struct. 36 (2003) 560–567.

doi:10.1007/BF02480834.

[60] Technical report 34, Concrete industrial ground floors: a guide to their design and construction, The Concrete Society, Surrey, UK, 2013.

Chapter 4 Post-cracking Tensile Behaviour of Blended Steel Fibre Reinforced Concrete

H. Hu, Z. Wang, F.P. Figueiredo, P. Papastergiou, M. Guadagnini, K. Pilakoutas, Post-cracking tensile behaviour of blended steel fibre reinforced concrete, Structural Concrete, 2018. **Submitted.**

Author contribution statement

Dr Papastergiou, Dr Guadagnini and Prof. Pilakoutas coordinated the Anagennisi project. Mr Wang and Dr Figueiredo contributed to the numerical analysis, in particular on determining mesh refinement and parameters adopted in FE modelling. All authors discussed the results and commented on the manuscript.

ABSTRACT

Fibre blends have the potential to improve the mechanical and sustainability credentials of steel fibre reinforced concrete (SFRC), but at which ratios these can work is not known a priori. This paper investigates the uniaxial tensile stress-strain ($\sigma - \varepsilon$) relationship of blended SFRC using Manufactured Steel Fibres (MSF) on their own, or blended with sorted steel fibres recycled from end-of-life tyres (RTSF), at total fibre dosages of 30, 35 and 45 kg/m^3. The accuracy of two $\sigma - \varepsilon$ relations proposed by RILEM TC 162-TDF and Model Code 2010 is assessed using the experimental results from concrete prisms. By using nonlinear finite element (FE) analysis, it is found that the RILEM approach can lead to significant overestimation (up to 72%) of peak flexural load and energy absorption capacity (up to 39%), whilst the Model Code 2010 can provide a rather accurate prediction of the energy absorption capacity and some overestimation (less than 34%) of the peak flexural load. Inverse FE analysis is used to determine indirectly the uniaxial tensile $\sigma - \varepsilon$ relations of the examined SFRC mixes, and a simplified trilinear relation for SFRC is proposed. It is concluded that the tensile strength of SFRC with RTSF at a low total fibre dosage is only marginally improved by fibre addition, and the post-cracking tensile strengths at different strains can be determined directly from residual flexural tensile strengths (f_{Ri}) of prisms.

This chapter consists of a "stand-alone" journal paper and includes a relevant bibliography at the end of the chapter. Additional information on FE mesh sensitivity analysis is presented in Appendix C.

4.1 Introduction

The mechanical properties of steel fibres recycled from end-of-life tyres have been studied since 1999 at The University of Sheffield [1–8]. Recycled Tyre Steel Fibres (RTSF, see Figure 4-1), as randomly distributed reinforcement in concrete is now a product used in industrial flooring. It has been shown that RTSF can improve the flexural strength and toughness of concrete, in particular at the initial stage of cracking. More significantly, for sustainability, LCA studies [9,10] show that the production of RTSF only requires up to 5% of the energy input compared to that of manufactured steel fibres (MSF). However, the current design guidelines for SFRC still do not consider the benefits of using fibre blends or RTSF only, and this becomes a main barrier to the wider use of RTSF in construction applications.

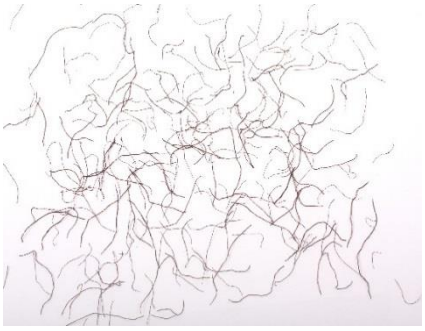

Figure 4-1: Reused Tyre Steel Fibres (RTSF) [8]

For a low dosage (<0.5% by volume) of steel fibres added in concrete, many studies [8,11–15] have suggested that fibre addition has an insignificant effect on the compressive strength of concrete. Existing design guidelines (e.g. RILEM TC 162-TDF [16] and Model Code 2010 [17]) mainly focus on the tensile properties of SFRC, as in most applications (e.g. pavements and tunnel linings), the material is subjected to bending. Since tensile tests on SFRC are difficult to execute and interpret [17–21] flexural tests on prisms or slabs are universally adopted to provide the nominal tensile properties of SFRC. Based on fracture parameters determined using 3-point notched prism tests, RILEM TC 162-TDF [16] proposes a trilinear stress-strain ($\sigma - \varepsilon$) relationship for SFRC, whilst Model Code 2010 [17] adopts a stress-crack opening ($\sigma - w$) law in uniaxial tension. The $\sigma - w$ relationships can be converted to $\sigma - \varepsilon$ by introducing a structural characteristic length l_{cs}. Nevertheless, these design guidelines (i.e. RILEM TC 162-TDF and Model Code 2010) rely on test results from SFRC using single-type fibres (i.e. MSF) and it is not

certain if they are also suitable for blended SFRC mixes. Compared with typical MSF, RTSF have a wide range of fibre length and aspect ratio distributions, as well as higher strength (≥2000 MPa) [5,22–26]. This paper will examine the suitability of these two constitutive models for fibre blends with RTSF. Comparisons are made between predicted load-deflection curves using FE analysis versus the experimental results. The research reported in this paper was undertaken as part of the FP7 EU-funded project "Anagennisi" [27], which aimed to develop uses for all tyre components in concrete. This numerical work is based on a previous experimental investigation on the fibre blends using RTSF [8], and it is found that the mechanical properties of blended mixes using RTSF vary depending on dosages, but are comparable with (or even better than) those of MSF-only mixes at the same fibre dosage.

The following section 4.2 summarises the characteristics of the tensile constitutive models for SFRC, as proposed by RILEM and Model Code 2010. Section 4.3 briefly reports the mechanical properties of the examined 10 SFRC mixes. Section 4.4 describes details of the FE modelling adopted, and uses the two constitutive models to predict the load-deflection characteristics, which are compared against the experimental results. The tensile $\sigma - \varepsilon$ relations for the examined SFRC mixes are then determined using inverse FE analysis, and a simplified trilinear $\sigma - \varepsilon$ relation for SFRC using RTSF (at low fibre dosage) is proposed. Key research findings are summarised in section 4.5.

4.2 Stress-strain models proposed by RILEM TC 162-TDF and Model code 2010

4.2.1 Concepts of flexural tensile strength ($f_{ctm,fl}$) and residual flexural tensile strength (f_R)

EN 14651:2005 [28] follows a testing methodology first adopted by RILEM [16], to characterise the flexural tensile behaviour of SFRC prisms. It uses the average load-CMOD (or –deflection) curve from 3-point notched prism tests (Figure 4-2) to extract several fracture parameters of SFRC mixes.

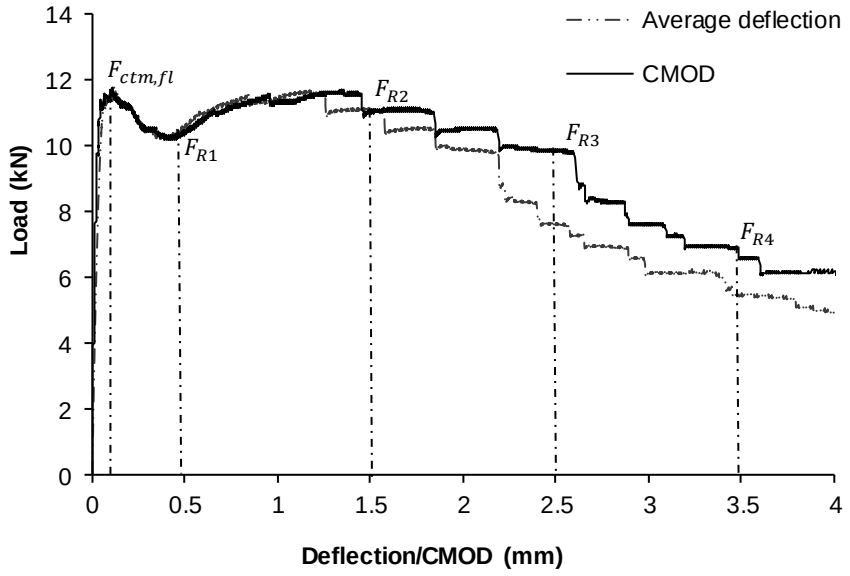

Figure 4-2: Definition of $f_{ctm,fl}$ and f_R values according to EN 14651:2005 [28]

The flexural tensile strength $f_{ctm,fl}$ is determined as the flexural stress corresponding to the maximum load $F_{ctm,fl}$ up to a CMOD of 0.05 mm. To characterise the post-cracking behaviour of SFRC, four residual flexural tensile strength parameters (f_{R1}, f_{R2}, f_{R3} and f_{R4}) are obtained from the post-cracking part of the curve at 0.5, 1.5, 2.5 and 3.5 mm of CMOD, respectively. The $f_{ctm,fl}$ and f_R values are calculated using the expressions below [28],

$$f_{ctm,fl} = \frac{3F_{ctm,fl}l}{2bh_{sp}^2}, f_{Ri} = \frac{3F_{Ri}l}{2bh_{sp}^2} \quad (4\text{-}1)$$

Where $F_{ctm,fl}$ (N) is the load corresponding to $f_{ctm,fl}$, and F_{Ri} (N) is the load at CMODs of 0.5, 1.5, 2.5 and 3.5 mm ($i = 1,2,3,4$), respectively. b is the width of the specimen, l is the span length and h_{sp} is the effective depth of the notched section.

4.2.2 The $\sigma - \varepsilon$ relationship proposed by RILEM TC 162-TDF

Figure 4-3 represents the trilinear $\sigma - \varepsilon$ relationship of SFRC in tension proposed by RILEM TC 162-TDF [16]. The key points in the diagram are defined by the expressions given below [16]:

$$\sigma_1 = 0.7f_{ctm,fl}(1.6 - d), \varepsilon_1 = \frac{\sigma_1}{E_c},$$

$$\sigma_2 = 0.45f_{R1}k_h, \varepsilon_2 = \varepsilon_1 + 0.1‰, \quad (4\text{-}2)$$

$$\sigma_3 = 0.37f_{R4}k_h, \varepsilon_3 = 25‰$$

Where d (in m) is the effective specimen depth, E_c (in MPa) is the average modulus of elasticity of SFRC and k_h is a size factor to accommodate the size effect of various SFRC structural elements. For the notched prisms, k_h=1 is suggested.

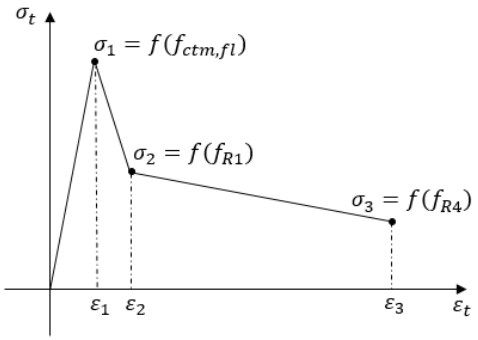

Figure 4-3: Trilinear $\sigma - \varepsilon$ diagram for SFRC, according to RILEM TC 162-TDF [16]

4.2.3 The $\sigma - \varepsilon$ relationship proposed by Model Code 2010.

Model Code 2010 provides both the $\sigma - w$ and $\sigma - \varepsilon$ relationship, and the latter being derived by adopting a suitable structural characteristic length l_{cs}. Since strain is used for design purposes, in this study, the models are compared using the $\sigma - \varepsilon$ relationship.

Model Code 2010 allows for both softening and hardening $\sigma - \varepsilon$ behaviour. For softening behaviour (see Figure 4-4 (a)), the same $\sigma - \varepsilon$ relationship proposed for plain concrete in uniaxial tension is used up to an intersection (σ_c) with the post-cracking tensile response of SFRC. For hardening behaviour (Figure 4-4 (b) and (c)), the $\sigma - \varepsilon$ relationship is defined using four branches, with an enhanced tensile strength of SFRC. The key points on the $\sigma - \varepsilon$ relationships can be determined by the following equations [17]:

$$\sigma_A = 0.9f_t, \varepsilon_A = \frac{\sigma_A}{E_c}, \sigma_B = f_t, \varepsilon_B = 0.00015,$$

$$\sigma_D = \sigma_{SLS} = 0.45f_{R1}, \varepsilon_{SLS} = \frac{CMOD_1}{l_{cs}}, \sigma_{A'} = 0.9\sigma_{SLS}, \varepsilon_{A'} = \frac{\sigma_{A'}}{E_c}, \quad (4\text{-}3)$$

$$\sigma_E = \sigma_{ULS} = \sigma_{SLS} - \frac{W_u}{CMOD_3}\ (\sigma_{SLS} - 0.5f_{R3} + 0.2f_{R1}),$$

$$\varepsilon_{ULS} = \frac{W_u}{l_{cs}} = \min(\varepsilon_{Fu}, \frac{2.5}{l_{cs}}), l_{cs} = \min(s_{rm}, y)\,, CMOD_1 = 0.5\ mm,$$

where f_t is the tensile strength of plain concrete, s_{rm} is the mean distance between cracks, $y = d$ is assumed for sections without traditional reinforcement under bending, $w_u \leq 2.5\ mm$ is the maximum crack opening accepted in structural design and for variable strain distribution along the cross-section $\varepsilon_{Fu} = 0.02$.

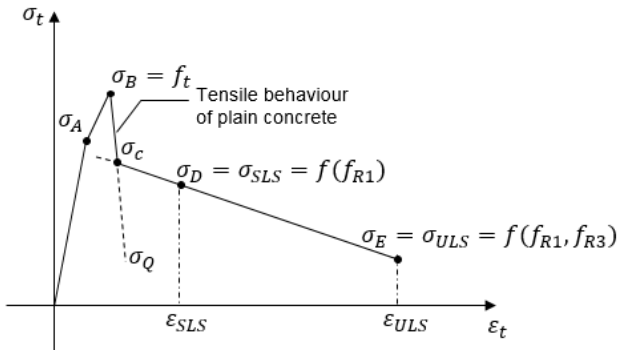

(a)

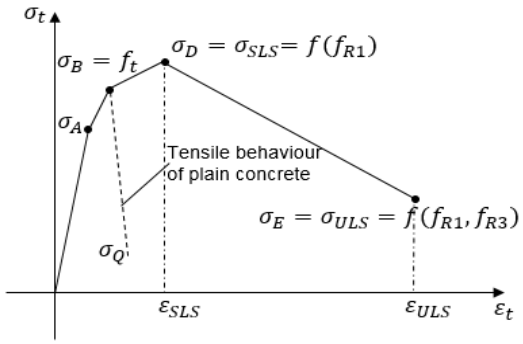

(b)

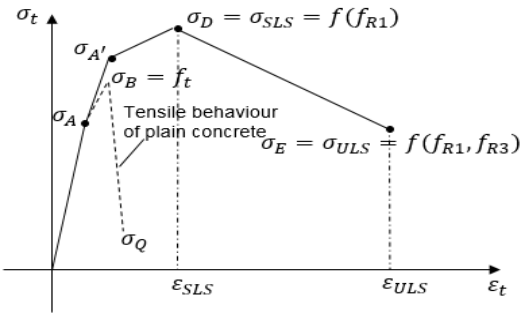

(c)

Figure 4-4: Tensile $\sigma - \varepsilon$ relations adopted by Model Code 2010 [17] for: (a) softening behaviour, (b) & (c) hardening behaviour

4.3 Experimental Programme

4.3.1 Materials and compositions

10 SFRC mixes at total fibre dosages of 30 kg/m^3 (volume fraction $V_f = 0.38\%$), 35 kg/m^3 ($V_f = 0.45\%$) and 45 kg/m^3 ($V_f = 0.57\%$) were examined. In these mixes, two types of undulated MSF (Figure 4-5 (a) and (b)) were used on their own, or blended with cleaned, classified and sorted RTSF (Figure 4-1). RTSF had a nominal diameter of 0.22 mm and a nominal tensile strength of around 2500 MPa [29]. Using a specially developed optical system [29], a length distribution analysis (Figure 4-5 (c)) shows that roughly 68% by mass of the RTSF had lengths in the range of 15-40 mm. For the two types of MSF used, MSF1 (diameter: 1.0 mm, length: 60 mm) has high tensile strength (nominal tensile strength of 1450 MPa), whilst MSF2 (diameter: 0.8 mm, length: 55 mm) has nominal strength of 1050 MPa. The concrete mix design comprised: 150 kg/m^3 of cement, 1097 kg/m^3 of coarse aggregates (4-20 mm), 804 kg/m^3 of fine aggregates (0-4 mm), 150 kg/m^3 of GGBS and 2.25 L/m^3 of plasticiser. The water cement ratio (w/c) was 0.55. More details of this experimental work can be found elsewhere [8].

Due to the large volume of concrete needed, the ready-mix concrete was cast in 5 separate batches. 6 plain concrete cubes and 6 prisms were manufactured for each batch. For each SFRC mix, either 6 or 12 prisms and 6 cubes were cast. Table 4-1 shows the details of the examined SFRC mixes, as well as the results of the compressive cube tests and flexural prism tests. Each mix is given a code based on the fibre type and dosage used. For example, 2M20R10 refers to a blended mix with 20 kg/m^3 of MSF2 and 10 kg/m^3 of RTSF.

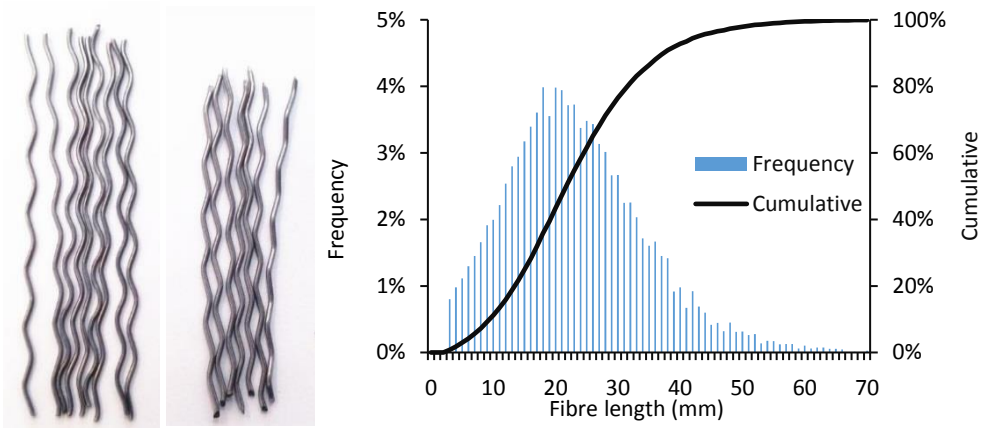

(a) (b) (c)

Figure 4-5: (a) MSF1, (b) MSF2 and (c) RTSF length distribution [8]

4.3.2 Compressive cube strength

The compressive strength f_{cu} of the examined SFRC mixes ranged from 41.8 MPa to 50.3 MPa, whilst the strength of the correspondent plain concrete was between 37.6 and 47.5 MPa. The variability found is considered typical for ready mixed concrete. Overall, the compressive strength of concrete was not affected dramatically either positively or negatively by the addition of steel fibres.

4.3.3 Results of SFRC prism tests

The flexural tests on prisms (150 mm x 150 mm x 550 mm) were performed according to EN 14651:2005 [28]. A notch at mid-span of each specimen was sawn one day before testing, and a clip gauge was used to measure the CMOD values. A yoke with two Linear Variable Differential Transformers (LVDTs) was used to measure central deflections. The average flexural modulus of elasticity (E_{fm}) for each SFRC mix was determined by utilising the results up to 40% of the peak load of the load-deflection curves. Table 4-1 reports the mean values of f_{cu}, E_{fm}, $f_{ctm,fl}$, and f_R for the examined SFRC mixes. The averaged (displacement based) load-deflection curves for the examined SFRC mixes are shown and discussed in section 4.4.2.

Table 4-1: Experimental results of the examined SFRC mixes

Total fibre dosage (kg/m³)	Mix code	Avg. f_{cu} (MPa) SFRC/Plain	E_{fm} (MPa)	$f_{ctm,fl}$ (MPa)	f_{R1} (MPa)	f_{R2} (MPa)	f_{R3} (MPa)	f_{R4} (MPa)
30	2M30	43.9/42.0	30500	3.8	3.6	3.4	2.9	2.4
	2M20R10	42.6/46.1	31500	3.8	3.7	3.6	3.1	2.5
	2M15R15	44.3/47.5	31200	3.3	3.4	3.2	2.8	2.3
	2M10R20	44.6/47.5	31600	3.3	3.1	2.7	2.4	2.1
	R30	41.8/37.6	29200	3.5	3.2	2.7	2.2	1.8
35	1M35	42.9/42.0	30100	3.7	3.8	4.0	3.7	3.3
45	1M45	41.9/42.0	29400	3.4	4.2	4.4	4.1	3.8
	1M35R10	42.8/46.1	29700	3.6	4.2	4.5	4.2	3.9
	1M22.5R22.5	50.3/47.5	34600	4.2	4.8	4.7	4.1	3.4
	1M10R35	44.5/39.9	32000	4.1	4.6	4.3	3.6	2.9

Although four residual flexural tensile strength parameters ($f_{R1}, f_{R2}, f_{R3}, f_{R4}$) are determined according to EN 14651: 2005, strong correlations (Figure 4-6) between f_{R1} and f_{R2}, f_{R3} and f_{R4} values for the tested SFRC prisms, were found [8]. This can lead to simpler design calculation.

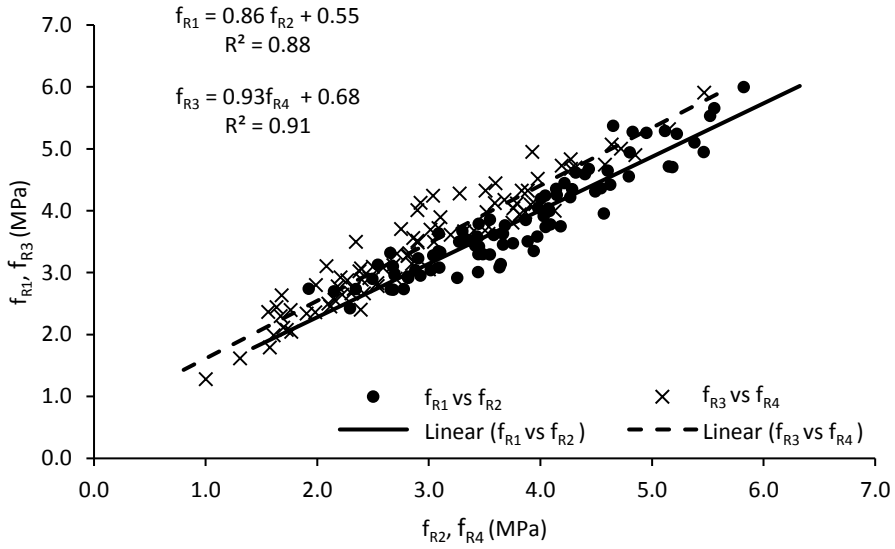

Figure 4-6: Relations between f_{R1} and f_{R2}, and between f_{R3} and f_{R4} [8]

4.4 Numerical research

4.4.1 FE Modelling

In this study, the FEA package, ABAQUS, was used to perform nonlinear analysis, as it allows the user to define a custom $\sigma - \varepsilon$ behaviour for concrete in tension [2]. A two-dimensional plane stress solid element (CPS4) with four nodes having two degrees of freedom, was chosen. A standard mesh sensitivity analysis (Appendix C) was carried out considering the influence of element size on the peak load and post-cracking behaviour of SFRC prisms. Figure 4-7 shows the variable finite element mesh adopted in the study, although the mesh may still be optimised to further increase computational efficiency.

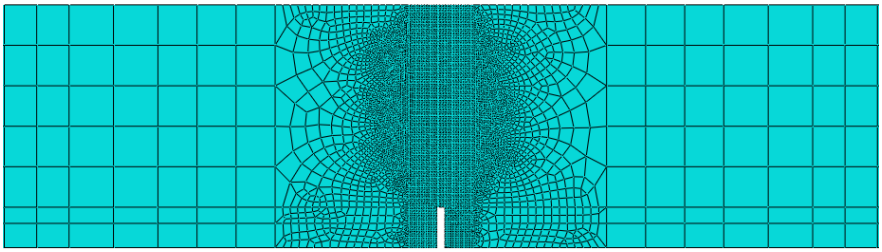

Figure 4-7: Mesh adopted for the finite element model

Three material models, Concrete Smeared Cracking (CSC), Brittle Cracking (BC) and Concrete Damaged Plasticity (CDP) are available in ABAQUS. Although Mobasher [30] suggests that all those three material models can be used for members dominated by tensile cracking, serious convergence issues were reported by several researchers [31,32] when SFRC prisms were modelled using the CSC model. Furthermore, the CDP model was preferred to the BC model, because the latter is only available for explicit dynamic or quasi-dynamic problems. Hence, the CDP model, which has been successfully applied in various numerical studies for SFRC [30–34], was adopted in this study.

4.4.1.1 Uniaxial compressive and tensile behaviour

In the CDP model, it is assumed that the main failure mechanisms of concrete are compressive crushing and tensile cracking, which relate to different degradation of the elastic stiffness in compression and tension, respectively. Under cyclic loading, a single degradation variable (d_c)

is used for the isotropic (scalar) stiffness reduction in compression whilst d_t is applied for tension. In addition, two equivalent plastic strains, $\tilde{\varepsilon}_c^{pl}$ and $\tilde{\varepsilon}_t^{pl}$, are adopted in the CDP model to characterise the compressive and tensile behaviour of cracked concrete, respectively. Figure 4-8 [35] shows the stress-strain relationship under (monotonic and cyclic) uniaxial compressive and tensile loading.

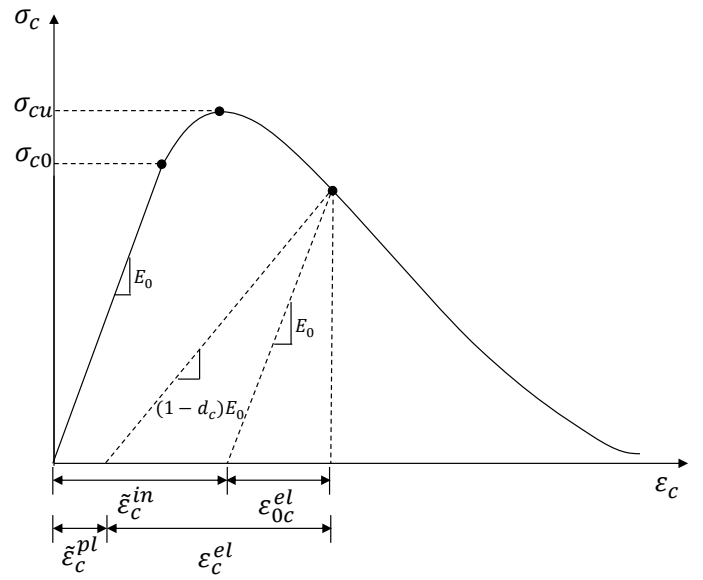

(a)

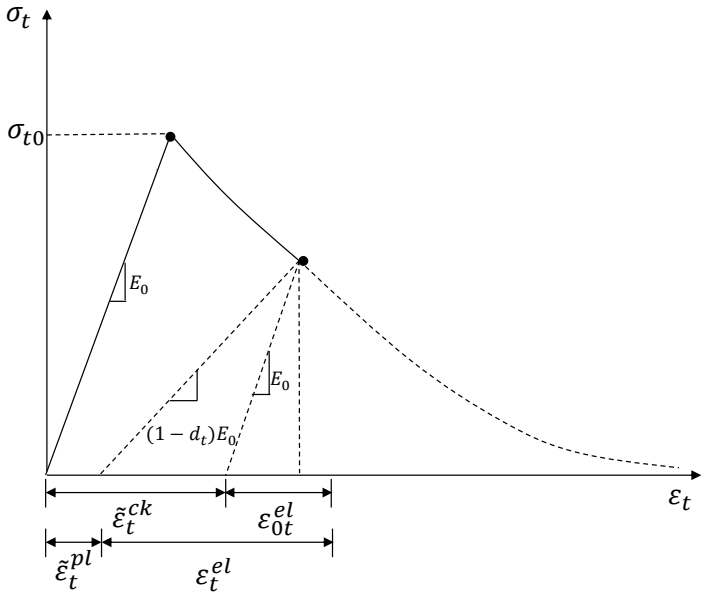

(b)

Figure 4-8: Uniaxial behaviour of concrete adopted in CDP model: (a) in compression, (b) in tension [35]

As reported in several studies [2,30,33], for SFRC prisms (with steel fibres up to dosages of 140 kg/m^3) under flexural loading, the compressive strain remains in the linear elastic region and the dominant failure mode is the tensile cracking of concrete. In this study, a perfectly plastic behaviour is considered after the peak stress, as shown in Figure 4-9. Where f_{cc} (in MPa) represents the SFRC mean compressive cylinder strength and $E_{cm} = E_{fm}$ (see Table 4-1) is assumed.

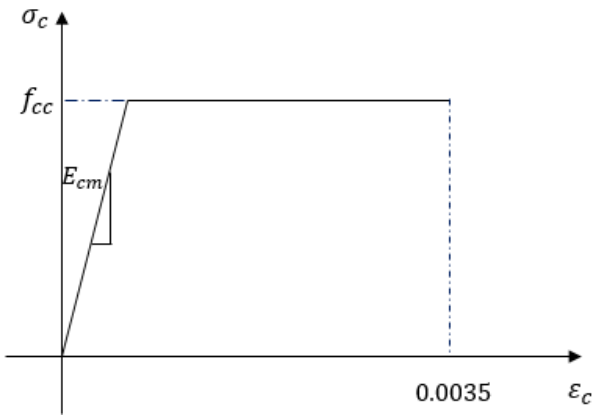

Figure 4-9: Compressive stress-strain relationship for concrete employed in this study

4.4.1.2 Yield condition and flow rule

The CDP model adopts a yield condition that was first developed by Lubliner et al. [36] and then modified by Lee and Fenves [37]. The ratio of biaxial to uniaxial compressive strength ($\frac{\sigma_{b0}}{\sigma_{c0}}$) and the ratio of the second stress invariant on the tensile meridian to that on the compressive meridian (K_c), are adopted in the CDP model to characterise the failure surface of concrete. For plain concrete, $\frac{\sigma_{b0}}{\sigma_{c0}}$ and K_c are usually assumed to be 1.15 and 2/3 respectively. In accordance with previous work [5,30,31,34] on numerical modelling of SFRC, the K_c value suggested for plain concrete was also adopted in this study for SFRC. However, the ratio $\frac{\sigma_{b0}}{\sigma_{c0}}$ slightly increases for SFRC reinforced with low dosages of steel fibres (0.5% by volume) [38] and as a result, a ratio of 1.2 was chosen in this study. Drucker-Prager hyperbolic function is used in the CDP model for the determination of the flow potential [35]. The dilation angle ψ and flow potential eccentricity ϵ are parameters used to define the flow rule. A dilation angle ψ =31° was adopted in this study

as suggested in literature [33] for SFRC reinforced with RTSF or MSF at a low total fibre dosage. An insignificant influence of steel fibres on this parameter was reported in the literature [39]. The eccentricity, ϵ=0.1, proposed by some researchers [30,31,33,34] for SFRC, was also adopted in this research. A small value of 0.00025 for the viscosity parameter was chosen since a small value was reported to provide better convergence for cracked concrete [34]. As the addition of steel fibres was found not to affect significantly the Poisson's ratio ν for compressive strengths lower than 85 MPa [38], a value of 0.2 was used in this study. Table 4-2 summarises the values of the parameters adopted in the FE modelling for SFRC [32].

Table 4-2: Parameters adopted in the FE modelling

Dilation angle ψ (°)	Eccentricity ϵ	$\frac{\sigma_{b0}}{\sigma_{c0}}$	K_c	Viscosity parameter	Poisson's ratio ν
31	0.1	1.2	0.667	0.0002	0.2

4.4.2 Evaluation of the $\sigma - \varepsilon$ relations proposed by RILEM TC 162-TDF and MODEL CODE 2010

By using the FE model described above in conjunction with the tensile $\sigma - \varepsilon$ relations proposed by RILEM and Model Code 2010 (see Figure 4-10), the respective load-deflection curves were derived for each of the tested SFRC mixes. The load-deflection curves derived using $\sigma - \varepsilon$ relations obtained by inverse analysis are also shown in the figure, as discussed later.

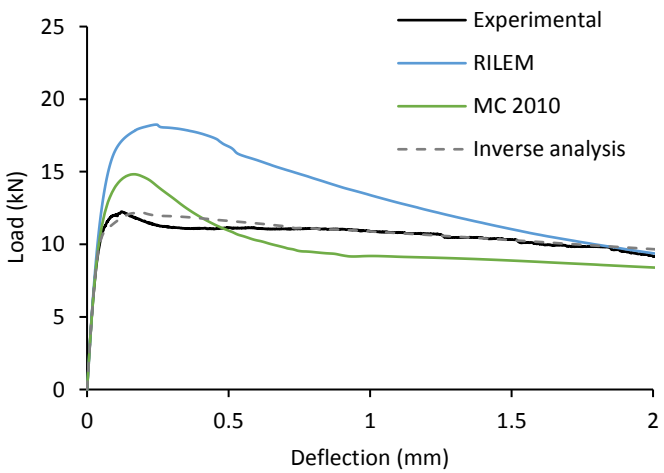

(a) Mix 2M30

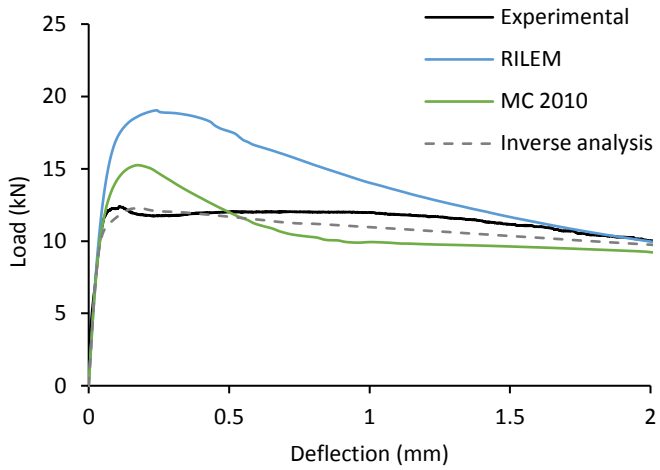

(b) Mix 2M20R10

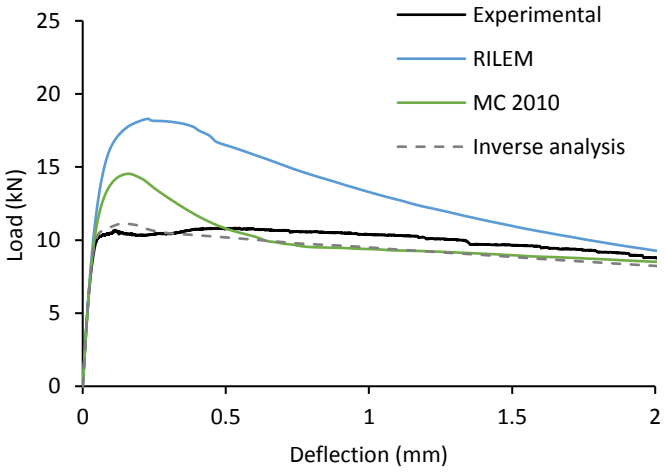

(c) Mix 2M15R15

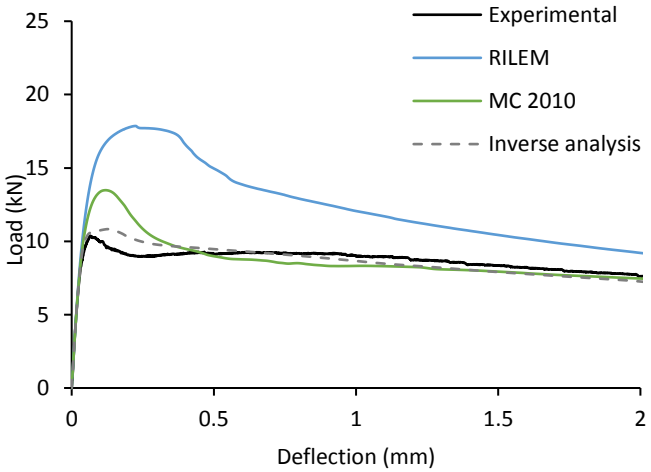

(d) Mix 2M10R20

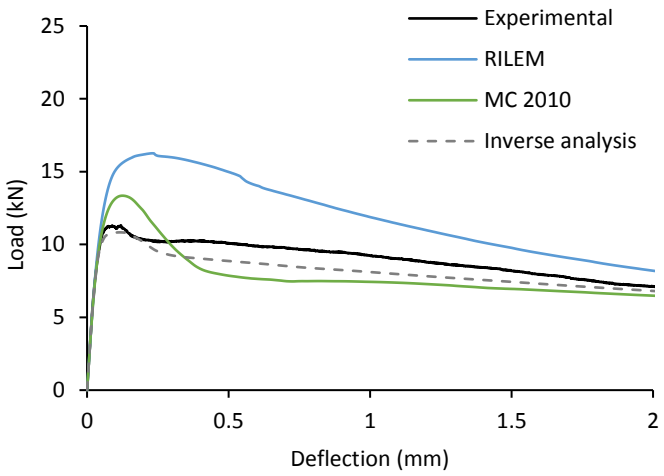

(e) Mix R30

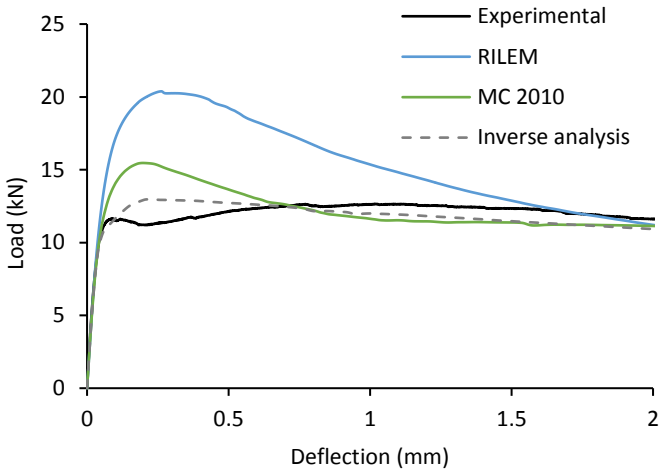

(f) Mix 1M35

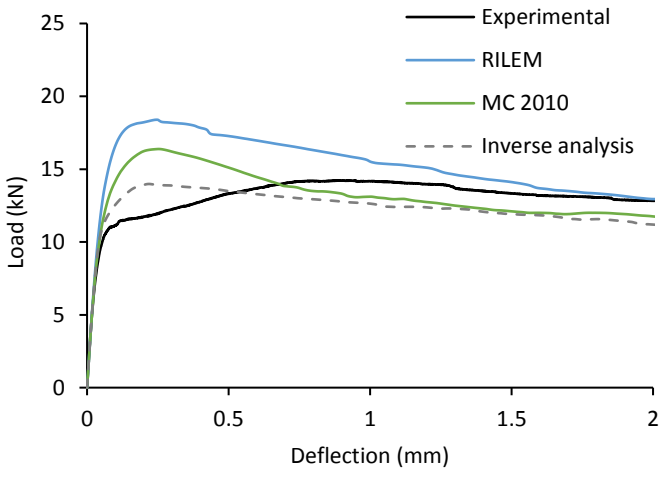

(g) Mix 1M45

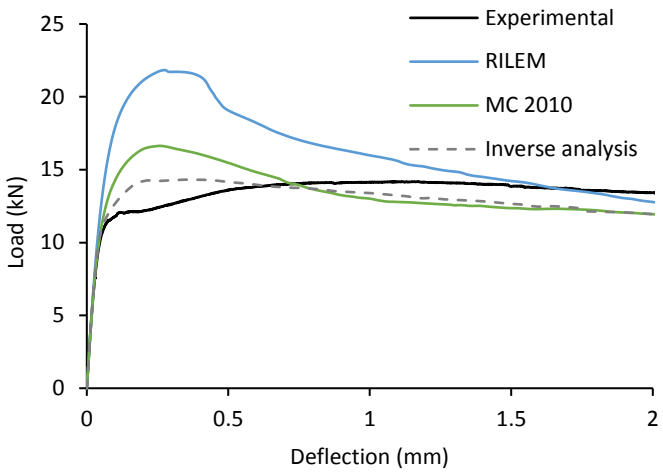

(h) Mix 1M35R10

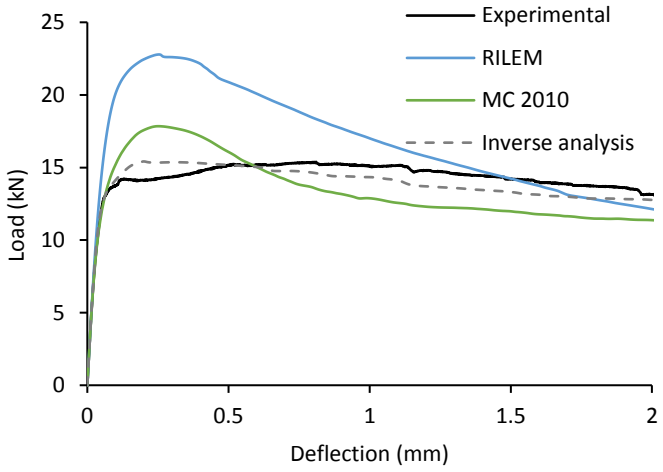

(i) Mix 1M22.5R22.5

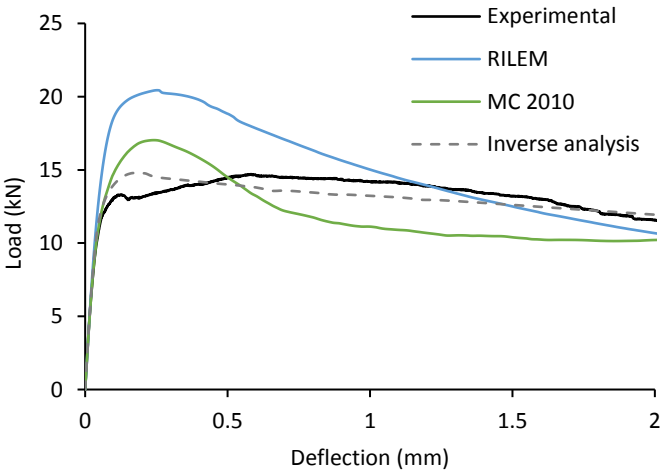

(j) Mix 1M10R35

Figure 4-10: Comparisons between experimental and predicted load-deflection curves for the examined SFRC mixes

In Figure 4-10, the load-deflection curves are shown up to a deflection of 2.0 mm, which is the value that corresponds to the ultimate limit strains (0.02 and 0.025) [2] proposed in the two design models. Table 4-3 shows the relative errors in the FE predictions for peak load and energy absorption (up to 2 mm).

Table 4-3: Errors in predicting peak load and energy absorption

Total dosage kg/m³	SFRC mix code	Error in peak load			Error in energy absorption		
		RILEM	MC 2010	Inverse analysis	RILEM	MC 2010	Inverse analysis
30	2M30	49%	21%	-1%	22%	-5%	2%
	2M20R10	53%	23%	-1%	19%	-5%	-2%
	2M15R15	69%	34%	3%	28%	0%	-5%
	2M10R20	72%	30%	4%	39%	1%	-1%
	R30	44%	18%	-4%	29%	-10%	-5%
35 or 45	1M35	61%	21%	2%	21%	1%	-3%
	1M45	29%	15%	-2%	13%	0%	-5%
	1M35R10	54%	17%	1%	15%	-2%	-4%
	1M22.5R22.5	48%	16%	0%	14%	-7%	-2%
	1M10R35	39%	16%	1%	11%	-9%	1%
Average error		52%	21%	0%	21%	-4%	-1%

It is clear that the two design models cannot capture well the flexural behaviour of SFRC. The RILEM model shows significant overestimations (up to 72%) of the peak flexural load and similar observations were reported in literature [2,3,12,32]. The overestimation of the flexural load continues up to deflections of about 1.5-2.0 mm, leading to significant overestimations of the energy absorption capacity up to 39% for 30 kg/m³ mixes, and up to 21% for mixes at 45 kg/m³. As the values of $\sigma_1 = 0.7 f_{ctm,fl}(1.6 - d)$ and $\sigma_2 = 0.45 f_{R1} k_h$ (see Figure 4-3) strongly influence the peak load of the predicted load-deflection curves, it is clear that the use of smaller values for the two parameters may lead to more accurate predictions of the peak load.

The Model Code approach provides a rather accurate prediction of the energy absorption capacity but does overestimate the peak flexural load up to 34%. For softening or slight hardening behaviour, Model Code 2010 assumes the tensile strength of SFRC (see Figure 4-4 (a) and (b)) to be the same as for plain concrete and, if that is correct, then the overestimation in peak load by the Model Code method is primarily due to the inaccurate estimation of $\sigma_D = \sigma_{SLS} = 0.45 f_{R1}$.

As errors in both models significantly reduce at displacements of 1.5-2.0 mm, it means that a residual flexural tensile strength (i.e. f_R) approach can still be used to predict the overall

behaviour of SFRC after cracking. Despite their inaccuracies, the RILEM relations are more convenient for practical purposes, since less key points are required to determine the $\sigma - \varepsilon$ curve. In particular, the determination of the intersection point in the Model Code relations is not straightforward, as the trilinear relationship for the behaviour of plain concrete and the relation for the post-cracking behaviour of each SFRC mix need to be determined separately.

It is clear that there is a need for a simplified $\sigma - \varepsilon$ model, which can provide more accurate predictions of the flexural behaviour of SFRC.

4.4.3 Inverse FE analysis

Inverse analysis, or back calculation, is a useful tool extensively used to determine best-fitting tensile stress-strain (or stress-crack) relations for SFRC from flexural tests [2,12,24,33,40–45]. According to Kooiman et al. [43], the inverse modelling procedure can be divided into four levels. The first level is the input level. On this level, assumptions of the uniaxial tensile and compressive behaviour of SFRC needs to be made, and usually, the shape of the uniaxial tensile stress-strain relation and the key strain values need to be determined. The second level is the numerical level where the FE analysis is performed under the consideration of the geometry of the tested specimen, boundary conditions and other material characteristics (e.g., Poisson's ratio). The third level is the level where the accuracy of the predicted load-deflection curve is checked. Compared to the experimental results, the relative errors in the FE predictions need to be calculated based on the given criteria (e.g. peak load) on this level. The fourth level is the output level. The uniaxial tensile stress-strain model for SFRC can be determined and further used in structural analysis while the given criteria are met. This inverse modelling procedure is adopted in this study.

Similar to the trilinear stress-strain relationship shown in Figure 4-3 (adopted by RILEM), Kooiman et al. [43], Barros et al. [12] and Neocleous et al. [3] have also suggested that the flexural behaviour of SFRC prisms with up to 140 kg/m^3 of MSF can be simulated well using a trilinear relation. A modified trilinear stress-strain ($\sigma' - \varepsilon'$) relation is proposed in this study for blended SFRC at low total fibre dosages. Three key points, ($\varepsilon_1', \sigma_1'$), ($\varepsilon_2', \sigma_2'$) and ($\varepsilon_3', \sigma_3'$) are used to determine the $\sigma' - \varepsilon'$ relationship. The strain values, $\varepsilon_1' = \frac{\sigma_1'}{E_c}$, $\varepsilon_2' = \varepsilon_1' + 0.002$ and $\varepsilon_3' = 0.025$, also used by Tlemat et al. [2], are adopted in this study. ε_1' defines the elastic portion of the load-deflection curve and the tensile contribution of the concrete. ε_2' is associated with the peak load and the behaviour of SFRC with only microcracks (SLS) [3], whilst ε_3' is used to define

the tail of the curve and represent the behaviour of SFRC at large cracks (ULS). Corresponding σ_i' (σ_1', σ_2' and σ_3') values for each mix are determined during the inverse analysis until small absolute error values ($\leq$ 5%) are achieved for the peak load and energy absorption up to 2 mm.

The results of the inverse analysis for all SFRC mixes is shown in Table 4-3. The small errors confirm that the trilinear $\sigma - \varepsilon$ relation is capable of providing accurate simulations of the flexural behaviour of SFRC, in particular blended SFRC using RTSF at a low total fibre dosage. Table 4-4 presents the σ_i' values defining the trilinear $\sigma - \varepsilon$ relations obtained from inverse analysis, and the graphical representation of the relations is shown in Figure 4-11. The single-type-fibre reinforced mixes are shown in solid lines in the figure, whilst the blended mixes are indicated in dashed lines.

Table 4-4: σ_i' values defining the trilinear $\sigma - \varepsilon$ relation, obtained from inverse analysis

Total fibre dosage (kg/m³)	SFRC mix code	Stress values (MPa)		
		σ_1'	σ_2'	σ_3'
30	2M30	1.95	0.95	0.90
	2M20R10	1.90	0.95	0.90
	2M15R15	1.90	0.90	0.60
	2M10R20	1.90	0.80	0.55
	R30	1.90	0.90	0.50
35 or 45	1M35	1.95	0.95	1.10
	1M45	2.06	1.15	1.20
	1M35R10	2.06	1.15	1.30
	1M22.5R22.5	2.22	1.35	1.35
	1M10R35	2.22	1.35	1.20

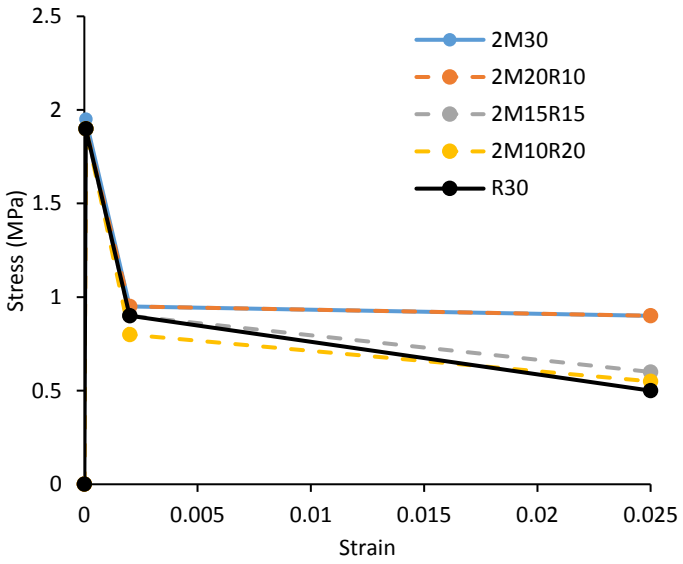

(a)

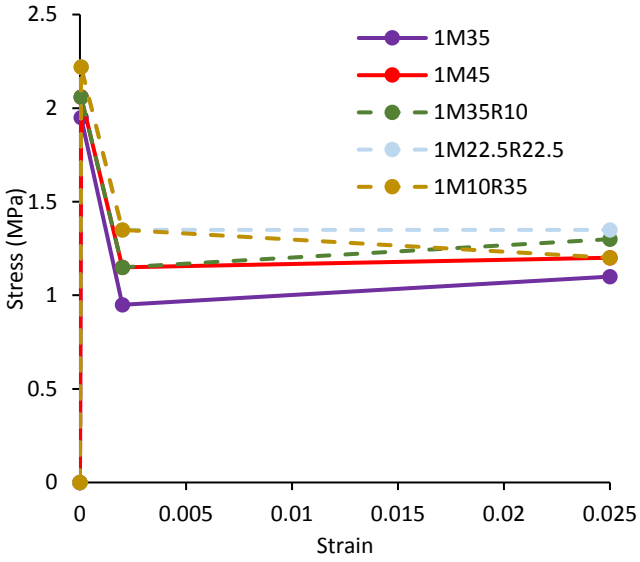

(b)

Figure 4-11: $\sigma - \varepsilon$ diagrams for the examined SFRC mixes at (a) 30 kg/m³ and (b) 45 kg/m³

To investigate the correlations between the actual tensile properties (σ_i' values) of SFRC and the nominal tensile properties ($f_{ctm,fl}$ and f_{Ri} values) derived from prism tests, several ratios, $\sigma_1'/f_{ctm,fl}$, σ_2'/f_{R1}, σ_2'/f_{R2}, σ_3'/f_{R3} and σ_3'/f_{R4}, were computed by dividing the σ_i' values by the corresponding fracture parameters f_j. Figure 4-12 shows the effect of the RTSF dosage on those ratios. It was found that σ_i' values overall correlate well with their corresponding $f_{ctm,fl}$ or f_{Ri} values. Although there is some variability, the strength ratios (σ_i'/f_j) are not affected much by

the RTSF dosage contained in the mixes. As a result, a simplified trilinear $\sigma - \varepsilon$ relationship for SFRC (using blended MSF and RTSF) can be developed from flexural tests.

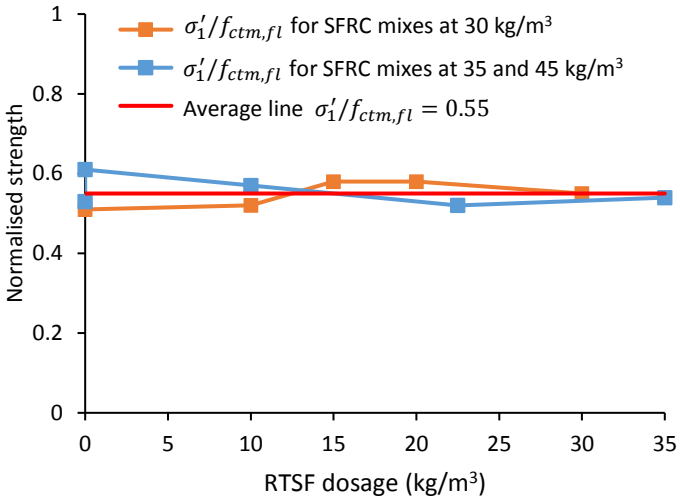

(a)

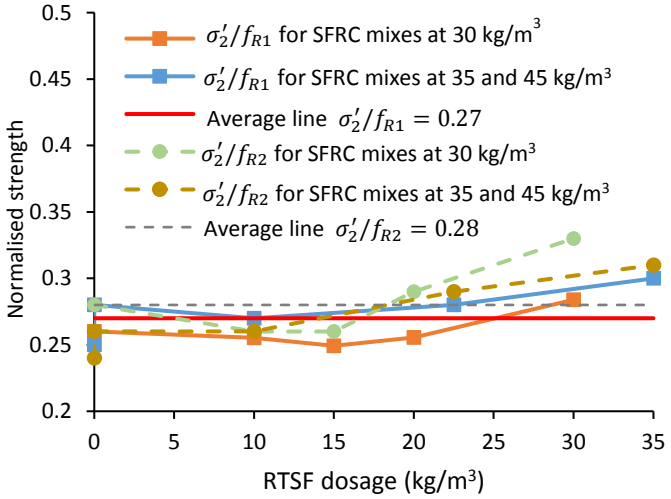

(b)

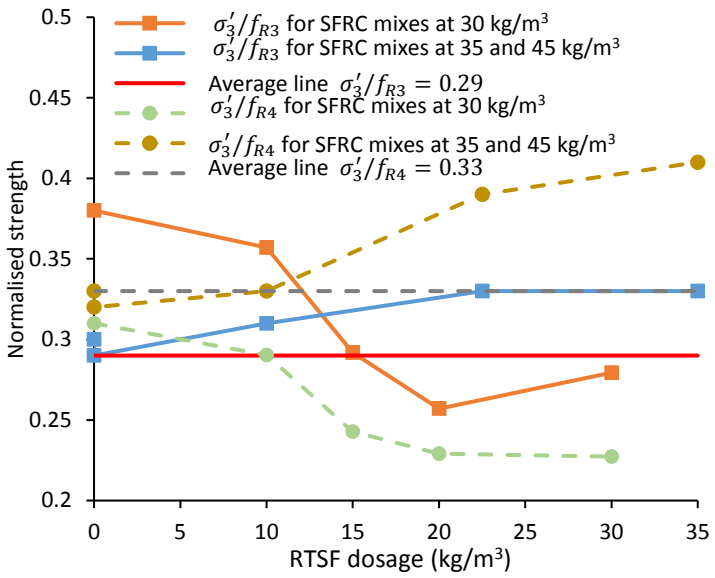

(c)

Figure 4-12: Relationship between RTSF dosage contained in each SFRC mix and different strength ratios

4.4.4 Proposed tensile stress-strain ($\sigma' - \varepsilon'$) relationship of SFRC

A simplified tri-linear $\sigma' - \varepsilon'$ relation is proposed for the tensile behaviour of SFRC (including blended SFRC), as given below:

$$\sigma_1' = 0.55 f_{ctm,fl}\ (COV = 6\%),\ \varepsilon_1' = \frac{\sigma_1'}{E_c};$$

$$\sigma_2' = 0.27 k_h\ f_{R1}\ (COV = 6\%),\ \varepsilon_2' = \varepsilon_1' + 0.002; \quad (4\text{-}4)$$

$$\sigma_3' = 0.29 k_h\ f_{R3}\ (COV = 13\%),\ \varepsilon_3' = \varepsilon_u' = 0.025;$$

Since this model was developed based on the EN 14651:2005 prisms with a standard geometry, the size effect was not addressed in this study, but size-dependent safety factors (e.g. k_h adopted in the RILEM approach) can be easily included.

4.4.4.1 Determined tensile strength, σ_1'

The determined tensile strength (σ_1') of SFRC with RTSF at a low total fibre dosage was around 55% of $f_{ctm,fl}$. Overall, the tensile strength of plain concrete (1.90 MPa, determined from inverse analysis) was only marginally increased by the fibre addition. A small strength

enhancement was seen for the 30 kg/m^3 mixes, whilst an enhancement of up to 17% was observed for the 45 kg/m^3 mixes. The two blended mixes 1M22.5R22.5 and 1M10R35 exhibited greater tensile strength (2.22 MPa) than mixes 1M35, 1M45 and 1M35R10 reinforced with higher dosages of MSF. This points to a synergetic performance of the two fibre types. The better distribution of short and thin RTSF can assist in arresting microcracks, whilst long and stiff MSF can be more effective in controlling larger cracks.

4.4.4.2 Post-cracking tensile strength, σ_2' and σ_3'

Post-cracking tensile strengths σ_2' and σ_3' were found to be about one third of the corresponding residual flexural tensile strength values (f_R). These values (0.27 for σ_2' and 0.29 for σ_3') are in good agreement with those suggested by Barros et al. [12], who proposed coefficients of 0.36 and 0.27 for SFRC using hooked ends MSF up to 45 kg/m^3 at a small (microcracking stage) and large (macrocracking stage) tensile strain, respectively. Mobasher et al. [41] also pointed out that a correction factor of 0.31 can be used to correlate the RILEM equivalent flexural tensile strength $f_{eq,3}$ and the tensile strength of cracked SFRC. In Model Code 2010, a coefficient of 1/3 is adopted in a simplified rigid-plastic model by scaling f_{R3} to the tensile strength of cracked SFRC at the ultimate limit state, f_{Ftu} (Figure 4-13). As seen in Figure 4-14 (a) (b) and (c), different stress distributions along the middle cross-section of the notched prisms are adopted in RILEM to determine three strength values, f_{Ri} (uncracked stage), σ_2 (microcracking stage) and σ_3 (macrocracking stage), respectively. Since f_R values are determined using linear elastic principles (Figure 4-14 (a)), it is clear that if used directly they will lead to a significant overestimation of the tensile strength of cracked SFRC which behaves in a nonlinear manner.

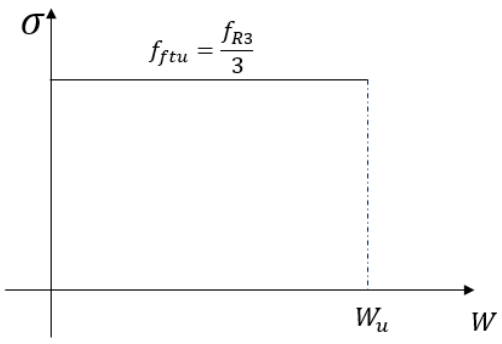

Figure 4-13: Simplified post-cracking stress-crack opening law adopted by Model Code 2010 [17]

As shown in Figure 4-6, f_{R1} and f_{R2}, as well as f_{R3} and f_{R4} of the tested SFRC prisms are strongly correlated. For the proposed $\sigma' - \varepsilon'$ relationship, it is confirmed that the use of f_{R1} and f_{R3} is sufficient to accurately represent the behaviour of SFRC at small and large cracks, respectively.

The post-cracking $\sigma - \varepsilon$ relations adopted in RILEM and Model code 2010 are based on the assumption that concrete remains linear in compression and perfectly plastic in tension with a predetermined neutral axis depth (Figure 4-14 (b) and (c)). Although these scalar values used in the two approaches could be used for design at specific limit states, they do not represent the true $\sigma - \varepsilon$ characteristics of SFRC, which are better captured by the proposed equations.

The larger COV value for σ_3' (see Equation 4-4) compared to the values for σ_1' and σ_2' (although all these COV values are generally small) indicates that at larger cracks the behaviour is more variable, as it is dominated by fibre distribution and orientation, as well as fibre pull out behaviour.

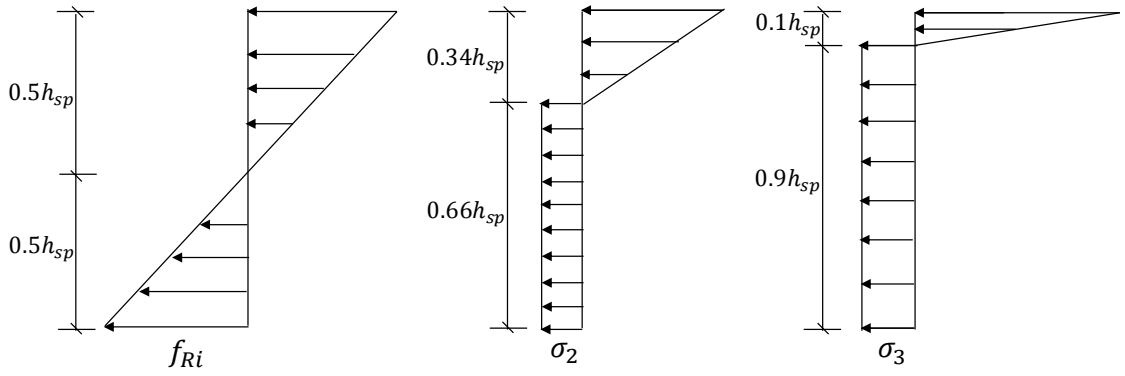

Figure 4-14: Stress distribution to determine: (a) f_{Ri}, (b) σ_2 and (c) σ_3 according to RILEM TC 162-TDF [16]

4.4.4.3 Ultimate limit strain ε_u'

Although the ultimate limit strain $\varepsilon_u' = \varepsilon_3' = 0.025$ (as also adopted in the RILEM model) corresponds only to a mid-span deflection of 2.0 mm and CMOD of about 2.5 mm, this strain value (0.025) is considered to be sufficient for structural design of SFRC at the ultimate limit state (ULS). Since ε_u' is about 10 times larger than ε_2' that corresponds to the peak load of the prisms, for a statically determinate element with a single hinge (crack), ε_u' will lead to a

curvature ductility of at least 5. The curvature ductility is determined by dividing the ultimate limit strain (ε_u') by the strain associated with the peak load (ε_2') while the neutral axis depth change is taken into account. This curvature ductility (equal or greater than 5) should be adequate for moment redistribution purposes, when plastic analysis is used.

4.5 Conclusions

Based on the test results of 10 SFRC mixes using MSF and RTSF at varying dosages, the accuracy of the uniaxial tensile $\sigma - \varepsilon$ relations proposed by RILEM and Model Code 2010 has been evaluated and a new uniaxial tensile $\sigma' - \varepsilon'$ relation for SFRC has been proposed. The main research findings are:

- The RILEM approach can lead to significant overestimation (up to 72%) of the peak flexural load and energy absorption capacity (up to 39%), whilst the Model Code 2010 can provide a rather accurate prediction of the energy absorption capacity and some overestimation (less than 35%) of the peak flexural load.

- The simplified trilinear stress-strain relationship ($\sigma' - \varepsilon'$) for SFRC proposed in this study can provide an accurate estimate of the peak load and energy absorption capacity of SFRC with RTSF at a low total fibre dosage.

- The tensile strength of SFRC with RTSF at a low total fibre dosage is only marginally improved by fibre addition, and the post-cracking tensile strengths at different strains can be determined directly from residual flexural tensile strengths (f_{Ri}) of prisms.

- However, it is noted that the proposed $\sigma' - \varepsilon'$ model is based on limited experimental data; further research on various aspects (e.g. fibre dosage and type) is still required to increase the range of validity of the proposed model.

References

[1] H. Tlemat, K. Pilakoutas, K. Neocleous, Stress-strain characteristic of SFRC using recycled fibres, Mater. Struct. 39 (2006) 365–377. doi:10.1617/s11527-005-9009-4.

[2] H. Tlemat, K. Pilakoutas, K. Neocleous, Modelling of SFRC using inverse finite element analysis, Mater. Struct. 39 (2006) 221–233. doi:10.1617/s11527-005-9010-y.

[3] K. Neocleous, H. Tlemat, K. Pilakoutas, Design issues for concrete reinforced with steel fibers, including fibers recovered from used tires, J. Mater. Civ. Eng. 18 (2006) 677–685. doi:10.1061/(ASCE)0899-1561(2006)18:5(677).

[4] A.G. Graeff, K. Pilakoutas, K. Neocleous, M.V.N.N. Peres, Fatigue resistance and cracking mechanism of concrete pavements reinforced with recycled steel fibres recovered from post-consumer tyres, Eng. Struct. 45 (2012) 385–395. doi:10.1016/j.engstruct.2012.06.030.

[5] N. Jafarifar, K. Pilakoutas, T. Bennett, Moisture transport and drying shrinkage properties of steel-fibre-reinforced-concrete, Constr. Build. Mater. 73 (2014) 41–50. doi:10.1016/j.conbuildmat.2014.09.039.

[6] K.H. Younis, K. Pilakoutas, Strength prediction model and methods for improving recycled aggregate concrete, Constr. Build. Mater. 49 (2013) 688–701. doi:10.1016/j.conbuildmat.2013.09.003.

[7] K.H. Younis, K. Pilakoutas, Assessment of post-restrained shrinkage mechanical properties of concrete, ACI Mater. J. 113 (2016) 267–276. doi:10.14359/51688699.

[8] H. Hu, P. Papastergiou, H. Angelakopoulos, M. Guadagnini, K. Pilakoutas, Mechanical properties of SFRC using blended manufactured and recycled tyre steel fibres, Constr. Build. Mater. 163 (2018) 376–389. doi:10.1016/j.conbuildmat.2017.12.116.

[9] H. Angelakopoulos, P Waldron, Tyre wire in Concrete Leading to Environmental sustainability. CIP Eco-innovation project, Twincletoes project - Layman's report, Twincon Ltd, Sheffield, UK, 2015.

[10] K. Neocleous, S.G. Maxineasa, L. Dumitrescu, K. Themistocleous, N. Taranu and D. Hadjimitsis, D1.6 Preliminary LCA. Anagennisi Project, Anagennisi: innovative use of all tyre components in concrete, 2014.

[11] R.F. Zollo, Fiber-reinforced concrete: an overview after 30 years of development, Cem. Concr. Compos. 19 (1997) 107–122. doi:10.1016/S0958-9465(96)00046-7.

[12] J. a. O. Barros, V.M.C.F. Cunha, A.F. Ribeiro, J.A.B. Antunes, Post-cracking behaviour of steel fibre reinforced concrete, Mater. Struct. 38 (2004) 47–56. doi:10.1617/14058.

[13] R.D. Neves, J.C.O. Fernandes de Almeida, Compressive behaviour of steel fibre reinforced concrete, Struct. Concr. 6 (2005) 1–8. doi:10.1680/stco.6.1.1.62458.

[14] E. Martinelli, A. Caggiano, H. Xargay, An experimental study on the post-cracking behaviour of Hybrid Industrial/Recycled Steel Fibre-Reinforced Concrete, Constr. Build. Mater. 94 (2015) 290–298. doi:10.1016/j.conbuildmat.2015.07.007.

[15] D. Bjegovic, A. Baricevic, S. Lakusic, D. Damjanovic, I. Duvnjak, Positive interaction of industrial and recycled steel fibres in fibre reinforced concrete, J. Civ. Eng. Manag. 19 (2013) S50–S60. doi:10.3846/13923730.2013.802710.

[16] Rilem Tc 162-Tdf, σ-ε-Design Method, Mater. Struct. 36 (2003) 560–567. doi:10.1007/BF02480834.

[17] F.I. du Béton, Fib Model Code for Concrete Structures 2010, Wilhelm Ernst & Sohn, Berlin, Germany, 2013.

[18] H. Tlemat, Steel fibres from waste tyres to concrete, testing, modelling and design, The University of Sheffield, Sheffield, UK, 2004.

[19] A.G. Graeff, Long-term performance of recycled steel fibre reinforced concrete for pavement applications, The University of Sheffield, UK, 2011.

[20] ACI 544.1R-96 (Reapproved 2002), State-of-the-art report on fiber reinforced concrete. American Concrete Institute, Michigan, US, 2002.

[21] A. Caratelli, A. Meda, Z. Rinaldi, Design according to MC2010 of a fibre-reinforced concrete tunnel in Monte Lirio, Panama, Struct. Concr. 13 (2012) 166–173. doi:10.1002/suco.201100034.

[22] M.A. Aiello, F. Leuzzi, G. Centonze, A. Maffezzoli, Use of steel fibres recovered from waste tyres as reinforcement in concrete: Pull-out behaviour, compressive and flexural strength, Waste Manag. 29 (2009) 1960–1970. doi:10.1016/j.wasman.2008.12.002.

[23] G. Centonze, M. Leone, M.A. Aiello, Steel fibers from waste tires as reinforcement in concrete: A mechanical characterization, Constr. Build. Mater. 36 (2012) 46–57. doi:10.1016/j.conbuildmat.2012.04.088.

[24] Z. Zamanzadeh, L. Lourenço, J. Barros, Recycled steel fibre reinforced concrete failing in bending and in shear, Constr. Build. Mater. 85 (2015) 195–207. doi:10.1016/j.conbuildmat.2015.03.070.

[25] H. Angelakopoulos, P. Papastergiou, K. Pilakoutas, Fibrous roller-compacted concrete with recycled materials - Feasibility study, Mag. Concr. Res. 67 (2015). doi:10.1680/macr.14.00246.

[26] G. Groli, A.P. Caldentey, A.G. Soto, Cracking performance of SCC reinforced with recycled fibres - an experimental study, Struct. Concr. 15 (2014) 136–153. doi:10.1002/suco.201300008.

[27] Anagennisi Project, Anagennisi: innovative use of all tyre components in concrete. http://anagennisi.org/wordpress/, 2014 (accessed 2017.07.20).

[28] BS EN 14651:2005, Test method for metallic fibre concrete - Measuring the flexural tensile strength (limit of proportionality (LOP), residual). British Standards Institution, London, UK, 2005.

[29] H. Angelakopoulos, Reused post-consumer tyre steel fibres in roller compacted concrete, The University of Sheffield, Sheffield, UK, 2016.

[30] B. Mobasher, Mechanics of fiber and textile reinforced cement, CRC Press, Florida, US, 2012.

[31] S. Oikonomou-mpegetis, Behaviour and design of steel fibre reinforced concrete slabs, Imperial College London, London, UK, 2012.

[32] W. Labib, An Experimental Study and Finite Element Analysis of Punching Shear Failure in Steel Fibre-Reinforced Concrete Ground-Suspended Floor Slabs, Liverpool John Moores University, Liverpool, UK, 2008.

[33] N. Jafarifar, K. Pilakoutas, H. Angelakopoulos, T. Bennett, Post-cracking tensile behaviour of steel-fibre-reinforced roller-compacted-concrete for FE modelling and design purposes, Mater. Construcción. 67 (2017) 122. doi:10.3989/mc.2017.06716.

[34] C. An, X. Castello, M. Duan, R.D. Toledo Filho, S.F. Estefen, Ultimate strength behaviour of sandwich pipes filled with steel fiber reinforced concrete, Ocean Eng. 55 (2012) 125–135. doi:10.1016/j.oceaneng.2012.07.033.

[35] Abaqus V. 6.14 Documentation, Dassault Systemes Simulia Corporation, 2014.

[36] J. Lubliner, J. Oliver, S. Oller, E. Oñate, A plastic-damage model for concrete, Int. J. Solids Struct. 25 (1989) 299–326. doi:10.1016/0020-7683(89)90050-4.

[37] J. Lee, G.L. Fenves, Plastic-Damage Model for Cyclic Loading of Concrete Structures, Eng Mech. 124 (1998) 892–900. doi:10.1061/(ASCE)0733-9399(1998)124:8(892).

[38] S. Swaddiwudhipong, P.E.C. Seow, Modelling of steel fiber-reinforced concrete under multi-axial loads, Cem. Concr. Res. 36 (2006) 1354–1361. doi:10.1016/j.cemconres.2006.03.008.

[39] X. Lu, C.-T.T. Hsu, Behavior of high strength concrete with and without steel fiber reinforcement in triaxial compression, Cem. Concr. Res. 36 (2006) 1679–1685. doi:10.1016/j.cemconres.2006.05.021.

[40] M. Bakhshi, C. Barsby, B. Mobasher, Comparative evaluation of early age toughness parameters in fiber reinforced concrete, Mater. Struct. Constr. 47 (2014) 853–872. doi:10.1617/s11527-013-0098-1.

[41] B. Mobasher, M. Bakhshi, C. Barsby, Backcalculation of residual tensile strength of regular and high performance fiber reinforced concrete from flexural tests, Constr. Build. Mater. 70 (2014) 243–253. doi:10.1016/j.conbuildmat.2014.07.037.

[42] C. Soranakom, B. Mobasher, Flexural design of fiber-reinforced concrete, ACI Mater. J. 106 (2009) 461–469.

[43] A.G. Kooiman, C. van der Veen, J.C. Walraven, Modelling the post-cracking behaviour of steel fibre reinforced concrete for structural design purposes, HERON, 45 (4) (2000), pp. 275-307

[44] G. Tiberti, F. Minelli, G. Plizzari, Reinforcement optimization of fiber reinforced concrete linings for conventional tunnels, Compos. Part B. 58 (2014) 199–207. doi:10.1016/j.compositesb.2013.10.012.

[45] ACI 544.8R-16, Report on indirect method to obtain stress-strain response of fiber-reinforced concrete (FRC). American Concrete Institute, Michigan, US, 2016.

Chapter 5 General Discussion, Conclusions & Recommendations for Future Work

This chapter presents a general discussion on the work presented in the previous chapters, followed by the main conclusions of this thesis and recommendations for future work.

5.1 General discussion

This section presents critical discussions on the experimental and numerical investigations presented in the previous chapters. Based on these discussions, recommendations for future work are summarised in Section 5.3.

5.1.1 Distribution and orientation of fibres in concrete

In Chapter 2 and 3, a high variability (up to 40% for prisms and 20% for round panels) of the fracture parameters (i.e. residual flexural tensile strength and energy absorption capacity) is found. This is most likely due to the inhomogeneous distribution and orientation of fibres that are affected by concrete mixing, flow of fresh concrete, vibration and wall effect caused by the formwork. Among these factors, the wall effect (in particular in small moulds) and the flow of fresh concrete are the most important ones. This to a certain extent was confirmed by the lower variability of the round panel tests. Nonetheless, the effort required in producing and testing the round panels is much more than for the prisms. Given the additional measurement of CMOD in the prism tests, it can be concluded that the prism tests are better suited to parametric examinations as conducted for this study.

5.1.2 RTSF supplied from different sources

RTSF can be obtained from different sources. Although the tensile strength of those RTSF is similar (from 2000-2600 MPa), they often exhibit different fibre length and aspect ratio distributions. This makes comparisons of the properties of SFRC using RTSF from different sources difficult, and it can be a barrier to the wider use of RTSF in concrete applications. It is strongly recommended that only classified RTSF are used in comparative studies and that the fibre length distribution is presented along with all studies utilising RTSF.

5.1.3 Failure mode of RTSF

As reported in Chapter 2, the failure mode of RTSF in flexural tests is considered to be a combination of fibre breakage and pull-out. However, further physical evidence of fibre breakage, in particular when using high aspect ratio RTSF in concrete, is still needed.

5.1.4 Effect of concrete type on the mechanical properties of SFRC

To allow direct comparisons of different SFRC mixes and to help to establish a robust experimental database, the same concrete mix design was used in this study. However, the mix design could still be optimised to maximise the contribution of recycled fibres, such as increasing

the critical fibre dosage in concrete and reducing air entrainment. The optimisation of the mix design can be made in several aspects, such as using different aggregate size, types and proportion, mixing sequences, as well as types and amount of cement replacement materials (e.g. GGBS) and superplasticiser.

Furthermore, as discussed in Chapter 2 and 3, the flexural performance of RTSF-only mixes is usually inferior to MSF-only mixes at the same fibre dosage. This can be explained by the fact that a large portion of RTSF lengths is smaller than the nominal size of typical coarse aggregates. Hence, the effect of the size of coarse aggregates on the properties of SFRC using RTSF needs to be further investigated.

5.1.5 Synergy in blended SFRC using RTSF

As reported in Chapter 2, positive synergy is derived from blended SFRC mixes containing 10 kg/m^3 of RTSF. This is normally attributed to the effectiveness of the different fibres at different cracks stages. However, an alternative cause for the positive synergy may be the better distribution of RTSF can lead to an improved fibre-matrix interfacial bond performance and thus increased pull-out resistance of MSF. However, additional scientific evidence is still required for these mechanisms.

Positive synergy is not observed for SFRC prisms using RTSC and RTSF (see Chapter 3). This may be due to the superior performance of the RTSC, but a rational scientific explanation is also needed.

Compared to the required slab thicknesses for blended SFRC using MSF and 10 kg/m^3 of RTSF (mixes B and H as shown in Figure 2-24), the recycled-fibre mixes using RTSC alone or blended with RTSF (shown in Figure 3-14) exhibit lower required slab thickness (5-12%) at the same total fibre dosage. The results again confirm that RTSF can be better blended with RTSC than MSF. The recycled-fibre mixes could enable concrete flooring applications with considerably less volume of concrete required, as well as significant environmental benefits (e.g. reduced energy input). Hence, to exploit the environmental benefits of recycled steel fibres, further investigations on the use of recycled fibres in more structural applications are required.

5.1.6 The uniaxial tensile stress-strain relations for blended SFRC

Using inverse analysis to determine $\sigma - \varepsilon$ equations for SFRC is sound (see Chapter 4), but the simplified model may not be suitable for higher dosages of blended steel fibres in concrete.

In addition, the proposed relations are derived from concrete prisms with standard depths of 150 mm. However, as reported in RILEM TC 162-TDF, the use of uniaxial $\sigma - \varepsilon$ relations (determined indirectly from flexural prism tests) could lead to severe overestimates of the carrying capacity of deep beams. This may be due to the size effect intrinsic to the model or inconsistent properties of SFRC from batch to batch, or a combination of both.

Compared to stress-crack width ($\sigma - w$) relations, stress strain ($\sigma - \varepsilon$) relations are better for design purposes, whilst there is a tendency to use both $\sigma - \varepsilon$ and $\sigma - w$ relations in recent standards (e.g. Italian Standard (CNR-DT-204), as the use of $\sigma - w$ relations can provide a better insight of the fracture behaviour of SFRC. However, a structural characteristic length has to be determined to convert $\sigma - \varepsilon$ to $\sigma - w$, and this adds extra uncertainty in the process.

5.2 Main conclusions

The main purpose of this research was to develop an in-depth understanding of the mechanical behaviour of blended SFRC using manufactured and recycled fibres from tyres at low total fibre dosages. Extensive experimental work on various blended concrete mixes using MSF and RTSF, as well as RTSF and RTSC has been conducted. Based on the experimental results, a simplified trilinear stress-strain relationship ($\sigma' - \varepsilon'$) for blended SFRC at low total fibre dosages is proposed. The main conclusions derived from each chapter are summarised below.

5.2.1 Mechanical properties of SFRC using blended MSF and RTSF (Ch. 2)

- MSF and RTSF hybrids do not significantly affect f_{cu} and E_{fm}.

- RTSF are more effective in controlling microcracks. As cracks open, the flexural behaviour of SFRC depends increasingly more on fibre-matrix interaction, fibre orientation and distribution.

- Owing to the nonhomogeneous fibre distribution of SFRC, the variability of the fracture parameters obtained from prism tests is up to 35%, and up to 20% for round panels. The MSF and RTSF hybridisation has little effect on the scatter of the fracture parameters.

- Strong correlations exist between f_{R1} and f_{R2}, f_{R3} and f_{R4} (for prisms), as well as E_5 and E_{10}, E_{20} and E_{40} (for round panels). Correlations in the flexural behaviour of the SFRC prisms and round panels are reported. Proposed equations could be used by engineers to convert fracture parameters from one test to the other, but a wide testing database is still required.

- Hybrid (MSF + RTSF) mixes containing 10 kg/m^3 of RTSF at total fibre dosages of 30 and 45 kg/m^3 offer significant synergetic effect. However, as the RTSF content increases, the performance drops below that of MSF-only mixes.
- It is noted that these research findings are based on limited experimental data, further research on various aspects (fibre dosage, fibre type and loading configuration, etc.) is still needed to increase the range of validity and expand the conclusions.

5.2.2 Mechanical properties of SFRC using blended RTSC and RTSF (Ch. 3)

- The tensile and pull-out properties of RTSC are similar to (or even better than) typical MSF.
- The critical embedment length of RTSC is found to be in the range of 25-40 mm, and thus the recommended length of RTSC ranges from 50 to 60 mm.
- Similar to MSF, recycled-fibre mixes (at low total dosages of RTSC on their own or blended with RTSF) do not significantly affect f_{cu} and E_{fm}.
- RTSC and RTSF have a marginal effect on the variability of the residual flexural tensile strength of SFRC. Compared with the resistance provided by the matrix itself prior to cracking, the post-cracking behaviour of SFRC relies increasingly on more variable parameters, such as fibre-matrix interaction and fibre distribution
- RTSF-only mixes are effective to MSF-only mixes at serviceability conditions. However, due to the smaller lengths and diameters of RTSF, their effectiveness at controlling cracks degrades gradually as cracks open.
- RTSC are more beneficial than MSF at arresting microcracks and bridging macrocracks. Moreover, RTSC are found better mobilised at larger crack widths and the post-cracking strength of recycled-fibre mixes (RTSC on their own or blended with RTSF) is significantly higher (up to 103%) than MSF-only mixes at the same total fibre dosage. Overall, the post-cracking performance of recycled fibre blends improves with increasing amounts of RTSC.
- It is noted that these research findings are based on limited experimental data, further research on various aspects (fibre dosage, fibre type and loading configuration, etc.) is still needed to increase the range of validity and expand the conclusions.

5.2.3 Post-cracking tensile behaviour of blended SFRC (Ch. 4)

- The RILEM approach can lead to significant overestimation (up to 72%) of the peak flexural load and energy absorption capacity (up to 39%), whilst the Model Code 2010 can provide a rather accurate prediction of the energy absorption capacity and some overestimation (less than 35%) of the peak flexural load.
- The simplified trilinear stress-strain relationship ($\sigma' - \varepsilon'$) for SFRC proposed in this study can provide an accurate estimate of the peak load and energy absorption capacity of SFRC with RTSF at a low total fibre dosage (up to 45 kg/m^3).
- The tensile strength of SFRC with RTSF at a low total fibre dosage is only marginally improved by fibre addition, and the post-cracking tensile strengths at different strains can be determined directly from residual flexural tensile strengths (f_{Ri}) of prisms.
- However, it is noted that the proposed $\sigma' - \varepsilon'$ model is based on limited experimental data; further research on various aspects (e.g. fibre dosage and type) is still required to increase the range of validity of the proposed model.

5.3 Recommendations for future work

The extensive (experimental and numerical) work presented in this study may contribute to the continuous growth of SFRC structural applications. However, as discussed in section 5.1, several aspects need to be further investigated, as described below.

5.3.1 Future experimental work

- Additional work on SFRC using higher dosages (>45 kg/m^3) of fibre blends (using MSF or RTSC and RTSF) needs to be undertaken.
- Further research on the wall effect and concrete flow in the fresh state is required. This could be achieved by casting large SFRC slabs and coring specimens (e.g. cylinders) at different positions (centre and edges). Specimens could be cut either parallel or perpendicular to the concrete flow direction and then fibre distribution of the notched planes could be determined through image analysis.
- Fibre pull-out tests (using fibres embedded in concrete at different angles) could be used to investigate the effect of fibre orientation on the fibre pull-out behaviour. To investigate the failure mode of RTSF, pull-out tests on RTSF at different embedment lengths could be performed. To confirm the beneficial effect of RTSF on enhancing the

pull-out resistance of MSF (or RTSC), pull-out tests could be undertaken on MSF (or RTSC) embedded in concrete reinforced with small amounts of RTSF.

- To rapidly categorise RTSF from different sources and reduce uncertainty in design, it is necessary to investigate the relationship between a certain range of aspect ratios of RTSF and the post-cracking strength of SFRC prisms using RTSF at certain dosages (in particular the critical dosage of RTSF, 30 kg/m^3).
- To increase the critical dosage of RTSF and RTSC in concrete, different concrete mix designs could be examined. Furthermore, to optimise the flexural performance of SFRC using RTSF, flexural tests on SFRC prisms using different sizes of coarse aggregates should be undertaken.

5.3.2 Improving the numerical investigation and the proposed $\sigma - \varepsilon$ model

- The suitability of the proposed $\sigma - \varepsilon$ model for blended SFRC using higher dosages (> 45 kg/m^3) of recycled fibres should be examined.
- The accuracy of the proposed model for deeper beams (> 150 mm) needs to be investigated. If necessary, a size-dependent factor should be introduced in the model.
- The inverse analysis undertaken (see Chapter 4) can be expanded to determine the stress-crack width ($\sigma - w$) relationship. Fracture mechanic principles should be used to determine the height and length of the fracture zone.

5.3.3 Exploiting the environmental benefits of recycled steel fibres

To further exploit the environmental benefits of recycled steel fibres, combinations of steel rebars (or meshes) and recycled fibres as reinforcement in concrete, as well as recycled fibres and recycled aggregates (e.g. recycled concrete aggregate), could be investigated.

In addition, the use of recycled steel fibres in more structural applications needs to be investigated, as given below:

- Water retaining structures (for crack control purposes);
- Pumped SFRC in insulated concrete formwork (fibres used as main reinforcement);
- Strong rooms to increase resistance to drilling, coring and blast.
- Strong bases for heavy machinery (complex static and dynamic loading), to eliminate shear reinforcement.

Appendix A:

Experimental results –Chapter 2

A.1 Mix design data

Mix Design Data

To: **TWINTEC LTD**
Unit 1, Prospect Park
Valley Drive
Rugby
Warwickshire CV21 1TF

Newbold Quarry
Lichfield Road
Staffordshire DE13 8EF

Tel: 01283714405
Fax: 01283714469

Site / Contract Address	**UNIVERSITY OF SHEFFIELD - SHEFFIELD** **University of Sheffield** **Civil Engineering Structures Lab** **Gate 2 Portobello Street** **Sheffield**	Plant: Contact: Our Ref: Account No: Issue Date: Issued By:	**SHEFFIELD ELITE** **Amanda Steven** **1265445** **160368** **31/10/14**

All mixes in accordance with BS 8500-2 (except proprietary mixes) unless otherwise agreed. Batch weight of materials calculated on as SSD basis for 1.0m3 of fresh compacted concrete. Mixes are quality controlled and actual mix proportions may vary in response to control systems.

Source Plant: **Sheffield Minimix**

C25/30 20mm CIIIA Pump Mix S2 Min 300 Max WCR 0.55			**Quantity / UOM**
PC Cement Rugby 52,5N CEMI	CEMEX	Rugby Works	150.000 KG
GGBS Holcim Germany	Holcim	Bremen	150.000 KG
4/20 Conc. Graded Gravel EN12620/PD6682-1 TC1 Newbold			1097.000 KG
0/4 Conc. Sand MP Gravel EN12620/PD6682-1 TD1 Woodhall			804.000 KG
Water (Cold)			

A/C Ratio	6.337	Actual WCR	.550
% Fines	42.294	Alkali (kg/m3)	2.865
Total Cementitious (kg/m3)	300.000	Chlorides	.060

A.2 Compressive strength (SFRC and plain concrete cubes)

			SFRC		Plain	
Mix	**Casting date**	**Testing date**	**Load (kN)**	**Stress (MPa)**	**Load (kN)**	**Stress (MPa)**
A	13/11/2014	19/12/2014 (37 days)	986.5	43.8	936.8	41.6
			945.5	42.0	967.5	43.0
			1028.2	45.7	931.6	41.4
AVG A			986.7	**43.9**	945.3	**42.0**
SD			41.4	**1.8**	19.4	**0.9**
B	18/11/2014	22/12/2014 (35 days)	902.8	40.1	1073.8	47.7
			971.8	43.2	1054.8	46.9
			998	44.4	986.2	43.8
AVG B			957.5	**42.6**	1038.3	**46.1**
SD			49.2	**2.2**	46.1	**2.0**
C	4/11/2014	15/12/2014 (42 days)	959.5	42.6	1088.2	48.4
			991.2	44.1	1041.6	46.3
			1042.3	46.3	1078.8	47.9
AVG C			997.7	**44.3**	1069.5	**47.5**
SD			41.8	**1.9**	24.6	**1.1**
D	4/11/2014	15/12/2014 (42 days)	1038.2	46.1	1088.2	48.4
			1014.6	45.1	1041.6	46.3
			954.5	42.4	1078.8	47.9
AVG D			1002.4	**44.6**	1069.5	**47.5**
SD			43.2	**1.9**	24.6	**1.1**

			SFRC		Plain	
Mix	**Casting date**	**Testing date**	**Load (kN)**	**Stress (MPa)**	**Load (kN)**	**Stress (MPa)**
E	20/11/2014	22/12/2014 (33 days)	988.5	43.9	928.7	41.3
			913.2	40.6	845.2	37.6
			916.8	40.7	762.8	33.9
AVG E			939.5	**41.8**	845.6	**37.6**
SD			42.5	**1.9**	83.0	**3.7**
F	13/11/2014	20/12/2014 (38 days)	998.5	44.4	936.8	41.6
			917.4	40.8	967.5	43.0
			980.2	43.6	931.6	41.4
AVG F			965.4	**42.9**	945.3	**42.0**
SD			42.5	**1.9**	19.4	**0.9**
G	13/11/2014	22/12/2014 (40 days)	943.6	41.9	936.8	41.6
			966.8	43.0	967.5	43.0
			920.4	40.9	931.6	41.4
AVG G			943.6	**41.9**	945.3	**42.0**
SD			23.2	**1.0**	19.4	**0.9**
H	18/11/2014	22/12/2014 (35 days)	959.4	42.6	1073.8	47.7
			966.7	43.0	1054.8	46.9
			963.5	42.8	986.2	43.8
AVG H			963.2	**42.8**	1038.3	**46.1**
SD			3.7	**0.2**	46.1	**2.0**
I	4/11/2014	15/12/2014 (42 days)	1114.7	49.5	1088.2	48.4
			1190.4	52.9	1041.6	46.3
			1088	48.4	1078.8	47.9
AVG I			1131.0	**50.3**	1069.5	**47.5**
SD			53.1	**2.4**	24.6	**1.1**
J	11/11/2014	18/12/2014 (38 days)	993.3	44.1	879.9	39.1
			1019.9	45.3	923.6	41.0
			991.1	44.0	887.3	39.4
AVG J			1001.4	**44.5**	896.9	**39.9**
SD			16.0	**0.7**	23.4	**1.0**

A.3 Residual flexural tensile strength (SFRC prisms)

A	f_R				B	f_R			
	f_{R1}	f_{R2}	f_{R3}	f_{R4}		f_{R1}	f_{R2}	f_{R3}	f_{R4}
A1	3.30	3.49	3.11	2.08	B1	3.42	3.45	2.91	2.47
A2	2.91	2.82	2.36	1.98	B2	5.24	5.23	4.83	4.27
A3	5.27	4.83	4.45	3.60	B3	3.23	2.91	2.66	2.42
A4	2.74	1.93	1.28	1.00	B4	3.04	3.02	2.40	1.76
A5	3.04	2.88	2.37	1.56	B5	3.34	3.09	2.63	1.68
A6	2.42	2.30	1.79	1.58	B6	3.76	3.68	3.50	2.35
A7	3.10	2.68	2.45	2.12	B7	3.91	4.03	3.08	2.59
A8	3.47	3.76	3.50	3.05	B8	4.04	4.07	3.28	2.81
A9	5.26	4.95	4.24	3.04	B9	3.79	3.45	3.10	2.50
A10	3.44	3.42	2.92	2.21	B10	3.85	3.55	3.02	2.38
A11	4.67	4.44	4.18	3.68	B11	4.24	4.05	3.31	2.72
A12	3.54	3.33	2.74	2.33	B12	2.73	2.78	2.66	2.31
Mean A	**3.60**	**3.40**	**2.95**	**2.35**	**Mean B**	**3.72**	**3.61**	**3.12**	**2.52**
Standard Deviation	0.95	0.96	0.99	0.83	Standard Deviation	0.65	0.68	0.63	0.65
COV (%)	**24.5**	**27.3**	**31.7**	**34.3**	**COV (%)**	**15.5**	**17.8**	**19.2**	**24.6**

C	f_R				D	f_R			
	f_{R1}	f_{R2}	f_{R3}	f_{R4}		f_{R1}	f_{R2}	f_{R3}	f_{R4}
C1	3.50	3.27	2.78	2.19	D1	2.73	2.35	2.05	1.77
C2	3.67	3.30	2.83	2.54	D2	2.90	2.50	2.30	1.67
C3	3.27	3.06	2.78	2.54	D3	2.73	2.68	2.44	1.64
C4	2.93	2.81	2.34	1.91	D4	3.33	3.11	2.90	2.70
C5	3.58	3.43	2.89	2.40	D5	4.02	3.93	3.58	2.96
C6	3.51	3.36	3.07	2.39	D6	3.08	3.10	2.50	2.10
Mean C	**3.41**	**3.21**	**2.78**	**2.33**	**Mean D**	**3.13**	**2.94**	**2.63**	**2.14**
Standard Deviation	0.27	0.23	0.24	0.24	Standard Deviation	0.49	0.58	0.54	0.57
COV (%)	**5.9**	**7.2**	**7.7**	**10.2**	**COV (%)**	**15.7**	**19.5**	**20.7**	**26.4**

E	f_R				F	f_R			
	f_{R1}	f_{R2}	f_{R3}	f_{R4}		f_{R1}	f_{R2}	f_{R3}	f_{R4}
E1	3.63	3.09	2.57	2.16	F1	3.29	3.55	3.12	2.68
E2	3.13	2.55	2.08	1.73	F2	3.13	3.65	3.90	3.11
E3	3.32	2.66	1.99	1.61	F3	4.95	5.47	4.68	4.28
E4	2.70	2.15	1.62	1.31	F4	3.30	3.45	3.68	3.41
E5	3.28	3.04	2.65	2.22	F5	2.91	3.26	3.03	2.91
E6	2.96	2.70	2.11	1.70	F6	3.77	4.69	4.52	3.98
					F7	4.42	4.63	4.13	2.93
					F8	2.73	2.66	2.40	2.39
					F9	4.45	4.22	3.67	3.32
					F10	4.04	3.98	3.81	3.75
					F11	4.36	4.55	3.94	3.82
					F12	3.75	4.18	4.01	2.90
Mean E	**3.17**	**2.70**	**2.17**	**1.79**	**Mean F**	**3.76**	**4.02**	**3.74**	**3.29**
Standard Deviation	0.32	0.34	0.38	0.35	Standard Deviation	0.70	0.76	0.64	0.57
COV (%)	**10.2**	**12.2**	**15.7**	**18.4**	**COV (%)**	**18.6**	**17.9**	**16.1**	**17.4**

G	f_R				H	f_R			
	f_{R1}	f_{R2}	f_{R3}	f_{R4}		f_{R1}	f_{R2}	f_{R3}	f_{R4}
G1	5.07	5.73	4.90	4.85	H1	4.61	4.32	4.04	3.76
G2	3.01	3.44	3.05	3.00	H2	5.53	5.52	5.32	5.15
G3	5.99	5.82	5.07	4.64	H3	4.71	5.15	4.73	4.19
G4	3.08	3.64	3.69	3.02	H4	5.61	6.32	5.91	5.47
G5	3.58	3.97	3.98	3.87	H5	4.55	4.79	4.70	4.31
G6	3.63	3.67	3.63	3.54	H6	5.10	5.38	5.00	4.72
G7	3.96	4.57	4.33	3.83	H7	3.35	3.94	3.74	3.54
G8	4.22	4.27	4.11	3.96	H8	2.95	2.93	2.80	1.99
G9	4.25	4.15	3.98	3.52	H9	4.00	4.08	4.10	3.91
G10	4.70	5.18	4.74	4.58	H10	3.45	3.67	3.14	2.85
G11	3.78	4.09	3.31	2.83	H11	3.50	3.89	4.00	4.13
G12	4.59	4.40	4.12	3.79	H12	3.61	3.58	3.52	2.90
Mean G	**4.15**	**4.41**	**4.08**	**3.78**	**Average H**	**4.25**	**4.46**	**4.25**	**3.91**
Standard Deviation	0.85	0.79	0.62	0.66	Standard Deviation	0.89	0.98	0.91	1.00
COV (%)	**18.5**	**16.9**	**14.1**	**17.4**	**COV (%)**	**21.3**	**21.3**	**21.2**	**24.2**

I	f_R				J	f_R			
	f_{R1}	f_{R2}	f_{R3}	f_{R4}		f_{R1}	f_{R2}	f_{R3}	f_{R4}
I1	4.65	4.61	4.28	3.28	J1	4.35	4.29	3.61	3.20
I2	5.65	5.56	4.95	3.93	J2	4.19	4.01	2.88	2.27
I3	4.94	4.80	3.72	3.09	J3	4.35	4.14	3.70	2.75
I4	5.67	4.70	4.12	3.59	J4	3.85	3.87	3.27	2.81
I5	4.31	4.49	4.33	3.89	J5	5.29	5.12	4.32	3.51
I6	3.74	4.05	3.49	2.90	J6	5.37	4.65	3.56	2.86
Mean I	**4.83**	**4.70**	**4.15**	**3.45**	**Mean J**	**4.57**	**4.35**	**3.56**	**2.90**
Standard Deviation	0.76	0.50	0.51	0.42	Standard Deviation	0.62	0.46	0.48	0.42
COV (%)	**15.2**	**10.2**	**11.4**	**11.3**	**COV (%)**	**13.6**	**10.2**	**12.4**	**13.4**

A.4 Prisms (after testing)

Specimen code name:		A1			
Notched Depth d_n	126	mm			
Depth, d	150	mm	Span, L	500	mm
Width, b	150	mm	Flexural strength	3.71	MPa

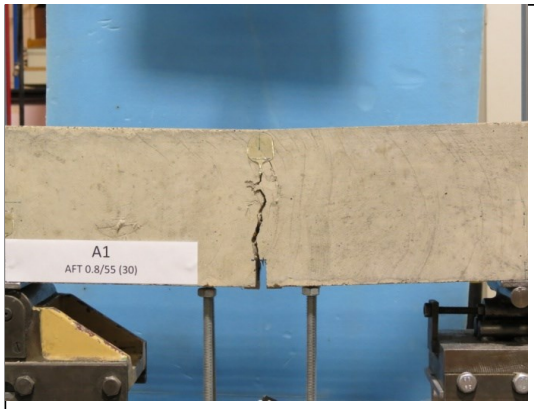

Bottom face of cast concrete

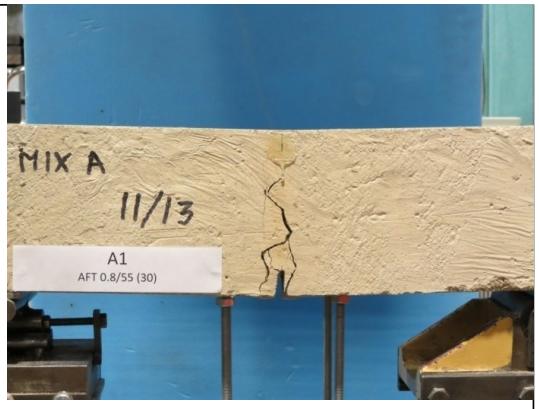

Top face of cast concrete

Crack zone of bottom face

Crack zone of top face

Stress-deformation graphs

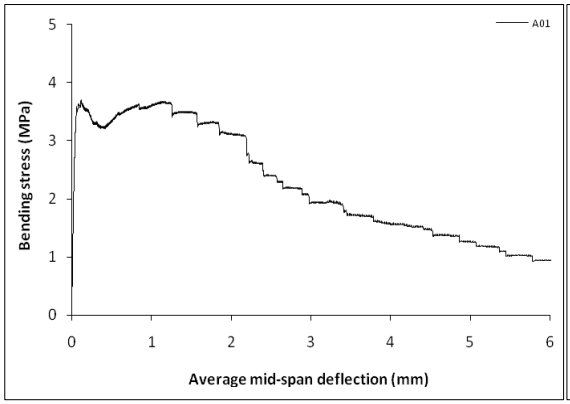

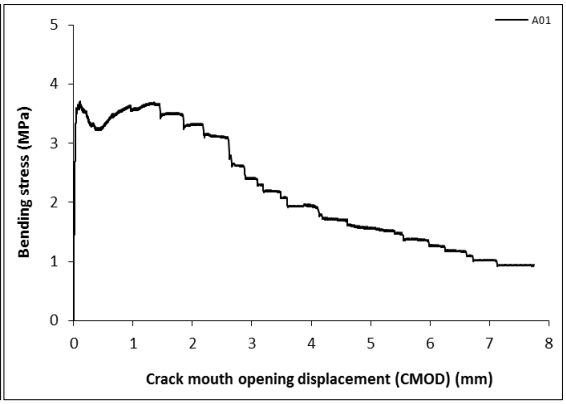

Specimen code name:			A2		
Notched Depth d_n	124	mm			
Depth, d	150	mm	Span, L	500	mm
Width, b	150	mm	Flexural strength	4.00	MPa

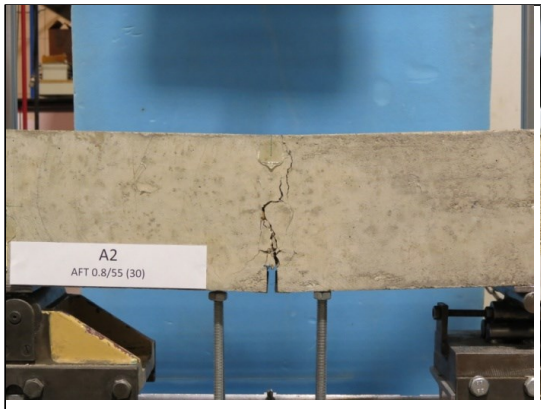

Bottom face of cast concrete

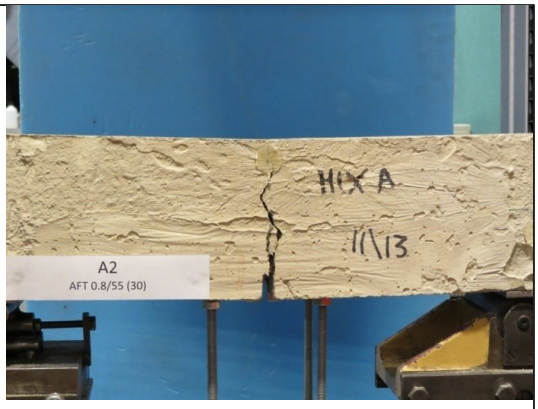

Top face of cast concrete

Crack zone of bottom face

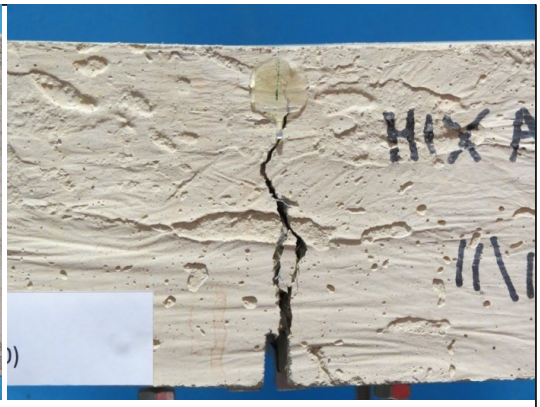

Crack zone of top face

Stress-deformation graphs

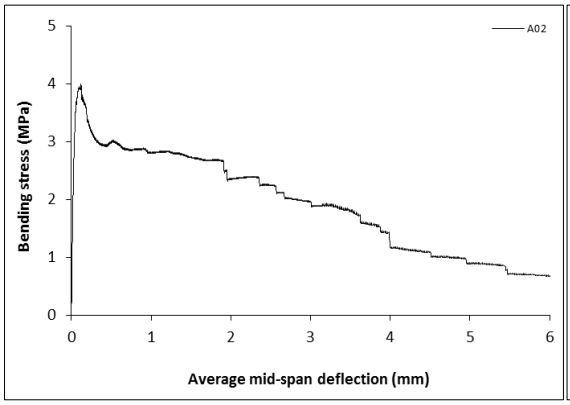

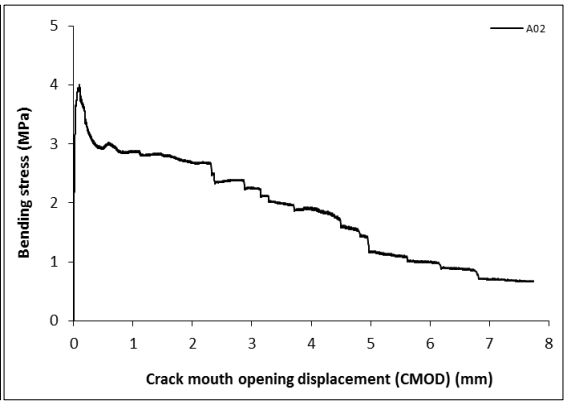

Specimen code name:		A3			
Notched Depth d_n	126	mm			
Depth, d	151	mm	Span, L	549	mm
Width, b	150	mm	Flexural strength	5.38	MPa

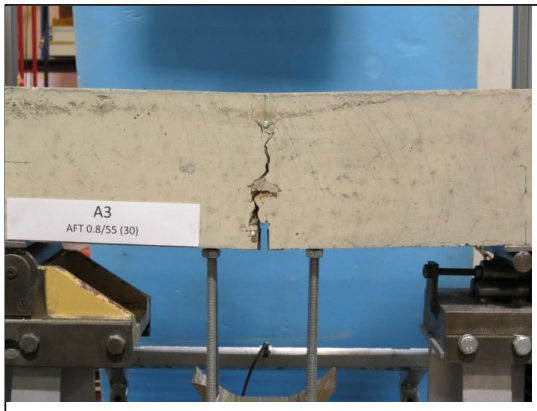

Bottom face of cast concrete

Top face of cast concrete

Crack zone of bottom face

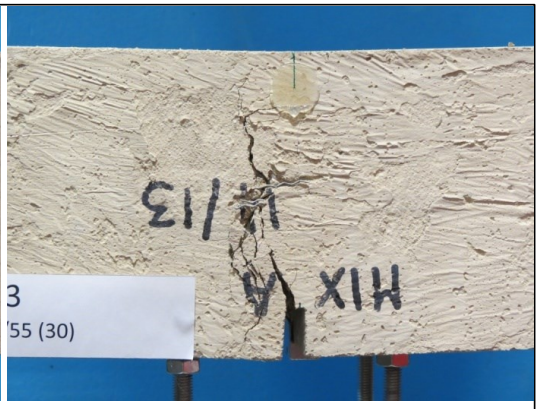

Crack zone of top face

Stress-deformation graphs

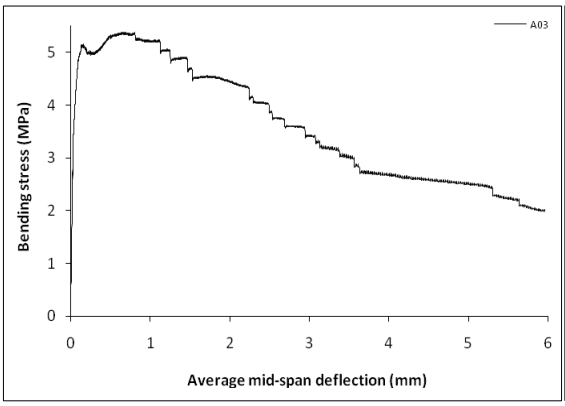

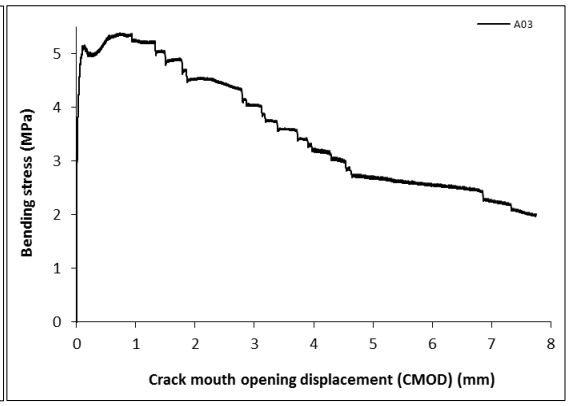

Specimen code name:		A4			
Notched Depth d_n	126	mm			
Depth, d	151	mm	Span, L	500	mm
Width, b	150	mm	Flexural strength	3.20	MPa

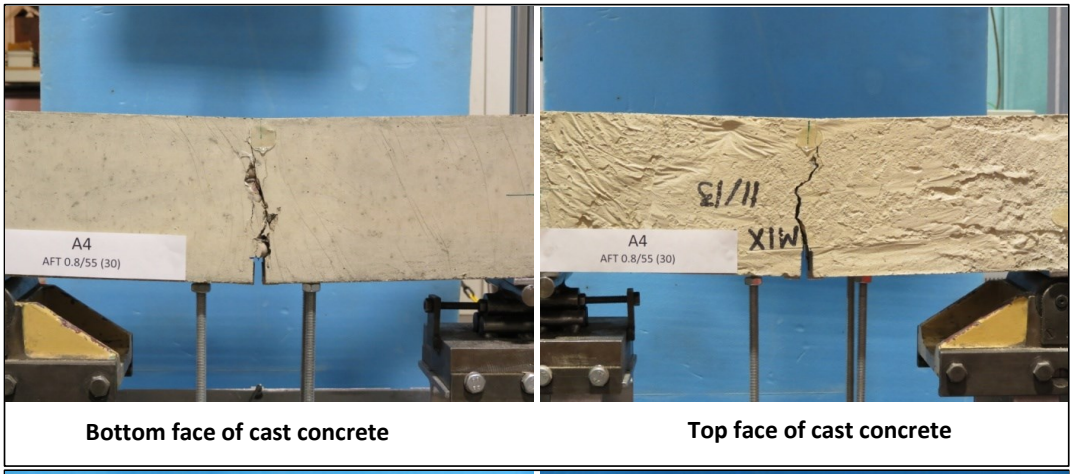

Bottom face of cast concrete | Top face of cast concrete

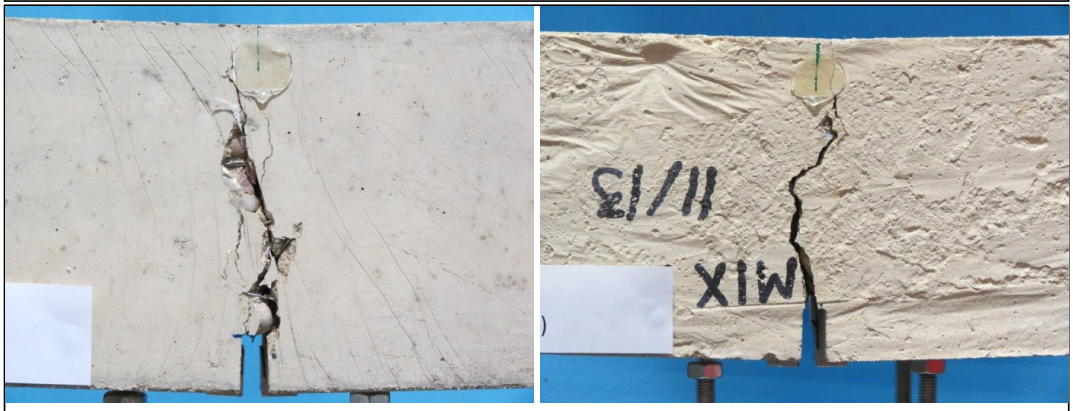

Crack zone of bottom face | Crack zone of top face

Stress-deformation graphs

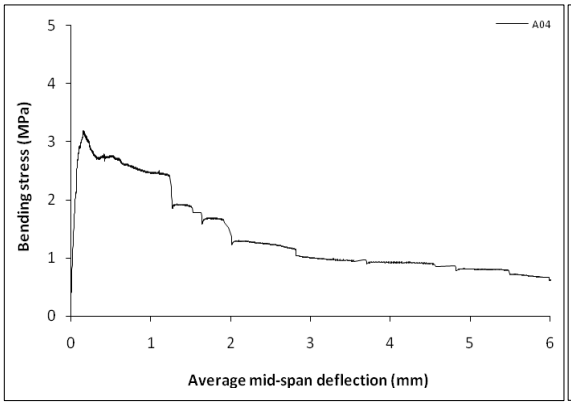

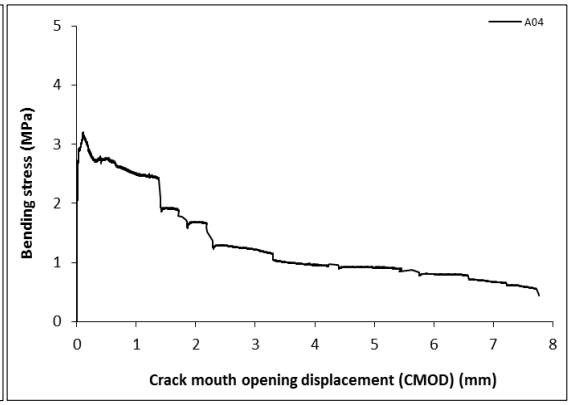

Specimen code name:		A5			
Notched Depth d_n	125	mm			
Depth, d	150	mm	Span, L	500	mm
Width, b	151	mm	Flexural strength	3.95	MPa

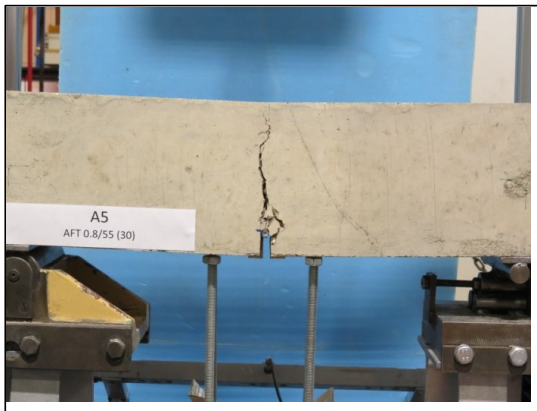

Bottom face of cast concrete

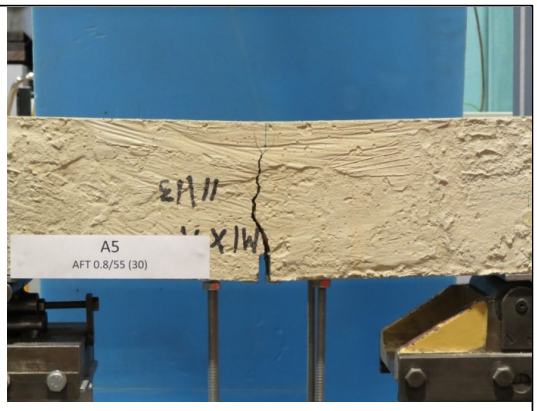

Top face of cast concrete

Photo Missing

Crack zone of bottom face

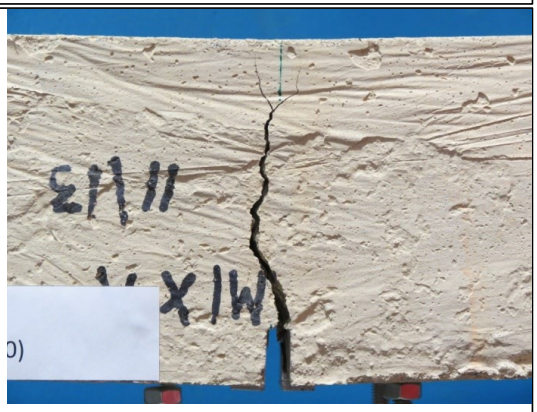

Crack zone of top face

Stress-deformation graphs

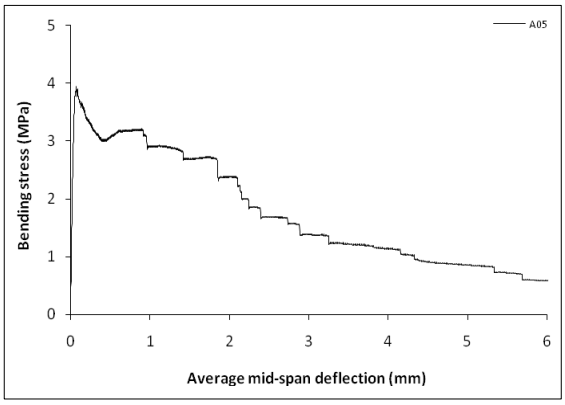

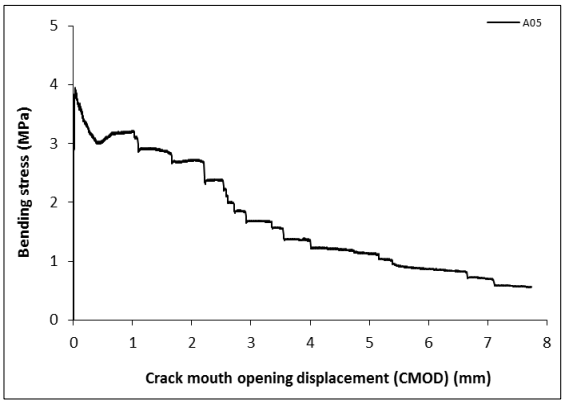

Specimen code name:		A6			
Notched Depth d_n	125	mm			
Depth, d	150	mm	Span, L	500	mm
Width, b	153	mm	Flexural strength	4.15	MPa

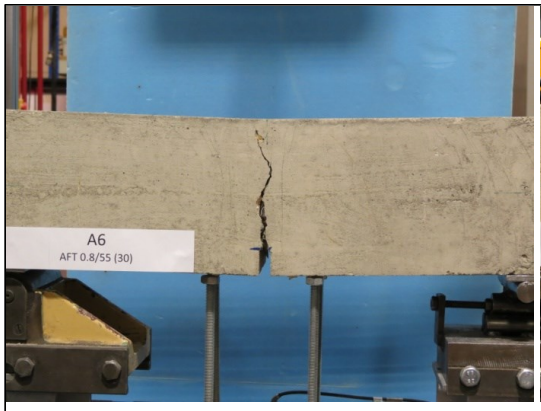

Bottom face of cast concrete

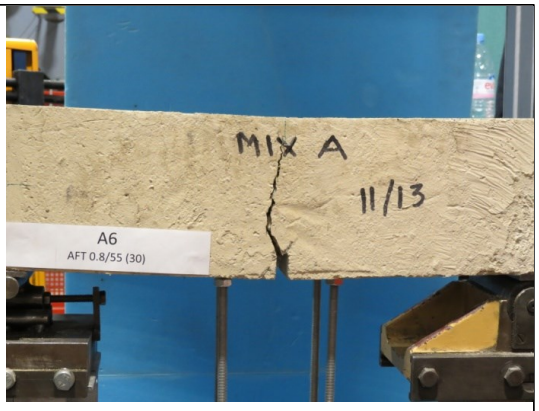

Top face of cast concrete

Crack zone of bottom face

Crack zone of top face

Stress-deformation graphs

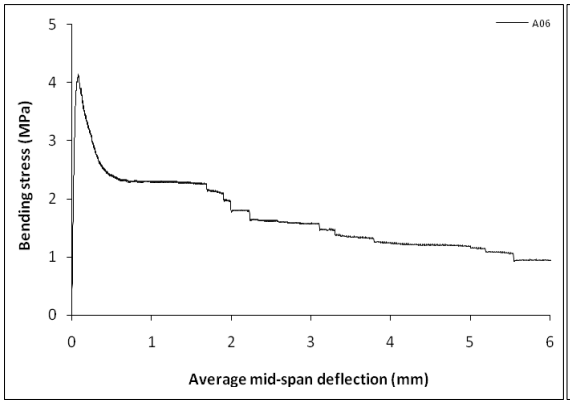

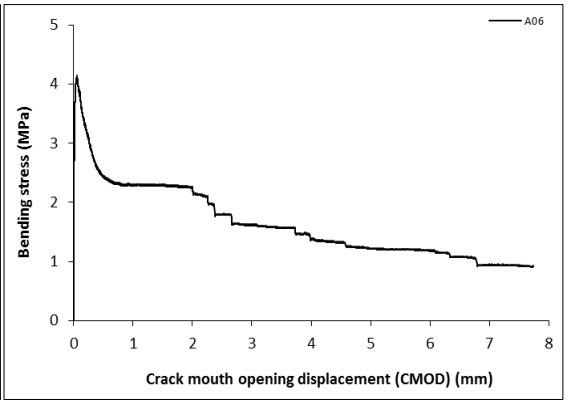

Specimen code name:		A7			
Notched Depth d_n	124	mm			
Depth, d	150	mm	Span, L	500	mm
Width, b	152	mm	Flexural strength	3.24	MPa

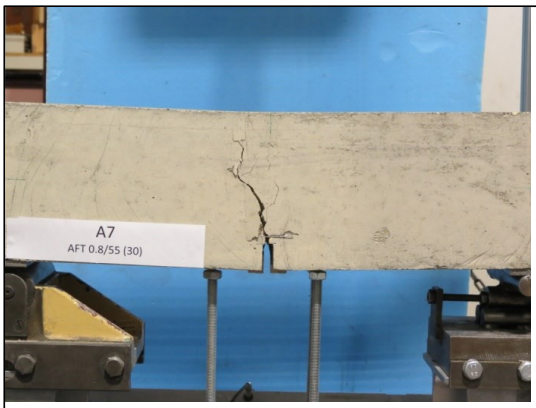

Bottom face of cast concrete

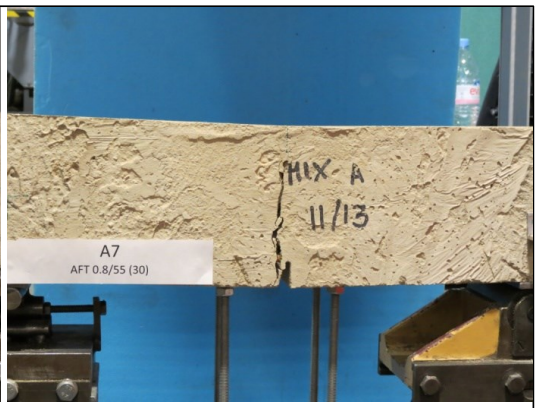

Top face of cast concrete

Crack zone of bottom face

Crack zone of top face

Stress-deformation graphs

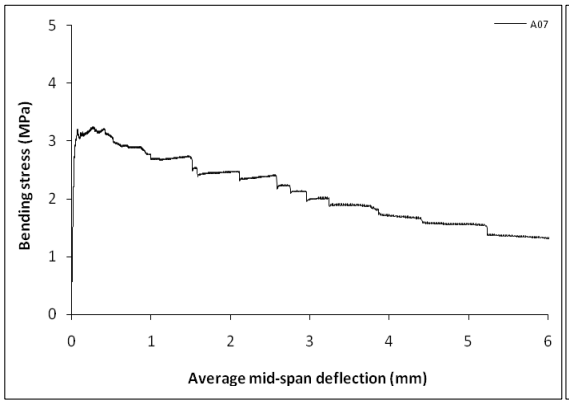

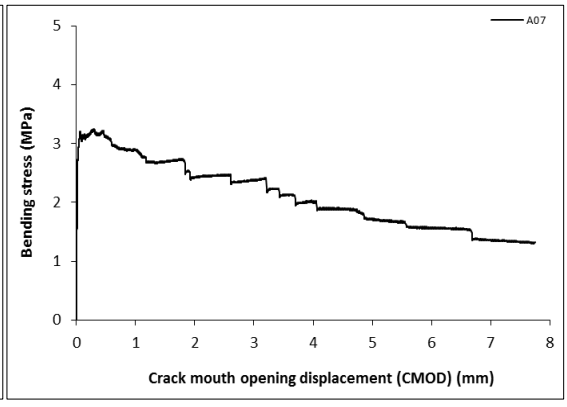

Specimen code name:			A8		
Notched Depth d_n	124	mm			
Depth, d	150	mm	Span, L	500	mm
Width, b	152	mm	Flexural strength	3.89	MPa

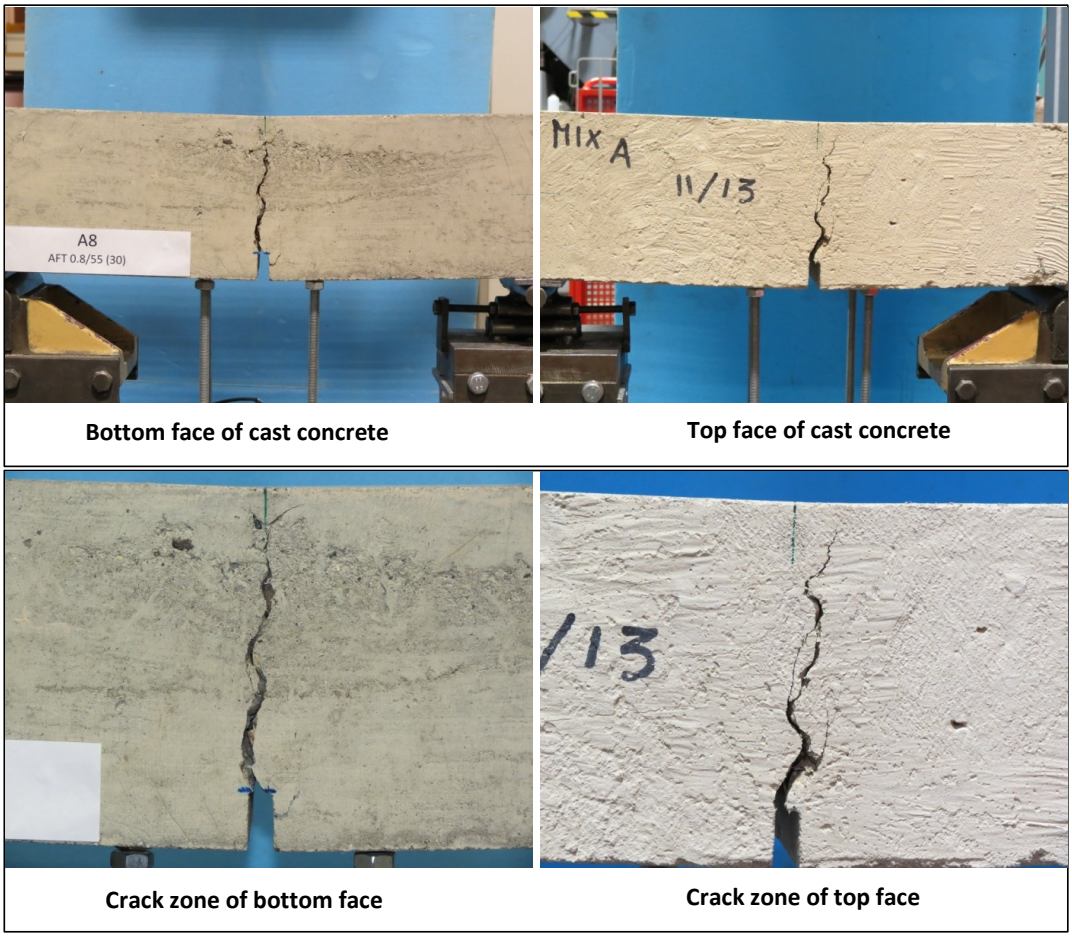

Bottom face of cast concrete | Top face of cast concrete

Crack zone of bottom face | Crack zone of top face

Stress-deformation graphs

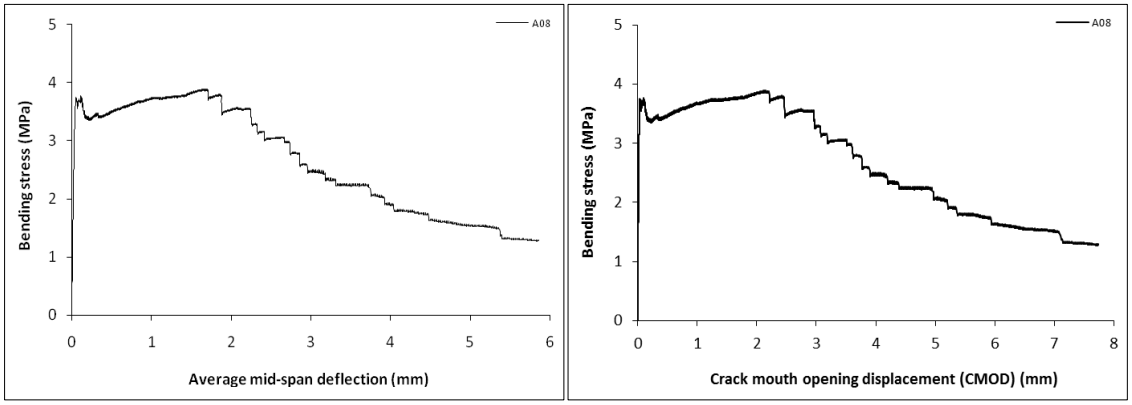

Specimen code name:			A9		
Notched Depth d_n	124	mm			
Depth, d	150	mm	Span, L	500	mm
Width, b	153	mm	Flexural strength	5.32	MPa

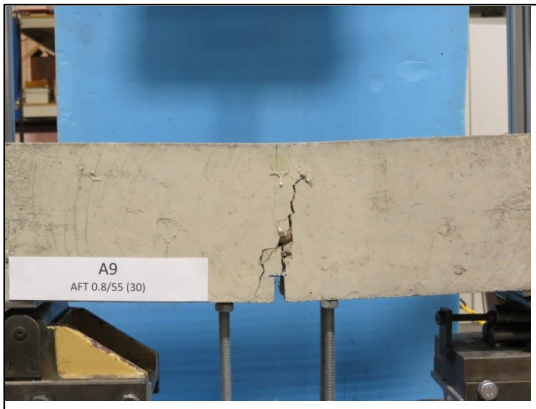

Bottom face of cast concrete

Top face of cast concrete

Crack zone of bottom face

Crack zone of top face

Stress-deformation graphs

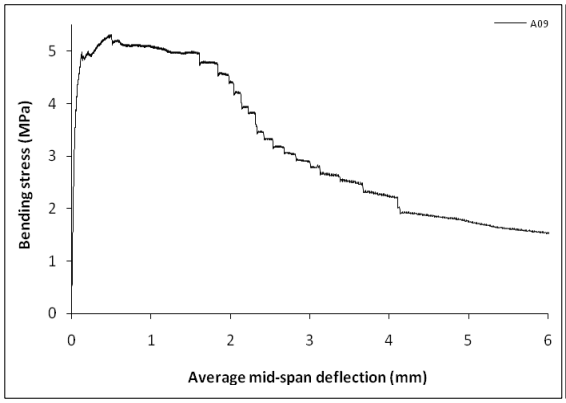

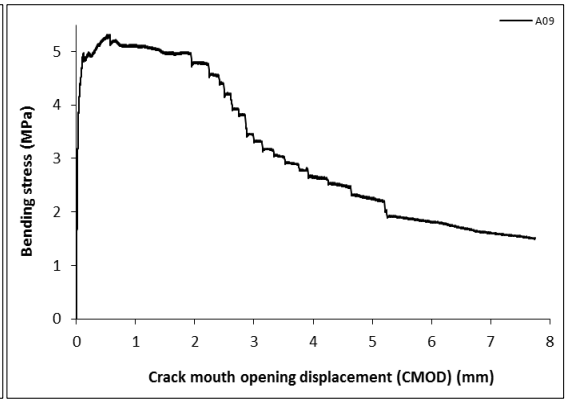

Specimen code name:			A10		
Notched Depth d_n	125	mm			
Depth, d	150	mm	Span, L	500	mm
Width, b	152	mm	Flexural strength	4.49	MPa

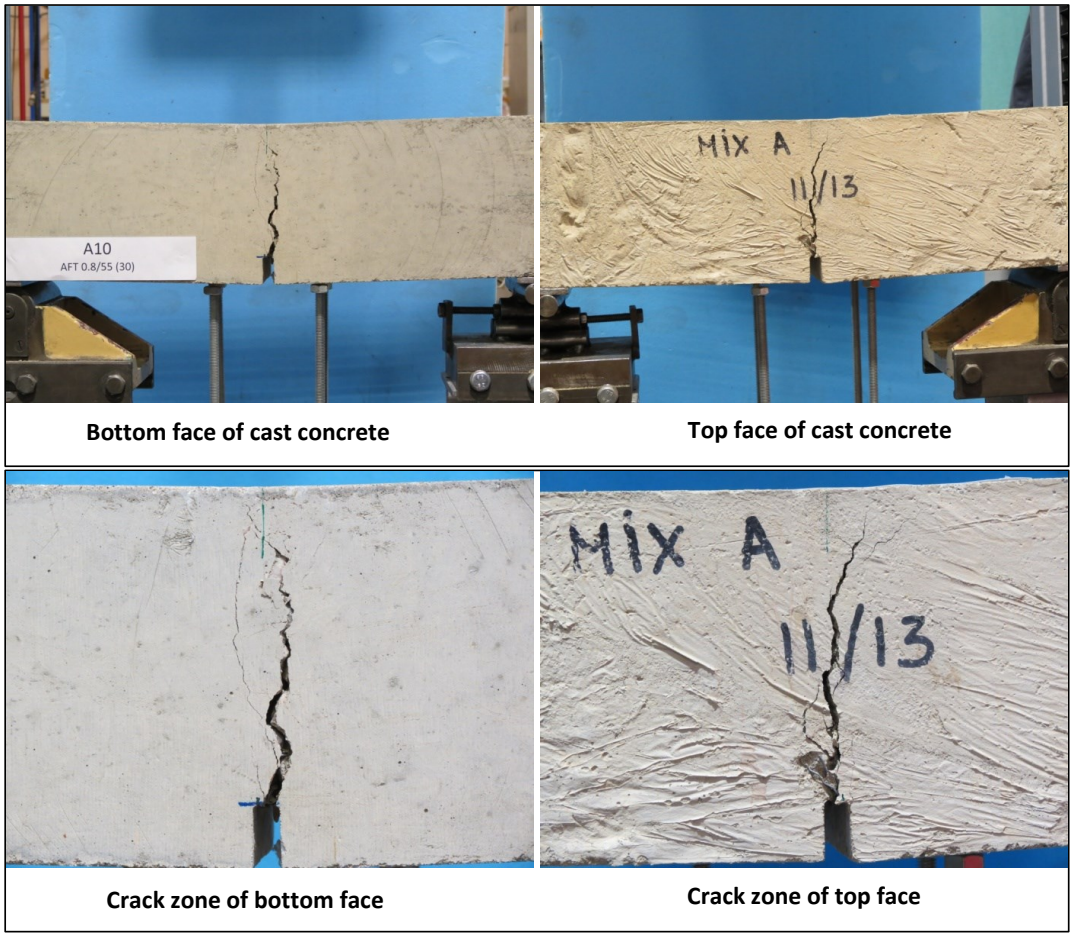

Bottom face of cast concrete

Top face of cast concrete

Crack zone of bottom face

Crack zone of top face

Stress-deformation graphs

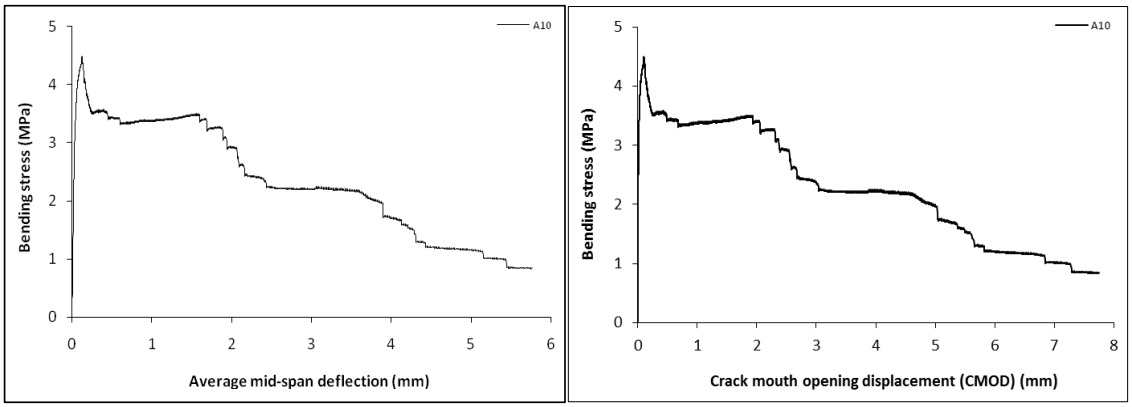

Specimen code name:		A11			
Notched Depth d_n	125	mm			
Depth, d	150	mm	Span, L	500	mm
Width, b	151	mm	Flexural strength	5.00	MPa

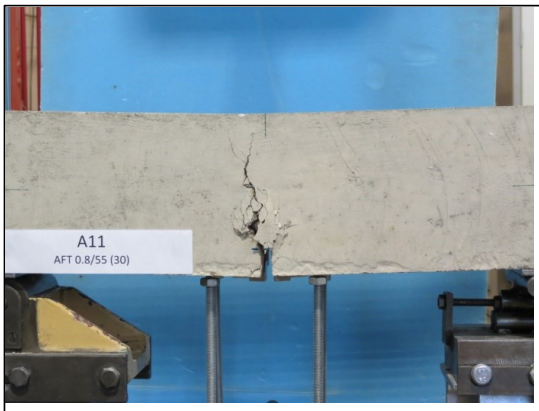

Bottom face of cast concrete

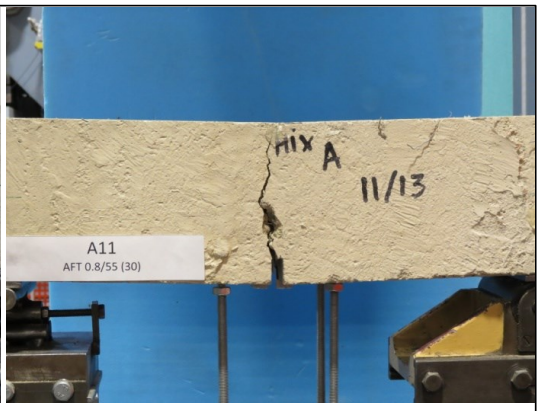

Top face of cast concrete

Crack zone of bottom face

Crack zone of top face

Stress-deformation graphs

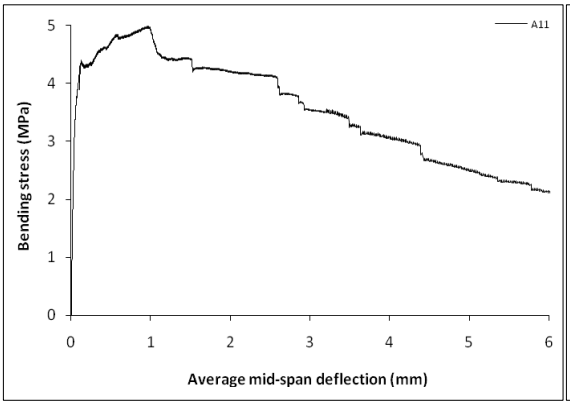

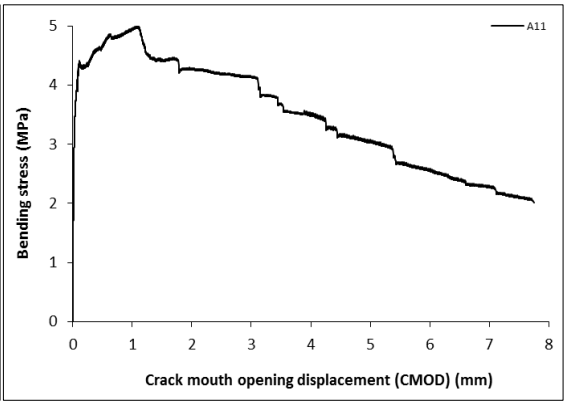

Specimen code name:		A12			
Notched Depth d_n	125	mm			
Depth, d	150	mm	Span, L	500	mm
Width, b	150	mm	Flexural strength	4.00	MPa

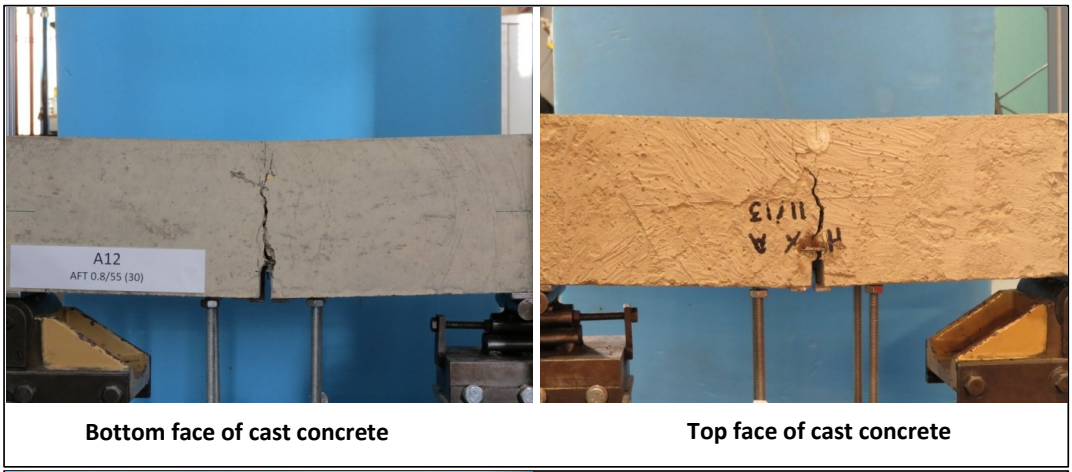

Bottom face of cast concrete | Top face of cast concrete

Crack zone of bottom face | Crack zone of top face

Stress-deformation graphs

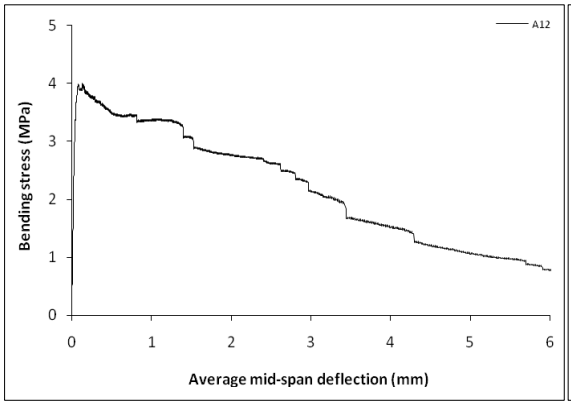

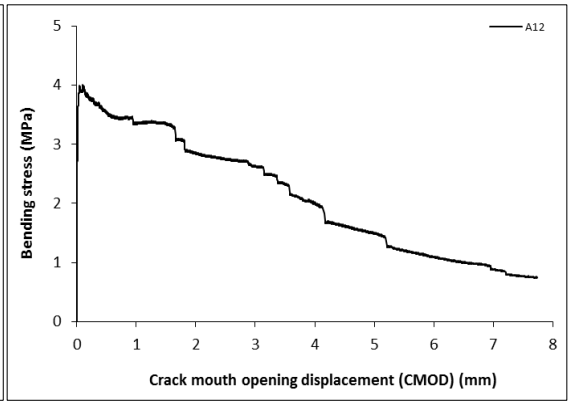

Mix:	A		
Notched Depth d_n	mm		
Depth, d	mm	Span, L	mm
Width, b	mm	Flexural strength	MPa

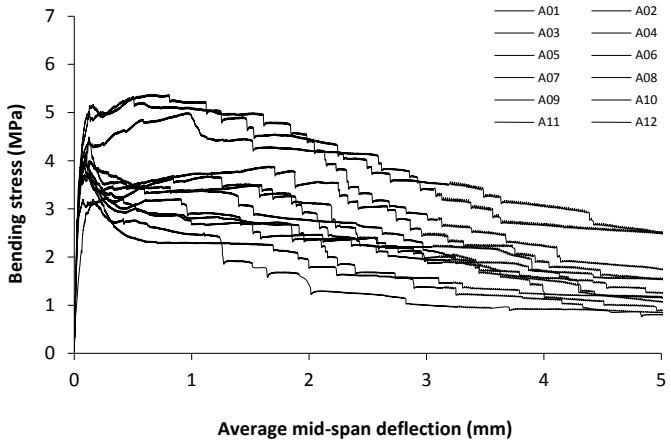

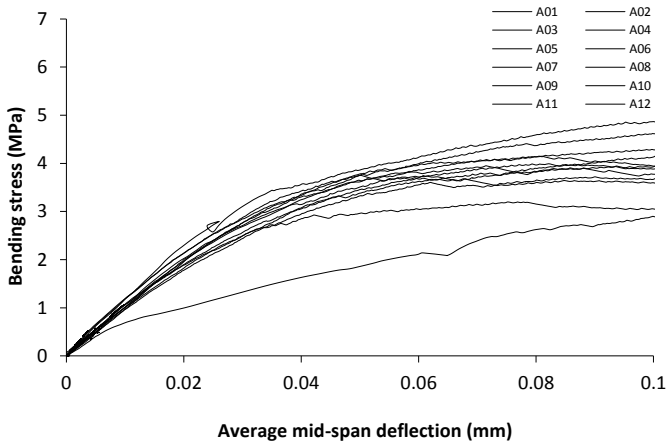

Specimen code name:		B1			
Notched Depth d_n	126	mm			
Depth, d	150	mm	Span, L	500	mm
Width, b	153	mm	Flexural strength	3.78	MPa

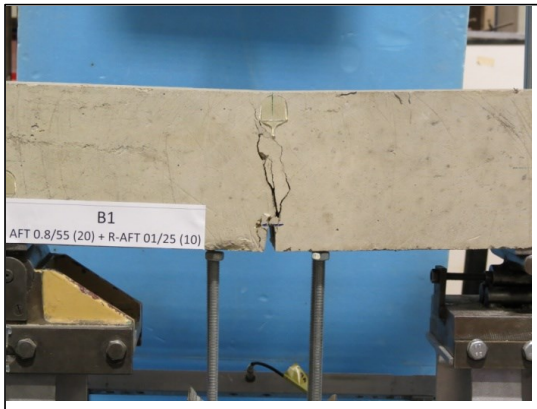

Bottom face of cast concrete

Top face of cast concrete

Crack zone of bottom face

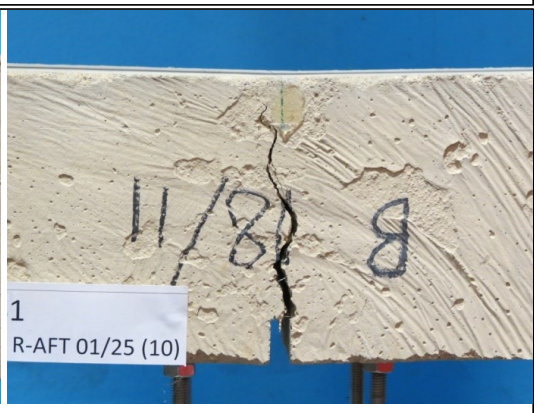

Crack zone of top face

Stress-deformation graphs

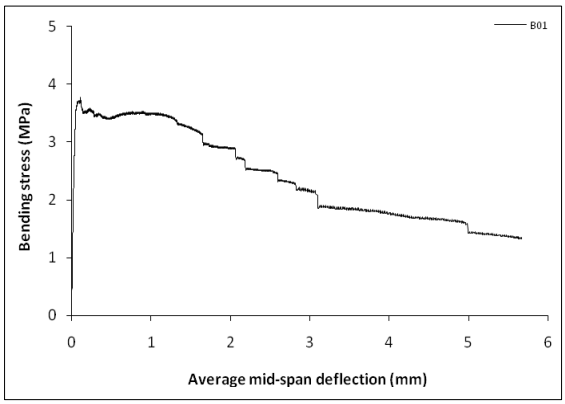

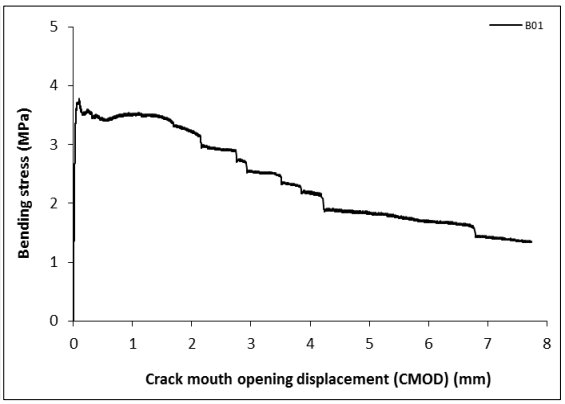

Specimen code name:		B2			
Notched Depth d_n	125	mm			
Depth, d	150	mm	Span, L	500	mm
Width, b	152	mm	Flexural strength	5.44	MPa

Crack zone of bottom face

Crack zone of top face

Stress-deformation graphs

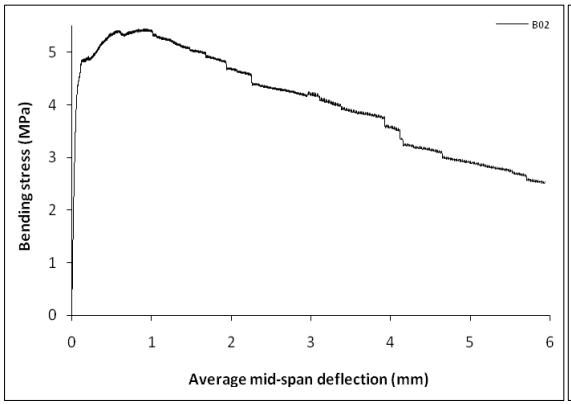

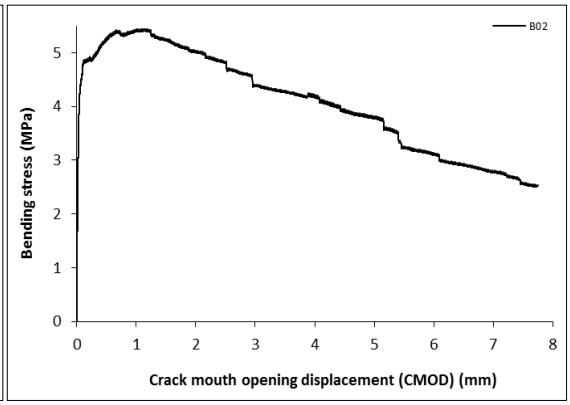

Specimen code name:		B3			
Notched Depth d_n	125	mm			
Depth, d	150	mm	Span, L	500	mm
Width, b	154	mm	Flexural strength	3.40	MPa

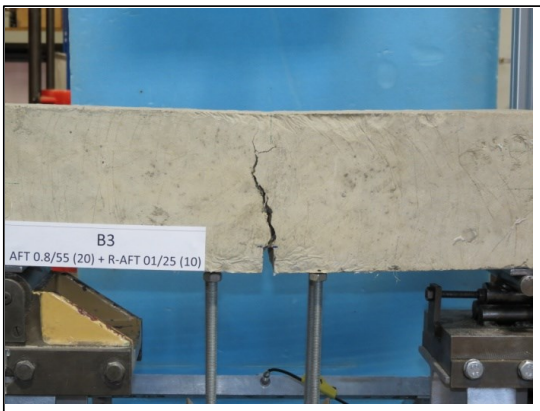

Bottom face of cast concrete

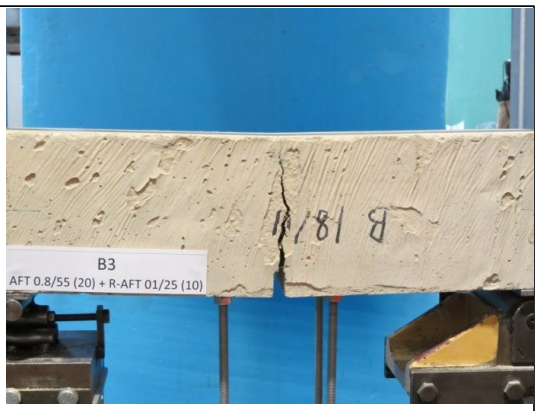

Top face of cast concrete

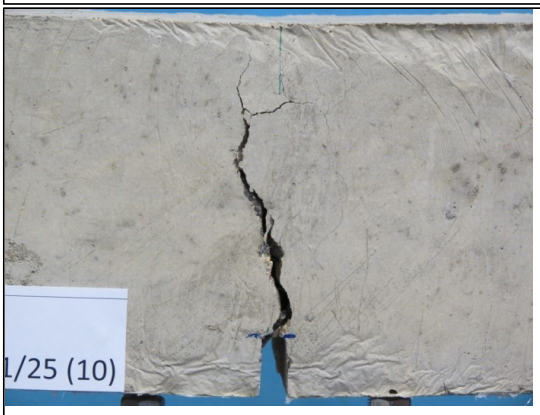

Crack zone of bottom face

Crack zone of top face

Stress-deformation graphs

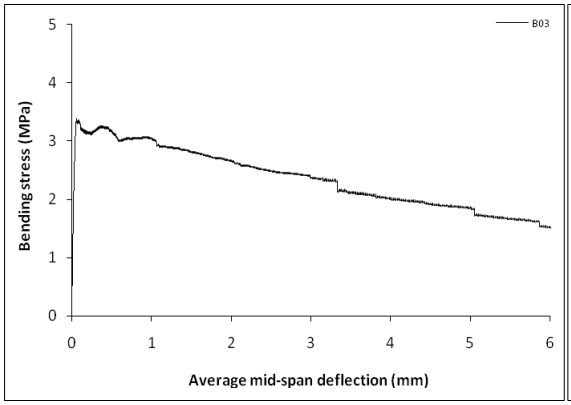

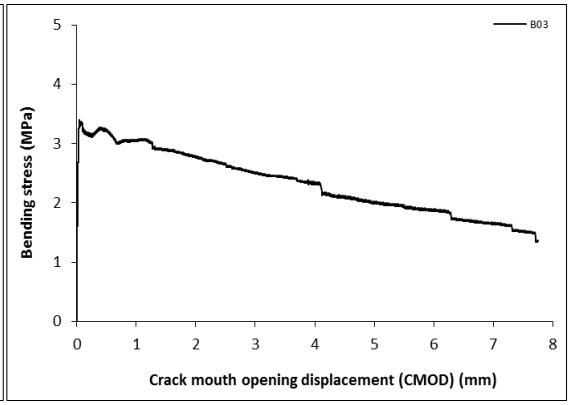

Specimen code name:		B4			
Notched Depth d_n	126	mm			
Depth, d	151	mm	Span, L	500	mm
Width, b	157	mm	Flexural strength	3.62	MPa

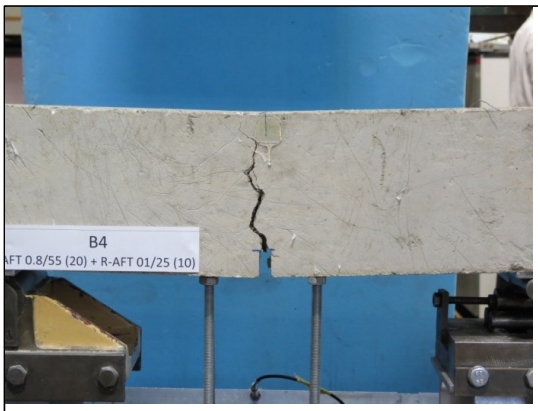

Bottom face of cast concrete

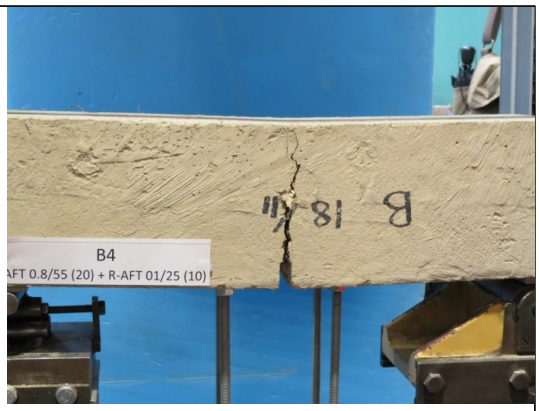

Top face of cast concrete

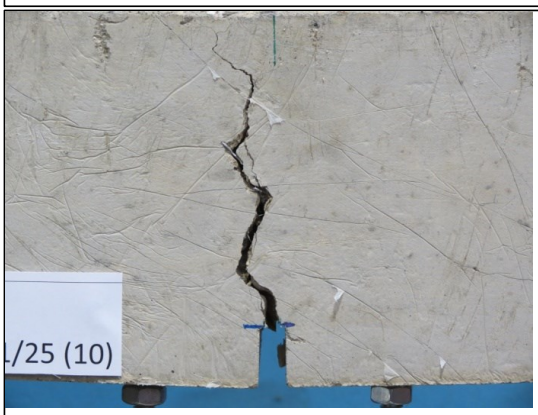

Crack zone of bottom face

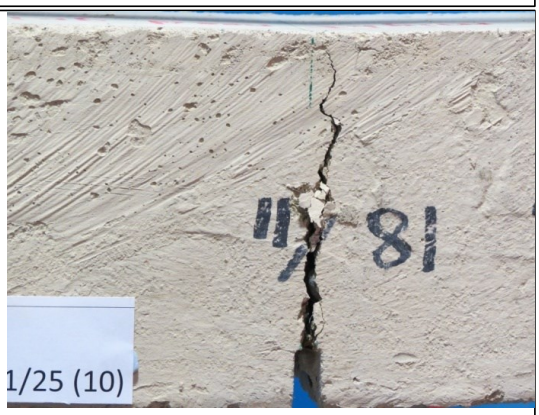

Crack zone of top face

Stress-deformation graphs

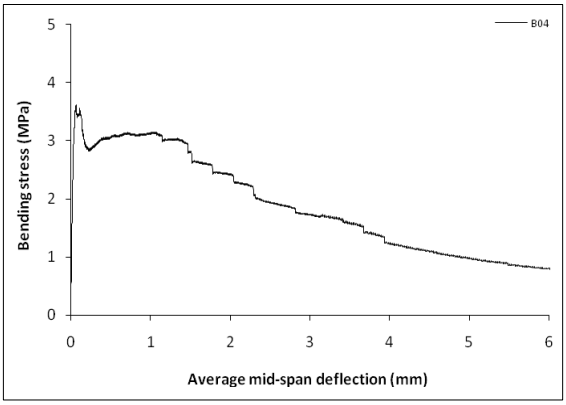

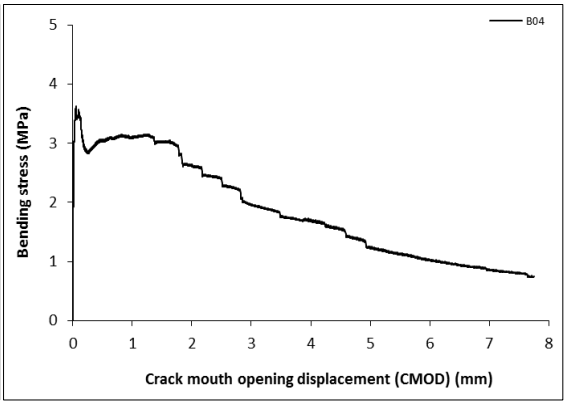

Specimen code name:		B5			
Notched Depth d_n	126	mm			
Depth, d	151	mm	Span, L	500	mm
Width, b	157	mm	Flexural strength	3.70	MPa

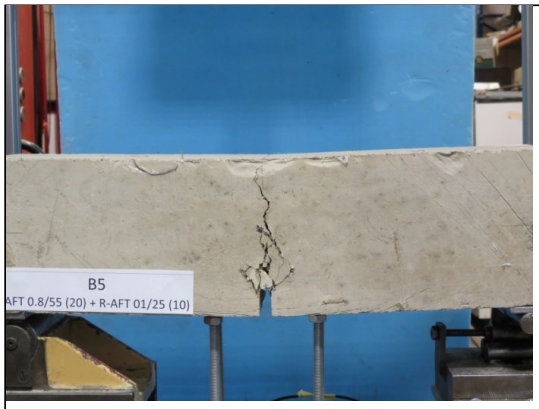

Bottom face of cast concrete

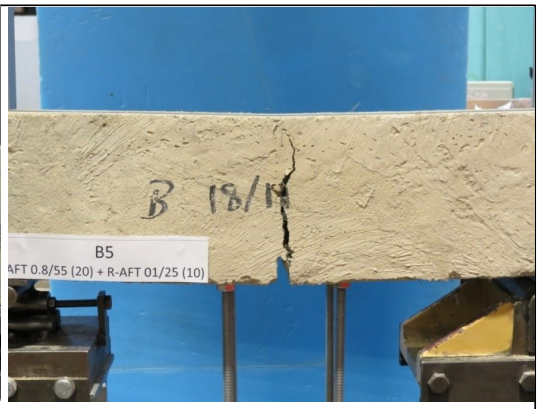

Top face of cast concrete

Crack zone of bottom face

Crack zone of top face

Stress-deformation graphs

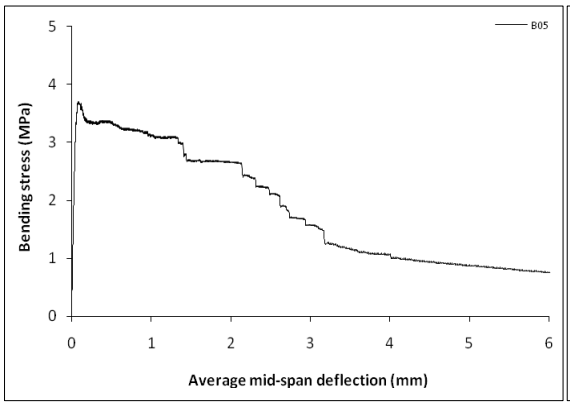

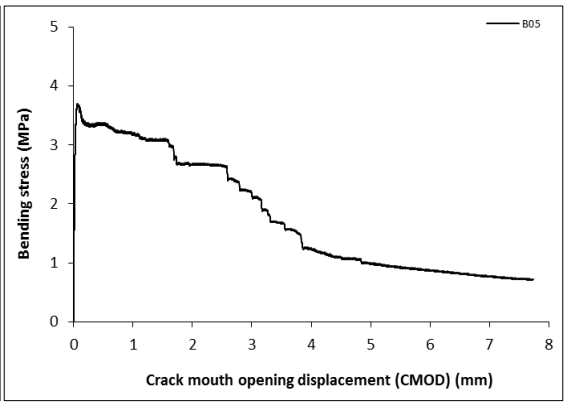

Specimen code name:		B6			
Notched Depth d_n	126	mm			
Depth, d	151	mm	Span, L	500	mm
Width, b	150	mm	Flexural strength	3.82	MPa

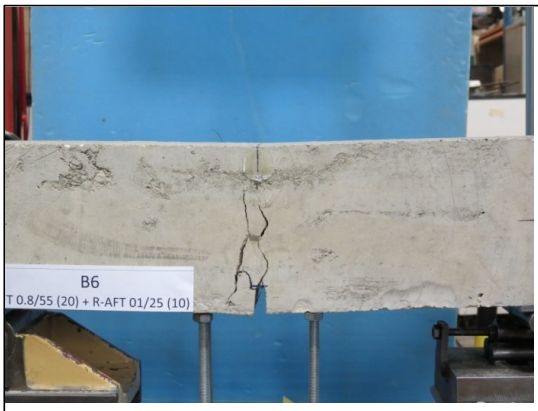

Bottom face of cast concrete

Top face of cast concrete

Crack zone of bottom face

Crack zone of top face

Stress-deformation graphs

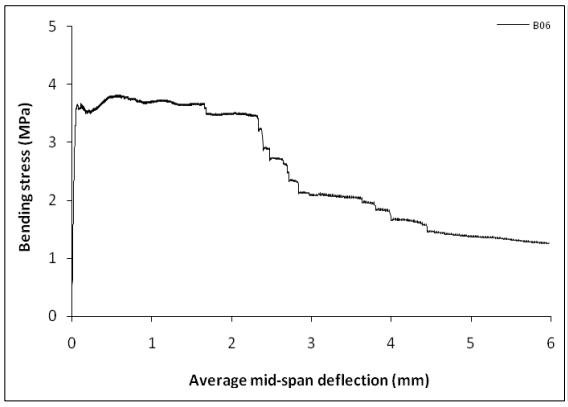

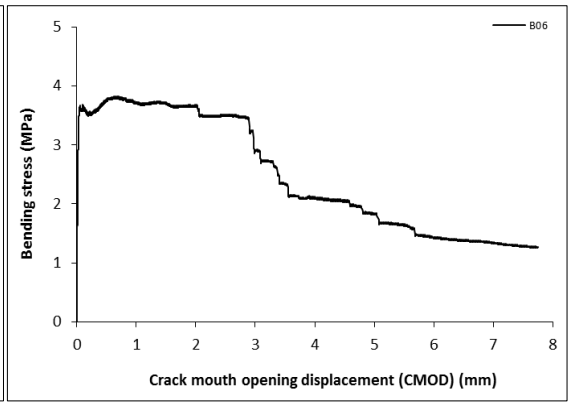

Specimen code name:		B7			
Notched Depth d_n	125	mm			
Depth, d	149	mm	Span, L	500	mm
Width, b	156	mm	Flexural strength	4.21	MPa

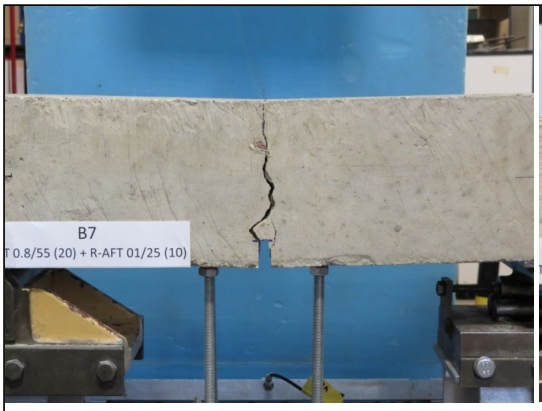

Bottom face of cast concrete

Top face of cast concrete

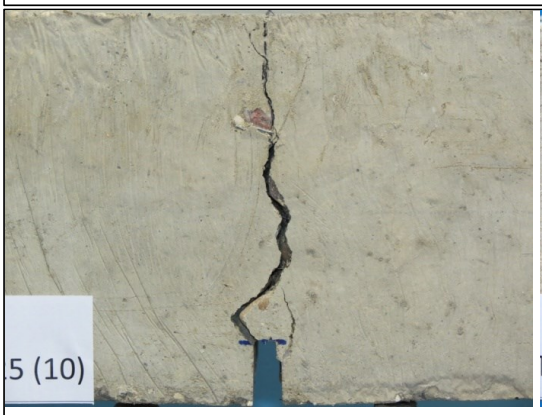

Crack zone of bottom face

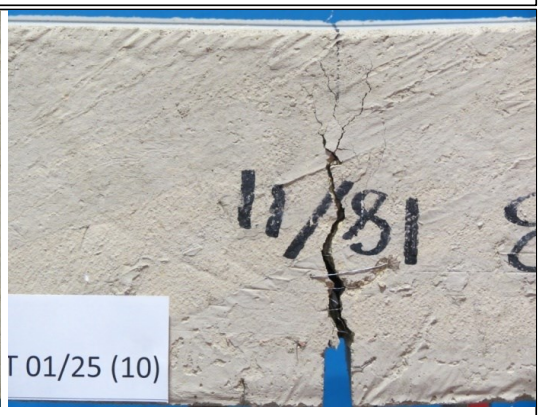

Crack zone of top face

Stress-deformation graphs

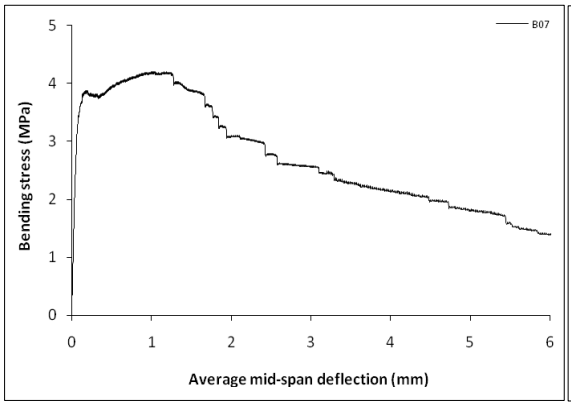

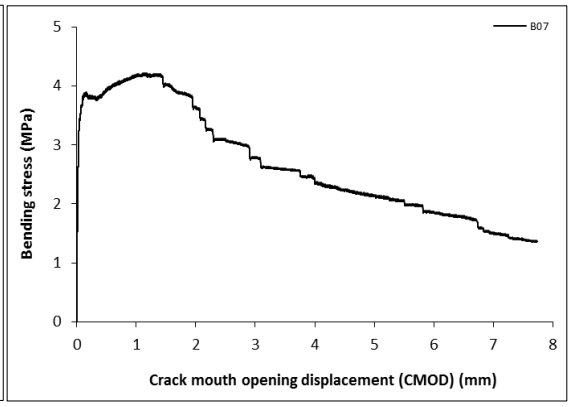

Specimen code name:		B8			
Notched Depth d_n	124	mm			
Depth, d	149	mm	Span, L	500	mm
Width, b	155	mm	Flexural strength	4.23	MPa

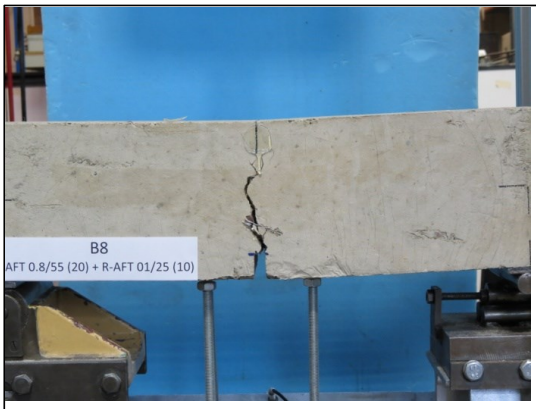

Bottom face of cast concrete

Top face of cast concrete

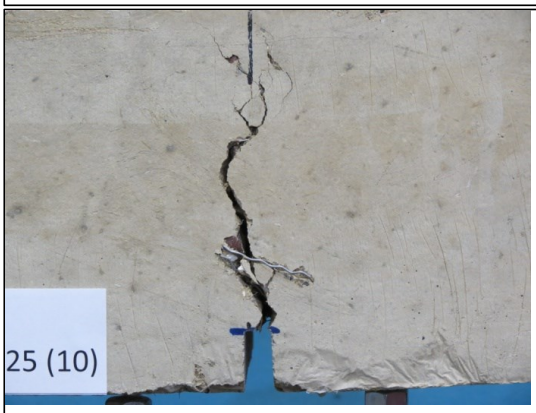

Crack zone of bottom face

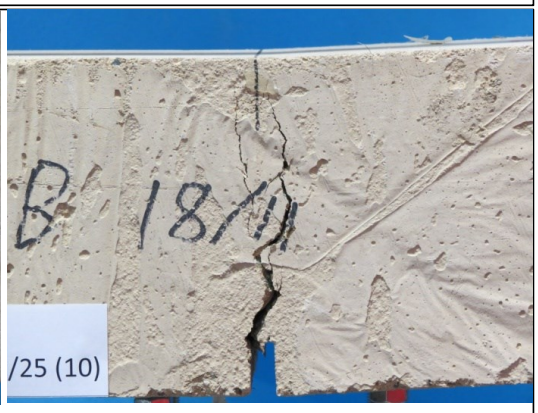

Crack zone of top face

Stress-deformation graphs

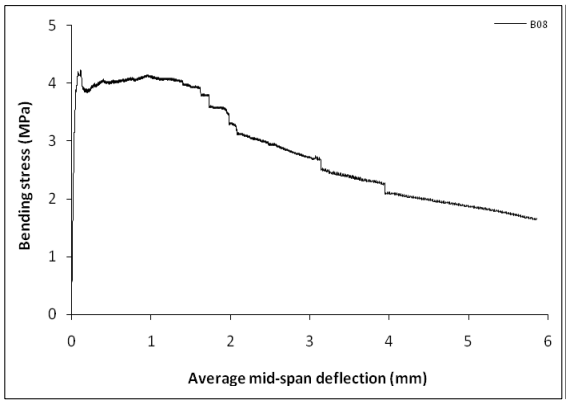

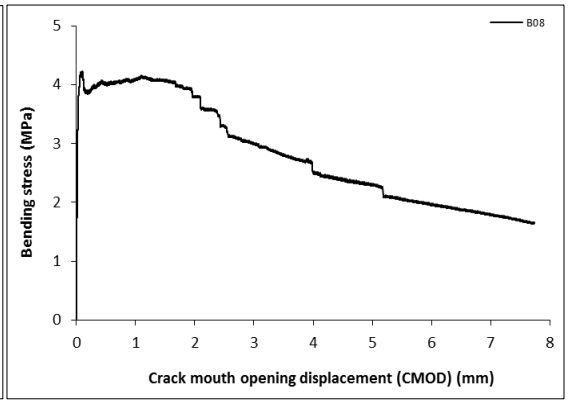

Specimen code name:		B9			
Notched Depth d_n	124	mm			
Depth, d	158	mm	Span, L	500	mm
Width, b	155	mm	Flexural strength	4.09	MPa

Bottom face of cast concrete

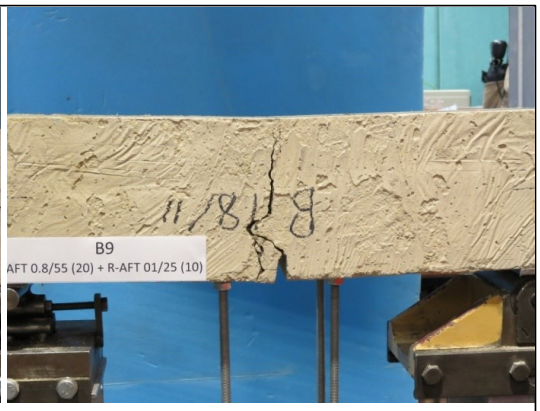

Top face of cast concrete

Crack zone of bottom face

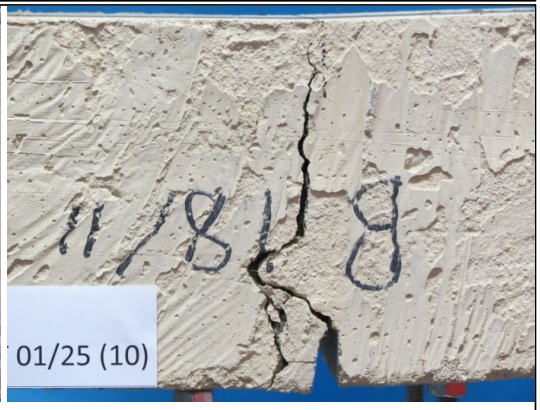

Crack zone of top face

Stress-deformation graphs

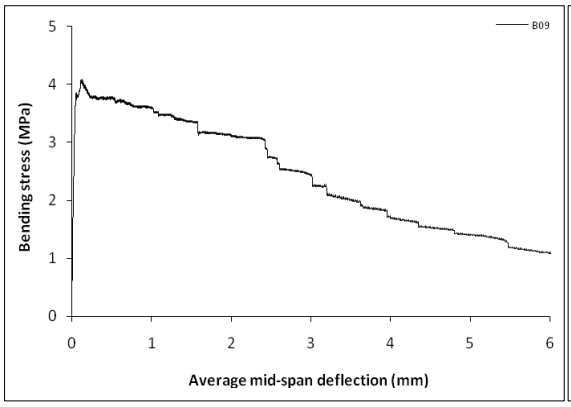

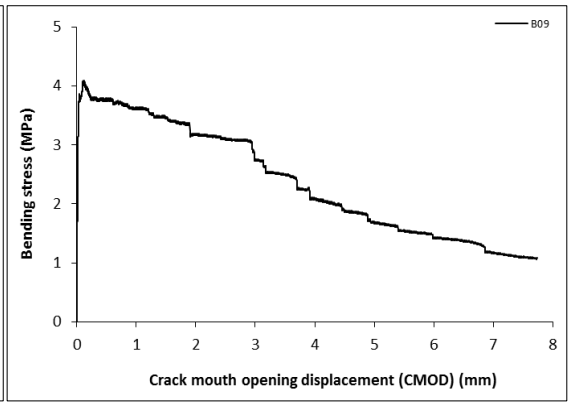

Specimen code name:		B10			
Notched Depth d_n	126	mm			
Depth, d	150	mm	Span, L	500	mm
Width, b	155	mm	Flexural strength	4.17	MPa

Bottom face of cast concrete

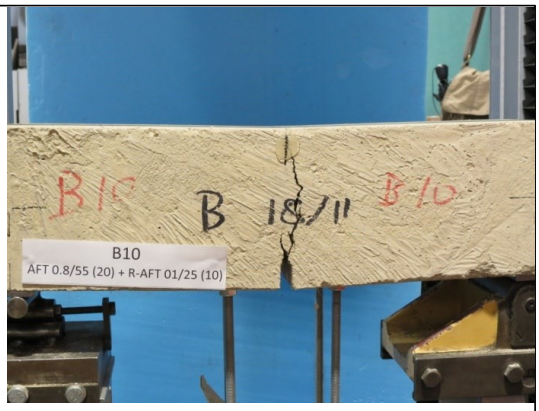

Top face of cast concrete

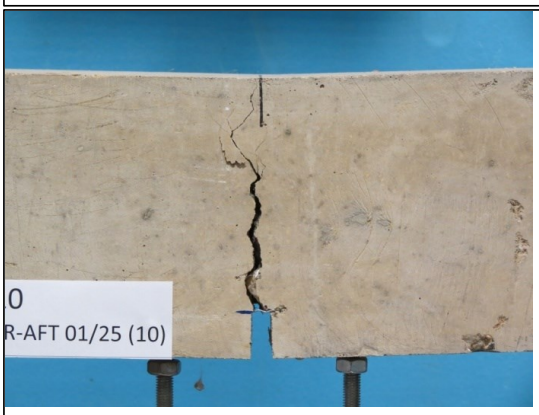

Crack zone of bottom face

Crack zone of top face

Stress-deformation graphs

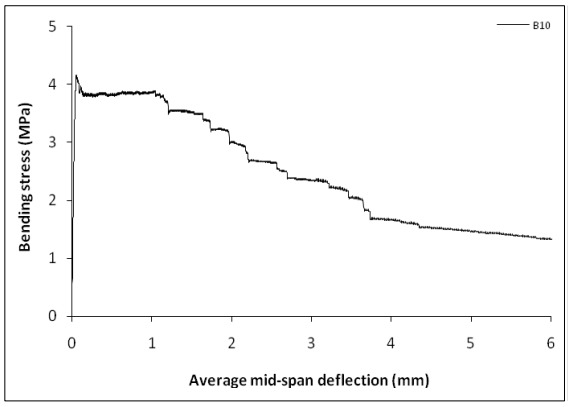

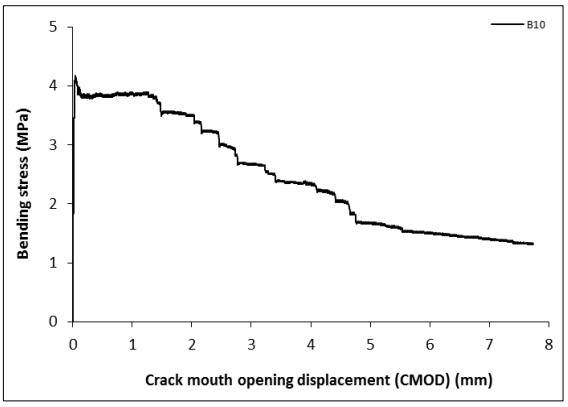

Specimen code name:		B11			
Notched Depth d_n	125	mm			
Depth, d	150	mm	Span, L	500	mm
Width, b	156	mm	Flexural strength	4.36	MPa

Bottom face of cast concrete

Top face of cast concrete

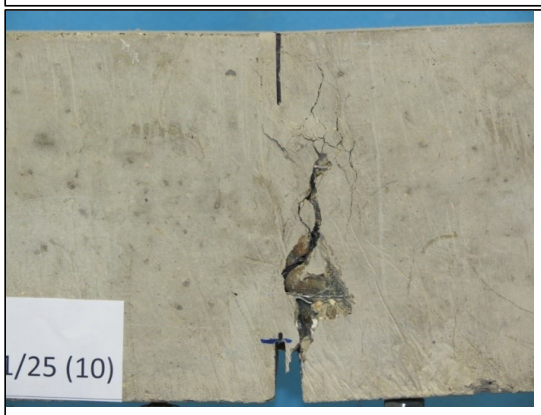

Crack zone of bottom face

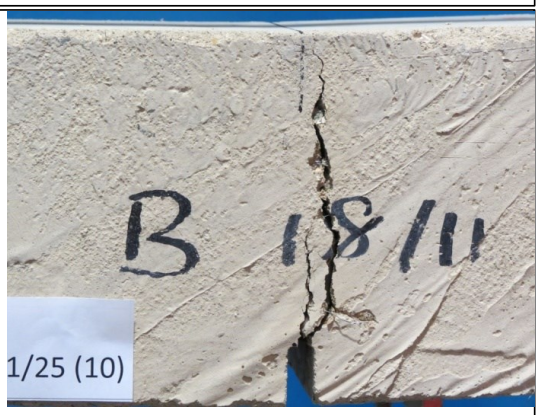

Crack zone of top face

Stress-deformation graphs

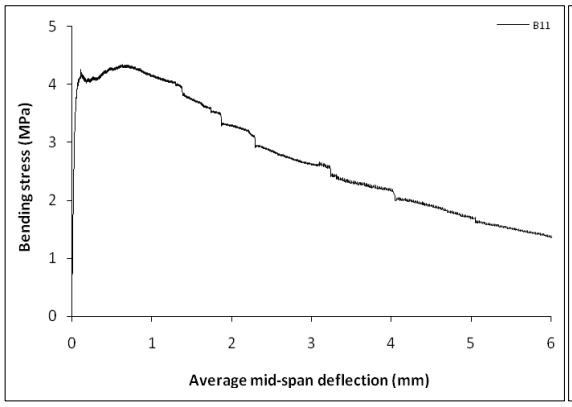

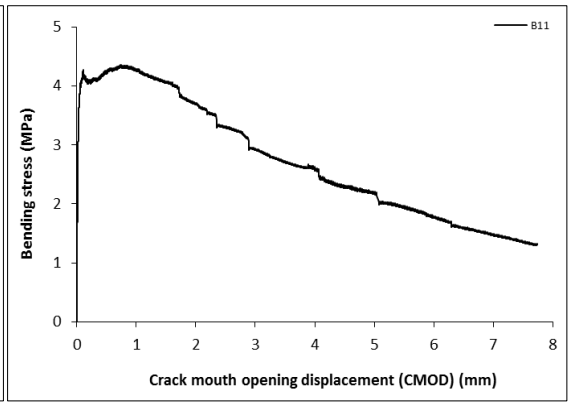

Specimen code name:		B12			
Notched Depth d_n	126	mm			
Depth, d	151	mm	Span, L	500	mm
Width, b	153	mm	Flexural strength	3.77	MPa

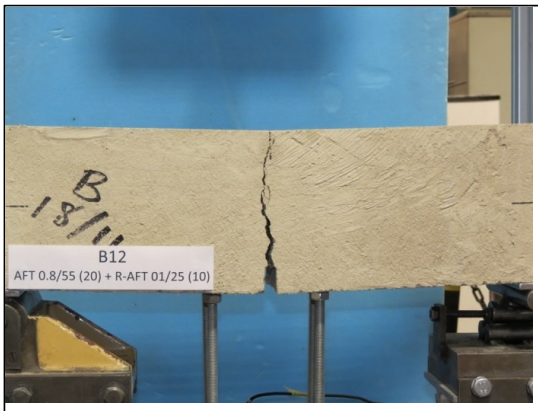

Bottom face of cast concrete

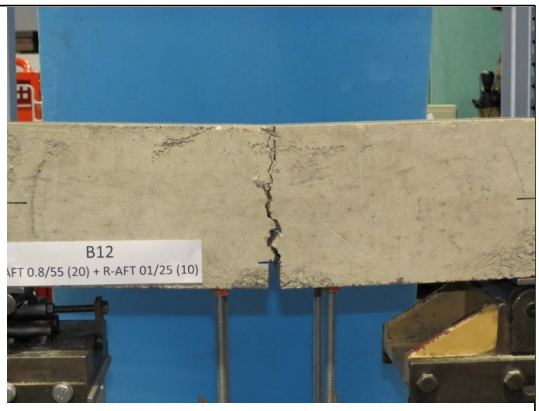

Top face of cast concrete

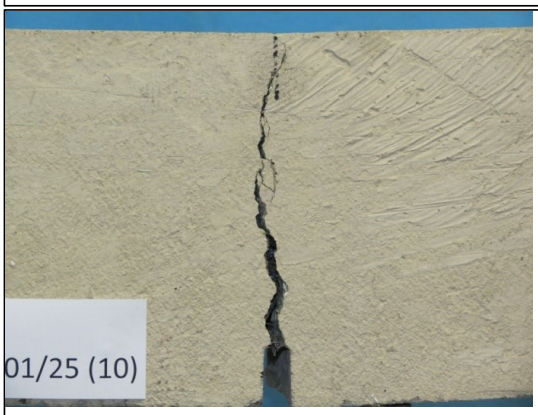

Crack zone of bottom face

Crack zone of top face

Stress-deformation graphs

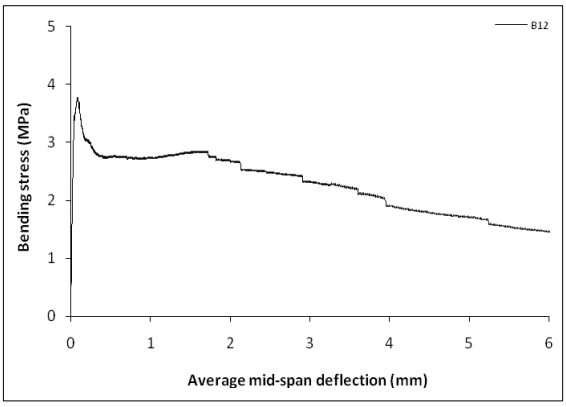

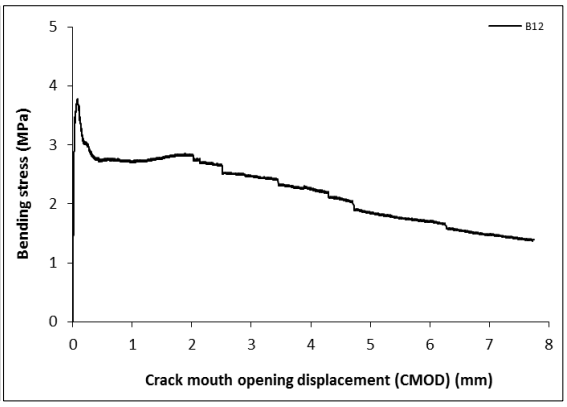

Mix:	B		
Notched Depth d_n	mm		
Depth, d	mm	Span, L	mm
Width, b	mm	Flexural strength	MPa

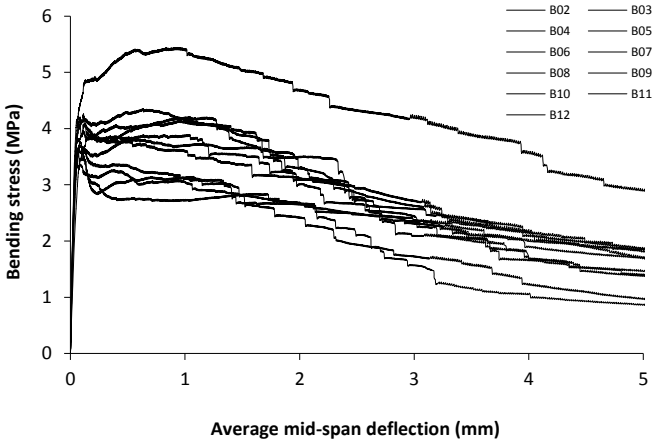

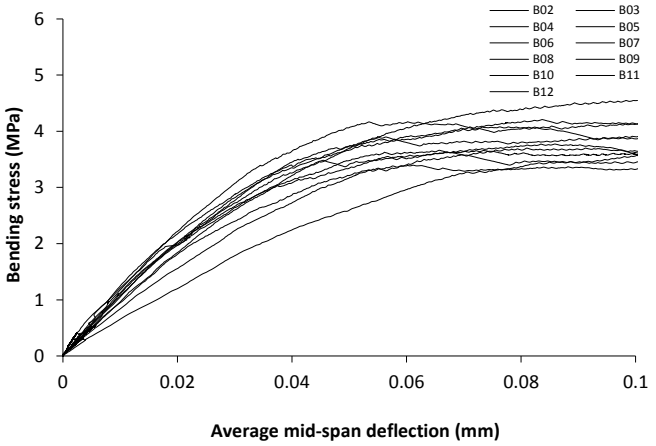

Specimen code name:		C1			
Notched Depth d_n	125	mm			
Depth, d	150	mm	Span, L	500	mm
Width, b	153	mm	Flexural strength	3.58	MPa

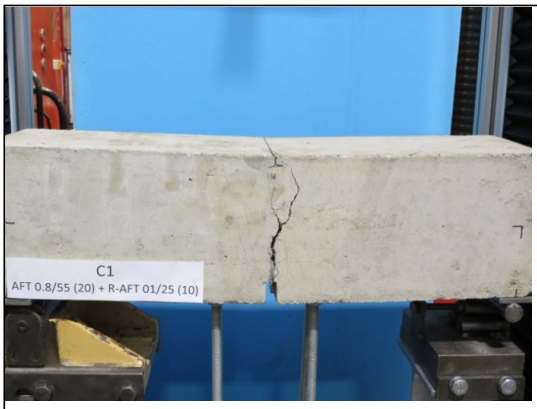

Bottom face of cast concrete

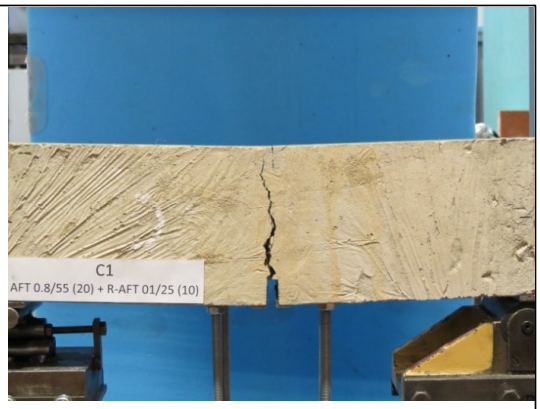

Top face of cast concrete

Crack zone of bottom face

Crack zone of top face

Stress-deformation graphs

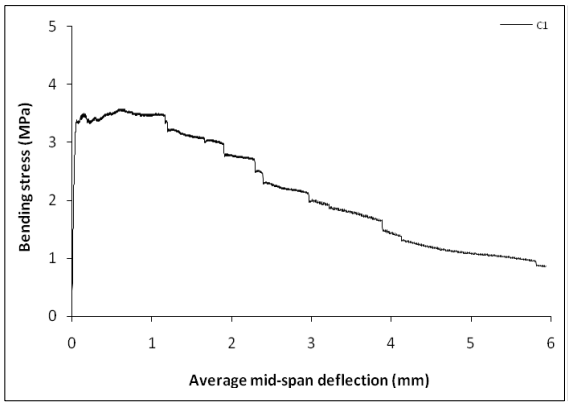

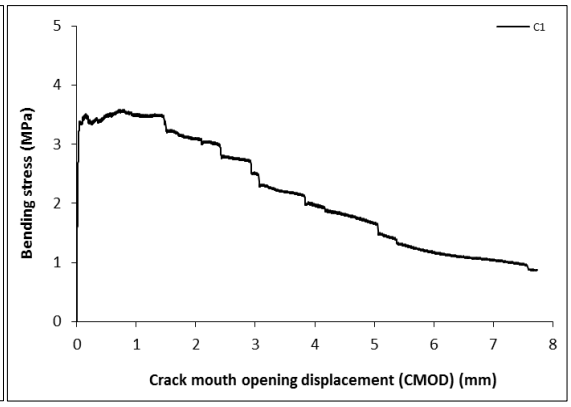

Specimen code name:		C2			
Notched Depth d_n	125	mm			
Depth, d	150	mm	Span, L	500	mm
Width, b	153	mm	Flexural strength	3.78	MPa

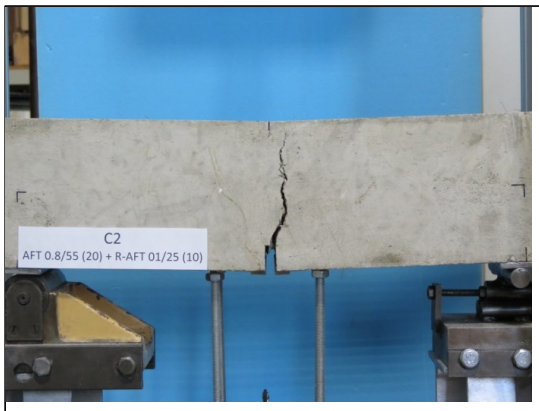

Bottom face of cast concrete

Top face of cast concrete

Crack zone of bottom face

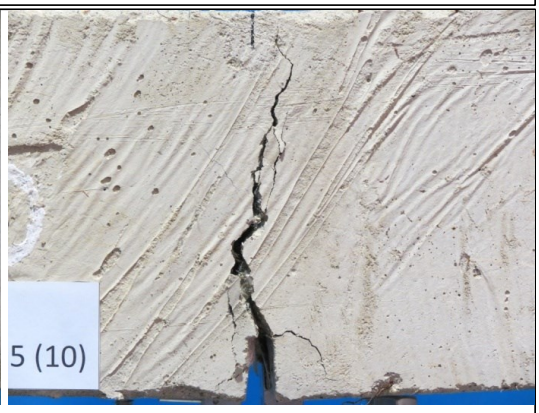

Crack zone of top face

Stress-deformation graphs

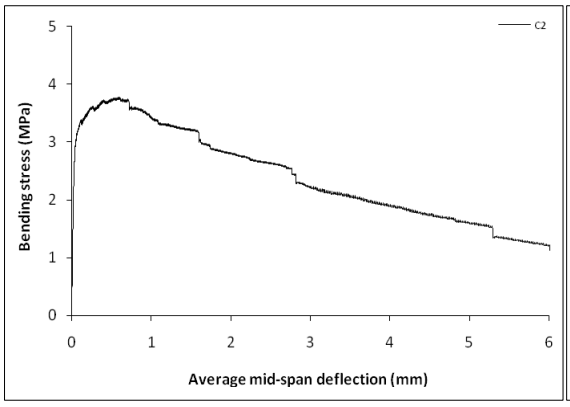

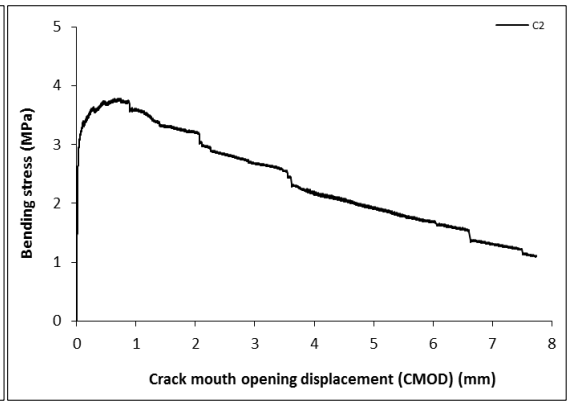

Specimen code name:		C3			
Notched Depth d_n	125	mm			
Depth, d	150	mm	Span, L	500	mm
Width, b	152	mm	Flexural strength	3.30	MPa

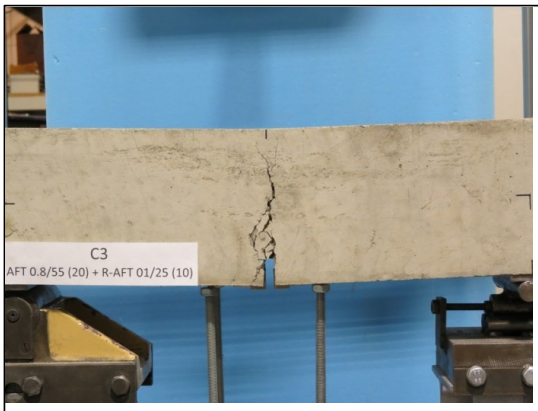

Bottom face of cast concrete

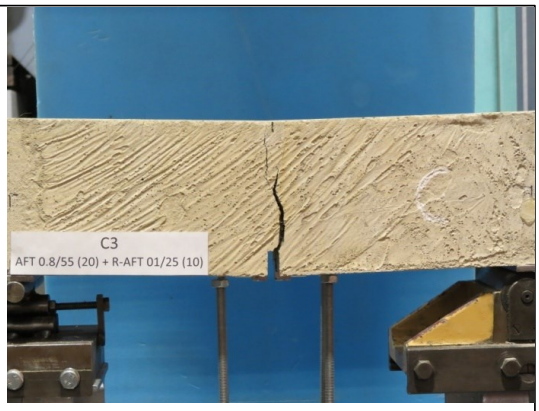

Top face of cast concrete

Crack zone of bottom face

Crack zone of top face

Stress-deformation graphs

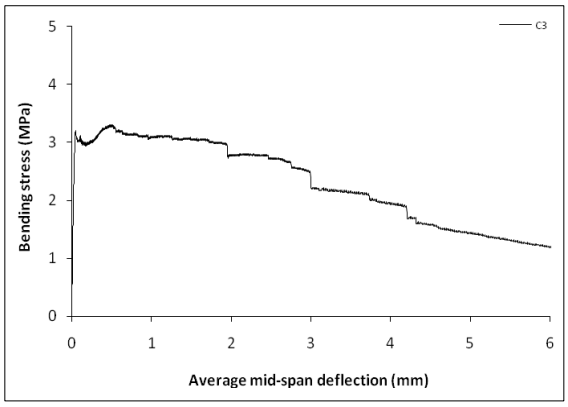

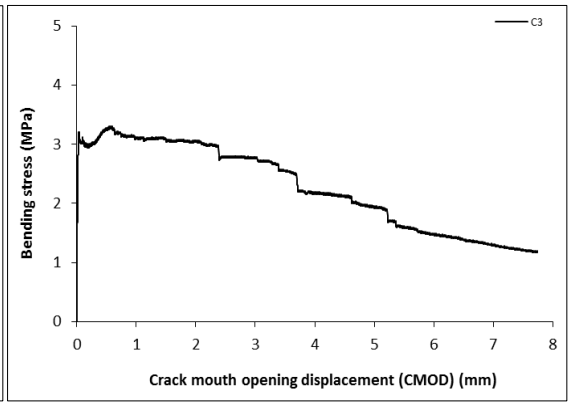

Specimen code name:		C4			
Notched Depth d_n	125	mm			
Depth, d	150	mm	Span, L	500	mm
Width, b	147	mm	Flexural strength	3.30	MPa

Bottom face of cast concrete

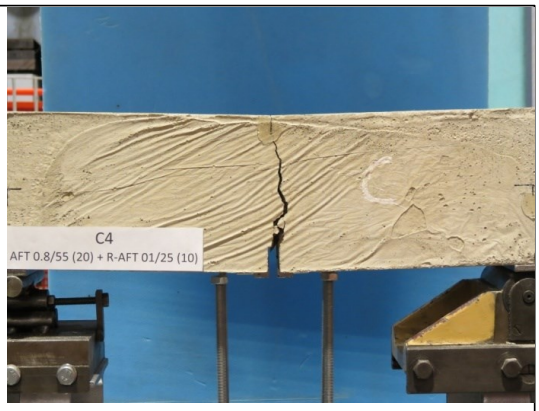

Top face of cast concrete

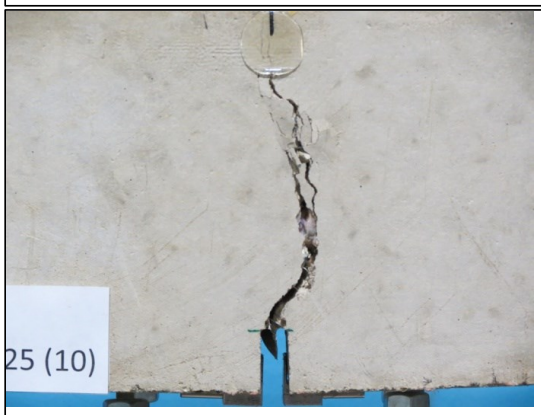

Crack zone of bottom face

Crack zone of top face

Stress-deformation graphs

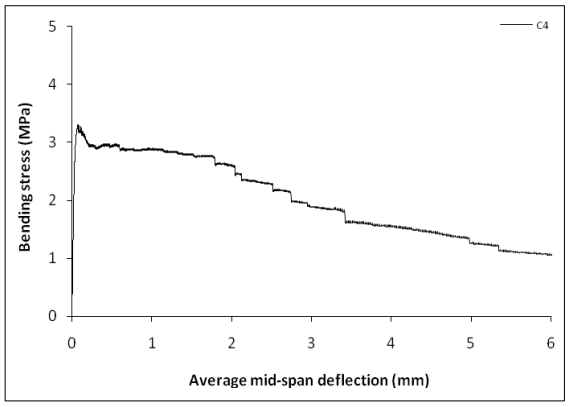

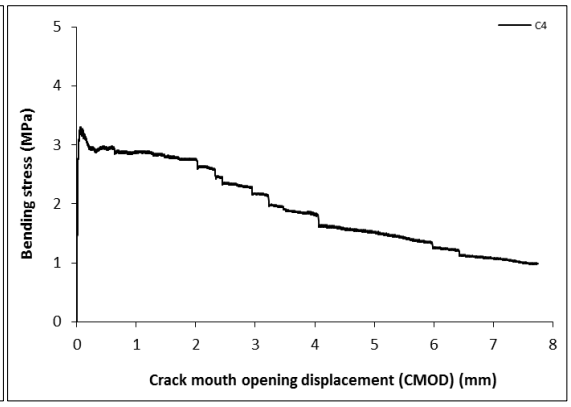

Specimen code name:		C5			
Notched Depth d_n	126	mm			
Depth, d	151	mm	Span, L	500	mm
Width, b	154	mm	Flexural strength	3.76	MPa

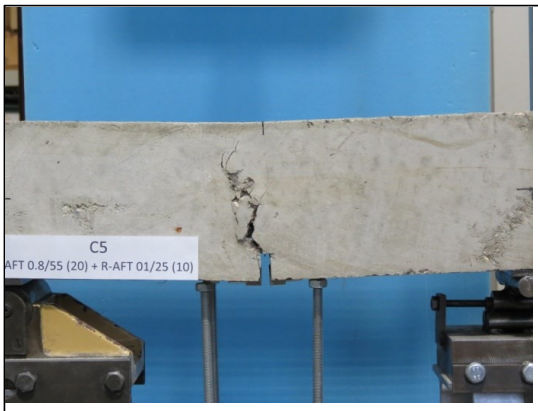

Bottom face of cast concrete

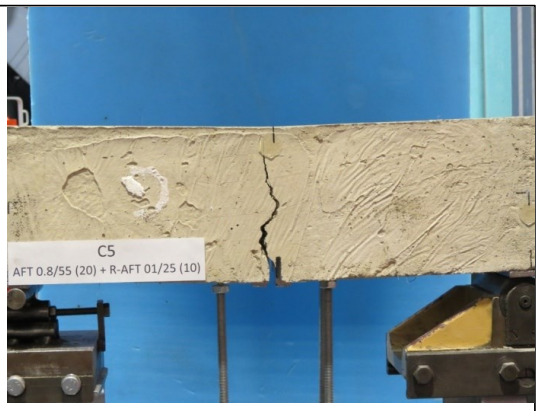

Top face of cast concrete

Crack zone of bottom face

Crack zone of top face

Stress-deformation graphs

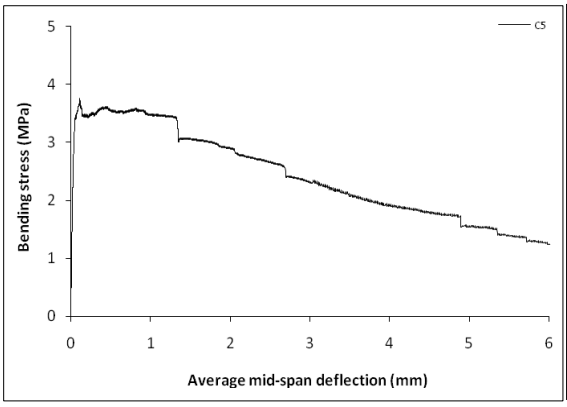

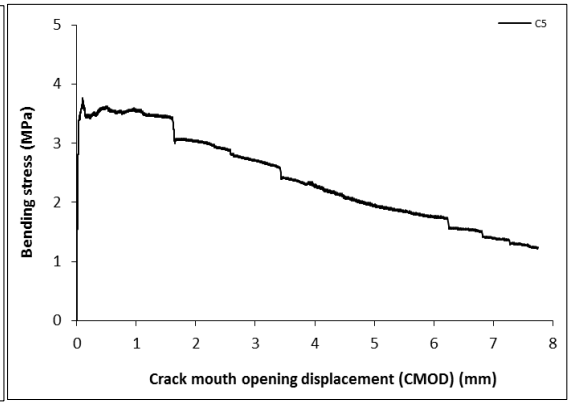

Specimen code name:		C6			
Notched Depth d_n	125	mm			
Depth, d	150	mm	Span, L	500	mm
Width, b	151	mm	Flexural strength	3.67	MPa

Bottom face of cast concrete

Top face of cast concrete

Crack zone of bottom face

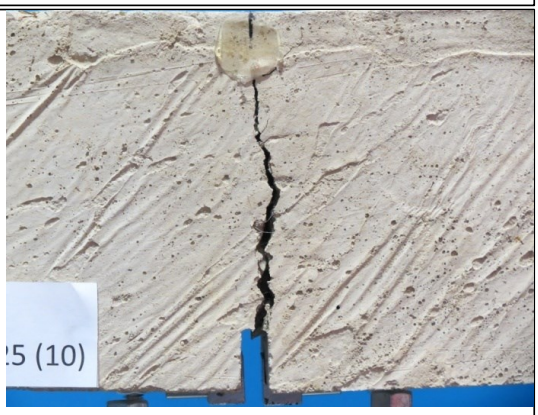

Crack zone of top face

Stress-deformation graphs

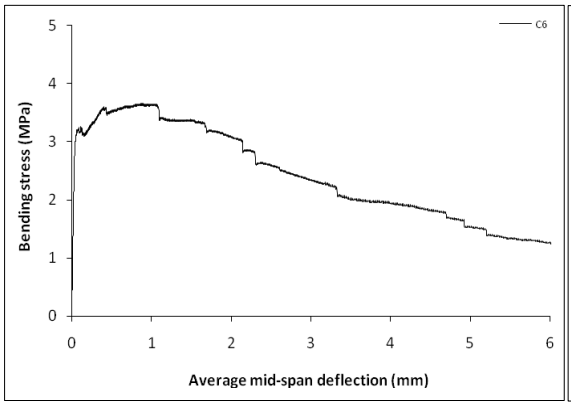

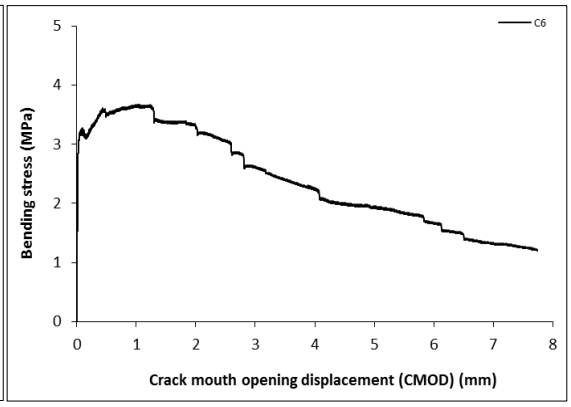

Mix:	C		
Notched Depth d_n	mm		
Depth, d	mm	Span, L	mm
Width, b	mm	Flexural strength	MPa

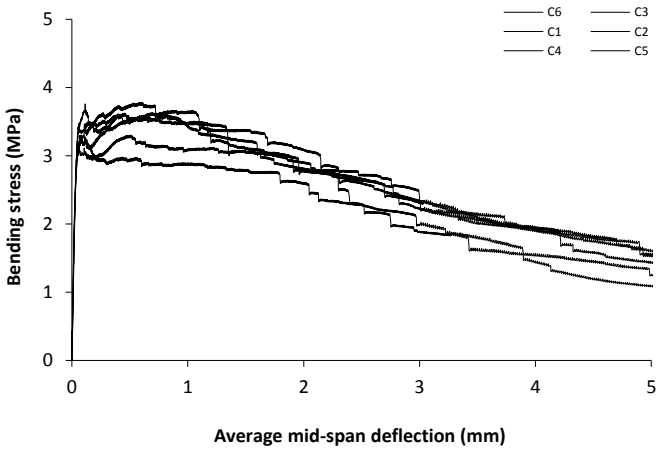

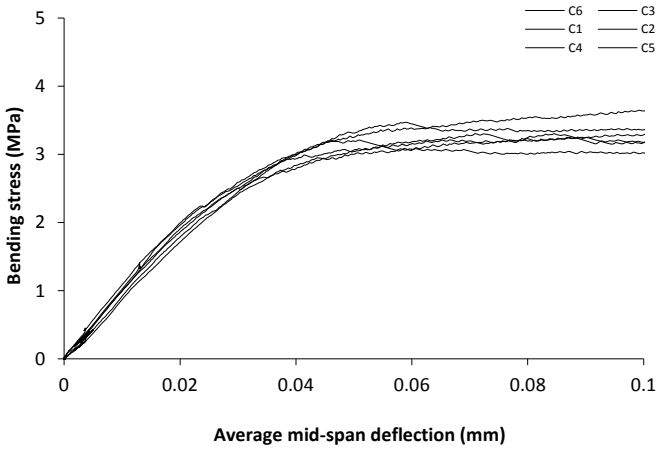

Specimen code name:		D1			
Notched Depth d_n	125	mm			
Depth, d	150	mm	Span, L	500	mm
Width, b	151	mm	Flexural strength	3.43	MPa

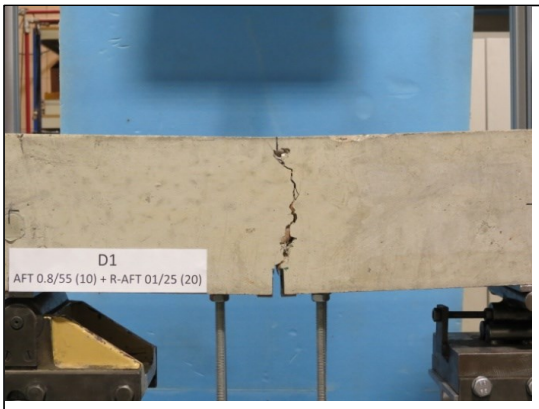

Bottom face of cast concrete

Top face of cast concrete

Crack zone of bottom face

Crack zone of top face

Stress-deformation graphs

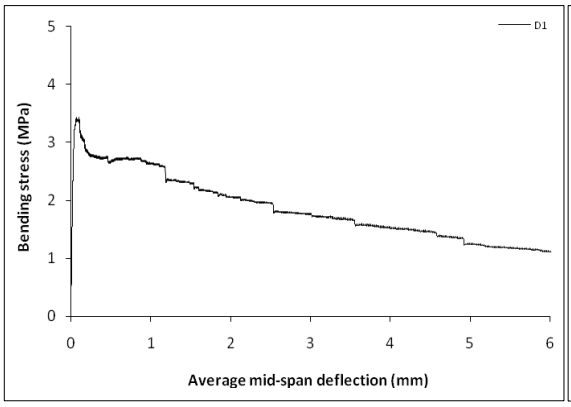

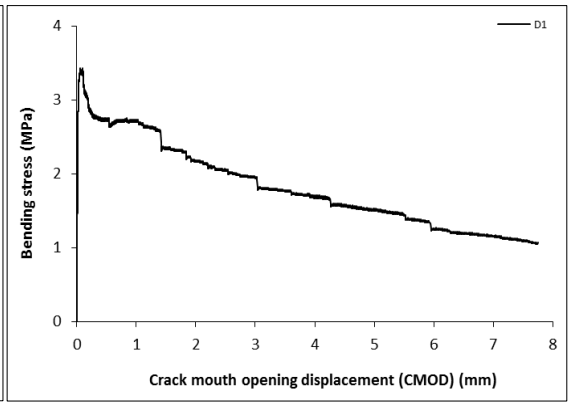

Specimen code name:		D2			
Notched Depth d_n	125	mm			
Depth, d	150	mm	Span, L	500	mm
Width, b	151	mm	Flexural strength	3.39	MPa

Bottom face of cast concrete

Top face of cast concrete

Crack zone of bottom face

Crack zone of top face

Stress-deformation graphs

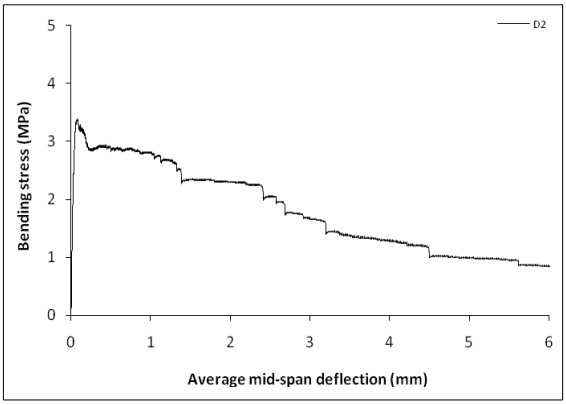

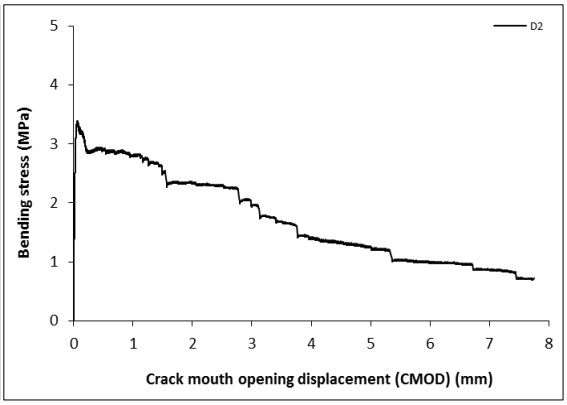

Specimen code name:		D3			
Notched Depth d_n	125	mm			
Depth, d	150	mm	Span, L	500	mm
Width, b	151	mm	Flexural strength	3.32	MPa

Bottom face of cast concrete

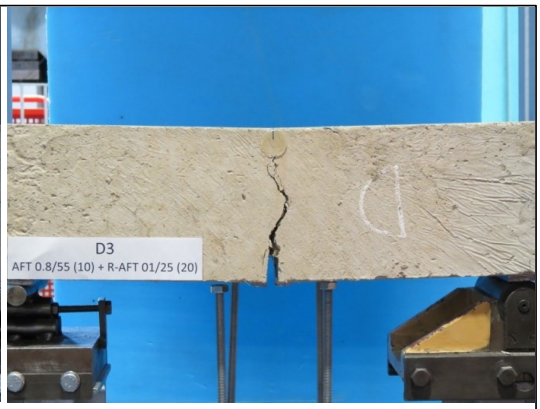

Top face of cast concrete

Crack zone of bottom face

Crack zone of top face

Stress-deformation graphs

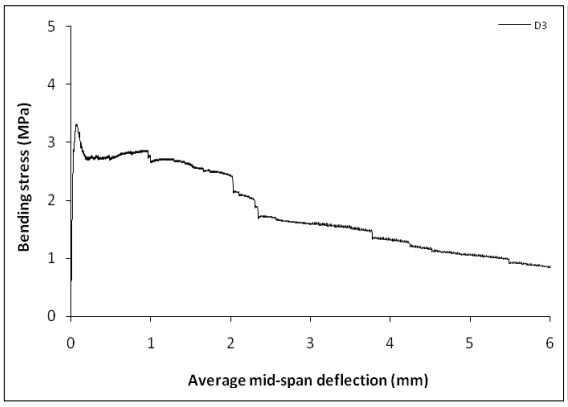

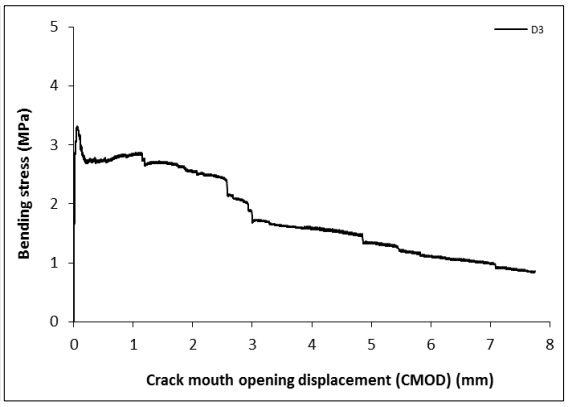

Specimen code name:		D4			
Notched Depth d_n	123	mm			
Depth, d	150	mm	Span, L	500	mm
Width, b	152	mm	Flexural strength	3.37	MPa

Bottom face of cast concrete

Top face of cast concrete

Crack zone of bottom face

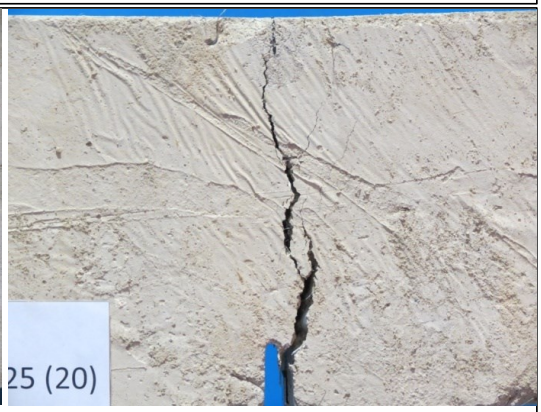

Crack zone of top face

Stress-deformation graphs

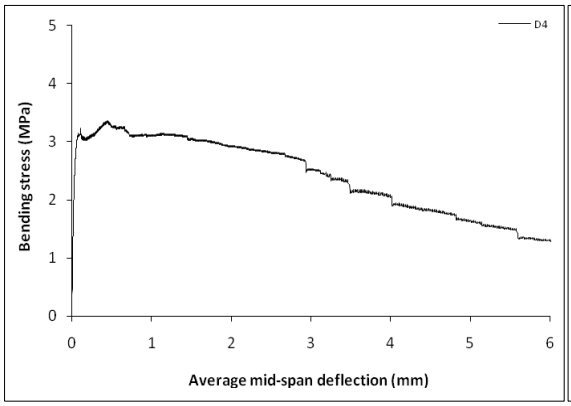

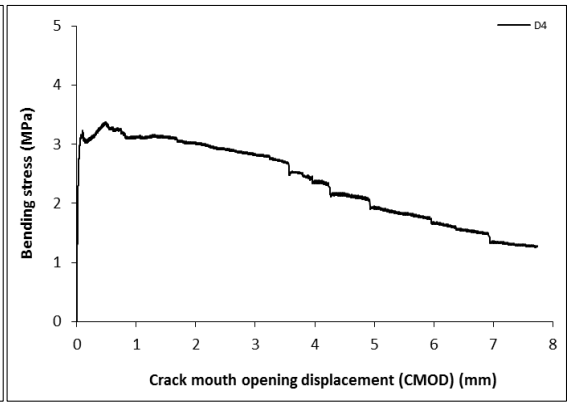

Specimen code name:		D6			
Notched Depth d_n	125	mm			
Depth, d	150	mm	Span, L	500	mm
Width, b	151	mm	Flexural strength	3.48	MPa

Bottom face of cast concrete

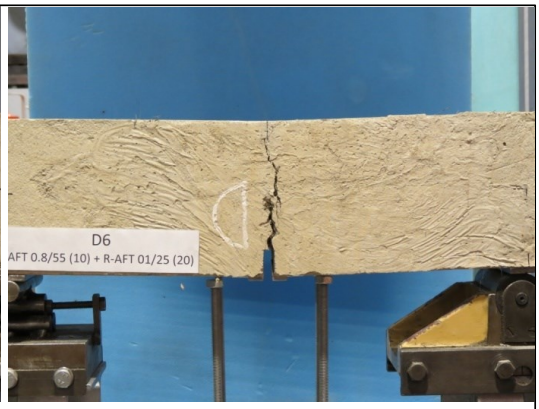

Top face of cast concrete

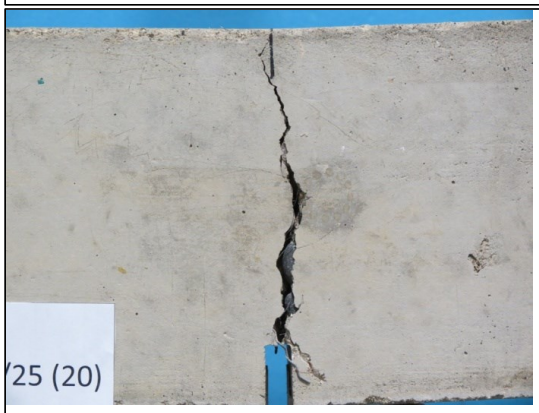

Crack zone of bottom face

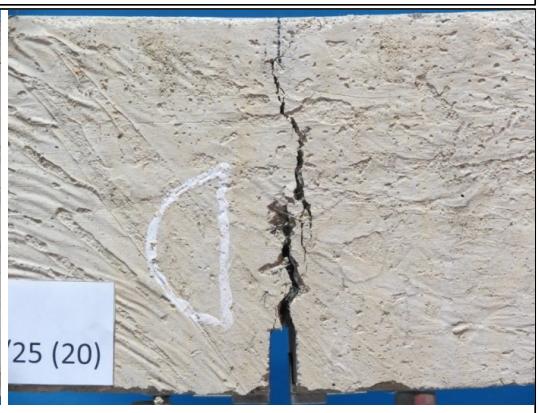

Crack zone of top face

Stress-deformation graphs

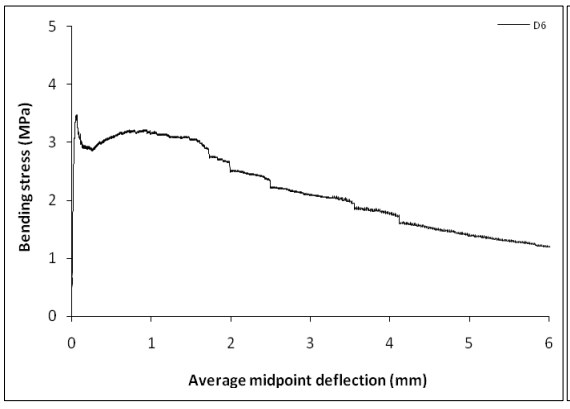

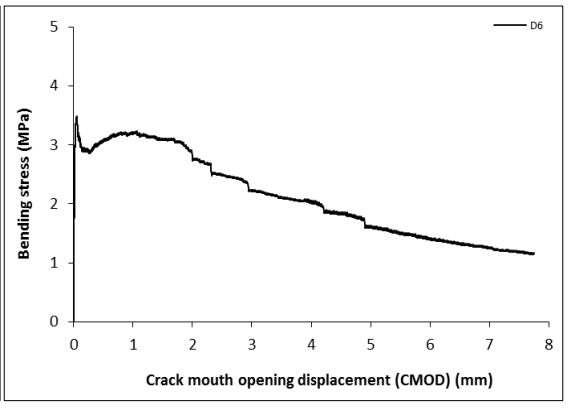

Mix:	D		
Notched Depth d_n	mm		
Depth, d	mm	Span, L	mm
Width, b	mm	Flexural strength	MPa

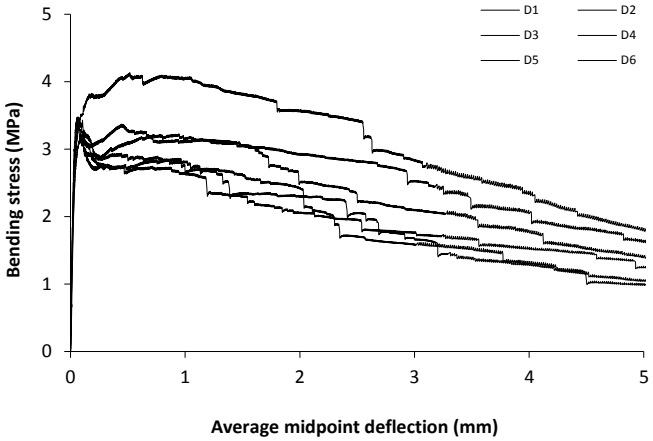

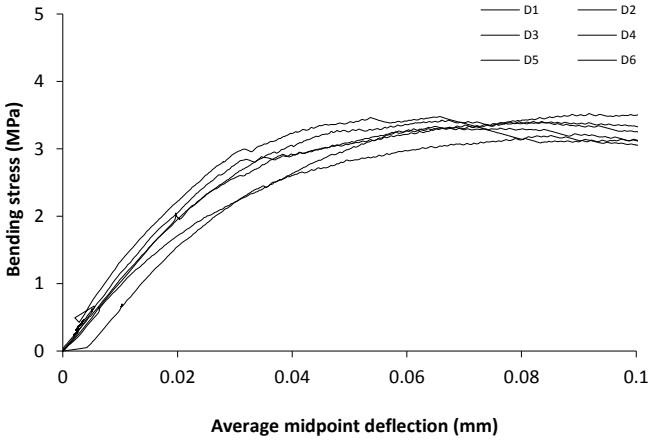

Specimen code name:		E1			
Notched Depth d_n	127	mm			
Depth, d	151	mm	Span, L	500	mm
Width, b	155	mm	Flexural strength	3.81	MPa

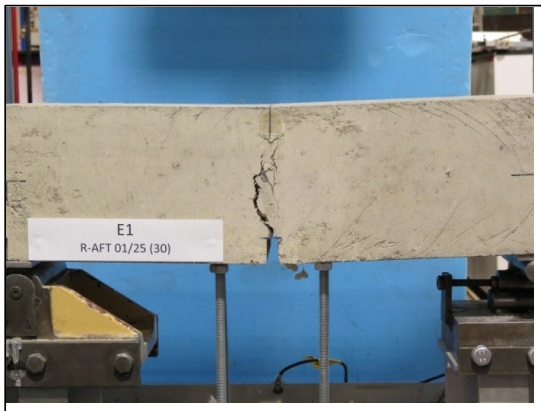

Bottom face of cast concrete

Top face of cast concrete

Crack zone of bottom face

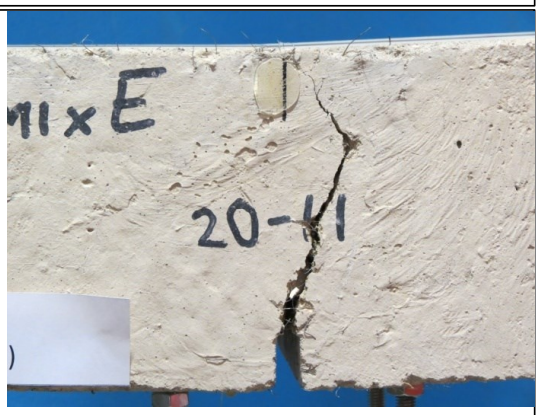

Crack zone of top face

Stress-deformation graphs

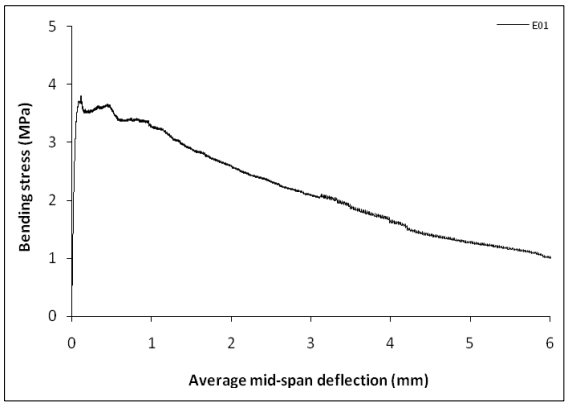

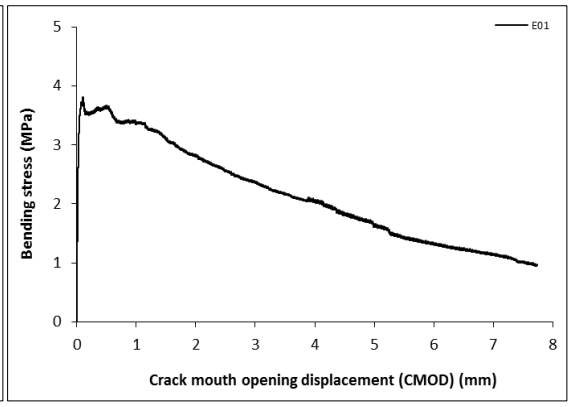

Specimen code name:		E2			
Notched Depth d_n	126	mm			
Depth, d	150	mm	Span, L	500	mm
Width, b	151	mm	Flexural strength	3.86	MPa

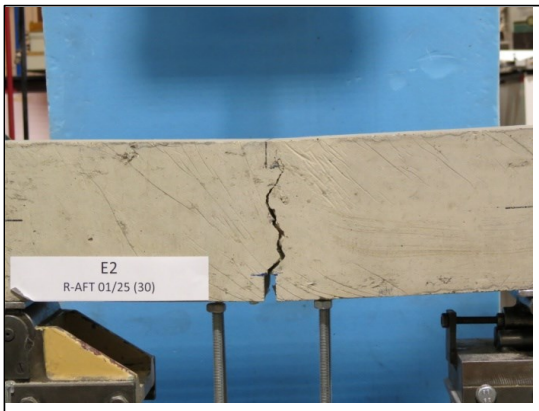

Bottom face of cast concrete

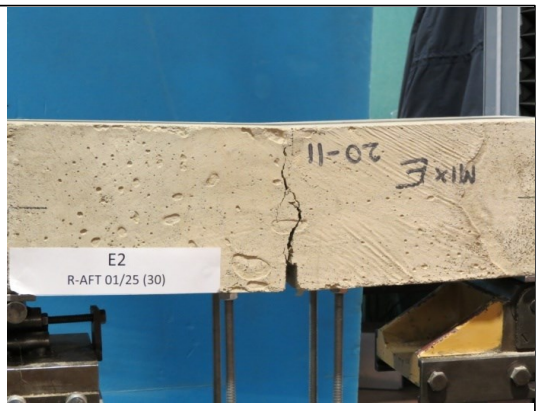

Top face of cast concrete

Crack zone of bottom face

Crack zone of top face

Stress-deformation graphs

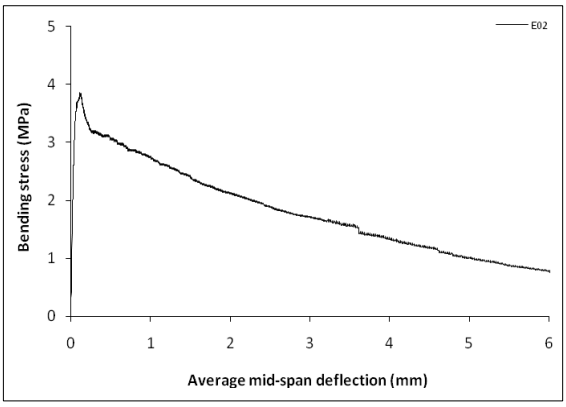

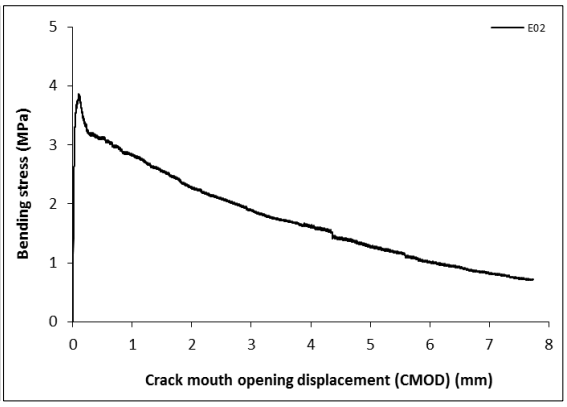

Specimen code name:		E3			
Notched Depth d_n	125	mm			
Depth, d	150	mm	Span, L	500	mm
Width, b	157	mm	Flexural strength	3.72	MPa

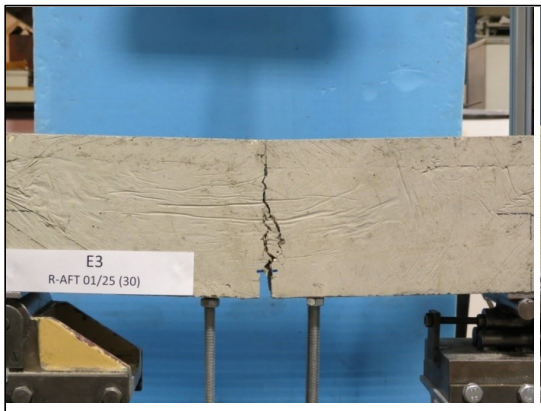

Bottom face of cast concrete

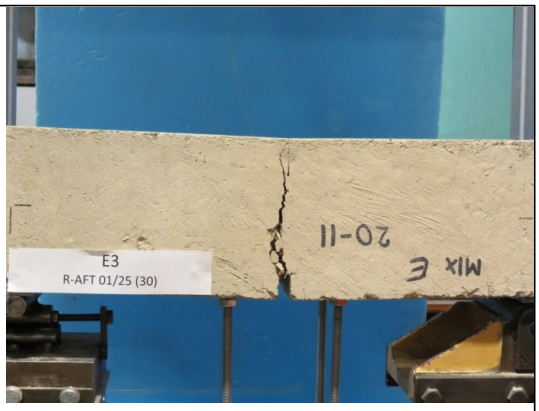

Top face of cast concrete

Crack zone of bottom face

Crack zone of top face

Stress-deformation graphs

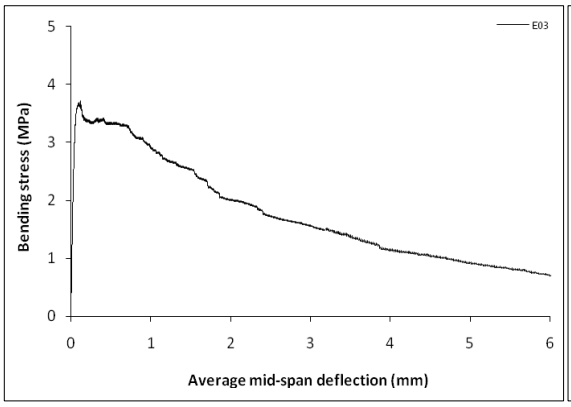

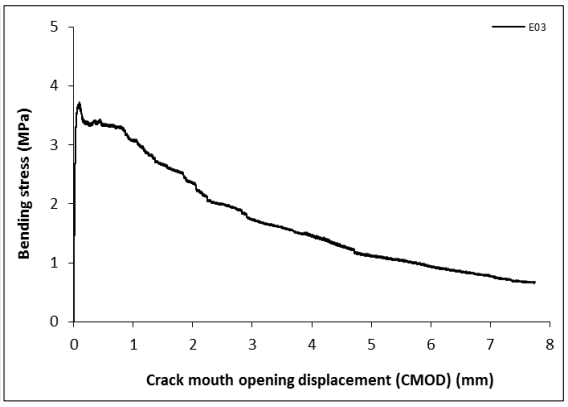

Specimen code name:		E4			
Notched Depth d_n	124	mm			
Depth, d	149	mm	Span, L	500	mm
Width, b	155	mm	Flexural strength	3.58	MPa

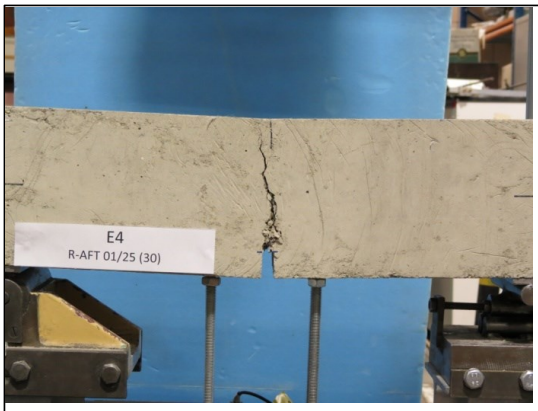

Bottom face of cast concrete

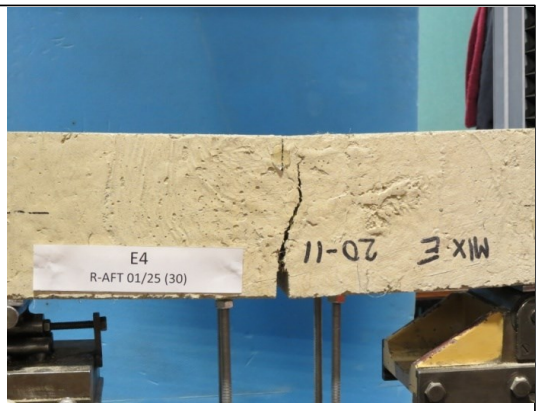

Top face of cast concrete

Crack zone of bottom face

Crack zone of top face

Stress-deformation graphs

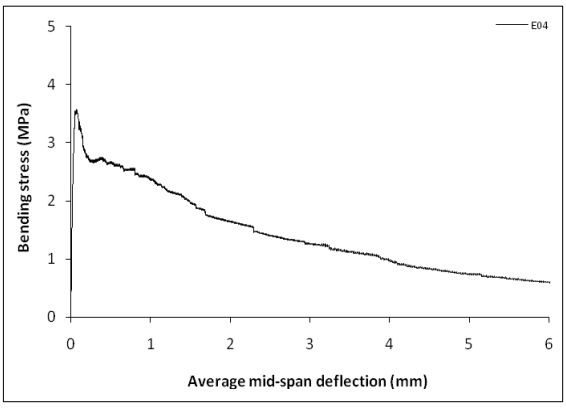

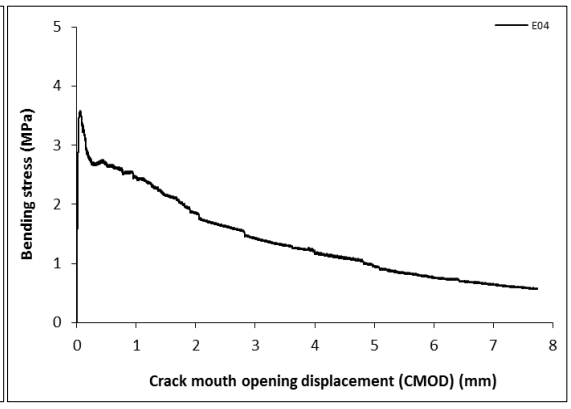

Specimen code name:		E5			
Notched Depth d_n	127	mm			
Depth, d	149	mm	Span, L	500	mm
Width, b	149	mm	Flexural strength	3.34	MPa

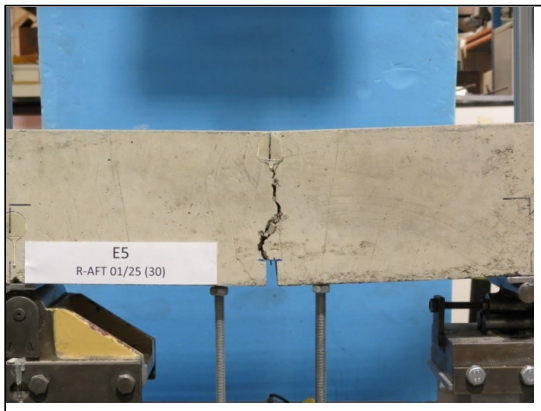

Bottom face of cast concrete

Top face of cast concrete

Crack zone of bottom face

Crack zone of top face

Stress-deformation graphs

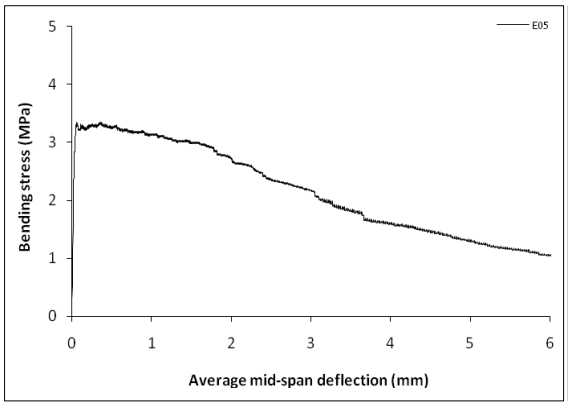

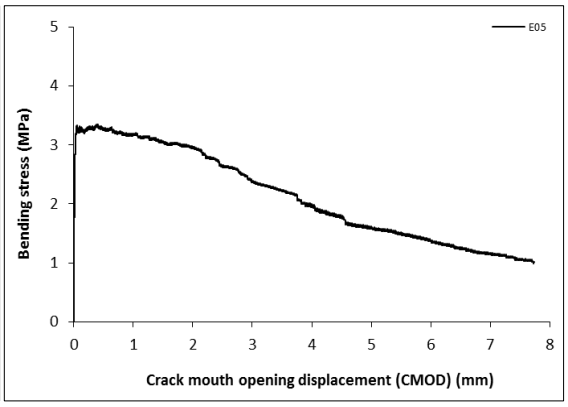

Specimen code name:		E6			
Notched Depth d_n	124	mm			
Depth, d	149	mm	Span, L	500	mm
Width, b	152	mm	Flexural strength	3.31	MPa

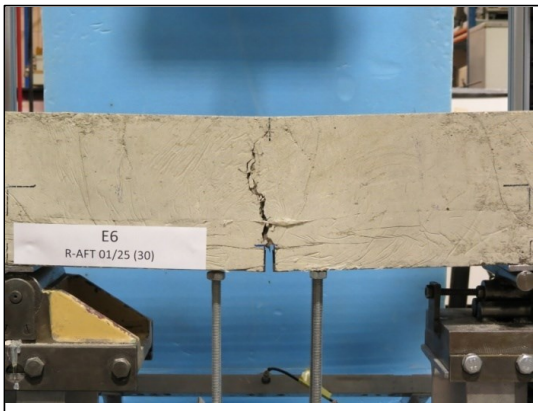

Bottom face of cast concrete

Top face of cast concrete

Crack zone of bottom face

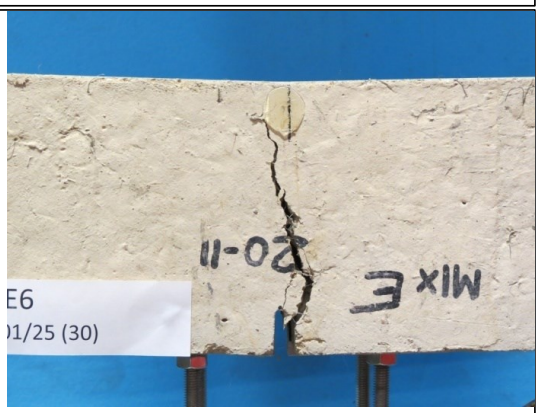

Crack zone of top face

Stress-deformation graphs

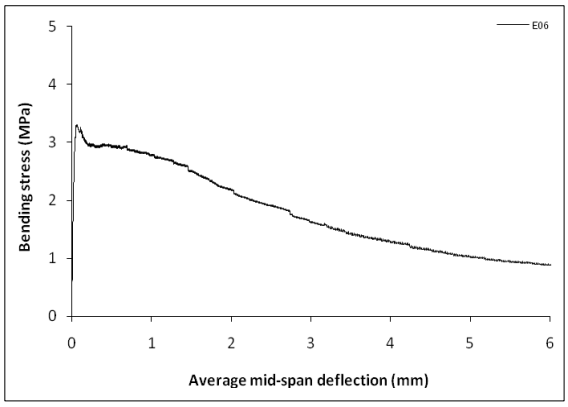

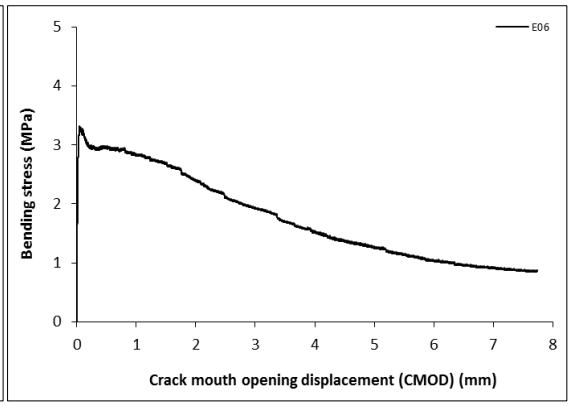

Mix:	E		
Notched Depth d_n	mm		
Depth, d	mm	Span, L	mm
Width, b	mm	Flexural strength	MPa

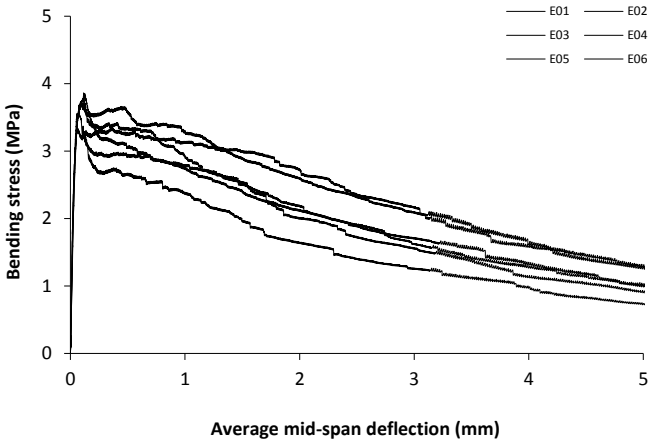

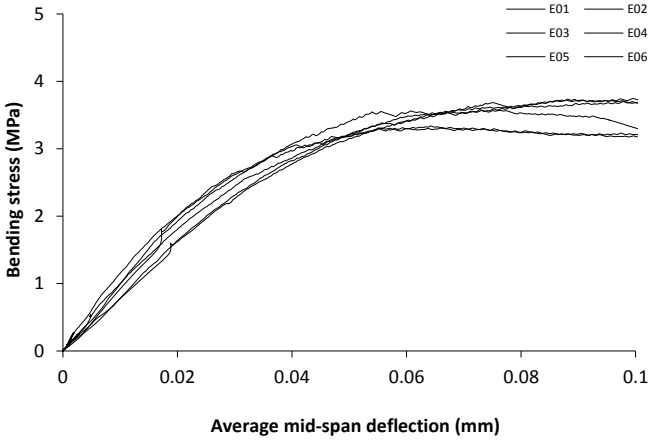

Specimen code name:		F1			
Notched Depth d_n	124	mm			
Depth, d	149	mm	Span, L	500	mm
Width, b	155	mm	Flexural strength	3.66	MPa

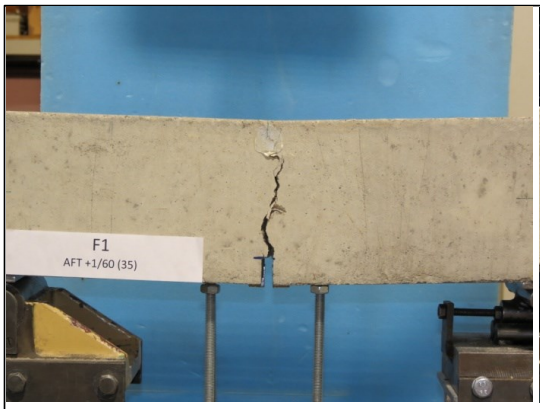

Bottom face of cast concrete

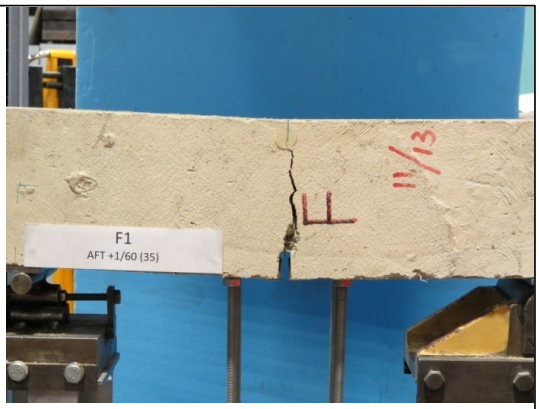

Top face of cast concrete

Crack zone of bottom face

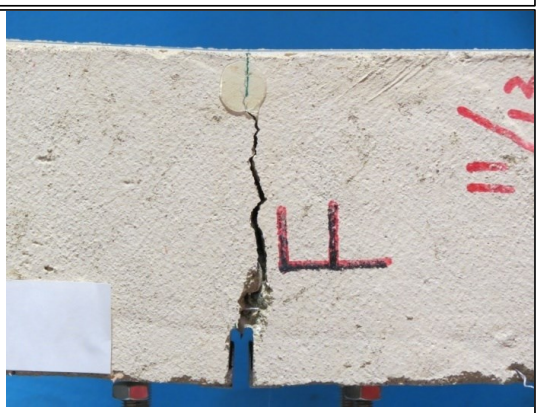

Crack zone of top face

Stress-deformation graphs

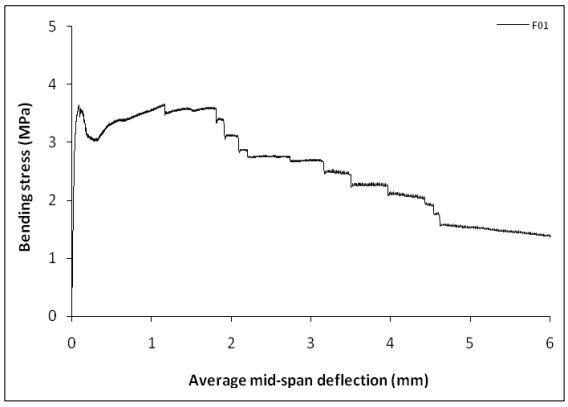

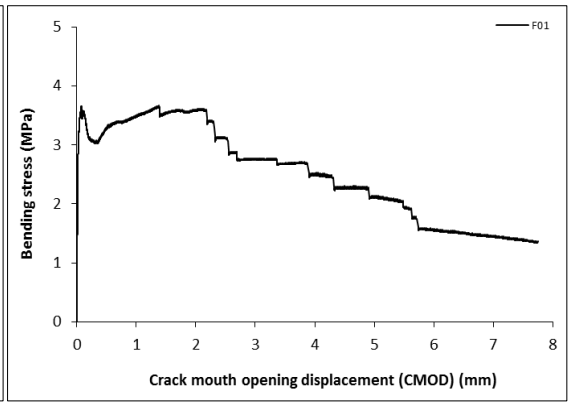

Specimen code name:		F2			
Notched Depth d_n	125	mm			
Depth, d	150	mm	Span, L	500	mm
Width, b	152	mm	Flexural strength	3.92	MPa

Bottom face of cast concrete

Top face of cast concrete

Crack zone of bottom face

Crack zone of top face

Stress-deformation graphs

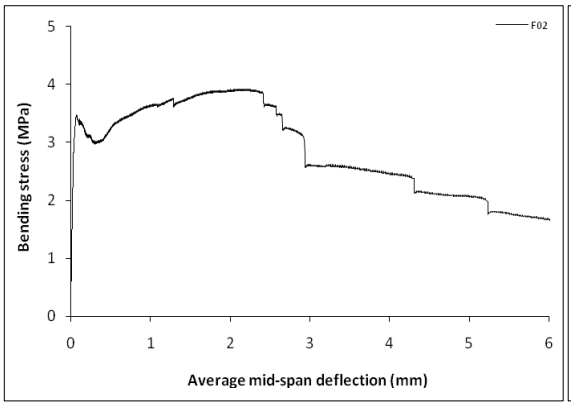

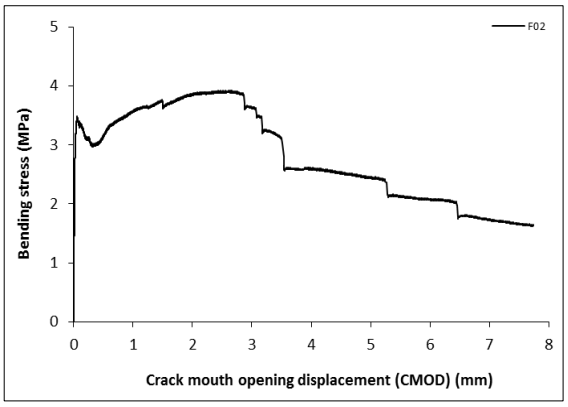

Specimen code name:		F3			
Notched Depth d_n	124	mm			
Depth, d	150	mm	Span, L	500	mm
Width, b	155	mm	Flexural strength	5.61	MPa

Bottom face of cast concrete

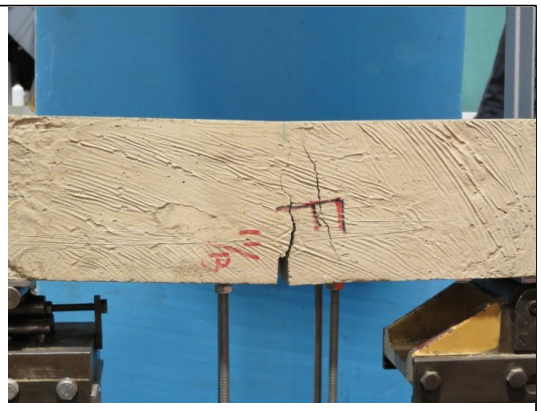

Top face of cast concrete

Crack zone of bottom face

Crack zone of top face

Stress-deformation graphs

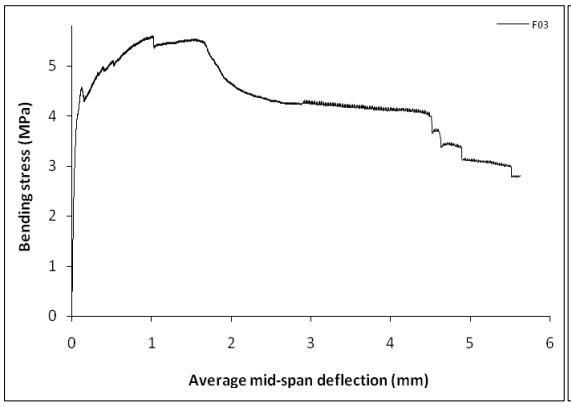

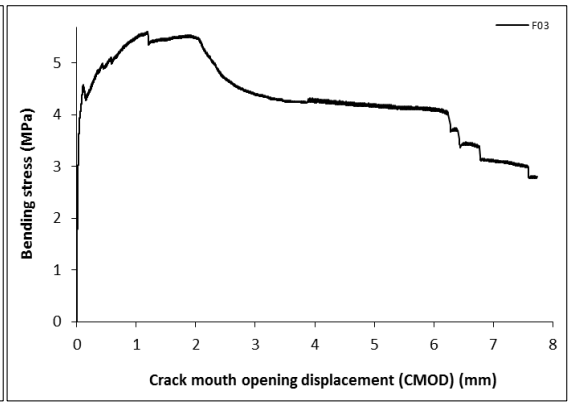

Specimen code name:		F4			
Notched Depth d_n	123	mm			
Depth, d	150	mm	Span, L	500	mm
Width, b	150	mm	Flexural strength	3.72	MPa

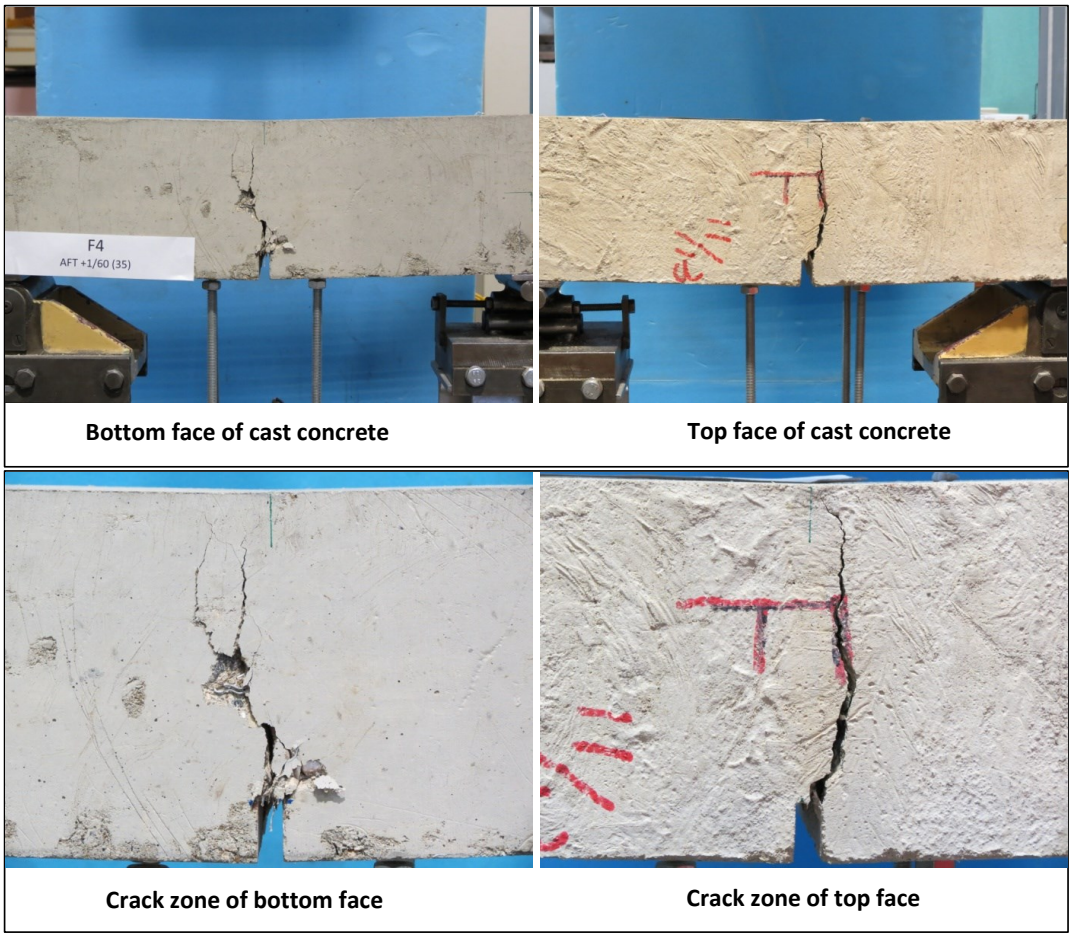

Stress-deformation graphs

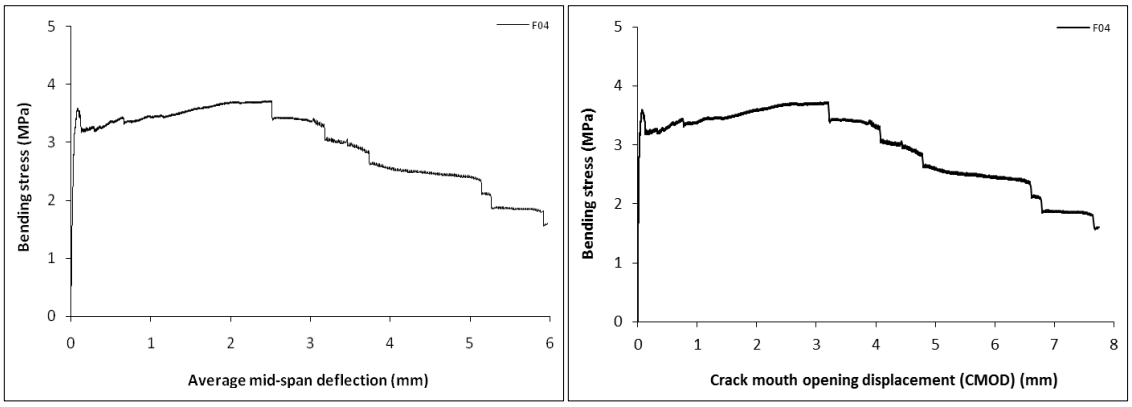

Specimen code name:		F5			
Notched Depth d_n	125	mm			
Depth, d	150	mm	Span, L	500	mm
Width, b	154	mm	Flexural strength	3.33	MPa

Bottom face of cast concrete

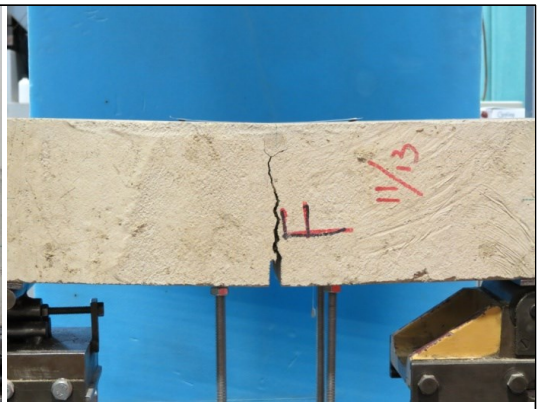

Top face of cast concrete

Crack zone of bottom face

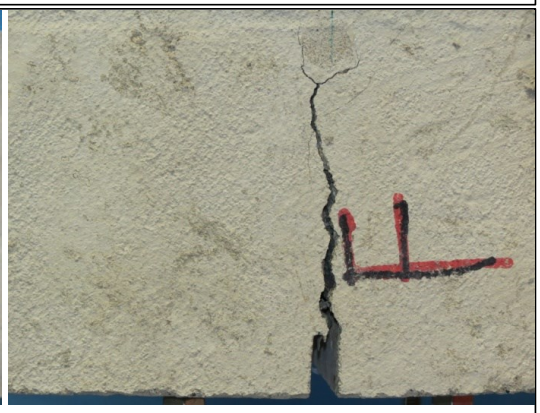

Crack zone of top face

Stress-deformation graphs

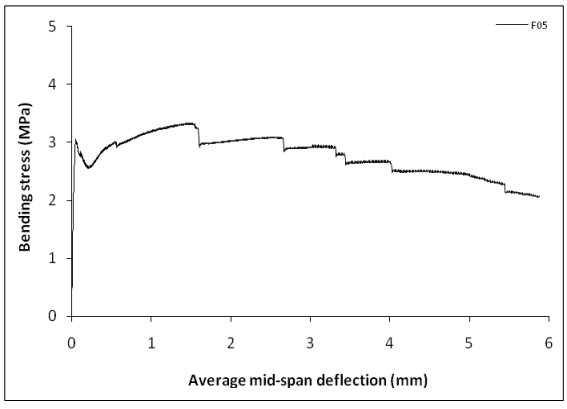

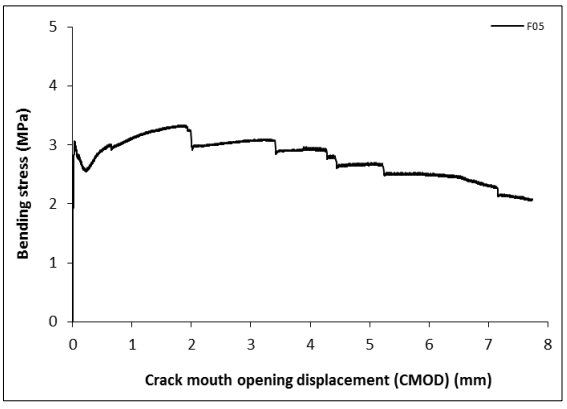

Specimen code name:		F6			
Notched Depth d_n	124	mm			
Depth, d	149	mm	Span, L	500	mm
Width, b	150	mm	Flexural strength	5.08	MPa

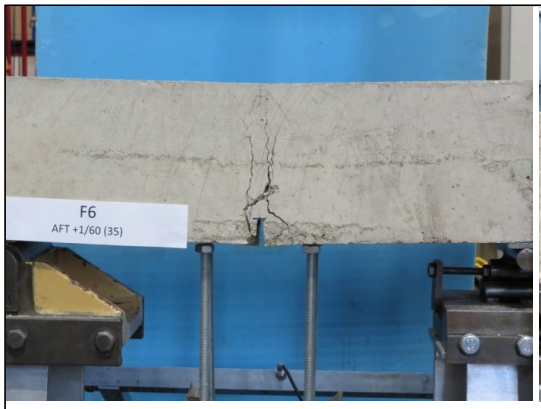

Bottom face of cast concrete

Top face of cast concrete

Crack zone of bottom face

Crack zone of top face

Stress-deformation graphs

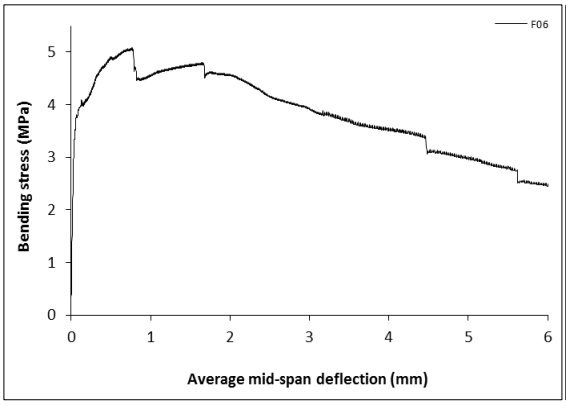

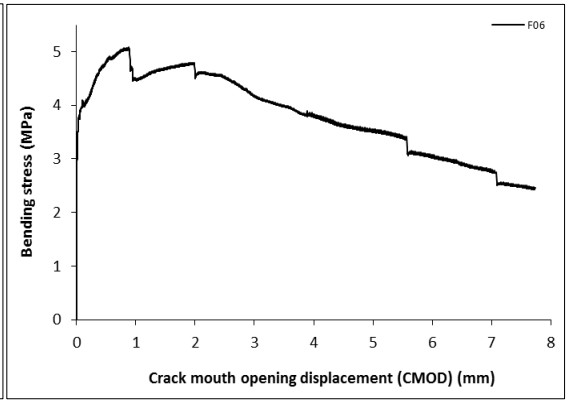

Specimen code name:		F7			
Notched Depth d_n	124	mm			
Depth, d	150	mm	Span, L	500	mm
Width, b	153	mm	Flexural strength	4.96	MPa

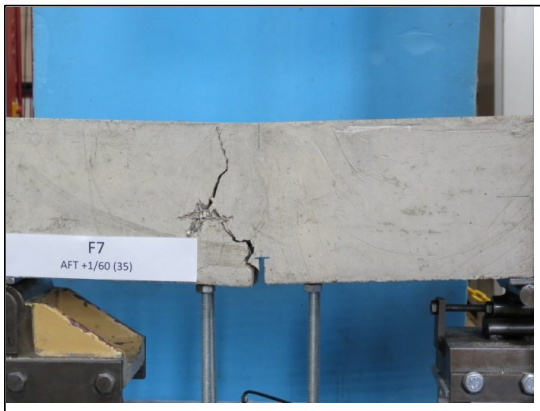

Bottom face of cast concrete

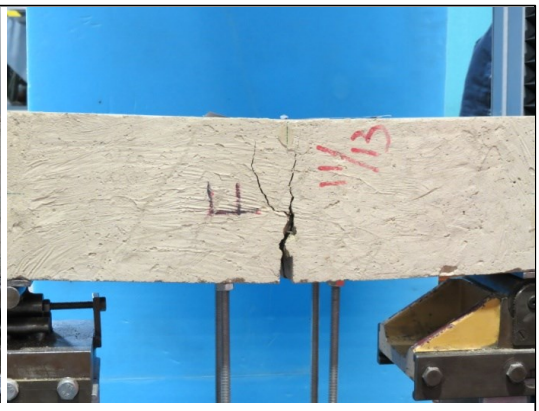

Top face of cast concrete

Crack zone of bottom face

Crack zone of top face

Stress-deformation graphs

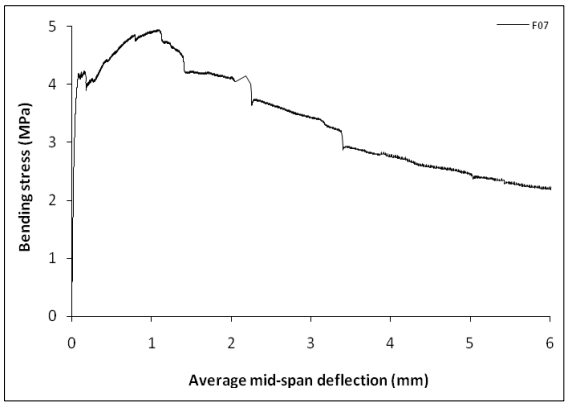

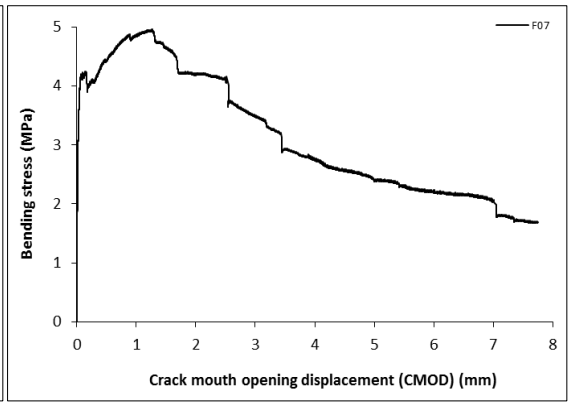

Specimen code name:		F8			
Notched Depth d_n	124	mm			
Depth, d	150	mm	Span, L	500	mm
Width, b	152	mm	Flexural strength	3.42	MPa

Bottom face of cast concrete

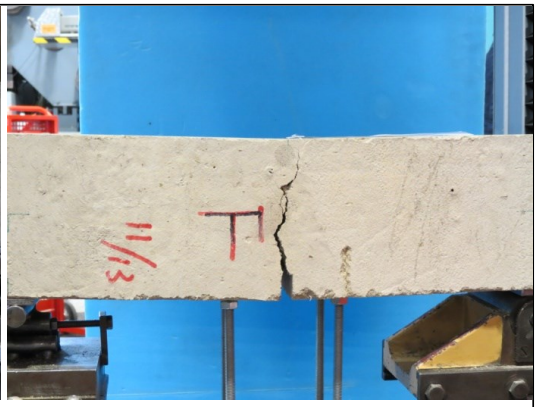

Top face of cast concrete

Crack zone of bottom face

Crack zone of top face

Stress-deformation graphs

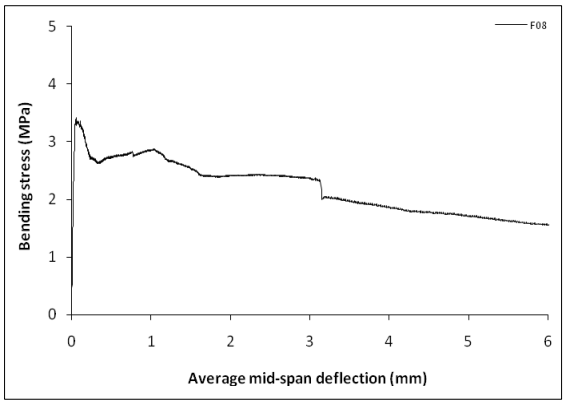

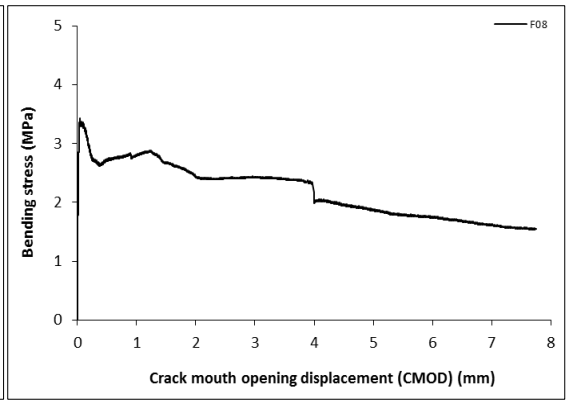

Specimen code name:		F9			
Notched Depth d_n	125	mm			
Depth, d	149	mm	Span, L	500	mm
Width, b	154	mm	Flexural strength	4.83	MPa

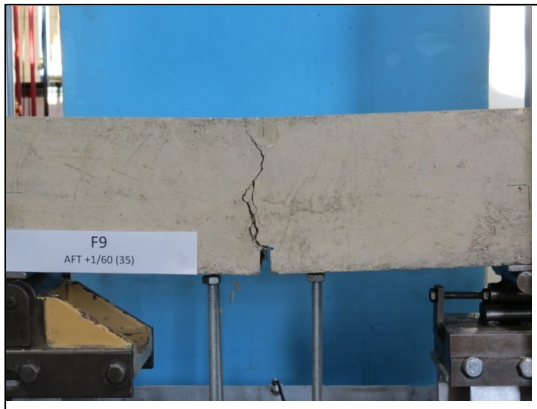

Bottom face of cast concrete

Top face of cast concrete

Crack zone of bottom face

Crack zone of top face

Stress-deformation graphs

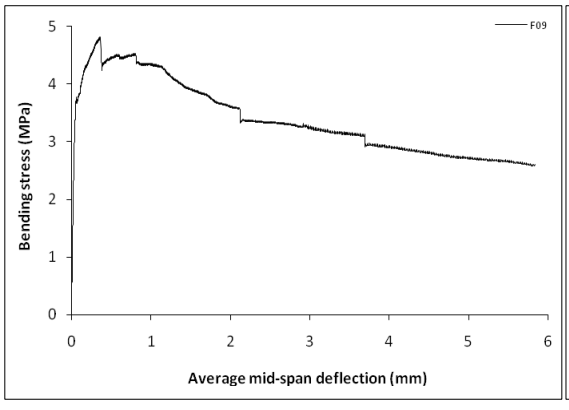

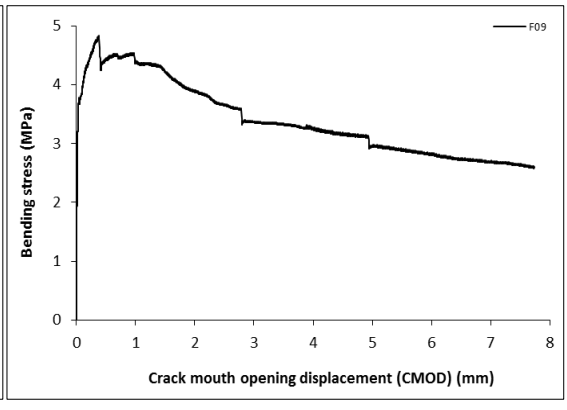

Specimen code name:		F10			
Notched Depth d_n	125	mm			
Depth, d	150	mm	Span, L	500	mm
Width, b	154	mm	Flexural strength	4.23	MPa

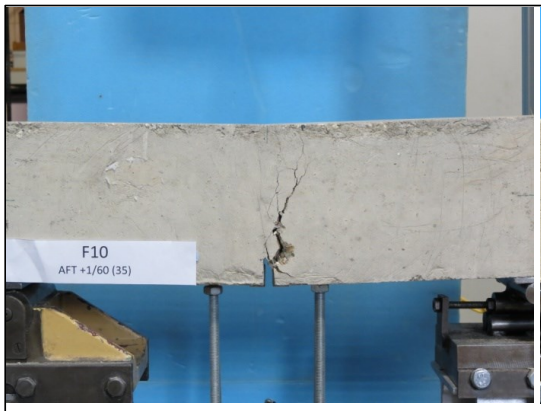

Bottom face of cast concrete

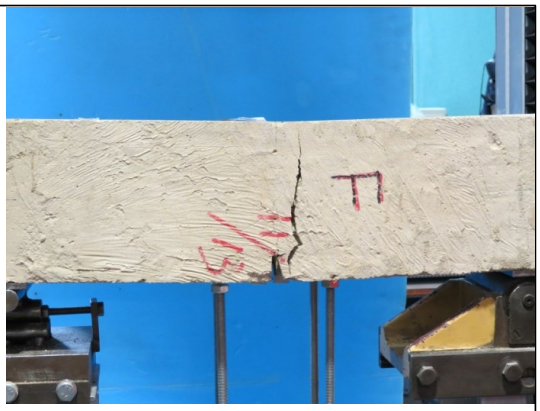

Top face of cast concrete

Crack zone of bottom face

Crack zone of top face

Stress-deformation graphs

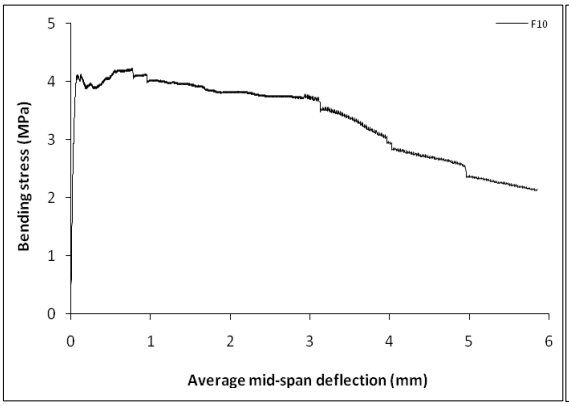

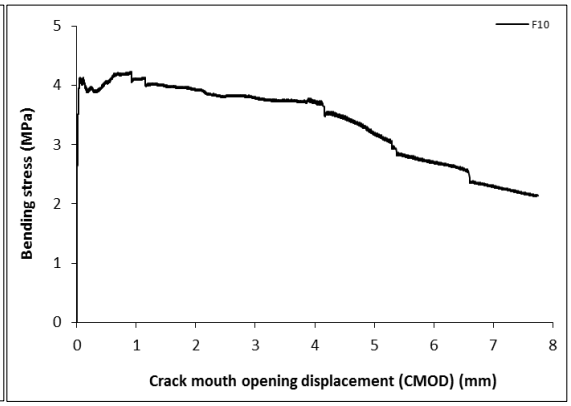

Specimen code name:		F11			
Notched Depth d_n	125	mm			
Depth, d	150	mm	Span, L	500	mm
Width, b	152	mm	Flexural strength	4.56	MPa

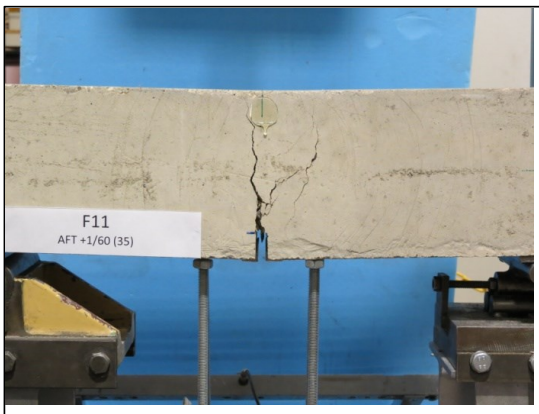

Bottom face of cast concrete

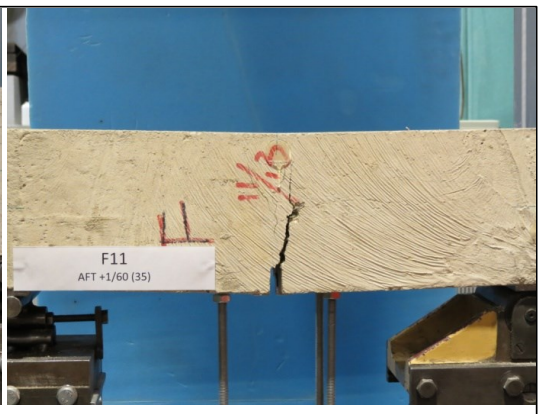

Top face of cast concrete

Crack zone of bottom face

Crack zone of top face

Stress-deformation graphs

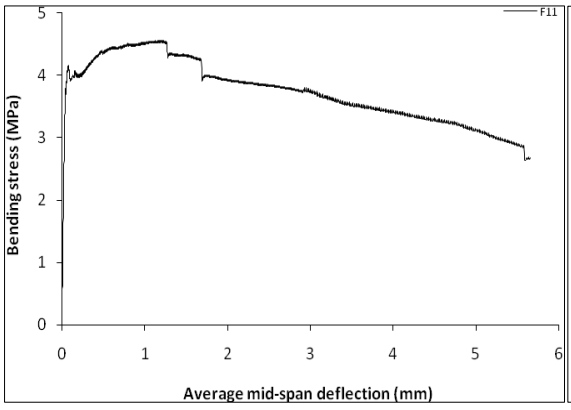

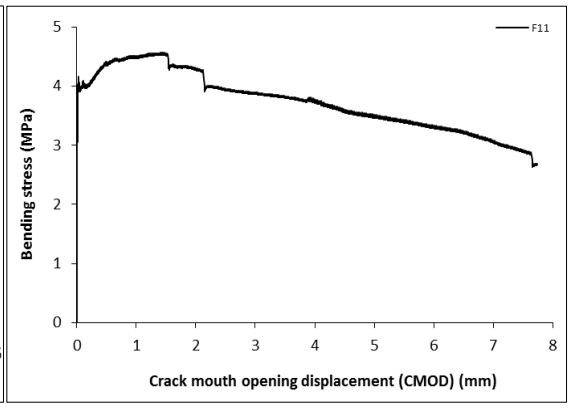

Specimen code name:		F12			
Notched Depth d_n	125	mm			
Depth, d	150	mm	Span, L	500	mm
Width, b	152	mm	Flexural strength	4.23	MPa

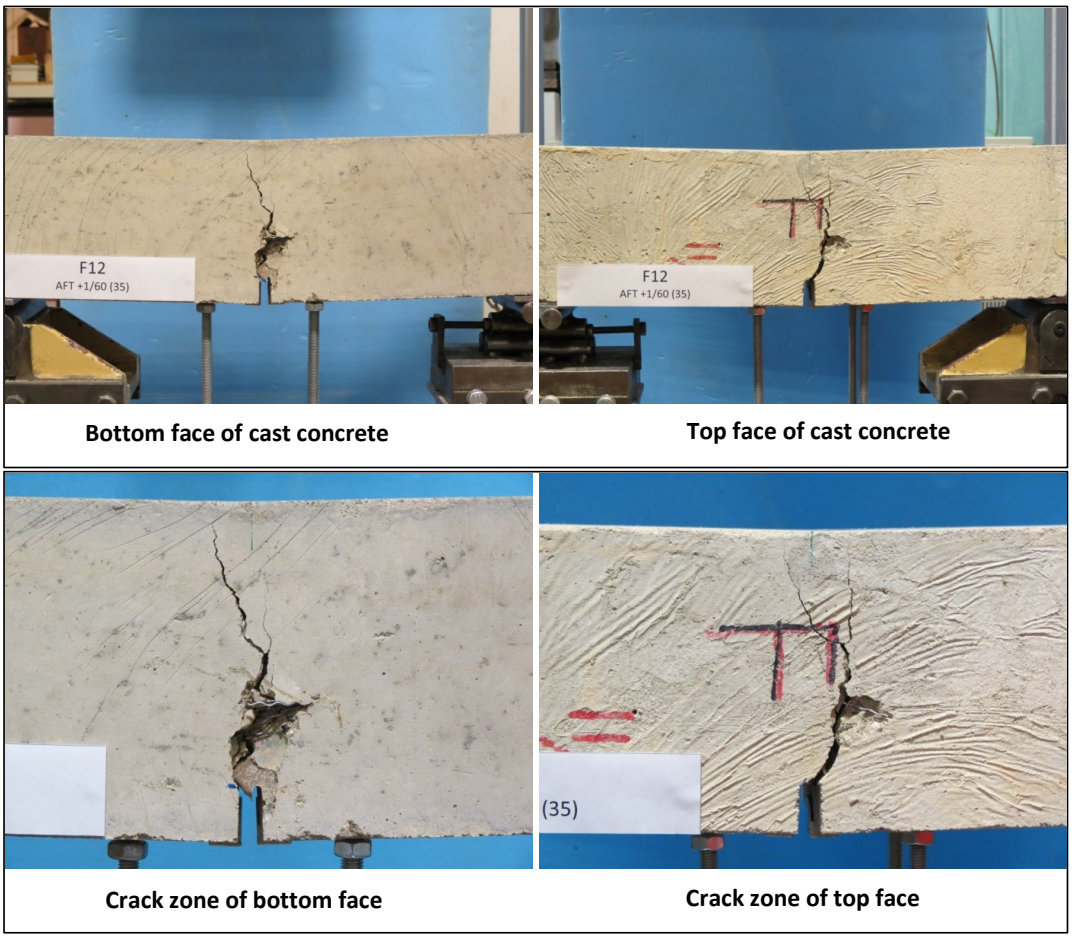

Bottom face of cast concrete | **Top face of cast concrete**

Crack zone of bottom face | **Crack zone of top face**

Stress-deformation graphs

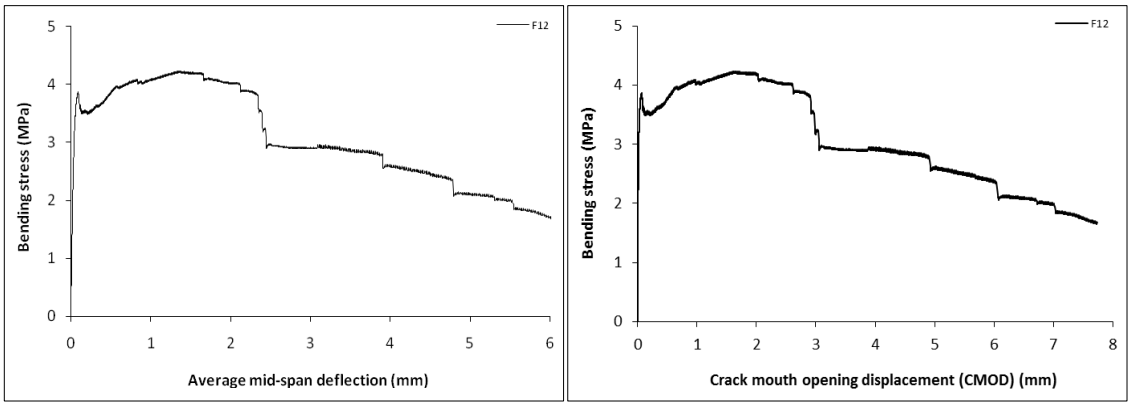

Mix:	F		
Notched Depth d_n	mm		
Depth, d	mm	Span, L	mm
Width, b	mm	Flexural strength	MPa

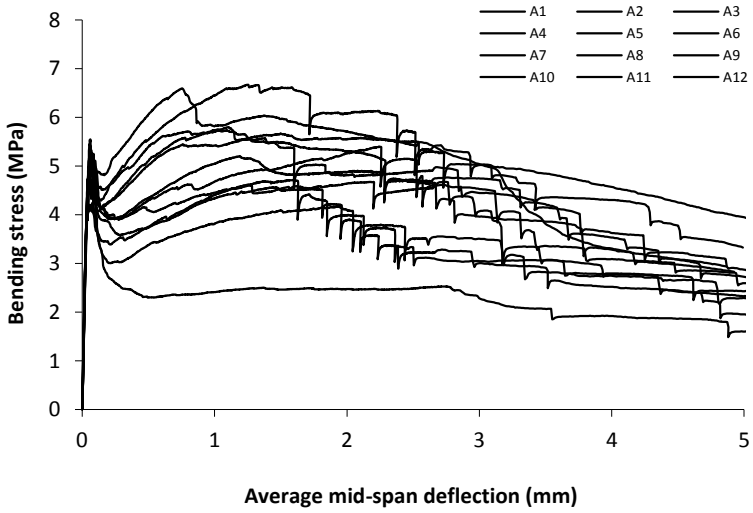

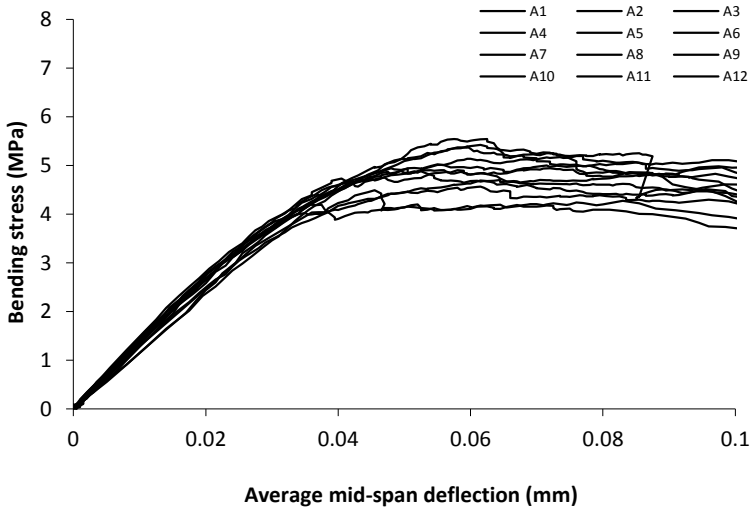

Specimen code name:		G1			
Notched Depth d_n	124	mm			
Depth, d	150	mm	Span, L	500	mm
Width, b	153	mm	Flexural strength	5.74	MPa

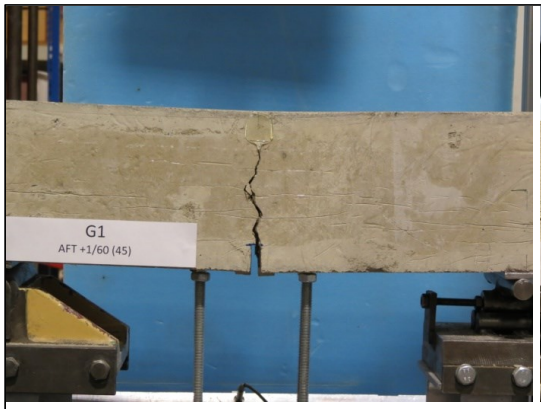

Bottom face of cast concrete

Top face of cast concrete

Crack zone of bottom face

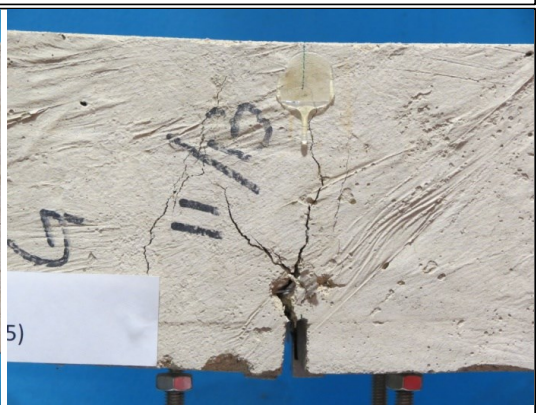

Crack zone of top face

Stress-deformation graphs

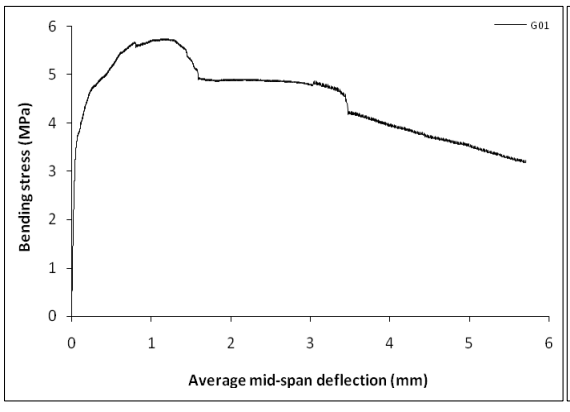

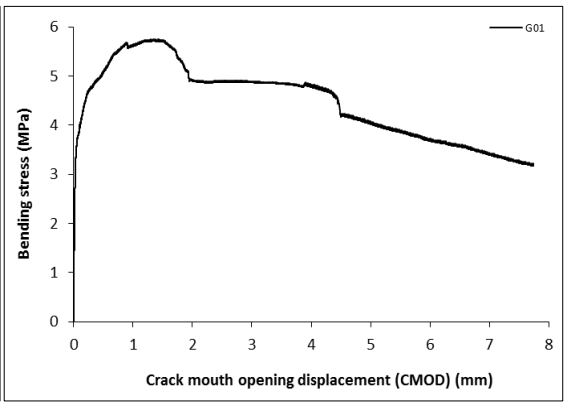

Specimen code name:		G2			
Notched Depth d_n	125	mm			
Depth, d	150	mm	Span, L	500	mm
Width, b	155	mm	Flexural strength	3.47	MPa

Bottom face of cast concrete

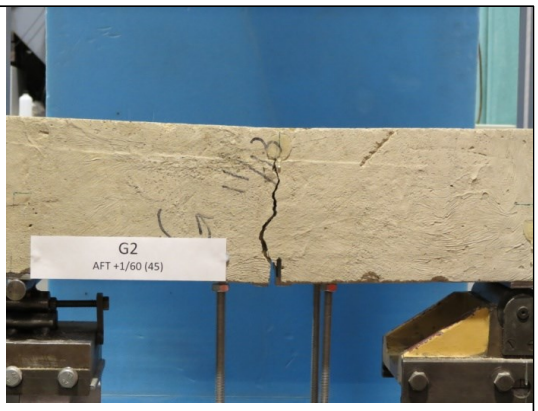

Top face of cast concrete

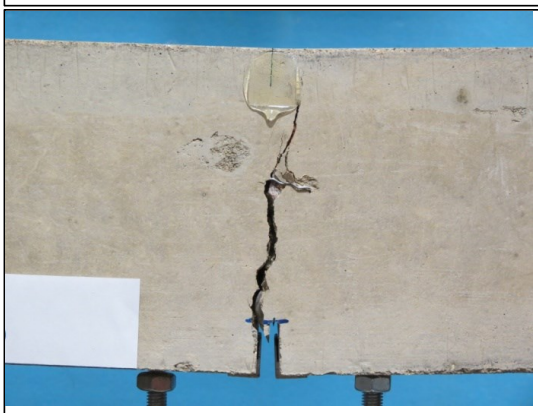

Crack zone of bottom face

Crack zone of top face

Stress-deformation graphs

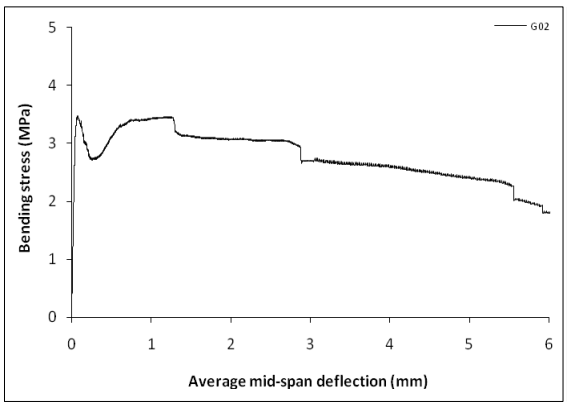

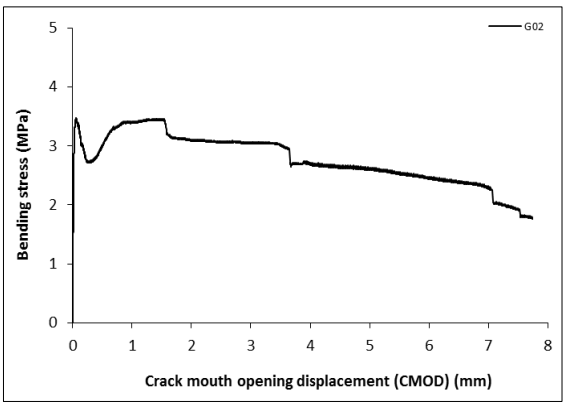

Specimen code name:		G3			
Notched Depth d_n	124	mm			
Depth, d	150	mm	Span, L	500	mm
Width, b	153	mm	Flexural strength	6.25	MPa

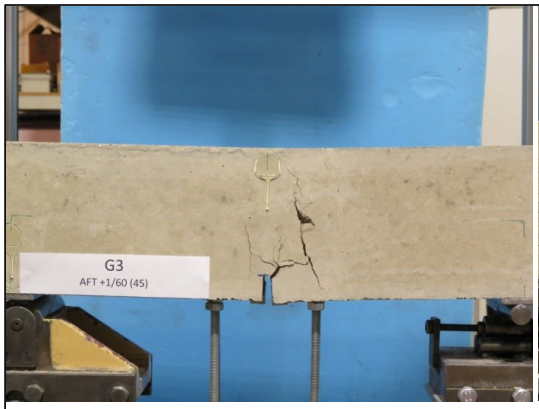

Bottom face of cast concrete

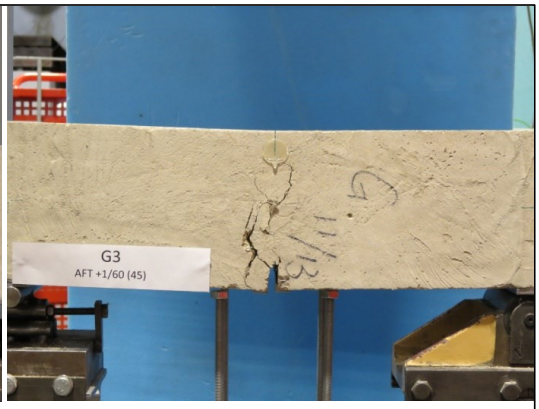

Top face of cast concrete

Crack zone of bottom face

Crack zone of top face

Stress-deformation graphs

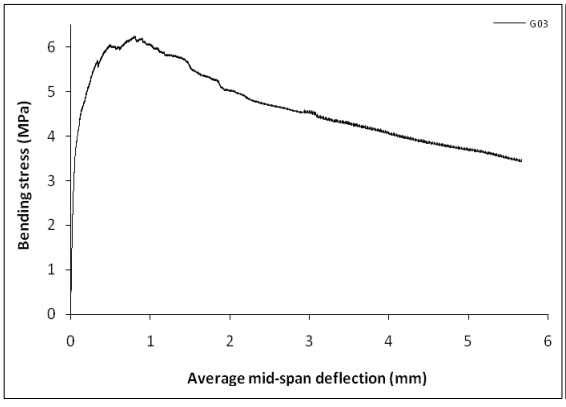

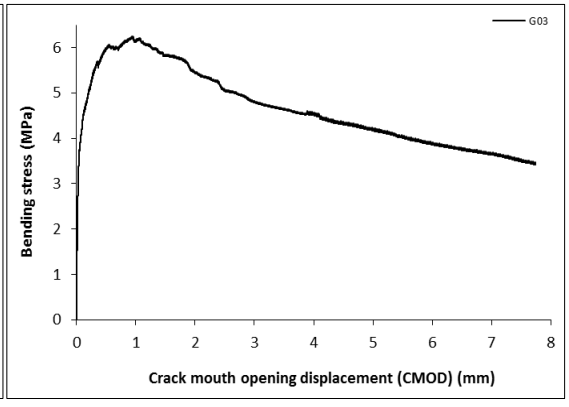

Specimen code name:		G4			
Notched Depth d_n	124	mm			
Depth, d	150	mm	Span, L	500	mm
Width, b	154	mm	Flexural strength	3.75	MPa

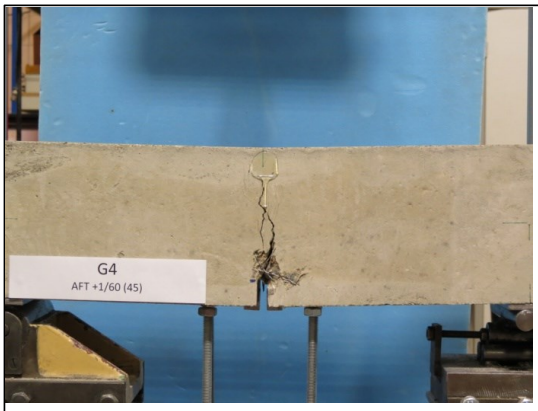

Bottom face of cast concrete

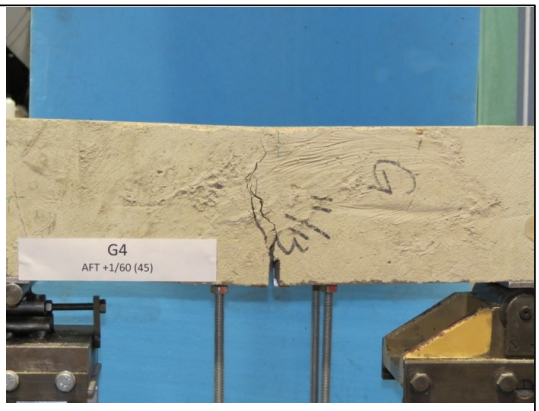

Top face of cast concrete

Crack zone of bottom face

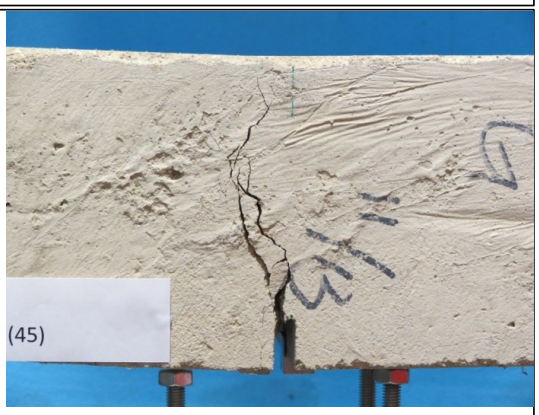

Crack zone of top face

Stress-deformation graphs

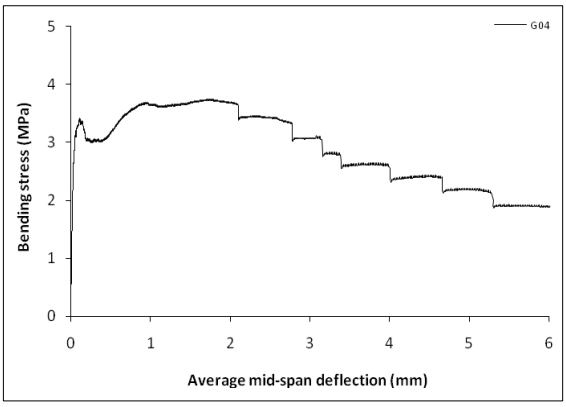

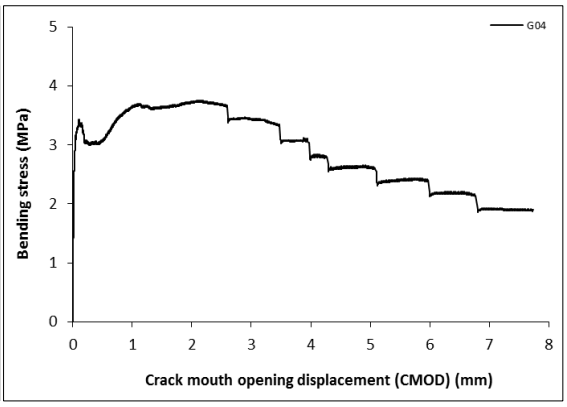

Specimen code name:		G5			
Notched Depth d_n	125	mm			
Depth, d	150	mm	Span, L	500	mm
Width, b	154	mm	Flexural strength	4.00	MPa

Bottom face of cast concrete

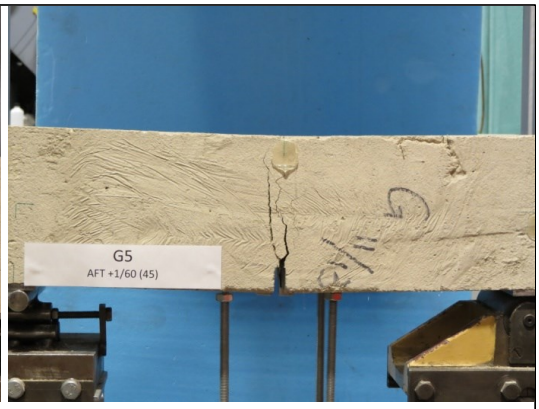

Top face of cast concrete

Crack zone of bottom face

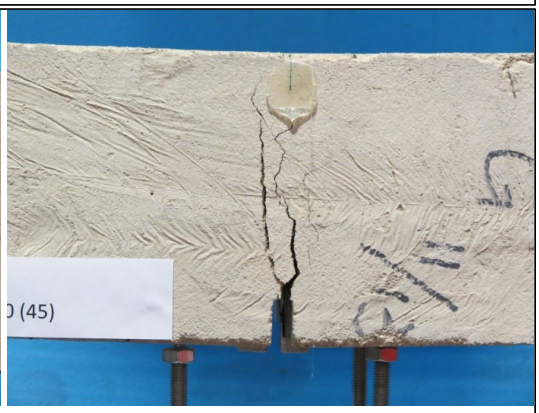

Crack zone of top face

Stress-deformation graphs

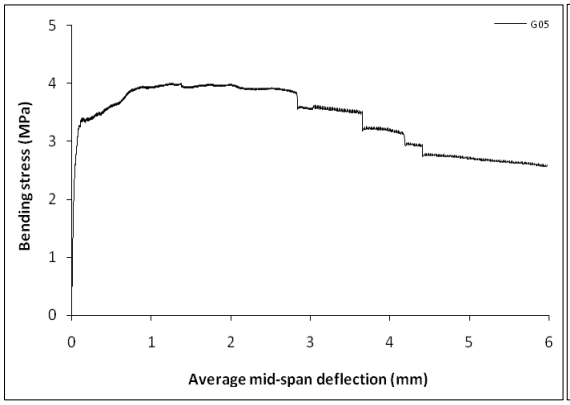

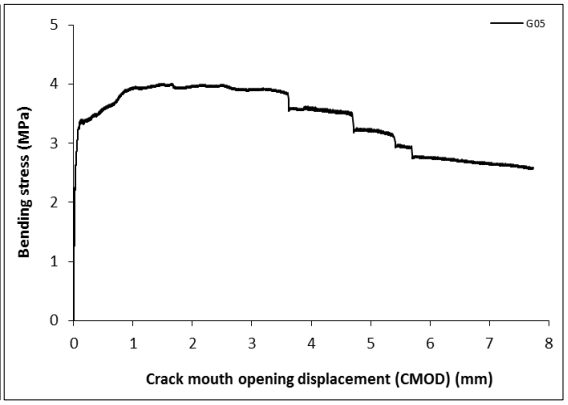

Specimen code name:		G6			
Notched Depth d_n	124	mm			
Depth, d	150	mm	Span, L	500	mm
Width, b	153	mm	Flexural strength	3.82	MPa

Bottom face of cast concrete

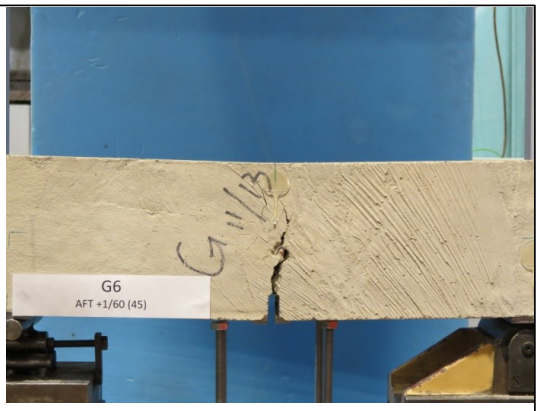

Top face of cast concrete

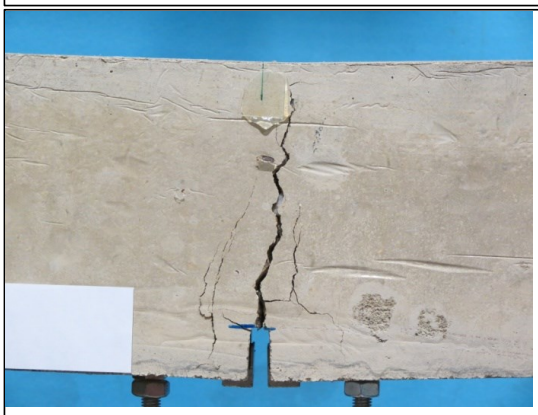

Crack zone of bottom face

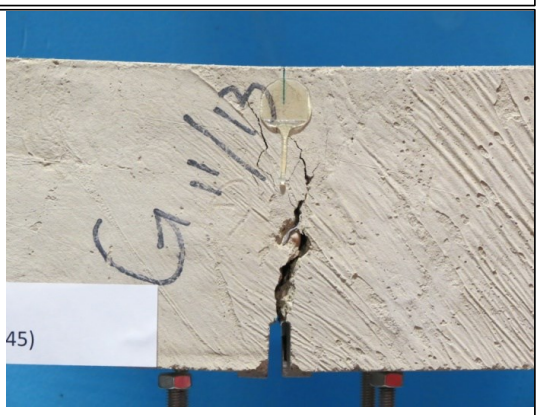

Crack zone of top face

Stress-deformation graphs

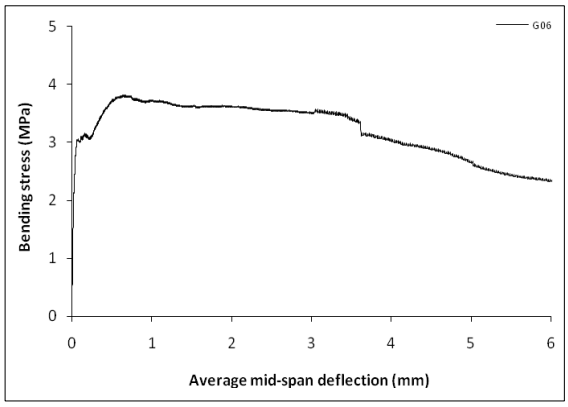

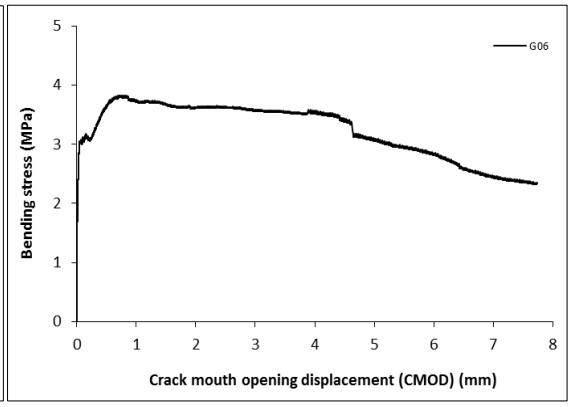

Specimen code name:		G7			
Notched Depth d_n	126	mm			
Depth, d	151	mm	Span, L	500	mm
Width, b	151	mm	Flexural strength	4.57	MPa

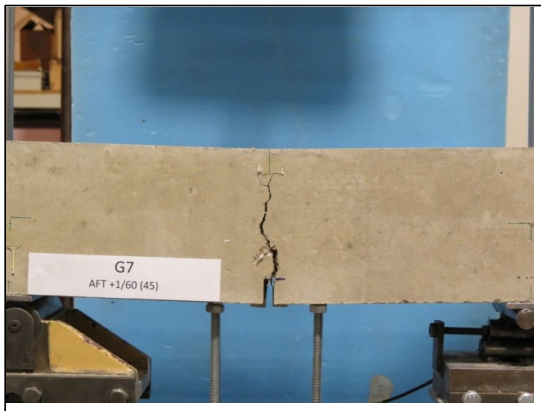

Bottom face of cast concrete

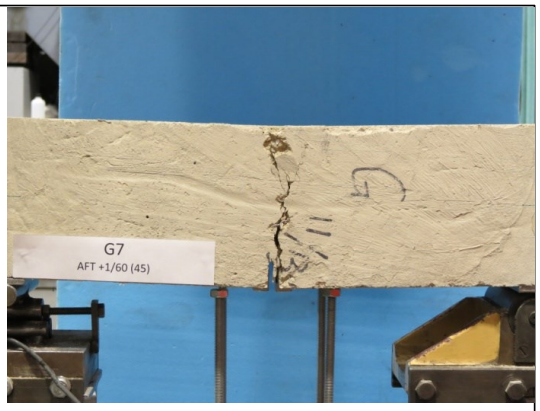

Top face of cast concrete

Crack zone of bottom face

Crack zone of top face

Stress-deformation graphs

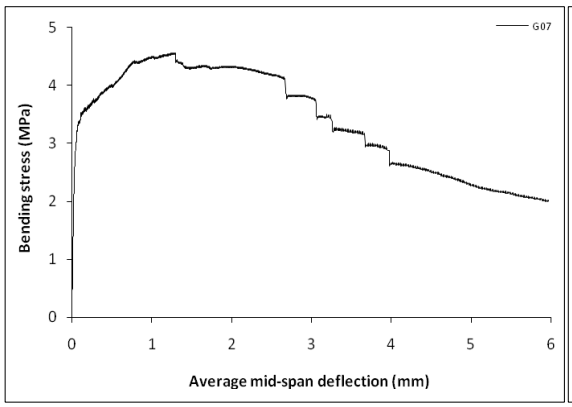

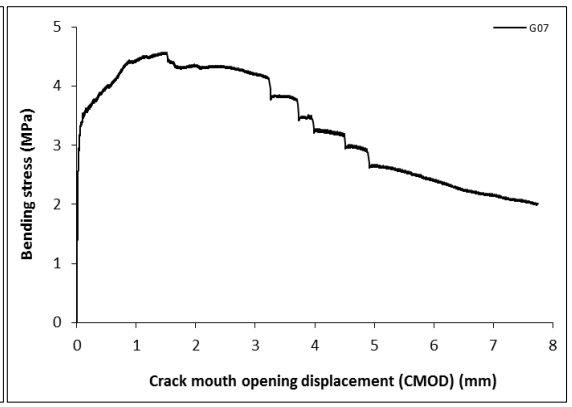

Specimen code name:		G8			
Notched Depth d_n	125	mm			
Depth, d	150	mm	Span, L	500	mm
Width, b	150	mm	Flexural strength	4.59	MPa

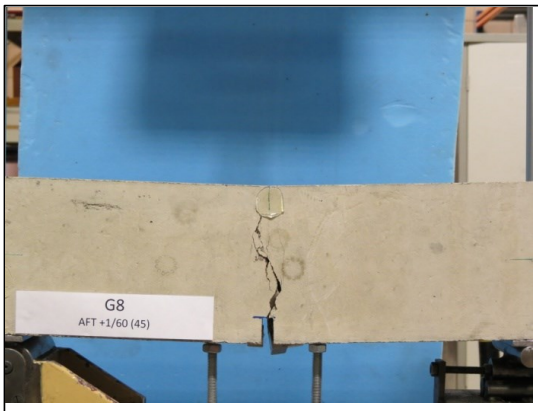

Bottom face of cast concrete

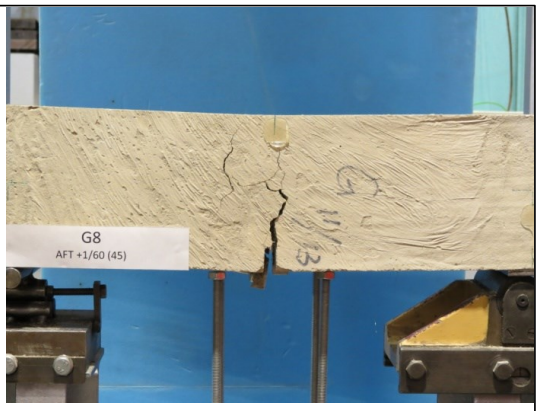

Top face of cast concrete

Crack zone of bottom face

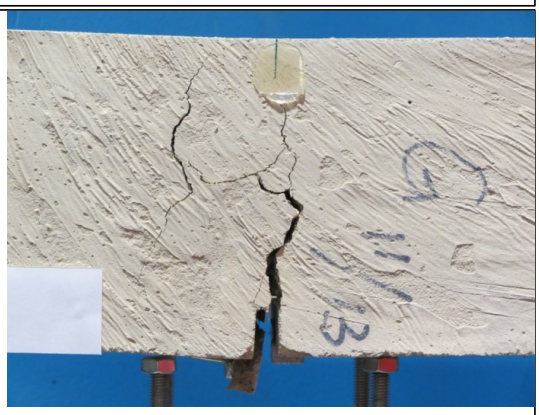

Crack zone of top face

Stress-deformation graphs

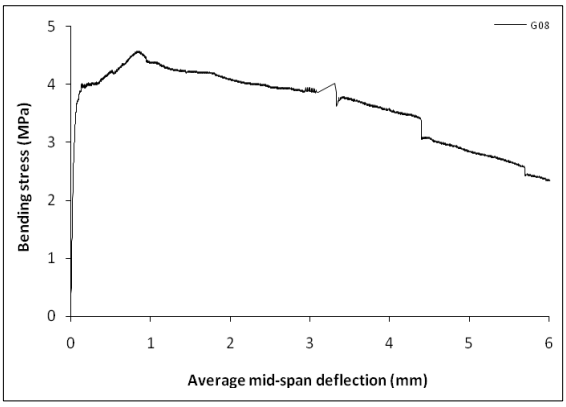

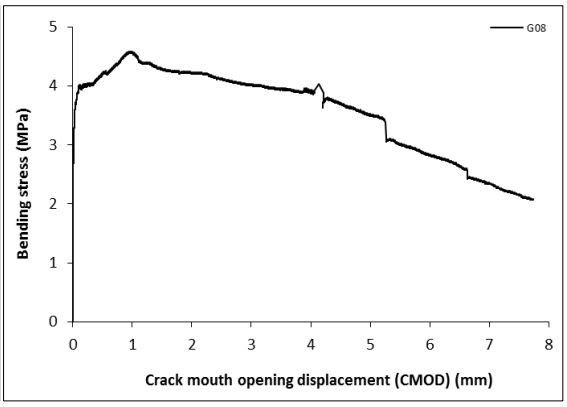

Specimen code name:		G9			
Notched Depth d_n	124	mm			
Depth, d	150	mm	Span, L	500	mm
Width, b	153	mm	Flexural strength	4.51	MPa

Bottom face of cast concrete

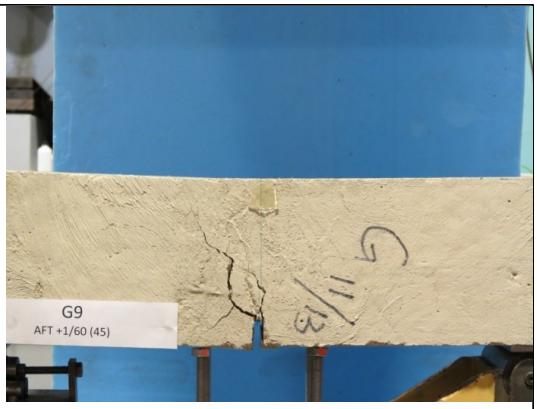

Top face of cast concrete

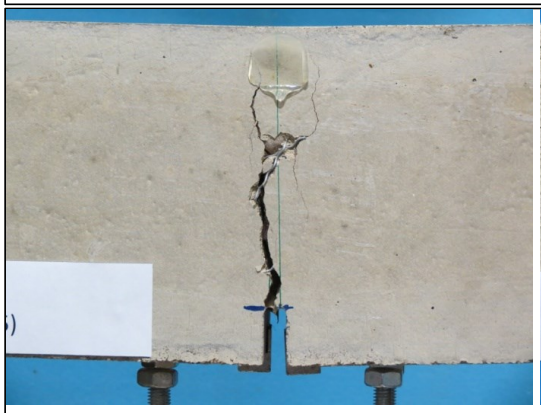

Crack zone of bottom face

Crack zone of top face

Stress-deformation graphs

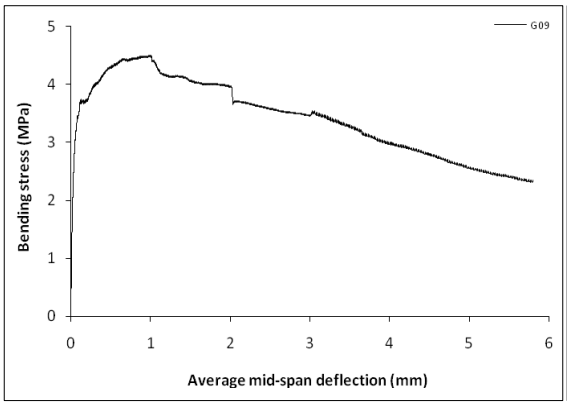

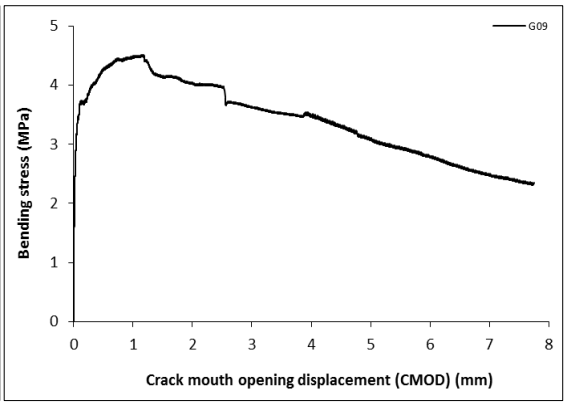

Specimen code name:		G10			
Notched Depth d_n	125	mm			
Depth, d	150	mm	Span, L	500	mm
Width, b	150	mm	Flexural strength	5.27	MPa

Bottom face of cast concrete

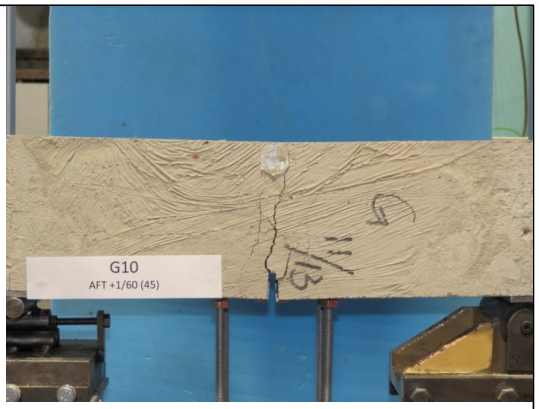

Top face of cast concrete

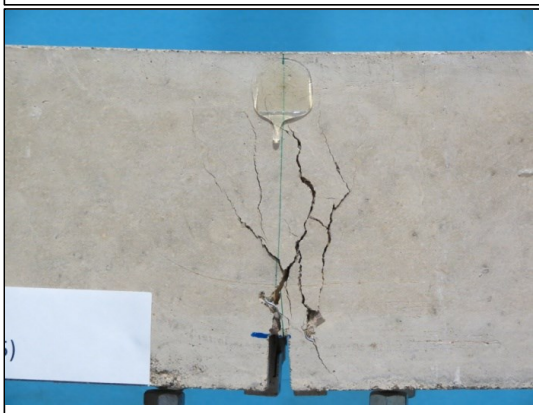

Crack zone of bottom face

Crack zone of top face

Stress-deformation graphs

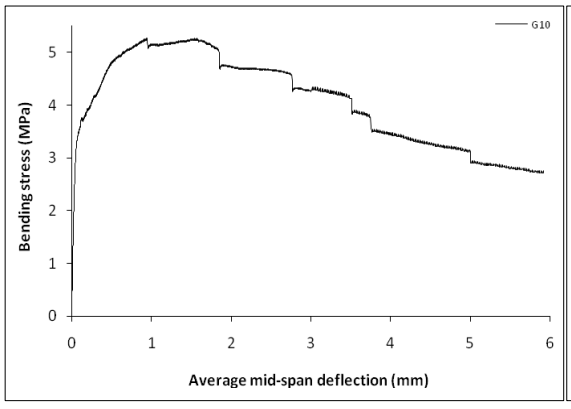

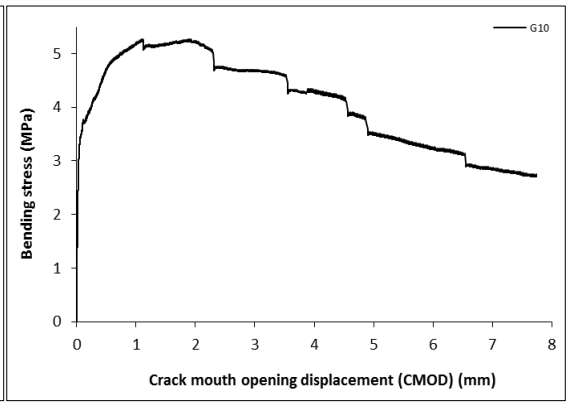

Specimen code name:		G11			
Notched Depth d_n	125	mm			
Depth, d	150	mm	Span, L	500	mm
Width, b	154	mm	Flexural strength	4.42	MPa

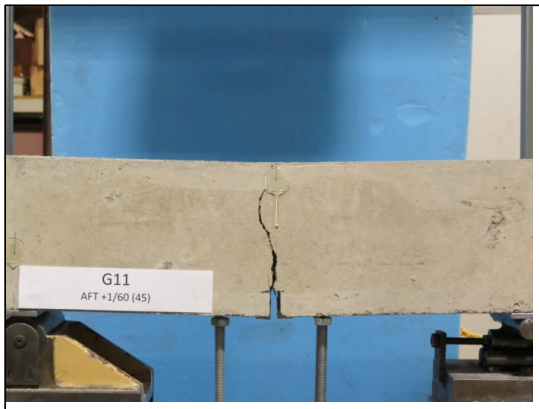

Bottom face of cast concrete

Top face of cast concrete

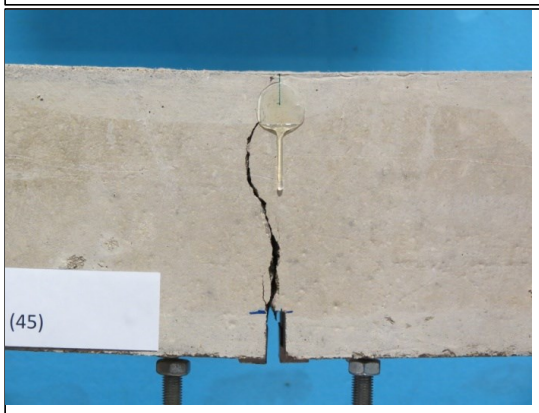

Crack zone of bottom face

Crack zone of top face

Stress-deformation graphs

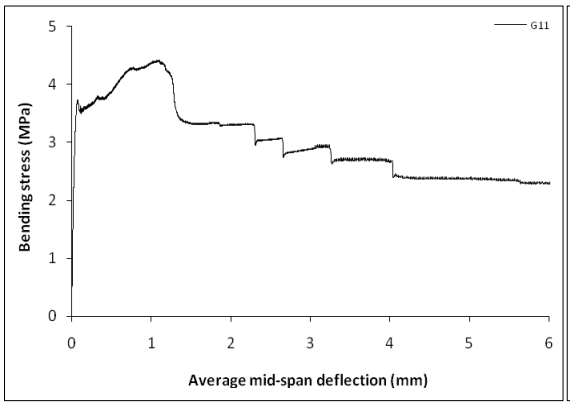

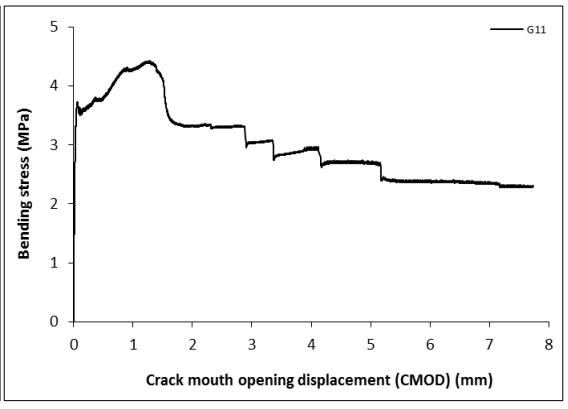

Specimen code name:		G12			
Notched Depth d_n	124	mm			
Depth, d	150	mm	Span, L	500	mm
Width, b	153	mm	Flexural strength	4.84	MPa

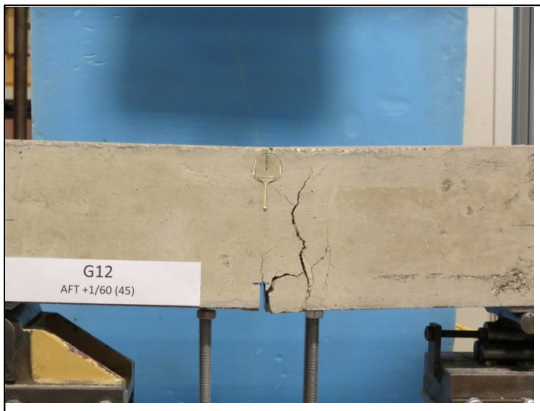

Bottom face of cast concrete

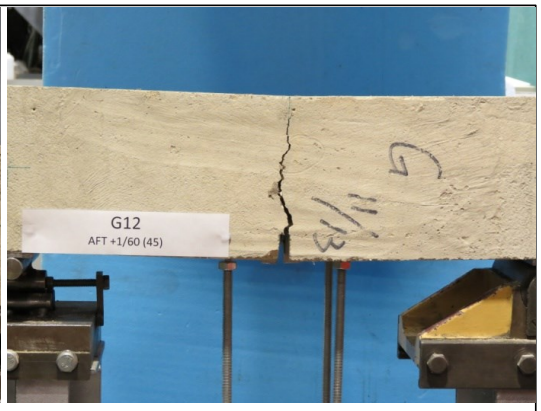

Top face of cast concrete

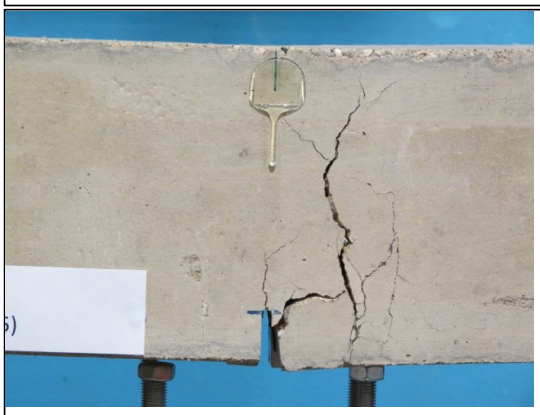

Crack zone of bottom face

Crack zone of top face

Stress-deformation graphs

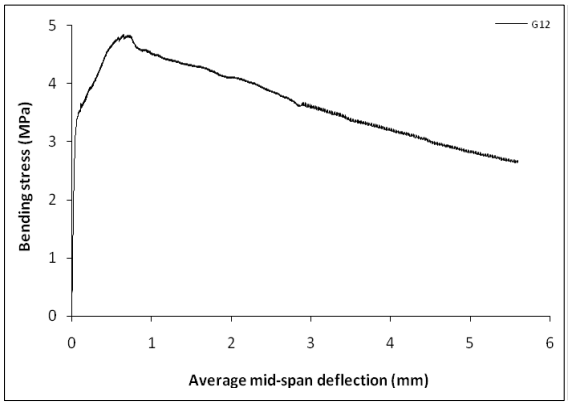

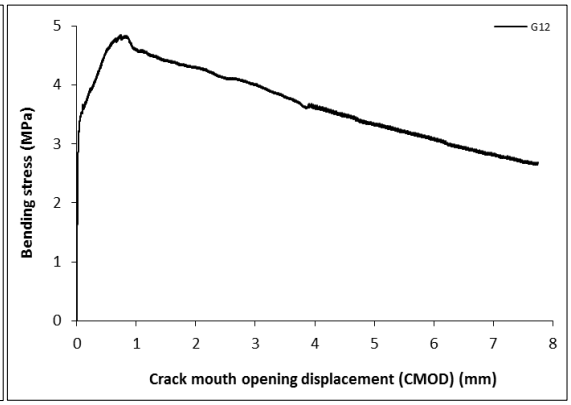

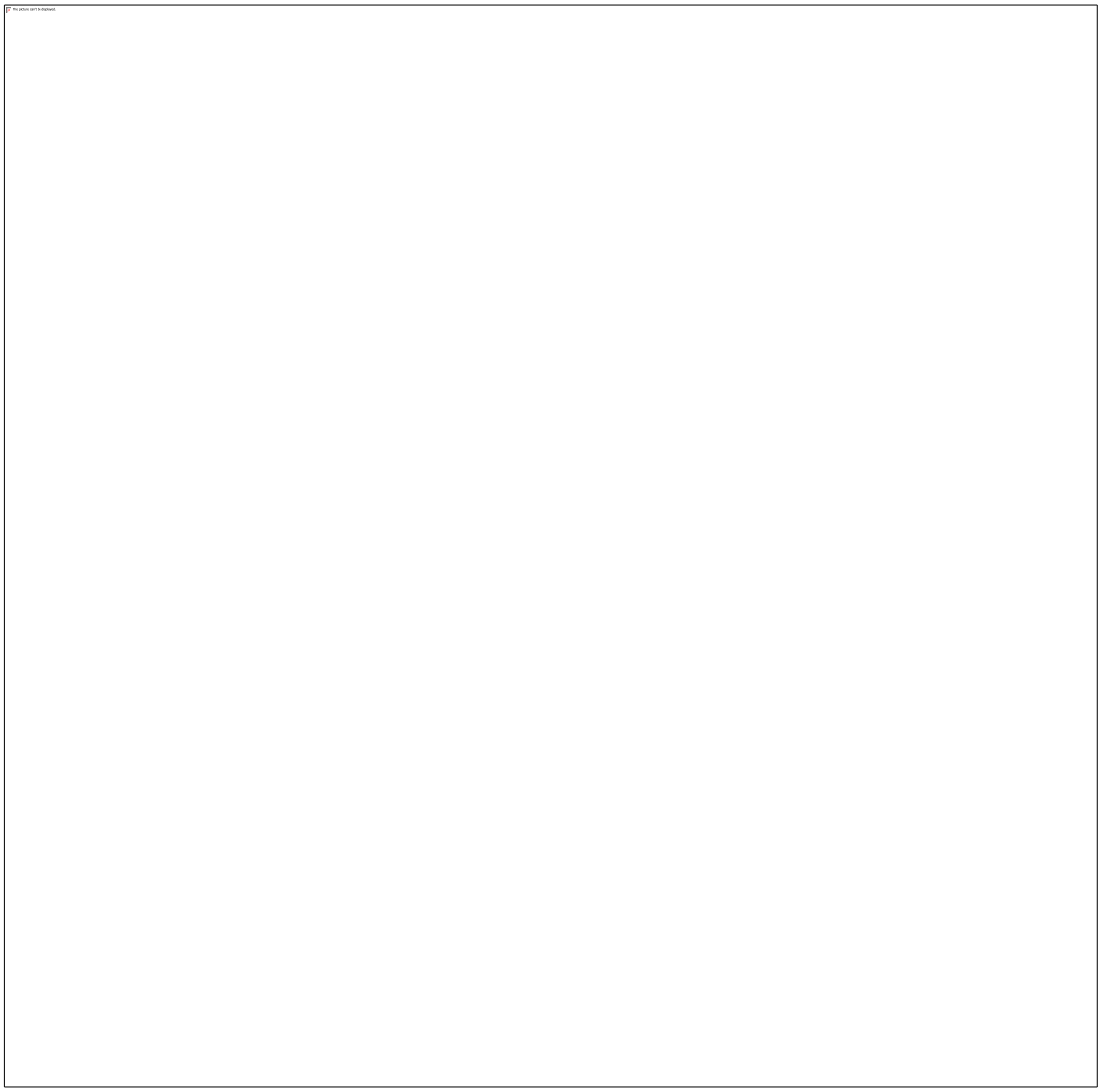
The picture can't be displayed.

Specimen code name:		H1			
Notched Depth d_n	122	mm			
Depth, d	149	mm	Span, L	500	mm
Width, b	151	mm	Flexural strength	4.68	MPa

Bottom face of cast concrete

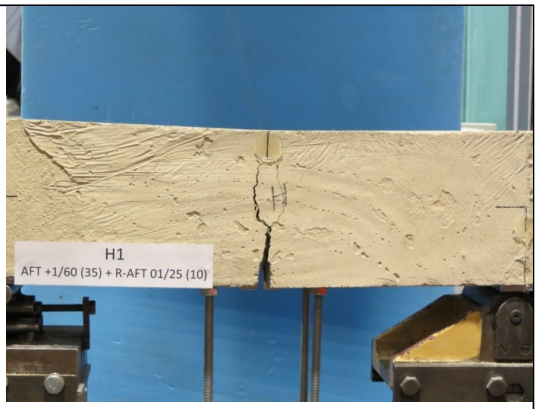

Top face of cast concrete

Crack zone of bottom face

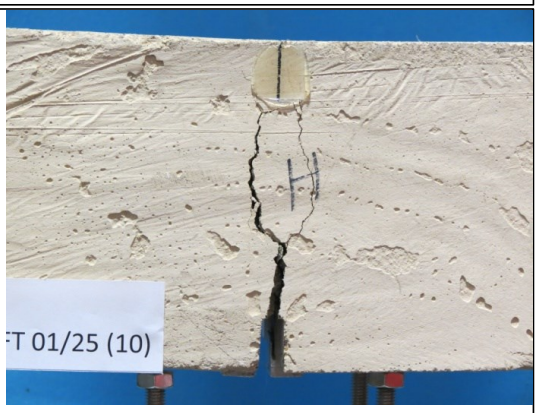

Crack zone of top face

Stress-deformation graphs

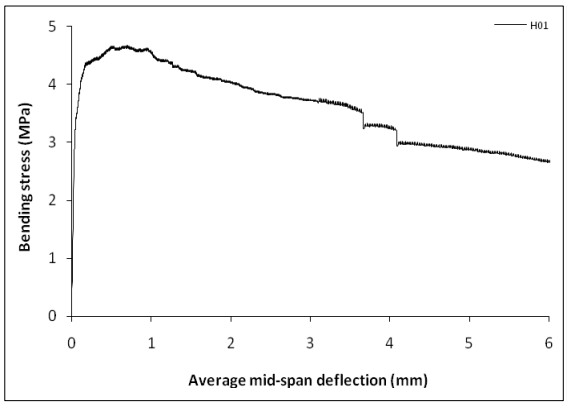

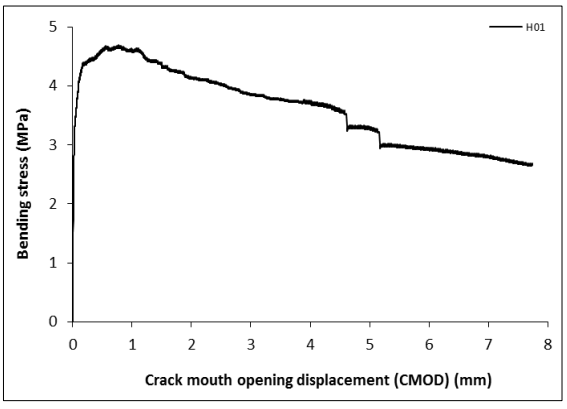

Specimen code name:		H2			
Notched Depth d_n	122	mm			
Depth, d	149	mm	Span, L	500	mm
Width, b	151	mm	Flexural strength	5.71	MPa

Bottom face of cast concrete

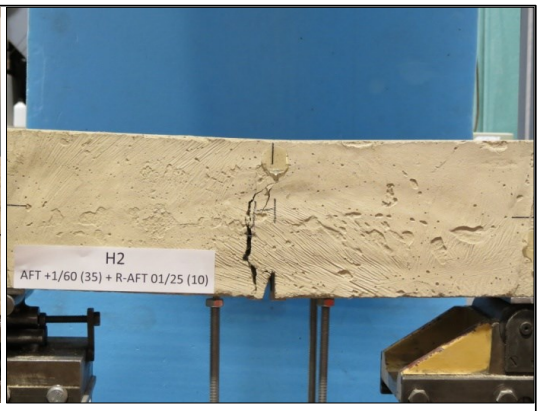

Top face of cast concrete

Crack zone of bottom face

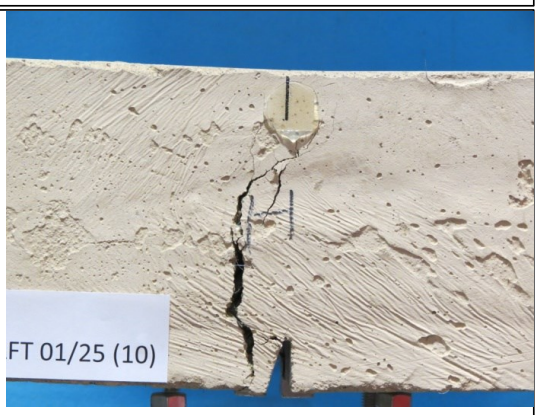

Crack zone of top face

Stress-deformation graphs

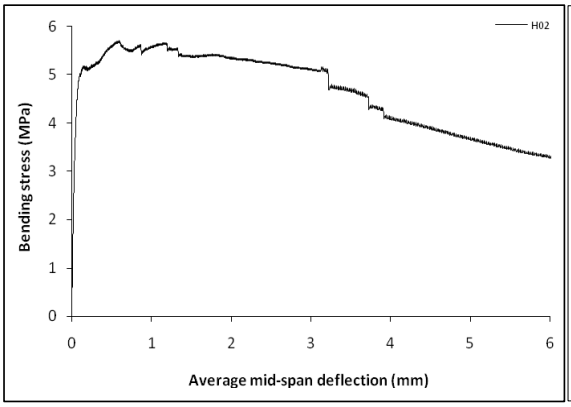

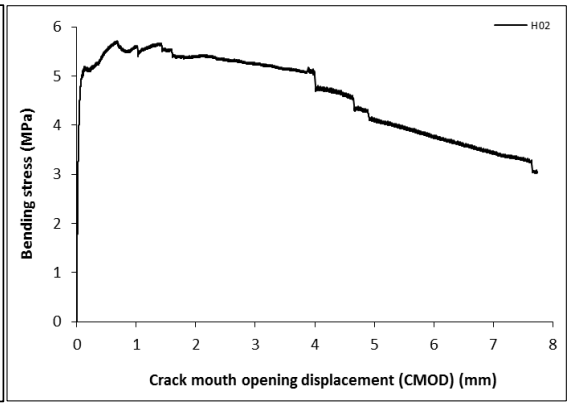

Specimen code name:		H3			
Notched Depth d_n	125	mm			
Depth, d	150	mm	Span, L	500	mm
Width, b	150	mm	Flexural strength	5.19	MPa

Bottom face of cast concrete

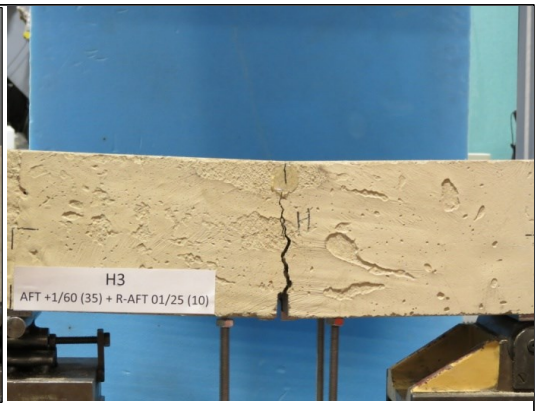

Top face of cast concrete

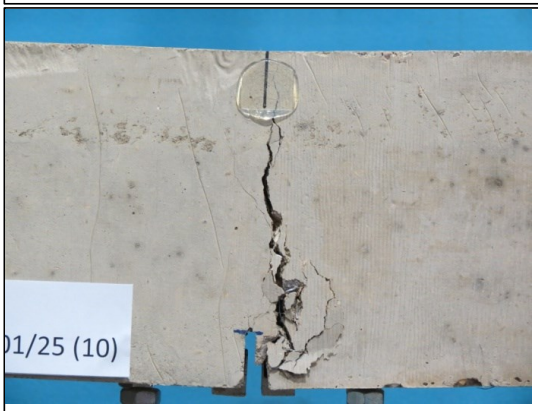

Crack zone of bottom face

Crack zone of top face

Stress-deformation graphs

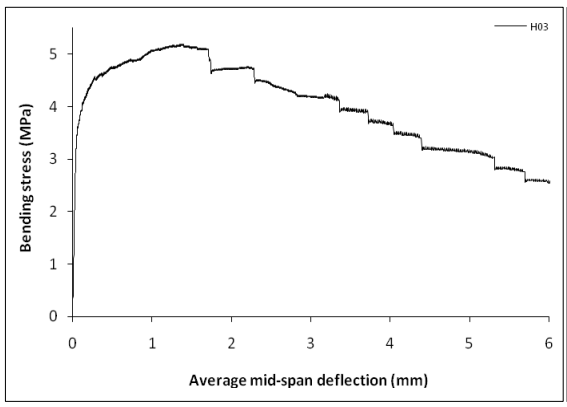

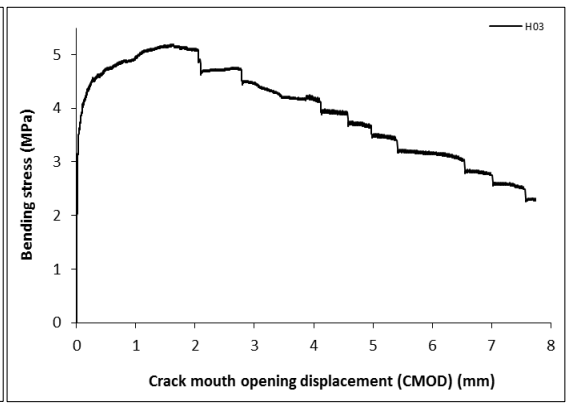

Specimen code name:		H4			
Notched Depth d_n	125	mm			
Depth, d	149	mm	Span, L	500	mm
Width, b	150	mm	Flexural strength	6.47	MPa

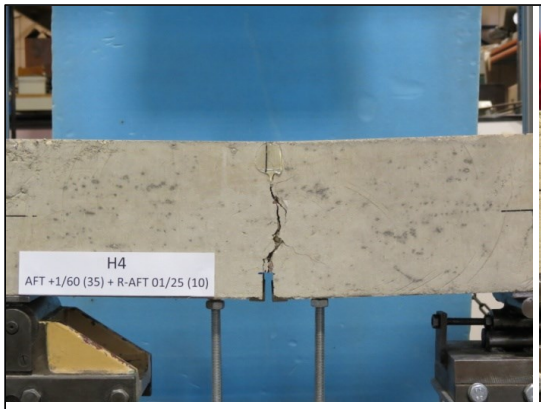

Bottom face of cast concrete

Top face of cast concrete

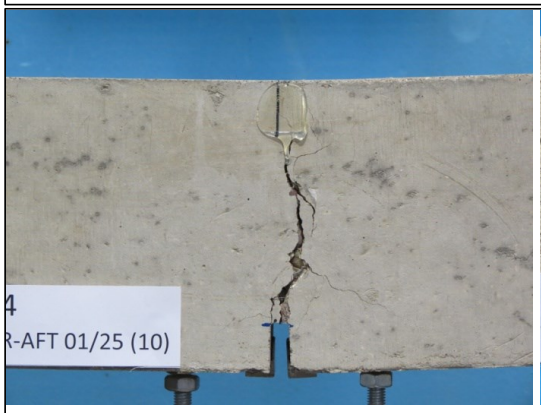

Crack zone of bottom face

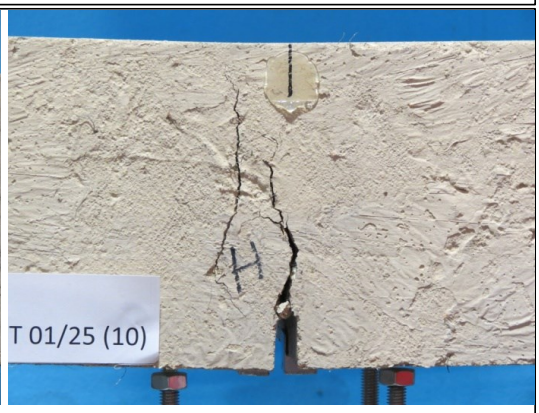

Crack zone of top face

Stress-deformation graphs

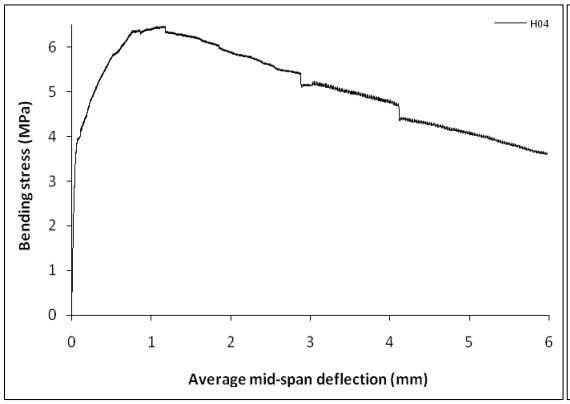

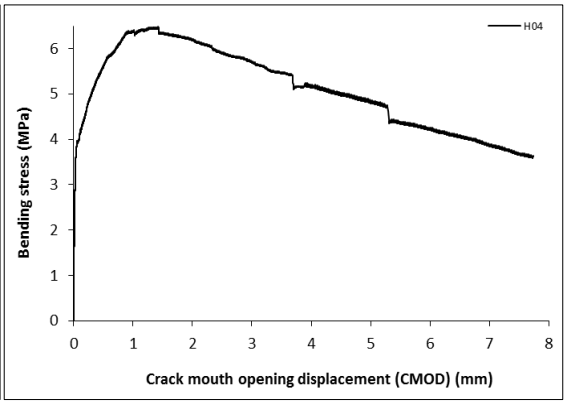

Specimen code name:		H5			
Notched Depth d_n	126	mm			
Depth, d	152	mm	Span, L	500	mm
Width, b	154	mm	Flexural strength	4.87	MPa

Bottom face of cast concrete

Top face of cast concrete

Crack zone of bottom face

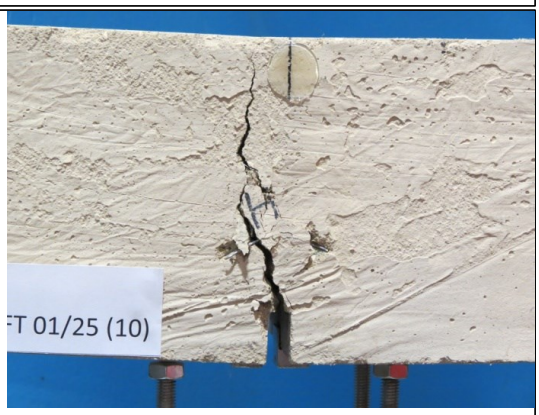

Crack zone of top face

Stress-deformation graphs

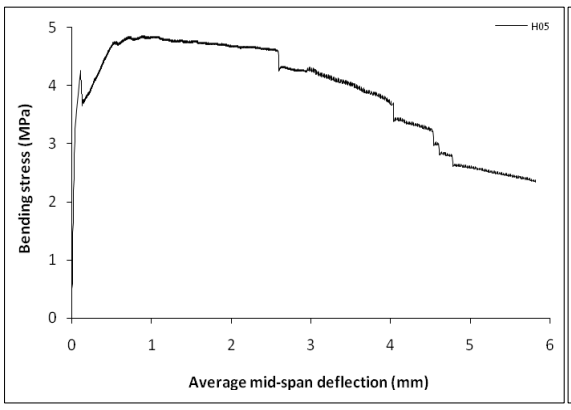

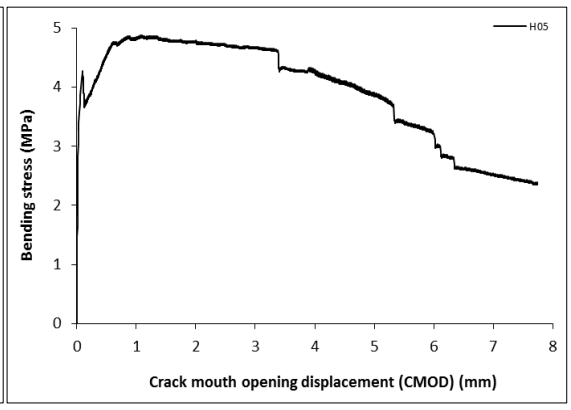

Specimen code name:		H6			
Notched Depth d_n	127	mm			
Depth, d	152	mm	Span, L	500	mm
Width, b	151	mm	Flexural strength	5.40	MPa

Bottom face of cast concrete

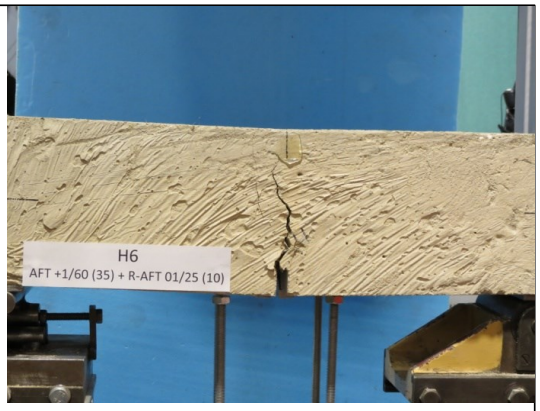

Top face of cast concrete

Crack zone of bottom face

Crack zone of top face

Stress-deformation graphs

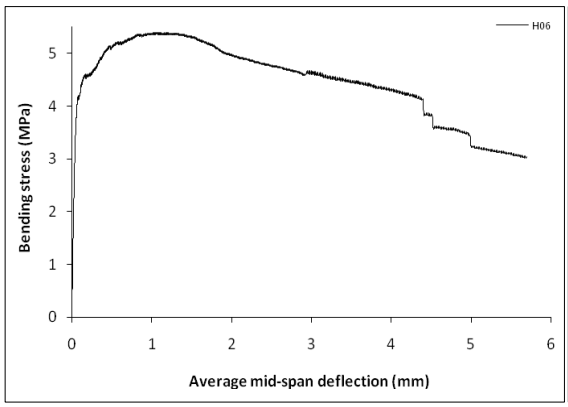

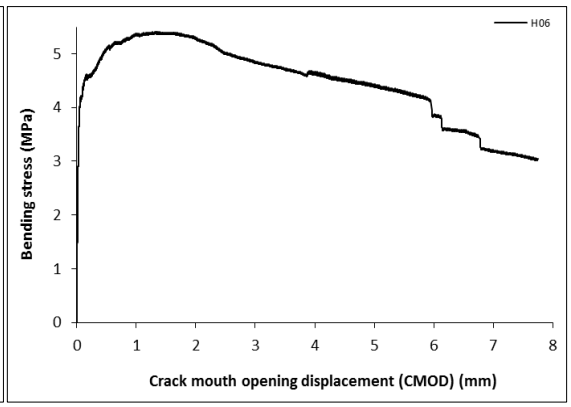

Specimen code name:		H7			
Notched Depth d_n	125	mm			
Depth, d	149	mm	Span, L	500	mm
Width, b	155	mm	Flexural strength	3.98	MPa

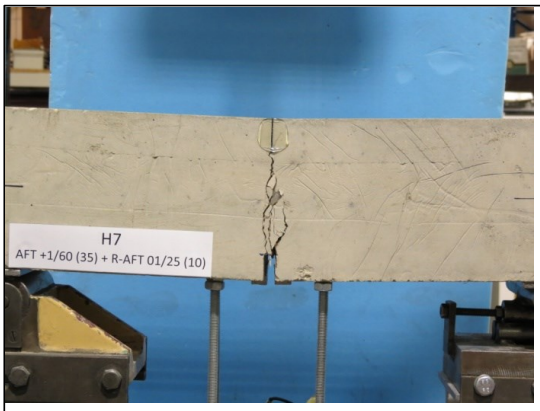

Bottom face of cast concrete

Top face of cast concrete

Crack zone of bottom face

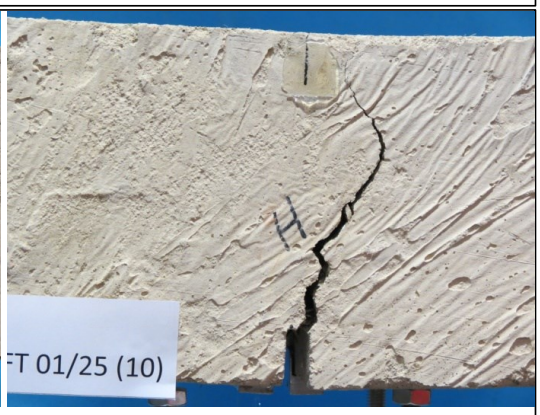

Crack zone of top face

Stress-deformation graphs

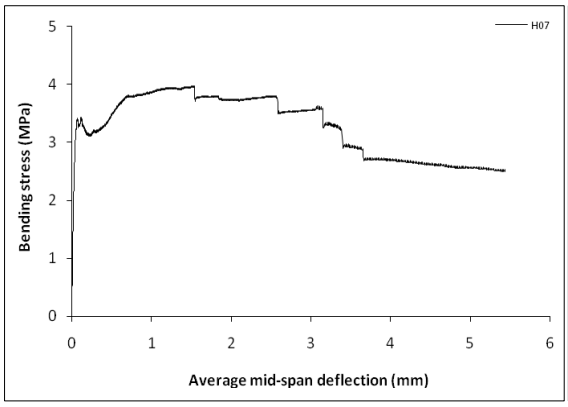

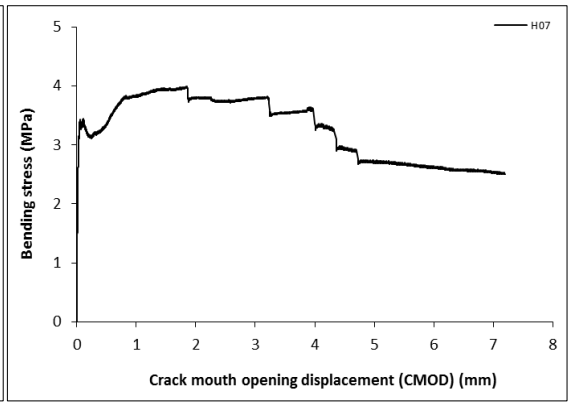

Specimen code name:		H8			
Notched Depth d_n	125	mm			
Depth, d	150	mm	Span, L	500	mm
Width, b	155	mm	Flexural strength	3.34	MPa

Bottom face of cast concrete

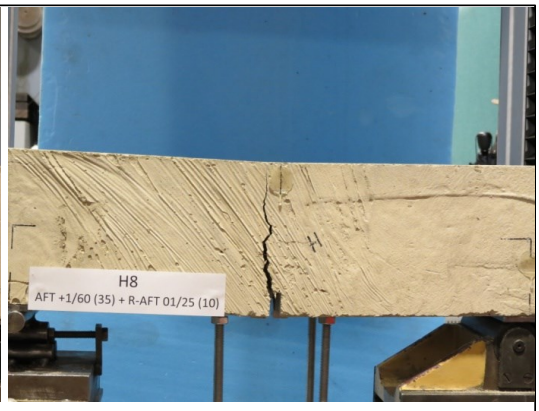

Top face of cast concrete

Crack zone of bottom face

Crack zone of top face

Stress-deformation graphs

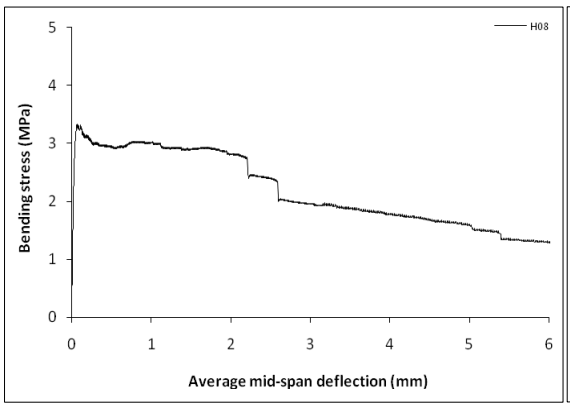

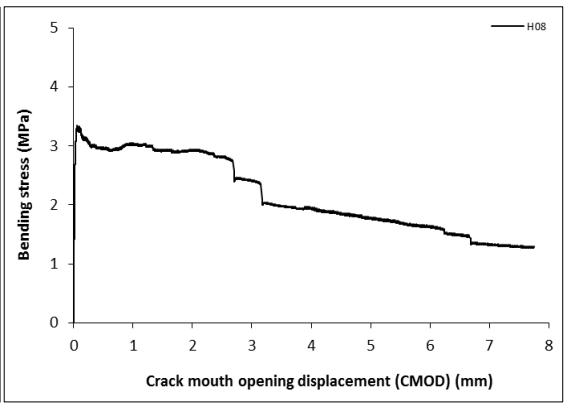

Specimen code name:		H9			
Notched Depth d_n	125	mm			
Depth, d	149	mm	Span, L	500	mm
Width, b	154	mm	Flexural strength	4.21	MPa

Bottom face of cast concrete

Top face of cast concrete

Crack zone of bottom face

Crack zone of top face

Stress-deformation graphs

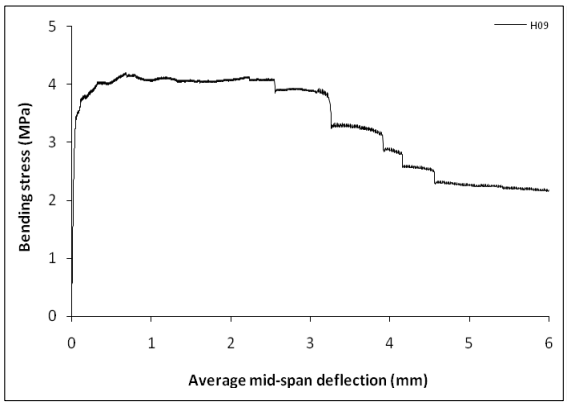

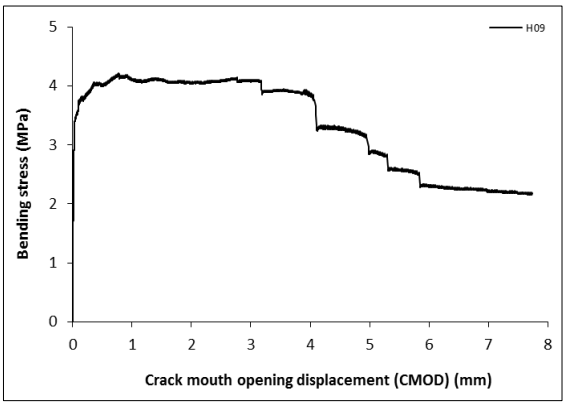

Specimen code name:		H10			
Notched Depth d_n	125	mm			
Depth, d	150	mm	Span, L	500	mm
Width, b	154	mm	Flexural strength	3.67	MPa

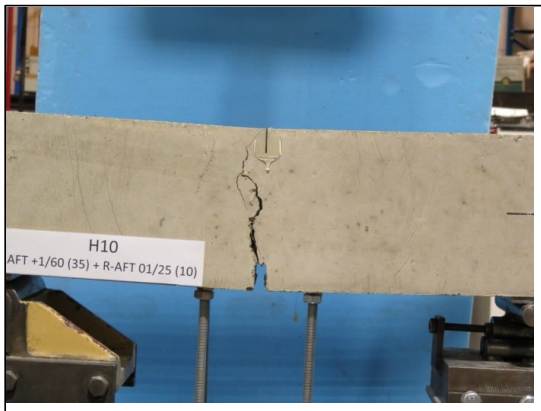

Bottom face of cast concrete

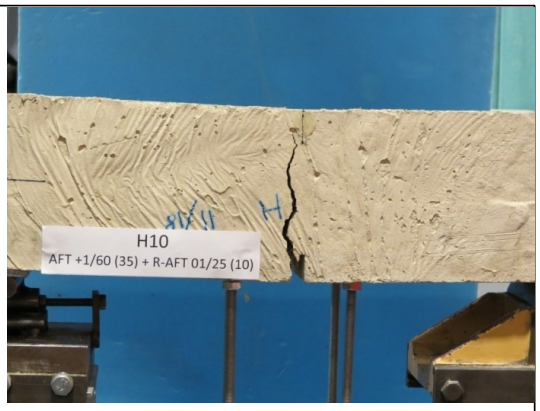

Top face of cast concrete

Crack zone of bottom face

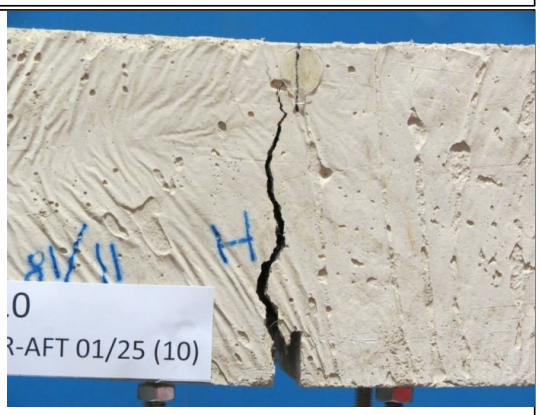

Crack zone of top face

Stress-deformation graphs

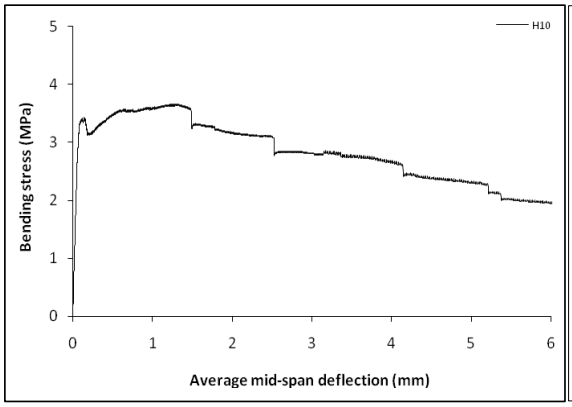

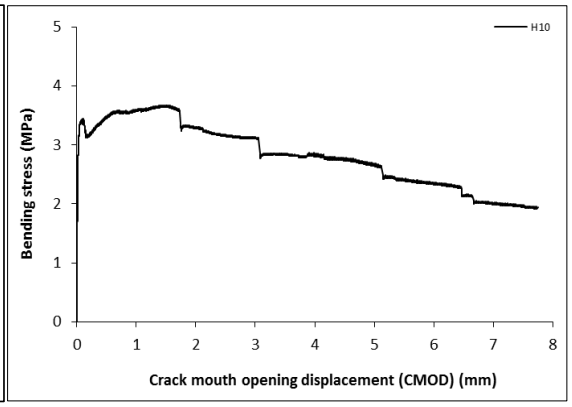

Specimen code name:		H11			
Notched Depth d_n	124	mm			
Depth, d	150	mm	Span, L	500	mm
Width, b	154	mm	Flexural strength	4.15	MPa

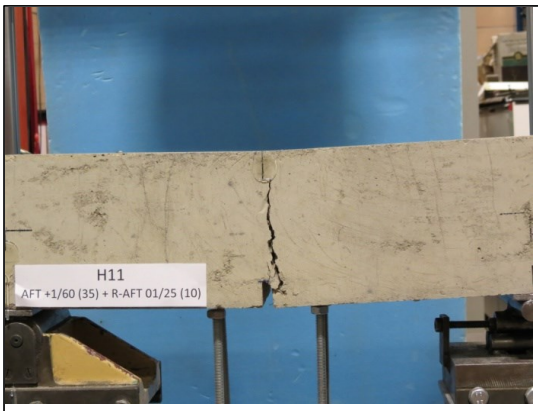

Bottom face of cast concrete

Top face of cast concrete

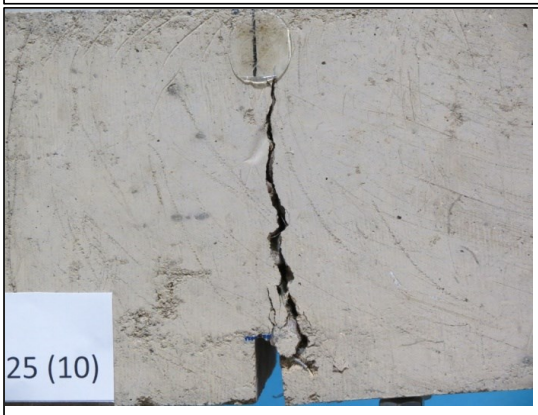

Crack zone of bottom face

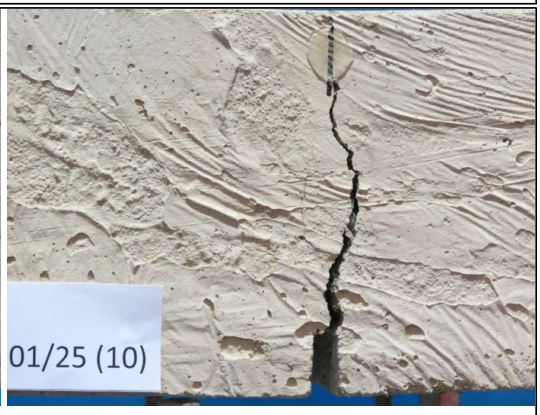

Crack zone of top face

Stress-deformation graphs

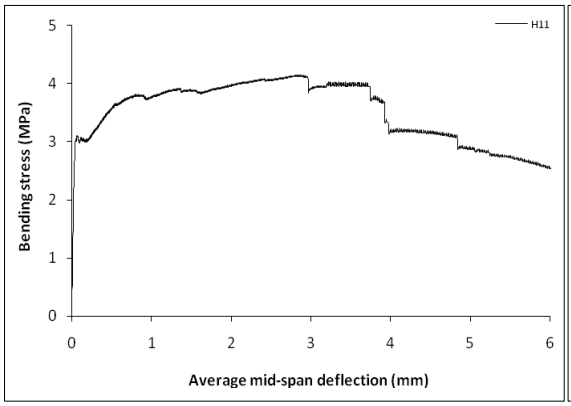

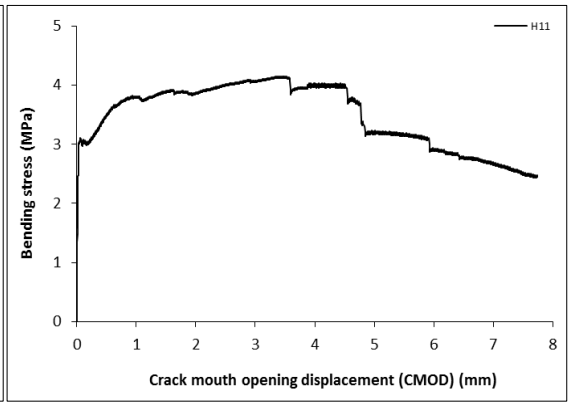

Specimen code name:		H12			
Notched Depth d_n	126	mm			
Depth, d	152	mm	Span, L	500	mm
Width, b	153	mm	Flexural strength	3.73	MPa

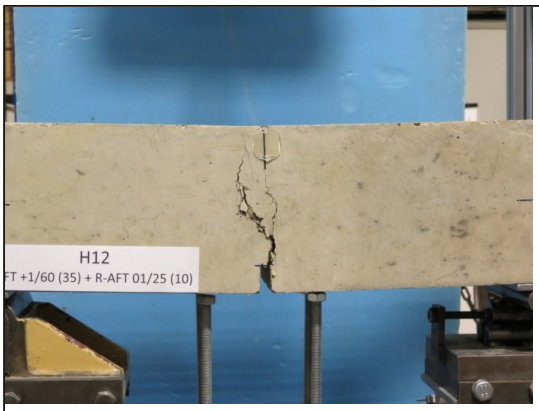

Bottom face of cast concrete

Top face of cast concrete

Crack zone of bottom face

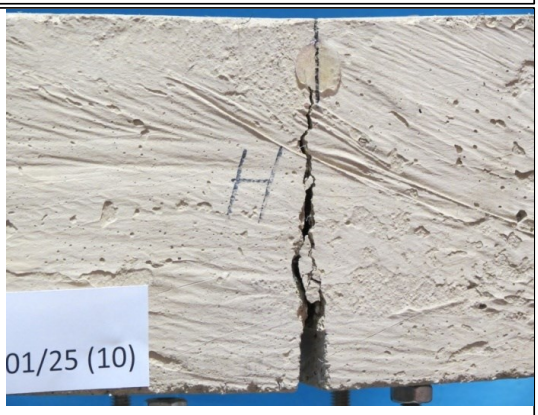

Crack zone of top face

Stress-deformation graphs

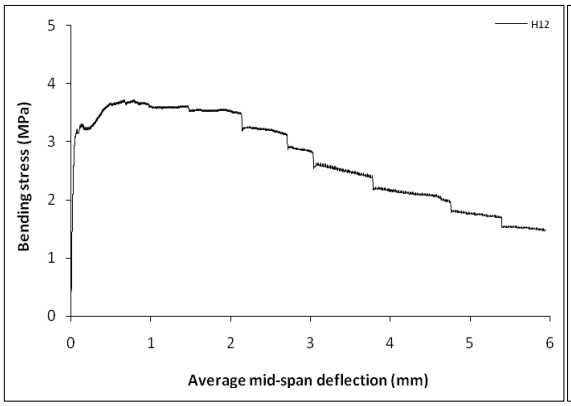

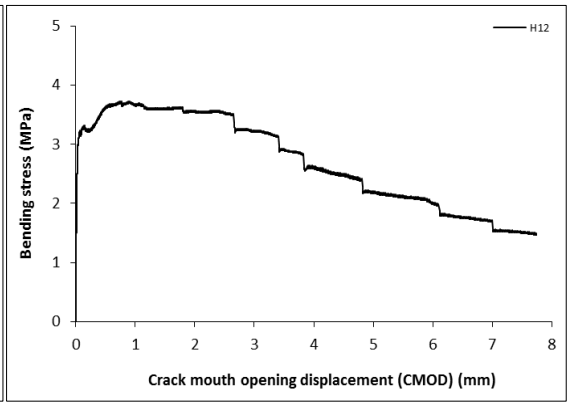

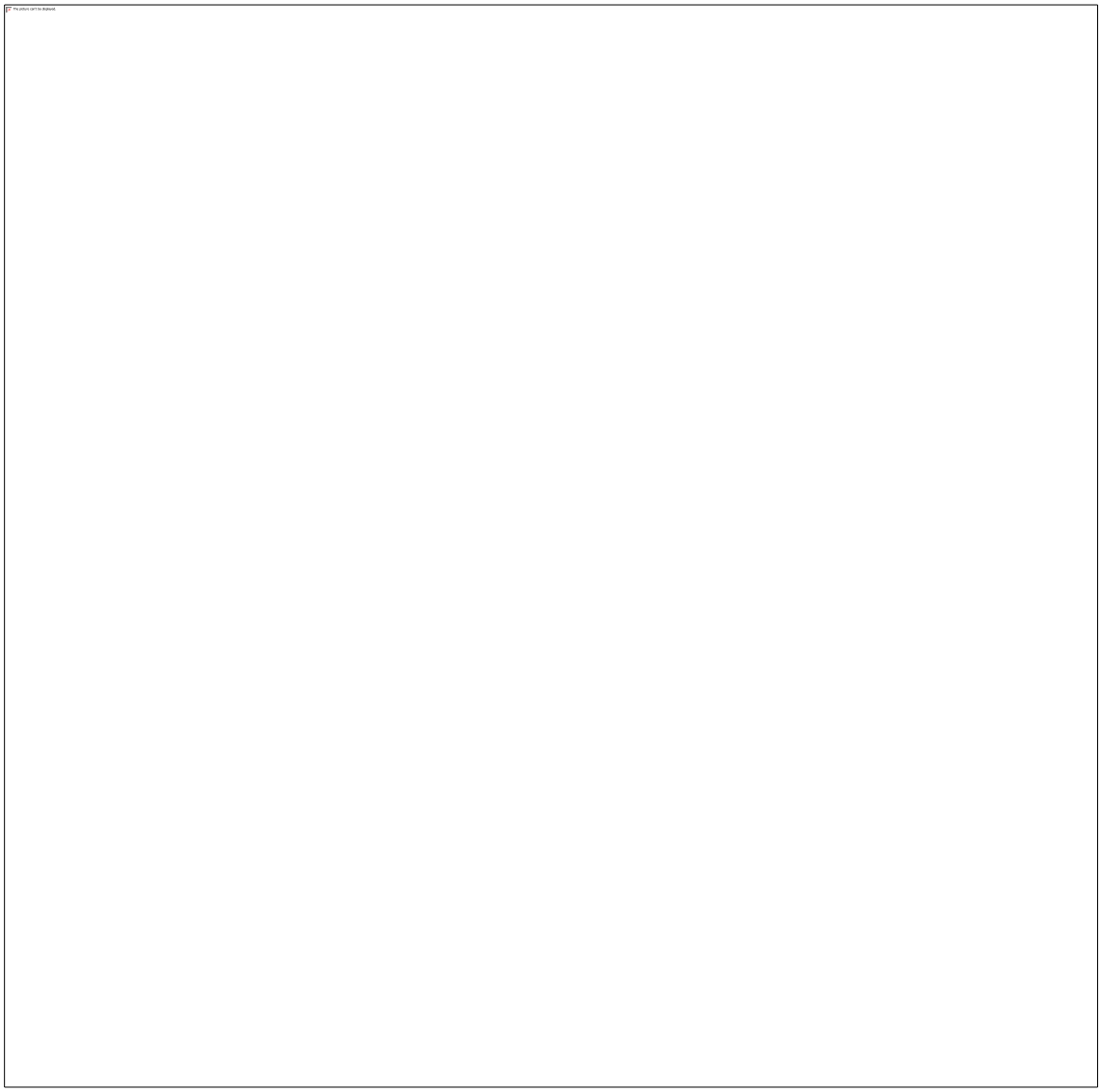

Specimen code name:		I1			
Notched Depth d_n	124	mm			
Depth, d	150	mm	Span, L	500	mm
Width, b	151	mm	Flexural strength	4.84	MPa

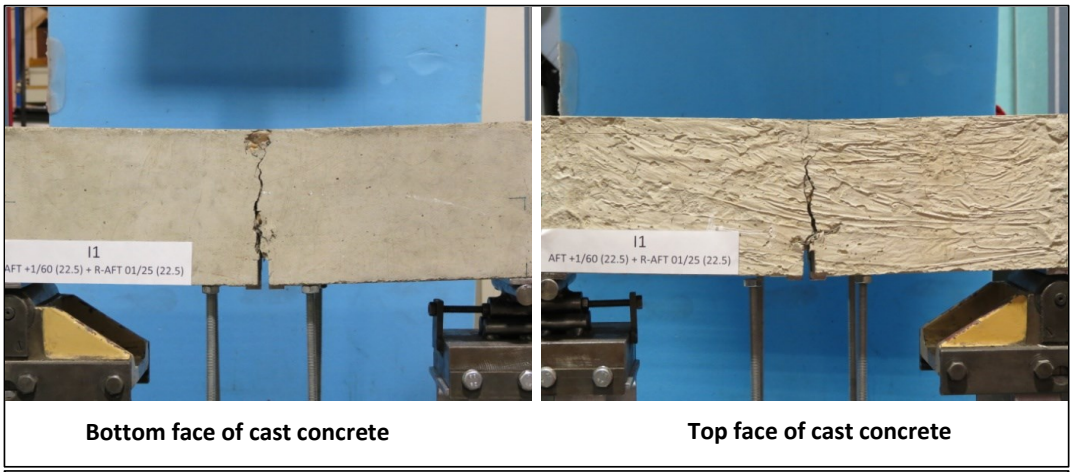

Bottom face of cast concrete **Top face of cast concrete**

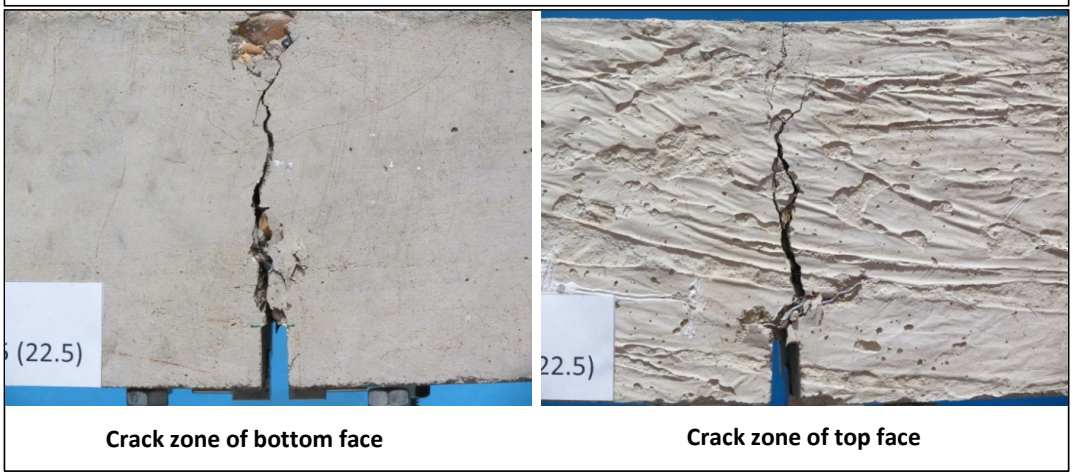

Crack zone of bottom face **Crack zone of top face**

Stress-deformation graphs

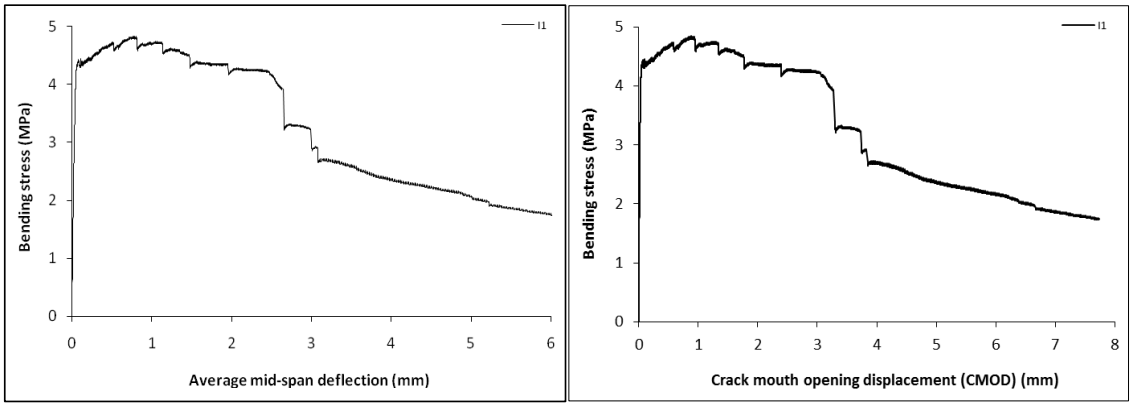

Specimen code name:		I2			
Notched Depth d_n	124	mm			
Depth, d	150	mm	Span, L	500	mm
Width, b	151	mm	Flexural strength	5.98	MPa

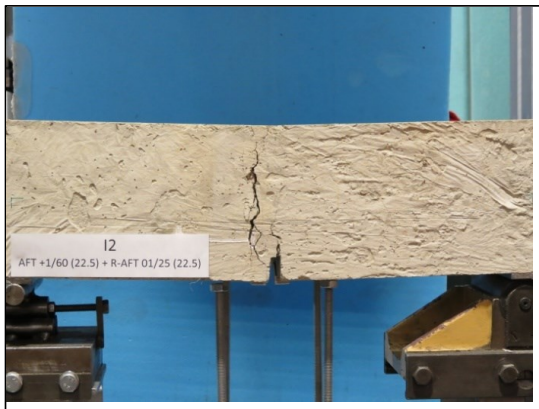

Bottom face of cast concrete

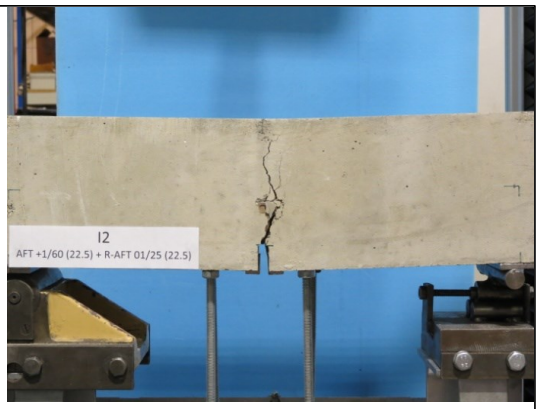

Top face of cast concrete

Crack zone of bottom face

Crack zone of top face

Stress-deformation graphs

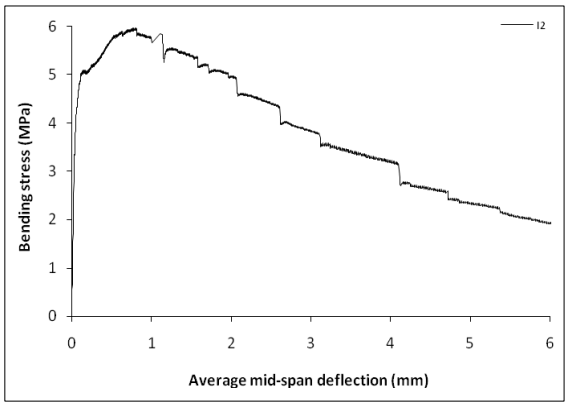

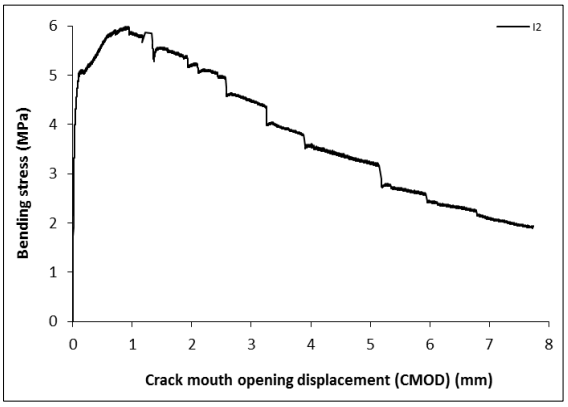

Specimen code name:		I3			
Notched Depth d_n	124	mm			
Depth, d	150	mm	Span, L	500	mm
Width, b	150	mm	Flexural strength	5.39	MPa

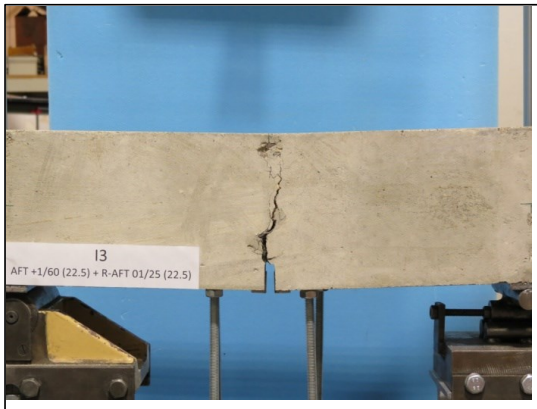

Bottom face of cast concrete

Top face of cast concrete

Crack zone of bottom face

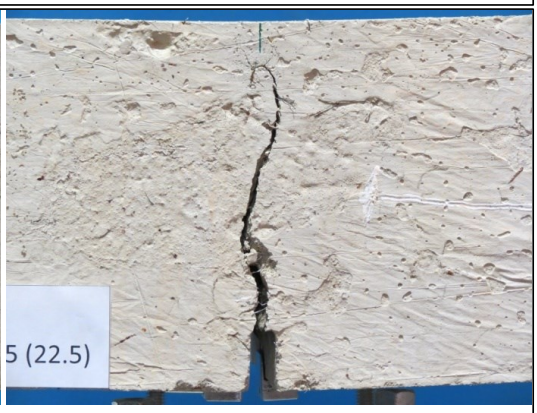

Crack zone of top face

Stress-deformation graphs

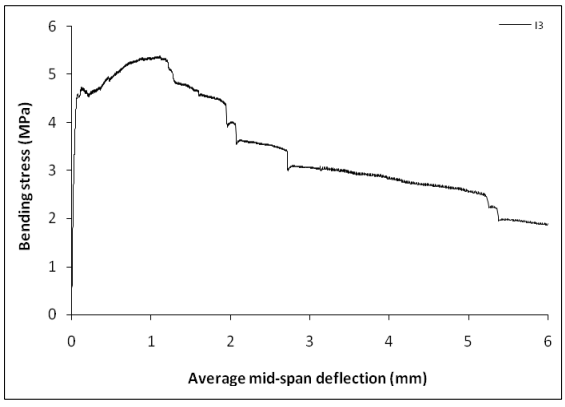

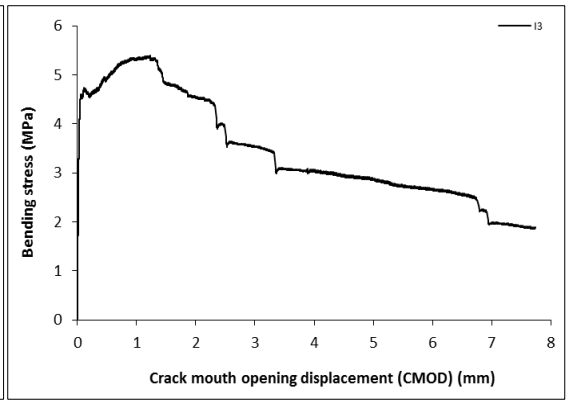

Specimen code name:		I4			
Notched Depth d_n	124	mm			
Depth, d	150	mm	Span, L	500	mm
Width, b	152	mm	Flexural strength	5.76	MPa

Bottom face of cast concrete

Top face of cast concrete

Crack zone of bottom face

Crack zone of top face

Stress-deformation graphs

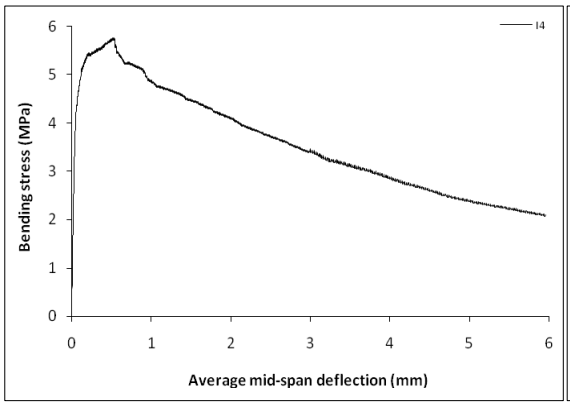

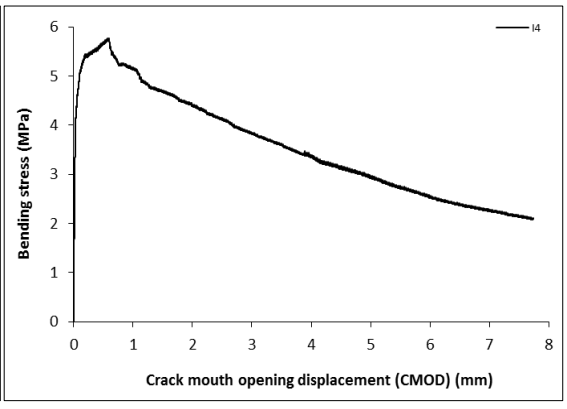

Specimen code name:		I5			
Notched Depth d_n	125	mm			
Depth, d	150	mm	Span, L	500	mm
Width, b	151	mm	Flexural strength	4.60	MPa

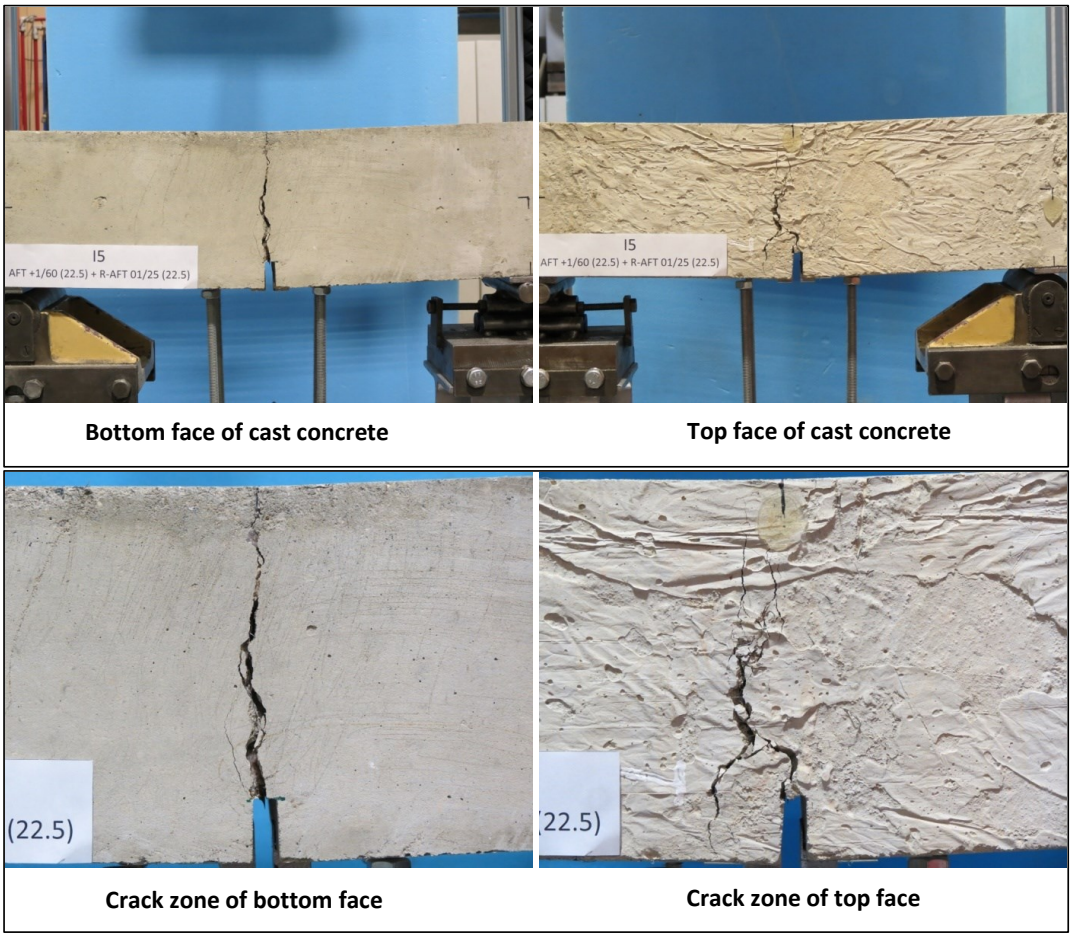

Bottom face of cast concrete | **Top face of cast concrete**

Crack zone of bottom face | **Crack zone of top face**

Stress-deformation graphs

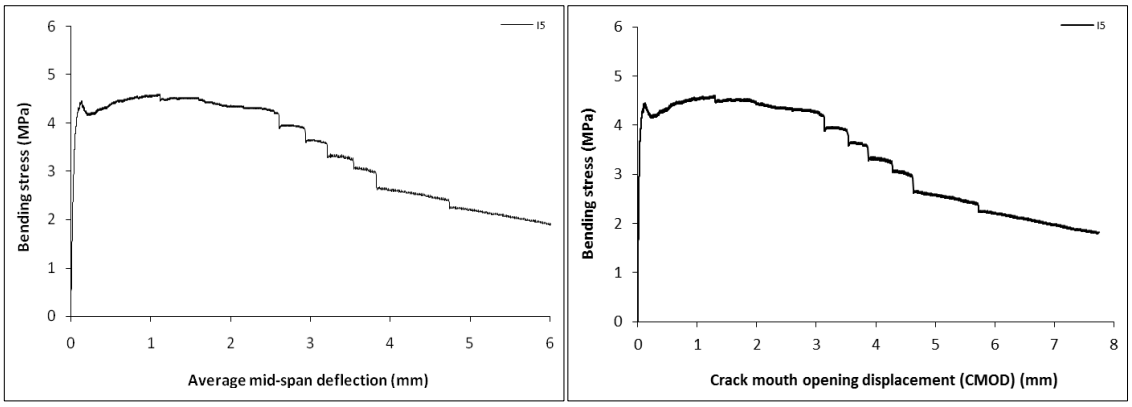

Specimen code name:		I6			
Notched Depth d_n	125	mm			
Depth, d	150	mm	Span, L	500	mm
Width, b	150	mm	Flexural strength	4.05	MPa

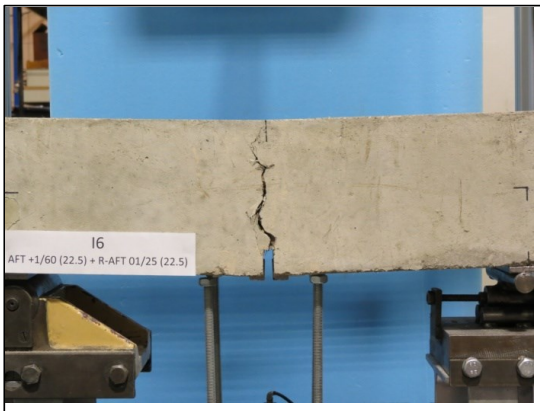

Bottom face of cast concrete

Top face of cast concrete

Crack zone of bottom face

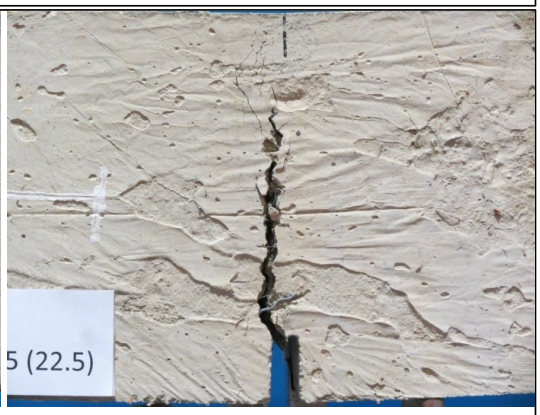

Crack zone of top face

Stress-deformation graphs

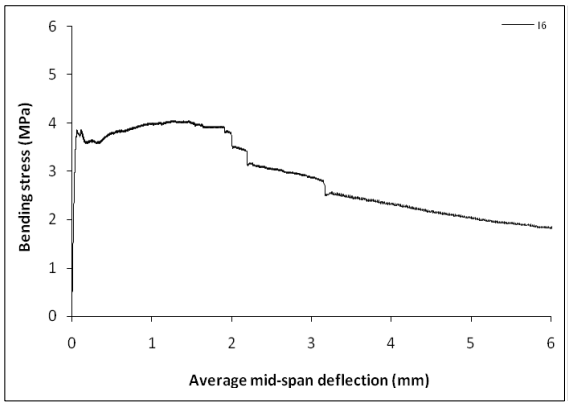

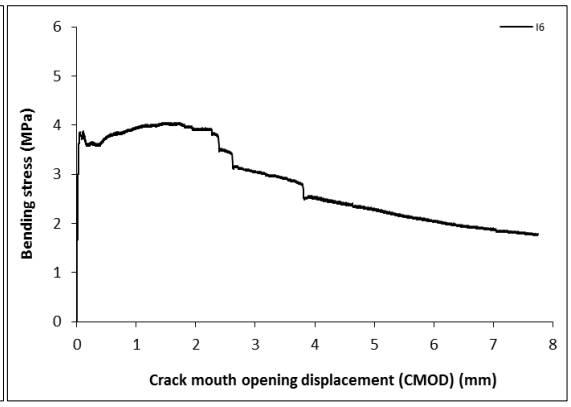

Mix:	I		
Notched Depth d_n	mm		
Depth, d	mm	Span, L	mm
Width, b	mm	Flexural strength	MPa

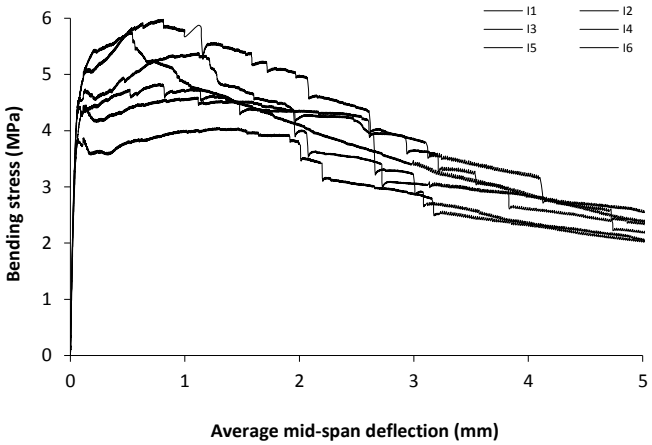

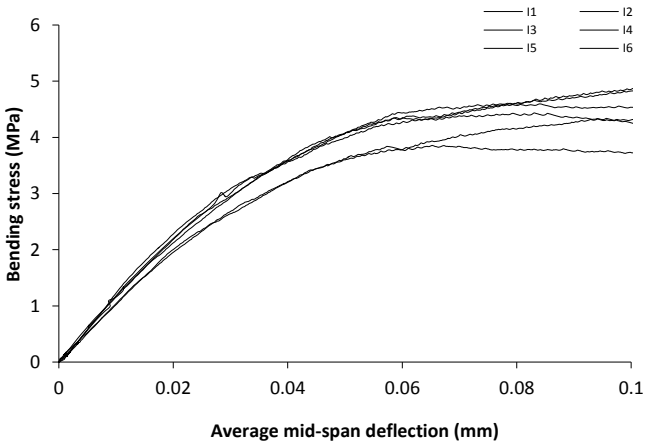

Specimen code name:		J1			
Notched Depth d_n	126	mm			
Depth, d	151	mm	Span, L	500	mm
Width, b	151	mm	Flexural strength	4.62	MPa

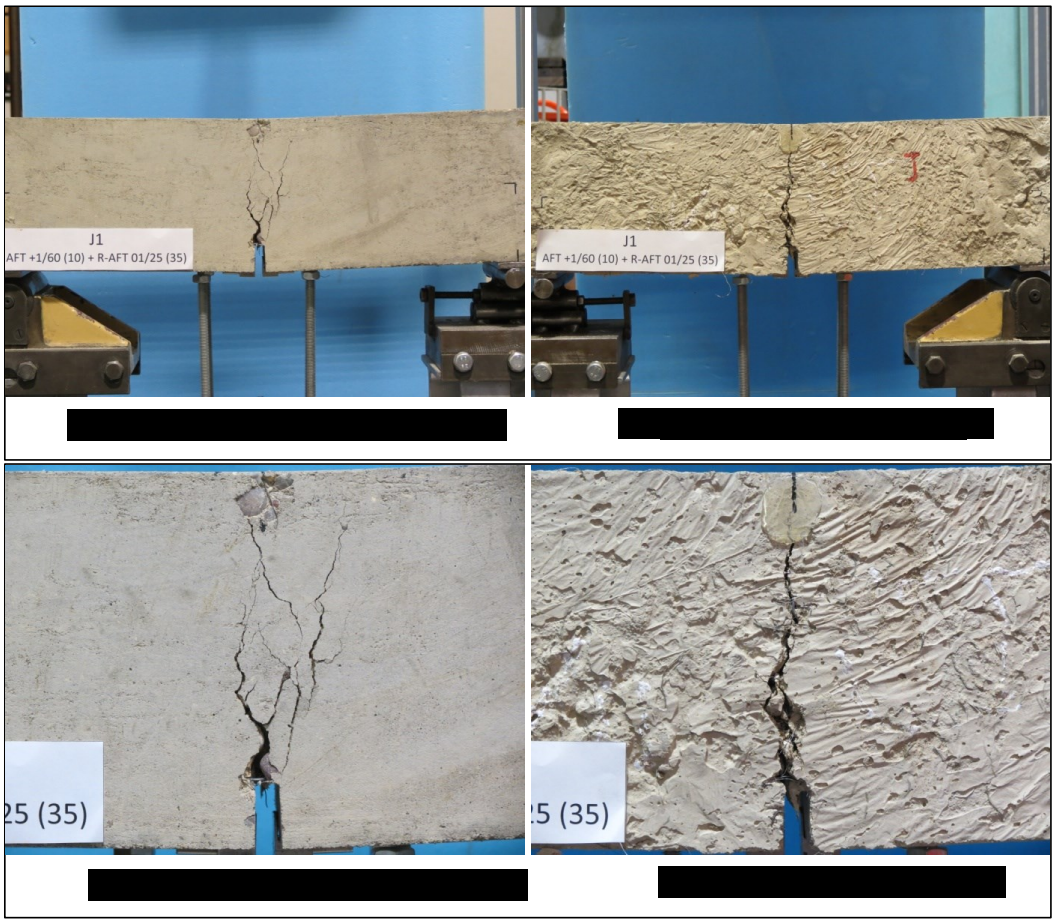

Stress-deformation graphs

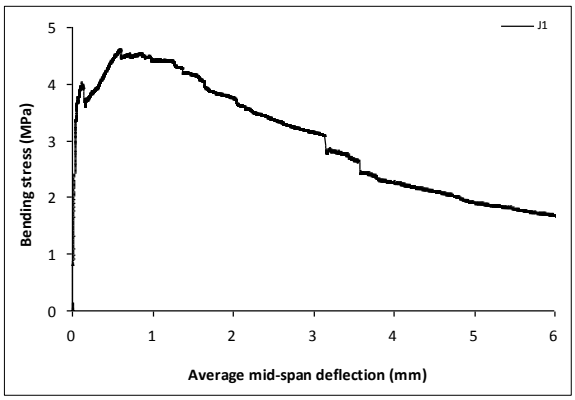

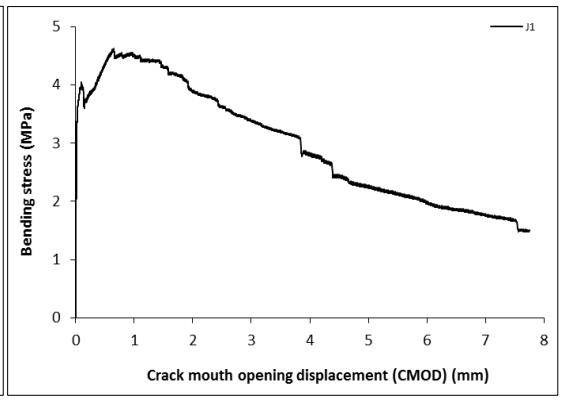

Specimen code name:		J2			
Notched Depth d_n	125	mm			
Depth, d	150	mm	Span, L	500	mm
Width, b	151	mm	Flexural strength	4.47	MPa

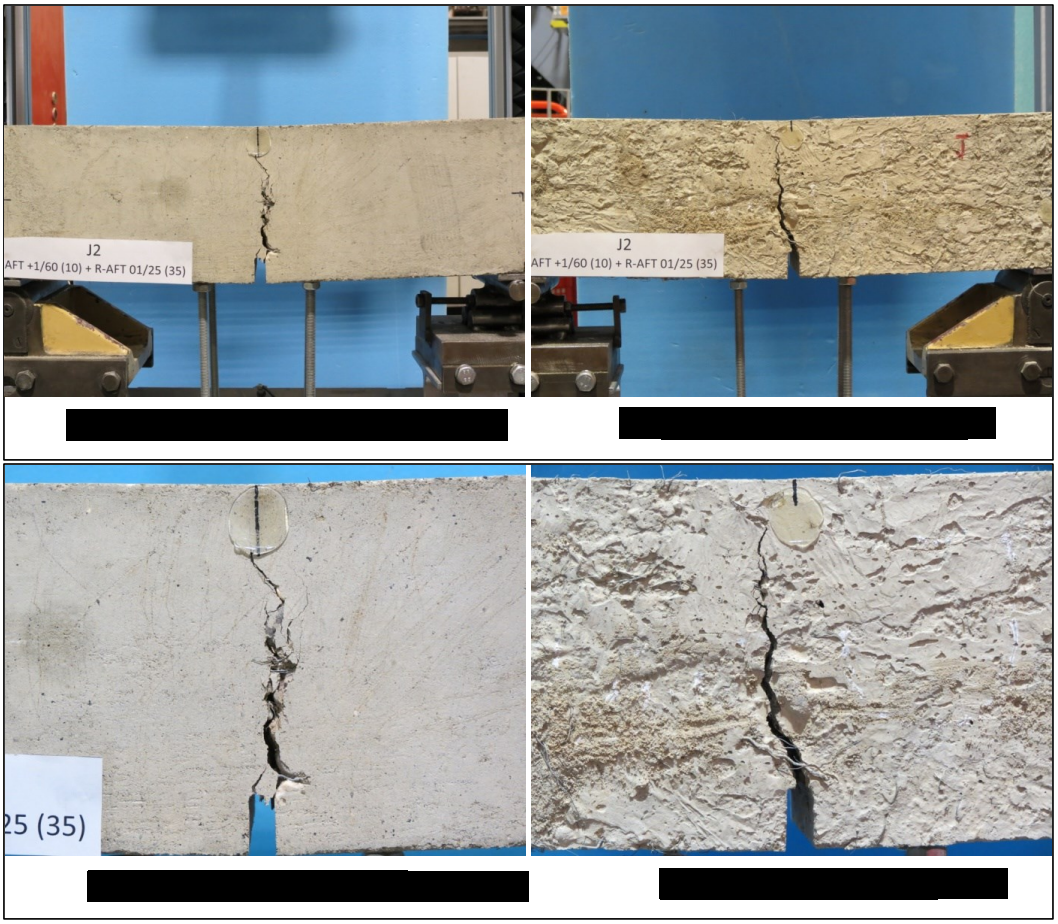

Stress-deformation graphs

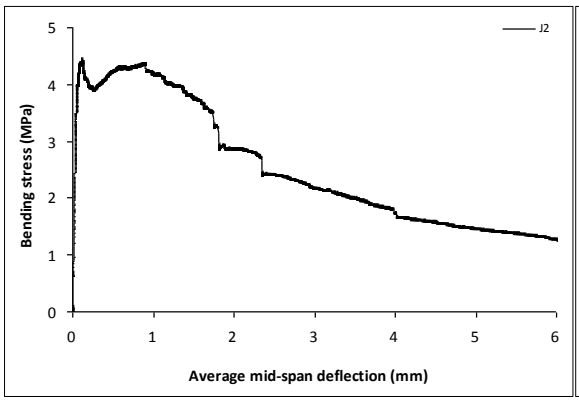

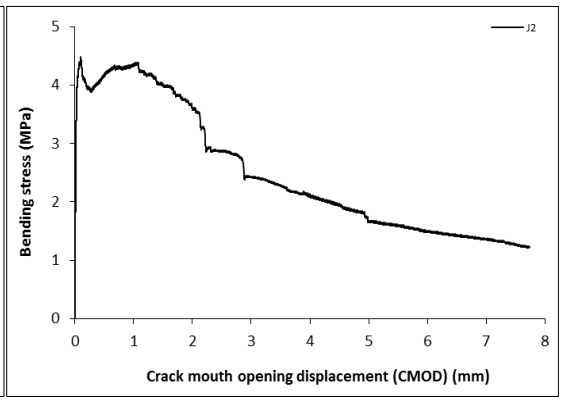

Specimen code name:		J3			
Notched Depth d_n	125	mm			
Depth, d	150	mm	Span, L	500	mm
Width, b	152	mm	Flexural strength	4.52	MPa

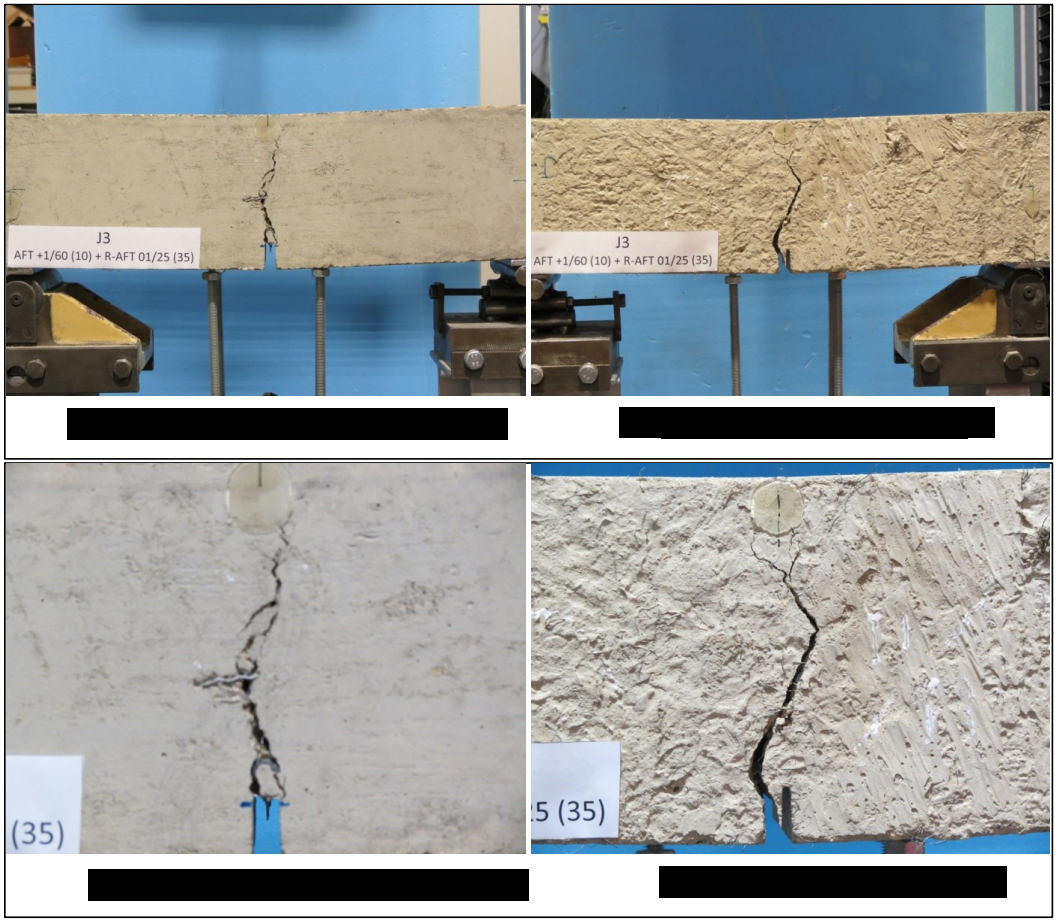

Stress-deformation graphs

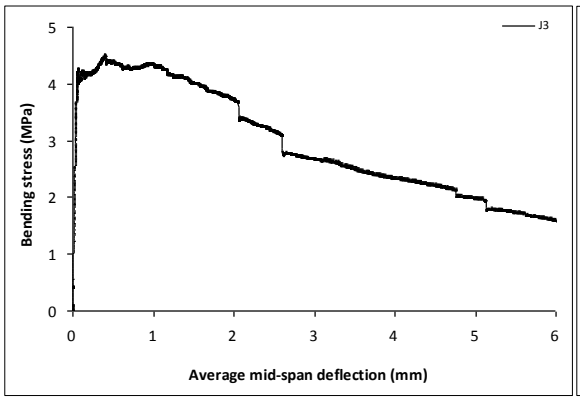

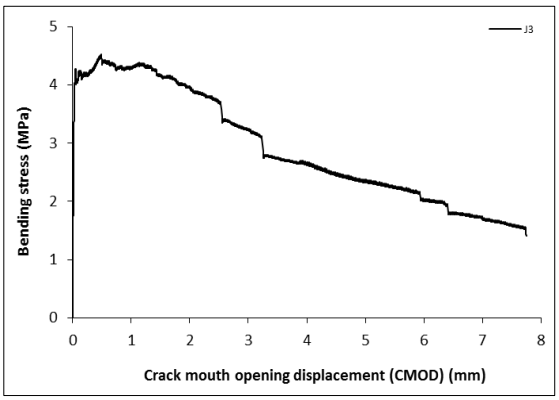

Specimen code name:		J4			
Notched Depth d_n	125	mm			
Depth, d	149	mm	Span, L	500	mm
Width, b	152	mm	Flexural strength	4.03	MPa

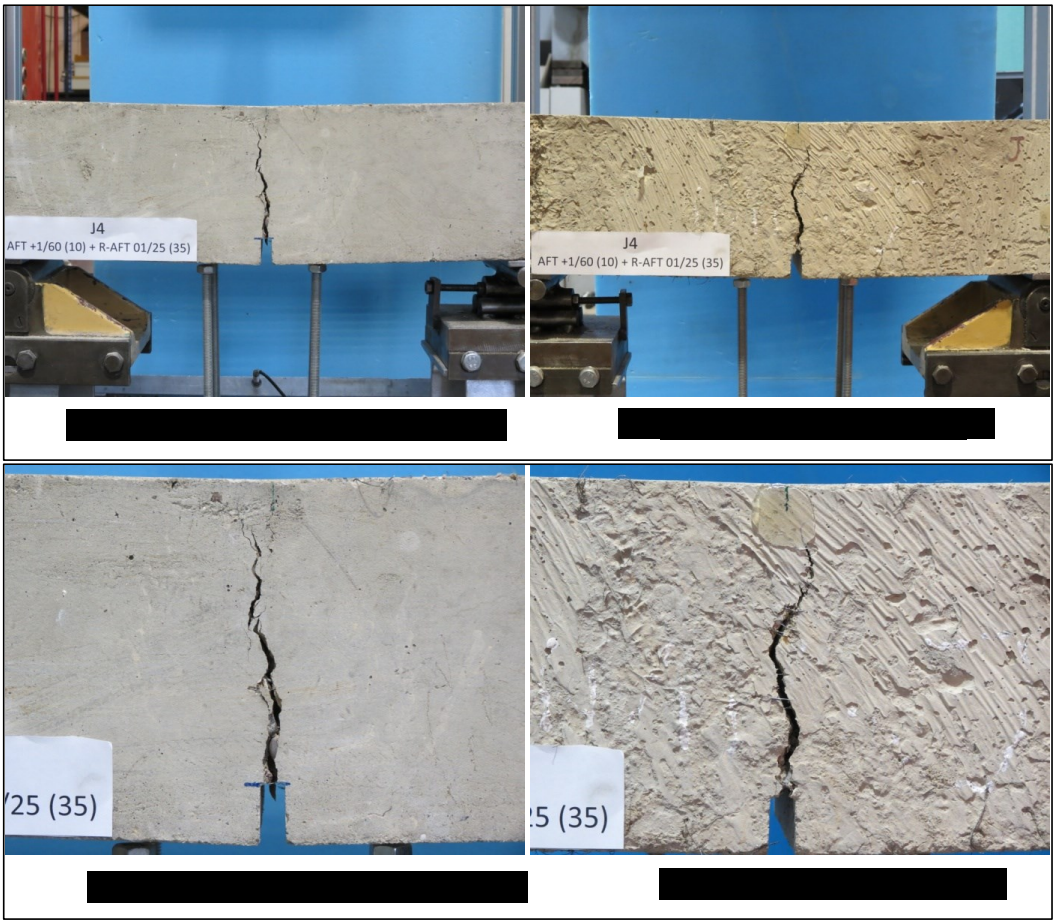

Stress-deformation graphs

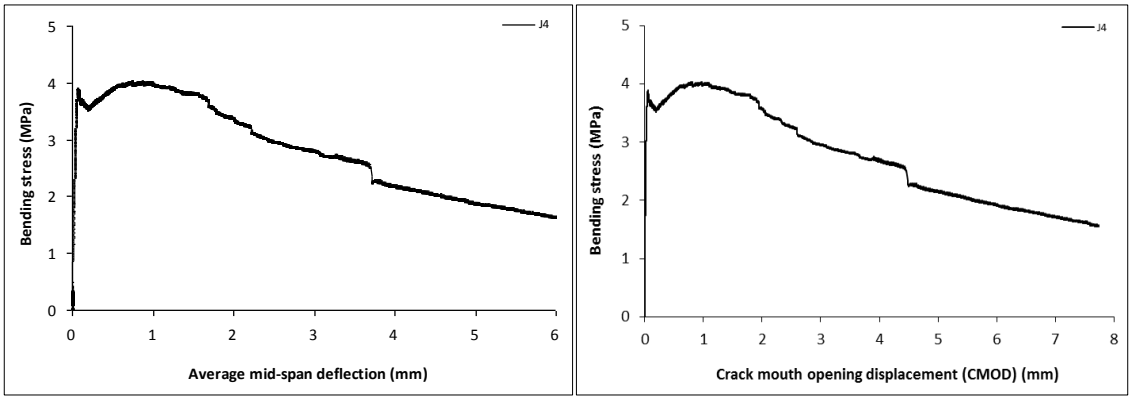

Specimen code name:		J5			
Notched Depth d_n	125	mm			
Depth, d	150	mm	Span, L	500	mm
Width, b	151	mm	Flexural strength	5.48	MPa

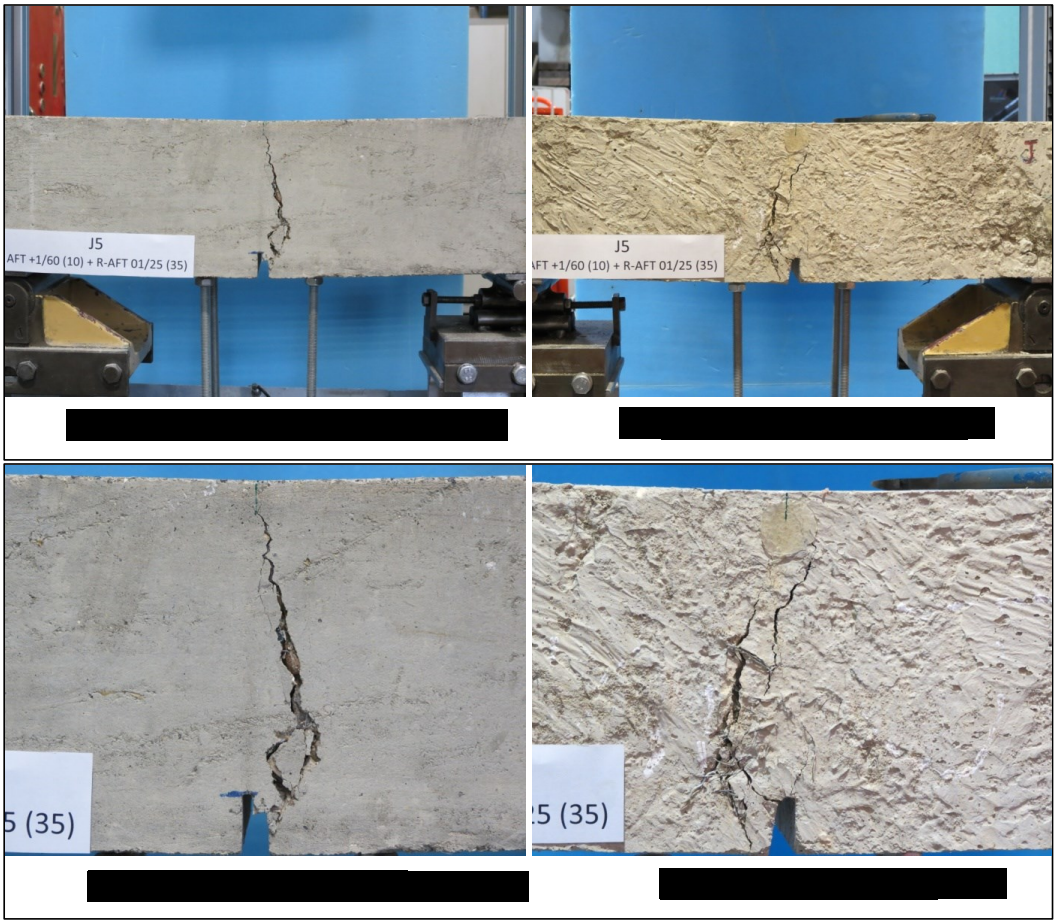

Stress-deformation graphs

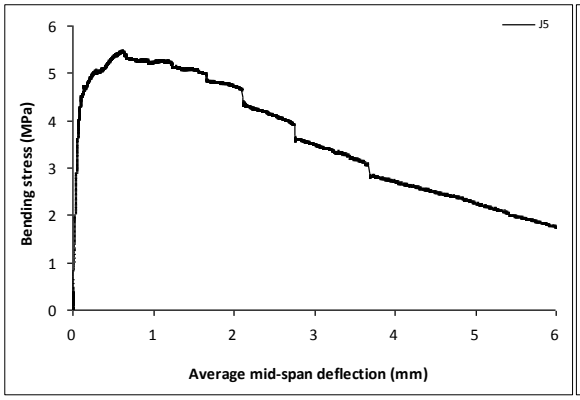

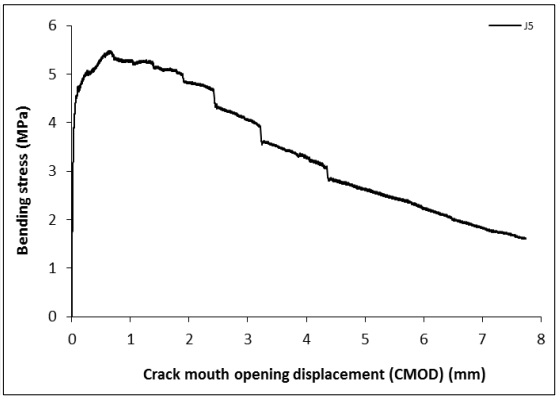

Specimen code name:		J6			
Notched Depth d_n	123	mm			
Depth, d	149	mm	Span, L	500	mm
Width, b	152	mm	Flexural strength	5.44	MPa

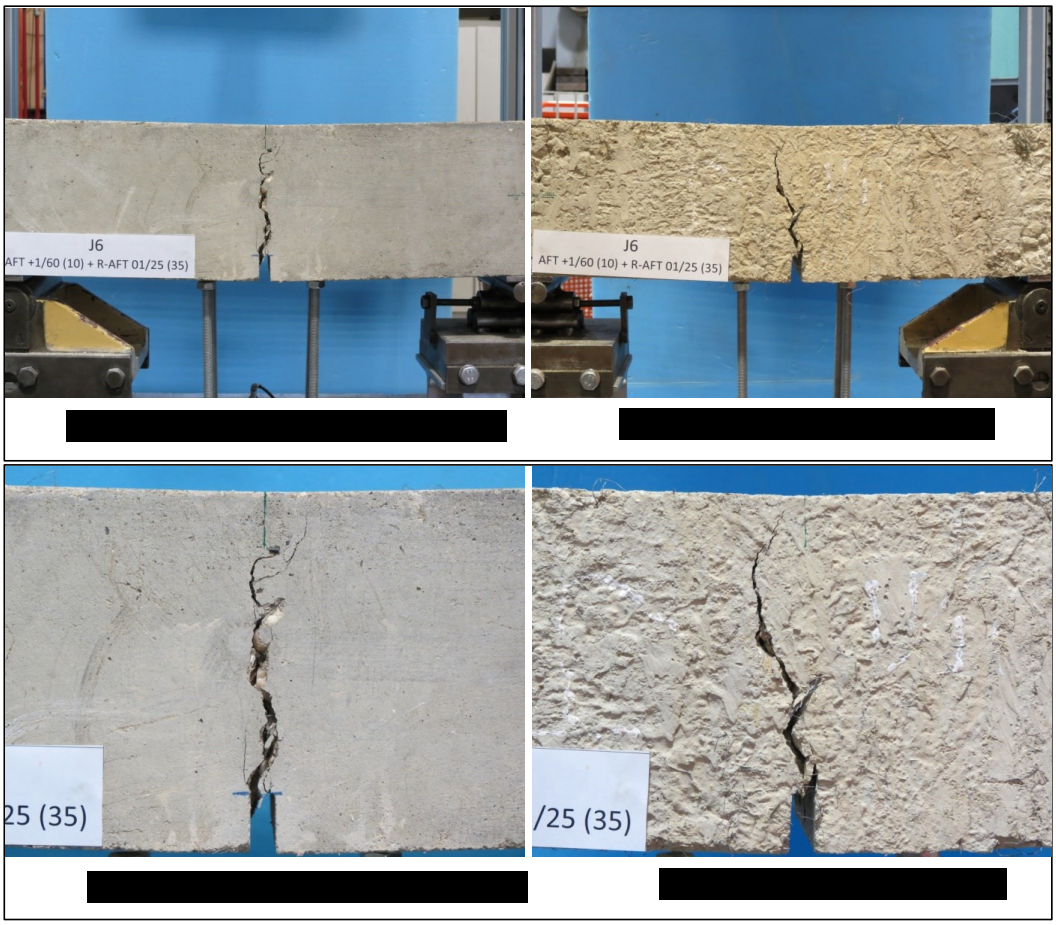

Stress-deformation graphs

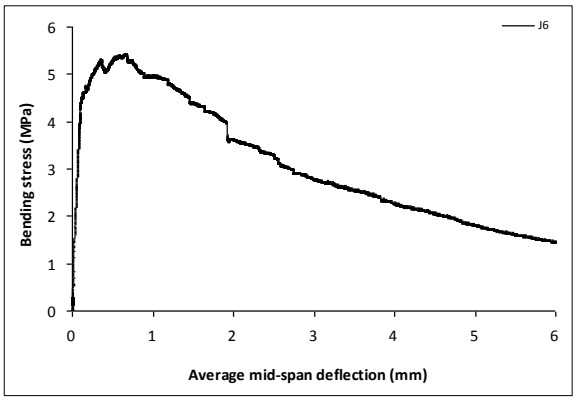

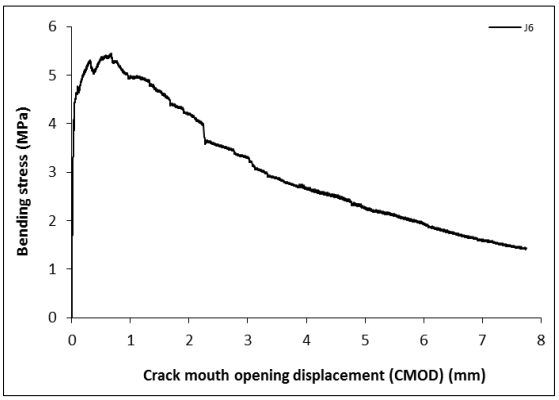

Mix:	J		
Notched Depth d_n	mm		
Depth, d	mm	Span, L	mm
Width, b	mm	Flexural strength	MPa

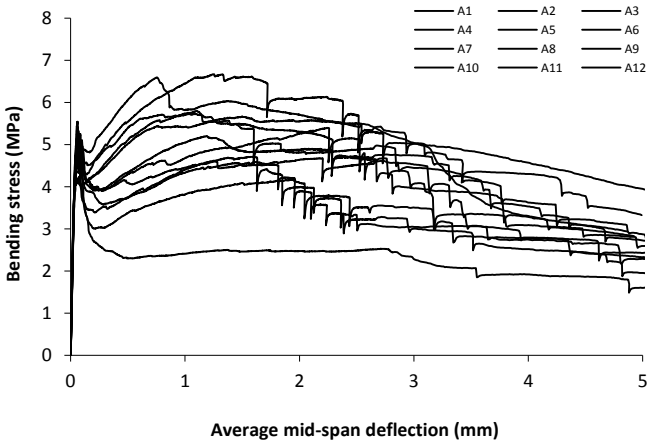

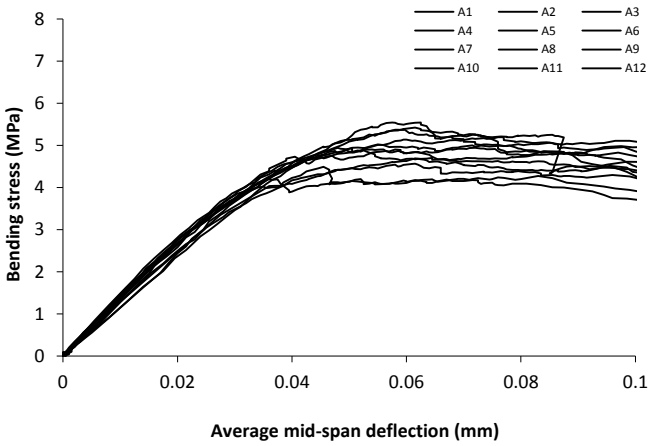

Specimen code name:		Plain 04/11-1			
Notched Depth d_n	125	mm			
Depth, d	150	mm	Span, L	500	mm
Width, b	151	mm	Flexural strength	3.19	MPa

Stress-deformation graphs

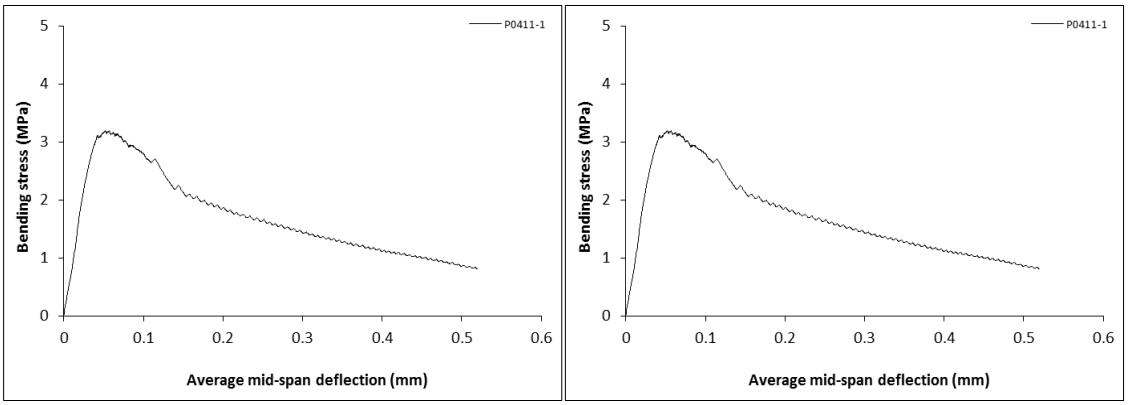

Specimen code name:		**Plain 04/11-2**			
Notched Depth d_n	123	mm			
Depth, d	149	mm	Span, L	500	mm
Width, b	152	mm	Flexural strength	2.88	MPa

Stress-deformation graphs

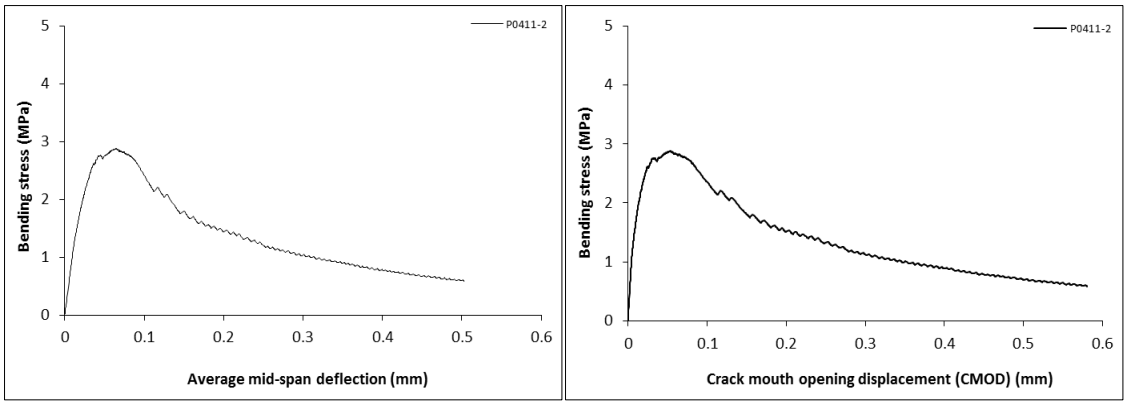

Specimen code name:		**Plain 04/11-3**			
Notched Depth d_n	126	mm			
Depth, d	151	mm	Span, L	500	mm
Width, b	153	mm	Flexural strength	3.01	MPa

Stress-deformation graphs

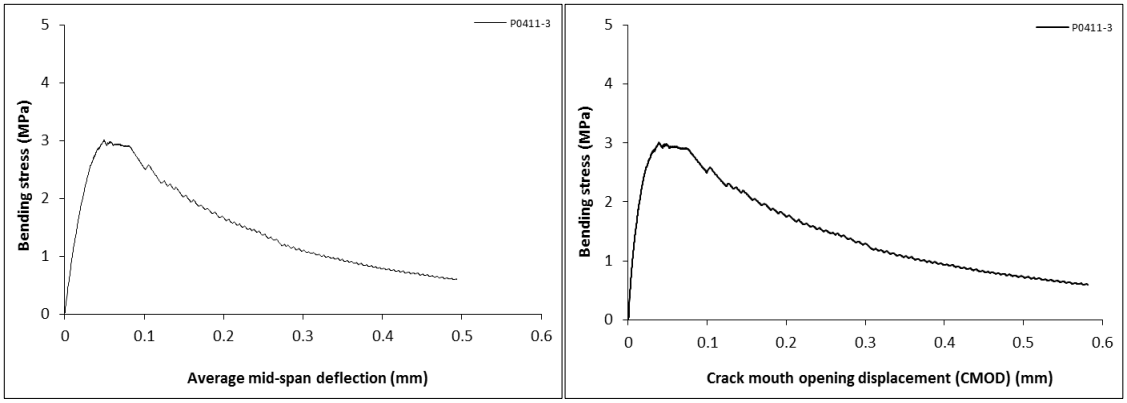

Specimen code name:		**Plain 04/11-4**			
Notched Depth d_n	124	mm			
Depth, d	149	mm	Span, L	500	mm
Width, b	152	mm	Flexural strength	3.32	MPa

Stress-deformation graphs

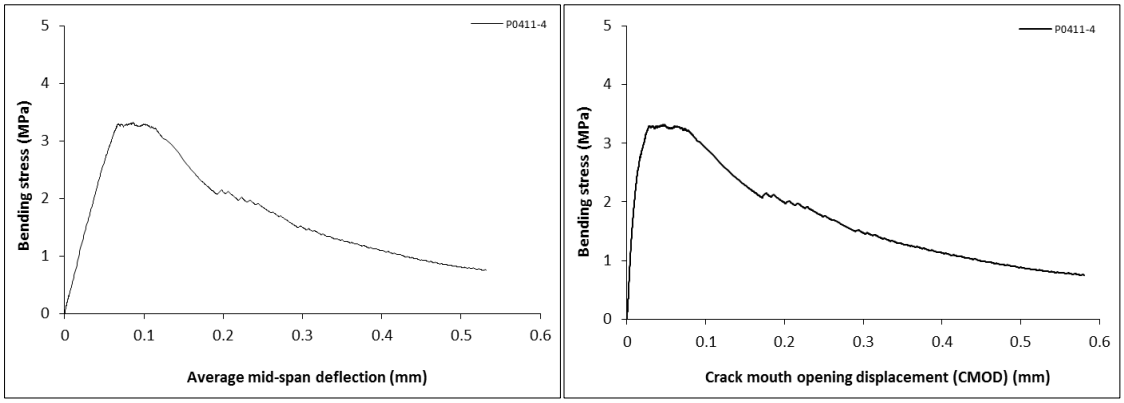

Specimen code name:		Plain 04/11-5			
Notched Depth d_n	124	mm			
Depth, d	150	mm	Span, L	500	mm
Width, b	154	mm	Flexural strength	2.90	MPa

Stress-deformation graphs

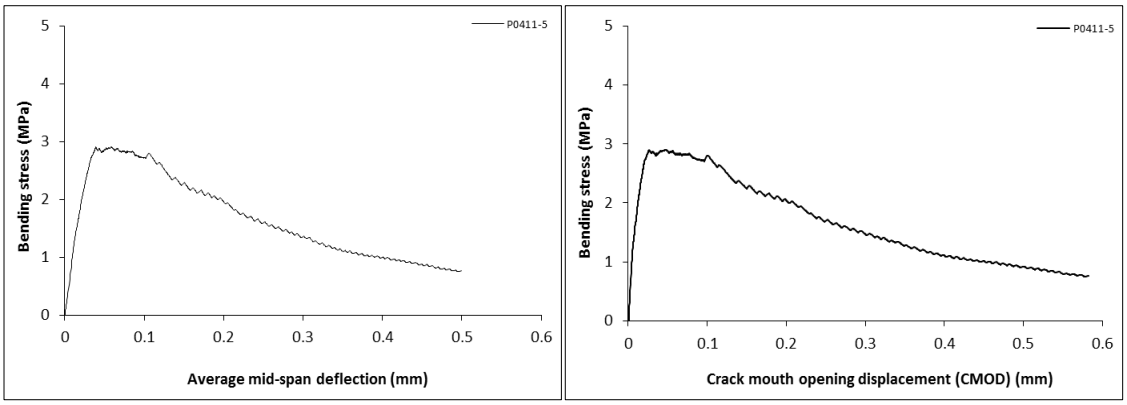

Specimen code name:		**Plain 04/11-6**			
Notched Depth d_n	124	mm			
Depth, d	150	mm	Span, L	500	mm
Width, b	151	mm	Flexural strength	2.92	MPa

Stress-deformation graphs

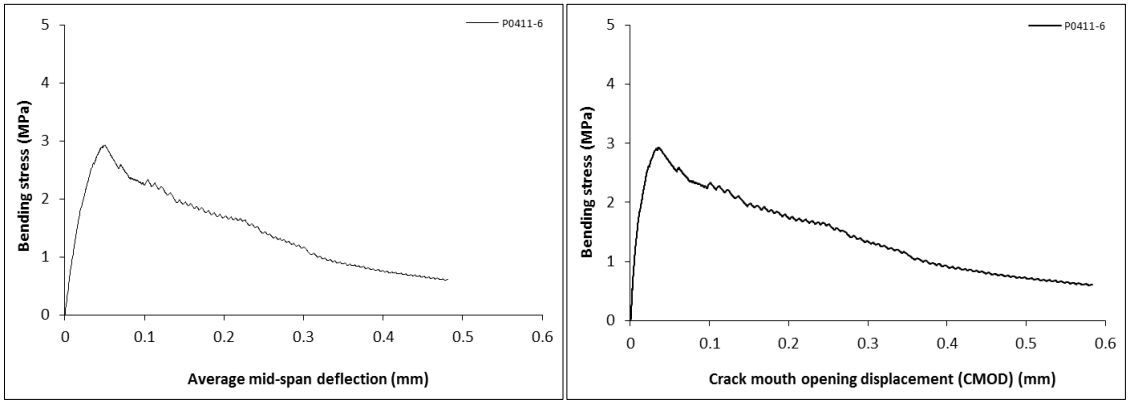

Mix:	**Plain 04/11**		
Notched Depth d_n	mm		
Depth, d	mm	Span, L	mm
Width, b	mm	Flexural strength	MPa

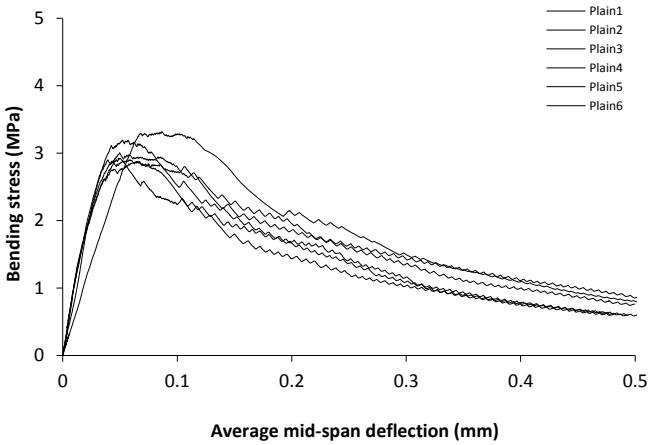

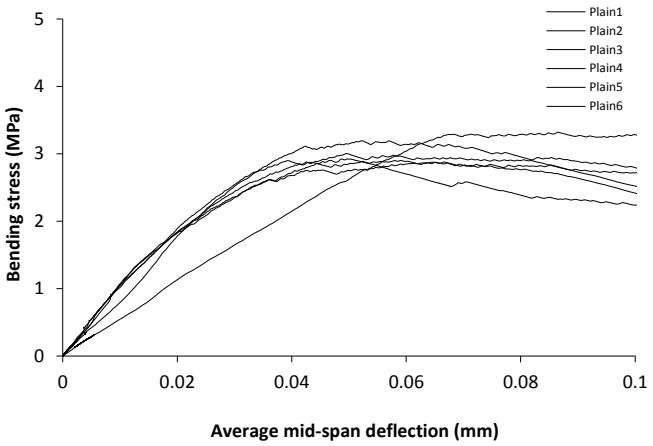

Specimen code name:		Plain 11/11-1			
Notched Depth d_n	124	mm			
Depth, d	150	mm	Span, L	500	mm
Width, b	154	mm	Flexural strength	3.26	MPa

Stress-deformation graphs

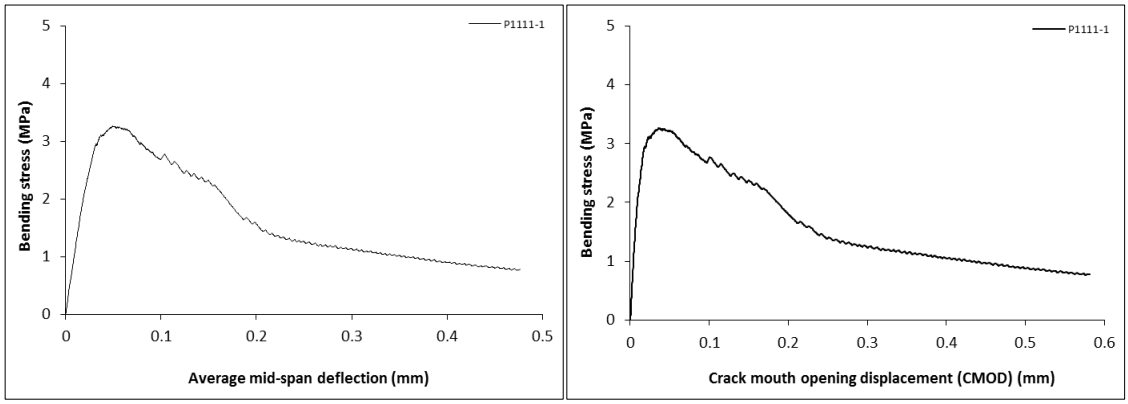

Specimen code name:		Plain 11/11-2			
Notched Depth d_n	125	mm			
Depth, d	150	mm	Span, L	500	mm
Width, b	154	mm	Flexural strength	2.92	MPa

Stress-deformation graphs

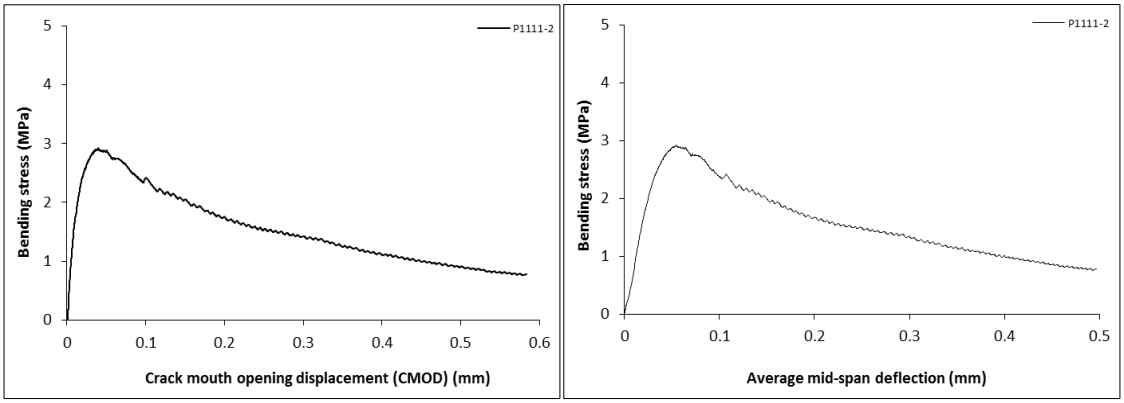

Specimen code name:		**Plain 11/11-3**			
Notched Depth d_n	125	mm			
Depth, d	150	mm	Span, L	500	mm
Width, b	152	mm	Flexural strength	3.58	MPa

Stress-deformation graphs

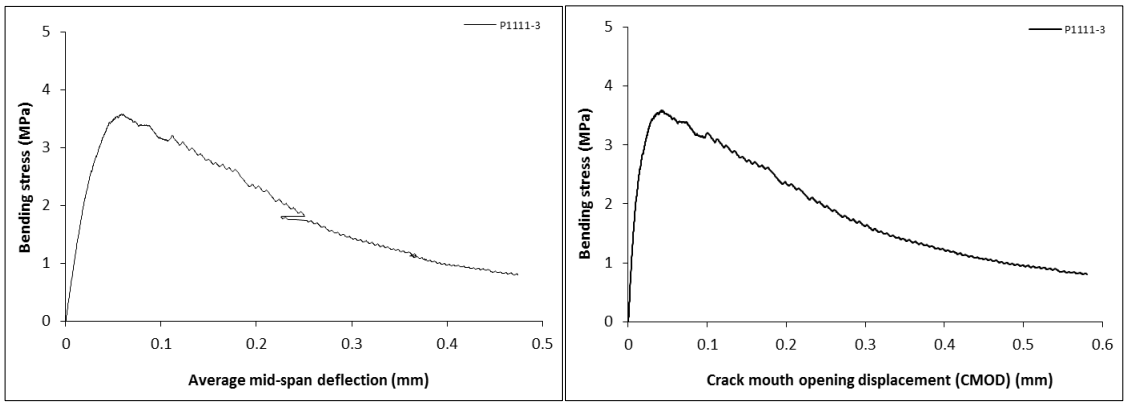

Specimen code name:		Plain 11/11-4			
Notched Depth d_n	125	mm			
Depth, d	150	mm	Span, L	500	mm
Width, b	151	mm	Flexural strength	3.48	MPa

Stress-deformation graphs

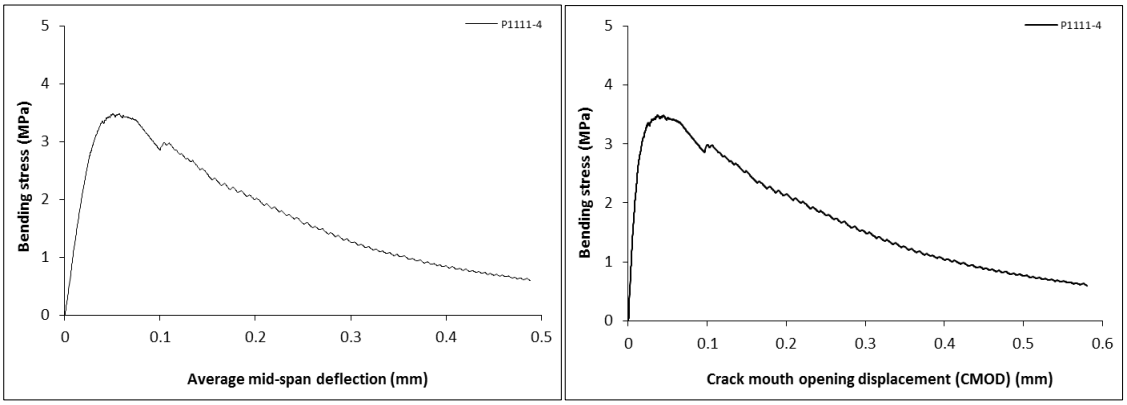

Specimen code name:		**Plain 11/11-5**			
Notched Depth d_n	126	mm			
Depth, d	151	mm	Span, L	500	mm
Width, b	152	mm	Flexural strength	3.09	MPa

Stress-deformation graphs

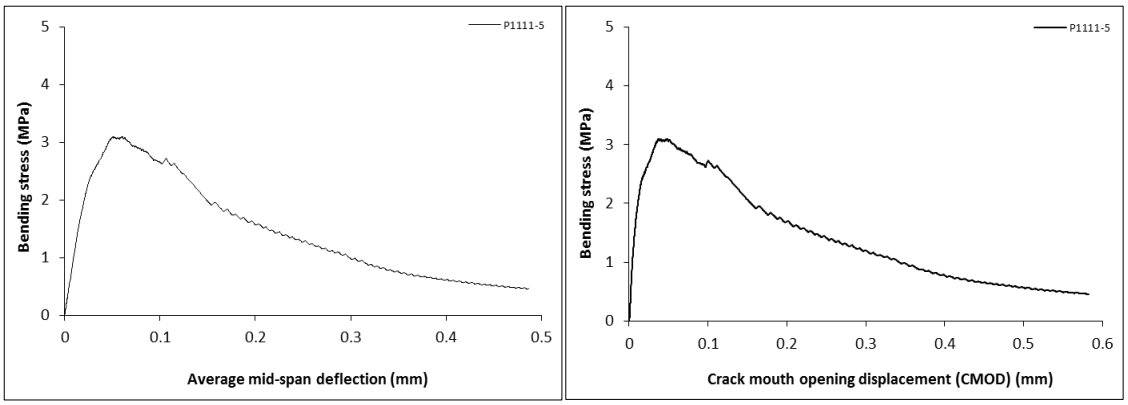

Mix:	**Plain 11/11**		
Notched Depth d_n	mm		
Depth, d	mm	Span, L	mm
Width, b	mm	Flexural strength	MPa

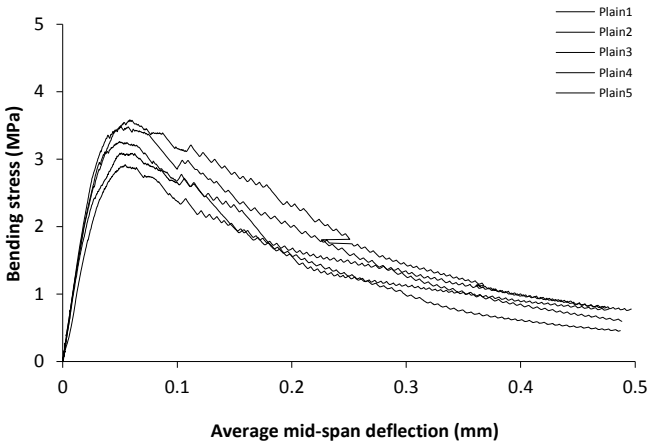

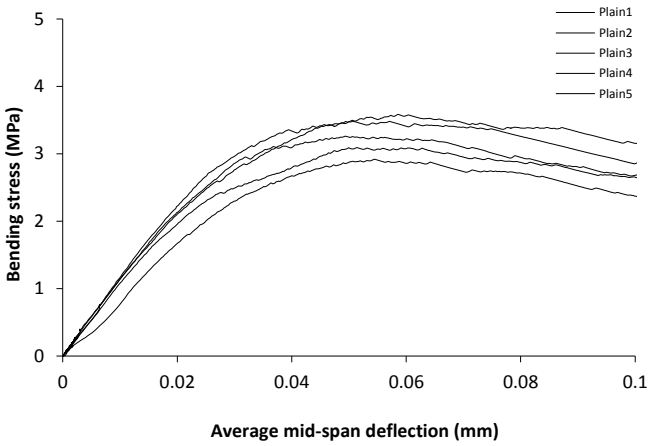

Specimen code name:		**Plain 13/11-1**			
Notched Depth d_n	124	mm			
Depth, d	150	mm	Span, L	500	mm
Width, b	151	mm	Flexural strength	2.82	MPa

Stress-deformation graphs

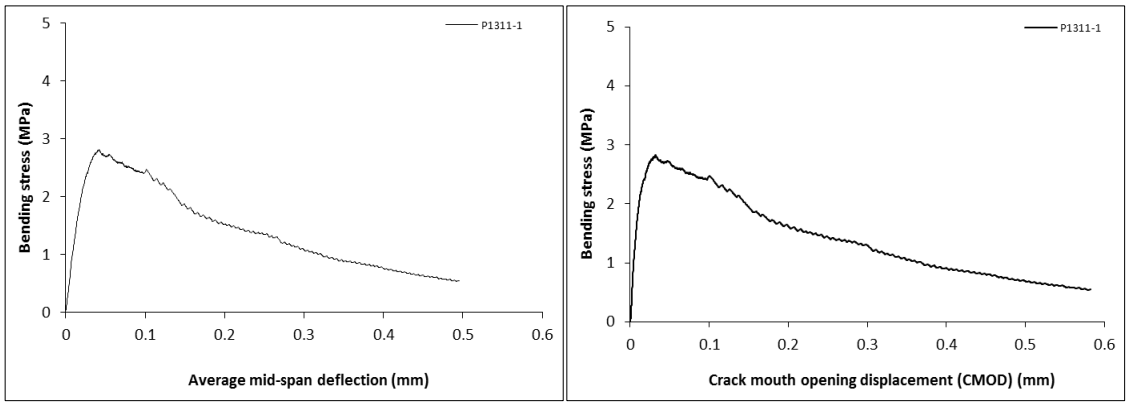

Specimen code name:		Plain 13/11-2			
Notched Depth d_n	124	mm			
Depth, d	149	mm	Span, L	500	mm
Width, b	154	mm	Flexural strength	3.32	MPa

Stress-deformation graphs

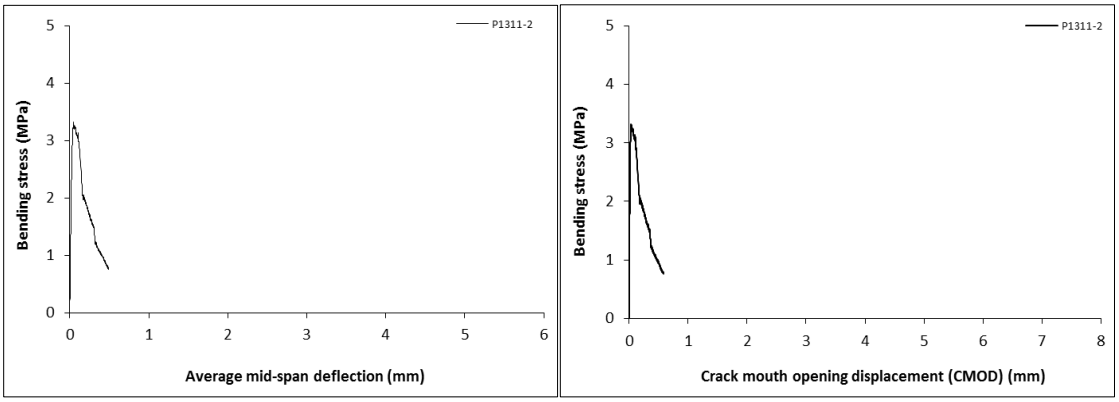

Specimen code name:		**Plain 13/11-3**			
Notched Depth d_n	124	mm			
Depth, d	149	mm	Span, L	500	mm
Width, b	151	mm	Flexural strength	2.80	MPa

Stress-deformation graphs

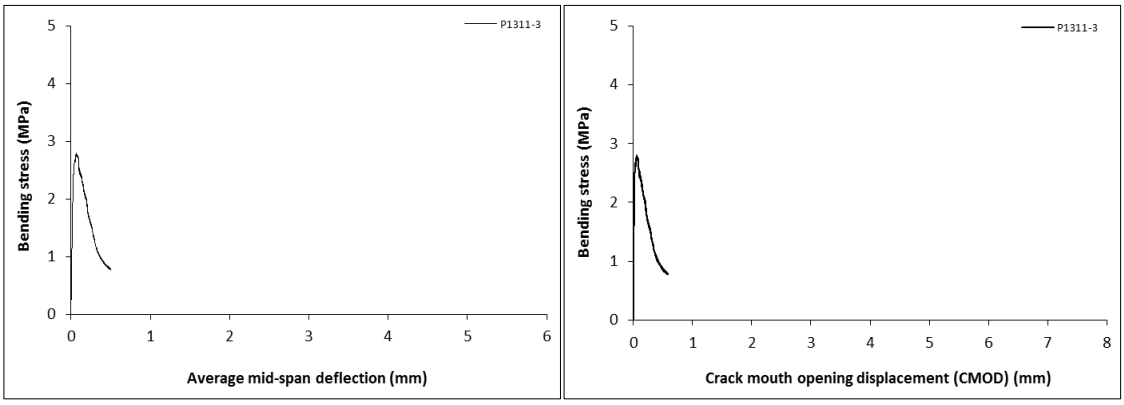

Specimen code name:		Plain 13/11-4			
Notched Depth d_n	124	mm			
Depth, d	150	mm	Span, L	500	mm
Width, b	153	mm	Flexural strength	3.42	MPa

Stress-deformation graphs

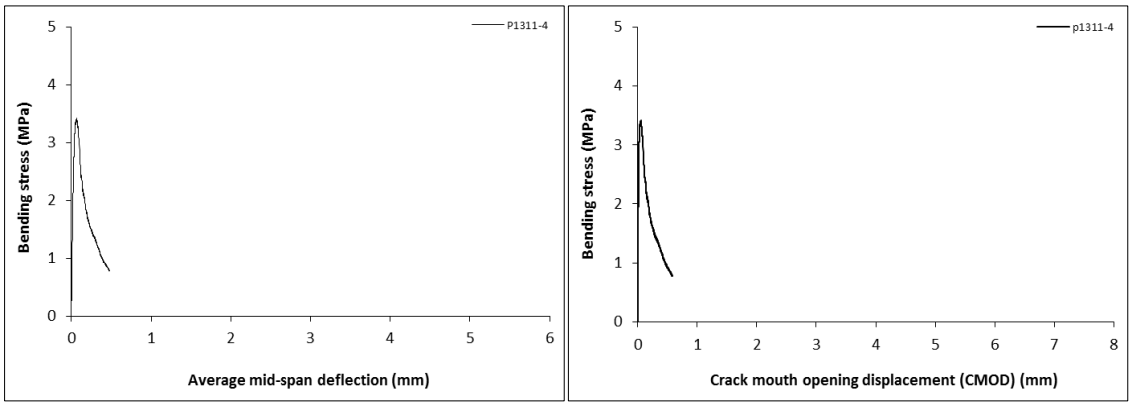

Specimen code name:		**Plain 13/11-5**			
Notched Depth d_n	127	mm			
Depth, d	153	mm	Span, L	500	mm
Width, b	151	mm	Flexural strength	3.12	MPa

Stress-deformation graphs

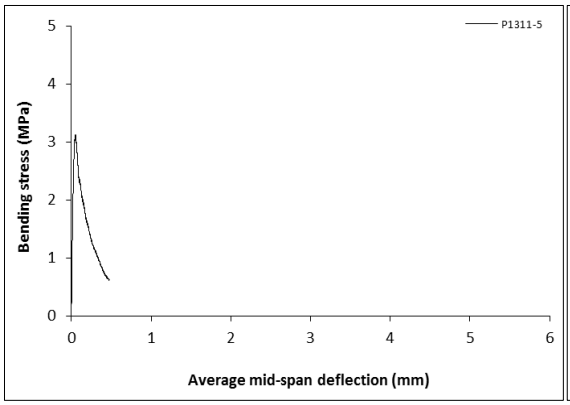

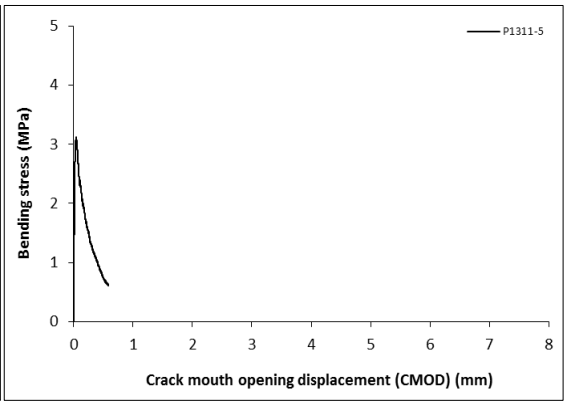

Specimen code name:		Plain 13/11-6			
Notched Depth d_n	124	mm			
Depth, d	149	mm	Span, L	500	mm
Width, b	151	mm	Flexural strength	2.93	MPa

Stress-deformation graphs

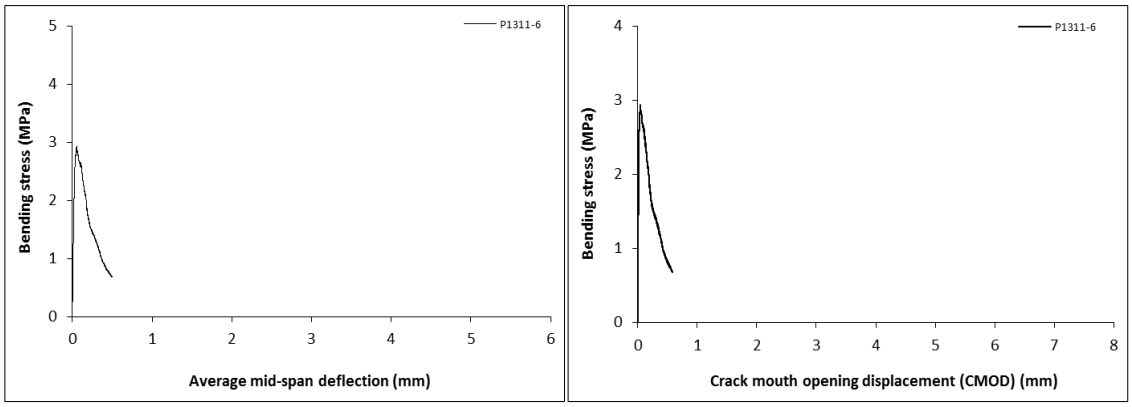

Mix:	Plain 13/11		
Notched Depth d_n	mm		
Depth, d	mm	Span, L	mm
Width, b	mm	Flexural strength	MPa

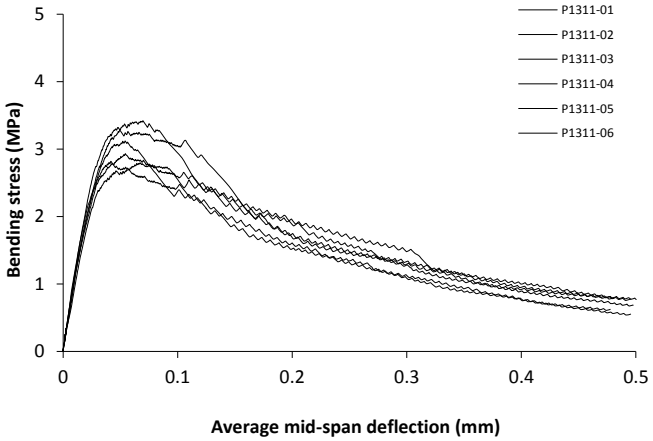

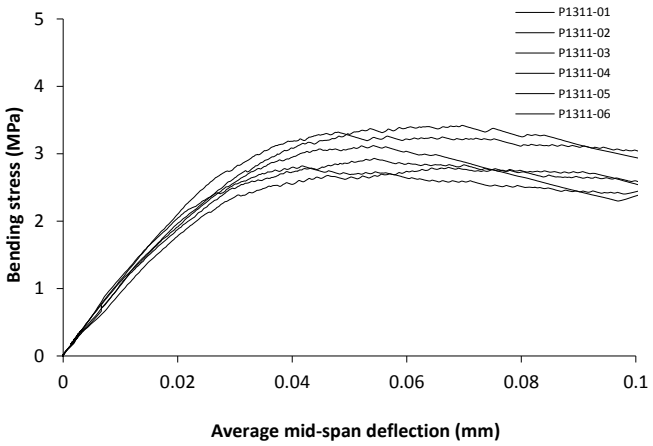

Specimen code name:		Plain 18/11-1			
Notched Depth d_n	124	mm			
Depth, d	149	mm	Span, L	500	mm
Width, b	153	mm	Flexural strength	3.17	MPa

Stress-deformation graphs

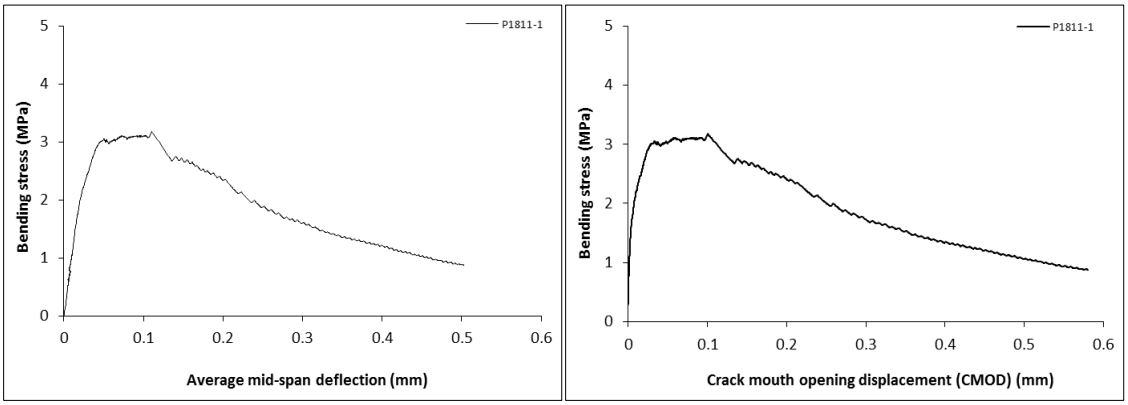

Specimen code name:		**Plain 18/11-2**			
Notched Depth d_n	124	mm			
Depth, d	149	mm	Span, L	500	mm
Width, b	154	mm	Flexural strength	3.13	MPa

Stress-deformation graphs

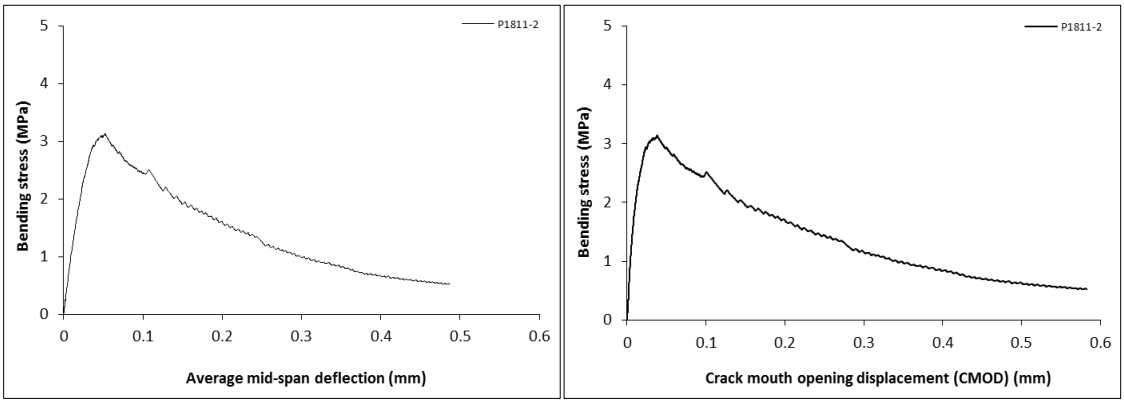

Specimen code name:		**Plain 18/11-3**			
Notched Depth d_n	126	mm			
Depth, d	151	mm	Span, L	500	mm
Width, b	152	mm	Flexural strength	3.08	MPa

Stress-deformation graphs

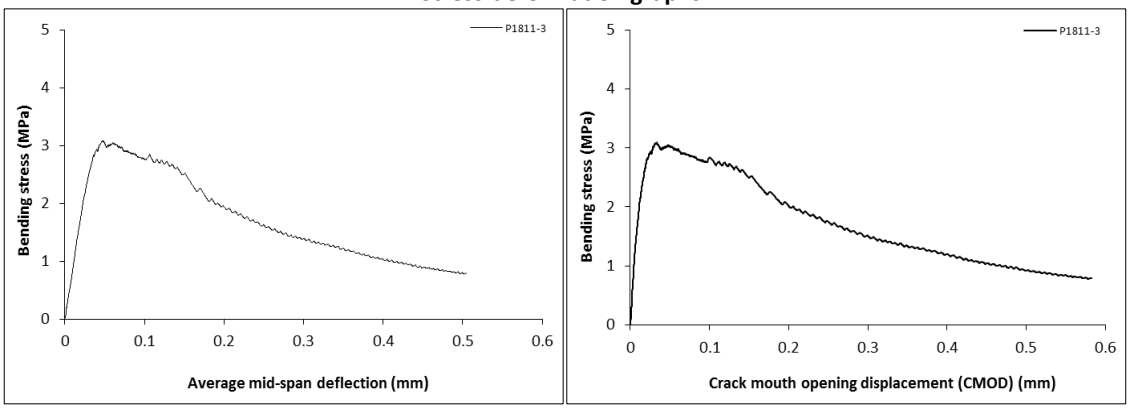

Specimen code name:		**Plain 18/11-4**			
Notched Depth d_n	124	mm			
Depth, d	149	mm	Span, L	500	mm
Width, b	152	mm	Flexural strength	3.57	MPa

Stress-deformation graphs

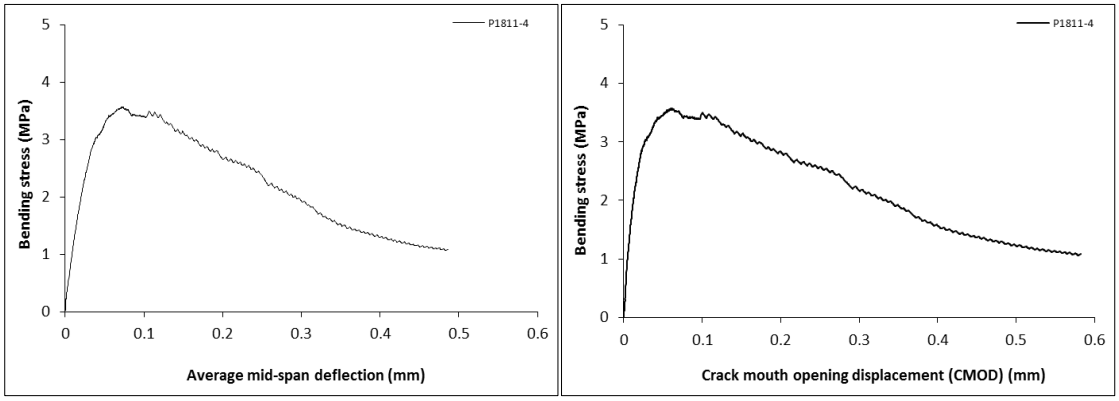

Specimen code name:		**Plain 18/11-5**			
Notched Depth d_n	127	mm			
Depth, d	152	mm	Span, L	500	mm
Width, b	150	mm	Flexural strength	2.89	MPa

Stress-deformation graphs

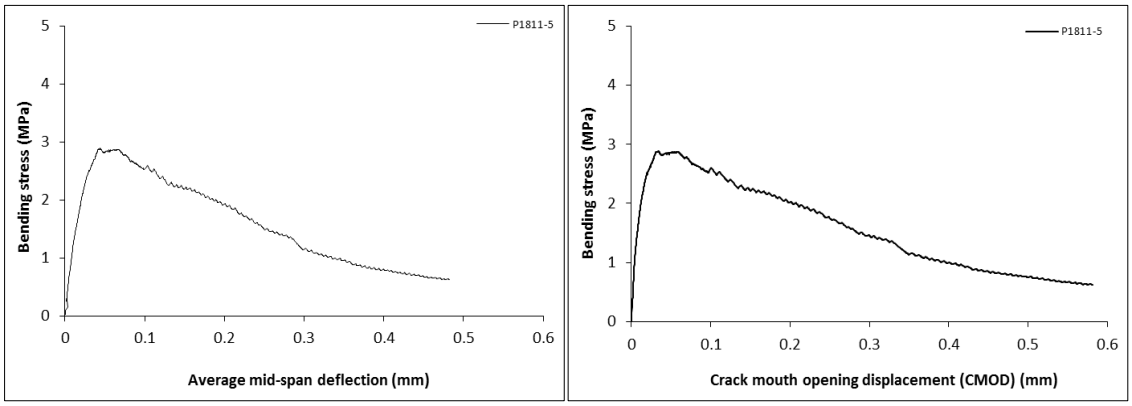

Specimen code name:		Plain 18/11-6			
Notched Depth d_n	125	mm			
Depth, d	149	mm	Span, L	500	mm
Width, b	151	mm	Flexural strength	3.44	MPa

Stress-deformation graphs

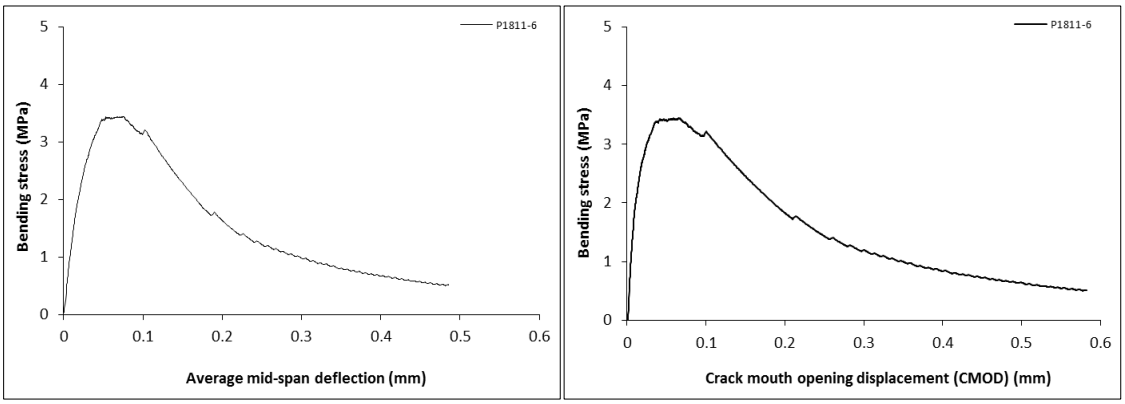

Mix:	Plain 18/11		
Notched Depth d_n	mm		
Depth, d	mm	Span, L	mm
Width, b	mm	Flexural strength	MPa

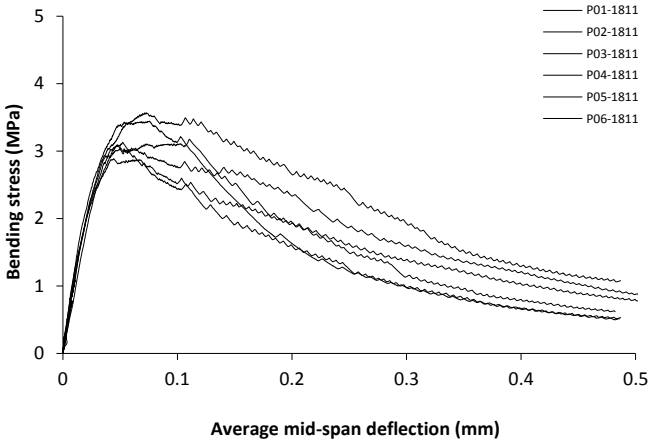

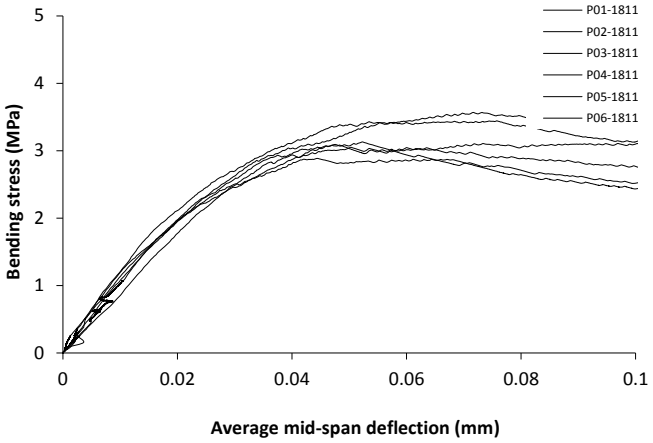

Specimen code name:		**Plain 20/11-1**			
Notched Depth d_n	126	mm			
Depth, d	150	mm	Span, L	500	mm
Width, b	155	mm	Flexural strength	2.82	MPa

Stress-deformation graphs

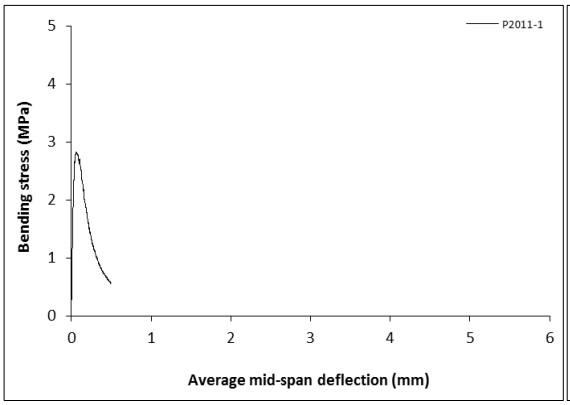

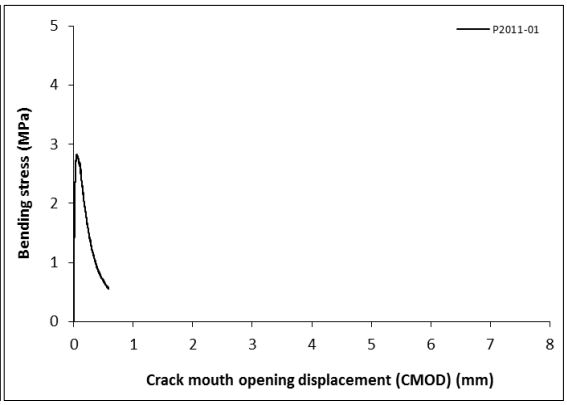

Specimen code name:		Plain 20/11-2			
Notched Depth d_n	125	mm			
Depth, d	149	mm	Span, L	500	mm
Width, b	154	mm	Flexural strength	3.25	MPa

Stress-deformation graphs

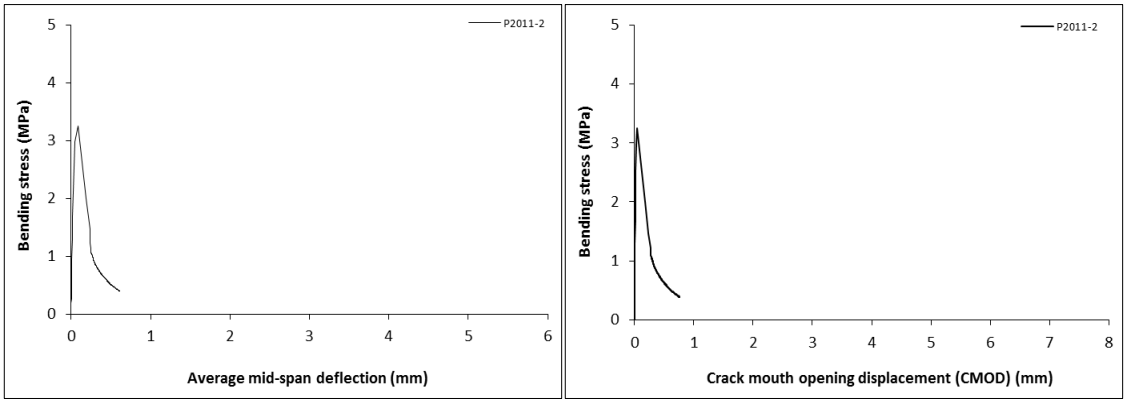

Specimen code name:		**Plain 20/11-3**			
Notched Depth d_n	126	mm			
Depth, d	149	mm	Span, L	500	mm
Width, b	150	mm	Flexural strength	3.29	MPa

Stress-deformation graphs

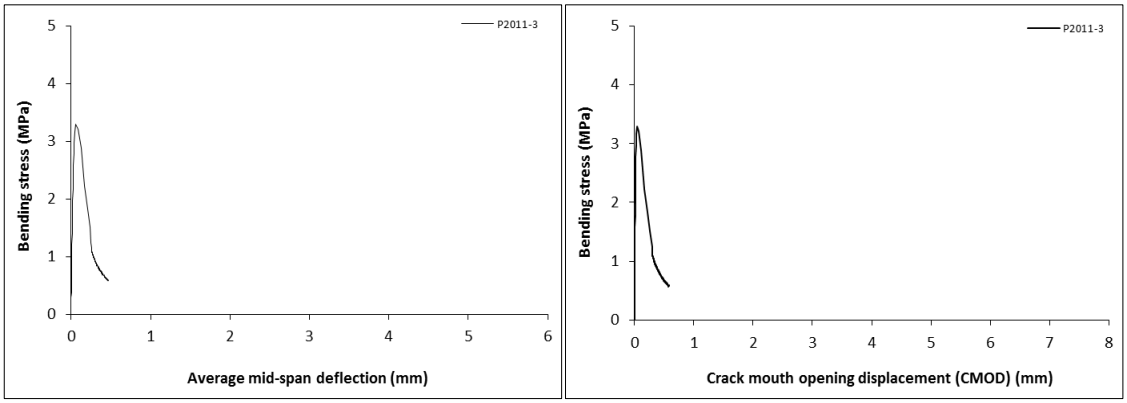

Specimen code name:		Plain 20/11-4			
Notched Depth d_n	126	mm			
Depth, d	150	mm	Span, L	500	mm
Width, b	157	mm	Flexural strength	3.10	MPa

Stress-deformation graphs

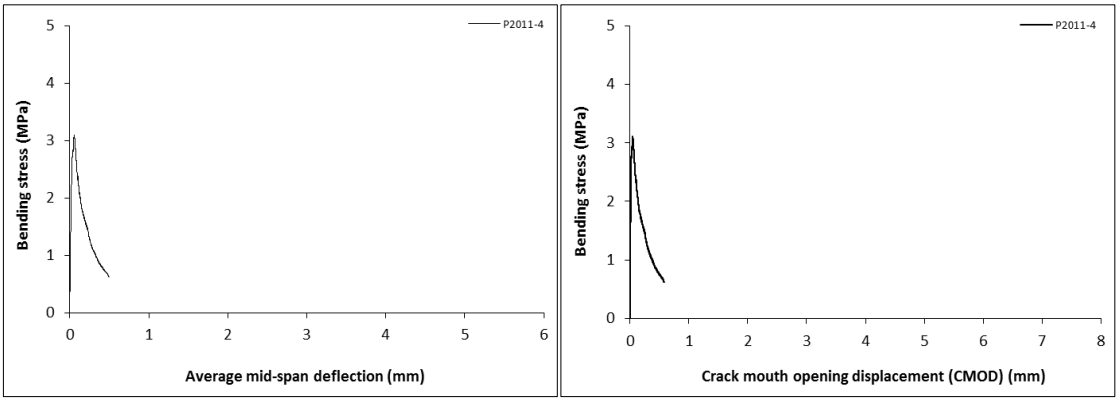

Specimen code name:		**Plain 20/11-5**			
Notched Depth d_n	128	mm			
Depth, d	156	mm	Span, L	500	mm
Width, b	150	mm	Flexural strength	2.36	MPa

Stress-deformation graphs

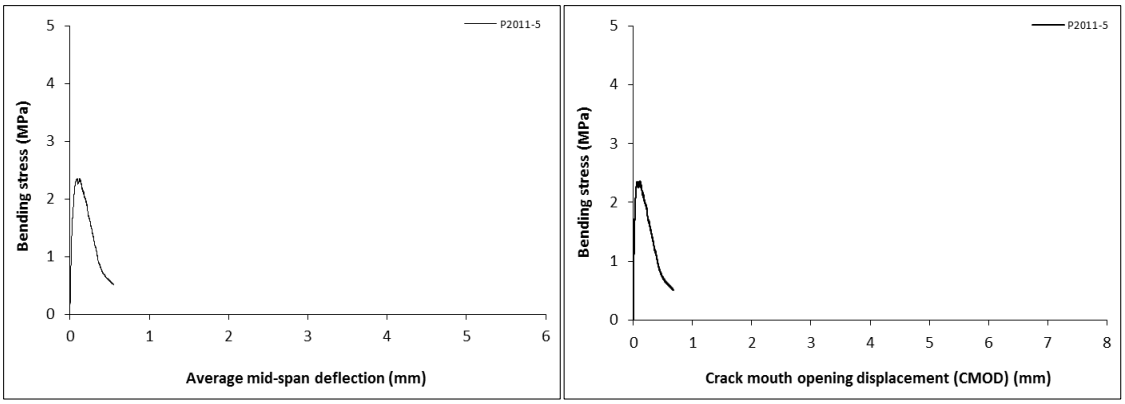

Specimen code name:		Plain 20/11-6			
Notched Depth d_n	123	mm			
Depth, d	151	mm	Span, L	500	mm
Width, b	155	mm	Flexural strength	3.13	MPa

Stress-deformation graphs

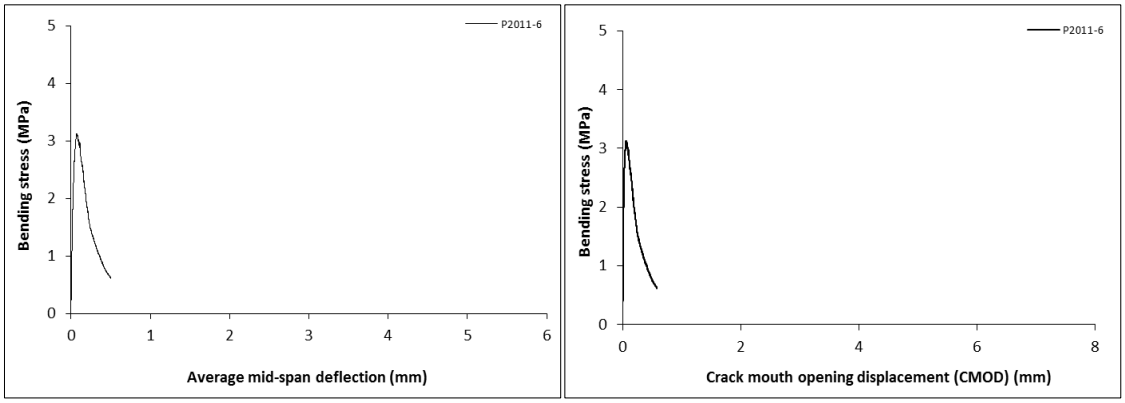

Mix:	Plain 20/11		
Notched Depth d_n	mm		
Depth, d	mm	Span, L	mm
Width, b	mm	Flexural strength	MPa

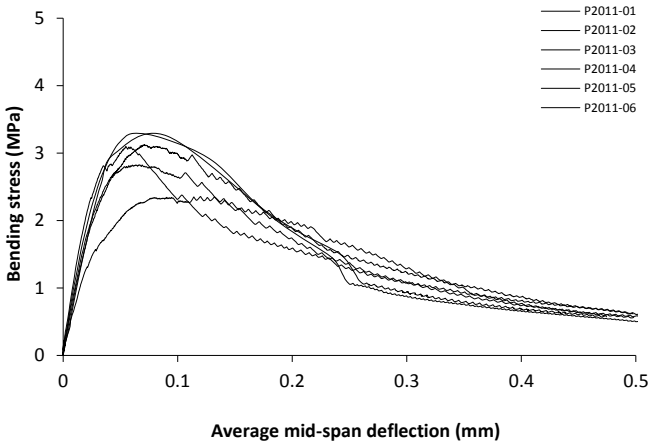

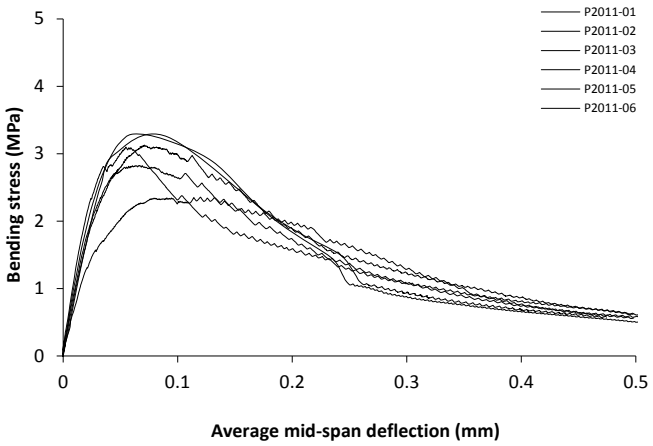

A.6 Energy absorption capacity (SFRC round panels)

		Fibre type and dosage	Max flexural load (kN)	Flexural strength (MPa)	Dissipated energy (Joule)			
					5 mm	10 mm	20 mm	40 mm
Mix A	Average	[A] – MSF2 (30)	24.1	3.7	74.0	123.7	179.7	228.7
	SD		1.6	0.0	3.2	8.8	15.2	24.7
Mix B	Average	[B] – MSF2 (20) + RTSF (10)	25.8	3.8	86.0	146.8	218.4	284.6
	SD		1.7	0.3	14.9	31.2	51.9	67.7
Mix C	Average	[C] - MSF2(15) + RTSF (15)	21.5	3.4	79.0	137.8	211.1	284.7
	SD		1.7	0.1	4.4	11.2	21.9	31.4
Mix D	Average	[D] - MSF2(10) + RTSF (20)	21.8	3.5	74.5	122.5	180.3	232.1
	SD		1.4	0.3	9.4	19.9	31.1	39.4
Mix E	Average	[E] - RTSF (30)	22.7	3.5	56.1	85.2	118.7	144.8
	SD		1.0	0.2	5.6	10.0	15.5	19.0
Mix F	Average	[F] - MSF1(35)	24.3	3.6	85.8	157.3	261.6	378.8
	SD		0.6	0.2	5.1	8.9	17.8	35.9
Mix G	Average	[G] - MSF1(45)	25.0	3.8	90.0	163.5	266.7	374.2
	SD		2.4	0.3	12.6	24.5	41.7	62.9
Mix H	Average	[H] - MSF1(35) + RTSF (10)	25.7	4.1	102.0	189.9	321.5	464.3
	SD		2.6	0.4	10.3	18.2	26.9	37.3
Mix I	Average	[I] - MSF1(22.5) + RTSF (22.5)	22.1	3.7	87.6	152.7	235.2	312.5
	SD		2.7	0.2	2.3	4.6	12.5	21.9
Mix J	Average	[J] - MSF1(10) + RTSF (35)	28.2	4.3	92.2	155.3	230.5	308.5
	SD		1.5	0.2	10.9	21.7	39.3	58.2

A.7 Round panels (after testing)

Specimen:			A1		
Depth, d	75.9	mm	Span, L	750	mm
Diameter, b	801.3	mm	Flexural strength	3.72	MPa

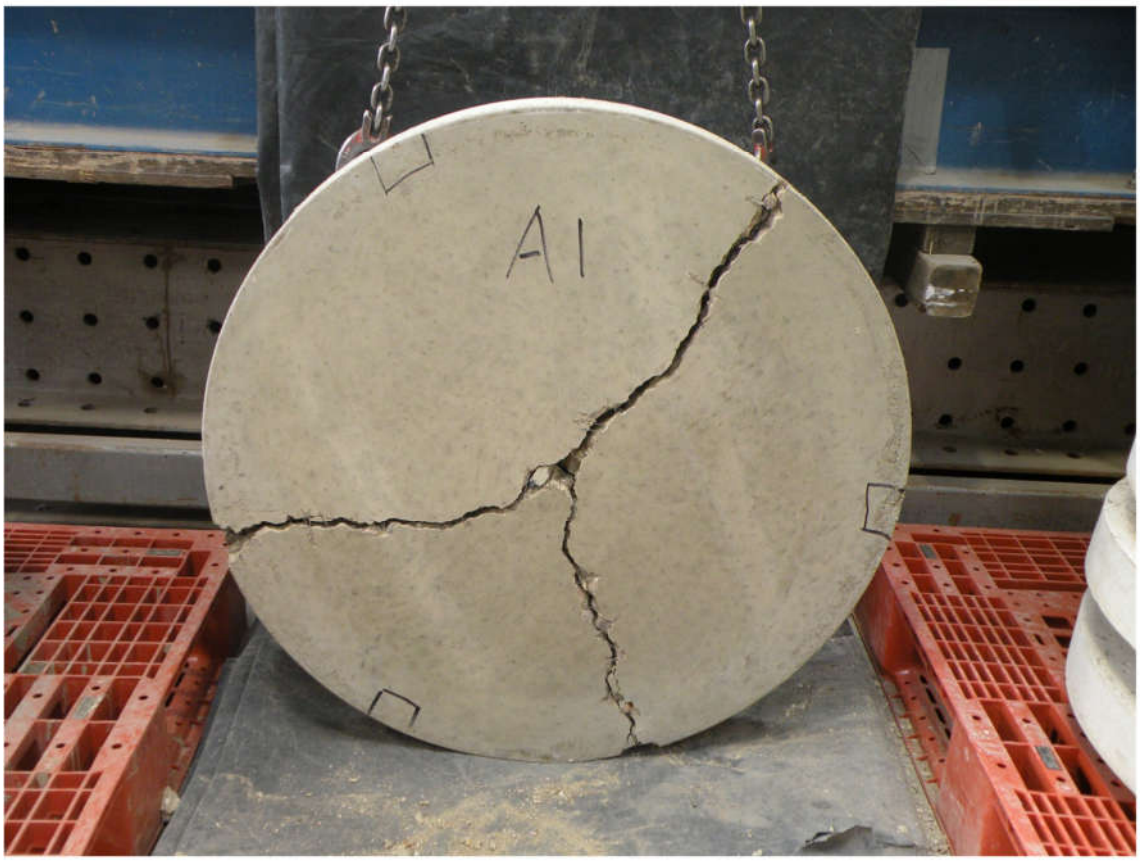

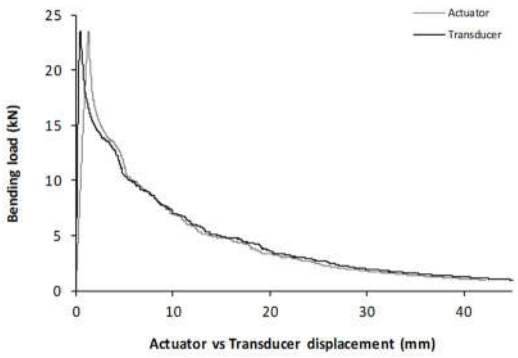

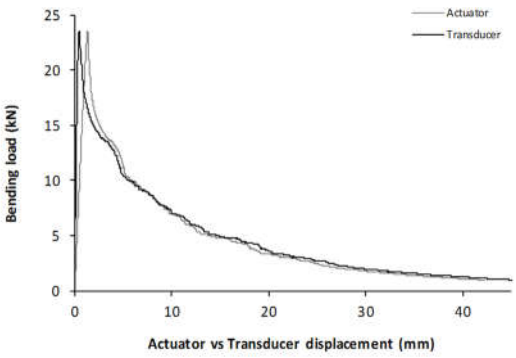

Specimen:			A2		
Depth, d	79.9	mm	Span, L	750	mm
Diameter	802	mm	Flexural strength	3.71	MPa

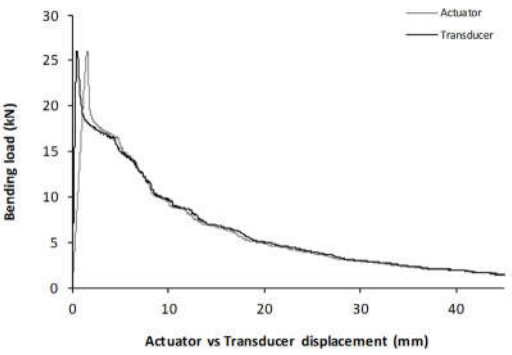

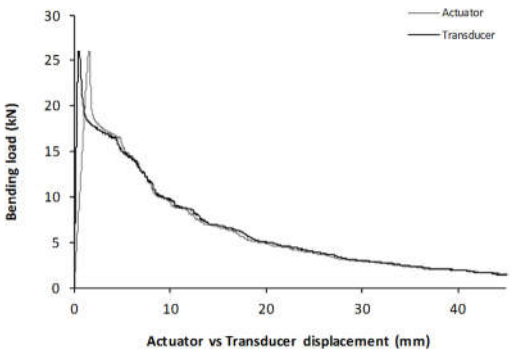

Specimen:			A3		
Depth, d	75.2	mm	Span, L	750	mm
Diameter	801.7	mm	Flexural strength	3.69	MPa

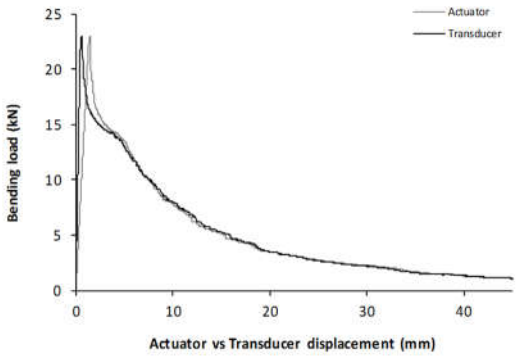

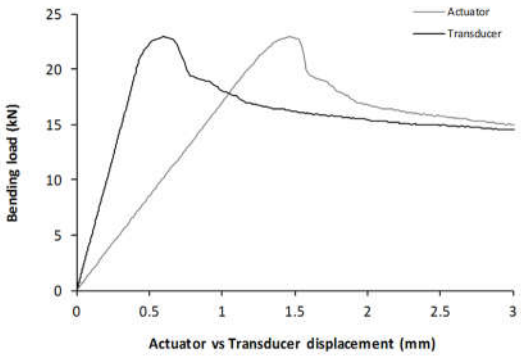

Mix:	A

Overall results

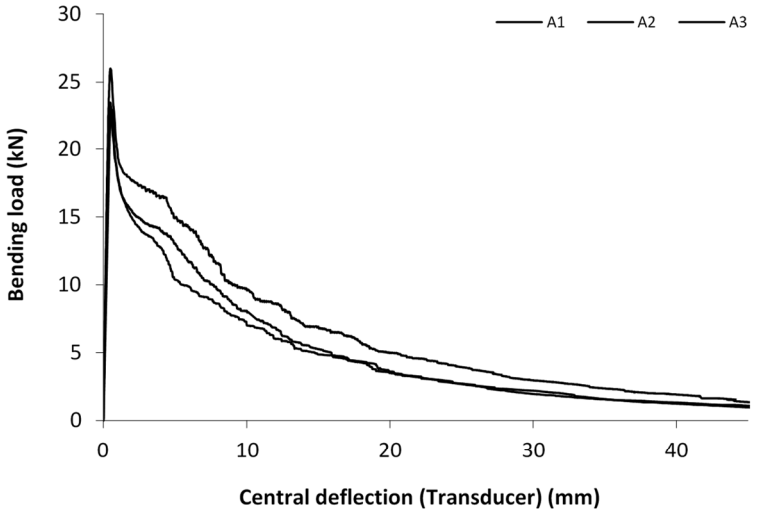

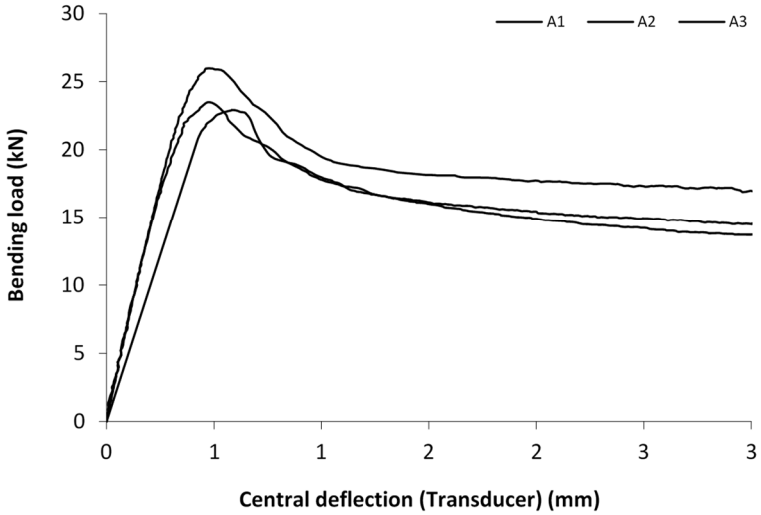

Specimen:			B1		
Depth, d	81.1	mm	Span, L	750	mm
Diameter	799	mm	Flexural strength	3.86	MPa

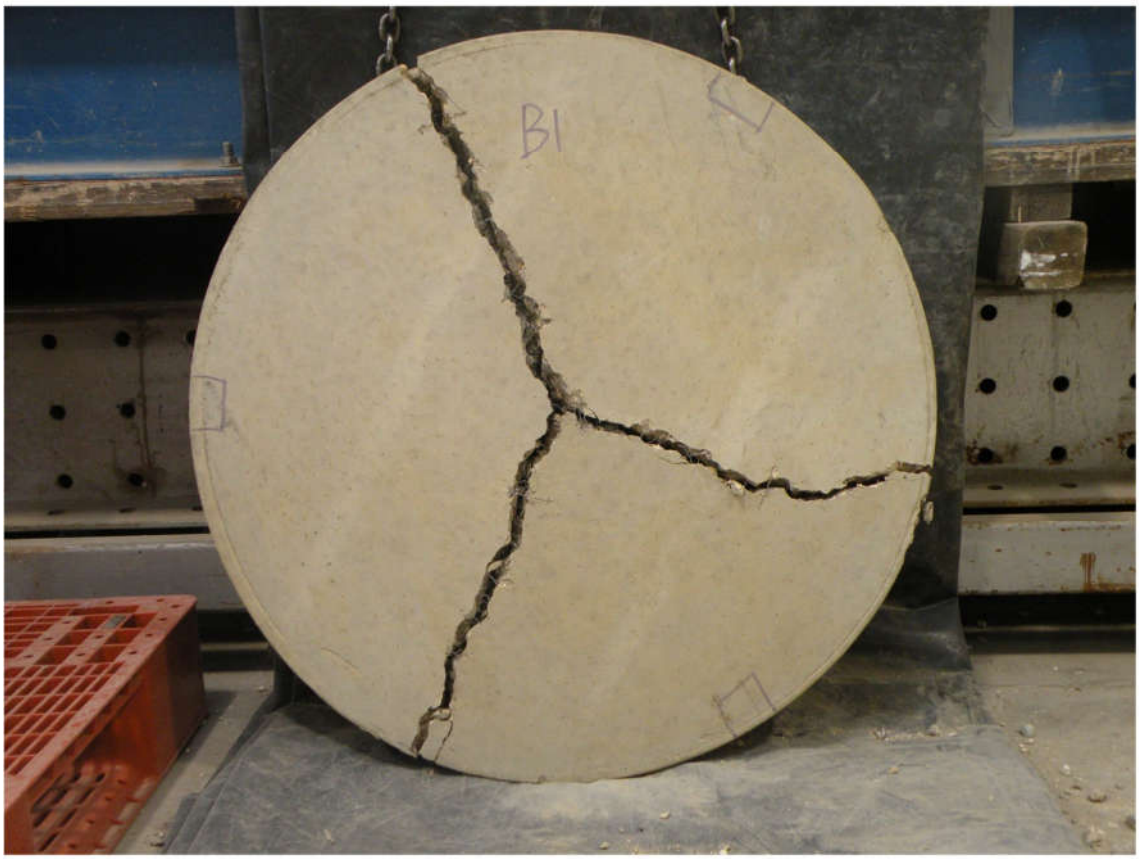

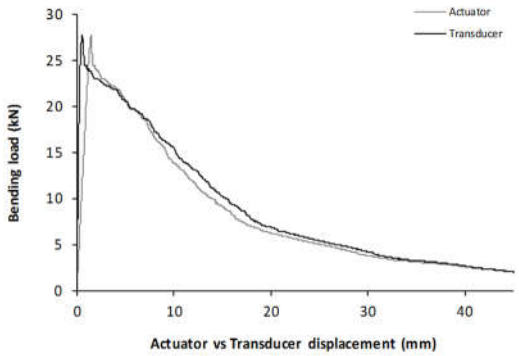

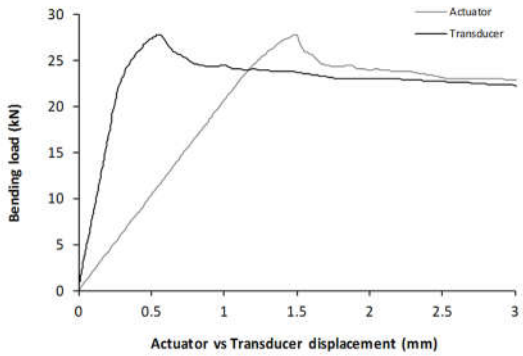

Specimen:			B2		
Depth, d	74.5	mm	Span, L	750	mm
Diameter	799	mm	Flexural strength	4.03	MPa

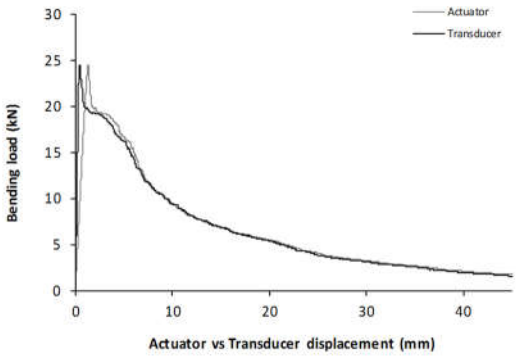

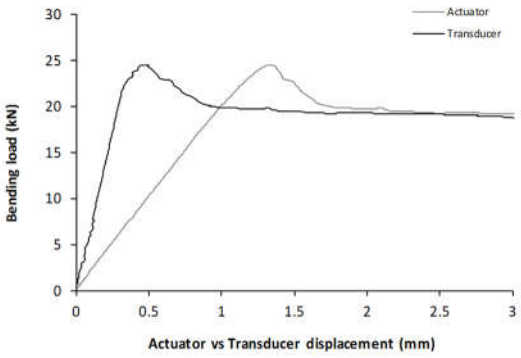

Specimen:			B3		
Depth, d	80.6	mm	Span, L	750	mm
Diameter	804.7	mm	Flexural strength	3.53	MPa

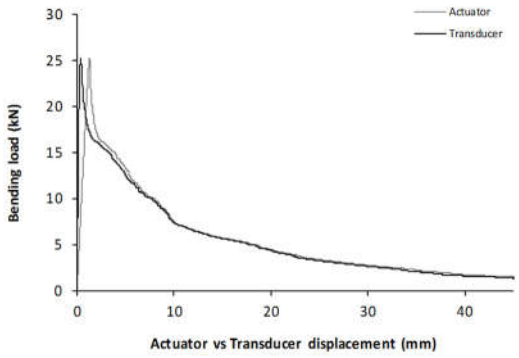

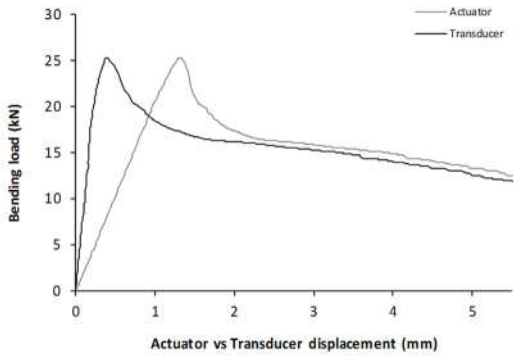

Mix:	B

Overall results

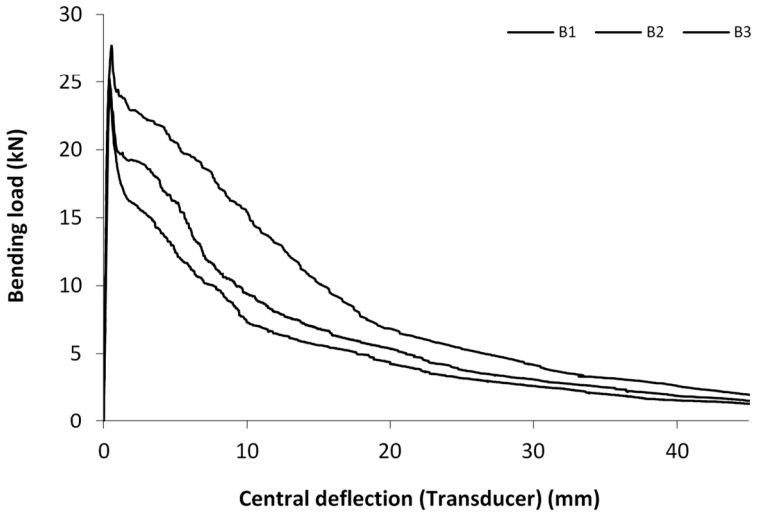

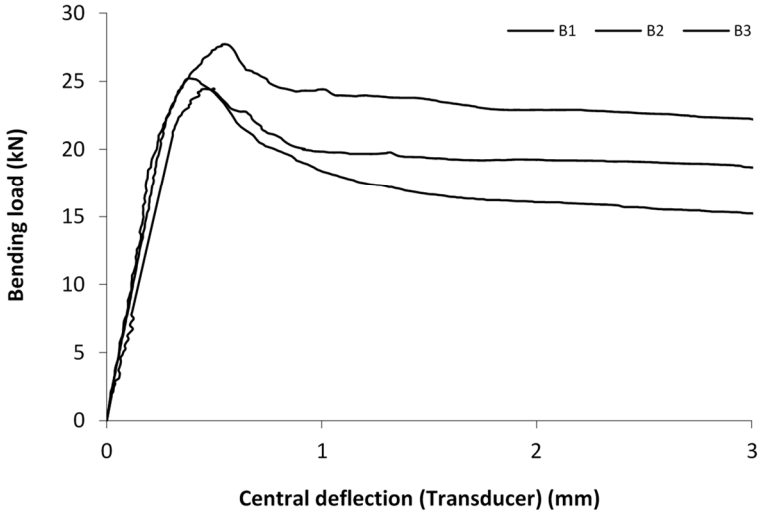

Specimen:			C1		
Depth, d	72.5	mm	Span, L	750	mm
Diameter	800.3	mm	Flexural strength	3.42	MPa

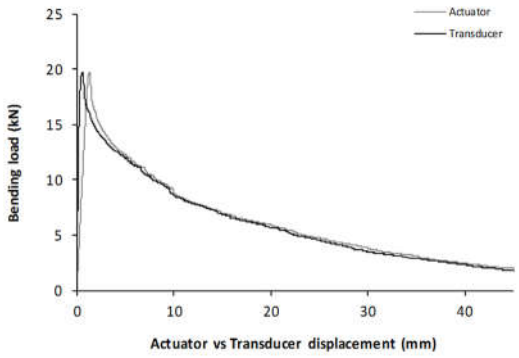

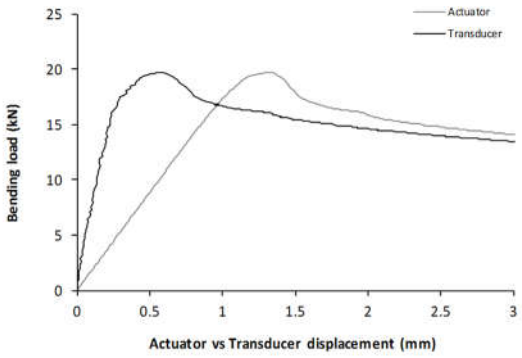

Specimen:			C2		
Depth, d	76	mm	Span, L	750	mm
Diameter	802.3	mm	Flexural strength	3.45	MPa

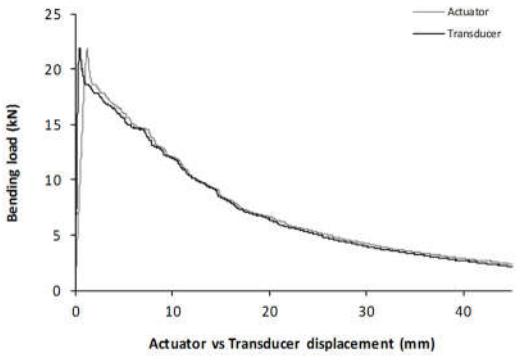

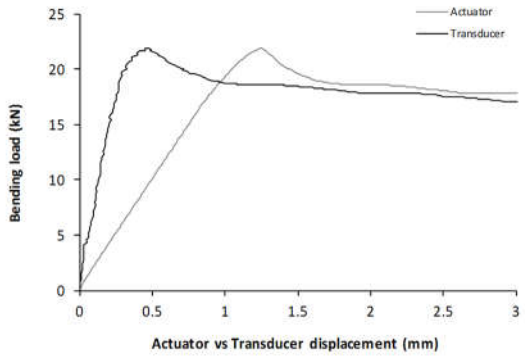

Specimen:			C3		
Depth, d	79.3	mm	Span, L	750	mm
Diameter	803	mm	Flexural strength	3.32	MPa

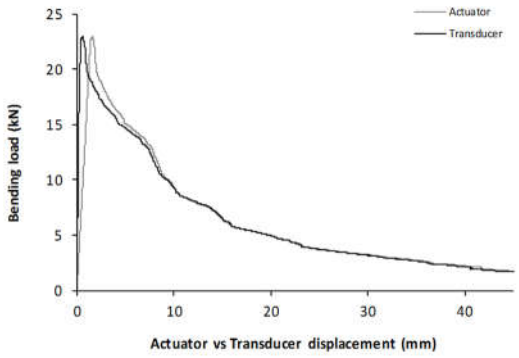

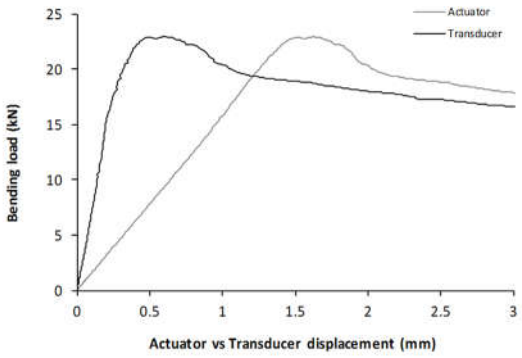

Mix:	C

Overall results

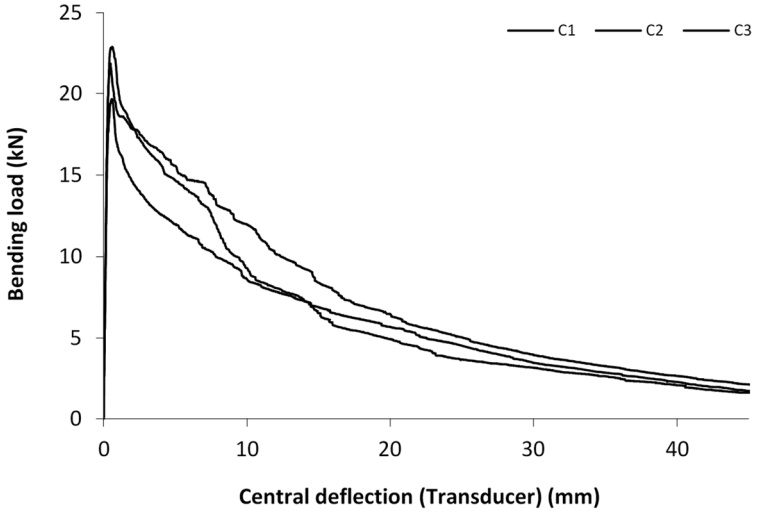

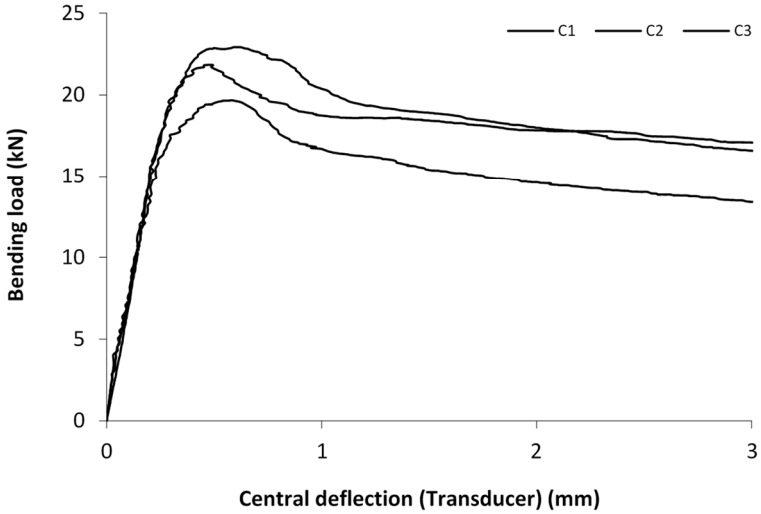

Specimen:			D1		
Depth, d	75.6	mm	Span, L	750	mm
Diameter	800.3	mm	Flexural strength	3.70	MPa

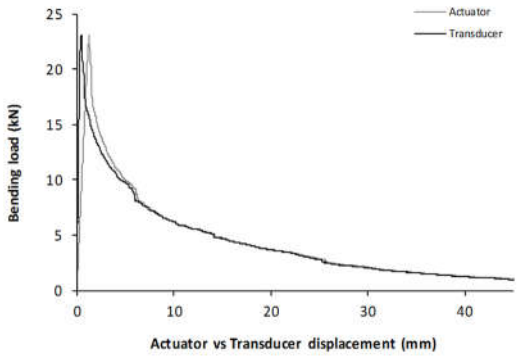

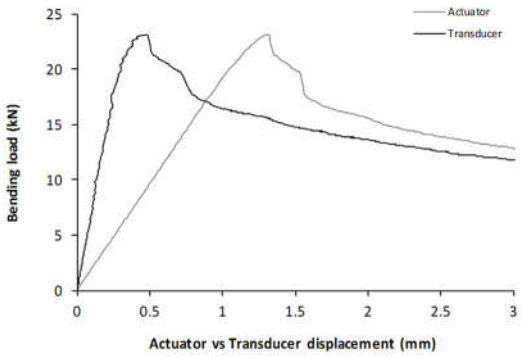

Specimen code name:			D2		
Depth, d	74.7	mm	Span, L	750	mm
Diameter	800.0	mm	Flexural strength	3.62	MPa

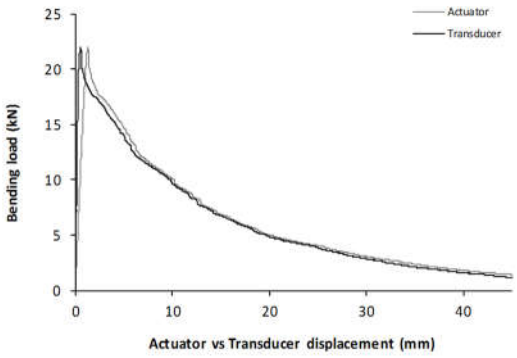

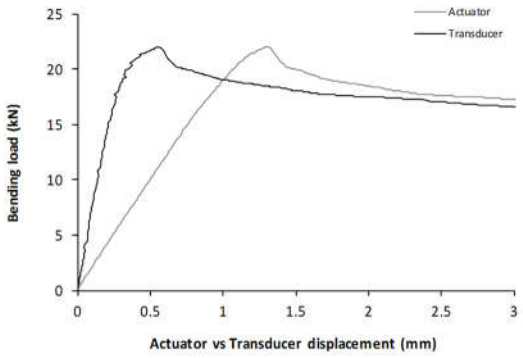

Specimen:			D3		
Depth, d	75.6	mm	Span, L	750	mm
Diameter	800.3	mm	Flexural strength	3.25	MPa

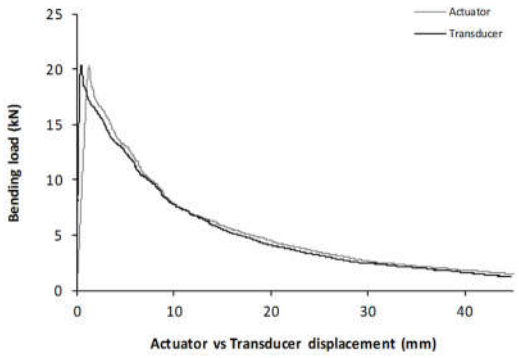

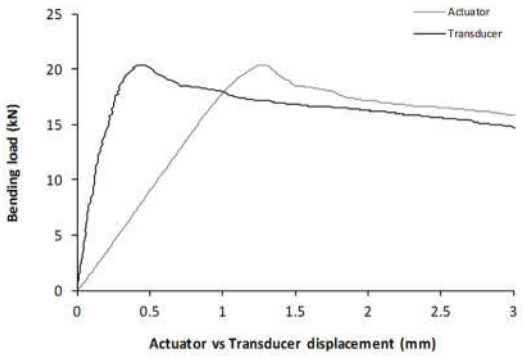

Mix:	D

Overall results

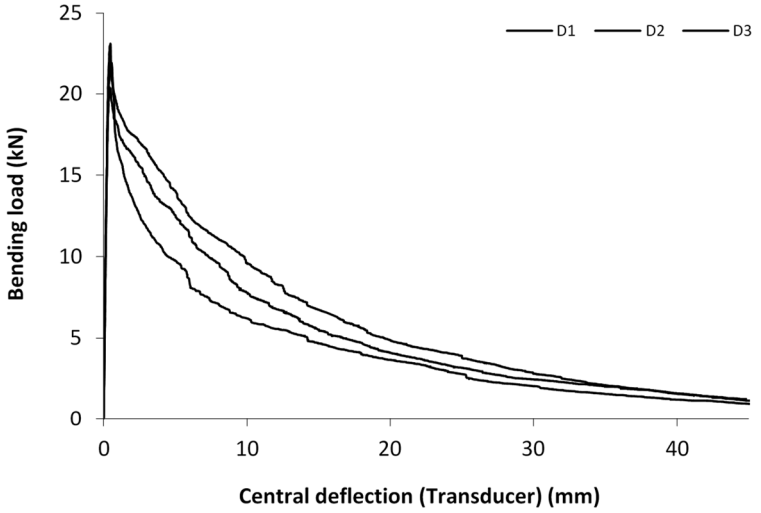

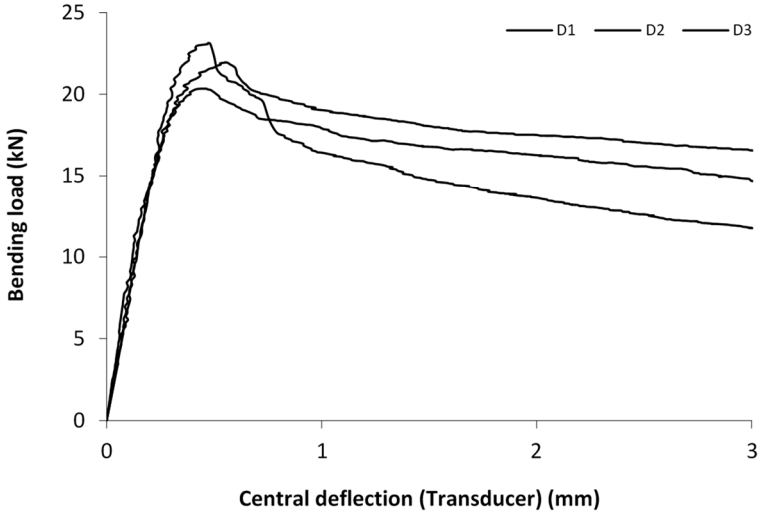

Specimen:			E1		
Depth, d	75.9	mm	Span, L	750	mm
Diameter	803.3	mm	Flexural strength	3.52	MPa

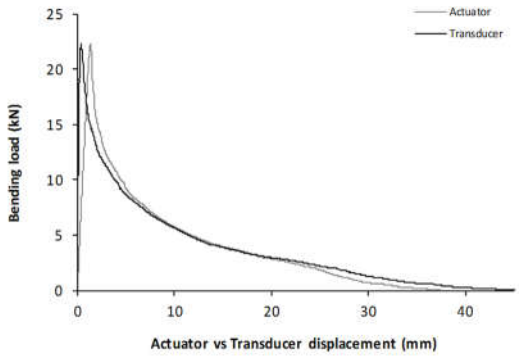

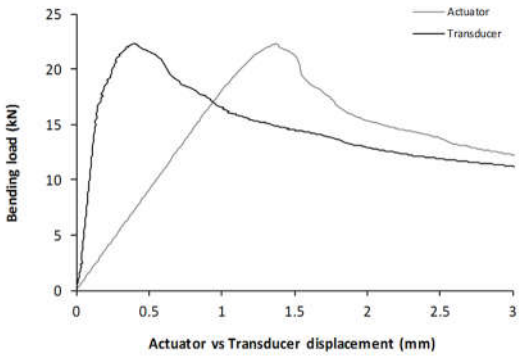

Specimen:			E2		
Depth, d	77.5	mm	Span, L	750	mm
Diameter	800.3	mm	Flexural strength	3.34	MPa

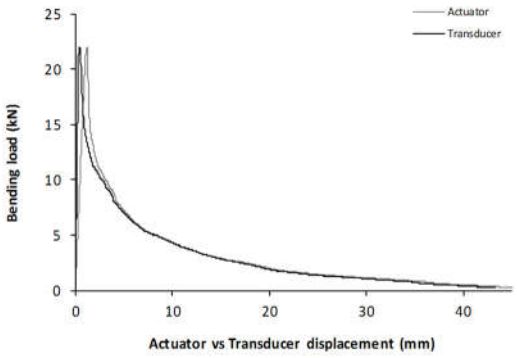

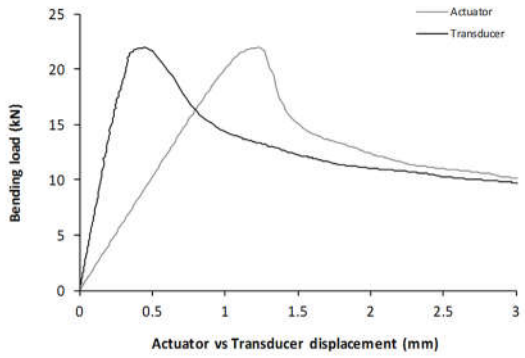

Specimen:			E3		
Depth, d	77.8	mm	Span, L	750	mm
Diameter	800	mm	Flexural strength	3.61	MPa

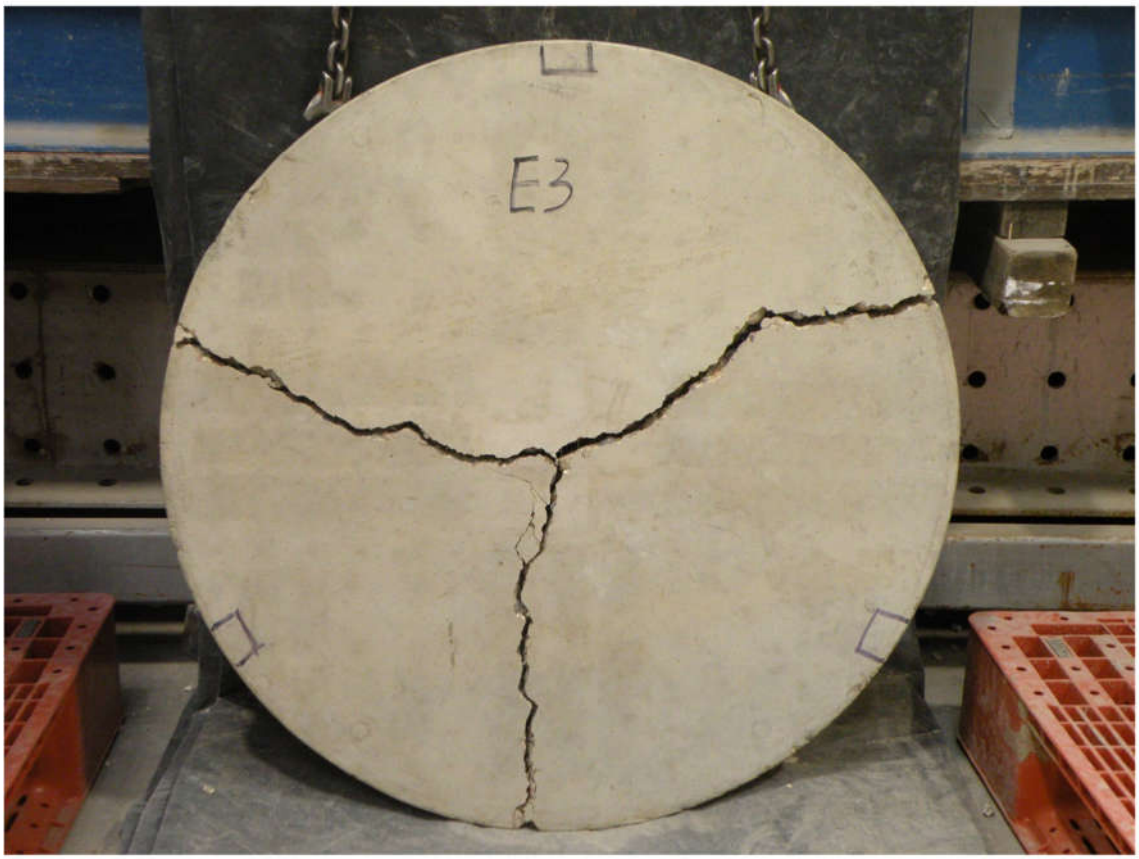

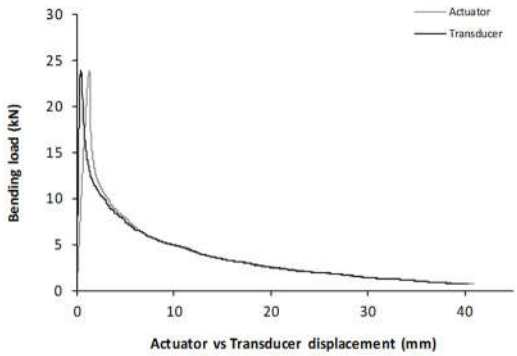

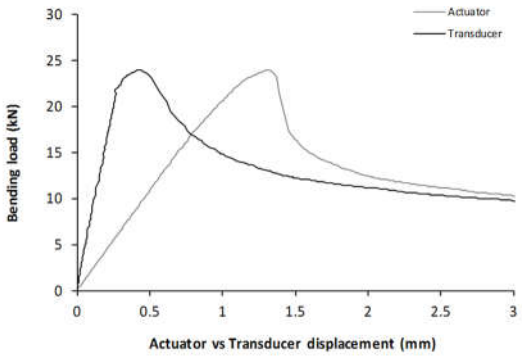

Mix:	E

Overall results

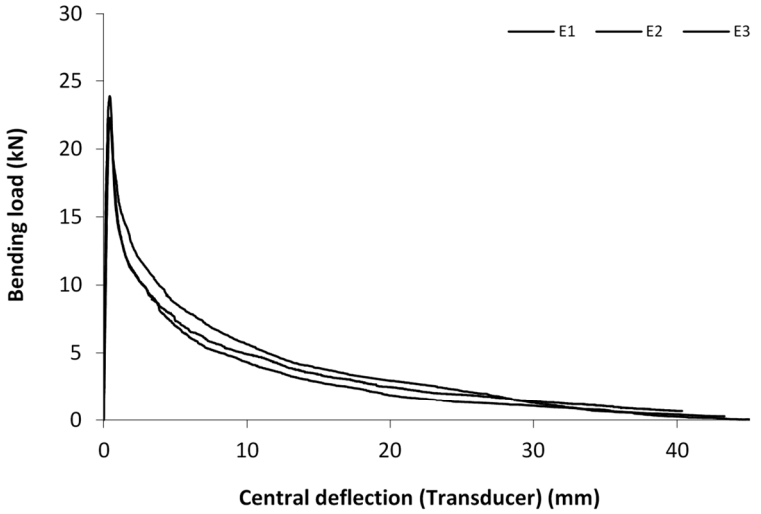

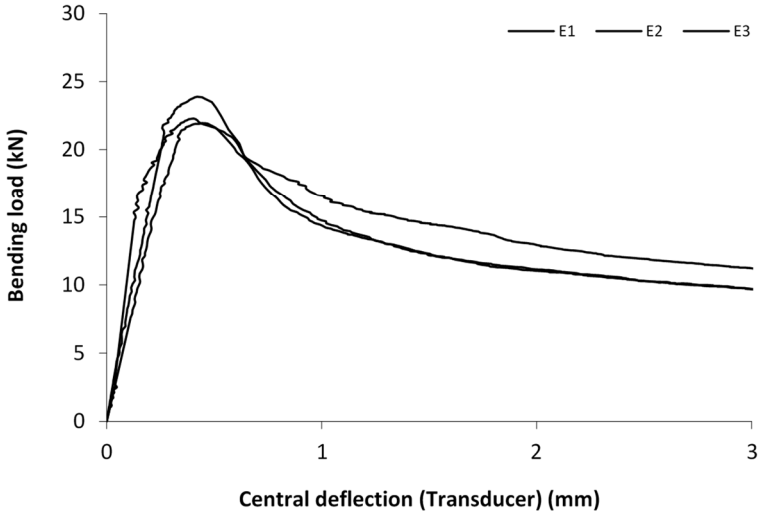

Specimen:			F1		
Depth, d	78.5	mm	Span, L	750	mm
Diameter	799	mm	Flexural strength	3.69	MPa

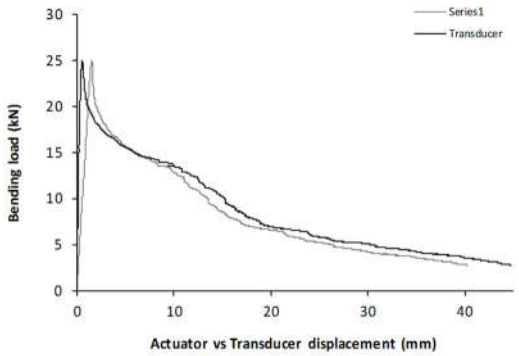

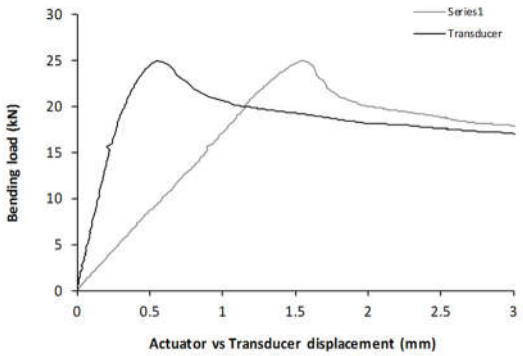

Specimen:			F2		
Depth, d	78.6	mm	Span, L	750	mm
Diameter	797	mm	Flexural strength	3.61	MPa

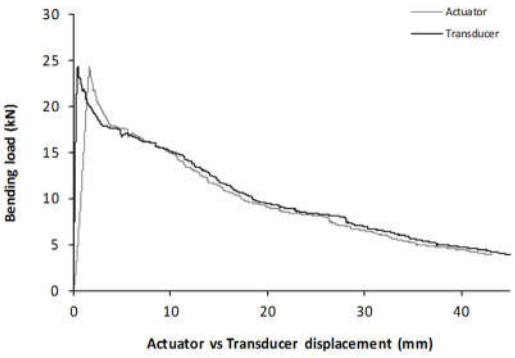

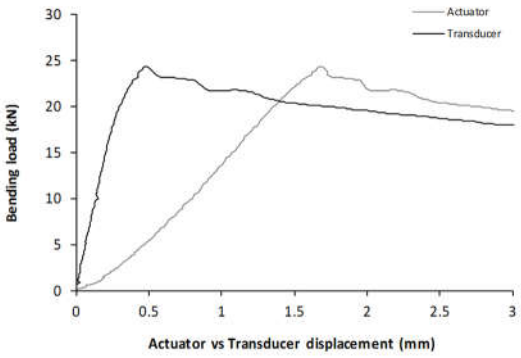

Specimen:			F3		
Depth, d	79.9	mm	Span, L	750	mm
Diameter	800	mm	Flexural strength	3.38	MPa

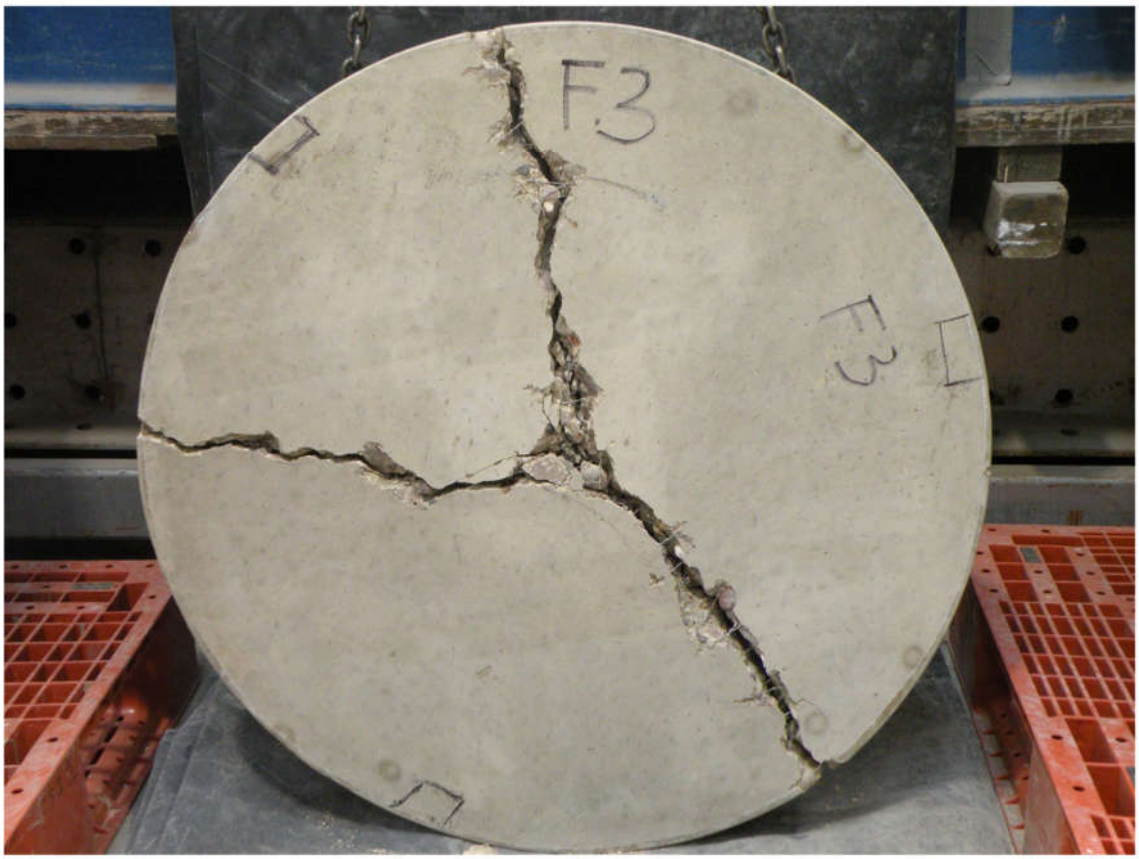

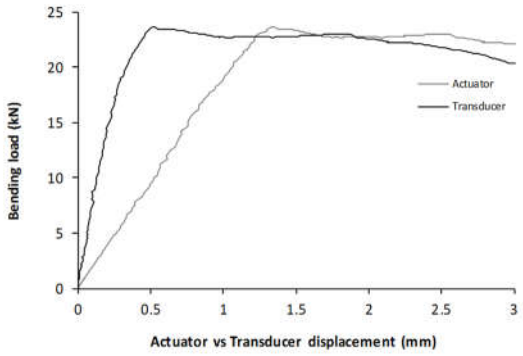

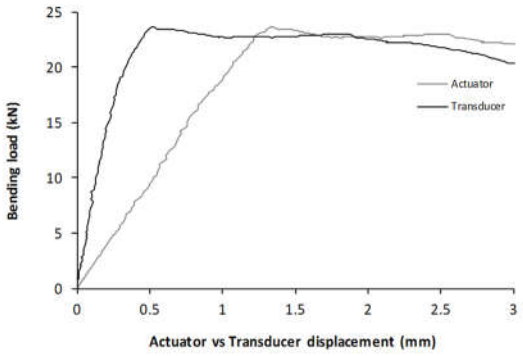

Mix:	F

Overall results

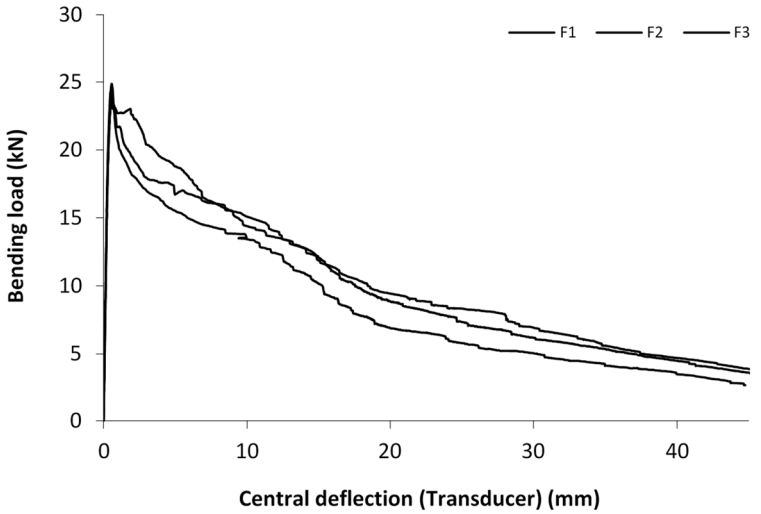

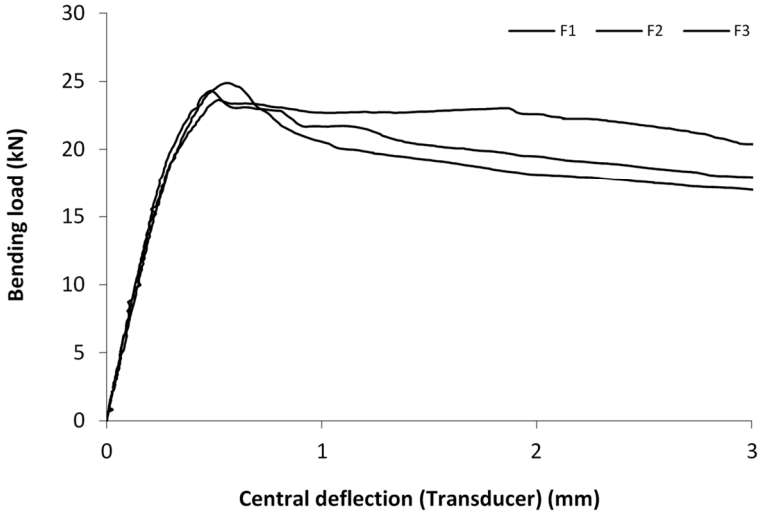

Specime:			G1		
Depth, d	78.8	mm	Span, L	750	mm
Diameter	801.3	mm	Flexural strength	4.04	MPa

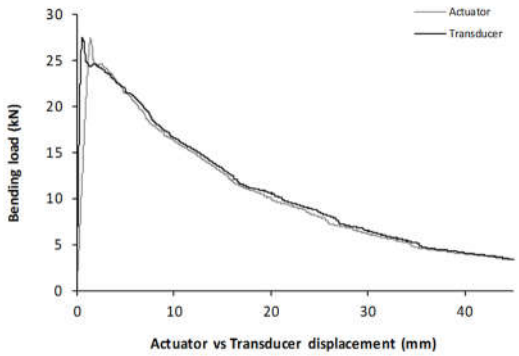

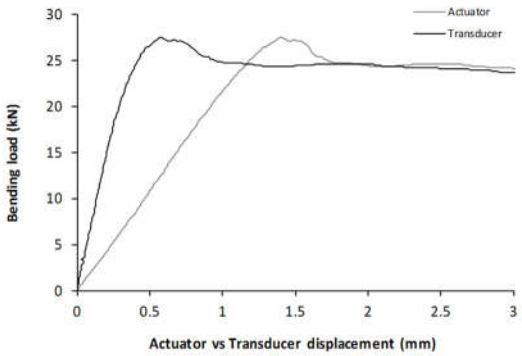

Specimen:			G2		
Depth, d	75.9	mm	Span, L	750	mm
Diameter	801	mm	Flexural strength	3.92	MPa

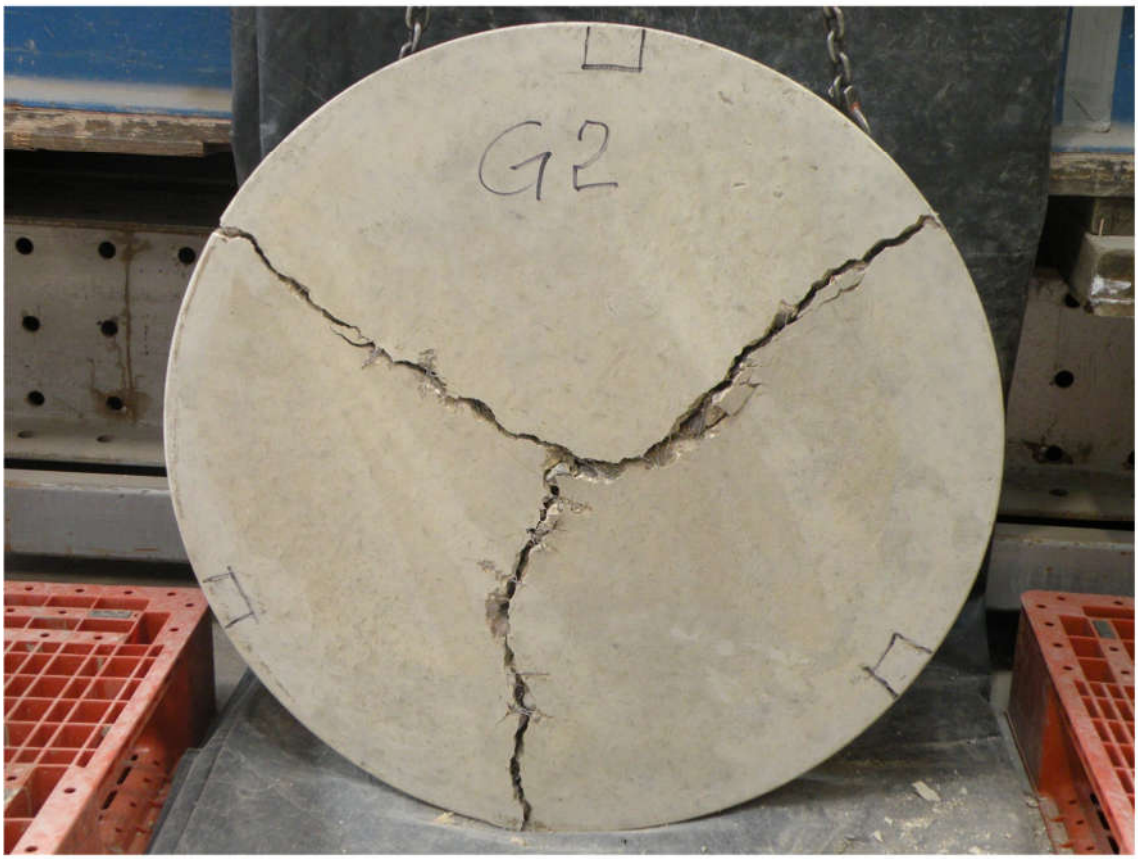

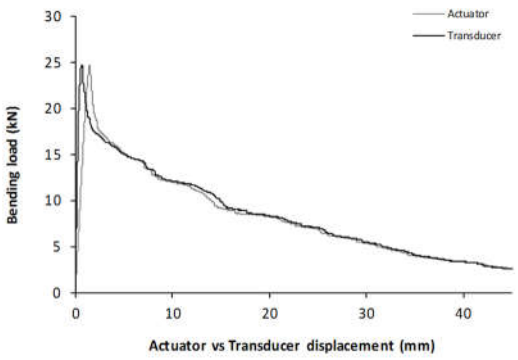

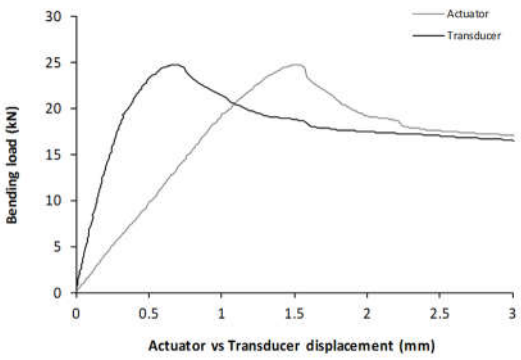

Specimen:			G3		
Depth, d	76.5	mm	Span, L	750	mm
Diameter	798	mm	Flexural strength	3.55	MPa

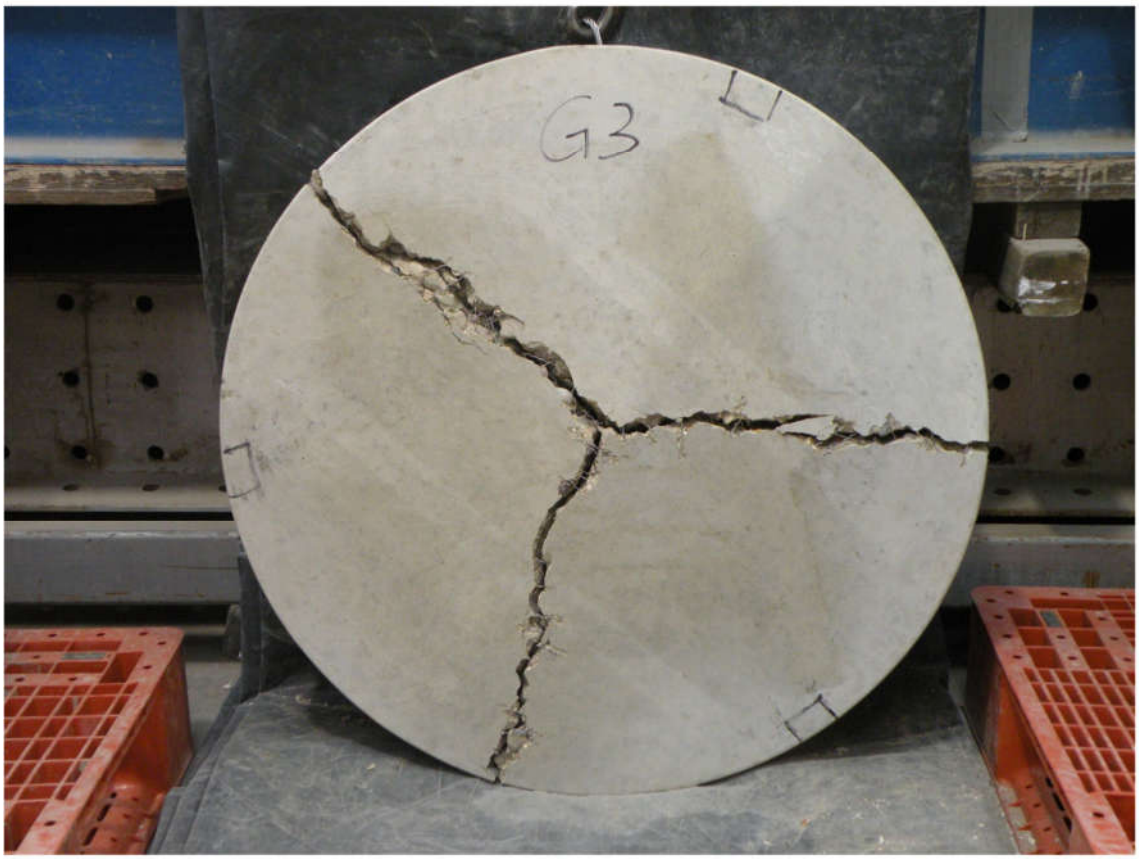

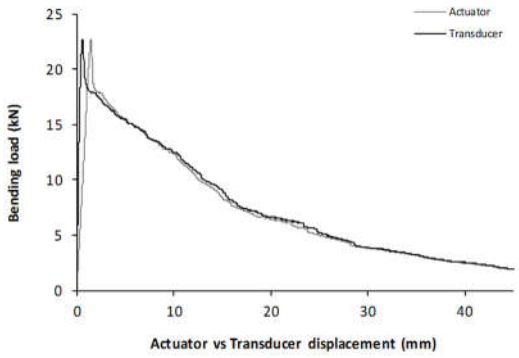

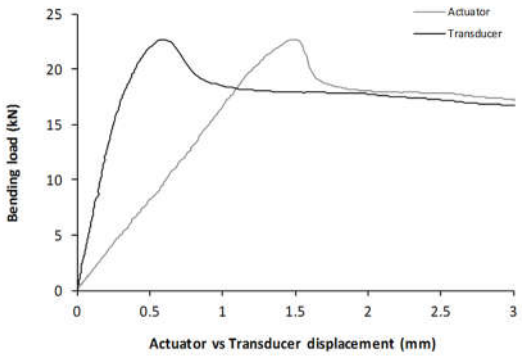

Mix:	G

Overall results

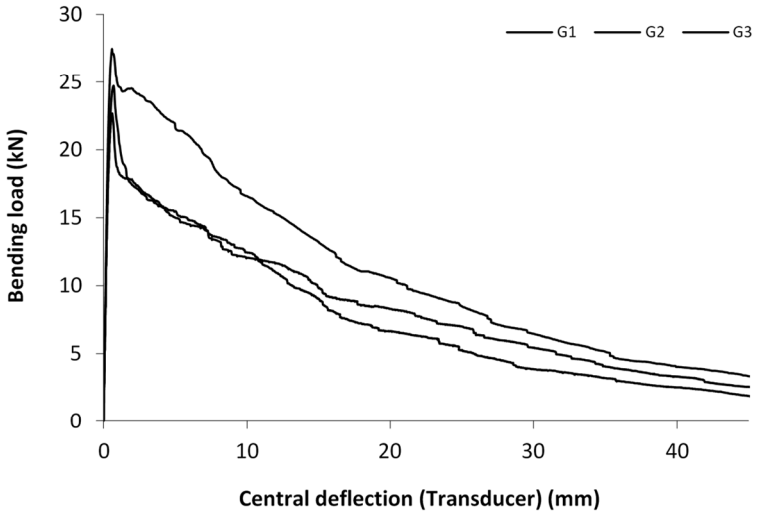

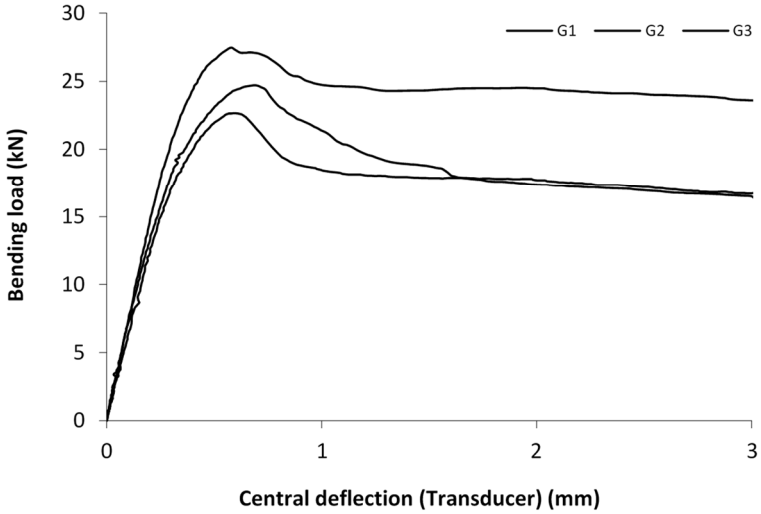

Specimen code name:			H1		
Depth, d	76.3	mm	Span, L	750	mm
Diameter	802	mm	Flexural strength	3.94	MPa

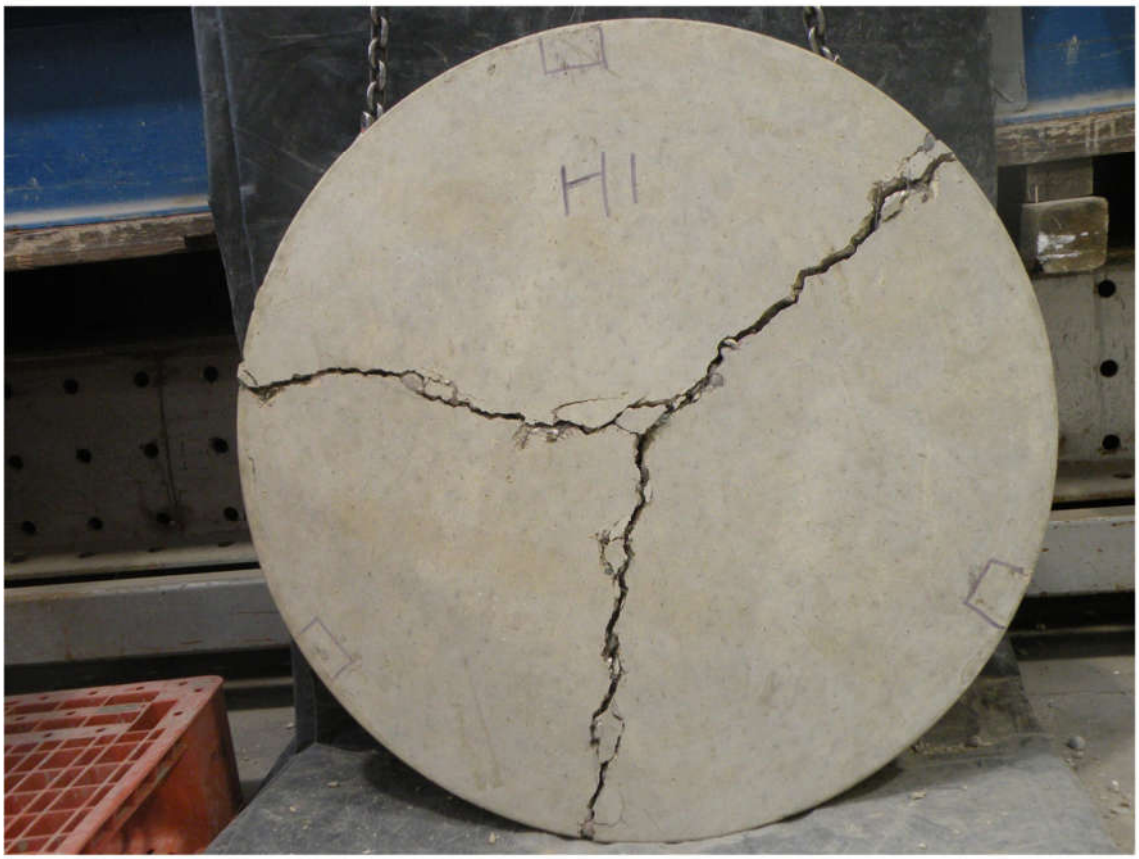

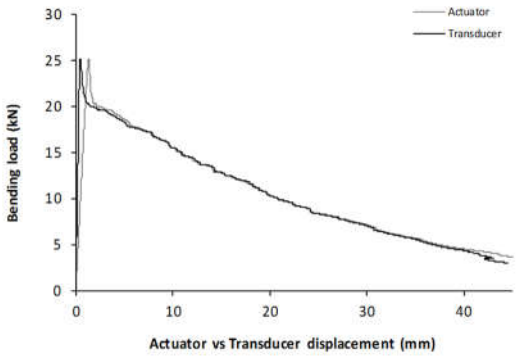

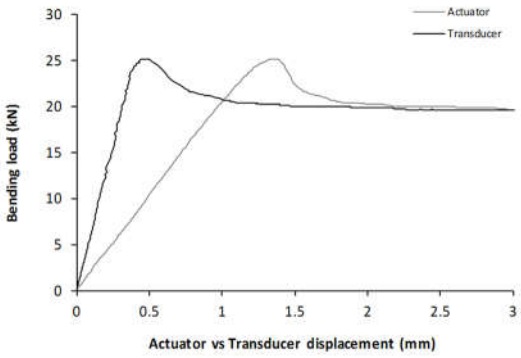

Specimen:			H2		
Depth, d	76.9	mm	Span, L	750	mm
Diameter	799	mm	Flexural strength	4.43	MPa

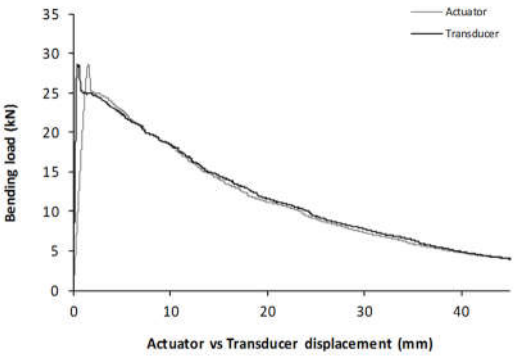

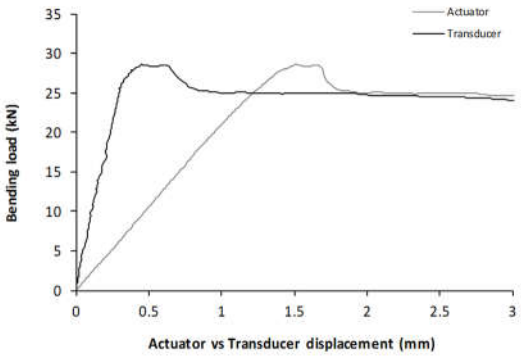

Specimen:			H3		
Depth, d	74.5	mm	Span, L	750	mm
Diameter	802.7	mm	Flexural strength	3.87	MPa

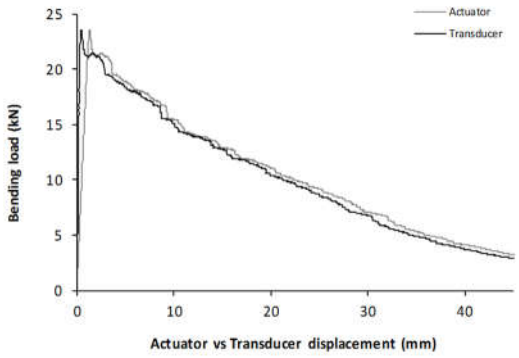

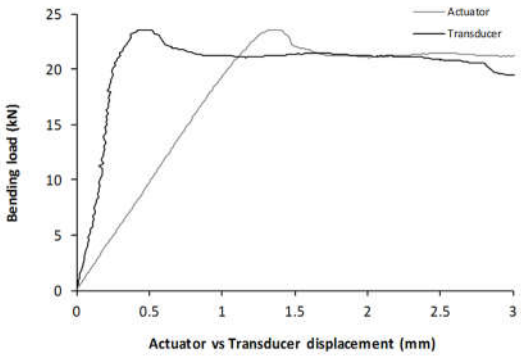

Mix:	H

Overall results

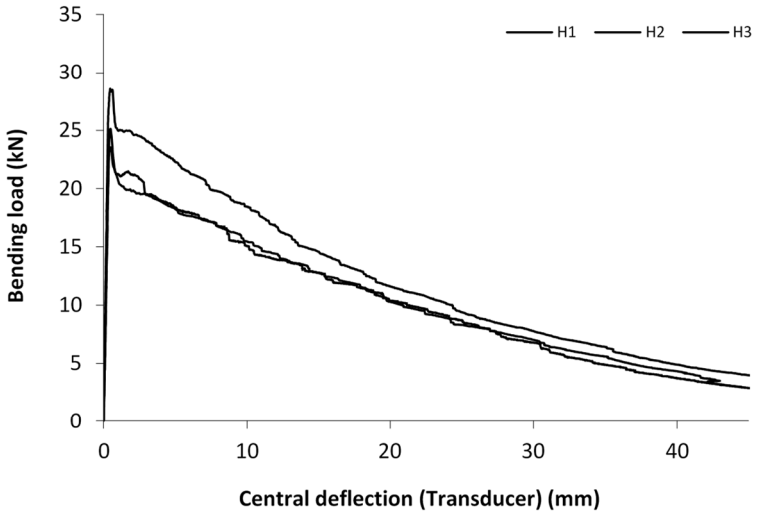

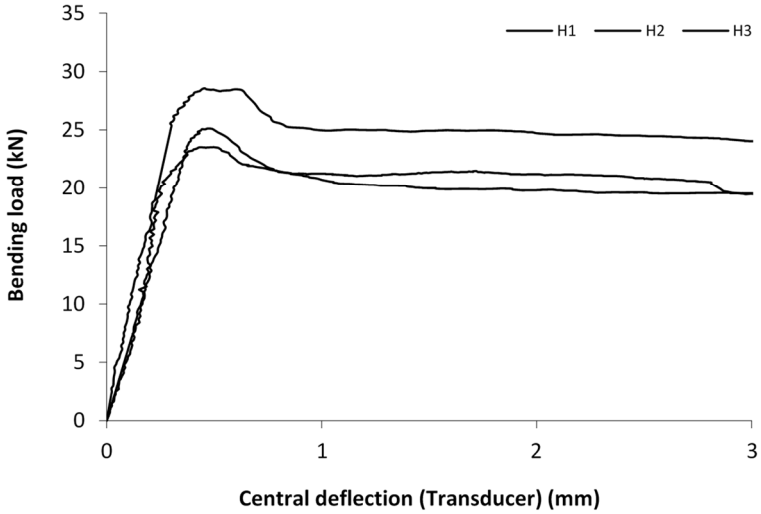

Specimen:			I1		
Depth, d	77.5	mm	Span, L	750	mm
Diameter	800.7	mm	Flexural strength	3.85	MPa

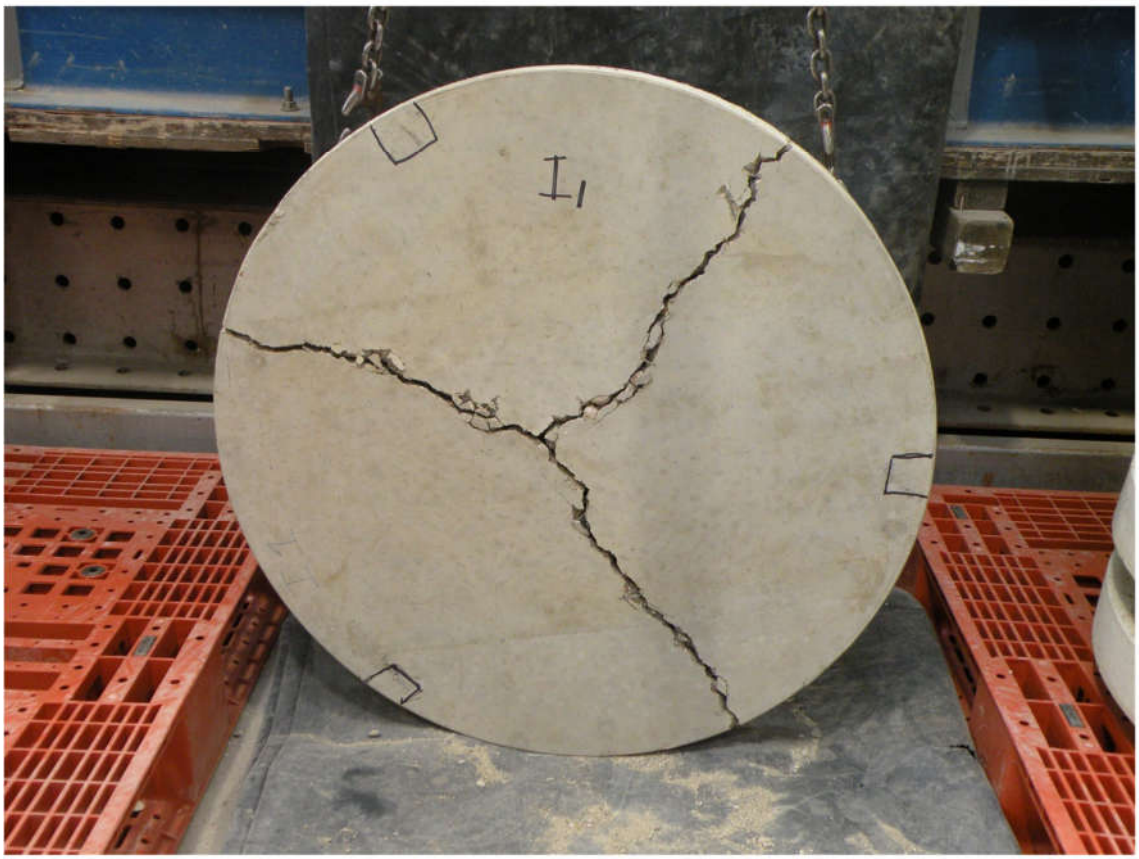

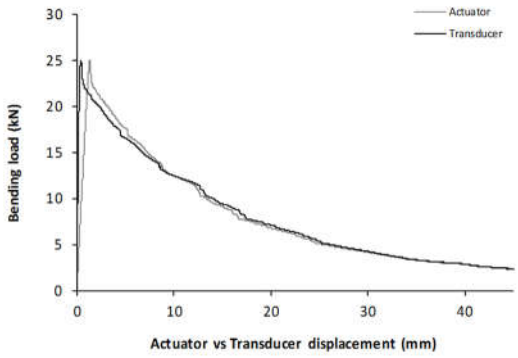

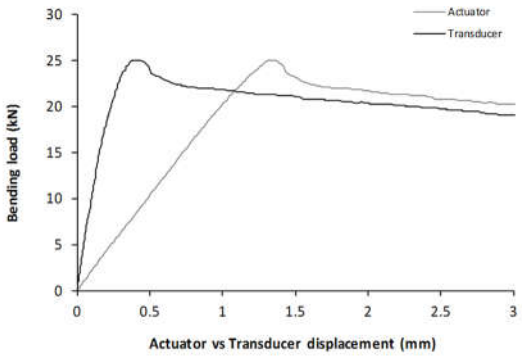

Specimen:			I2		
Depth, d	71.2	mm	Span, L	750	mm
Diameter	797.7	mm	Flexural strength	3.61	MPa

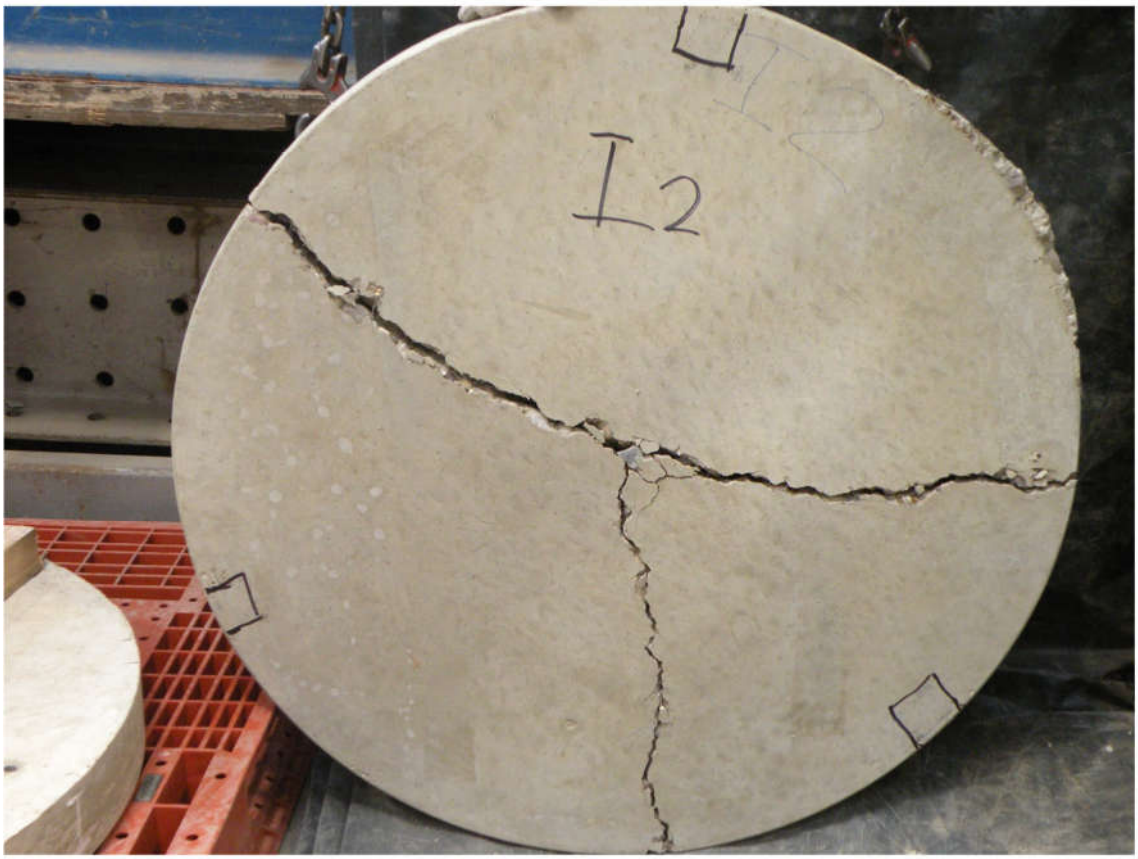

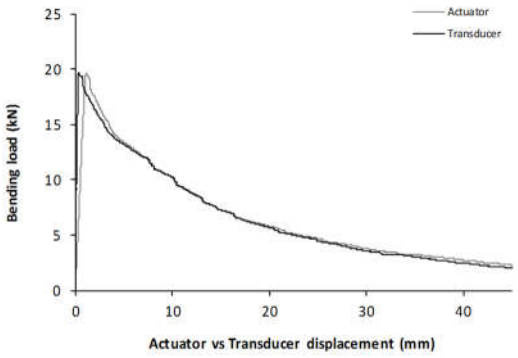

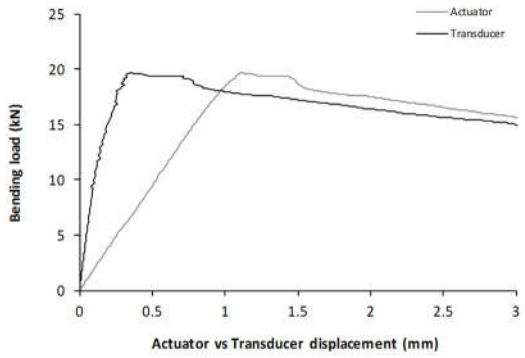

Specimen:			I3		
Depth, d	75.4	mm	Span, L	750	mm
Diameter	799.7	mm	Flexural strength	3.51	MPa

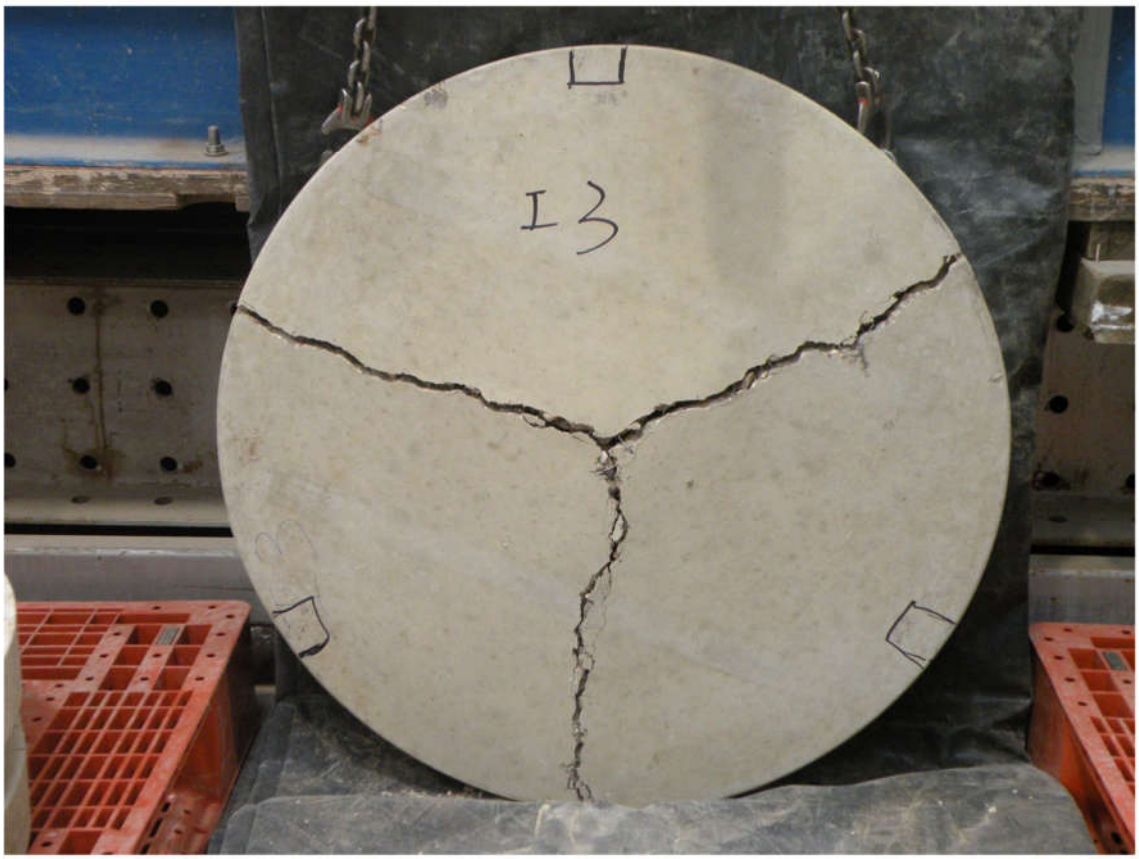

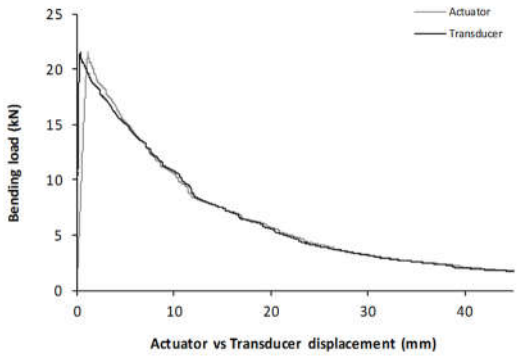

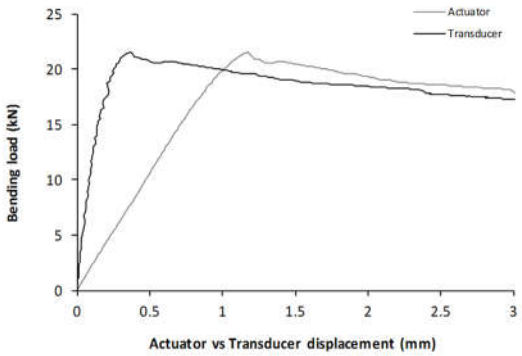

Mix: I

Overall results

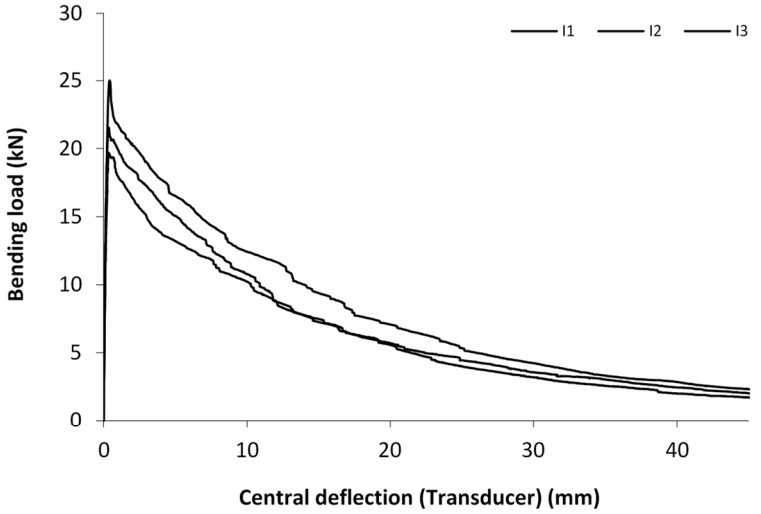

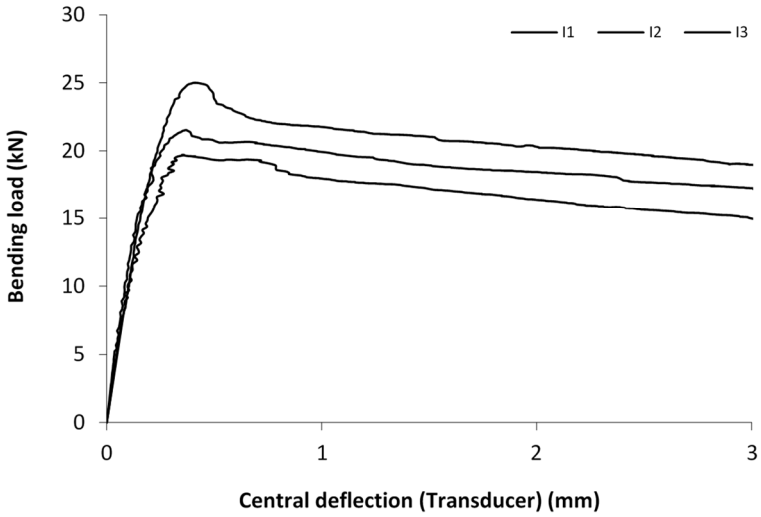

Specimen:			J1		
Depth, d	73.4	mm	Span, L	750	mm
Diameter	801	mm	Flexural strength	4.50	MPa

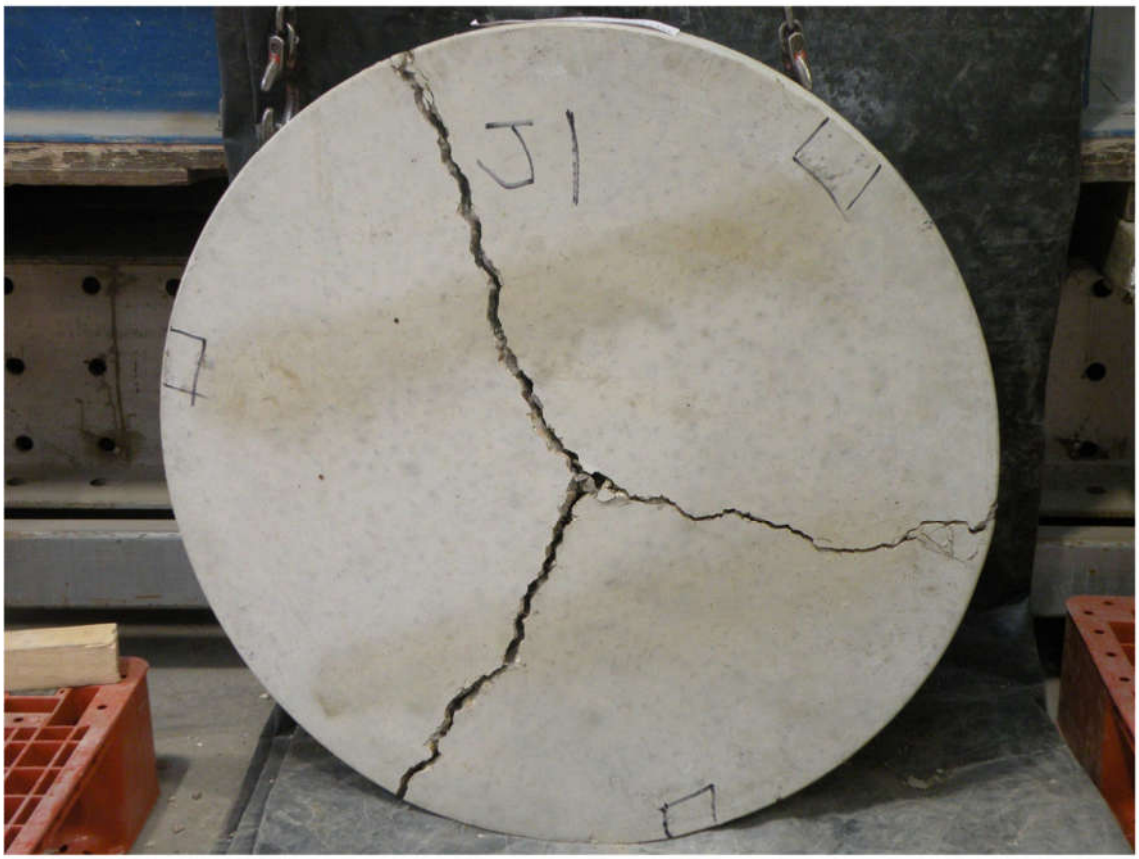

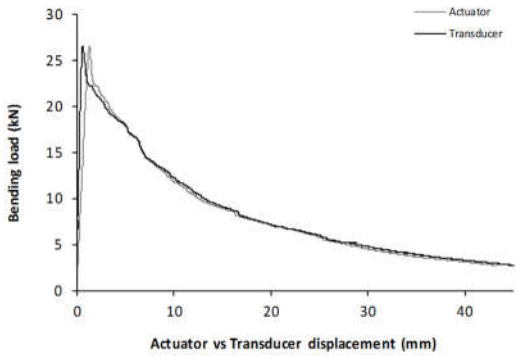

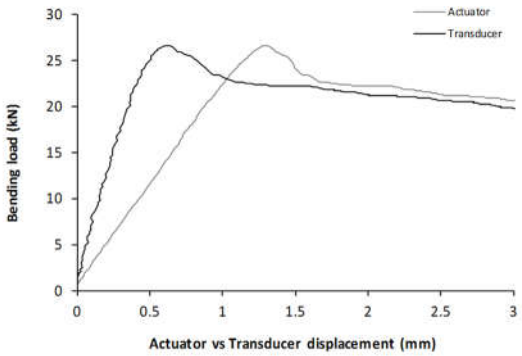

Specimen:			J2		
Depth, d	80.2	mm	Span, L	750	mm
Diameter	803.3	mm	Flexural strength	4.11	MPa

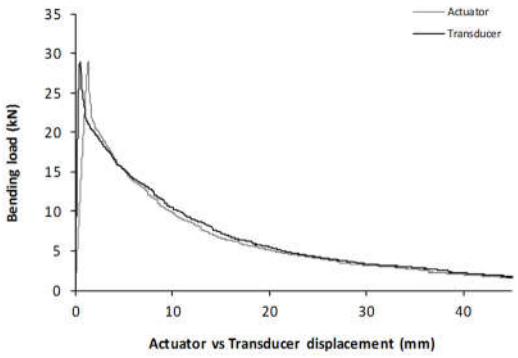

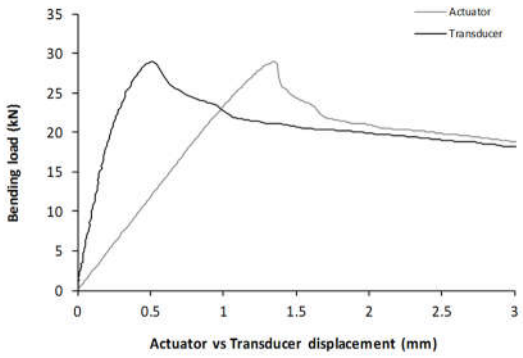

Specimen:			J3		
Depth, d	77.7	mm	Span, L	750	mm
Diameter	799.3	mm	Flexural strength	4.43	MPa

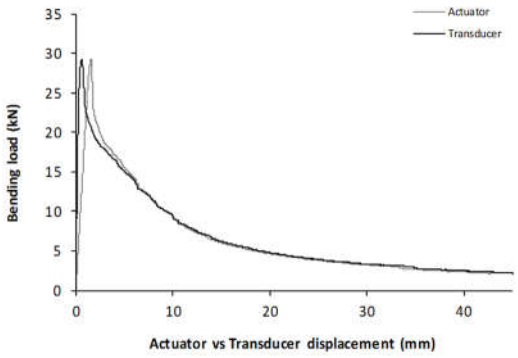

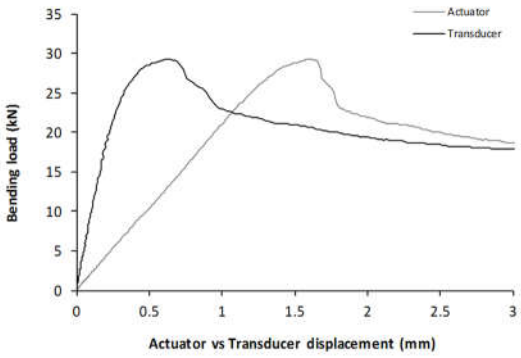

Mix:	J

Overall results

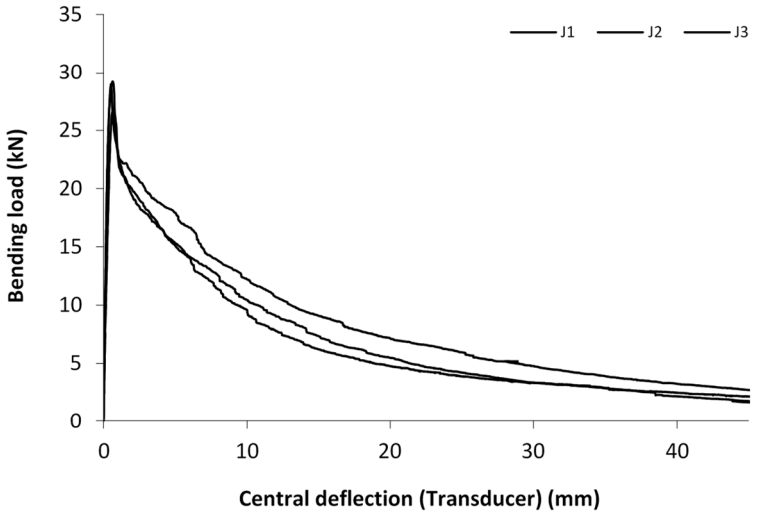

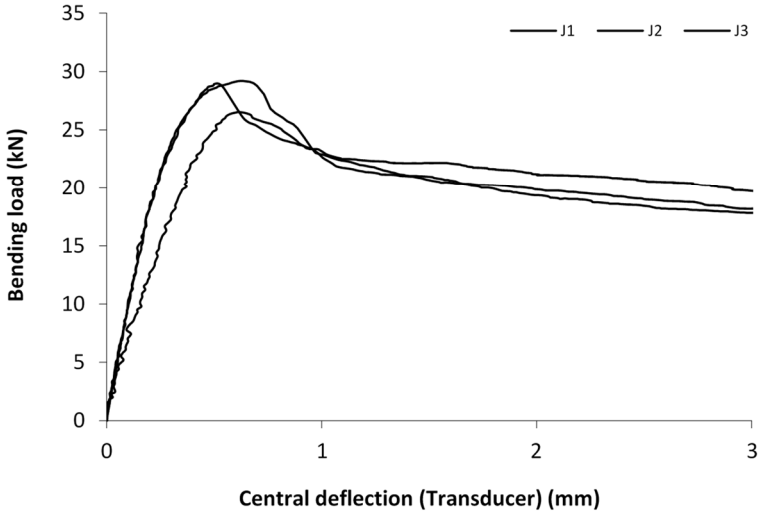

Appendix B:

Experimental results –Chapter 3

B.1 Tensile strength of RTSC

RTSC								
Specimen no	**Ultimate tensile load (kN)**	**Cord Diameter (mm) - As measured by calliper**	**Nominal Cord Area (mm^2)**	**Tensile Strength (MPa)**	**No of Filaments**	**Filament Diameter (mm)**	**Nominal Cord Area (mm^2) - Based on the total filament area**	**Tensile Stress (MPa)**
1	1.100	0.75	0.442	2490	12	0.2	0.377	2918
2	1.102			2494				2923
3	1.122			2540				2976
4	1.160			2626				3077
5	1.101			2492				2920
6	1.208			2734				3204
7	1.207			2732				3202
8	1.137			2574				3016
9	1.125			2546				2984
10	1.128			2553				2992
11	1.225			2773				3249
12	1.139			2578				3021
13	1.151			2605				3053
14	1.140			2580				3024
15	1.007			2279				2671
16	1.145			2592				3037
17	1.122			2540				2976
18	1.224			2771				3247
19	1.209			2737				3207
20	1.204			2725				3194
21	1.217			2755				3228
22	1.214			2748				3220
23	1.184			2680				3141

24	1.164			2635				3088
25	1.113			2519				2952
26	1.108			2508				2939
27	1.125			2546				2984
28	1.174			2657				3114
29	1.174			2657				3114
30	1.195			2705				3170
AVG	**1.154**			**2612**				**3061**

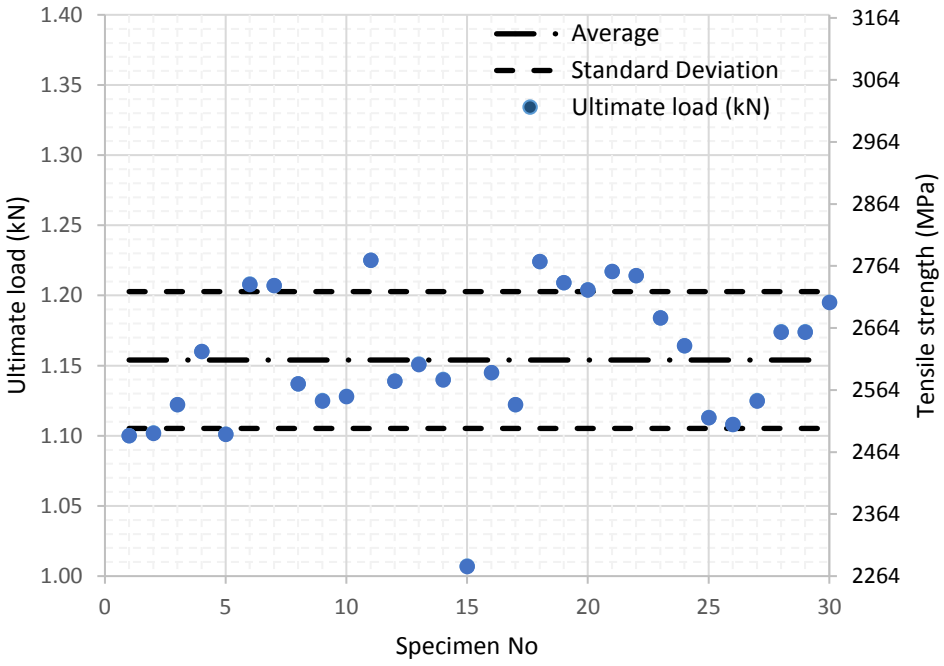

Figure B-1: Tensile strength of RTSC (based on the cord diameters measured by calliper)

B.2 Concrete mix Design (for pull-out tests)

Target concrete strength: C28/35
Cement (CEMII 42.5): 335 kg/m^3
Water: 185 kg/m^3
w/c: 0.55
Superplasticiser (Twinflow): 1.5 lt/m^3

Aggregates
Fines: 847 kg/m^3
Gravel 10mm: 491 kg/m^3
Gravel 14mm: 532 kg/m^3

B.3 Compressive and splitting tensile strength of concrete (for pull-out tests)

Table B-2: Compressive concrete strength (6 specimens) (loading rate: 0.5 MPa/s)

Cylinder no.	Density (kg/m^3)	Compressive strength (MPa)
1	2366.2	28.0
2	2170.5	25.4
3	2283.3	25.6
4	2309.5	21.5
5	2366.3	31.3
6	2387.1	21.6
Average	**2313.8**	**25.6**
STD	**73.4**	**3.4**

Table B-3: Splitting tensile concrete strength (6 specimens) (loading rate: 0.04 MPa/s)

Cylinder no.	Density (kg/m^3)	Splitting tensile strength (MPa)
1	2345	2.8
2	2406.5	3.2
3	2402.3	3.7
4	2389	2.8
5	2333.4	2.8
6	2382.7	3.8
Average	**2376.5**	**3.2**
STD	**27.7**	**0.4**

B.4 Failure load for RTSC with different embedment lengths

Table B-4: Failure load for RTSC with embedment length=10 mm

Specimen	Cord embedment length (mm)	Ultimate Load (N)	Failure Mode
1	10	359.39	Pull out
2	10	723.89	Pull out
3	10	244.87	Pull out
4	10	393.95	Pull out
5	10	220.00	Pull out
6	10	615.11	Pull out
Average Force (N)		**426.20**	
Standard Deviation (N)		**202.59**	

Table B-5: Failure load for RTSC with embedment length=25 mm

Specimen no.	Cord embedment length (mm)	Ultimate Load (N)	Failure Mode
1	25	549.75	Pull out
2	25	787.94	Pull out
3	25	690.07	Pull out
4	25	719.20	Pull out
5	25	778.69	Pull out
6	25	643.83	Pull out
Average Force (N)		**695.20**	
Standard Deviation (N)		**81.60**	

Table B-6: Failure load for RTSC with embedment length=40 mm

Specimen no.	Cord embedment length (mm)	Ultimate Load (N)	Failure Mode
1	40	1256.69	Cord Rupture
2	40	1102.05	Cord Rupture
3	40	1037.58	Cord Rupture
4	40	778.63	Pull-Out
5	40	926.43	Pull-Out
6	40	1159.36	Cord Rupture
Average Force (N)		**853.25/1139.30***	
Standard Deviation (N)		**102.25/125.10***	

* Results for specimens failed due to cord rupture

B.5 Compressive strength (SFRC and plain concrete cubes)

Mix	Casting date	Testing date	Load (kN)	Stress (MPa)
A – MSF2 (30)	**17/11/2015**	**09/02/2016 (84 days)**	1189.1	53.2
			989.6	42.6
			1154.4	51.3
			1091.7	48.5
			1156.4	50.4
			1101.9	48.3
AVG B			**1113.9**	**49.1**
SD				**3.1**
B – RTSC (20) + RTSF(10)	**17/11/2015**	**09/02/2016 (84 days)**	1106.6	47.0
			1177.1	51.6
			1162.0	50.6
			1113.7	47.9
			1074.5	47.8
			1124.7	48.7
AVG C			**1126.4**	**48.9**
SD				**1.7**
C – RTSC (30)	**17/11/2015**	**09/02/2016 (84 days)**	1167.1	50.2
			1246.5	52.6
			974.9	41.7
			1256.1	53.3
			1172.8	49.2
			1184.3	51.6
AVG A			**1167.0**	**49.8**
SD				**3.9**
D - RTSF (30)	**17/11/2015**	**09/02/2016 (84 days)**	1061.1	45.0
			1101.5	46.8
			1184.0	51.3
			1105.4	48.8
			1104.4	47.5
			1146.3	49.3

AVG D			**1117.1**	**48.1**
SD				**2.0**
P - Plain concrete 1*	**17/11/2015**	**09/02/2016 (84 days)**	1158.8	51.5
			996.8	44.3
			1012.5	45.2
			1053.0	46.8
			1014.8	45.1
			1080.2	48.0
AVG P			**1139.5**	**46.2**
SD				**2.4**

*Batch number

Mix	**Casting date**	**Testing date**	**Load (kN)**	**Stress (MPa)**
E – MSF1 (45)	**24/11/2015**	**01/02/2016 (69 days)**	1167.9	50.7
			1121.6	48.6
			1061.0	45.2
			1095.4	47.1
			1163.4	50.4
			1126.0	47.8
AVG F			**1122.6**	**48.3**
SD				**1.9**
F - RTSC (22.5) + RTSF (22.5)	**24/11/2015**	**01/02/2016 (69 days)**	1292.6	56.3
			1265.4	55.5
			1282.1	55.7
			1322.5	57.8
			1302.0	56.5
			1207.4	52.6
AVG G			**1278.7**	**55.7**
SD				**1.6**
G - RTSC (35) + RTSF (10)	**24/11/2015**	**01/02/2016 (69 days)**	1104.4	48.4
			1137.4	48.3
			1146.2	49.6
			1109.2	48.3
			1107.7	48.6

			1083.9	46.9
AVG H			**1114.8**	**48.4**
SD				**0.8**
H - RTSC (45)	**24/11/2015**	**01/02/2016 (69 days)**	1101.8	47.5
			1119.7	48.1
			1091.3	46.9
			1058.2	46.0
			1118.5	48.6
			1066.7	46.0
AVG E			**1092.7**	**47.2**
SD				**1.0**
P - Plain concrete 2*	**24/11/2015**	**01/02/2016 (69 days)**	1017.3	44.9
			1150.2	50.8
			1070.5	47.3
			991.8	44.1
			1037.7	46.1
			1083.0	48.1
AVG P			**1042.5**	**45.8**
SD				**2.7**

*Batch number

B.6 Residual flexural tensile strength (SFRC prisms)

A	f_R				B	f_R			
	f_{R1}	f_{R2}	f_{R3}	f_{R4}		f_{R1}	f_{R2}	f_{R3}	f_{R4}
A1	4.37	4.57	3.26	2.75	B1	3.57	4.30	3.87	3.04
A2	3.83	3.99	3.70	3.36	B2	5.47	6.04	5.54	4.18
A3	3.49	3.41	2.88	2.41	B3	5.84	6.34	5.84	4.56
A4	4.65	4.40	3.96	3.36	B4	3.93	4.01	3.89	3.51
A5	5.50	5.63	4.78	3.99	B5	7.26	7.11	6.94	5.99
A6	3.86	3.98	3.89	3.02	B6	6.01	6.89	4.48	3.82
A7	3.88	4.31	3.92	3.68	B7	5.01	5.05	4.45	3.91
A8	3.36	3.27	2.99	2.68	B8	4.97	5.47	4.49	3.62
A9	3.57	4.05	3.98	3.29	B9	4.89	5.75	5.04	4.05
A10	3.89	3.50	3.16	2.47	B10	4.70	5.51	4.55	3.49
A11	3.83	4.18	3.65	3.54	B11	6.06	5.96	5.75	5.04
A12	5.05	5.01	4.32	3.87	B12	5.89	7.12	6.40	5.90
Mean A	**4.1**	**4.2**	**3.7**	**3.2**	**Mean B**	**5.3**	**5.8**	**5.1**	**4.3**
Standard Deviation	0.66	0.67	0.56	0.54	Standard Deviation	1.01	1.01	0.99	0.94
COV (%)	15	15	14	15	**COV (%)**	18	17	19	21

C	f_R				D	f_R			
	f_{R1}	f_{R2}	f_{R3}	f_{R4}		f_{R1}	f_{R2}	f_{R3}	f_{R4}
C1	7.10	7.52	7.76	7.27	D1	2.32	1.66	1.20	1.03
C 2	5.86	6.15	5.99	5.85	D 2	2.29	1.69	1.48	1.31
C 3	8.06	8.52	8.03	7.33	D 3	3.64	3.10	2.09	1.71
C 4	6.84	7.23	7.09	6.60	D 4	2.76	1.97	1.66	1.19
C 5	6.48	7.76	7.58	6.59	D 5	3.09	2.68	2.22	1.79
C 6	5.82	7.18	6.81	5.91	D 6	3.13	2.36	1.85	1.46
C 7	6.34	7.95	7.71	7.03	D 7	3.79	3.02	2.27	1.79
C 8	6.32	7.59	6.36	5.01	D 8	5.54	4.82	3.80	3.00
C 9	7.70	8.00	7.78	6.83	D 9	3.68	2.78	2.06	1.37
C 10	6.98	7.26	6.69	6.07	D10	4.31	3.88	3.05	2.56
C 11	6.58	7.87	7.68	7.32	D 11	3.19	2.43	2.03	1.67
C 12	5.64	6.72	6.58	6.00	D12	3.29	2.39	1.86	1.57
Mean C	**6.6**	**7.5**	**7.2**	**6.5**	**Mean D**	**3.4**	**2.7**	**2.1**	**1.7**

Standard Deviation	0.74	0.63	0.67	0.73	Standard Deviation	0.89	0.91	0.70	0.56
COV (%)	11	8	9	11	**COV (%)**	25	32	31	32

E	**f_R**				**F**	**f_R**			
	f_{R1}	**f_{R2}**	**f_{R3}**	**f_{R4}**		**f_{R1}**	**f_{R2}**	**f_{R3}**	**f_{R4}**
E1	4.14	4.20	3.54	2.93	F1	4.94	5.53	5.10	3.56
E2	4.31	4.89	3.81	3.26	F2	5.79	6.56	6.00	5.60
E3	4.31	4.89	3.81	3.26	F3	5.13	5.92	5.34	4.68
E4	3.52	3.63	3.36	3.20	F4	5.84	6.44	5.82	5.08
E5	3.56	3.64	3.31	3.13	F5	5.70	6.42	6.48	5.75
E6	4.52	4.41	3.87	3.42	F6	7.02	7.42	6.57	5.79
E7	3.89	3.72	3.64	3.16	F7	5.43	6.26	5.88	5.38
E8	4.42	4.84	4.21	3.48	F8	7.05	7.76	7.33	6.14
E9	3.74	3.94	3.61	3.21	F9	4.26	4.36	4.34	3.52
E10	5.28	4.92	4.45	4.10	F10	7.08	7.78	7.28	6.18
E11	4.68	4.06	3.71	3.34	F11	5.17	5.36	5.21	4.31
E12	3.97	3.60	3.34	3.13	F12	5.37	6.43	6.04	5.21
Mean E	**4.2**	**4.2**	**3.7**	**3.3**	**Mean F**	**5.7**	**6.4**	**5.9**	**5.1**
Standard Deviation	0.51	0.54	0.44	0.43	Standard Deviation	0.90	1.00	0.88	0.91
COV (%)	12	12	12	13	**COV (%)**	15	15	14	17

G	**f_R**				**H**	**f_R**			
	f_{R1}	**f_{R2}**	**f_{R3}**	**f_{R4}**		**f_{R1}**	**f_{R2}**	**f_{R3}**	**f_{R4}**
G1	5.04	5.40	5.38	4.41	H1	6.11	7.31	6.73	6.28
G2	6.14	6.89	6.51	5.63	H2	6.99	8.15	7.88	7.35
G3	6.54	6.42	6.33	5.90	H3	6.76	7.00	6.42	5.71
G4	3.55	3.55	3.31	2.91	H4	7.73	8.44	7.72	6.56
G5	5.44	6.45	5.33	4.99	H5	6.53	6.96	6.68	6.05
G6	6.95	7.37	6.85	6.34	H6	6.92	7.14	6.81	6.02
G7	6.88	7.75	7.62	6.90	H7	6.76	8.23	7.18	6.19
G8	6.94	7.84	8.03	7.37	H8	N/A	N/A	N/A	N/A
G9	7.24	7.99	7.44	7.13	H9	6.21	7.36	7.12	6.41
G10	7.07	7.52	6.94	6.51	H10	8.51	9.46	8.74	7.98
G11	6.81	7.83	7.20	6.39	H11	6.83	8.27	8.23	7.44
G12	5.00	5.54	4.45	4.09	H12	7.24	8.34	7.92	6.67

Mean G	**6.1**	**6.7**	**6.3**	**5.7**	**Average H**	**7.0**	**7.9**	**7.4**	**6.6**
Standard Deviation	1.14	1.34	1.40	1.36	Standard Deviation	0.68	0.78	0.74	0.70
COV (%)	18	19	21	23	**COV (%)**	9	9	10	10

B.7 Prisms (after testing)

Specimen code name:		A1 (B1)	MSF2 (30)		
Notched Depth dn	125	mm			
Depth, d	150	mm	Span, L	500	mm
Width, b	147	mm	Flexural strength	4.67	MPa

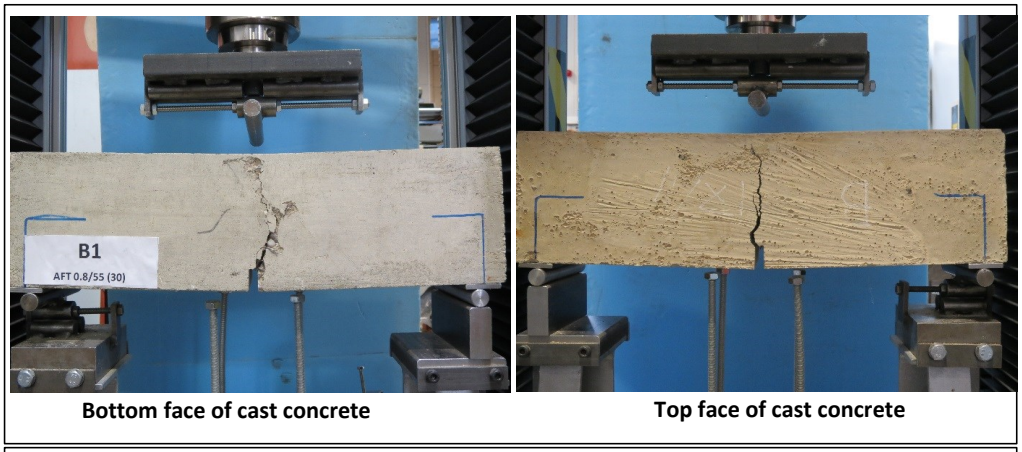

Bottom face of cast concrete

Top face of cast concrete

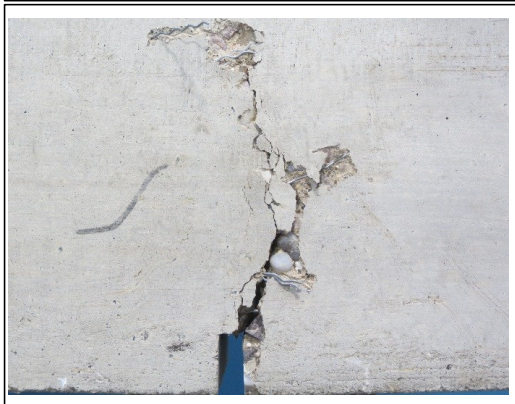

Crack zone of bottom face

Crack zone of top face

Stress-deformation graphs

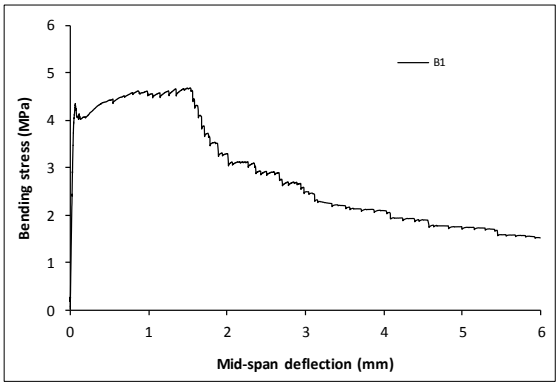

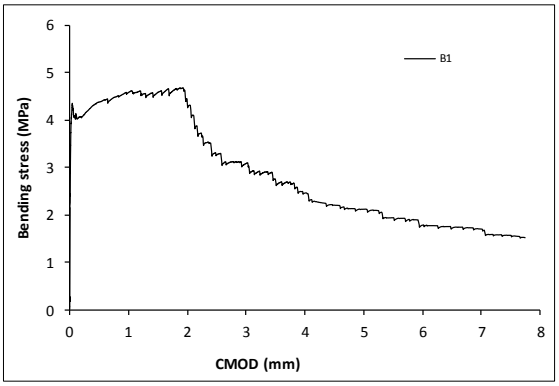

Specimen code name:		A2 (B2)	MSF2 (30)		
Notched Depth dn	123.75	mm			
Depth, d	149.5	mm	Span, L	500	mm
Width, b	147.25	mm	Flexural strength	4.04	MPa

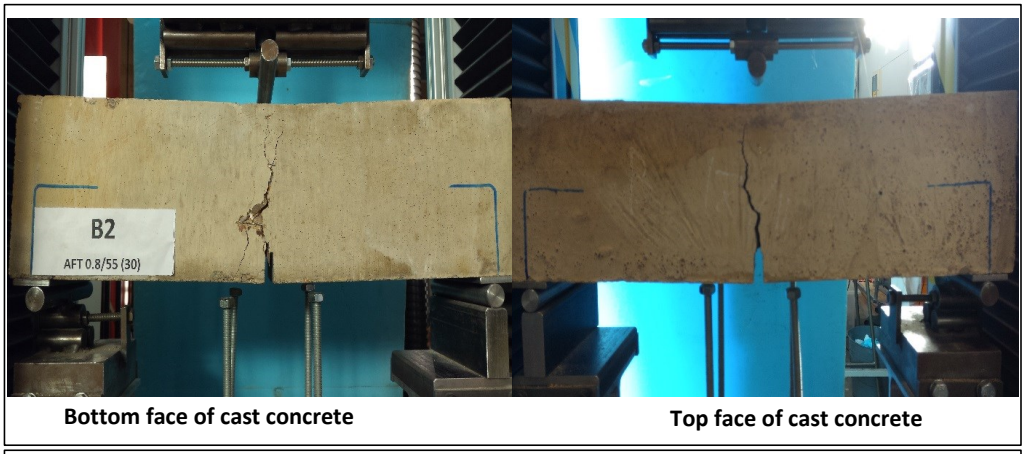

Bottom face of cast concrete | Top face of cast concrete

Crack zone of bottom face | Crack zone of top face

Stress-deformation graphs

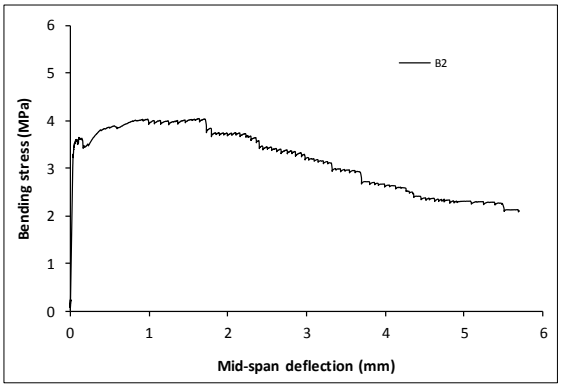

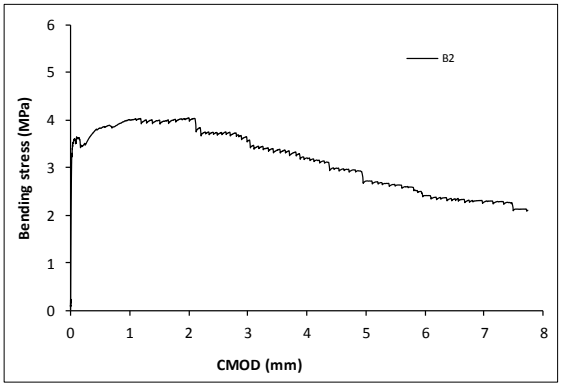

Specimen code name:		A3 (B3)	MSF2 (30)		
Notched Depth dn	124.5	mm			
Depth, d	150.5	mm	Span, L	500	mm
Width, b	146.25	mm	Flexural strength	4.56	MPa

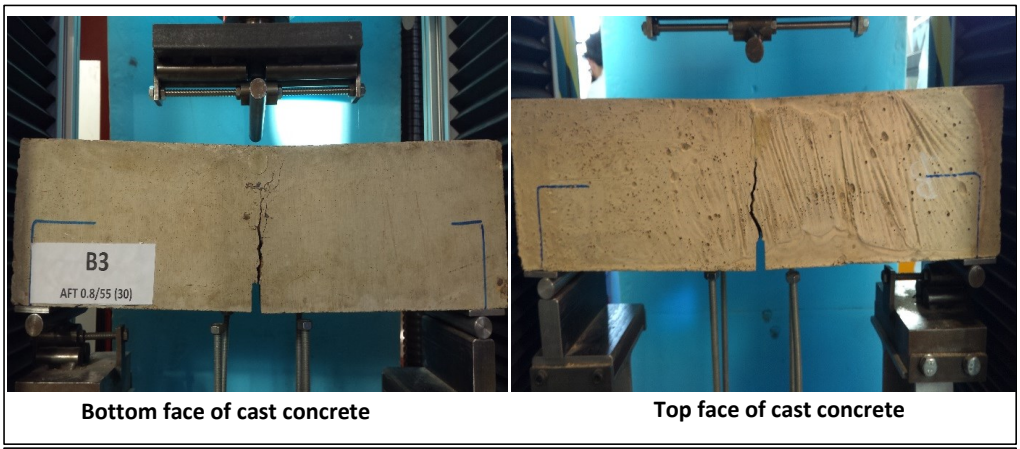

Bottom face of cast concrete | Top face of cast concrete

Crack zone of bottom face | Crack zone of top face

Stress-deformation graphs

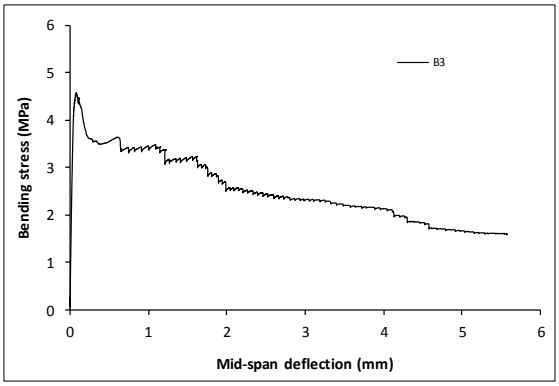

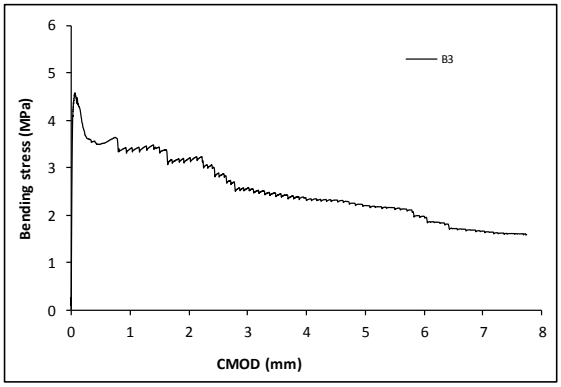

Specimen code name:		A4 (B4)	MSF2 (30)		
Notched Depth dn	123.75	mm			
Depth, d	150	mm	Span, L	500	mm
Width, b	148	mm	Flexural strength	4.97	MPa

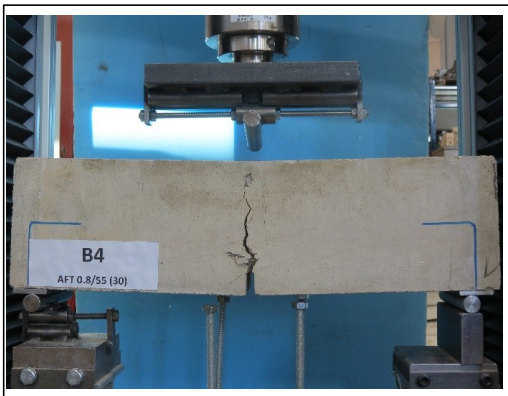

Bottom face of cast concrete

Top face of cast concrete

Crack zone of bottom face

Crack zone of top face

Stress-deformation graphs

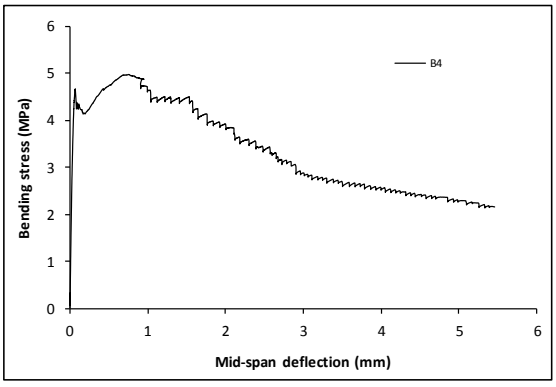

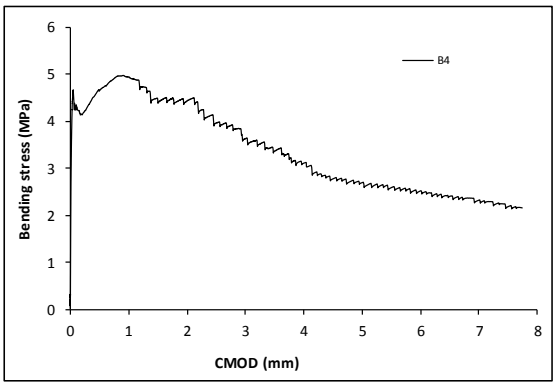

Specimen code name:		A5 (B5)	MSF2 (30)		
Notched Depth dn	123.75	mm			
Depth, d	149.5	mm	Span, L	500	mm
Width, b	150	mm	Flexural strength	5.99	MPa

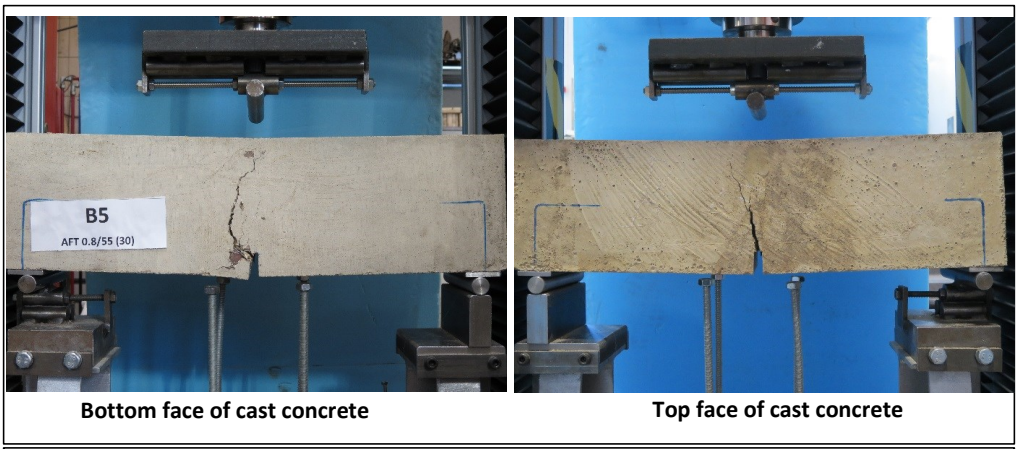

Bottom face of cast concrete | Top face of cast concrete

Crack zone of bottom face | Crack zone of top face

Stress-deformation graphs

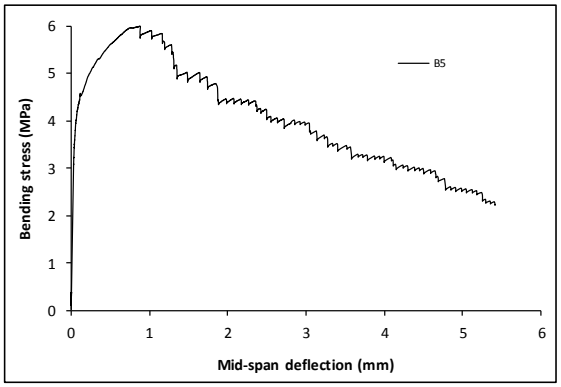

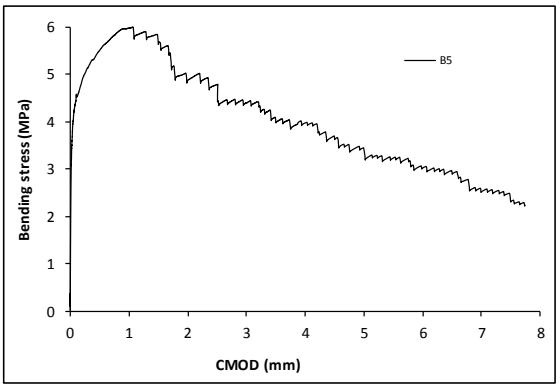

Specimen code name:		A6 (B6)	MSF2 (30)		
Notched Depth dn	124.25	mm			
Depth, d	150	mm	Span, L	500	mm
Width, b	150.25	mm	Flexural strength	4.13	MPa

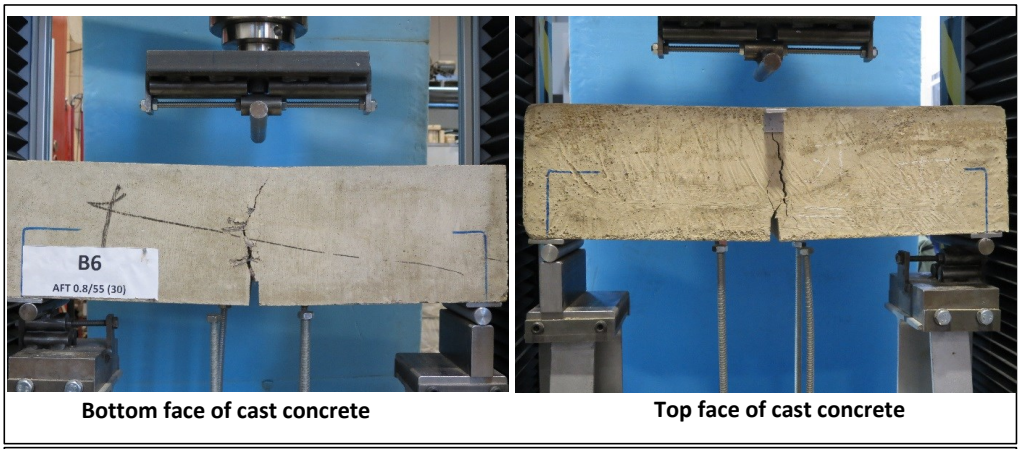

Bottom face of cast concrete | Top face of cast concrete

Crack zone of bottom face | Crack zone of top face

Stress-deformation graphs

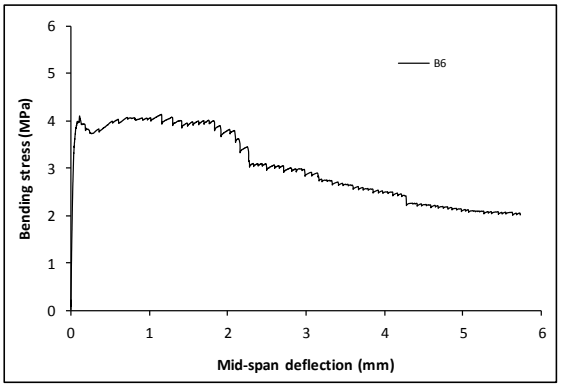

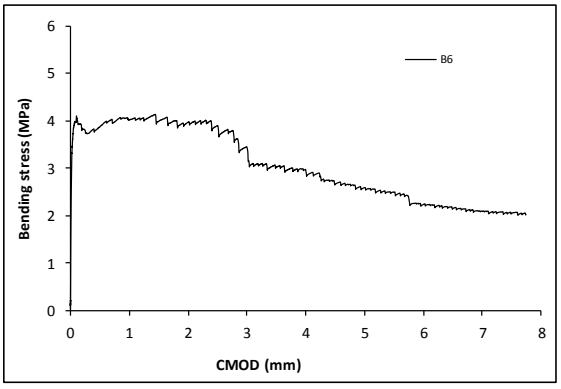

Specimen code name:		A7 (B7)	MSF2 (30)		
Notched Depth dn	124.75	mm			
Depth, d	150	mm	Span, L	500	mm
Width, b	150.25	mm	Flexural strength	4.36	MPa

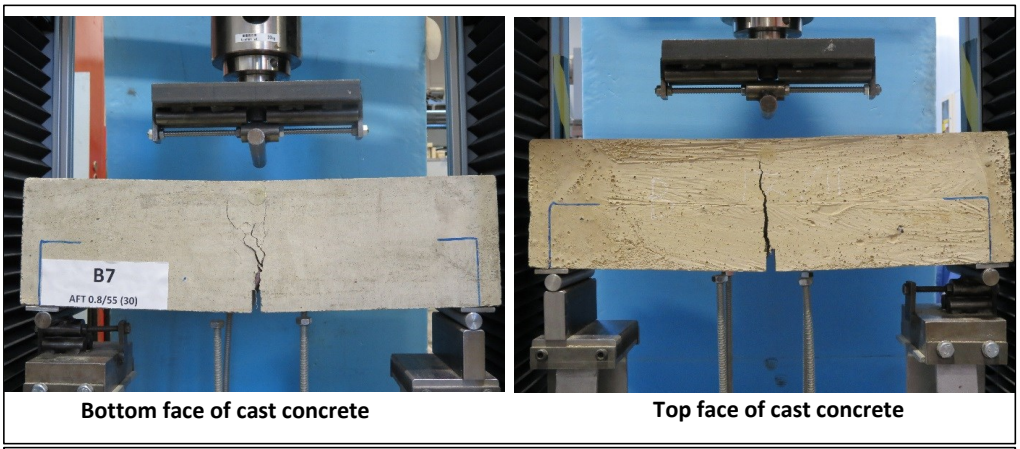

Bottom face of cast concrete | Top face of cast concrete

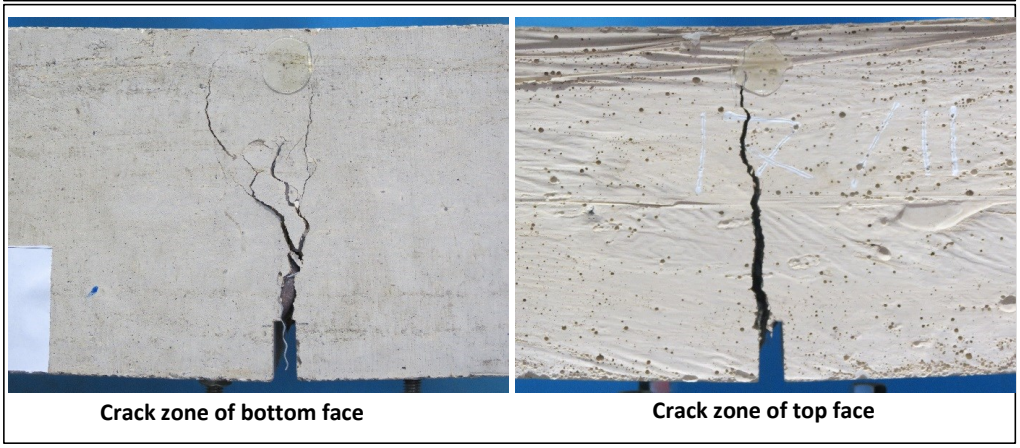

Crack zone of bottom face | Crack zone of top face

Stress-deformation graphs

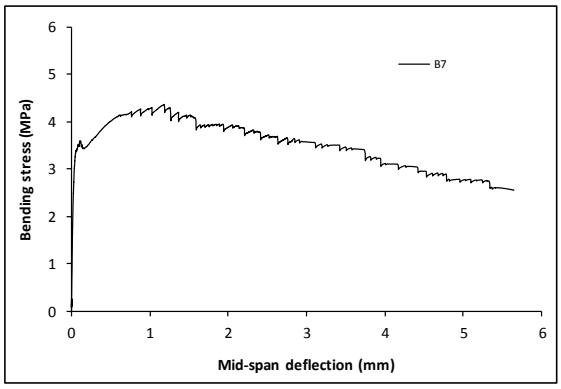

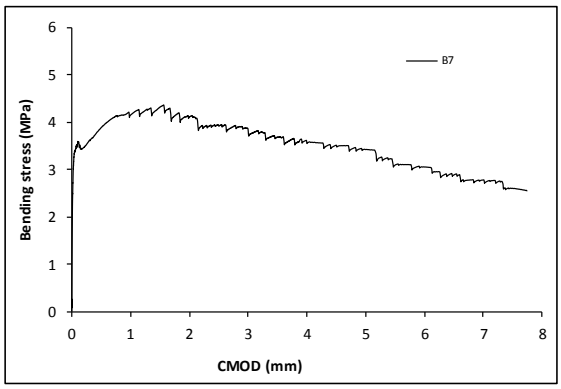

Specimen code name:		A8 (B8)	MSF2 (30)		
Notched Depth dn	125	mm			
Depth, d	149.25	mm	Span, L	500	mm
Width, b	149.5	mm	Flexural strength	3.94	MPa

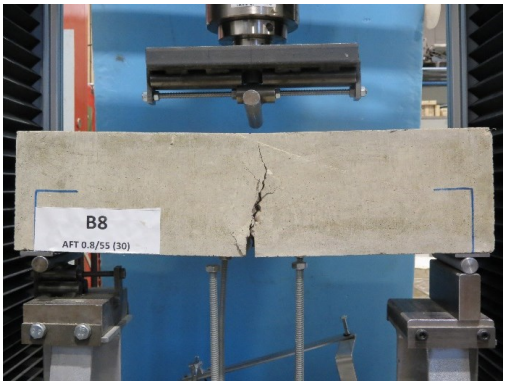

Bottom face of cast concrete

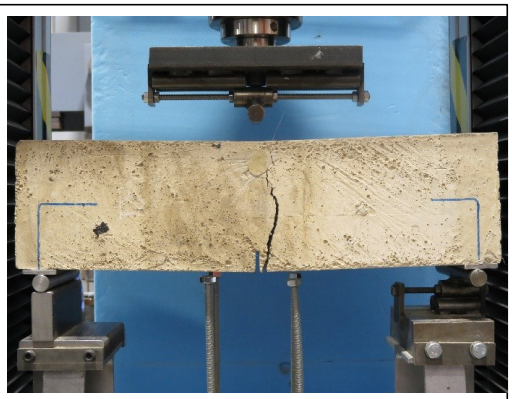

Top face of cast concrete

Crack zone of bottom face

Crack zone of top face

Stress-deformation graphs

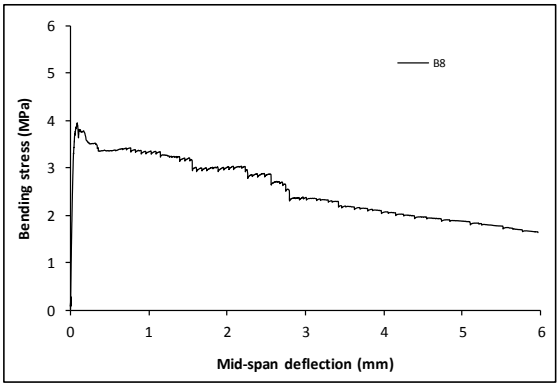

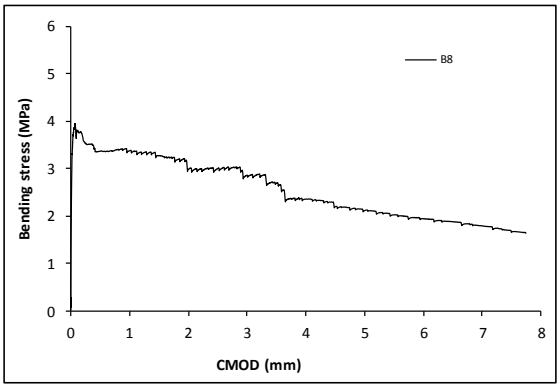

Specimen code name:		A9 (B9)	MSF2 (30)		
Notched Depth dn	125	mm			
Depth, d	150.25	mm	Span, L	500	mm
Width, b	147.25	mm	Flexural strength	4.10	MPa

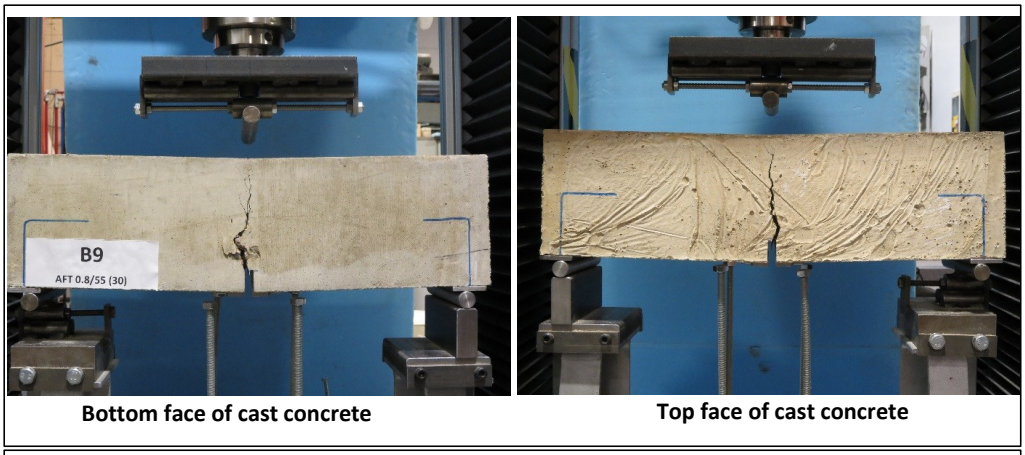

Bottom face of cast concrete

Top face of cast concrete

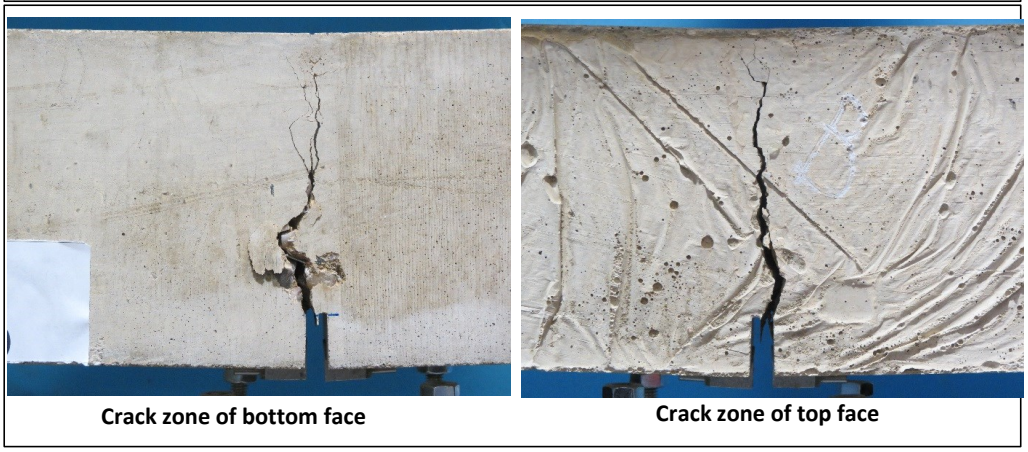

Crack zone of bottom face

Crack zone of top face

Stress-deformation graphs

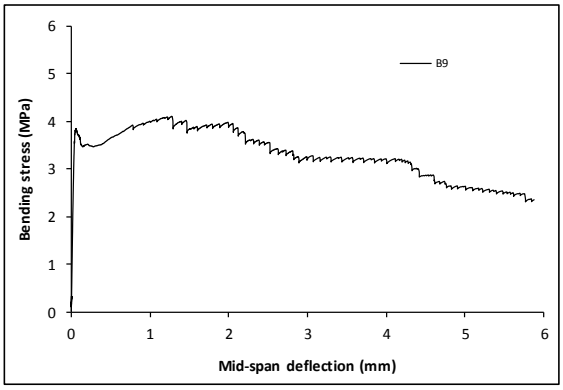

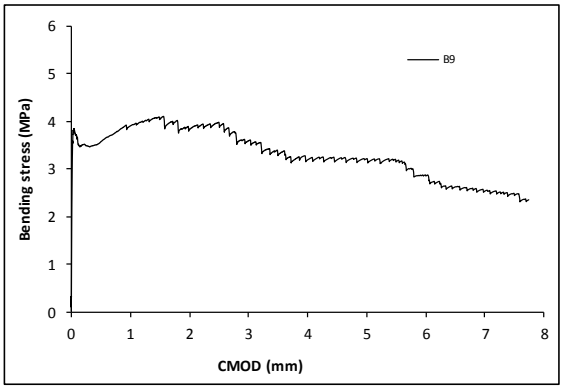

Specimen code name:		A10 (B10)	MSF2 (30)		
Notched Depth dn	124.75	mm			
Depth, d	149.75	mm	Span, L	500	mm
Width, b	148	mm	Flexural strength	4.40	MPa

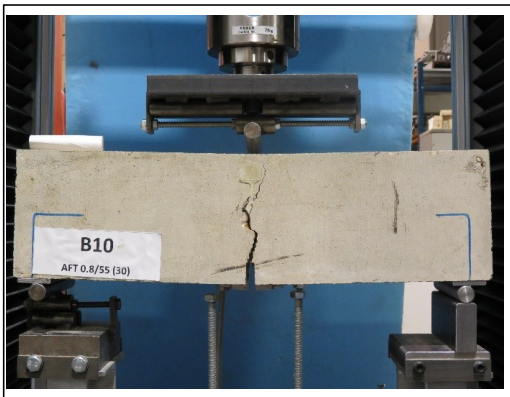

Bottom face of cast concrete

Top face of cast concrete

Crack zone of bottom face

Crack zone of top face

Stress-deformation graphs

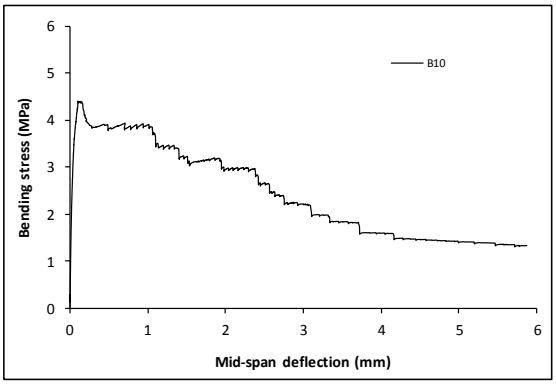

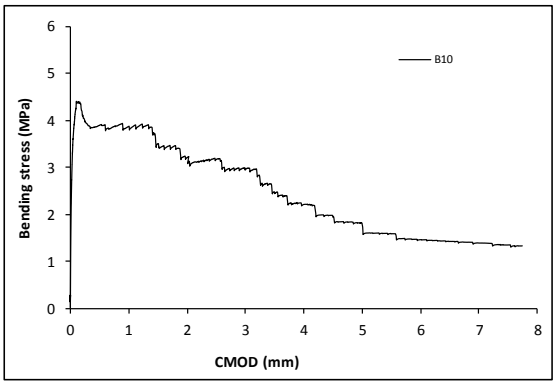

Specimen code name:		**A11 (B11)**	MSF2 (30)		
Notched Depth dn	124.75	mm			
Depth, d	150	mm	Span, L	500	mm
Width, b	147.75	mm	Flexural strength	4.33	MPa

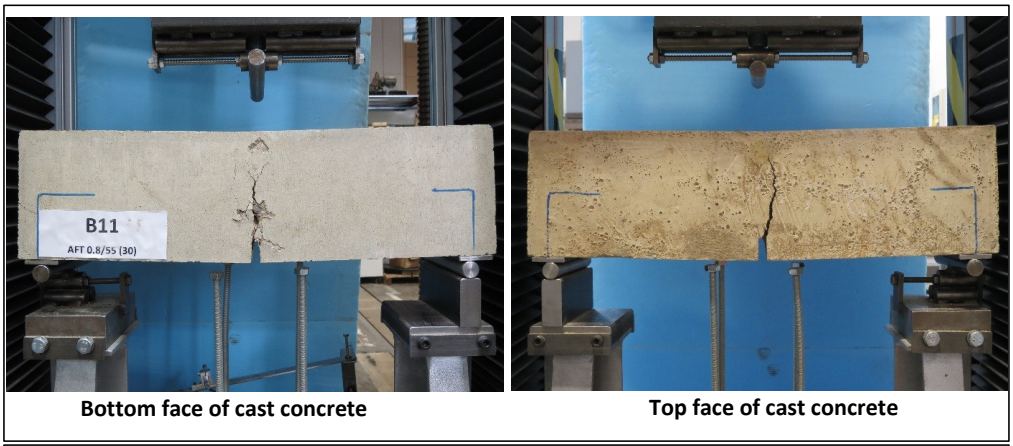

Bottom face of cast concrete **Top face of cast concrete**

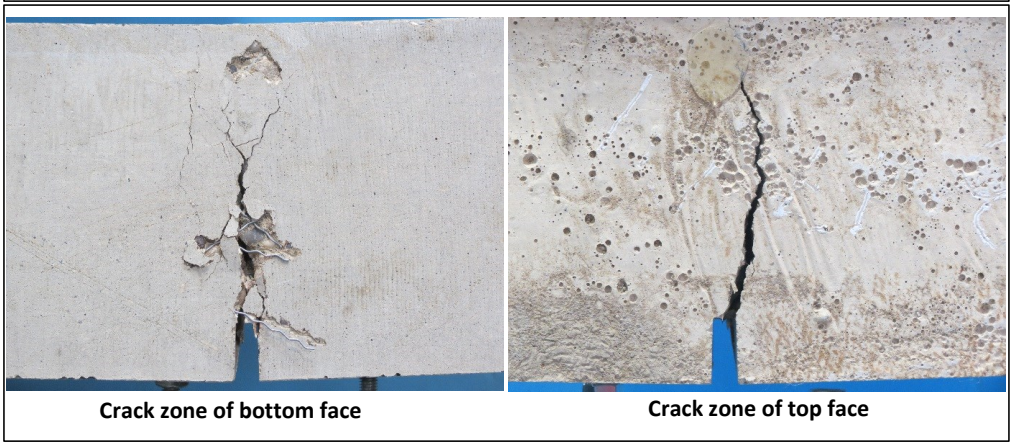

Crack zone of bottom face **Crack zone of top face**

Stress-deformation graphs

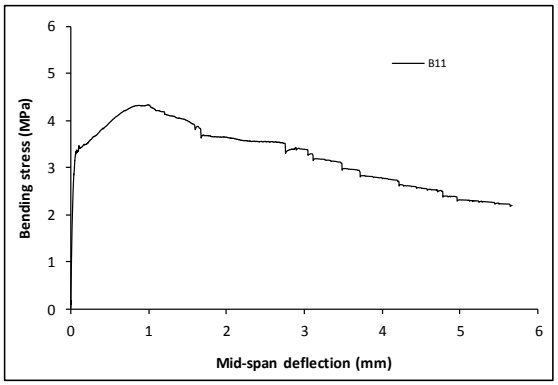

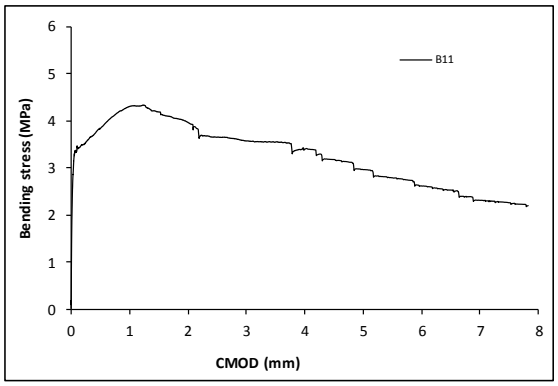

Specimen code name:		**A12 (B12)**	MSF2 (30)		
Notched Depth dn	124.5	mm			
Depth, d	150	mm	Span, L	500	mm
Width, b	149.25	mm	Flexural strength	5.32	MPa

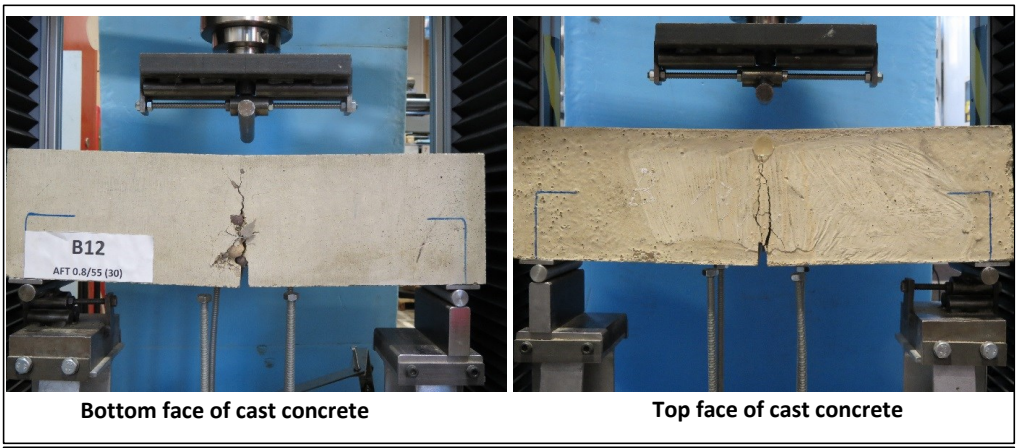

Bottom face of cast concrete **Top face of cast concrete**

Crack zone of bottom face **Crack zone of top face**

Stress-deformation graphs

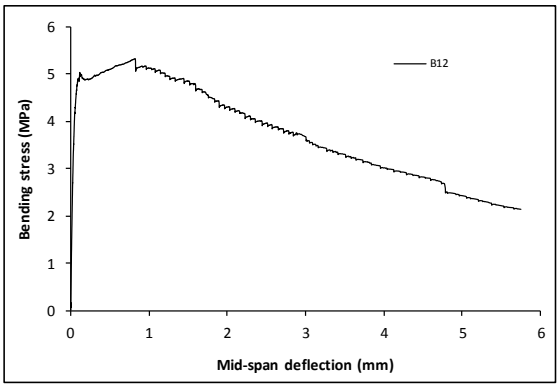

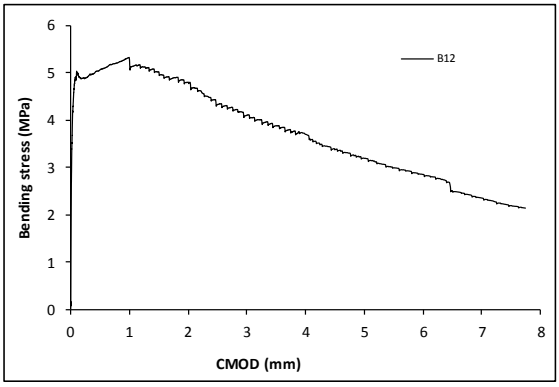

Mix:	**A (B)**	MSF2 (30)	
Notched Depth dn	mm		
Depth, d	mm	Span, L	mm
Width, b	mm	Flexural strength	MPa

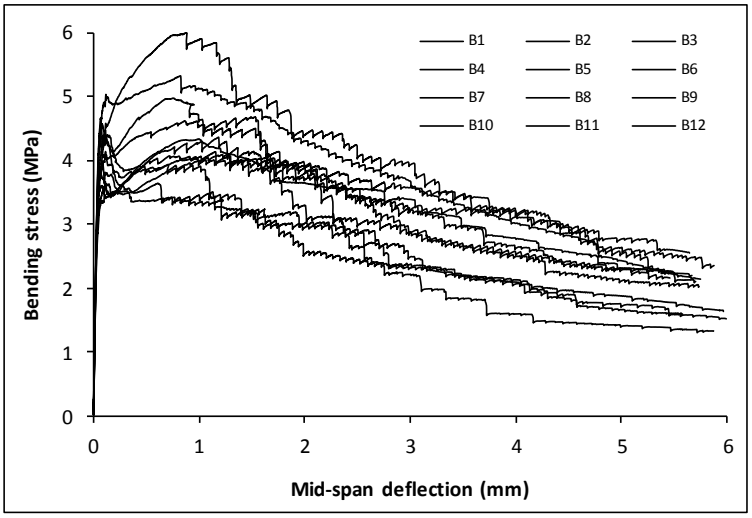

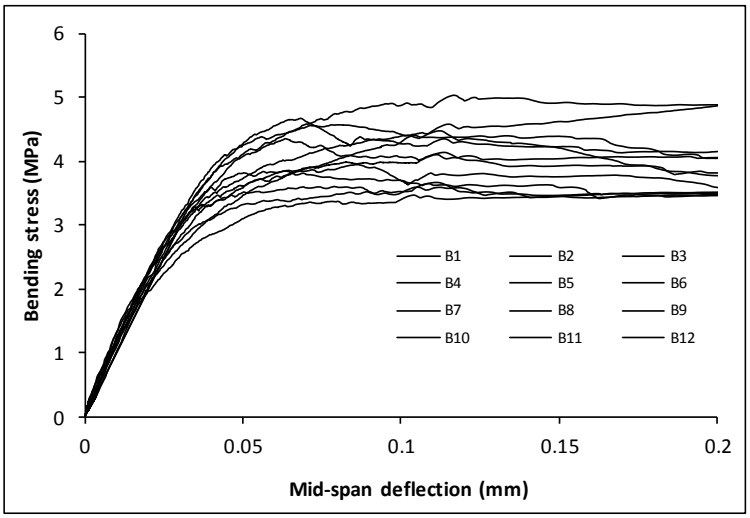

Specimen code name:		B1 (C1)	RTSC (20) + RTSF (10)		
Notched Depth dn	124.75	mm			
Depth, d	150.25	mm	Span, L	500	mm
Width, b	152.5	mm	Flexural strength	4.48	MPa

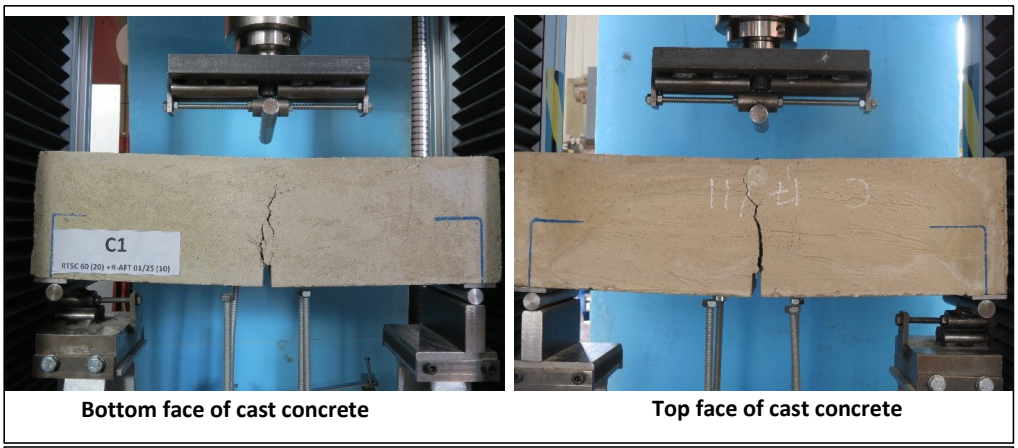

Bottom face of cast concrete

Top face of cast concrete

Crack zone of bottom face

Crack zone of top face

Stress-deformation graphs

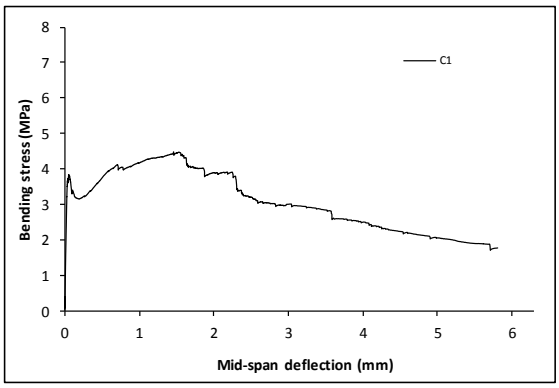

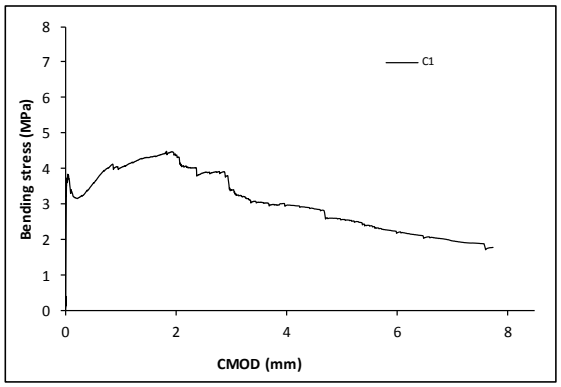

Specimen code name:		B2 (C2)	RTSC (20) + RTSF (10)		
Notched Depth dn	125.75	mm			
Depth, d	151	mm	Span, L	500	mm
Width, b	156	mm	Flexural strength	6.21	MPa

Bottom face of cast concrete

Top face of cast concrete

Crack zone of bottom face

Crack zone of top face

Stress-deformation graphs

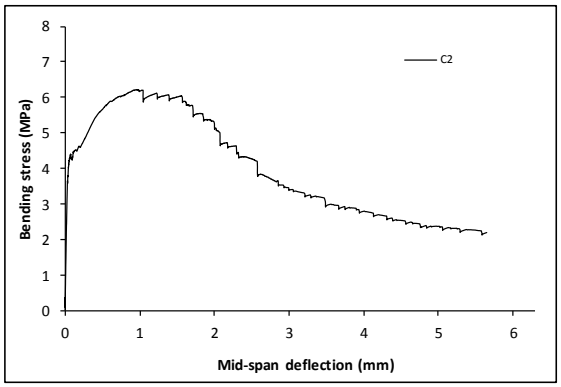

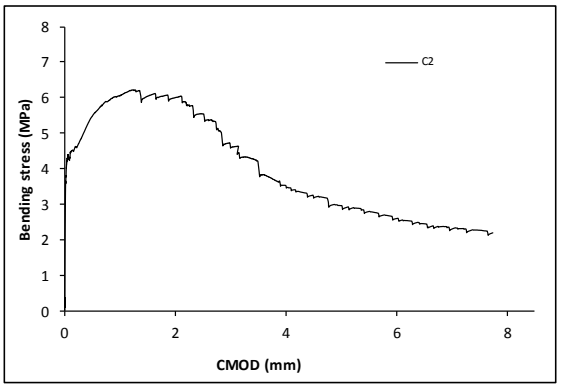

Specimen code name:		B3 (C3)	RTSC (20) + RTSF (10)		
Notched Depth dn	124.75	mm			
Depth, d	150	mm	Span, L	500	mm
Width, b	152	mm	Flexural strength	6.50	MPa

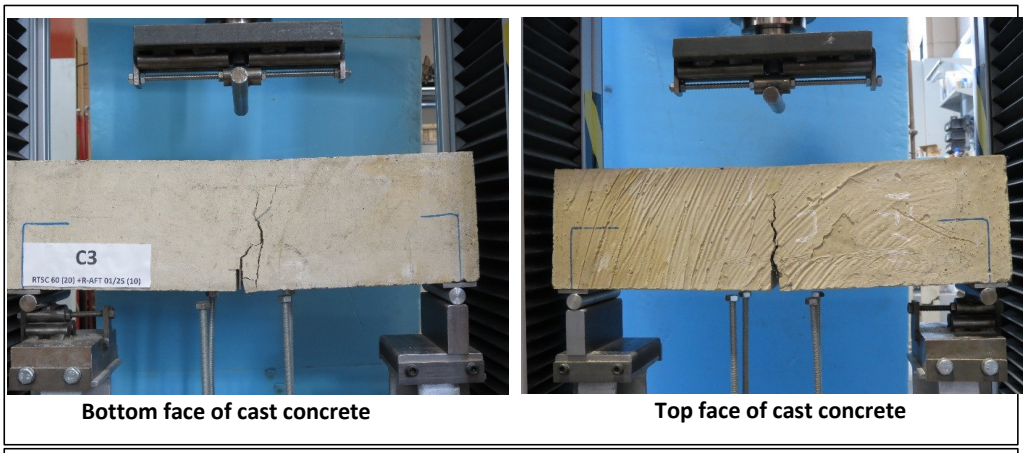

Bottom face of cast concrete

Top face of cast concrete

Crack zone of bottom face

Crack zone of top face

Stress-deformation graphs

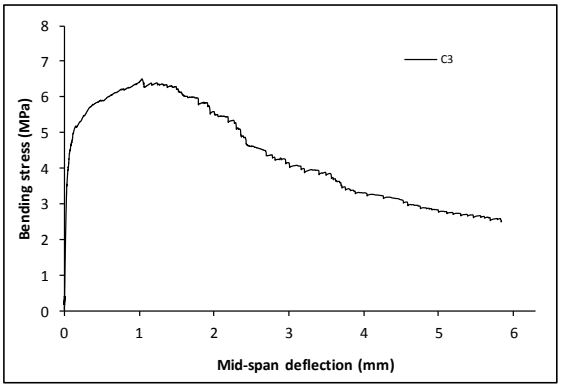

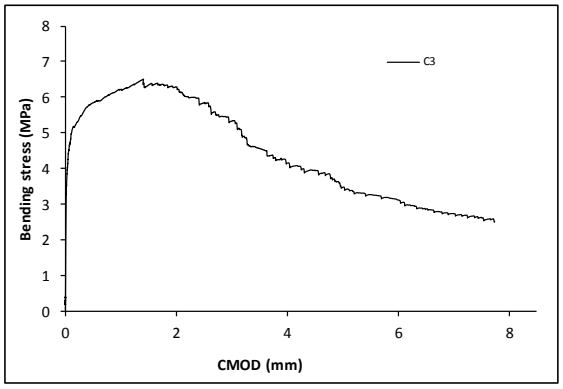

Specimen code name:		B4 (C4)	RTSC (20) + RTSF (10)		
Notched Depth dn	125	mm			
Depth, d	150.75	mm	Span, L	500	mm
Width, b	154	mm	Flexural strength	4.36	MPa

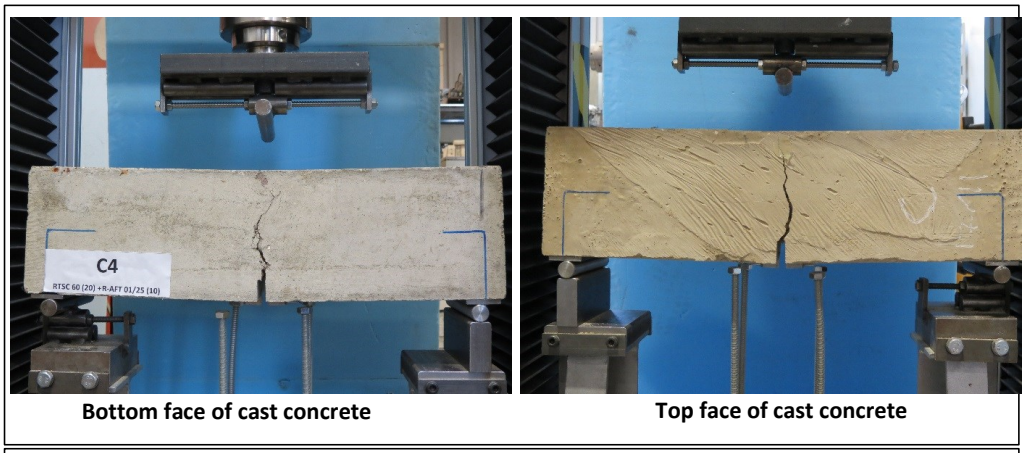

Bottom face of cast concrete | Top face of cast concrete

Crack zone of bottom face | Crack zone of top face

Stress-deformation graphs

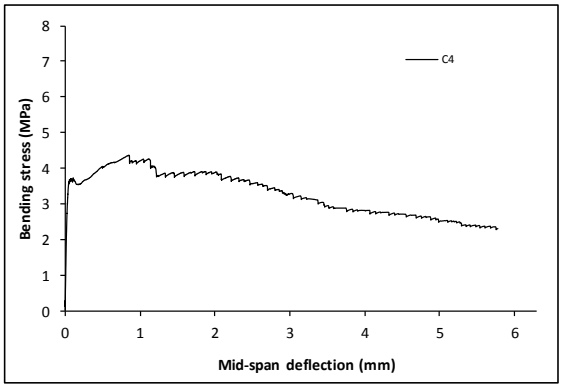

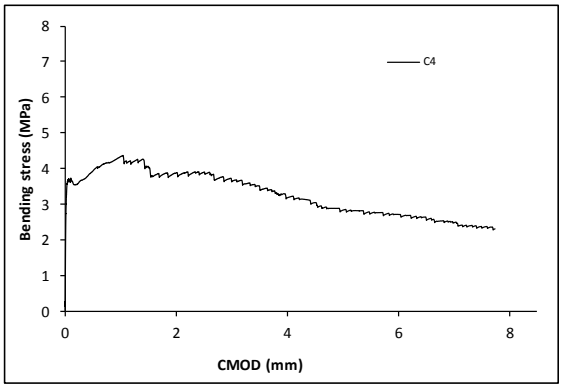

Specimen code name:		B5 (C5)	RTSC (20) + RTSF (10)		
Notched Depth dn	123.5	mm			
Depth, d	149.25	mm	Span, L	500	mm
Width, b	154.5	mm	Flexural strength	7.62	MPa

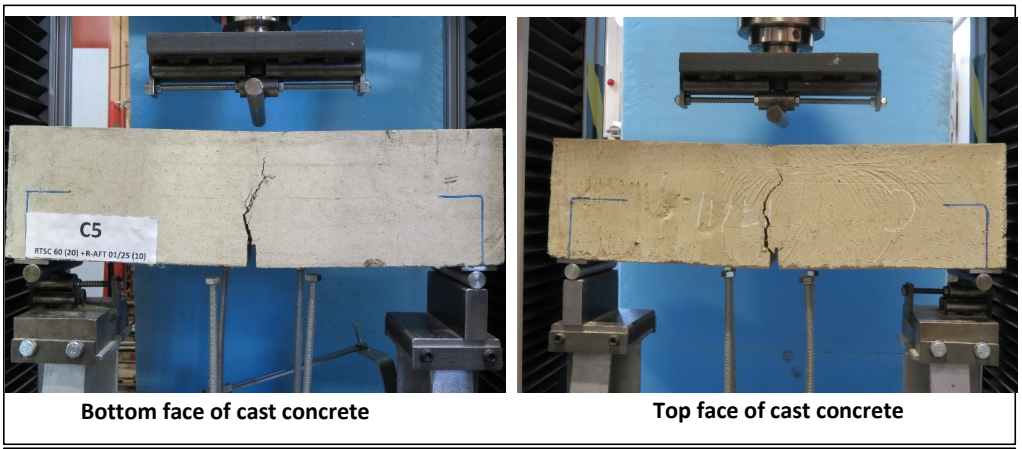

Bottom face of cast concrete | Top face of cast concrete

Crack zone of bottom face | Crack zone of top face

Stress-deformation graphs

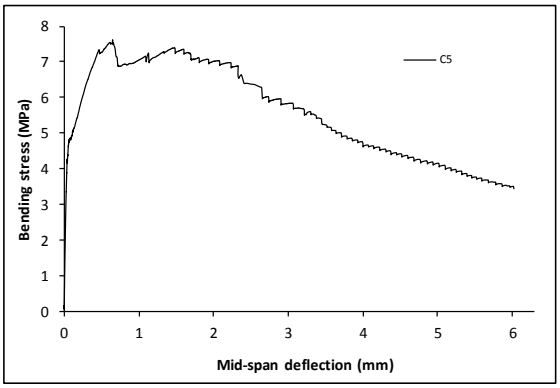

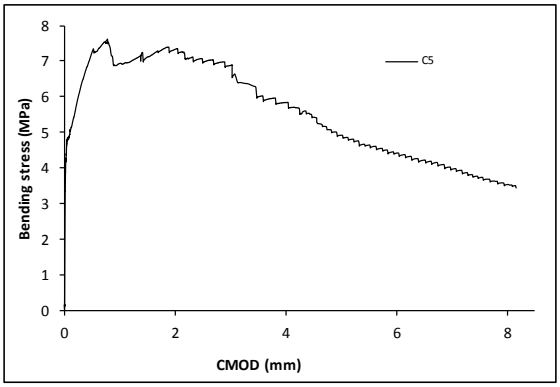

Specimen code name:		B6 (C6)	RTSC (20) + RTSF (10)		
Notched Depth dn	125	mm			
Depth, d	150.75	mm	Span, L	500	mm
Width, b	153.5	mm	Flexural strength	7.47	MPa

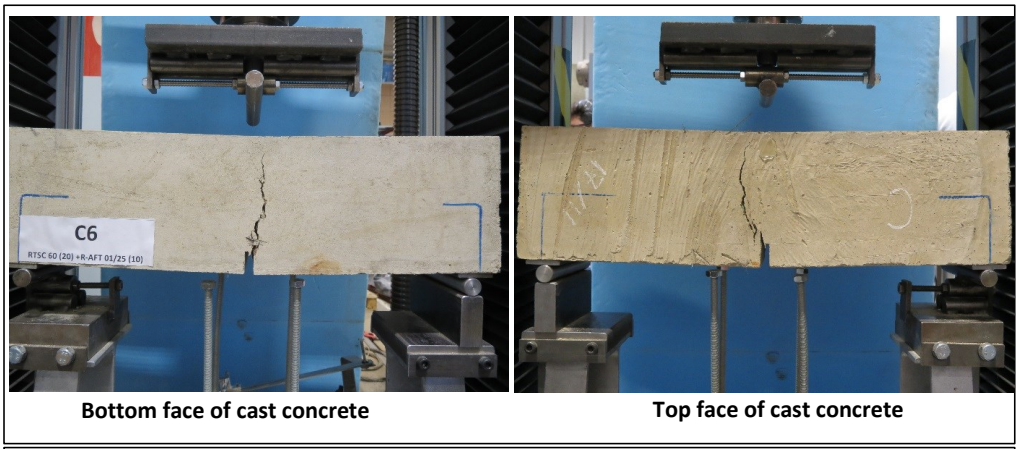

Bottom face of cast concrete | Top face of cast concrete

Crack zone of bottom face | Crack zone of top face

Stress-deformation graphs

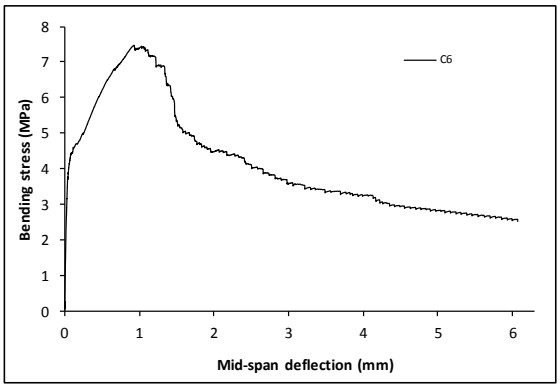

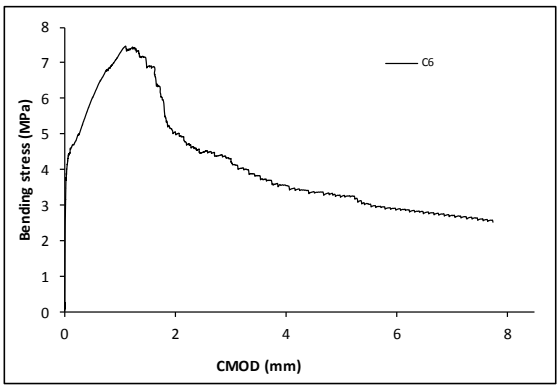

Specimen code name:		B7 (C7)	RTSC (20) + RTSF (10)		
Notched Depth dn	125.75	mm			
Depth, d	150.25	mm	Span, L	500	mm
Width, b	154.5	mm	Flexural strength	5.48	MPa

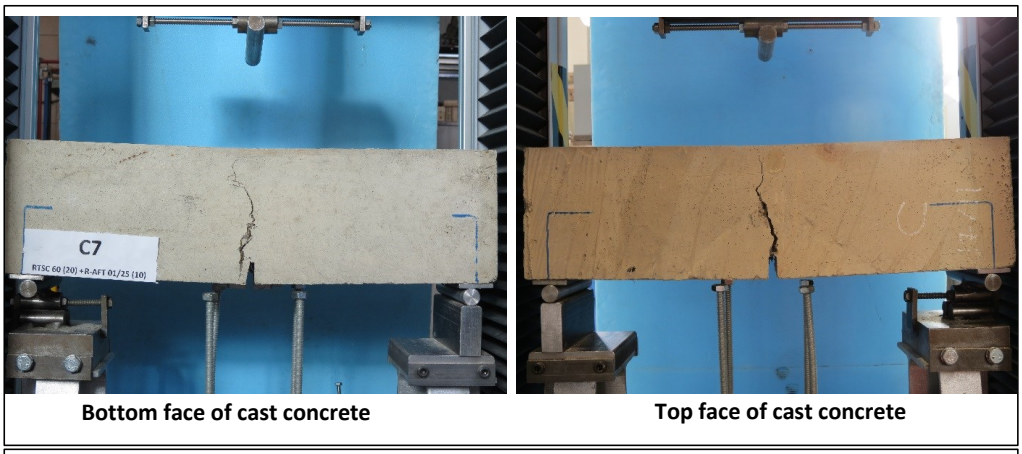

Bottom face of cast concrete | Top face of cast concrete

Crack zone of bottom face | Crack zone of top face

Stress-deformation graphs

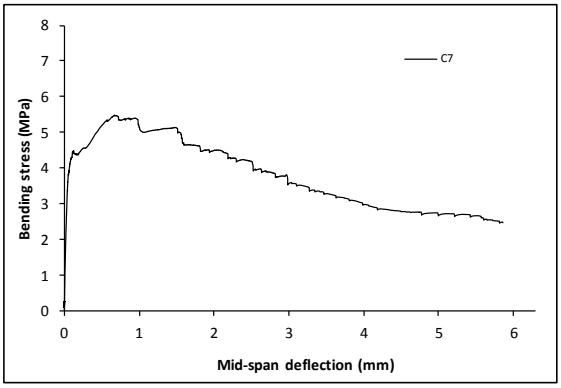

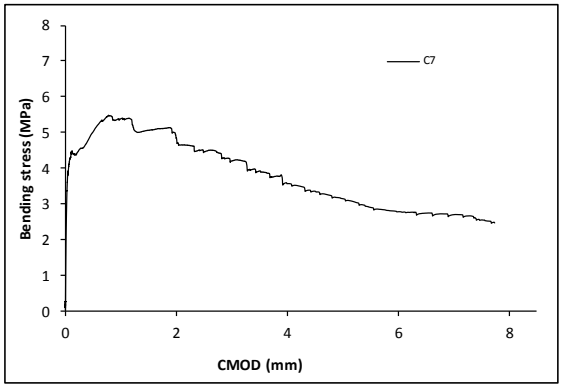

Specimen code name:		B8 (C8)	RTSC (20) + RTSF (10)		
Notched Depth dn	124.25	mm			
Depth, d	149	mm	Span, L	500	mm
Width, b	152	mm	Flexural strength	5.90	MPa

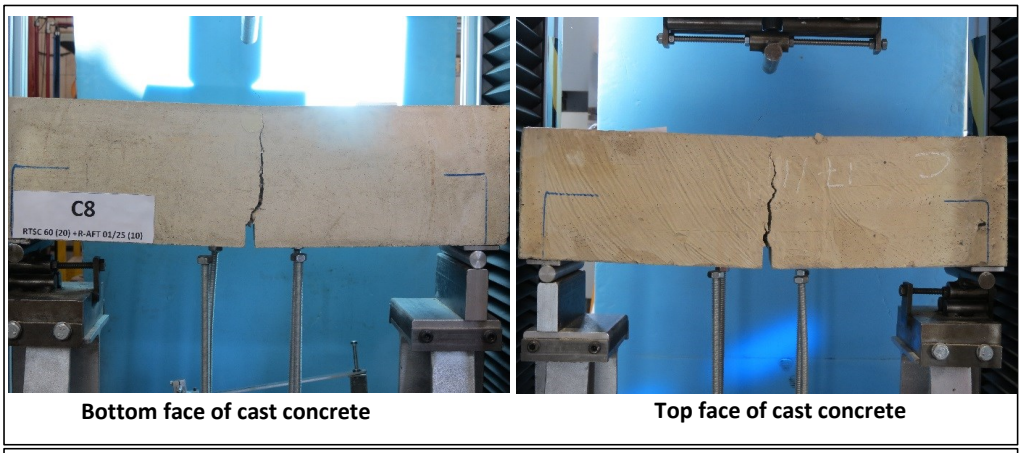

Bottom face of cast concrete | Top face of cast concrete

Crack zone of bottom face | Crack zone of top face

Stress-deformation graphs

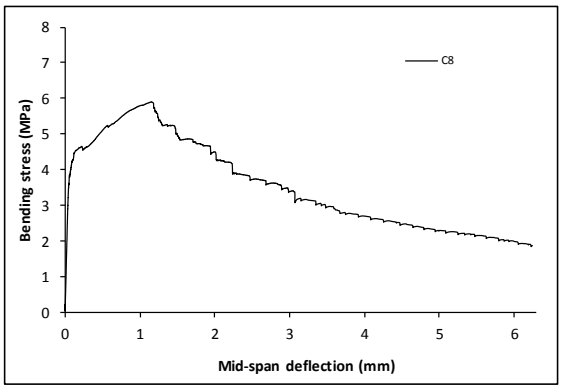

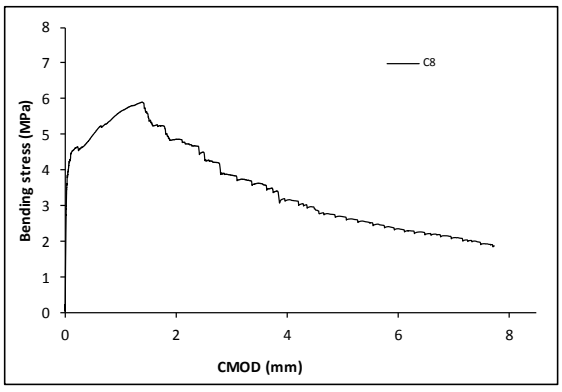

Specimen code name:		B9 (C9)	RTSC (20) + RTSF (10)		
Notched Depth dn	124	mm			
Depth, d	150	mm	Span, L	500	mm
Width, b	152	mm	Flexural strength	5.87	MPa

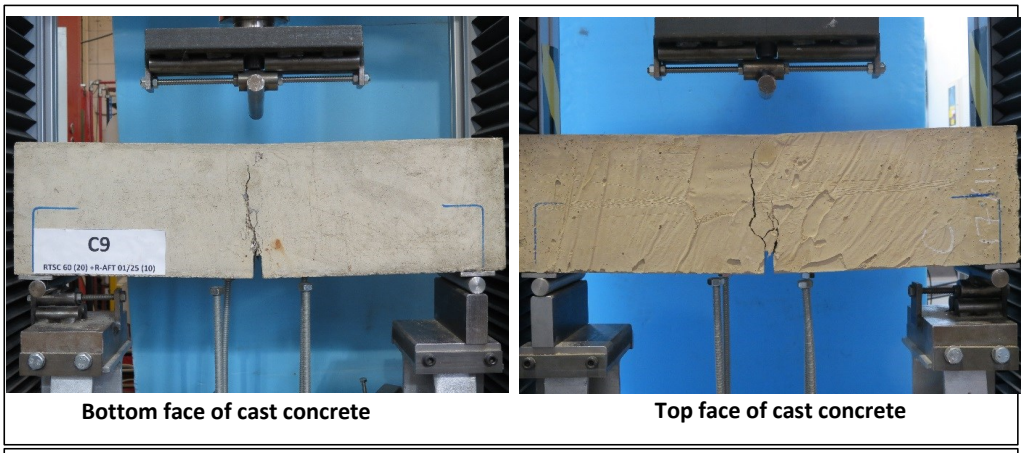

Bottom face of cast concrete | Top face of cast concrete

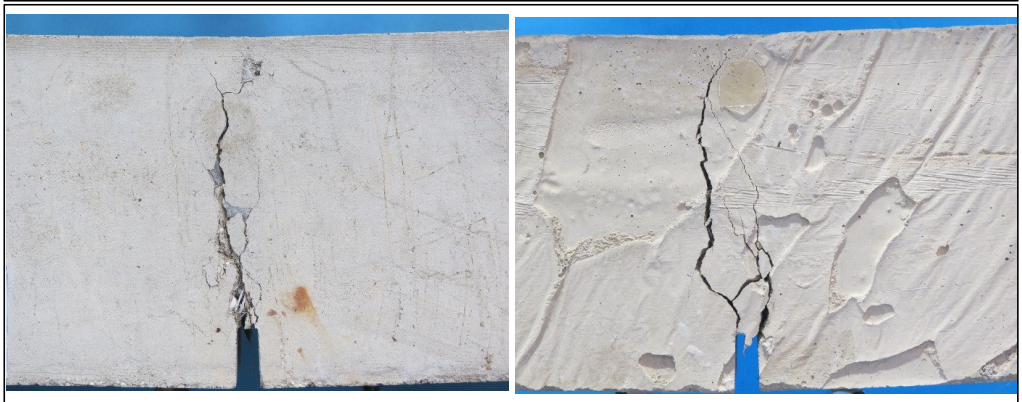

Crack zone of bottom face | Crack zone of top face

Stress-deformation graphs

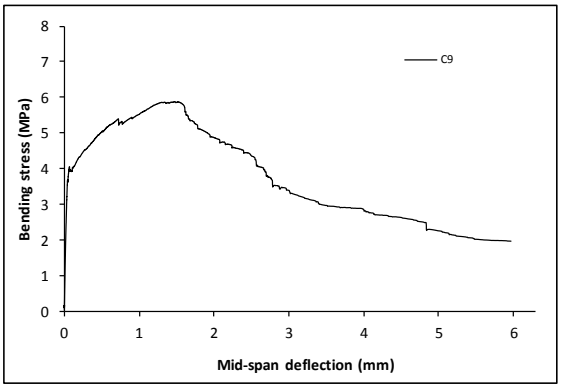

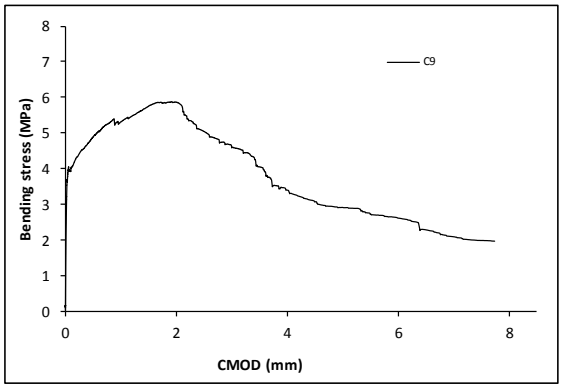

Specimen code name:		B10 (C10)	RTSC (20) + RTSF (10)		
Notched Depth dn	124.5	mm			
Depth, d	150.25	mm	Span, L	500	mm
Width, b	155.25	mm	Flexural strength	5.54	MPa

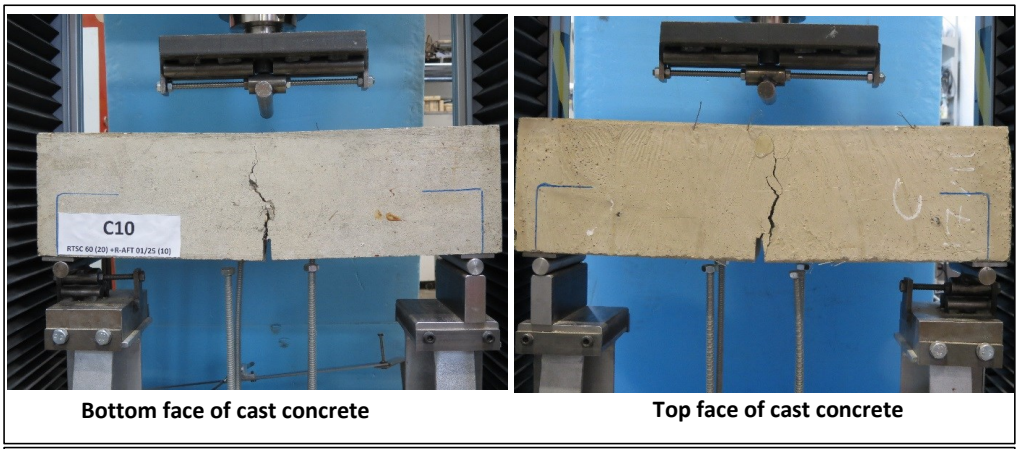

Bottom face of cast concrete | Top face of cast concrete

Crack zone of bottom face | Crack zone of top face

Stress-deformation graphs

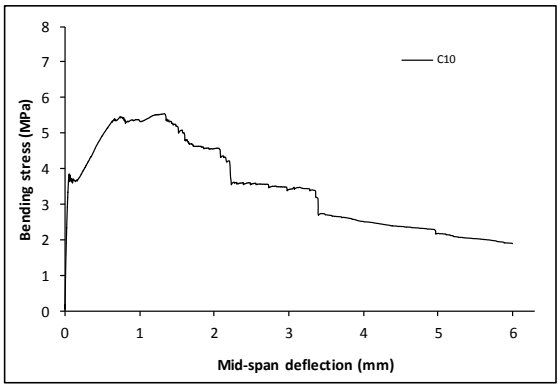

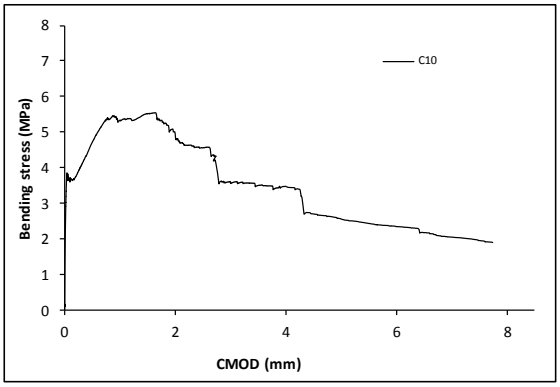

Specimen code name:		B11 (C11)	RTSC (20) + RTSF (10)		
Notched Depth dn	124.25	mm			
Depth, d	150	mm	Span, L	500	mm
Width, b	153.75	mm	Flexural strength	6.47	MPa

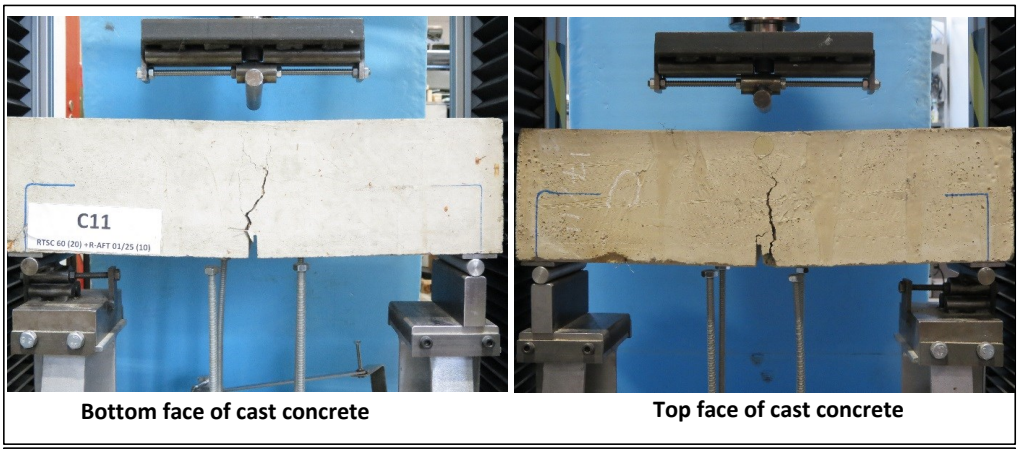

Bottom face of cast concrete | Top face of cast concrete

Crack zone of bottom face | Crack zone of top face

Stress-deformation graphs

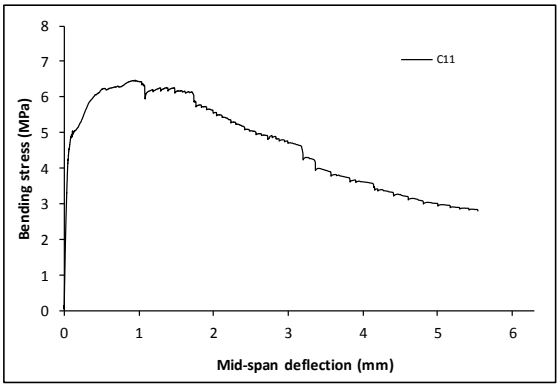

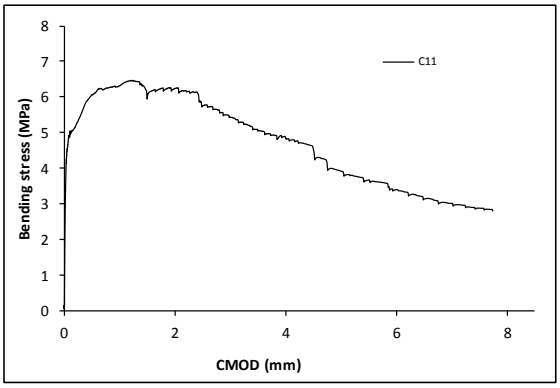

Specimen code name:		B12 (C12)	RTSC (20) + RTSF (10)		
Notched Depth dn	124.25	mm			
Depth, d	150	mm	Span, L	500	mm
Width, b	155	mm	Flexural strength	7.23	MPa

Bottom face of cast concrete

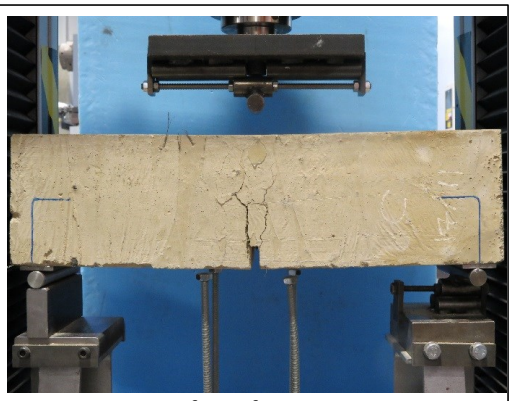

Top face of cast concrete

Crack zone of bottom face

Crack zone of top face

Stress-deformation graphs

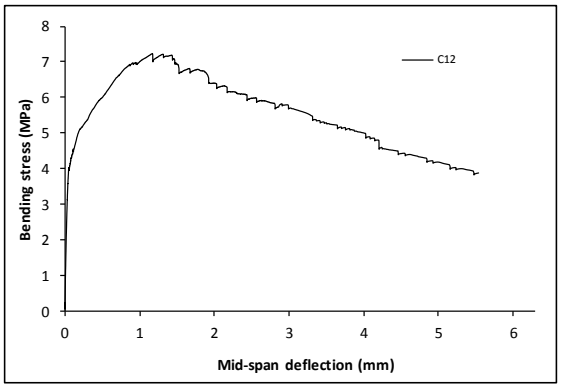

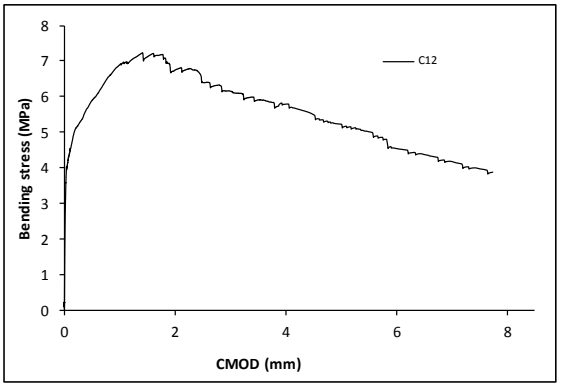

Mix:	**B (C)**	RTSC (20) + RTSF (10)	
Notched Depth dn	mm		
Depth, d	mm	Span, L	mm
Width, b	mm	Flexural strength	MPa

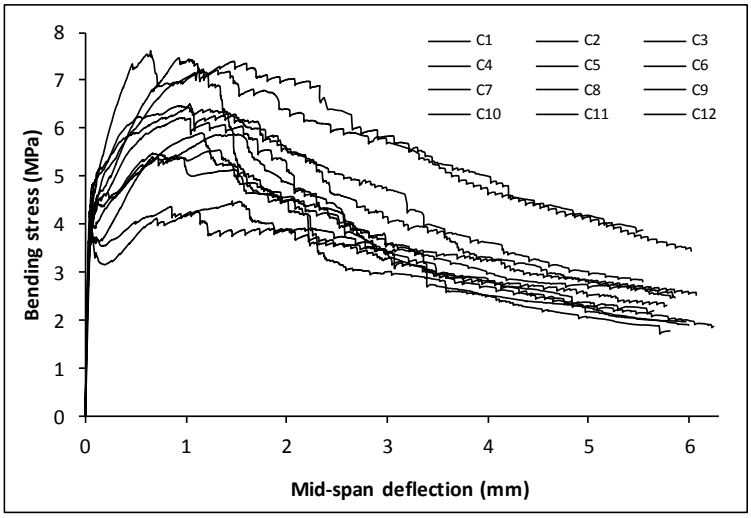

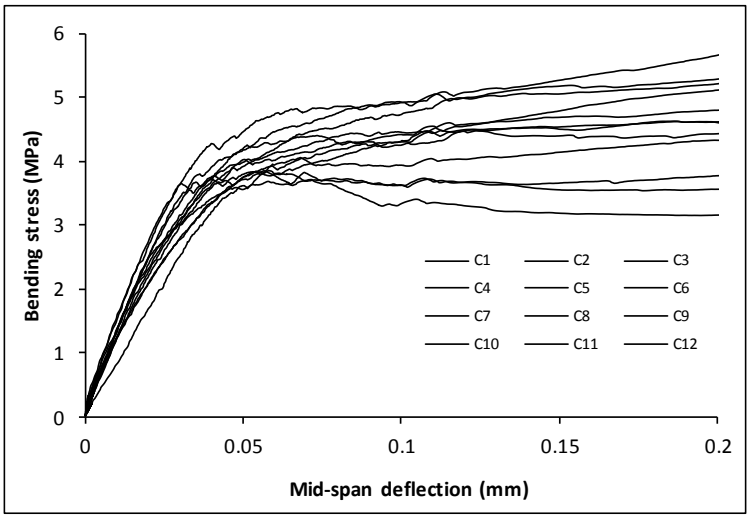

Specimen code name:		C1 (A1)	RTSC (30)		
Notched Depth dn	125.5	mm			
Depth, d	151	mm	Span, L	500	mm
Width, b	156	mm	Flexural strength	7.77	MPa

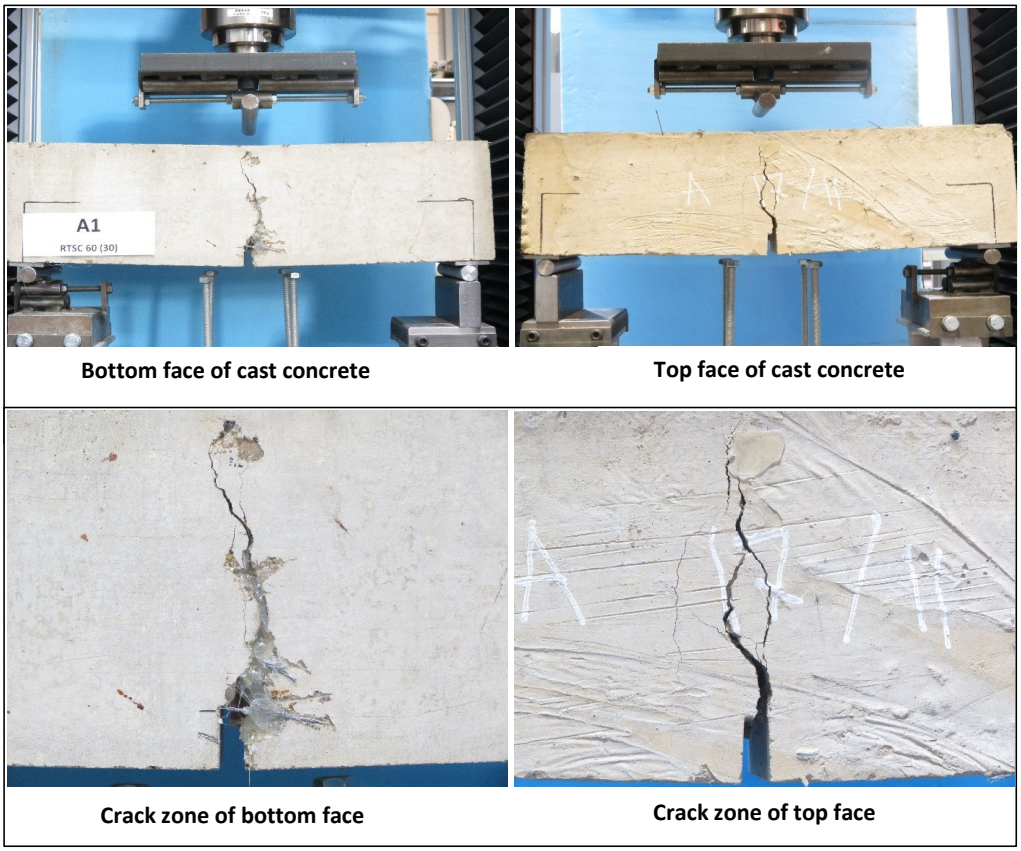

Bottom face of cast concrete | Top face of cast concrete

Crack zone of bottom face | Crack zone of top face

Stress-deformation graphs

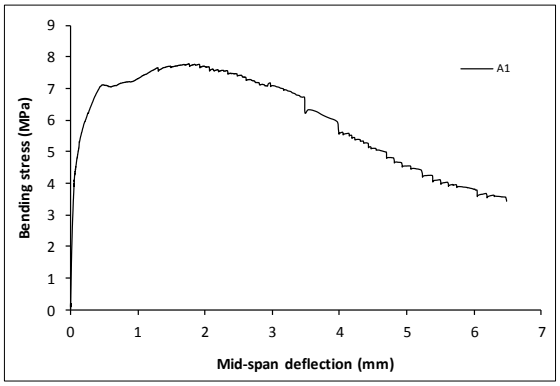

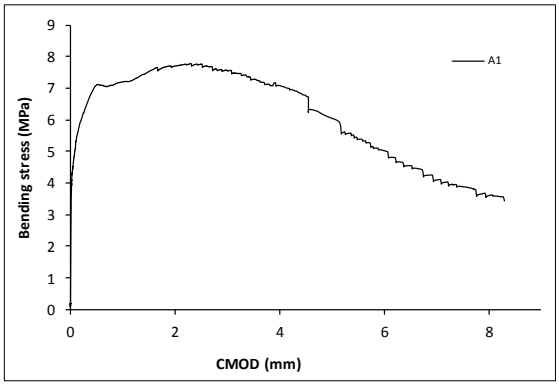

Specimen code name:		C2 (A2)	RTSC (30)		
Notched Depth dn	124	mm			
Depth, d	151	mm	Span, L	500	mm
Width, b	156.5	mm	Flexural strength	6.27	MPa

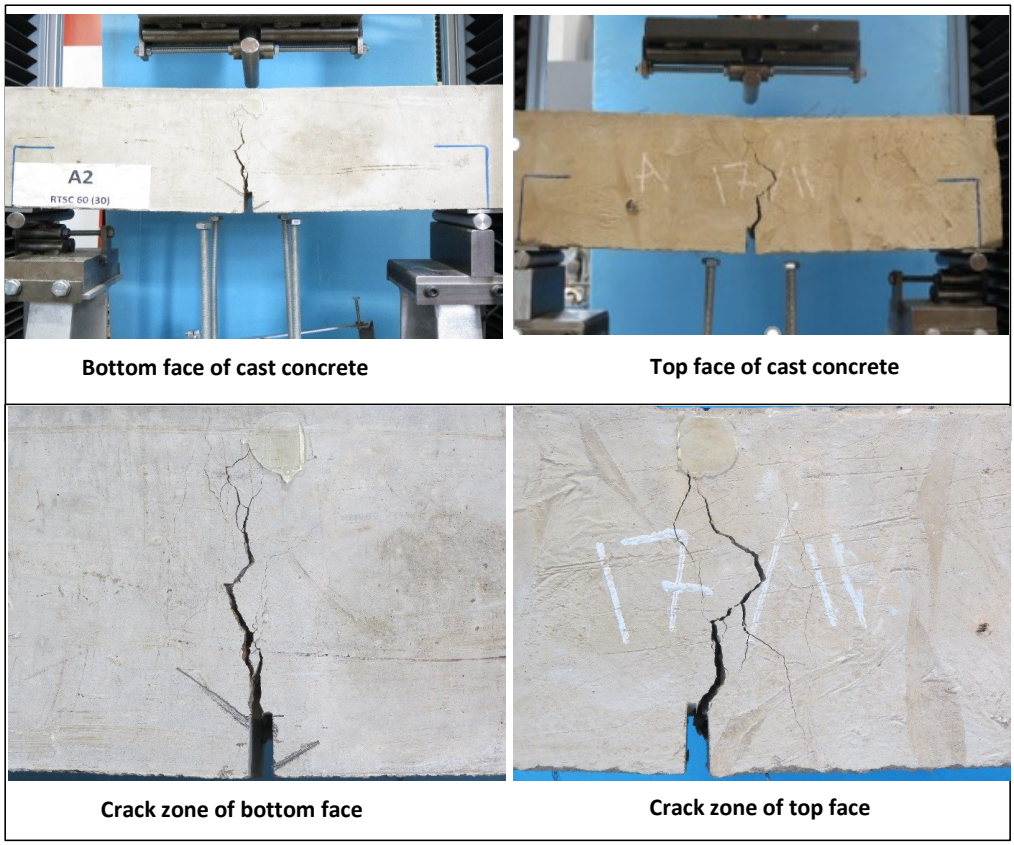

Bottom face of cast concrete | Top face of cast concrete

Crack zone of bottom face | Crack zone of top face

Stress-deformation graphs

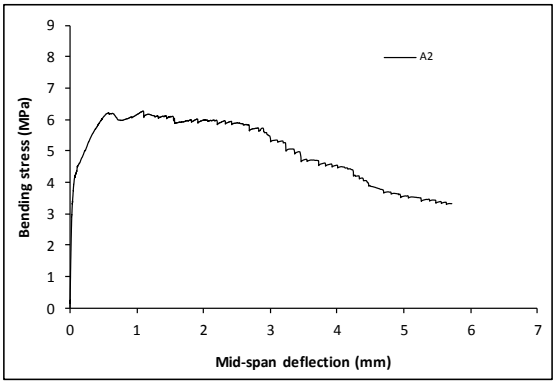

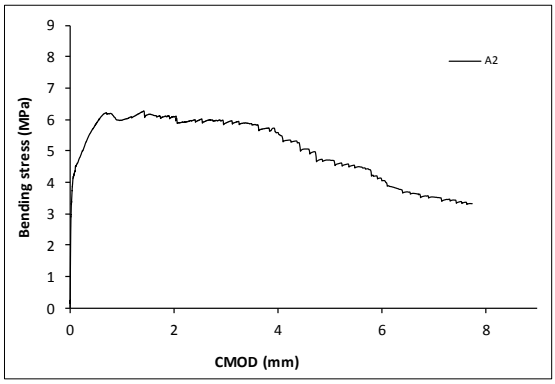

Specimen code name:		C3 (A3)	RTSC (30)		
Notched Depth dn	125.5	mm			
Depth, d	150	mm	Span, L	500	mm
Width, b	156.5	mm	Flexural strength	8.64	MPa

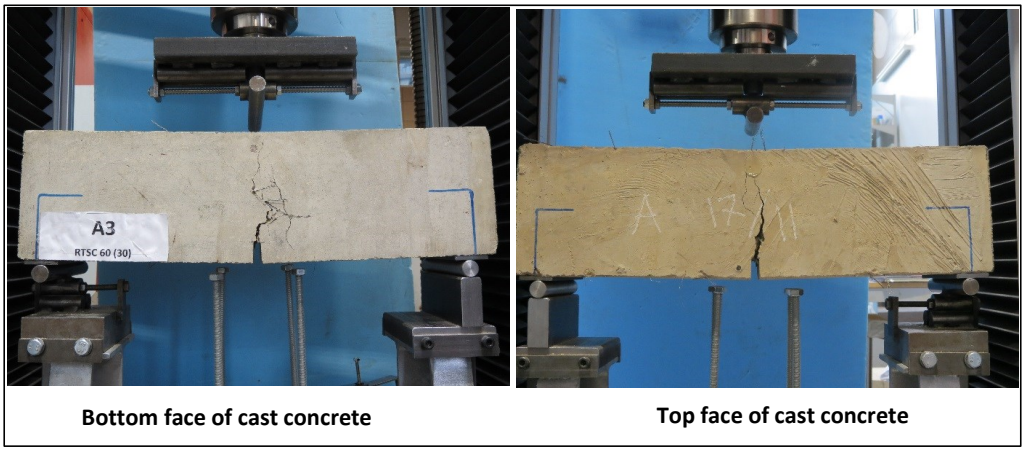

Bottom face of cast concrete | Top face of cast concrete

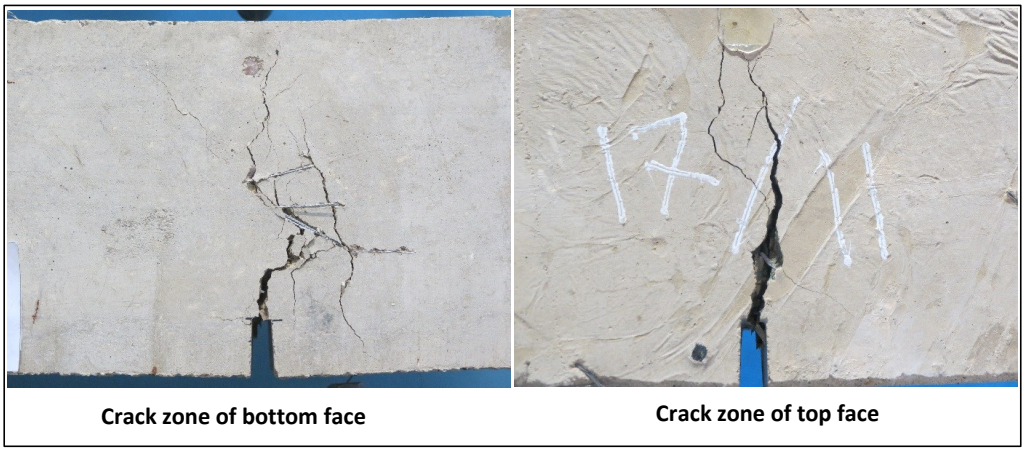

Crack zone of bottom face | Crack zone of top face

Stress-deformation graphs

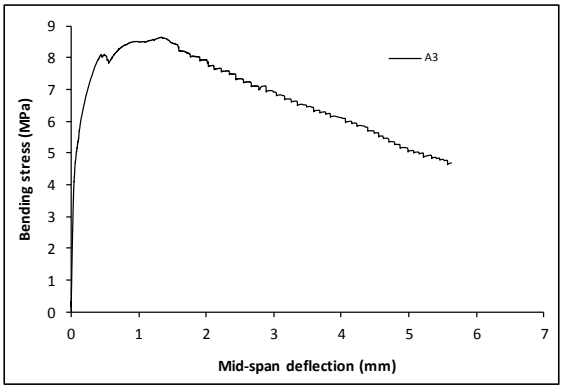

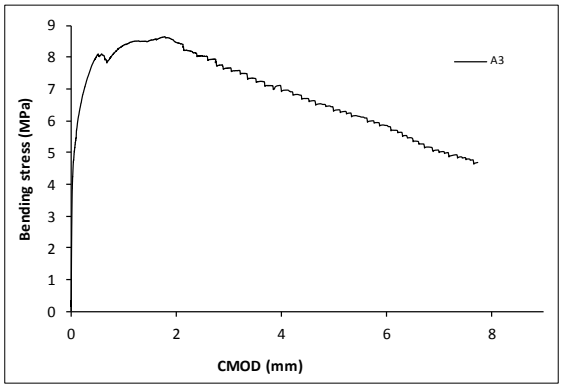

Specimen code name:		C4 (A4)	RTSC (30)		
Notched Depth dn	125.25	mm			
Depth, d	150	mm	Span, L	500	mm
Width, b	157	mm	Flexural strength	7.55	MPa

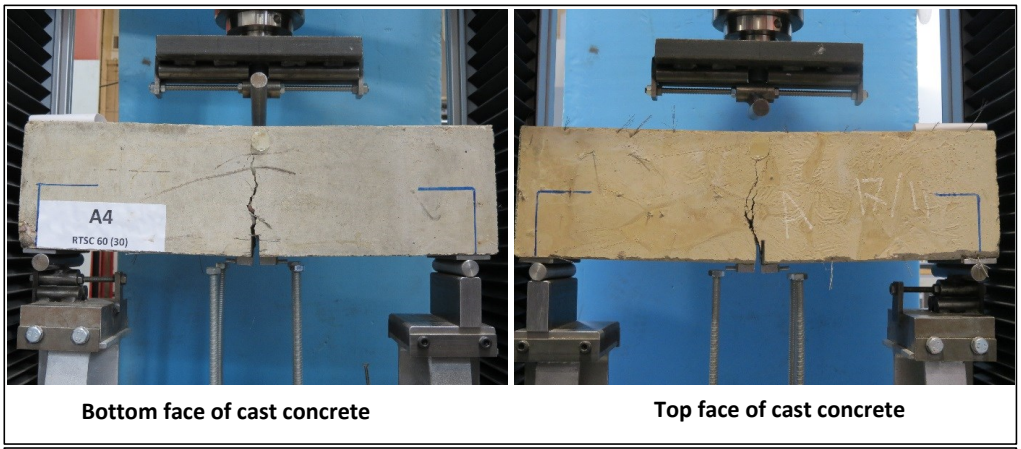

Bottom face of cast concrete | Top face of cast concrete

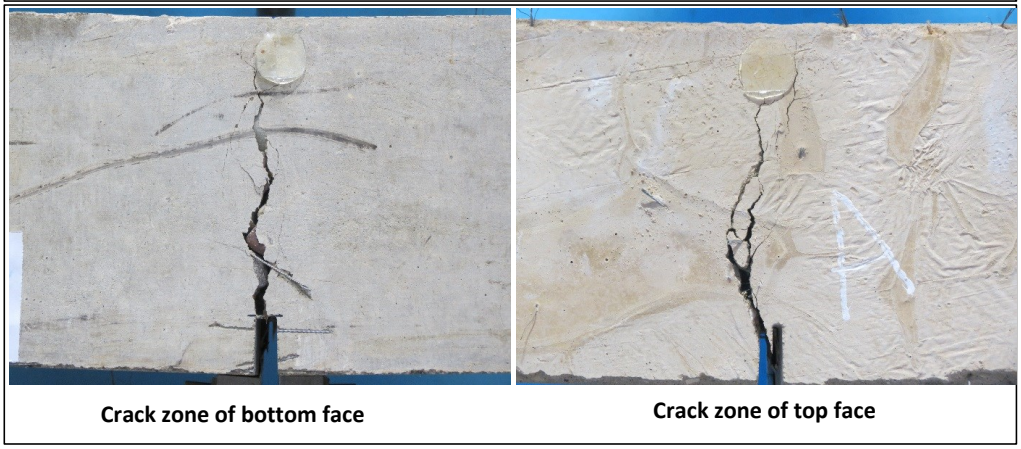

Crack zone of bottom face | Crack zone of top face

Stress-deformation graphs

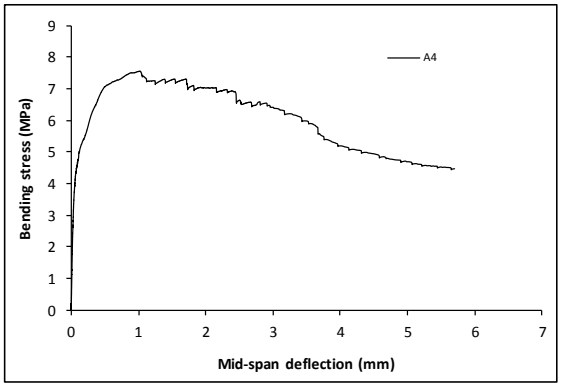

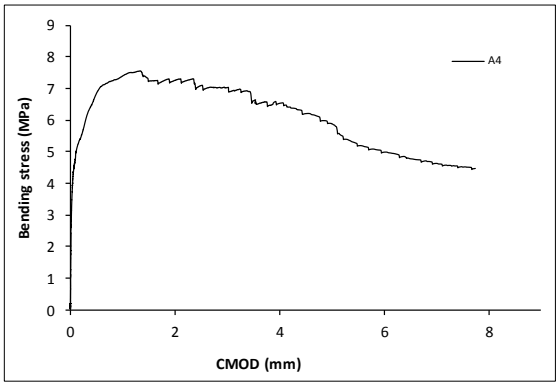

Specimen code name:		C5 (A5)	RTSC (30)		
Notched Depth dn	124	mm			
Depth, d	150	mm	Span, L	500	mm
Width, b	156.75	mm	Flexural strength	8.00	MPa

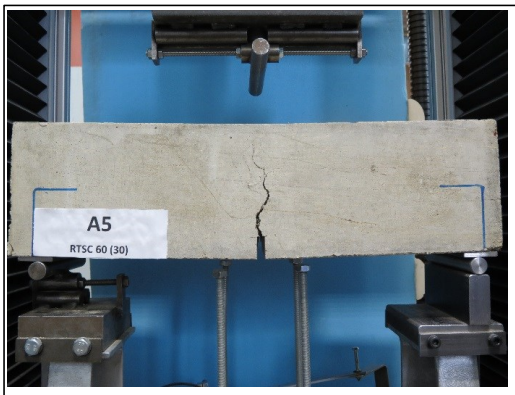

Bottom face of cast concrete

Top face of cast concrete

Crack zone of bottom face

Crack zone of top face

Stress-deformation graphs

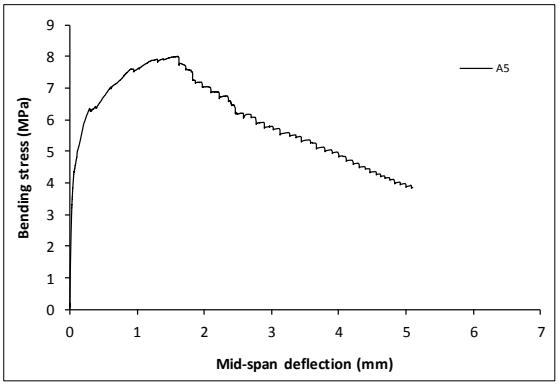

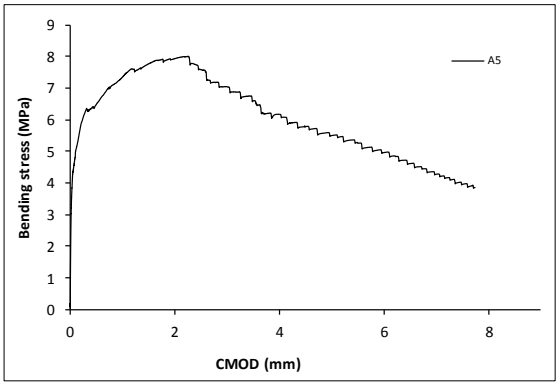

Specimen code name:		C6 (A6)	RTSC (30)		
Notched Depth dn	125.75	mm			
Depth, d	151	mm	Span, L	500	mm
Width, b	150	mm	Flexural strength	7.33	MPa

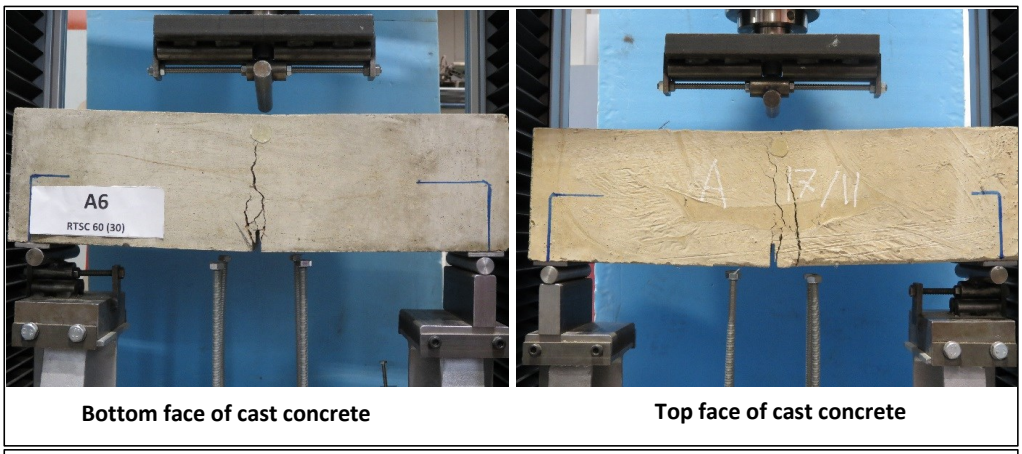

Bottom face of cast concrete | Top face of cast concrete

Crack zone of bottom face | Crack zone of top face

Stress-deformation graphs

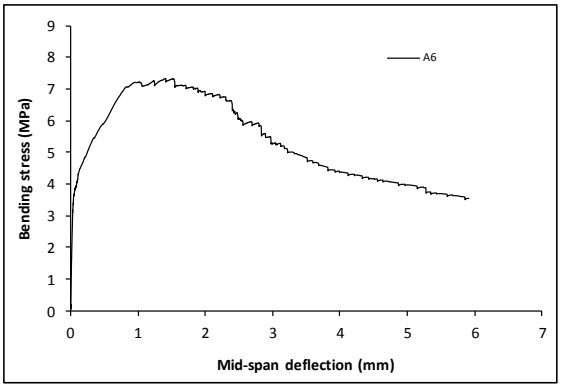

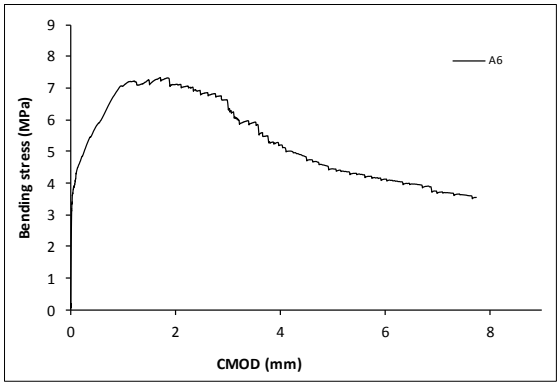

Specimen code name:		C7 (A7)	RTSC (30)		
Notched Depth dn	125	mm			
Depth, d	150.5	mm	Span, L	500	mm
Width, b	152	mm	Flexural strength	8.13	MPa

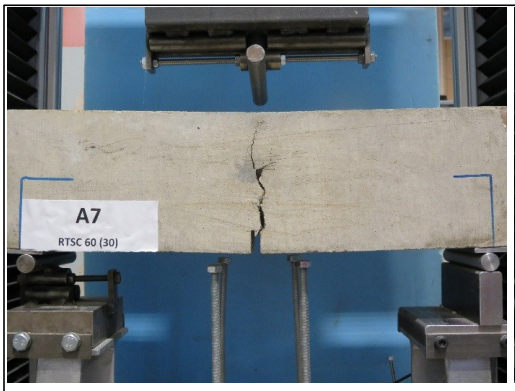

Bottom face of cast concrete

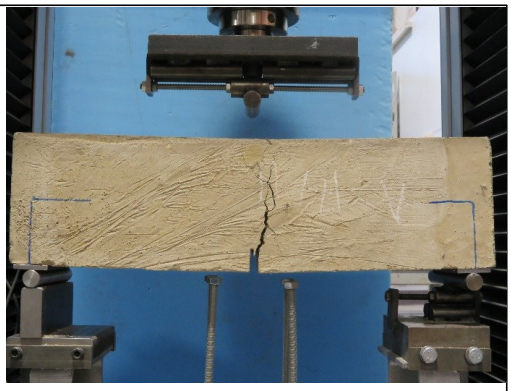

Top face of cast concrete

Crack zone of bottom face

Crack zone of top face

Stress-deformation graphs

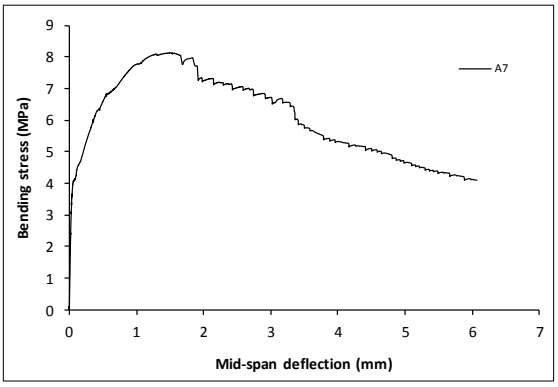

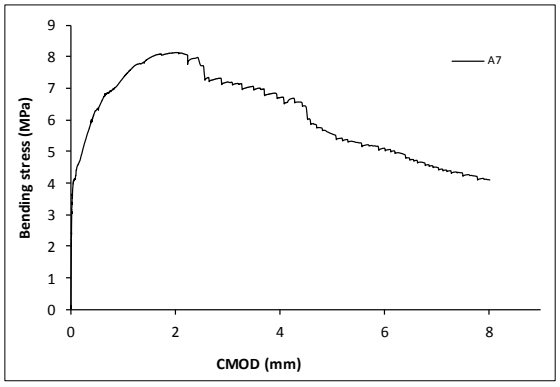

Specimen code name:		C8 (A8)	RTSC (30)		
Notched Depth dn	125	mm			
Depth, d	151.5	mm	Span, L	500	mm
Width, b	153	mm	Flexural strength	7.62	MPa

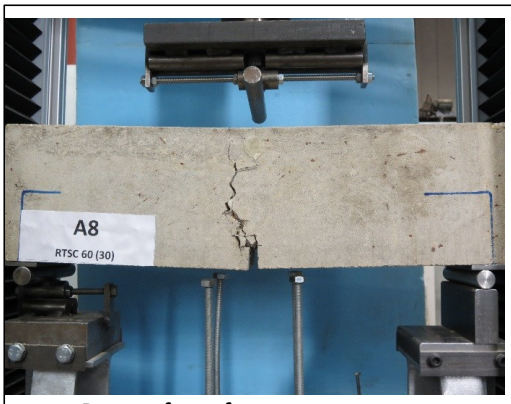

Bottom face of cast concrete

Top face of cast concrete

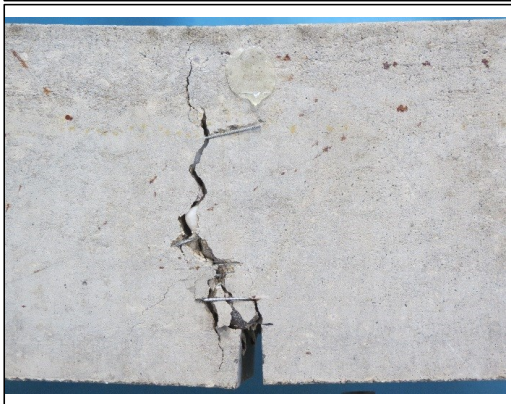

Crack zone of bottom face

Crack zone of top face

Stress-deformation graphs

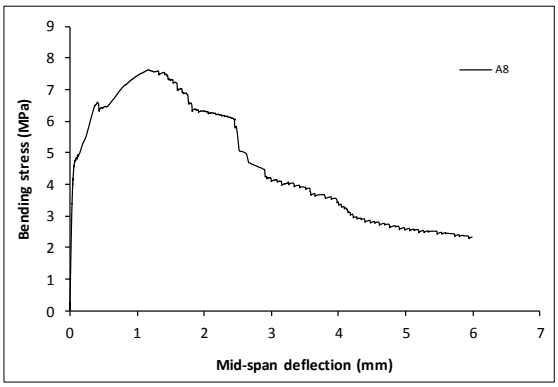

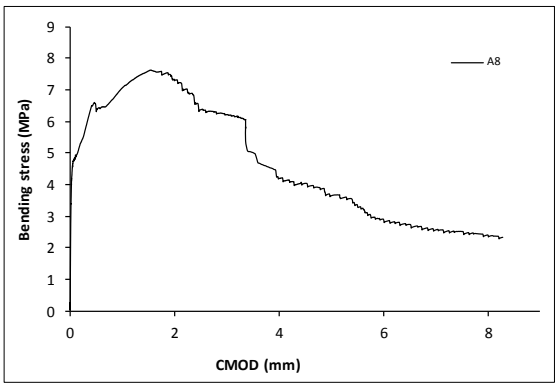

Specimen code name:		C9 (A9)	RTSC (30)		
Notched Depth dn	124.5	mm			
Depth, d	150	mm	Span, L	500	mm
Width, b	156	mm	Flexural strength	8.06	MPa

Bottom face of cast concrete

Top face of cast concrete

Crack zone of bottom face

Crack zone of top face

Stress-deformation graphs

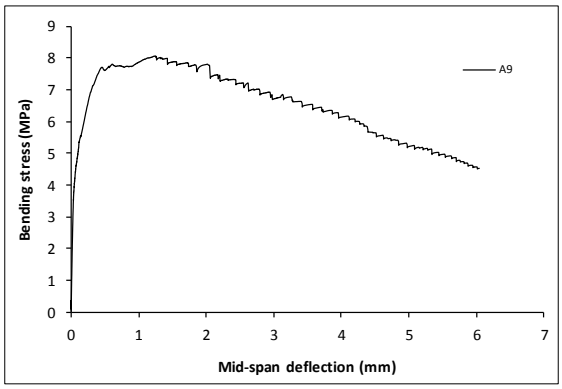

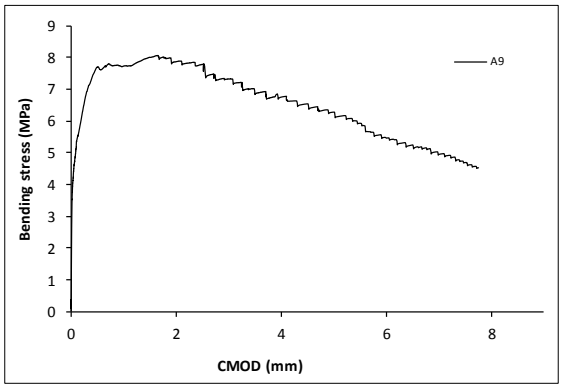

Specimen code name:		C10 (A10)	RTSC (30)		
Notched Depth dn	123.75	mm			
Depth, d	151	mm	Span, L	500	mm
Width, b	155.5	mm	Flexural strength	7.47	MPa

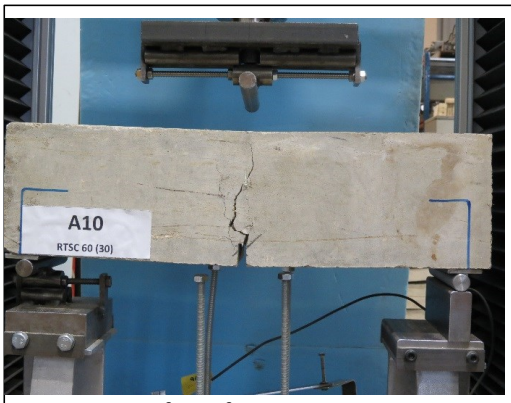

Bottom face of cast concrete

Top face of cast concrete

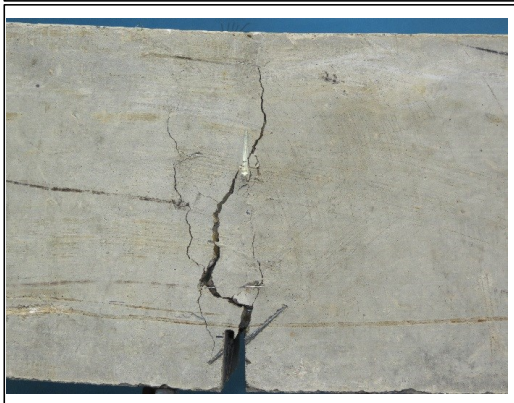

Crack zone of bottom face

Crack zone of top face

Stress-deformation graphs

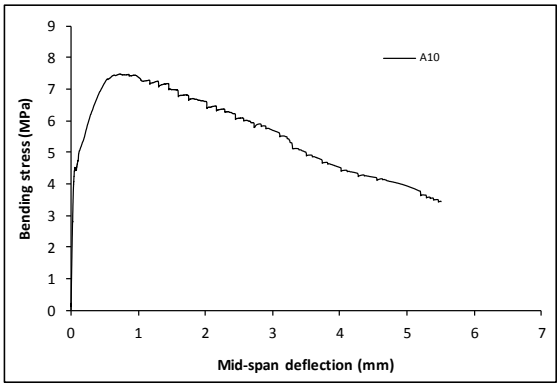

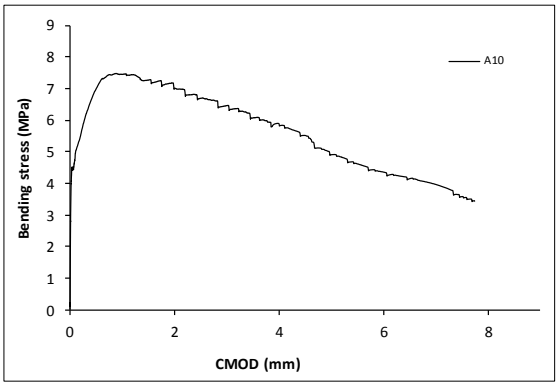

Specimen code name:		C11 (A11)	RTSC (30)		
Notched Depth dn	124.75	mm			
Depth, d	150.75	mm	Span, L	500	mm
Width, b	153.75	mm	Flexural strength	7.93	MPa

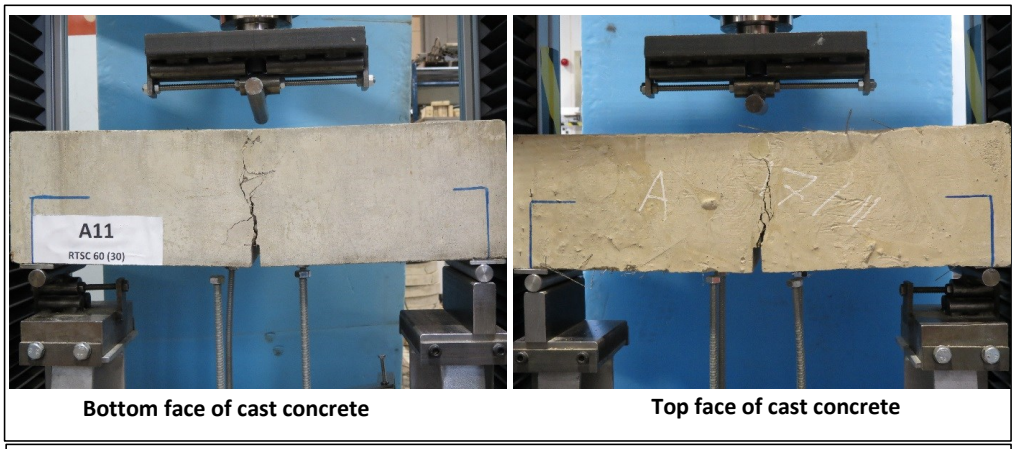

Bottom face of cast concrete

Top face of cast concrete

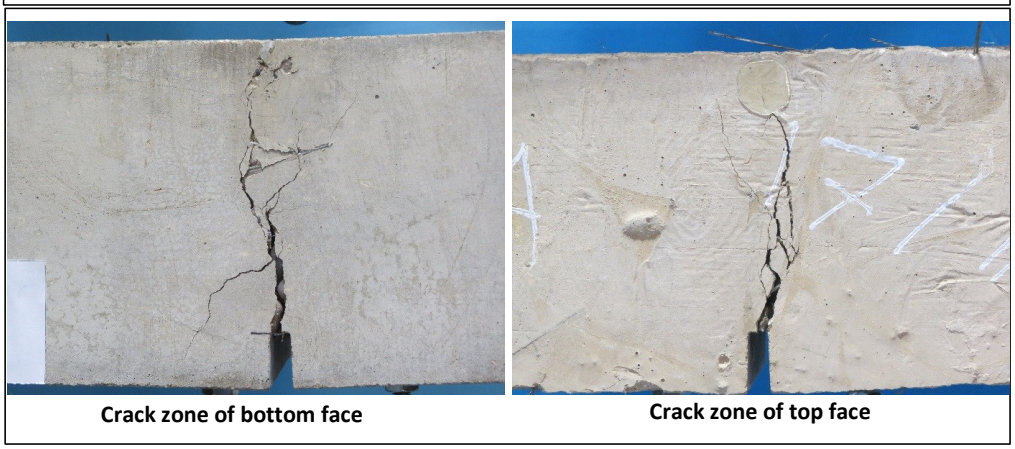

Crack zone of bottom face

Crack zone of top face

Stress-deformation graphs

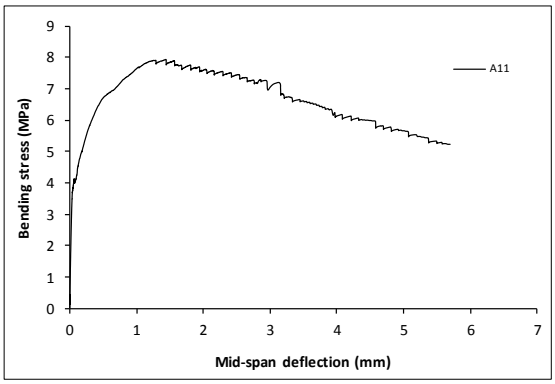

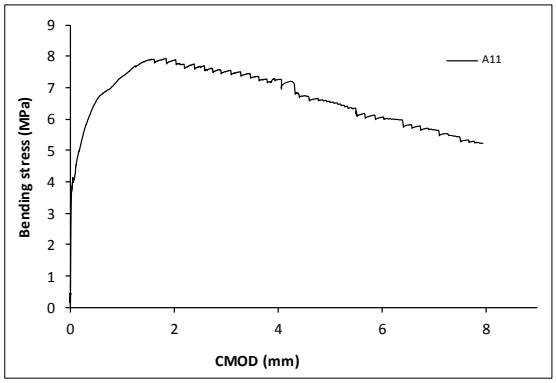

Specimen code name:		C12 (A12)	RTSC (30)		
Notched Depth dn	124.25	mm			
Depth, d	150	mm	Span, L	500	mm
Width, b	155	mm	Flexural strength	6.78	MPa

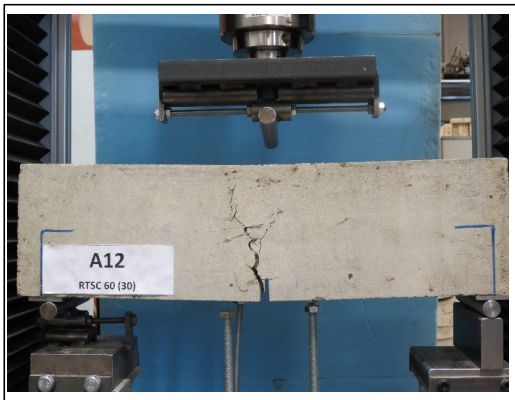

Bottom face of cast concrete

Top face of cast concrete

Crack zone of bottom face

Crack zone of top face

Stress-deformation graphs

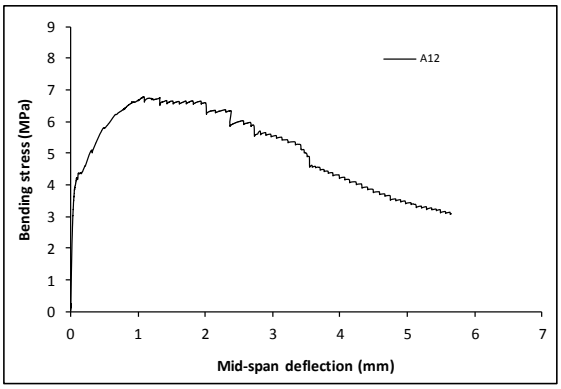

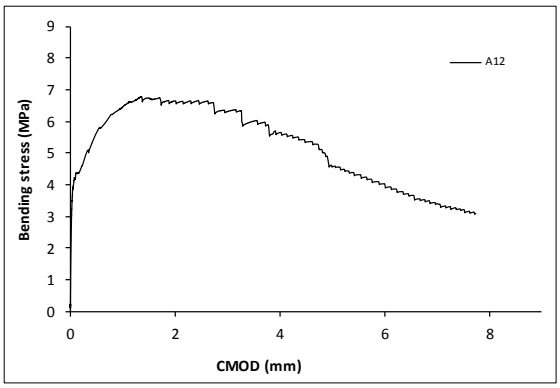

Mix:	**C (A)**	RTSC (30)	
Notched Depth dn	mm		
Depth, d	mm	Span, L	mm
Width, b	mm	Flexural strength	MPa

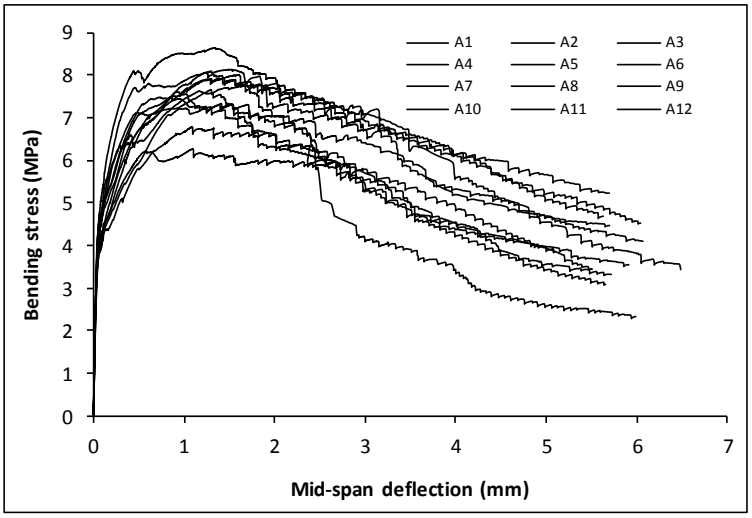

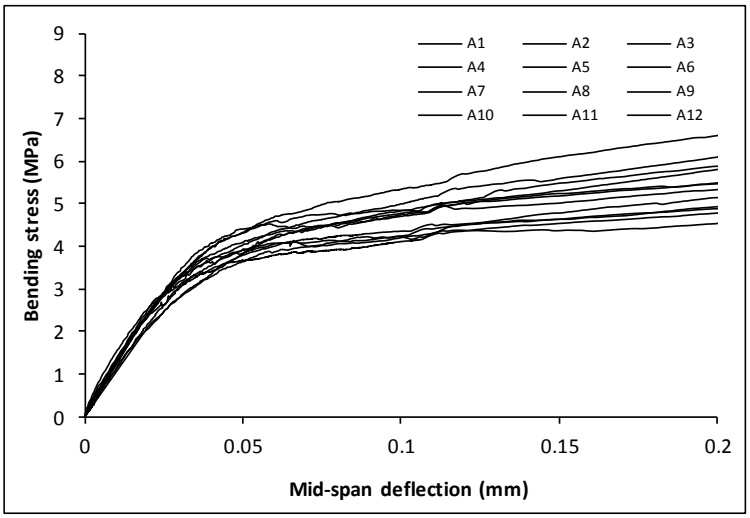

Specimen code name:		D1	RTSF (30)		
Notched Depth dn	124.5	mm			
Depth, d	150.25	mm	Span, L	500	mm
Width, b	154.25	mm	Flexural strength	3.44	MPa

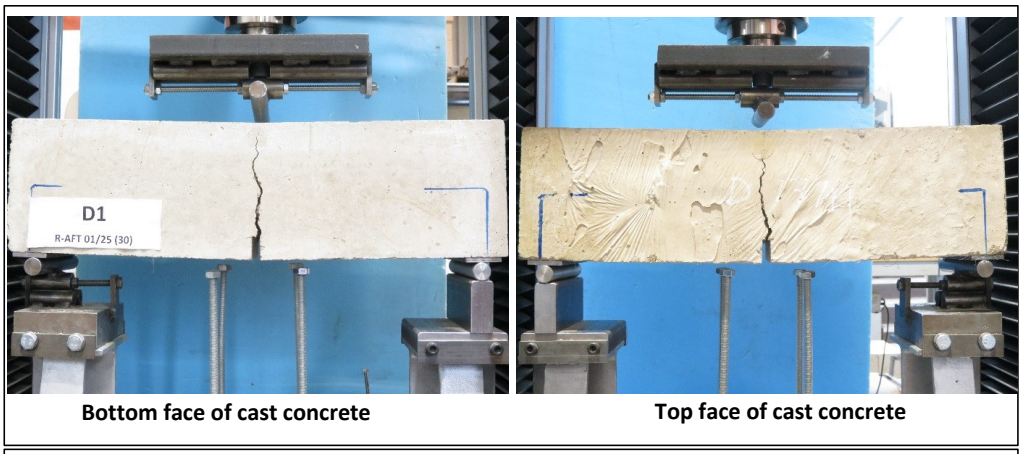

Bottom face of cast concrete | Top face of cast concrete

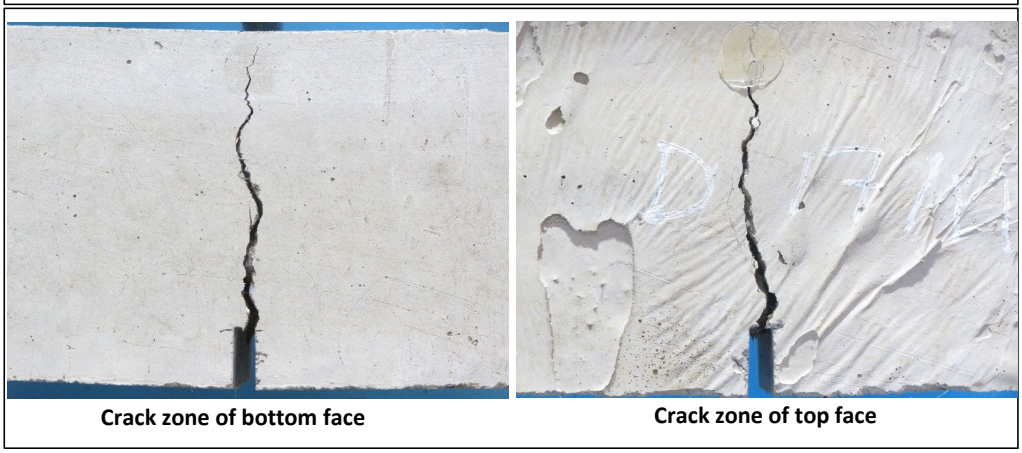

Crack zone of bottom face | Crack zone of top face

Stress-deformation graphs

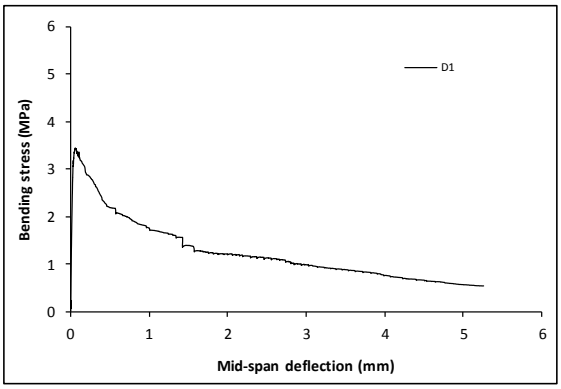

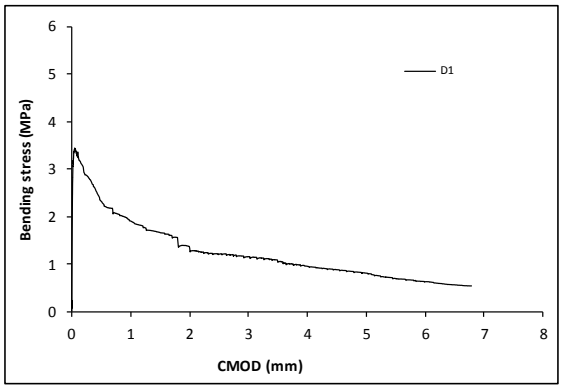

Specimen code name:		D2	RTSF (30)		
Notched Depth dn	123.5	mm			
Depth, d	150	mm	Span, L	500	mm
Width, b	157	mm	Flexural strength	3.40	MPa

Bottom face of cast concrete

Top face of cast concrete

Crack zone of bottom face

Crack zone of top face

Stress-deformation graphs

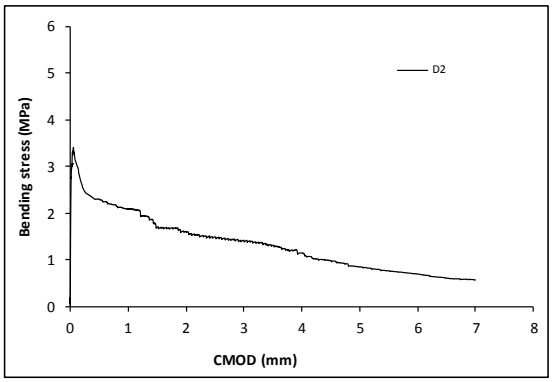

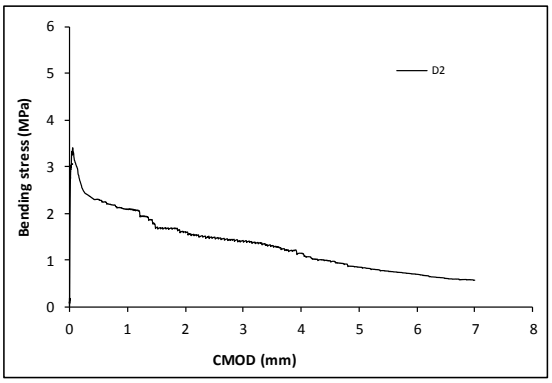

Specimen code name:		D3	RTSF (30)		
Notched Depth dn	125	mm			
Depth, d	151	mm	Span, L	500	mm
Width, b	154.75	mm	Flexural strength	3.99	MPa

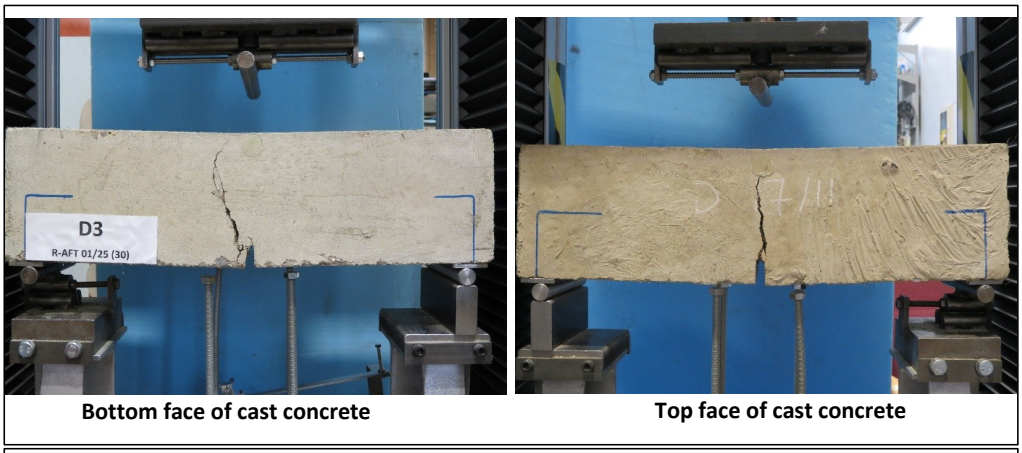

Bottom face of cast concrete | Top face of cast concrete

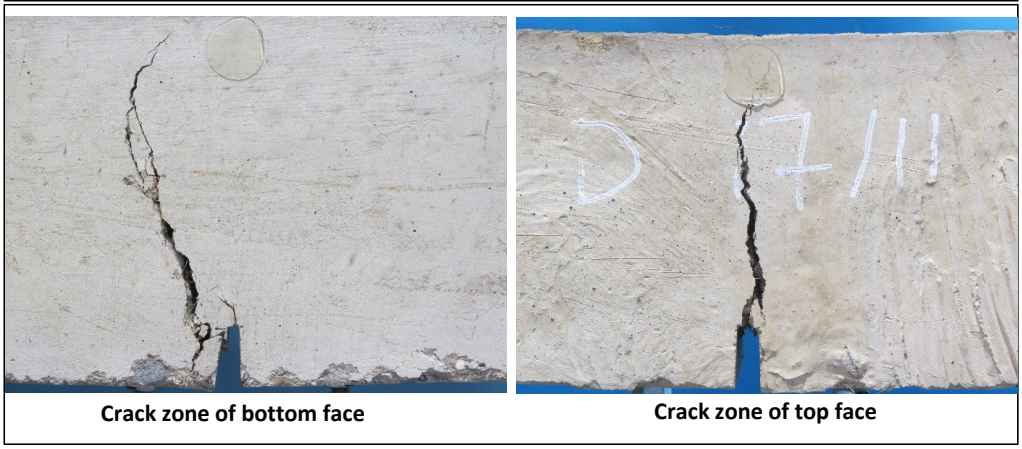

Crack zone of bottom face | Crack zone of top face

Stress-deformation graphs

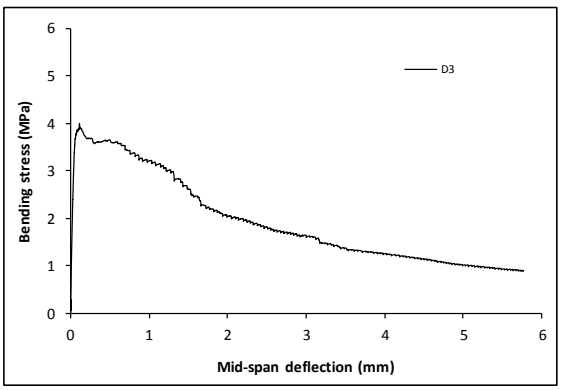

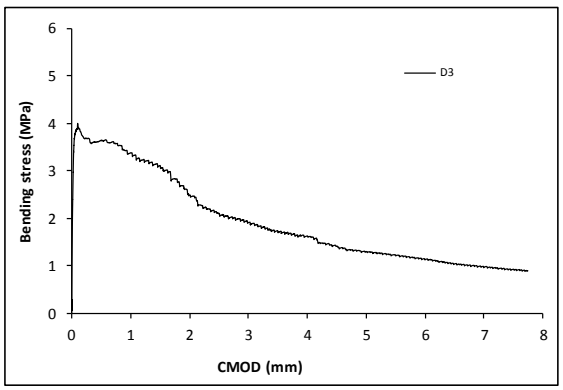

Specimen code name:		D4	RTSF (30)		
Notched Depth dn	125.5	mm			
Depth, d	151.25	mm	Span, L	500	mm
Width, b	153.25	mm	Flexural strength	3.31	MPa

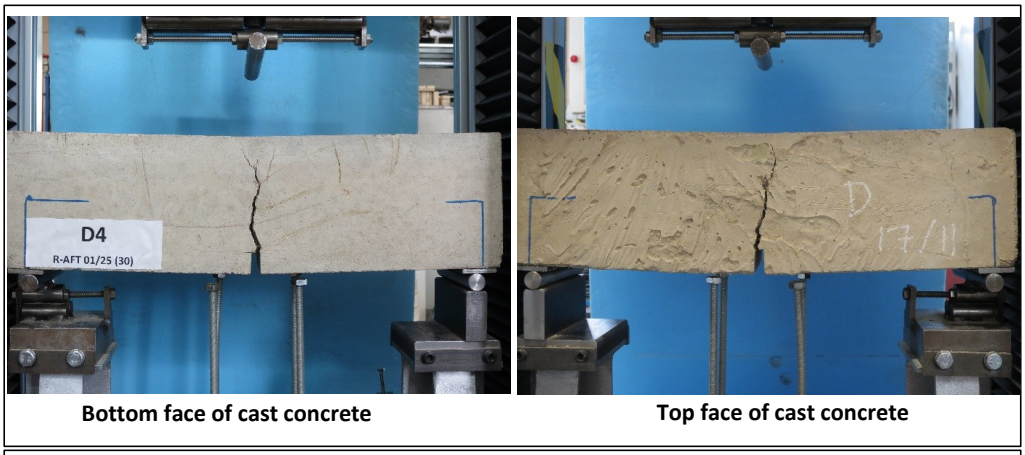

Bottom face of cast concrete | Top face of cast concrete

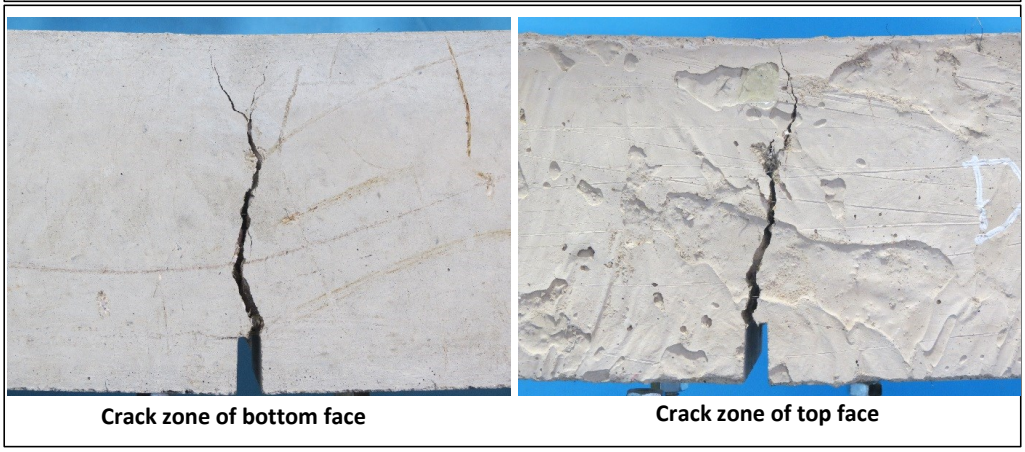

Crack zone of bottom face | Crack zone of top face

Stress-deformation graphs

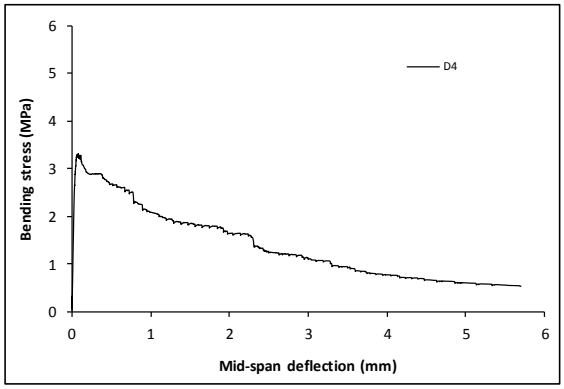

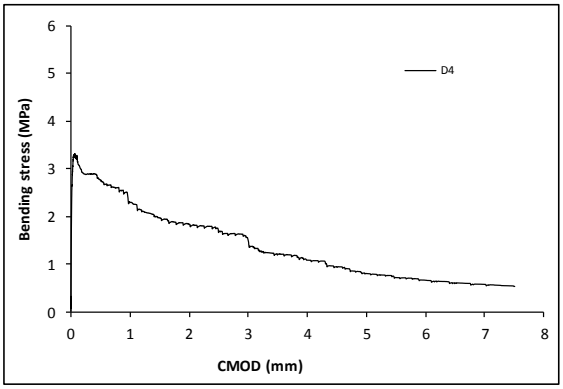

Specimen code name:		D5	RTSF (30)		
Notched Depth dn	126	mm			
Depth, d	151.5	mm	Span, L	500	mm
Width, b	153.5	mm	Flexural strength	3.36	MPa

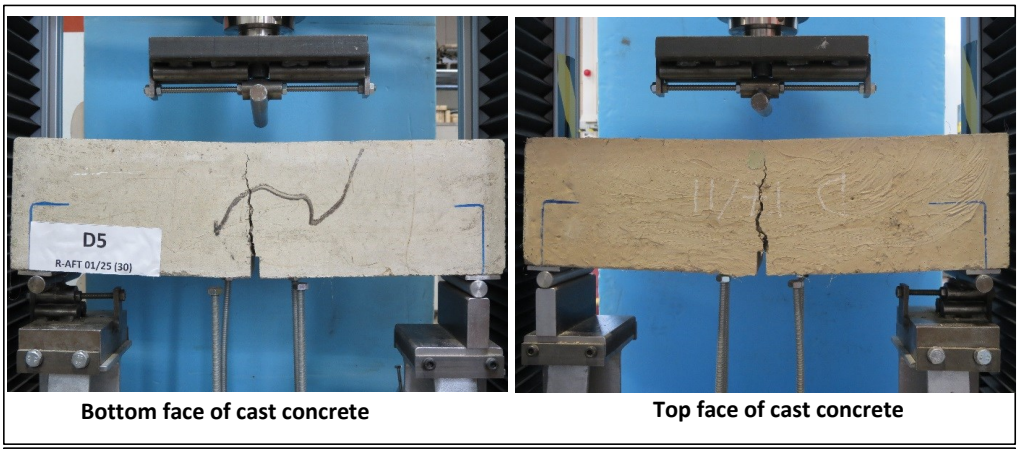

Bottom face of cast concrete | Top face of cast concrete

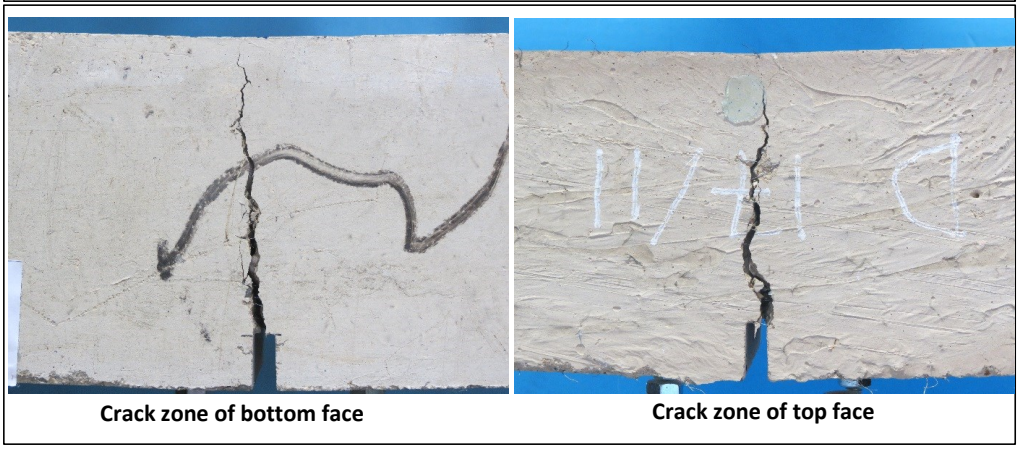

Crack zone of bottom face | Crack zone of top face

Stress-deformation graphs

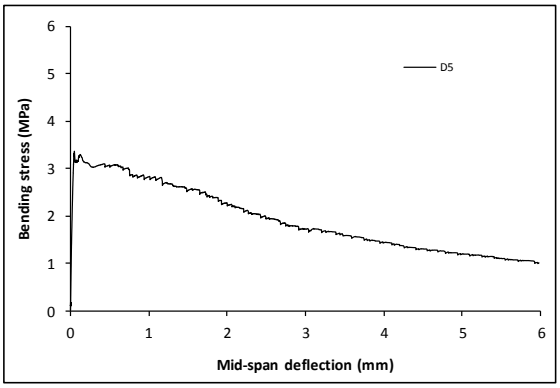

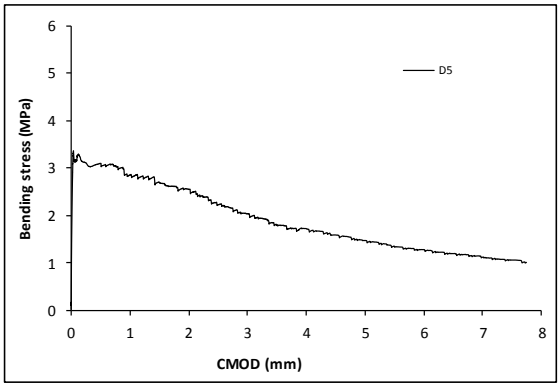

Specimen code name:		D6	RTSF (30)		
Notched Depth dn	125.5	mm			
Depth, d	150	mm	Span, L	500	mm
Width, b	156.25	mm	Flexural strength	3.64	MPa

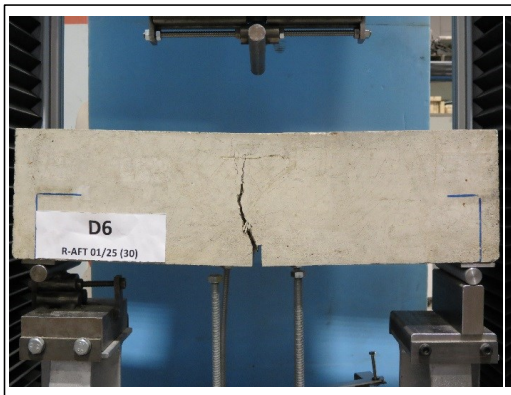

Bottom face of cast concrete

Top face of cast concrete

Crack zone of bottom face

Crack zone of top face

Stress-deformation graphs

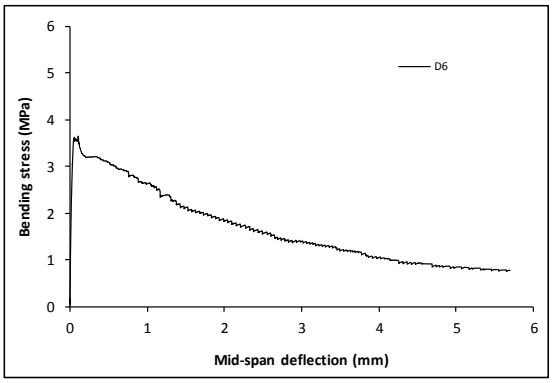

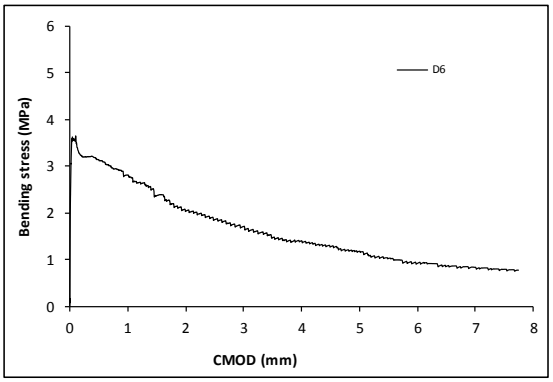

Specimen code name:		D7	RTSF (30)		
Notched Depth dn	124.75	mm			
Depth, d	150	mm	Span, L	500	mm
Width, b	158	mm	Flexural strength	4.10	MPa

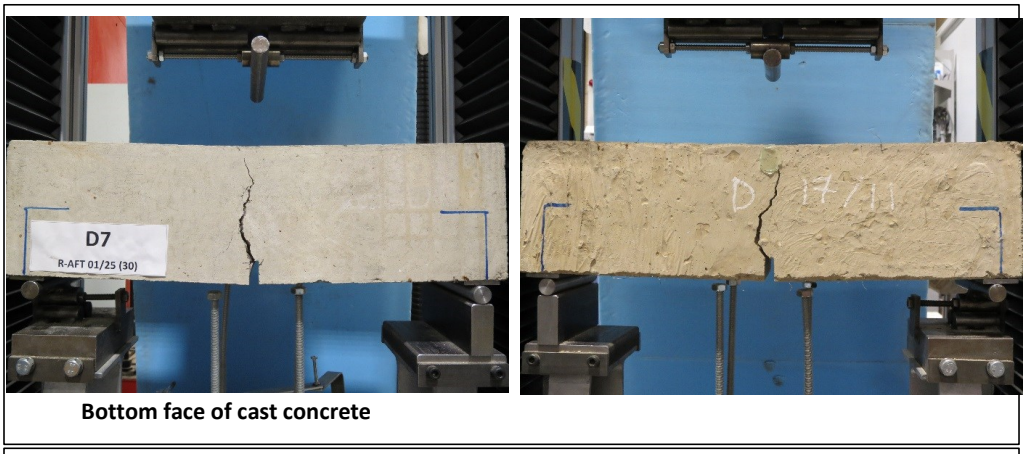

Bottom face of cast concrete

Crack zone of bottom face

Crack zone of top face

Stress-deformation graphs

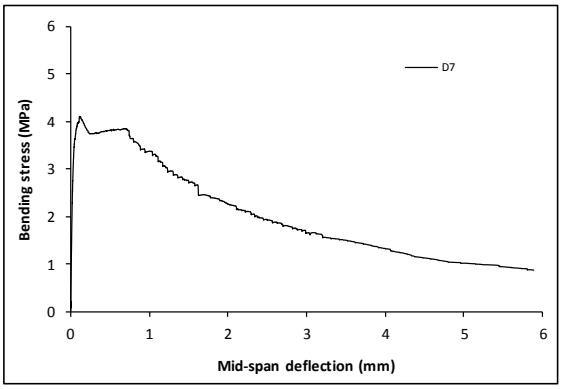

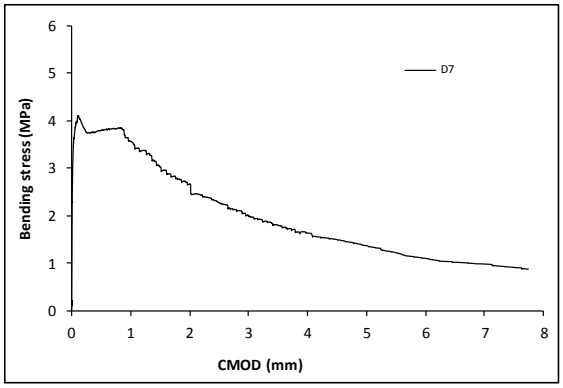

Specimen code name:		D8	RTSF (30)		
Notched Depth dn	124.25	mm			
Depth, d	151.75	mm	Span, L	500	mm
Width, b	153.75	mm	Flexural strength	5.70	MPa

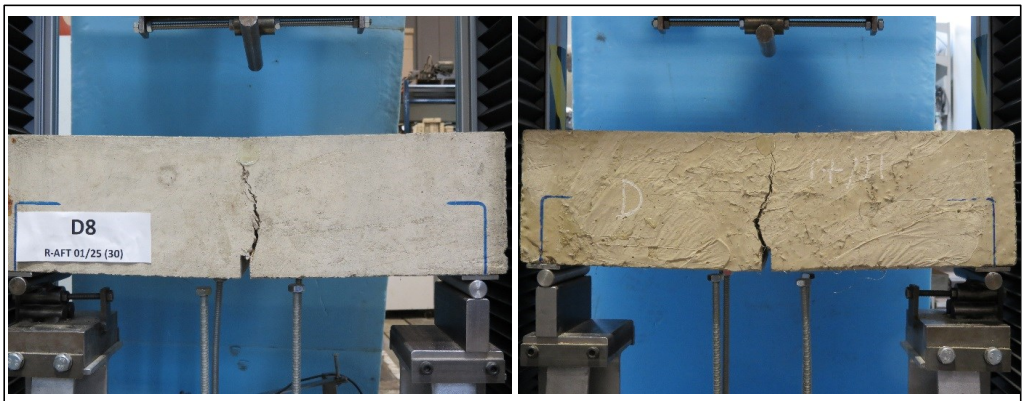

Bottom face of cast concrete

Top face of cast concrete

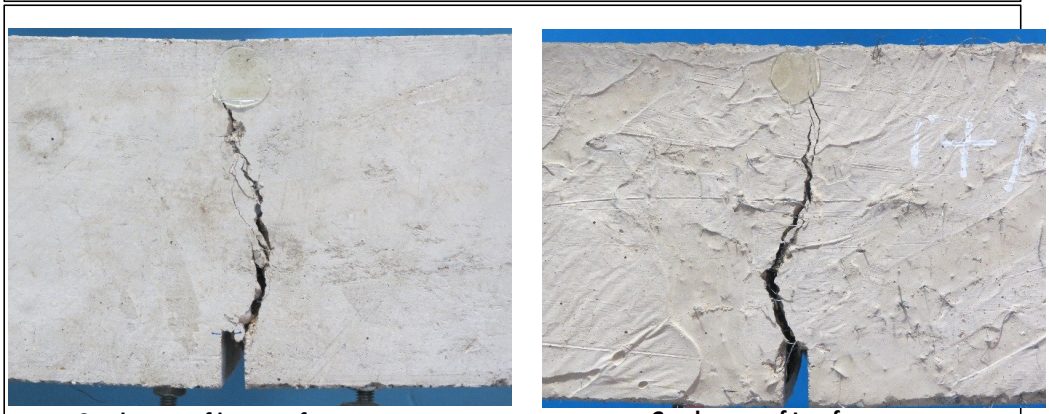

Crack zone of bottom face

Crack zone of top face

Stress-deformation graphs

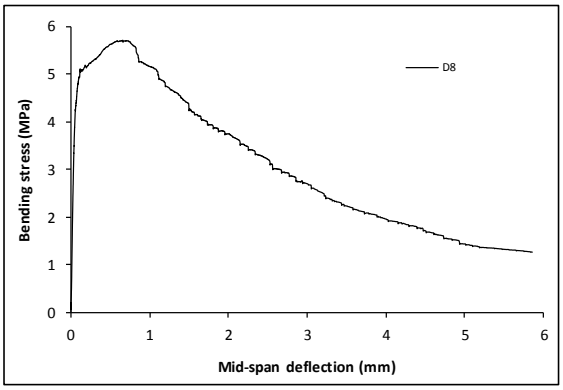

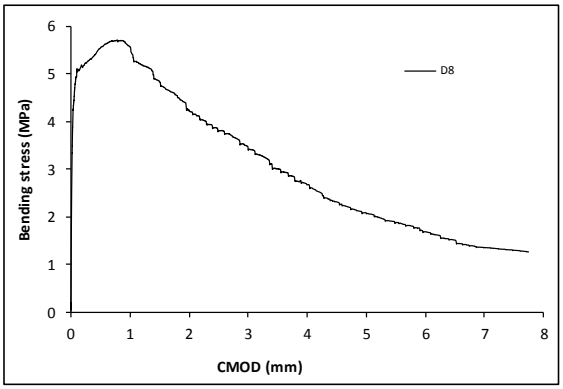

Specimen code name:		D9	RTSF (30)		
Notched Depth dn	125.25	mm			
Depth, d	150.25	mm	Span, L	500	mm
Width, b	156.5	mm	Flexural strength	4.53	MPa

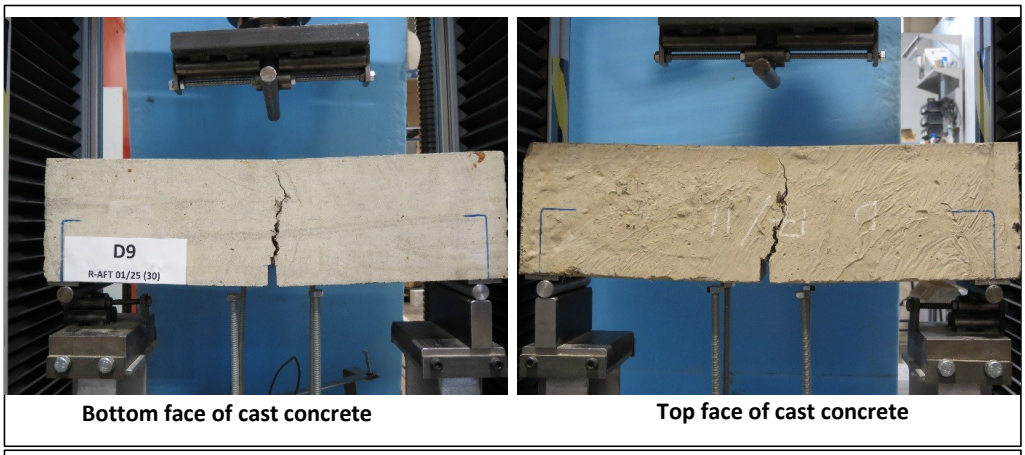

Bottom face of cast concrete | Top face of cast concrete

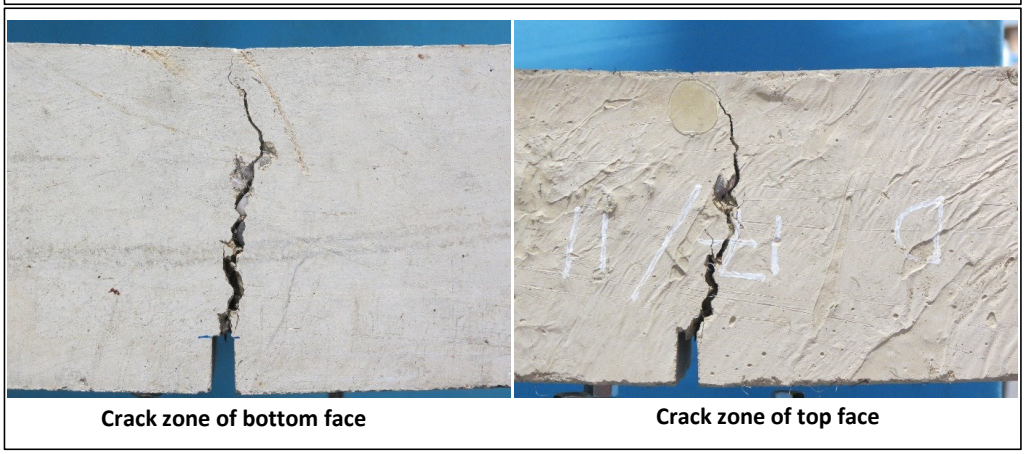

Crack zone of bottom face | Crack zone of top face

Stress-deformation graphs

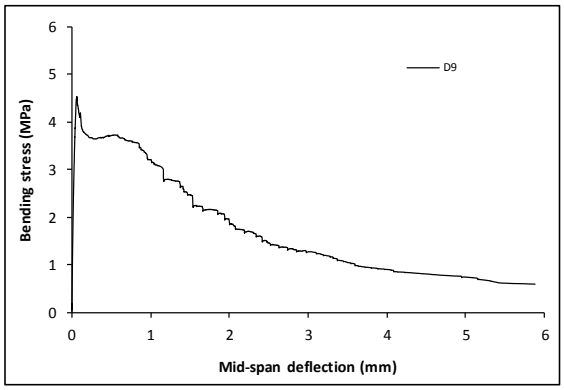

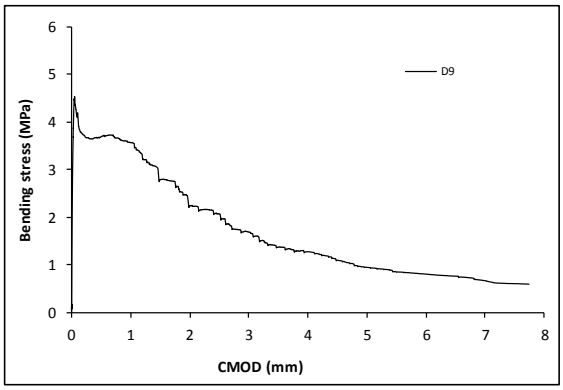

Specimen code name:		D10	RTSF (30)		
Notched Depth dn	124.75	mm			
Depth, d	150.75	mm	Span, L	500	mm
Width, b	157.5	mm	Flexural strength	4.42	MPa

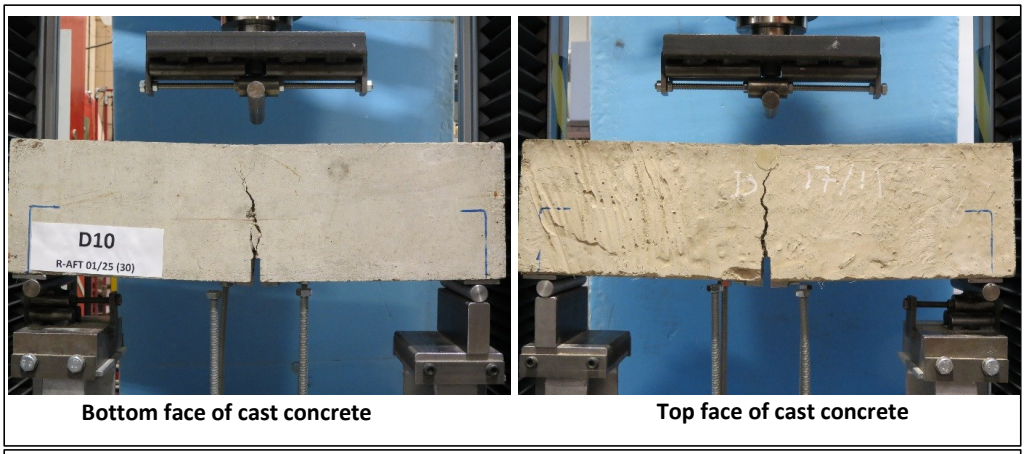

Bottom face of cast concrete | Top face of cast concrete

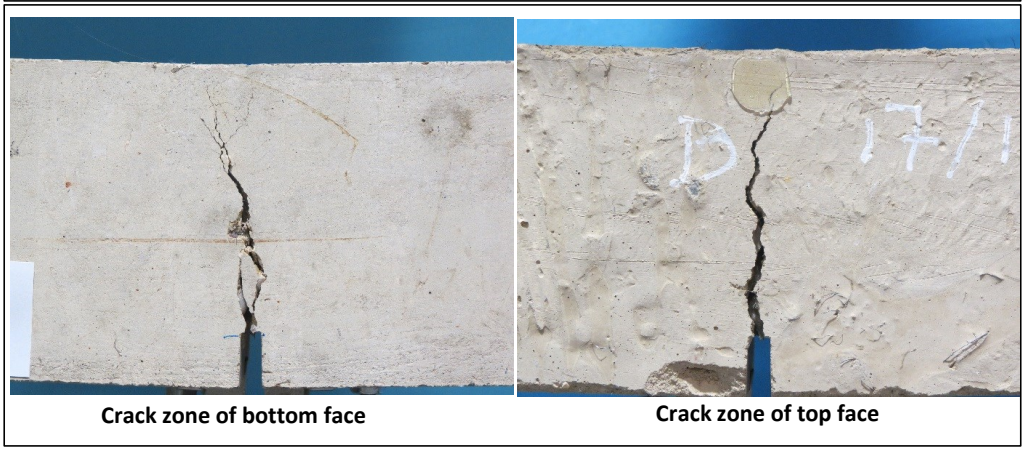

Crack zone of bottom face | Crack zone of top face

Stress-deformation graphs

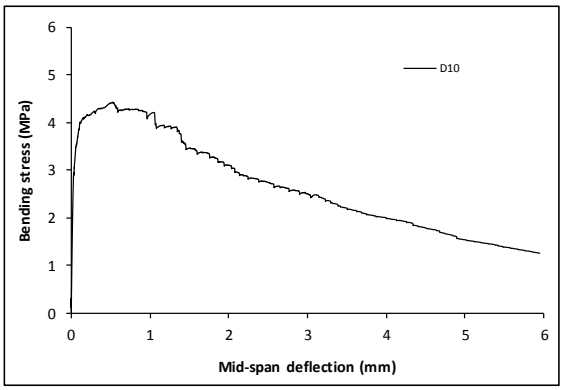

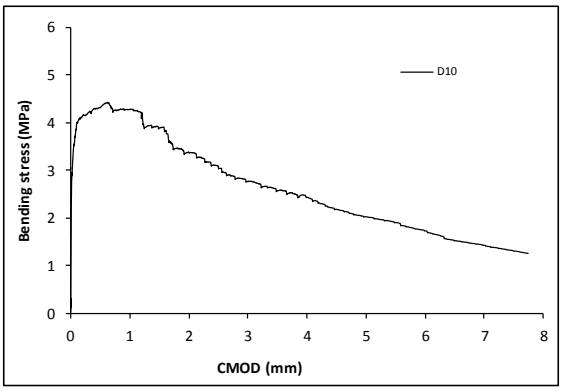

Specimen code name:		D11	RTSF (30)		
Notched Depth dn	124.25	mm			
Depth, d	149.5	mm	Span, L	500	mm
Width, b	155.25	mm	Flexural strength	3.91	MPa

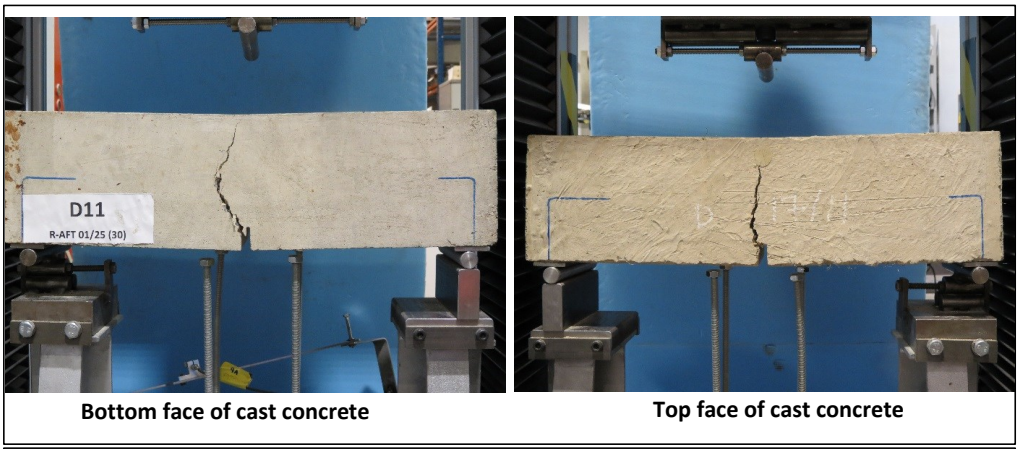

Bottom face of cast concrete | Top face of cast concrete

Crack zone of bottom face | Crack zone of top face

Stress-deformation graphs

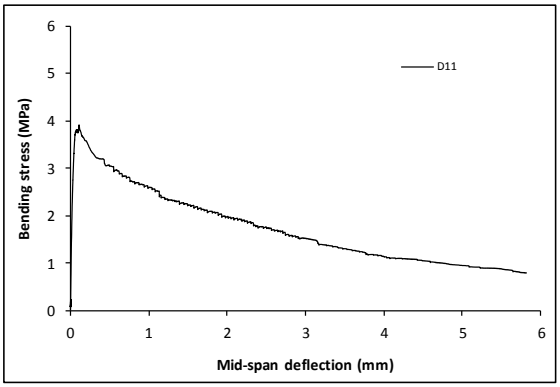

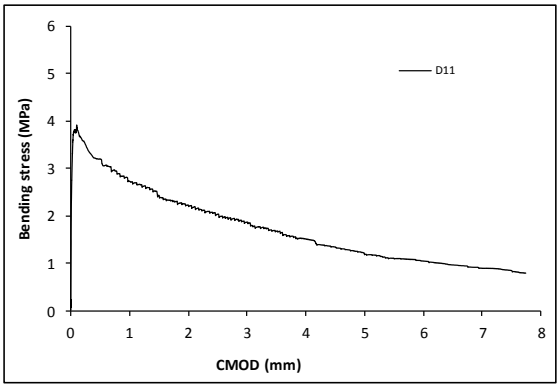

Specimen code name:		D12	RTSF (30)		
Notched Depth dn	124.75	mm			
Depth, d	150	mm	Span, L	500	mm
Width, b	157.75	mm	Flexural strength	3.91	MPa

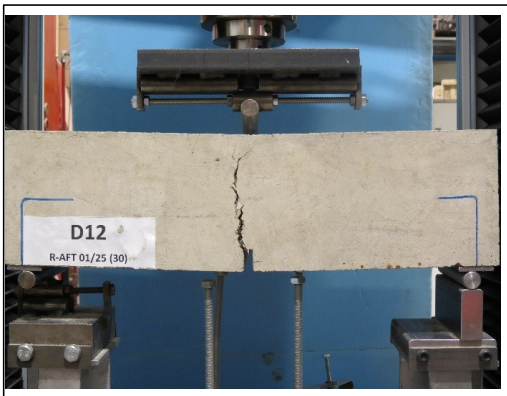

Bottom face of cast concrete

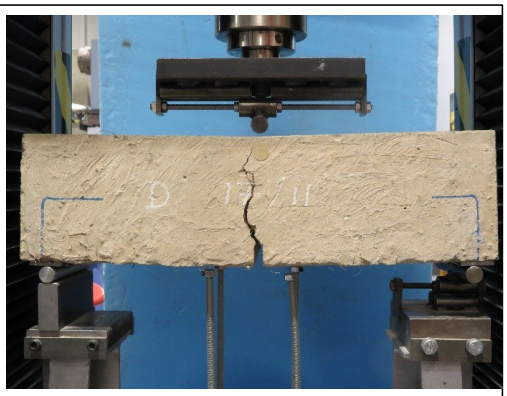

Top face of cast concrete

Crack zone of bottom face

Crack zone of top face

Stress-deformation graphs

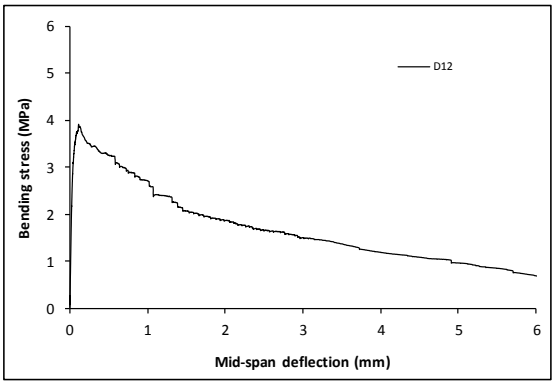

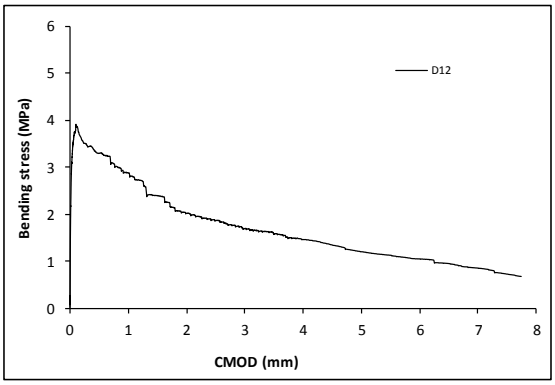

Mix:	D	RTSF (30)	
Notched Depth dn	mm		
Depth, d	mm	Span, L	mm
Width, b	mm	Flexural strength	MPa

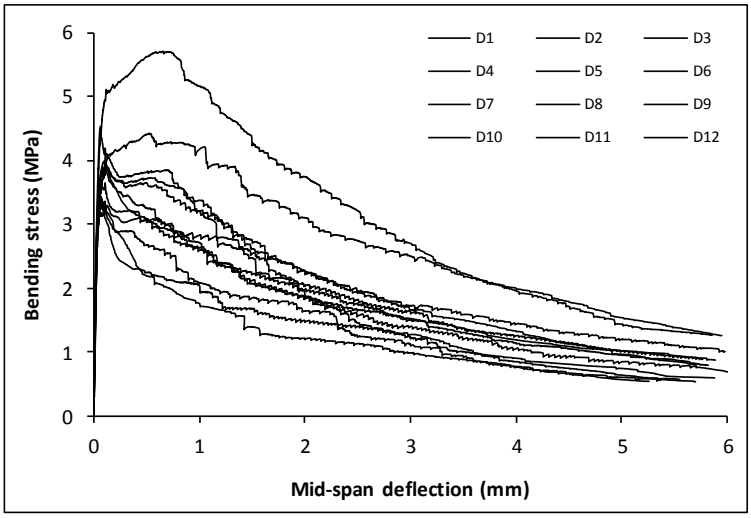

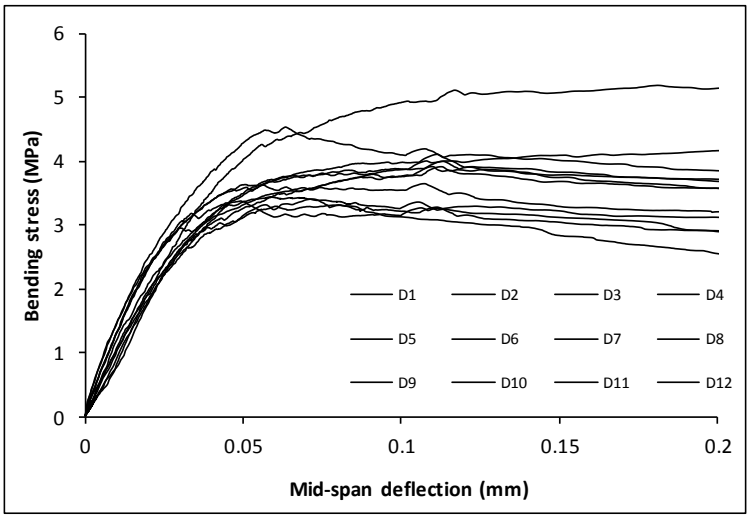

Specimen code name:		P1-1	Plain		
Notched Depth dn	124.5	mm			
Depth, d	149.25	mm	Span, L	500	mm
Width, b	152.75	mm	Flexural strength	3.73	MPa

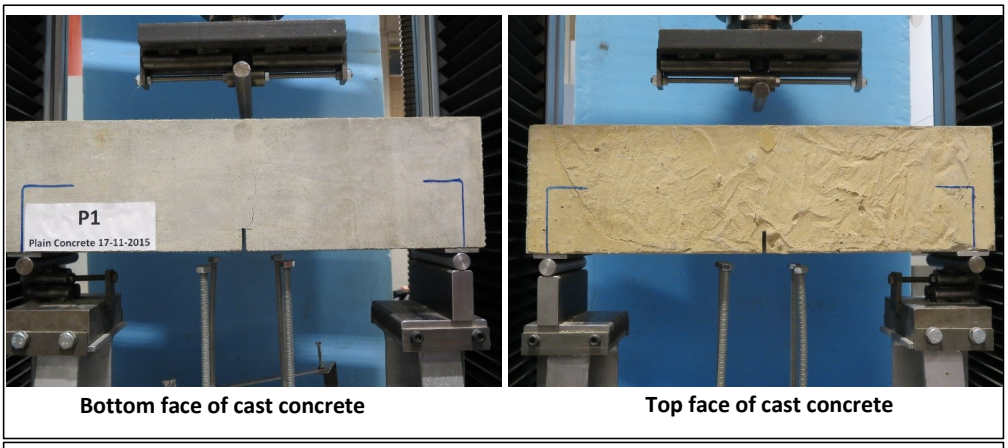

Bottom face of cast concrete | Top face of cast concrete

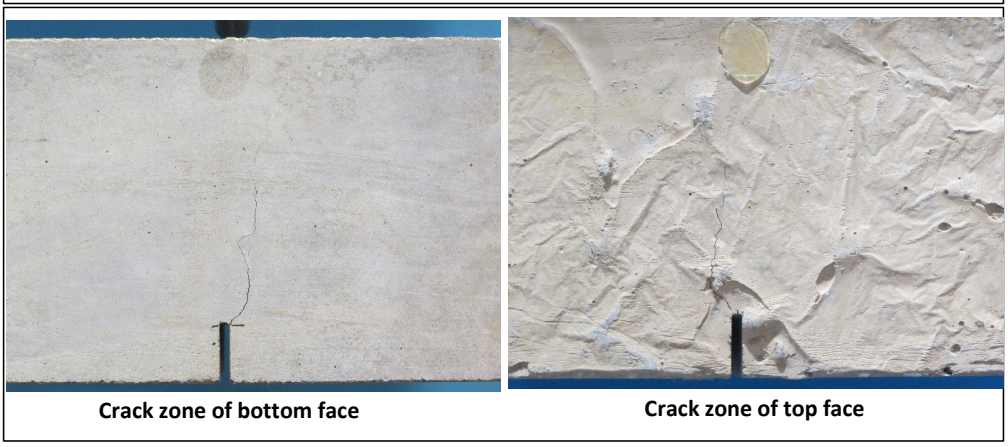

Crack zone of bottom face | Crack zone of top face

Stress-deformation graphs

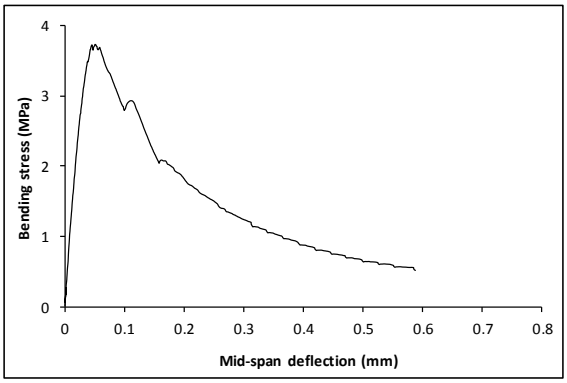

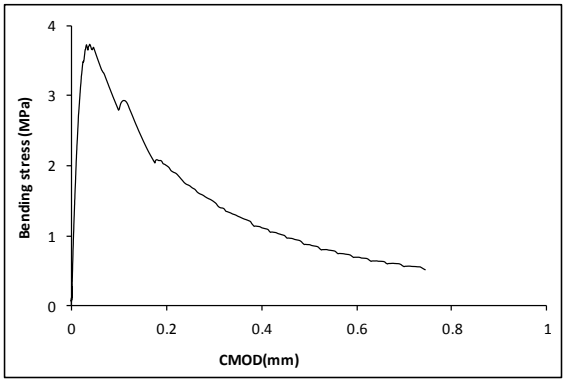

Specimen code name:		P1-2	Plain		
Notched Depth dn	123.5	mm			
Depth, d	150.25	mm	Span, L	500	mm
Width, b	152	mm	Flexural strength	3.70	MPa

Bottom face of cast concrete

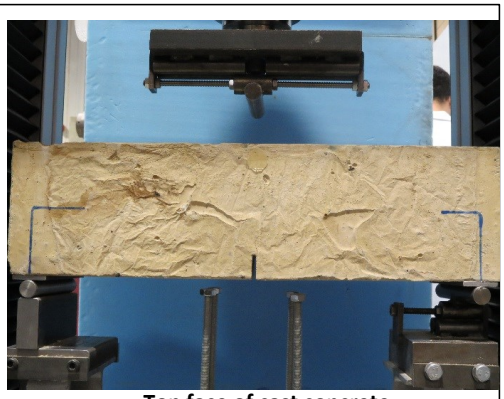

Top face of cast concrete

Crack zone of bottom face

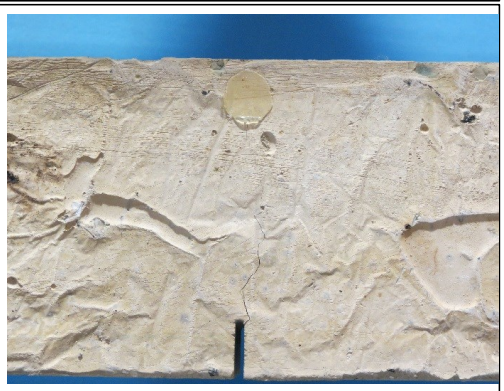

Crack zone of top face

Stress-deformation graphs

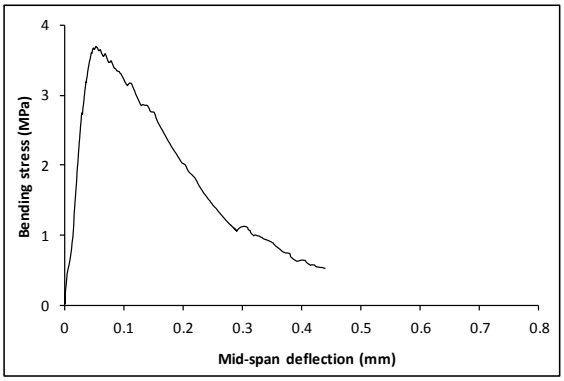

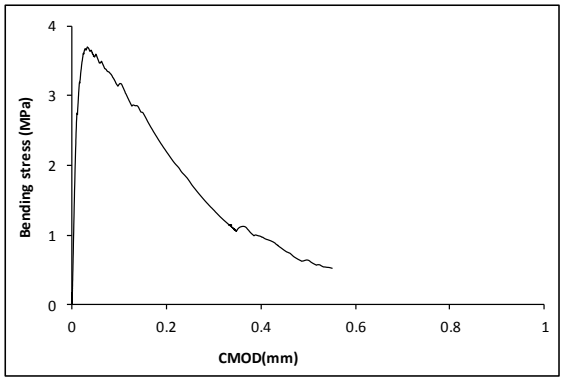

Specimen code name:		P1-3	Plain		
Notched Depth dn	124.5	mm			
Depth, d	150	mm	Span, L	500	mm
Width, b	152	mm	Flexural strength	3.60	MPa

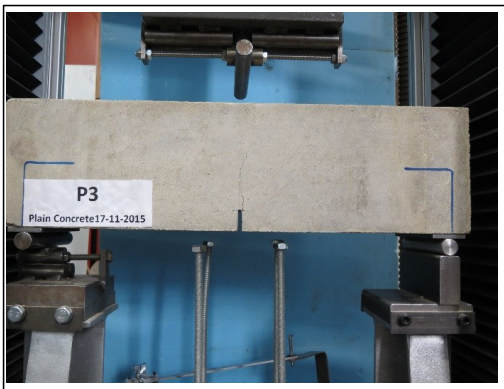

Bottom face of cast concrete

Top face of cast concrete

Crack zone of bottom face

Crack zone of top face

Stress-deformation graphs

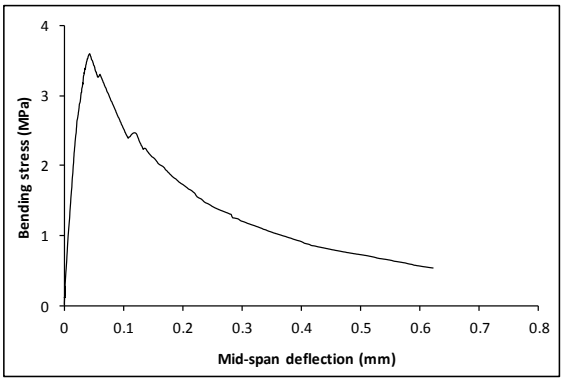

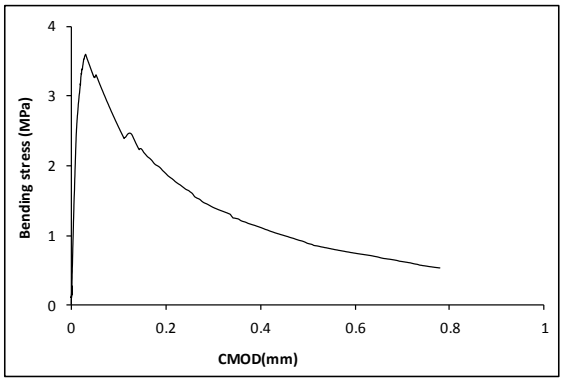

Specimen code name:		P1-4	Plain		
Notched Depth dn	124	mm			
Depth, d	149.5	mm	Span, L	500	mm
Width, b	150.5	mm	Flexural strength	3.41	MPa

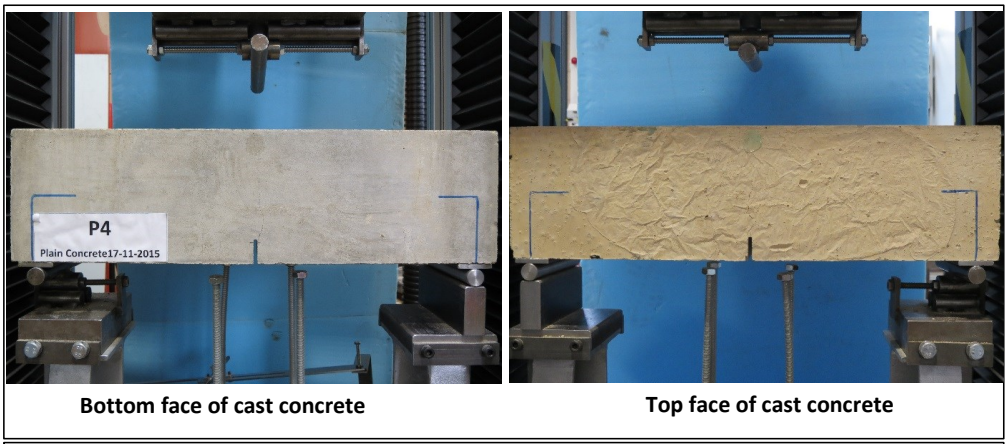

Bottom face of cast concrete | Top face of cast concrete

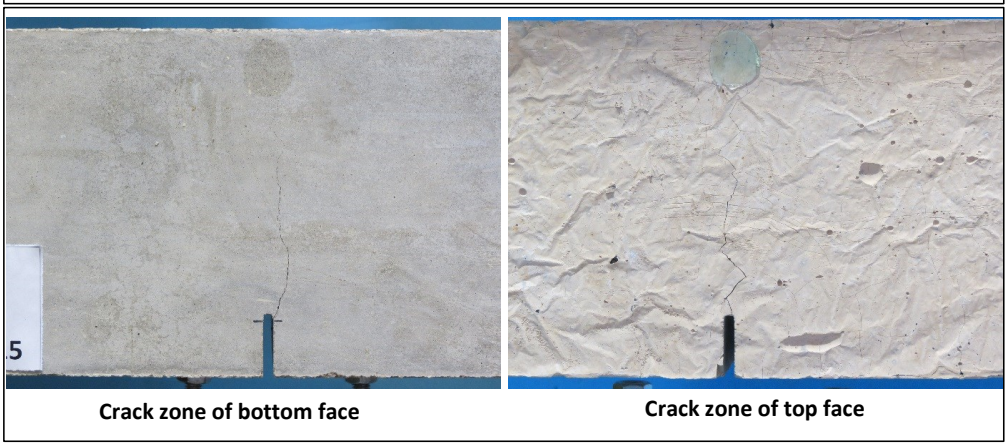

Crack zone of bottom face | Crack zone of top face

Stress-deformation graphs

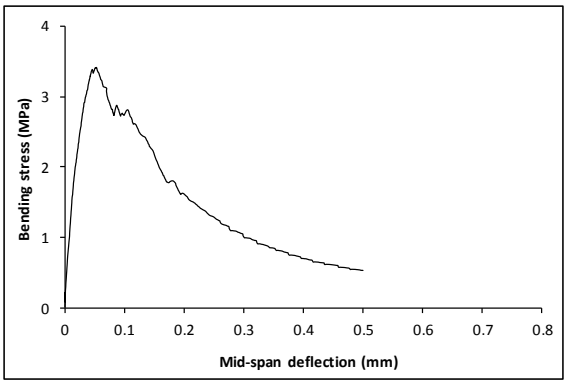

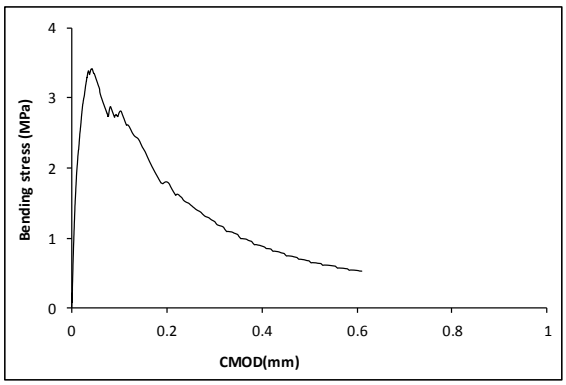

Specimen code name:		P1-5	Plain		
Notched Depth dn	125	mm			
Depth, d	150	mm	Span, L	500	mm
Width, b	151	mm	Flexural strength	3.24	MPa

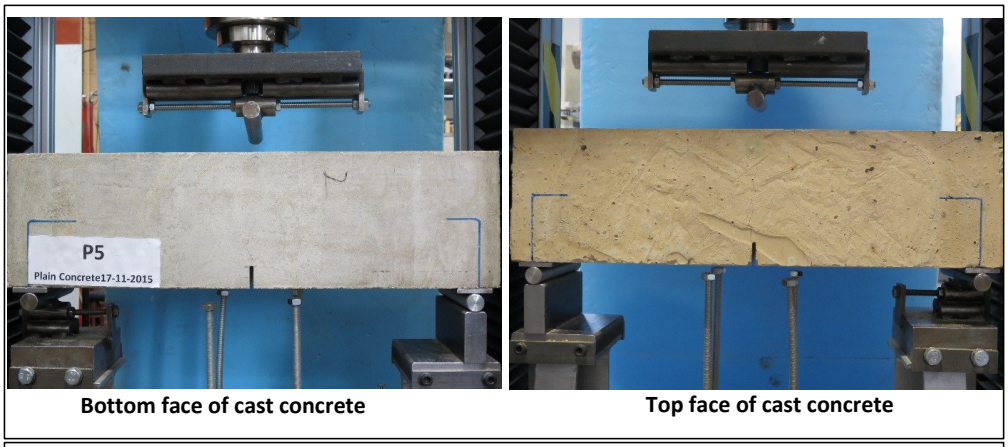

Bottom face of cast concrete | Top face of cast concrete

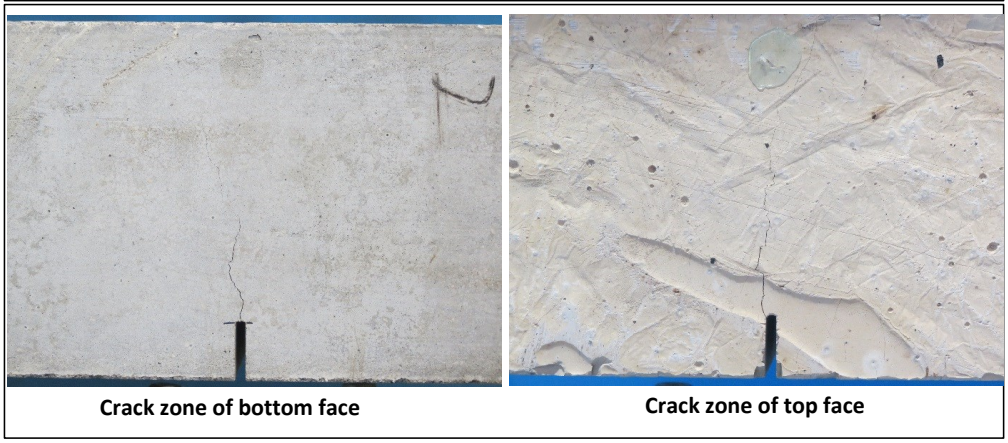

Crack zone of bottom face | Crack zone of top face

Stress-deformation graphs

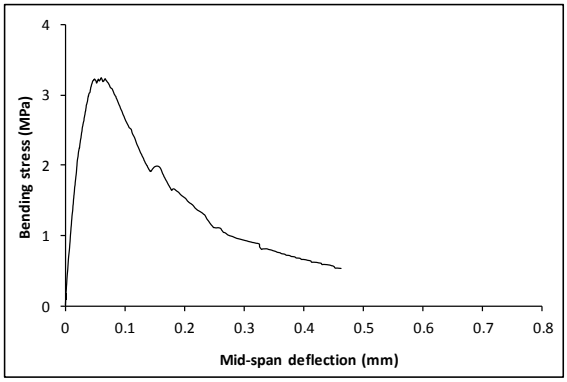

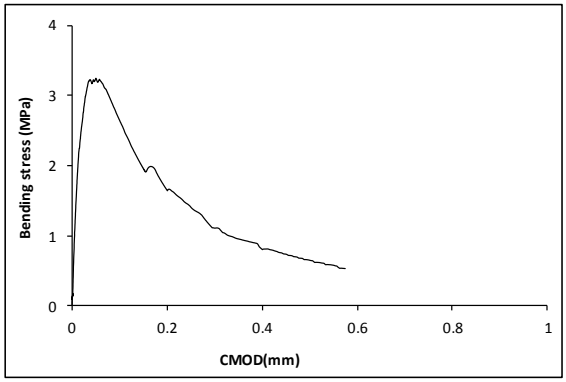

Specimen code name:		P1-6	Plain		
Notched Depth dn	123.75	mm			
Depth, d	150.25	mm	Span, L	500	mm
Width, b	152	mm	Flexural strength	3.71	MPa

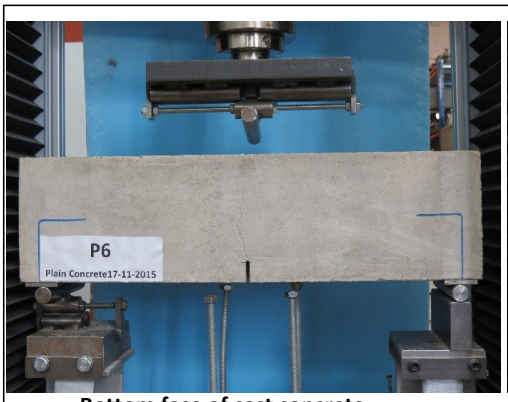

Bottom face of cast concrete

Top face of cast concrete

Crack zone of bottom face

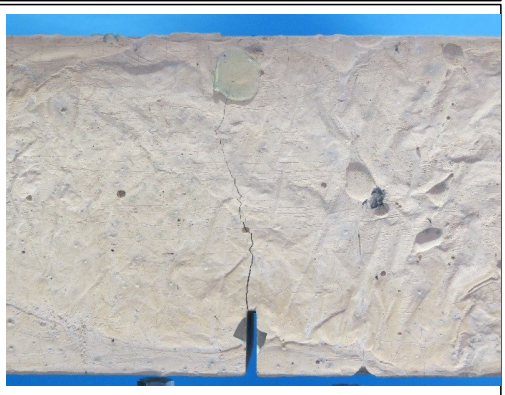

Crack zone of top face

Stress-deformation graphs

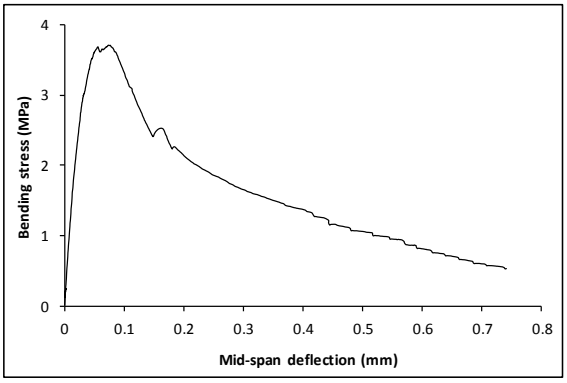

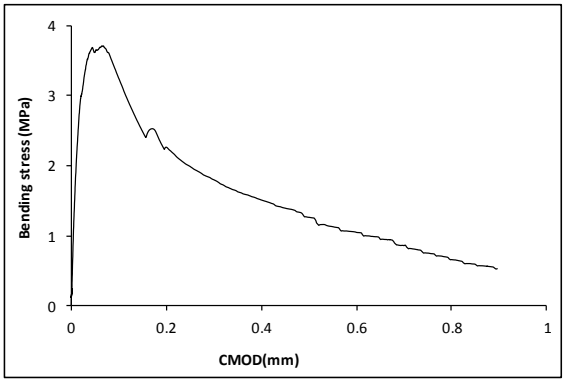

Mix:	**P1**	Plain	
Notched Depth dn	mm		
Depth, d	mm	Span, L	mm
Width, b	mm	Flexural strength	MPa

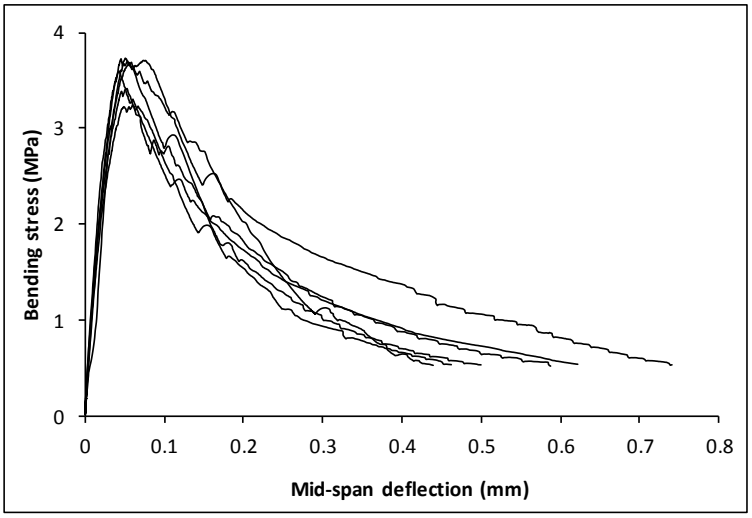

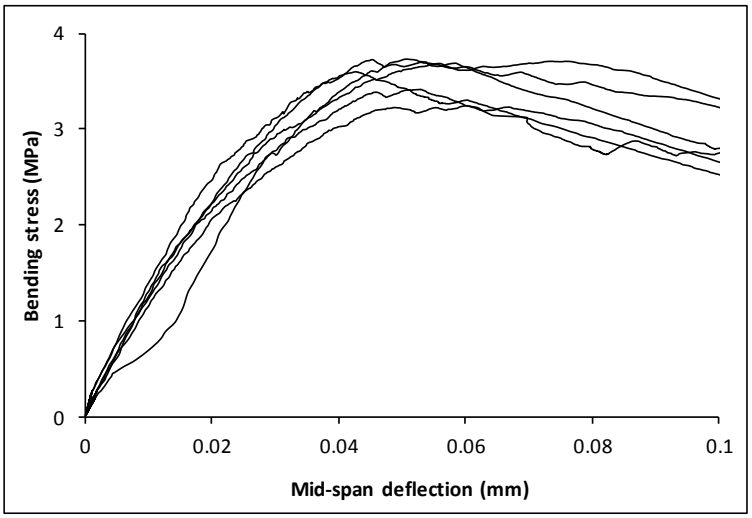

Specimen code name:		E1 (F1)	MSF1 (45)		
Notched Depth dn	124.5	mm			
Depth, d	150	mm	Span, L	500	mm
Width, b	154	mm	Flexural strength	4.52	MPa

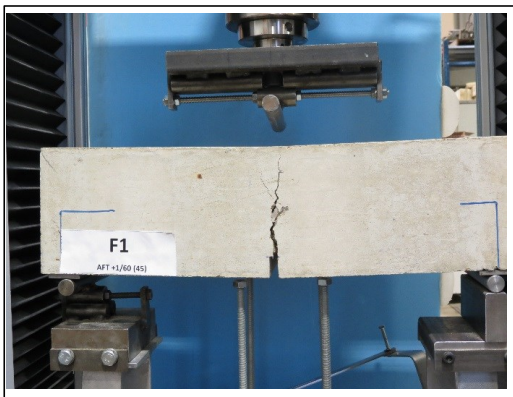

Bottom face of cast concrete

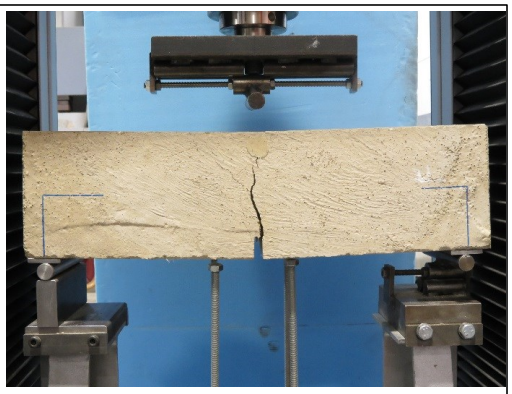

Top face of cast concrete

Crack zone of bottom face

Crack zone of top face

Stress-deformation graphs

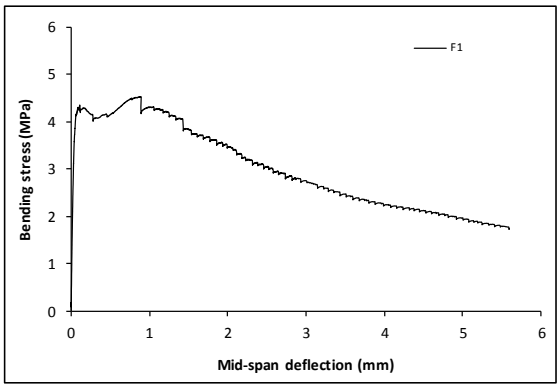

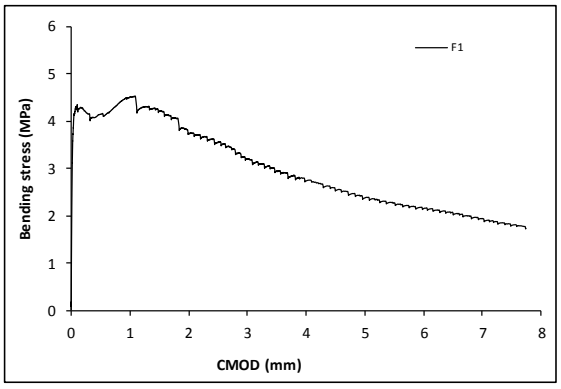

Specimen code name:		E2 (F2)	MSF1 (45)		
Notched Depth dn	125.25	mm			
Depth, d	151	mm	Span, L	500	mm
Width, b	152.5	mm	Flexural strength	5.05	MPa

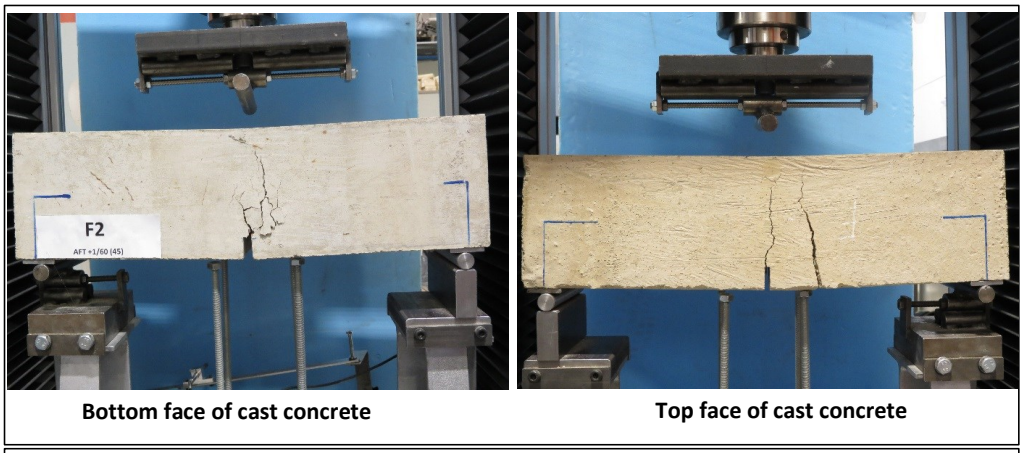

Bottom face of cast concrete | Top face of cast concrete

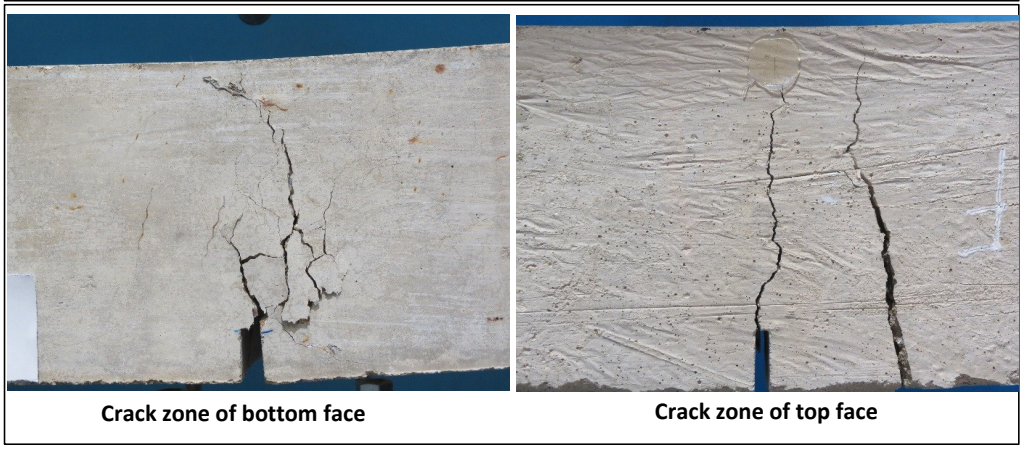

Crack zone of bottom face | Crack zone of top face

Stress-deformation graphs

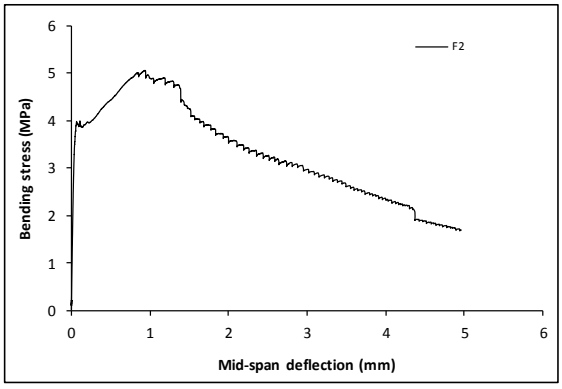

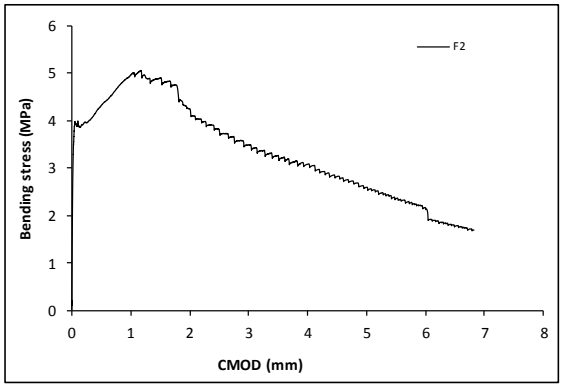

Specimen code name:		E3 (F3)	MSF1 (45)		
Notched Depth dn	125	mm			
Depth, d	150	mm	Span, L	500	mm
Width, b	153	mm	Flexural strength	5.06	MPa

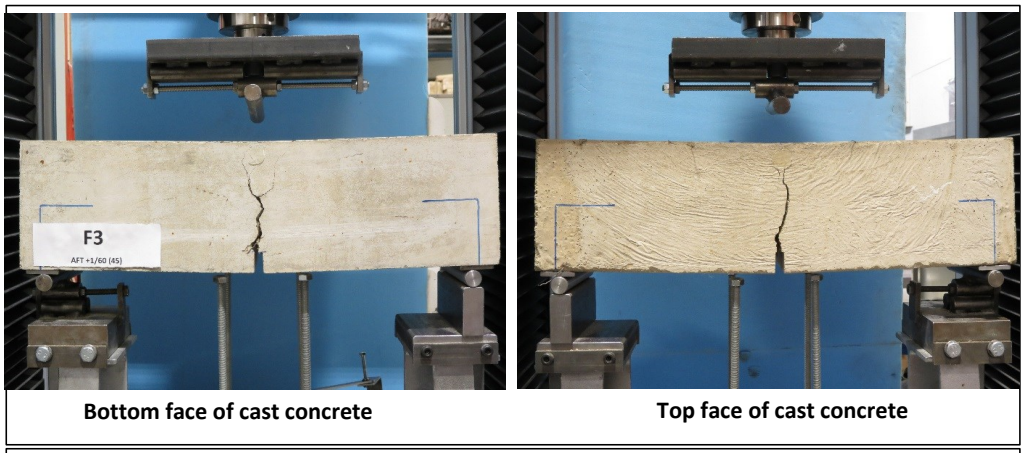

Bottom face of cast concrete | Top face of cast concrete

Crack zone of bottom face | Crack zone of top face

Stress-deformation graphs

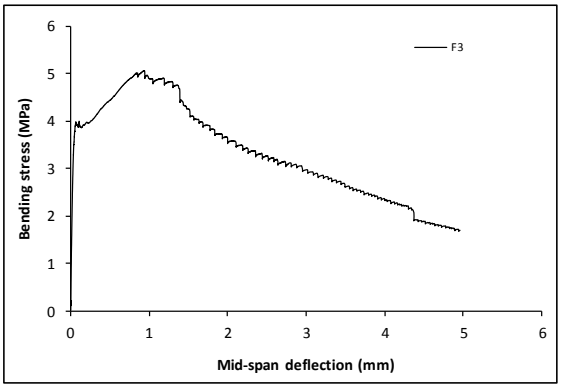

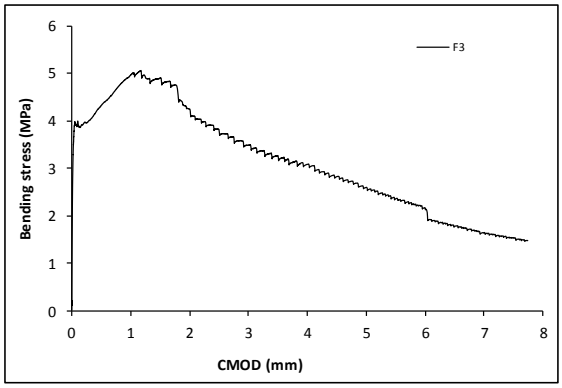

Specimen code name:		E4 (F4)	MSF1 (45)		
Notched Depth dn	124.5	mm			
Depth, d	150.5	mm	Span, L	500	mm
Width, b	152.25	mm	Flexural strength	3.93	MPa

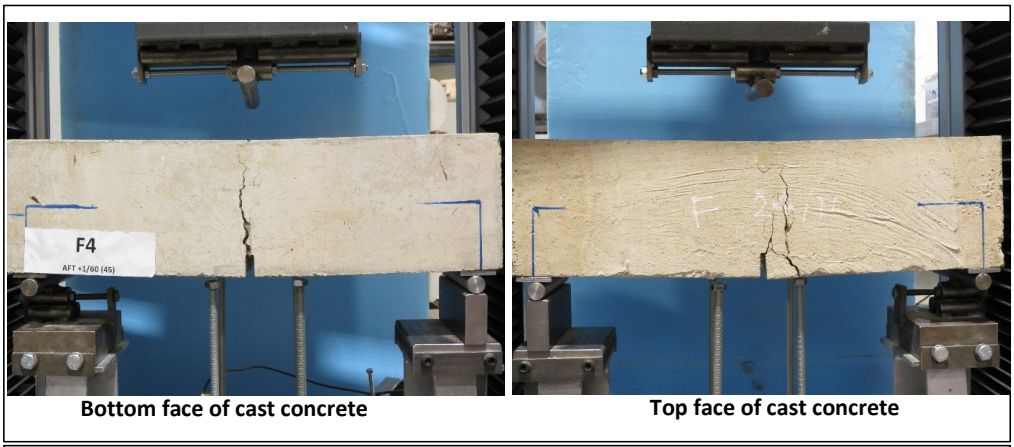

Bottom face of cast concrete | Top face of cast concrete

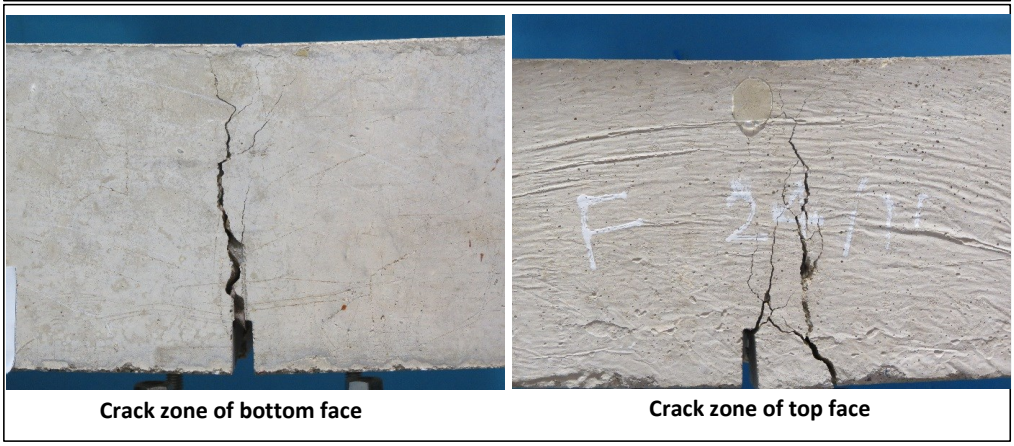

Crack zone of bottom face | Crack zone of top face

Stress-deformation graphs

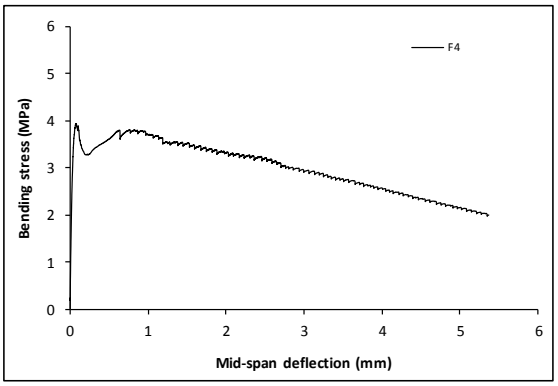

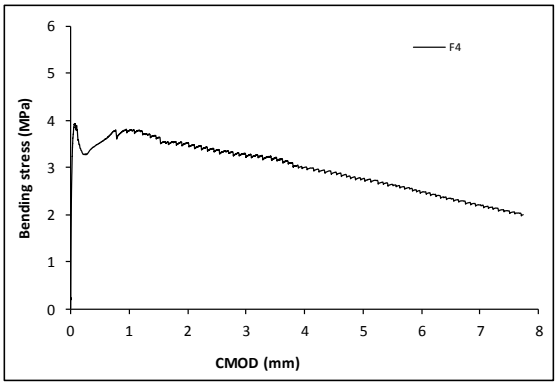

Specimen code name:		E5 (F5)	MSF1 (45)		
Notched Depth dn	125.5	mm			
Depth, d	150	mm	Span, L	500	mm
Width, b	152.25	mm	Flexural strength	3.78	MPa

Bottom face of cast concrete

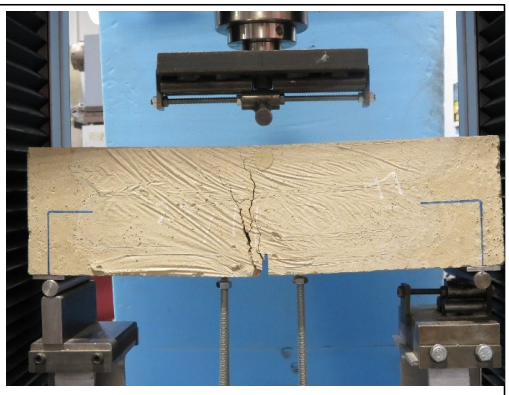

Top face of cast concrete

Crack zone of bottom face

Crack zone of top face

Stress-deformation graphs

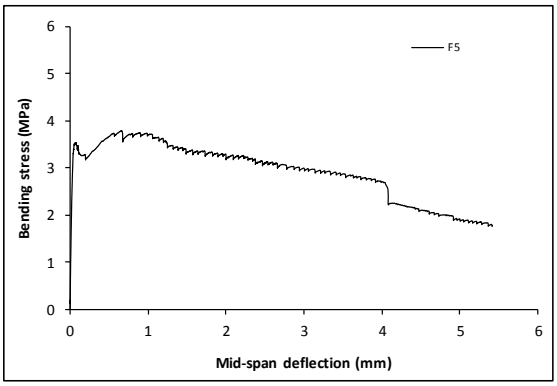

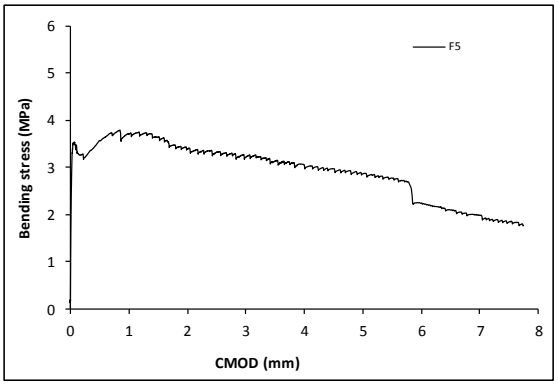

Specimen code name:		E6 (F6)	MSF1 (45)		
Notched Depth dn	124.25	mm			
Depth, d	150.25	mm	Span, L	500	mm
Width, b	153	mm	Flexural strength	4.70	MPa

Bottom face of cast concrete

Top face of cast concrete

Crack zone of bottom face

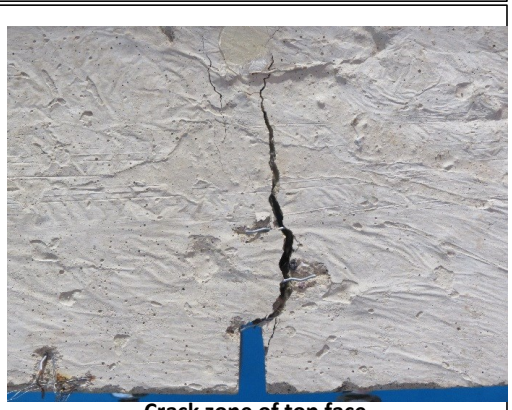

Crack zone of top face

Stress-deformation graphs

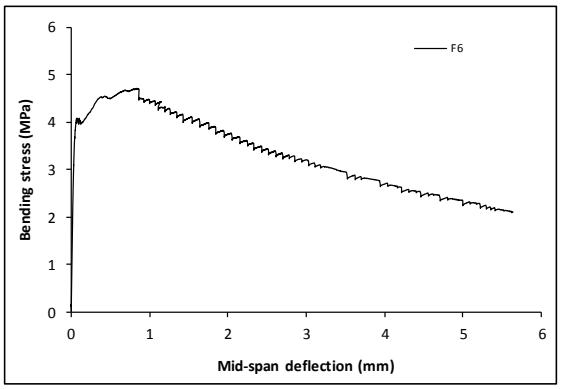

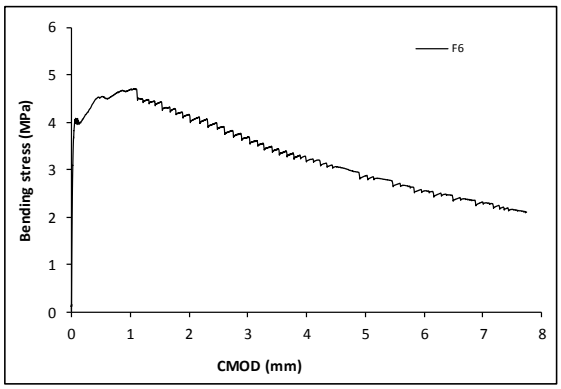

Specimen code name:		E7 (F7)	MSF1 (45)		
Notched Depth dn	125.25	mm			
Depth, d	150.5	mm	Span, L	500	mm
Width, b	154	mm	Flexural strength	3.90	MPa

Bottom face of cast concrete

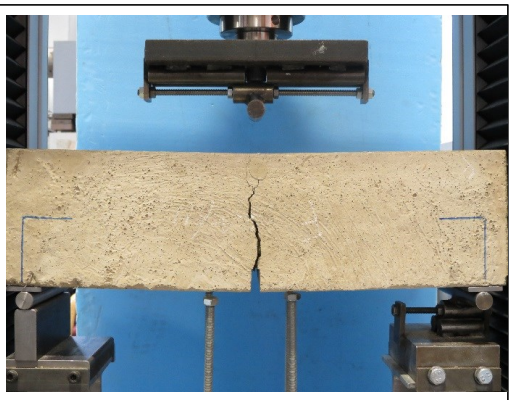

Top face of cast concrete

Crack zone of bottom face

Crack zone of top face

Stress-deformation graphs

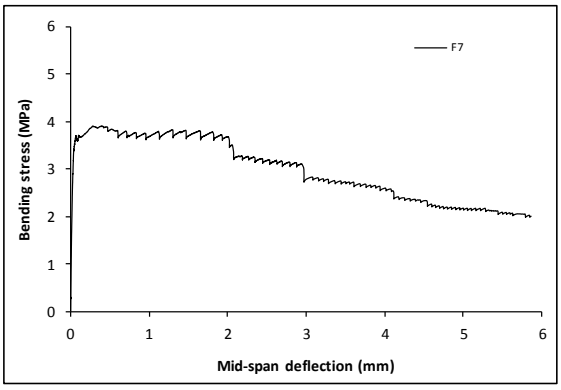

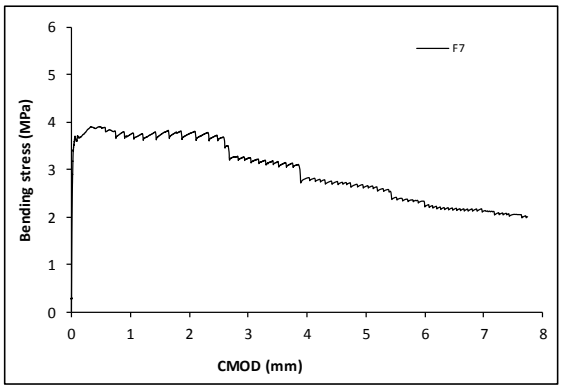

Specimen code name:		E8 (F8)	MSF1 (45)		
Notched Depth dn	126	mm			
Depth, d	150	mm	Span, L	500	mm
Width, b	154	mm	Flexural strength	5.27	MPa

Bottom face of cast concrete

Top face of cast concrete

Crack zone of bottom face

Crack zone of top face

Stress-deformation graphs

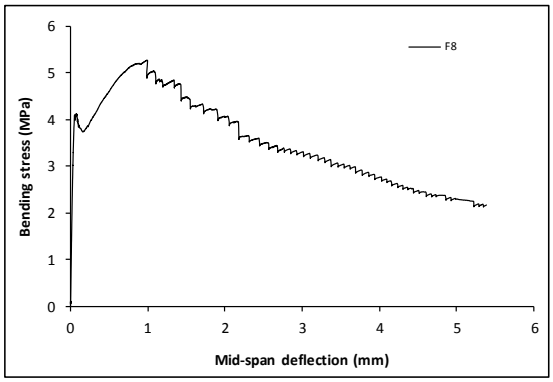

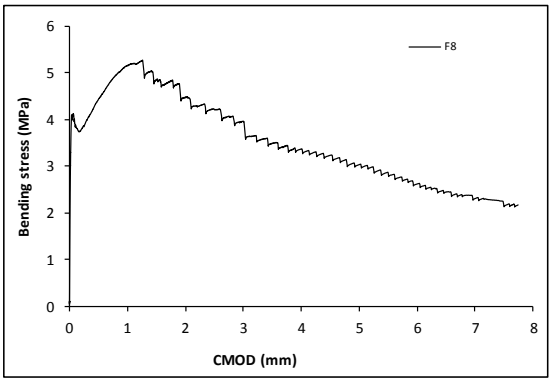

Specimen code name:		E9 (F9)	MSF1 (45)		
Notched Depth dn	126	mm			
Depth, d	150	mm	Span, L	500	mm
Width, b	152.5	mm	Flexural strength	4.12	MPa

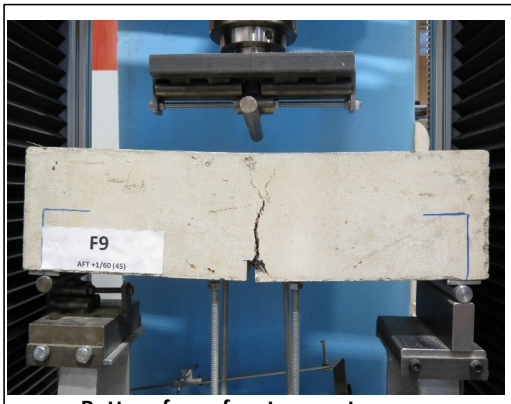

Bottom face of cast concrete

Top face of cast concrete

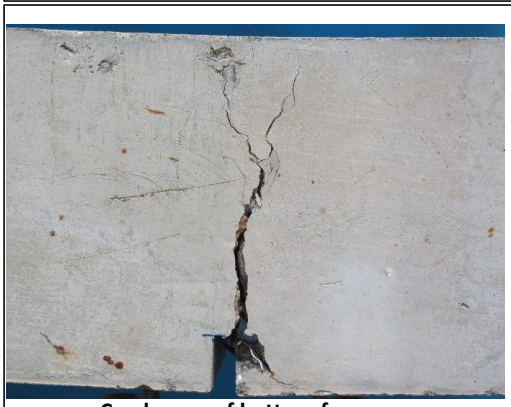

Crack zone of bottom face

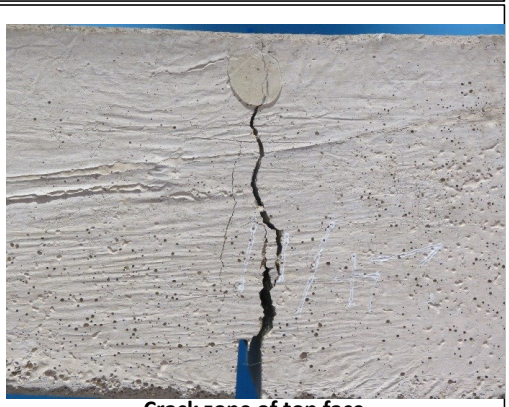

Crack zone of top face

Stress-deformation graphs

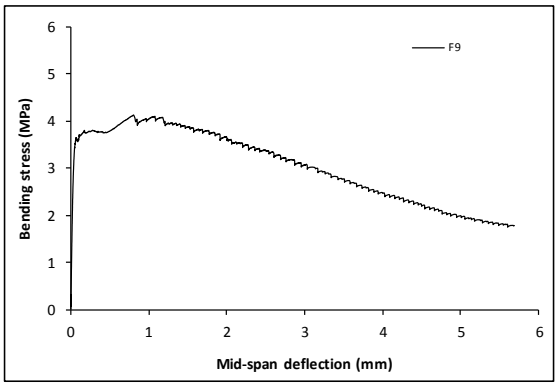

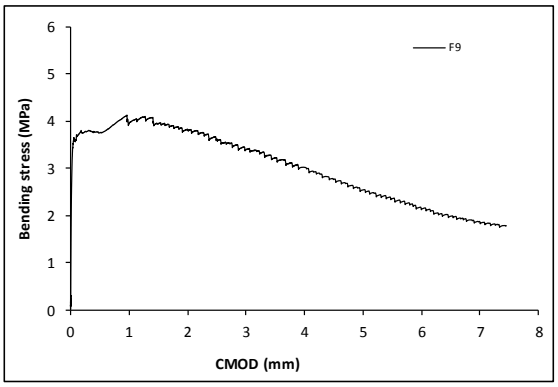

Specimen code name:		E10 (F10)	MSF1 (45)		
Notched Depth dn	126	mm			
Depth, d	150	mm	Span, L	500	mm
Width, b	153	mm	Flexural strength	5.50	MPa

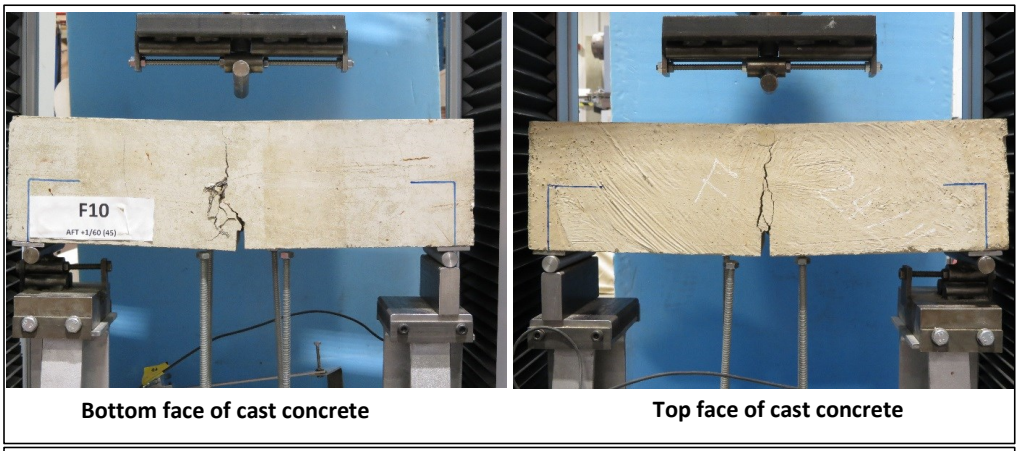

Bottom face of cast concrete

Top face of cast concrete

Crack zone of bottom face

Crack zone of top face

Stress-deformation graphs

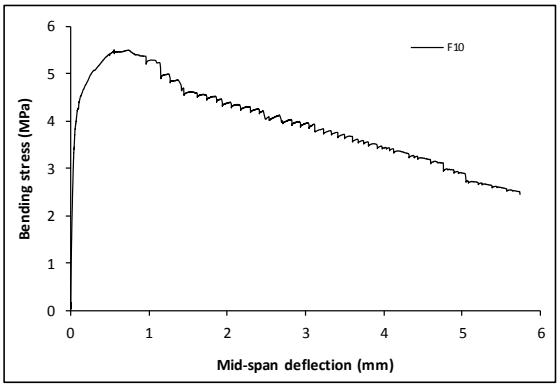

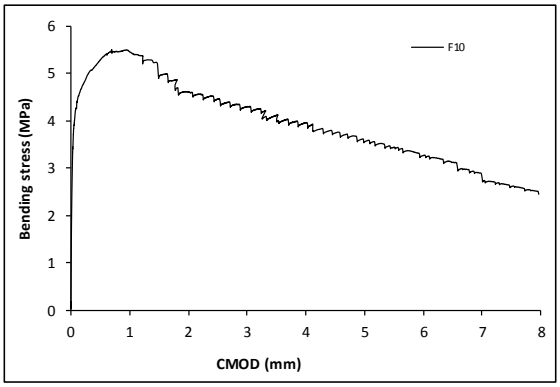

Specimen code name:		E11 (F11)	MSF1 (45)		
Notched Depth dn	125.25	mm			
Depth, d	150	mm	Span, L	500	mm
Width, b	151.25	mm	Flexural strength	4.71	MPa

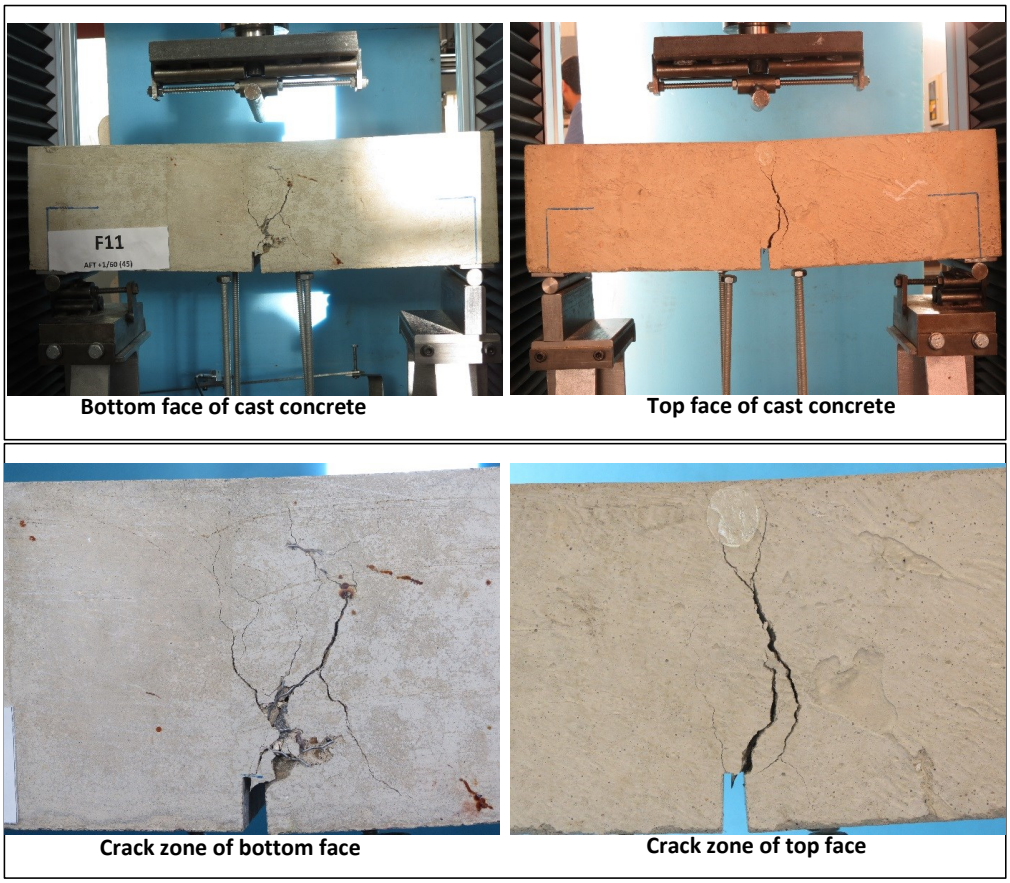

Stress-deformation graphs

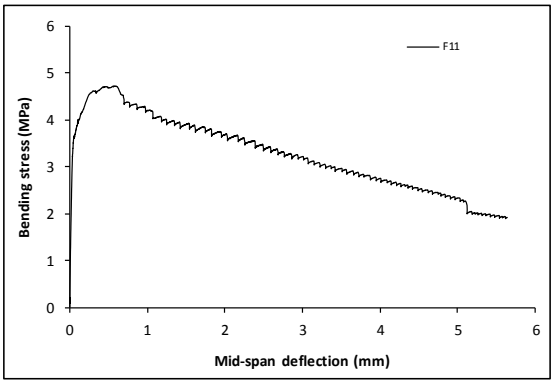

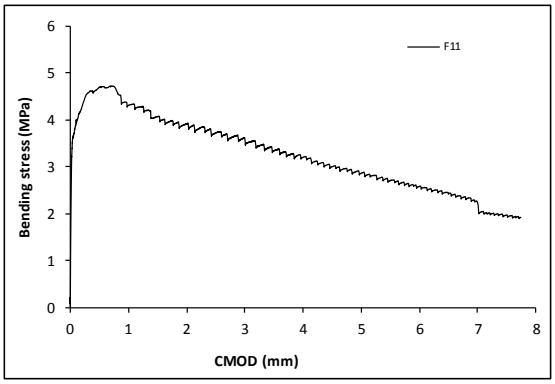

Specimen code name:		E12 (F12)	MSF1 (45)		
Notched Depth dn	123.5	mm			
Depth, d	150	mm	Span, L	500	mm
Width, b	151.75	mm	Flexural strength	4.03	MPa

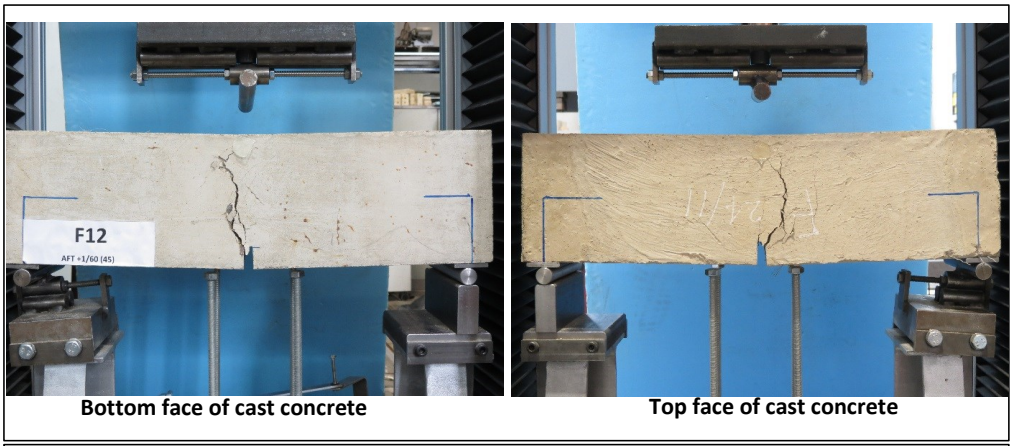

Bottom face of cast concrete | Top face of cast concrete

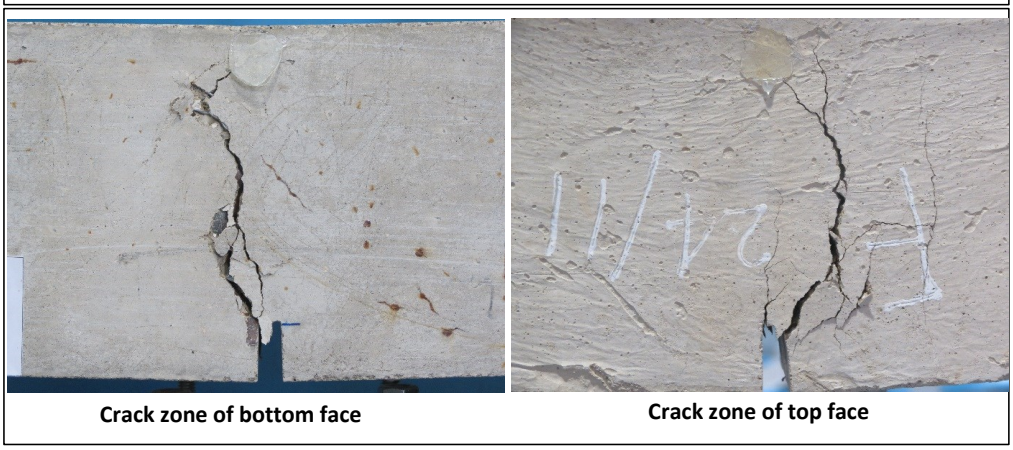

Crack zone of bottom face | Crack zone of top face

Stress-deformation graphs

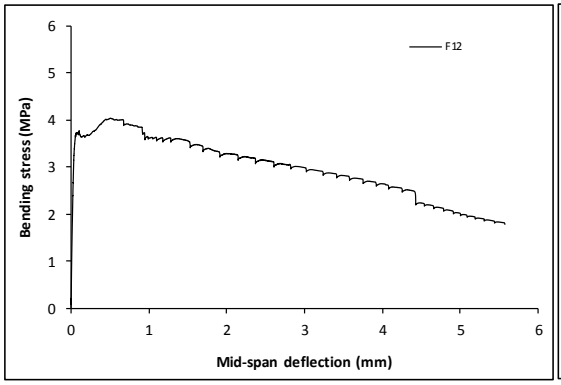

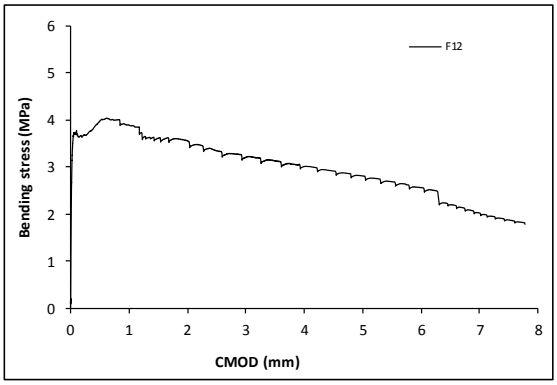

Mix:	**E (F)**	MSF1 (45)	
Notched Depth dn	mm		
Depth, d	mm	Span, L	mm
Width, b	mm	Flexural strength	MPa

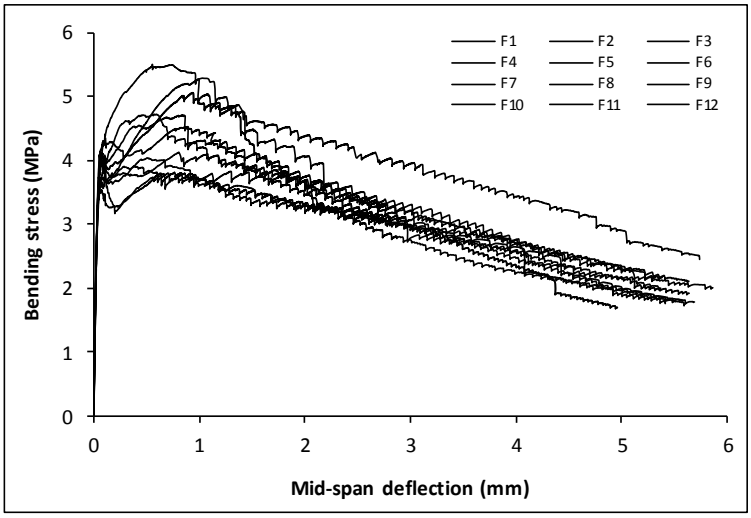

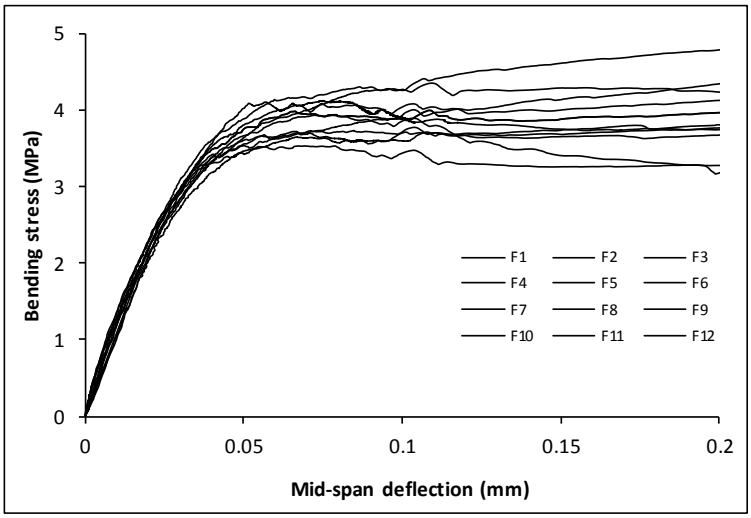

Specimen code name:		F1 (G1)	RTSC (22.5) + RTSF (22.5)		
Notched Depth dn	123.5	mm			
Depth, d	150	mm	Span, L	500	mm
Width, b	151	mm	Flexural strength	5.56	MPa

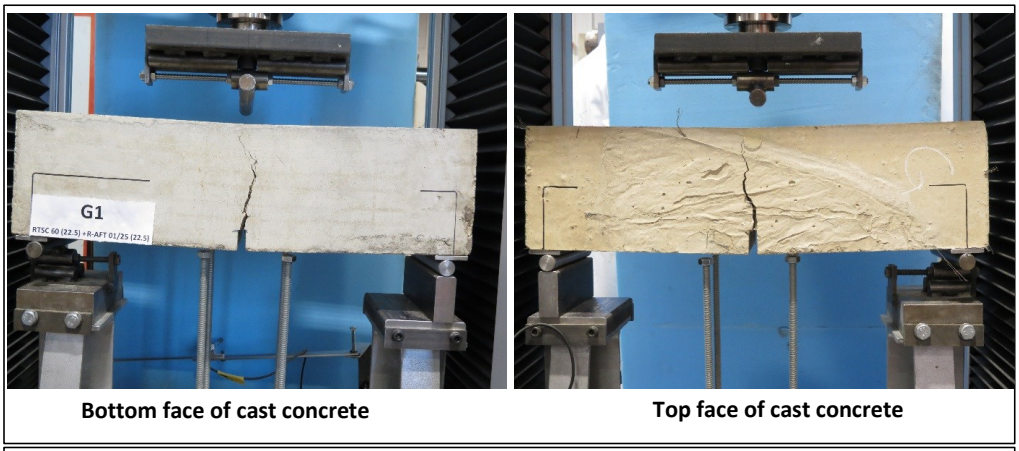

Bottom face of cast concrete | Top face of cast concrete

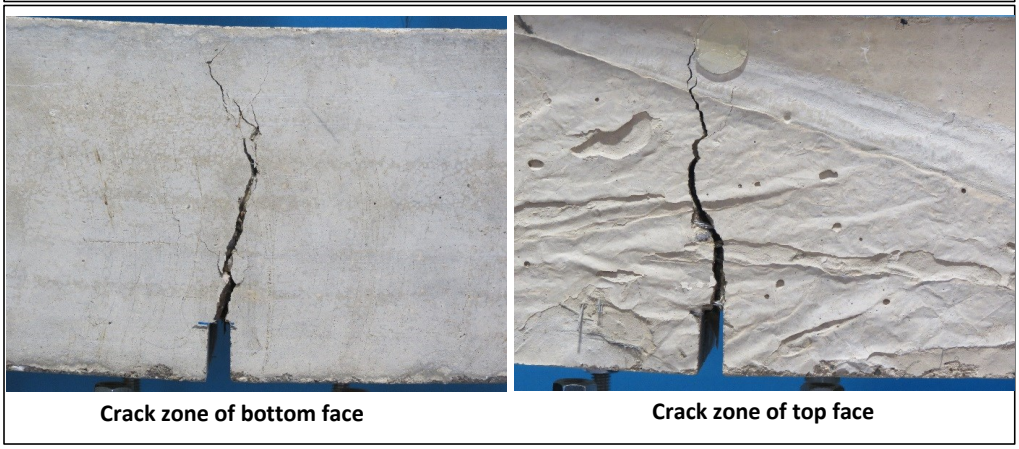

Crack zone of bottom face | Crack zone of top face

Stress-deformation graphs

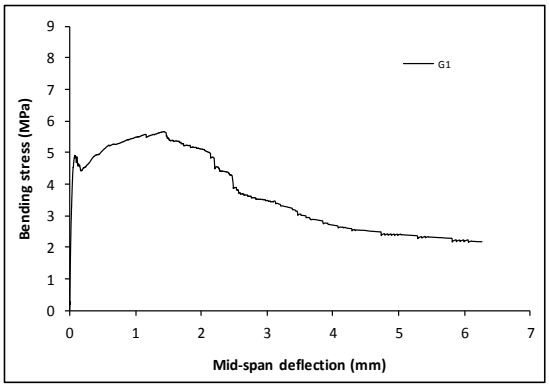

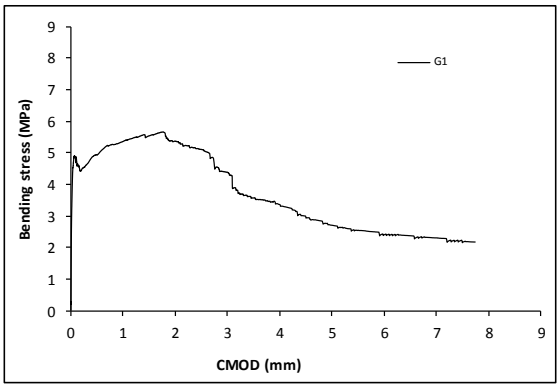

Specimen code name:		F2 (G2)	RTSC (22.5) + RTSF (22.5)		
Notched Depth dn	124	mm			
Depth, d	150	mm	Span, L	500	mm
Width, b	152	mm	Flexural strength	6.82	MPa

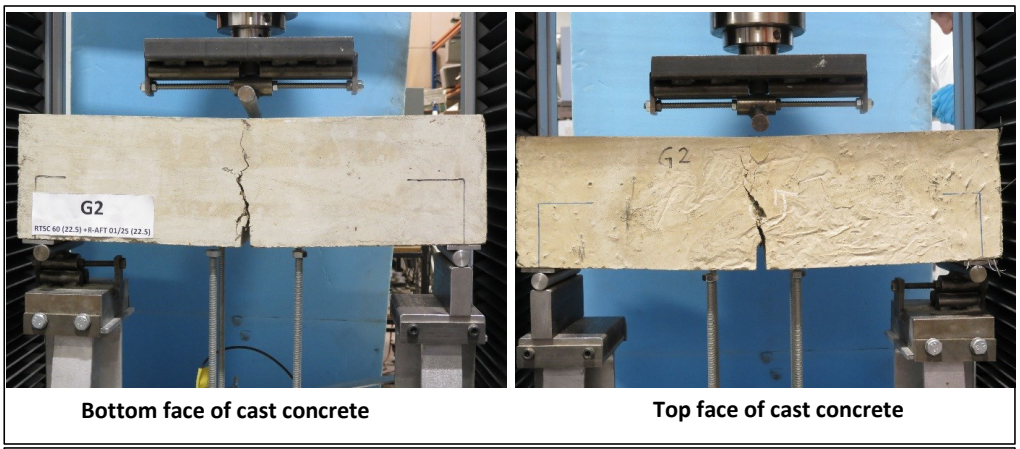

Bottom face of cast concrete | Top face of cast concrete

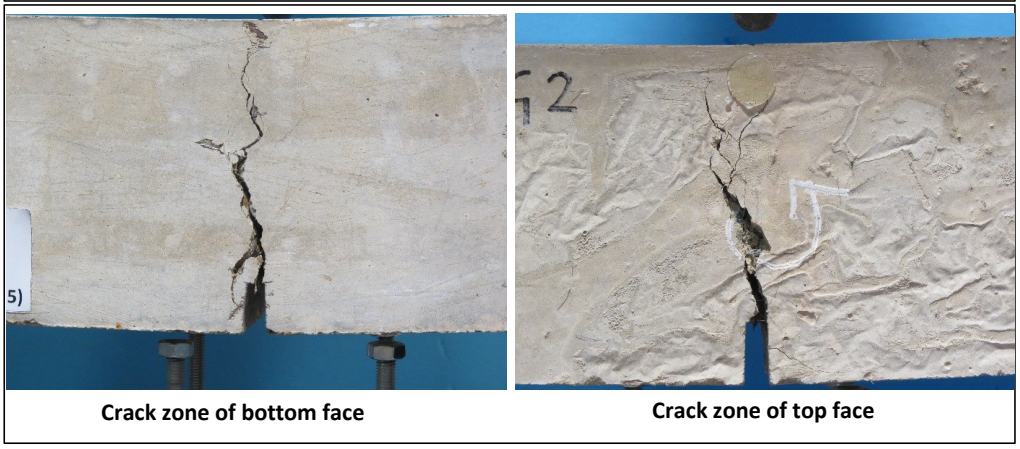

Crack zone of bottom face | Crack zone of top face

Stress-deformation graphs

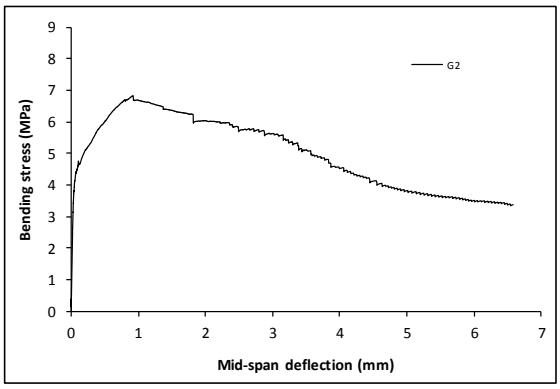

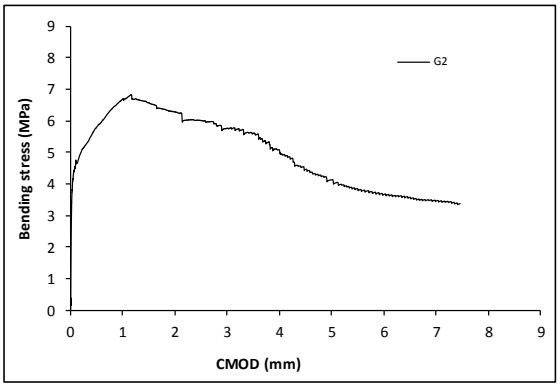

Specimen code name:		F3 (G3)	RTSC (22.5) + RTSF (22.5)		
Notched Depth dn	122.5	mm			
Depth, d	150.5	mm	Span, L	500	mm
Width, b	153	mm	Flexural strength	5.97	MPa

Bottom face of cast concrete

Top face of cast concrete

Crack zone of bottom face

Crack zone of top face

Stress-deformation graphs

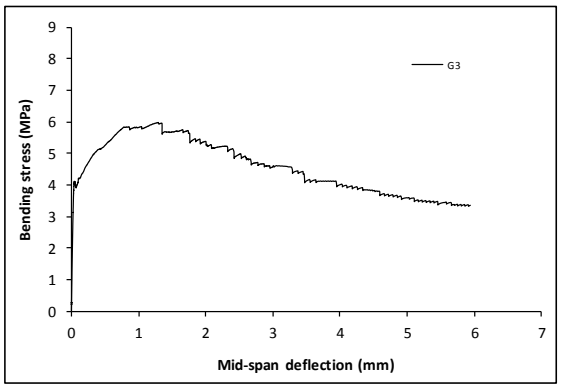

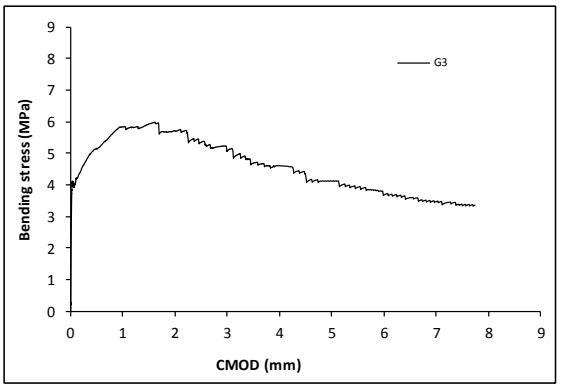

Specimen code name:		F4 (G4)	RTSC (22.5) + RTSF (22.5)		
Notched Depth dn	123.5	mm			
Depth, d	150	mm	Span, L	500	mm
Width, b	152	mm	Flexural strength	6.76	MPa

Bottom face of cast concrete

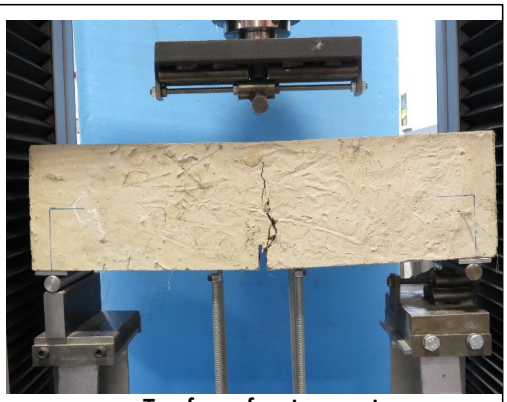

Top face of cast concrete

Crack zone of bottom face

Crack zone of top face

Stress-deformation graphs

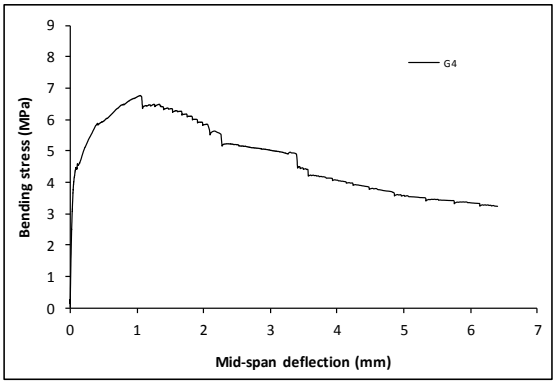

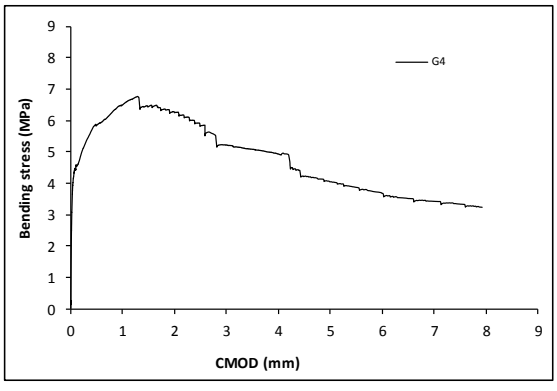

Specimen code name:		F5 (G5)	RTSC (22.5) + RTSF (22.5)		
Notched Depth dn	123.5	mm			
Depth, d	150	mm	Span, L	500	mm
Width, b	150.5	mm	Flexural strength	6.91	MPa

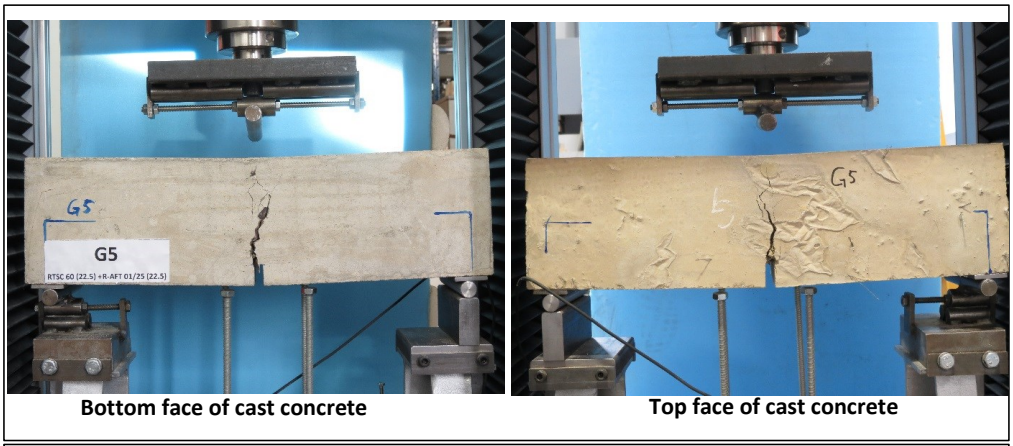

Bottom face of cast concrete | Top face of cast concrete

Crack zone of bottom face | Crack zone of top face

Stress-deformation graphs

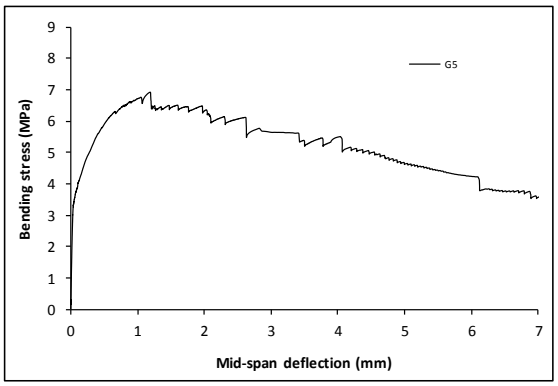

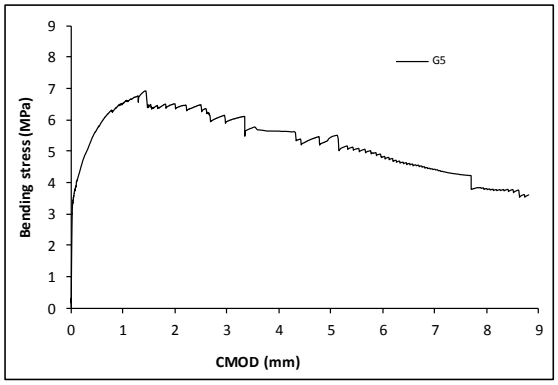

Specimen code name:		F6 (G6)	RTSC (22.5) + RTSF (22.5)		
Notched Depth dn	123.5	mm			
Depth, d	150	mm	Span, L	500	mm
Width, b	152	mm	Flexural strength	7.46	MPa

Bottom face of cast concrete

Top face of cast concrete

Crack zone of bottom face

Crack zone of top face

Stress-deformation graphs

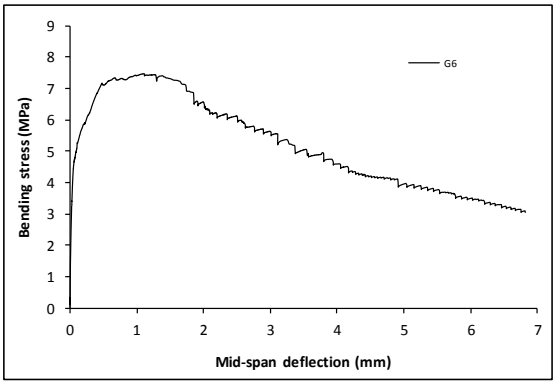

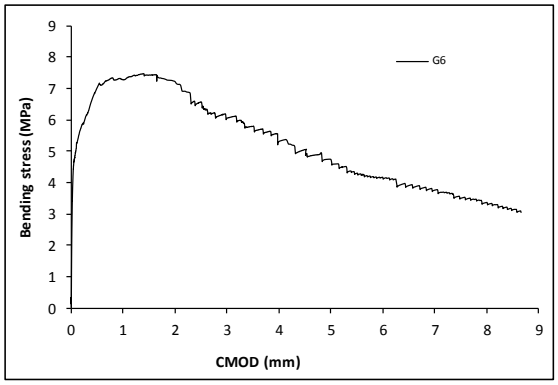

Specimen code name:		F7 (G7)	RTSC (22.5) + RTSF (22.5)		
Notched Depth dn	124.5	mm			
Depth, d	150	mm	Span, L	500	mm
Width, b	151.75	mm	Flexural strength	6.41	MPa

Bottom face of cast concrete

Top face of cast concrete

Crack zone of bottom face

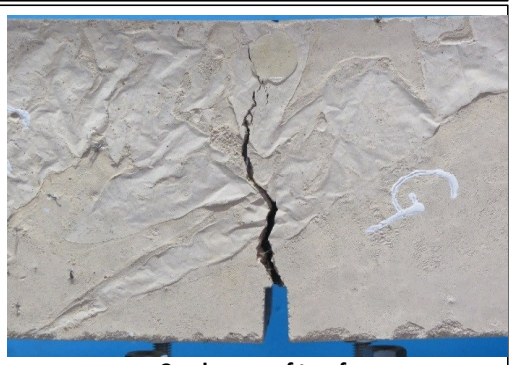

Crack zone of top face

Stress-deformation graphs

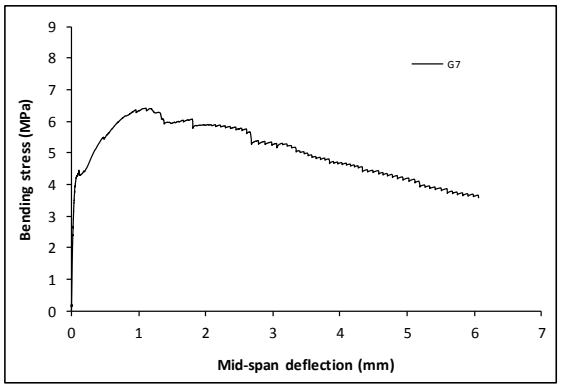

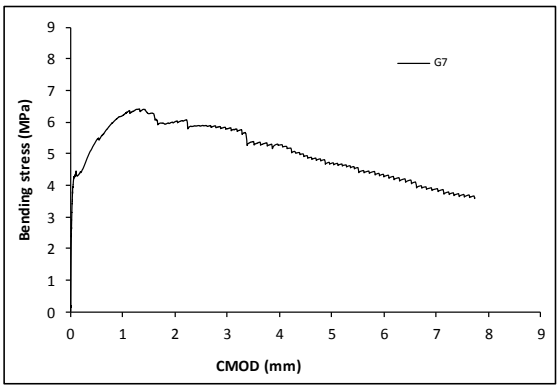

Specimen code name:		F8 (G8)	RTSC (22.5) + RTSF (22.5)		
Notched Depth dn	124	mm			
Depth, d	150	mm	Span, L	500	mm
Width, b	150.25	mm	Flexural strength	7.80	MPa

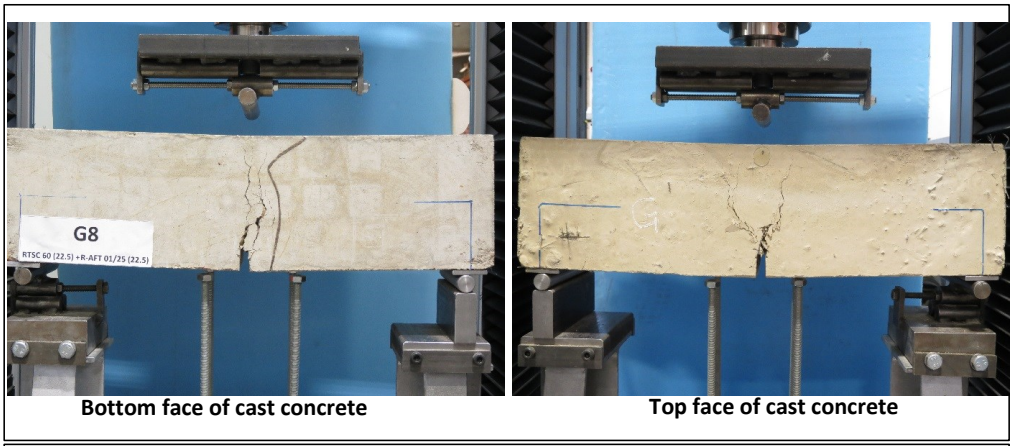

Bottom face of cast concrete | Top face of cast concrete

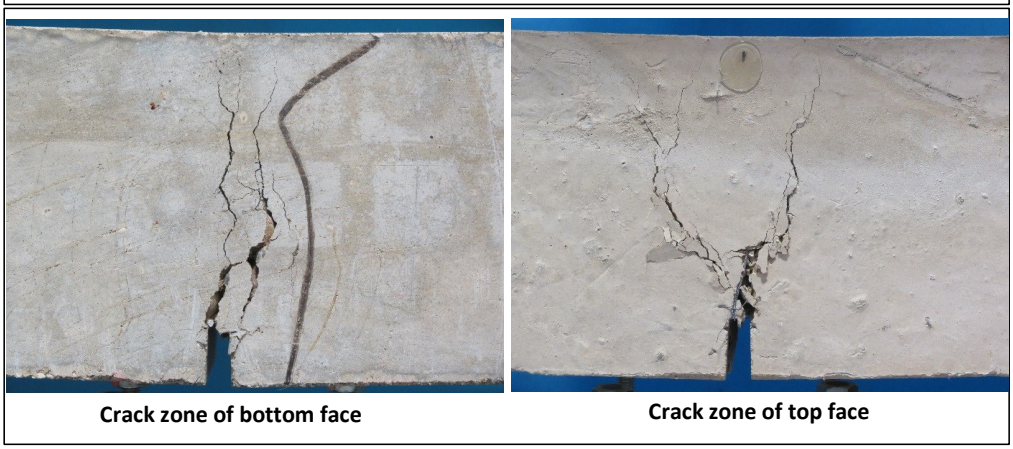

Crack zone of bottom face | Crack zone of top face

Stress-deformation graphs

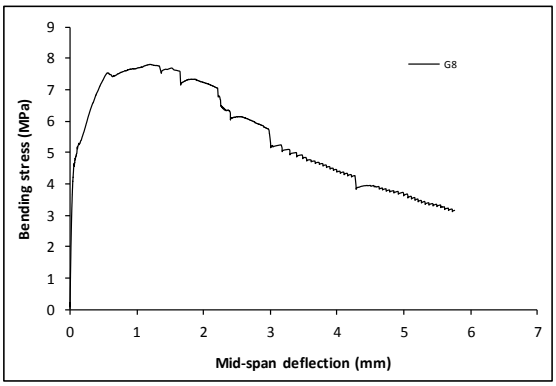

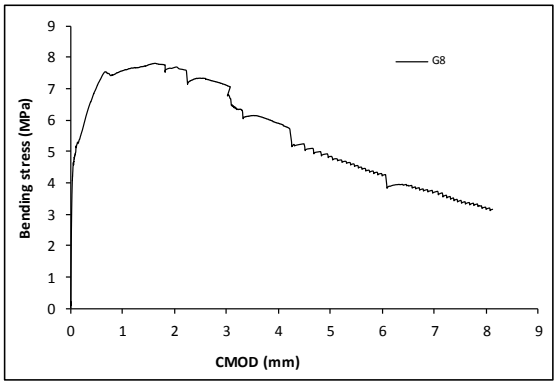

Specimen code name:		F9 (G9)	RTSC (22.5) + RTSF (22.5)		
Notched Depth dn	126.25	mm			
Depth, d	150	mm	Span, L	500	mm
Width, b	151	mm	Flexural strength	5.25	MPa

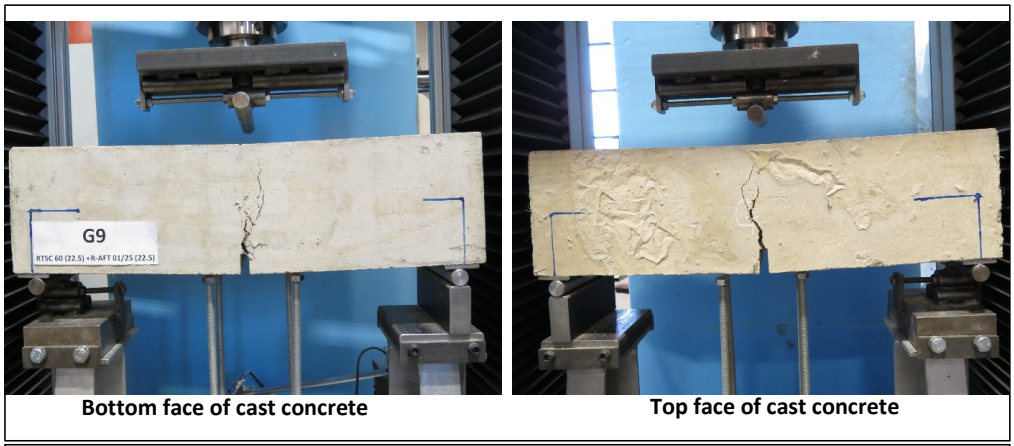

Bottom face of cast concrete | Top face of cast concrete

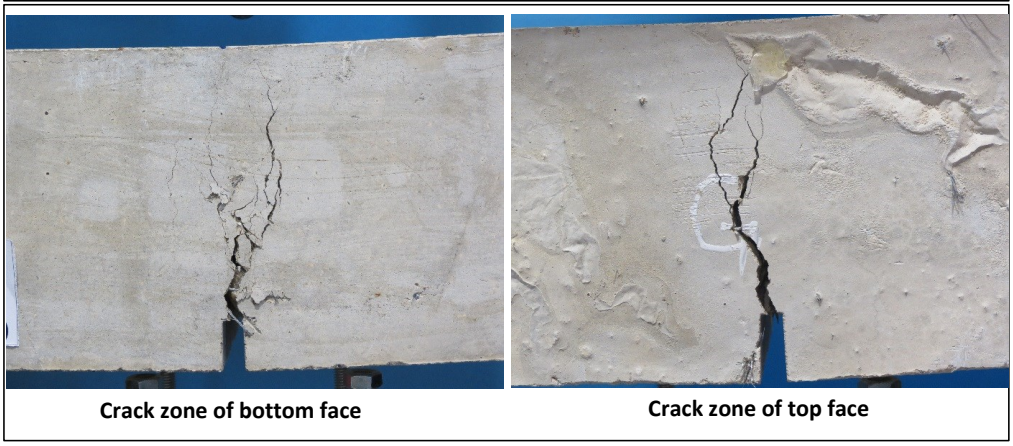

Crack zone of bottom face | Crack zone of top face

Stress-deformation graphs

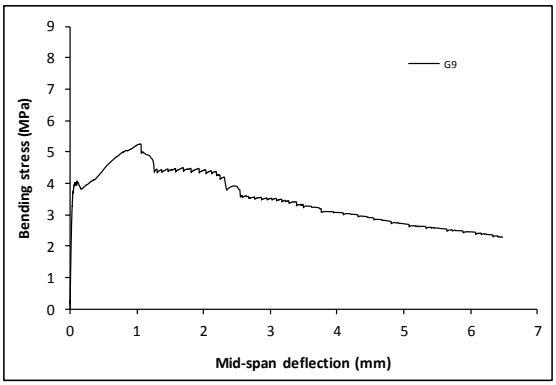

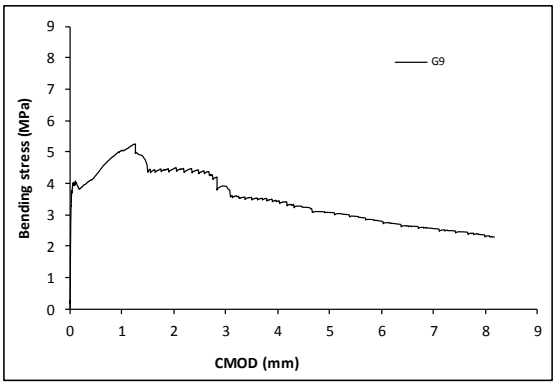

Specimen code name:		F10 (G10)	RTSC (22.5) + RTSF (22.5)		
Notched Depth dn	123	mm			
Depth, d	150	mm	Span, L	500	mm
Width, b	152.5	mm	Flexural strength	8.29	MPa

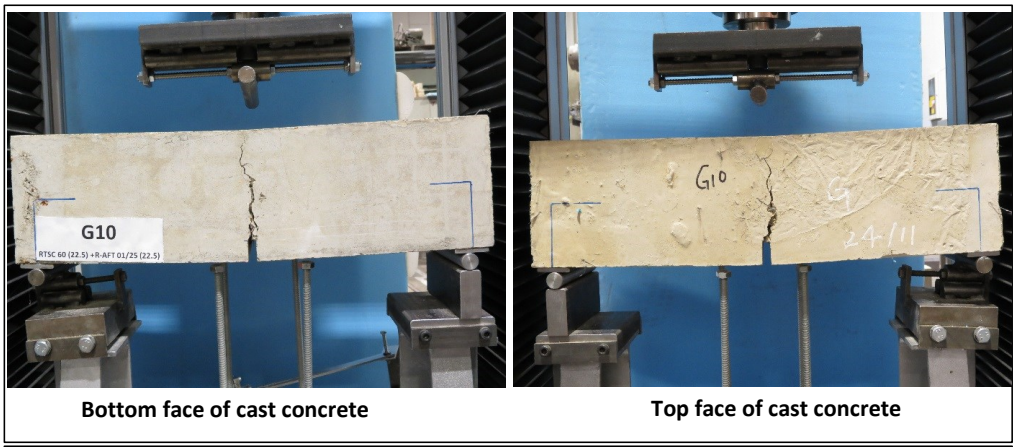

Bottom face of cast concrete | Top face of cast concrete

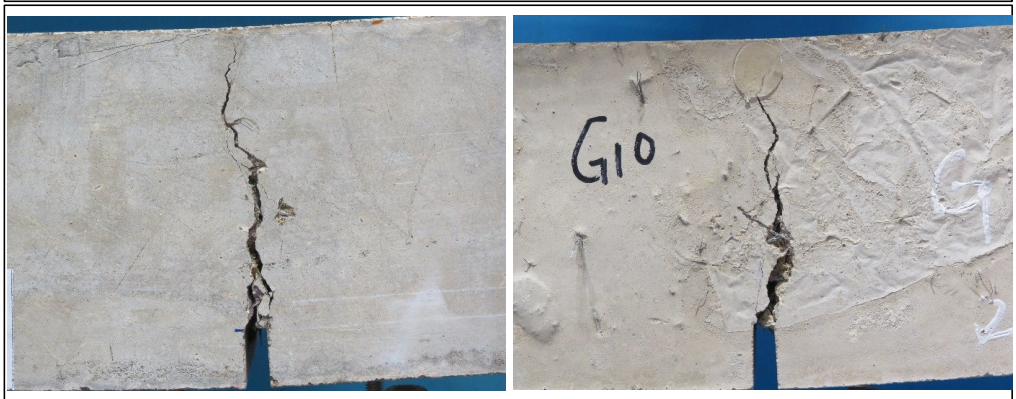

Crack zone of bottom face | Crack zone of top face

Stress-deformation graphs

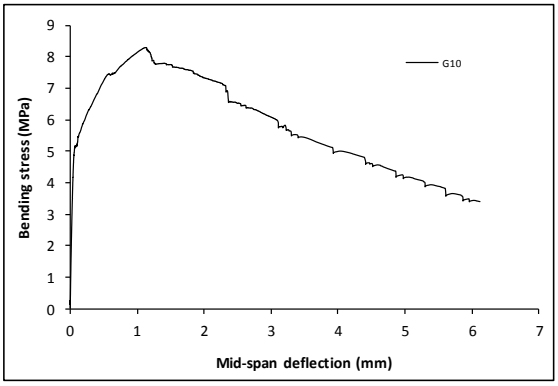

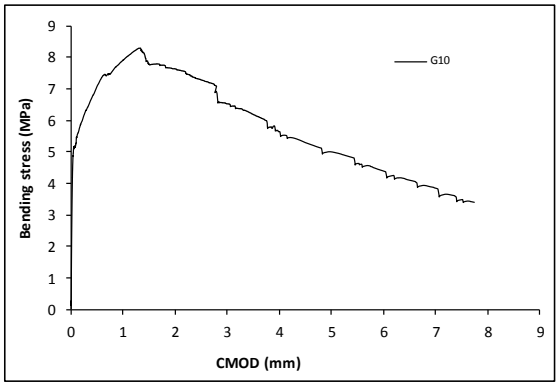

Specimen code name:		F11 (G11)	RTSC (22.5) + RTSF (22.5)		
Notched Depth dn	124	mm			
Depth, d	149.5	mm	Span, L	500	mm
Width, b	153.25	mm	Flexural strength	5.67	MPa

Bottom face of cast concrete

Top face of cast concrete

Crack zone of bottom face

Crack zone of top face

Stress-deformation graphs

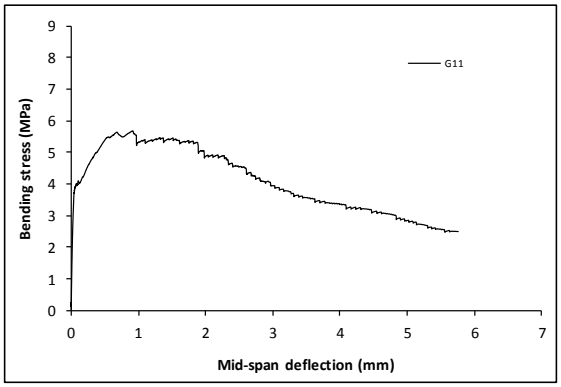

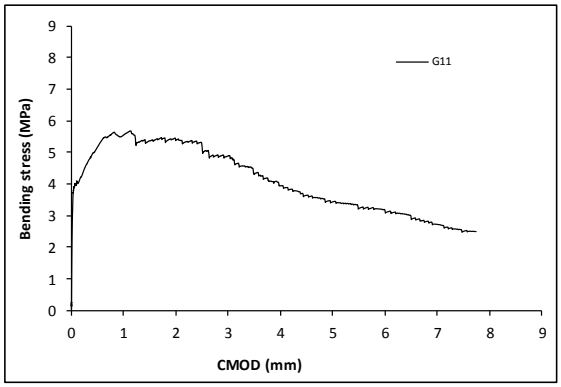

Specimen code name:		F12 (G12)	RTSC (22.5) + RTSF (22.5)		
Notched Depth dn	123.5	mm			
Depth, d	151	mm	Span, L	500	mm
Width, b	151.75	mm	Flexural strength	6.47	MPa

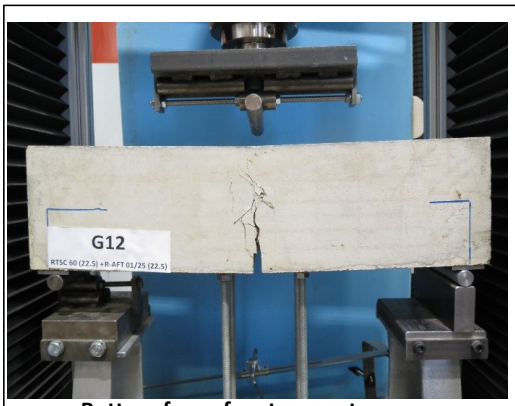

Bottom face of cast concrete

Top face of cast concrete

Crack zone of bottom face

Crack zone of top face

Stress-deformation graphs

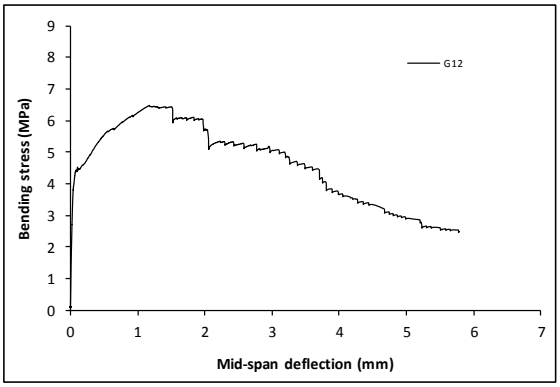

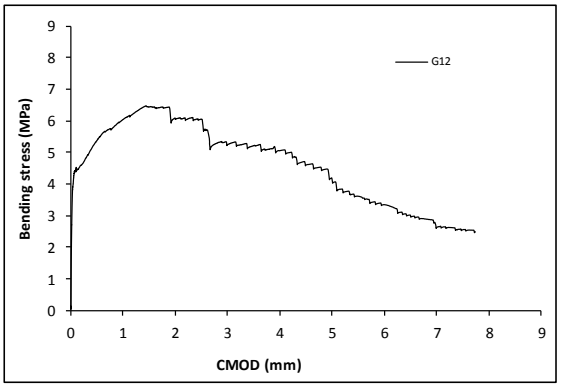

Mix:	**F (G)**	RTSC (22.5) + RTSF (22.5)	
Notched Depth dn	mm		
Depth, d	mm	Span, L	mm
Width, b	mm	Flexural strength	MPa

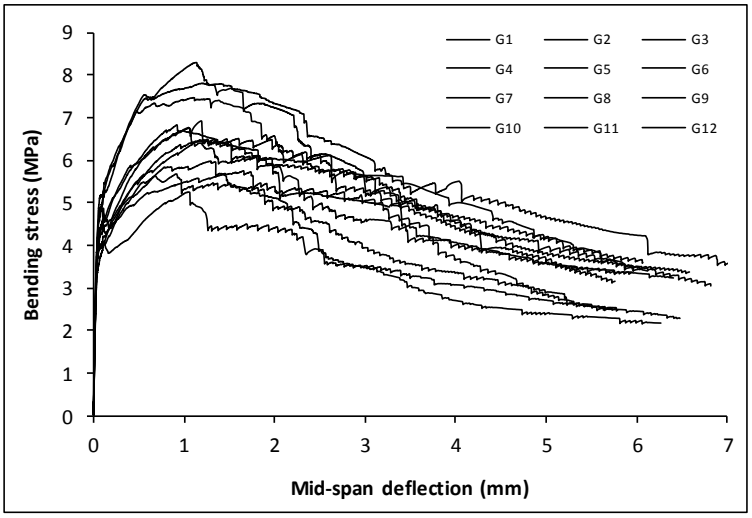

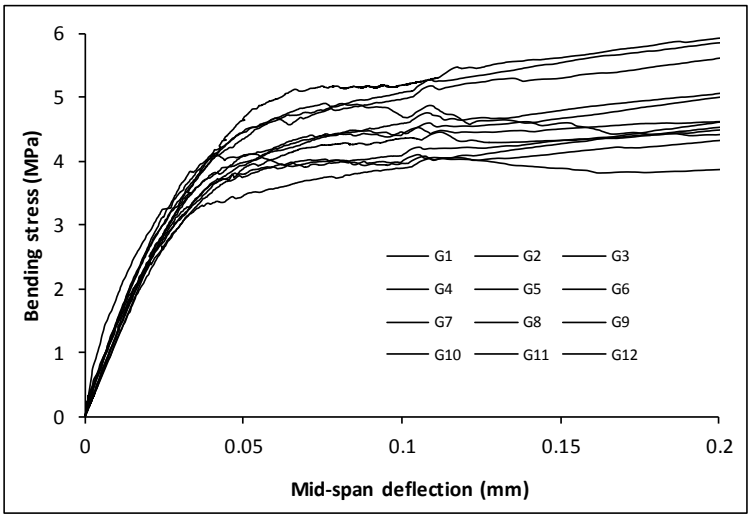

Specimen code name:		G1 (H1)	RTSC (35) + RTSF (10)		
Notched Depth dn	123	mm			
Depth, d	150	mm	Span, L	500	mm
Width, b	152.25	mm	Flexural strength	5.90	MPa

Bottom face of cast concrete

Top face of cast concrete

Crack zone of bottom face

Crack zone of top face

Stress-deformation graphs

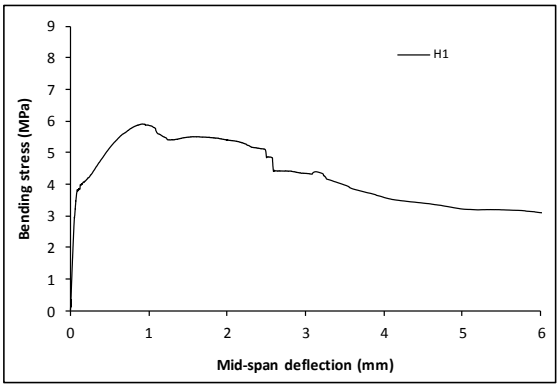

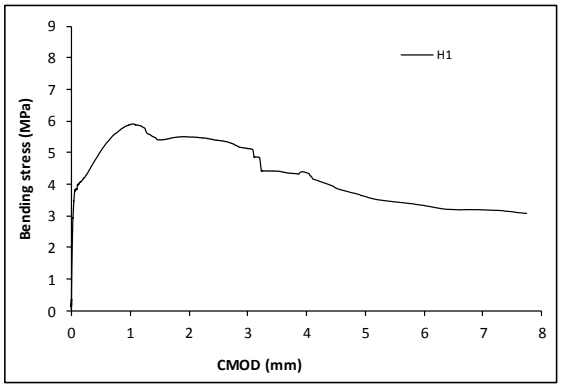

Specimen code name:		G2 (H2)	RTSC (35) + RTSF (10)		
Notched Depth dn	123.25	mm			
Depth, d	150	mm	Span, L	500	mm
Width, b	151	mm	Flexural strength	7.23	MPa

Bottom face of cast concrete

Top face of cast concrete

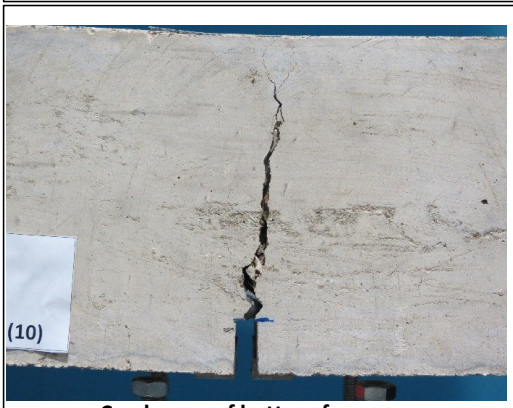

Crack zone of bottom face

Crack zone of top face

Stress-deformation graphs

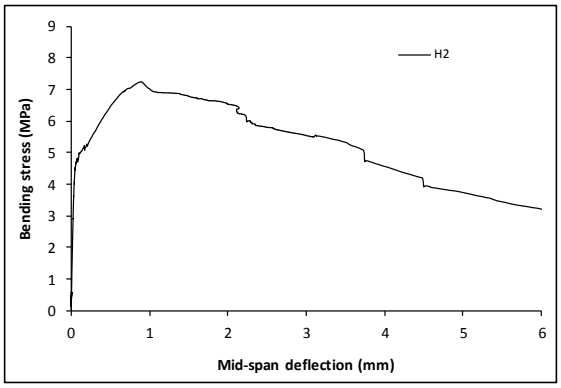

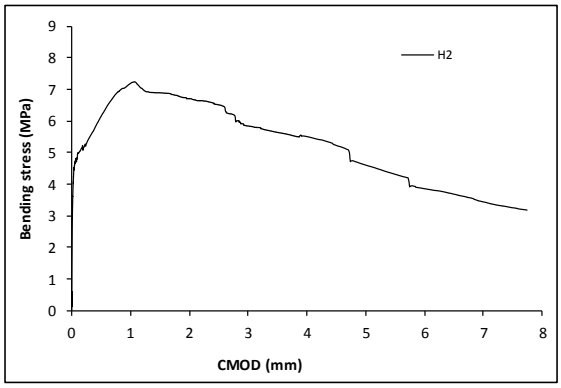

Specimen code name:		G3 (H3)	RTSC (35) + RTSF (10)		
Notched Depth dn	124.75	mm			
Depth, d	150	mm	Span, L	500	mm
Width, b	154.5	mm	Flexural strength	6.65	MPa

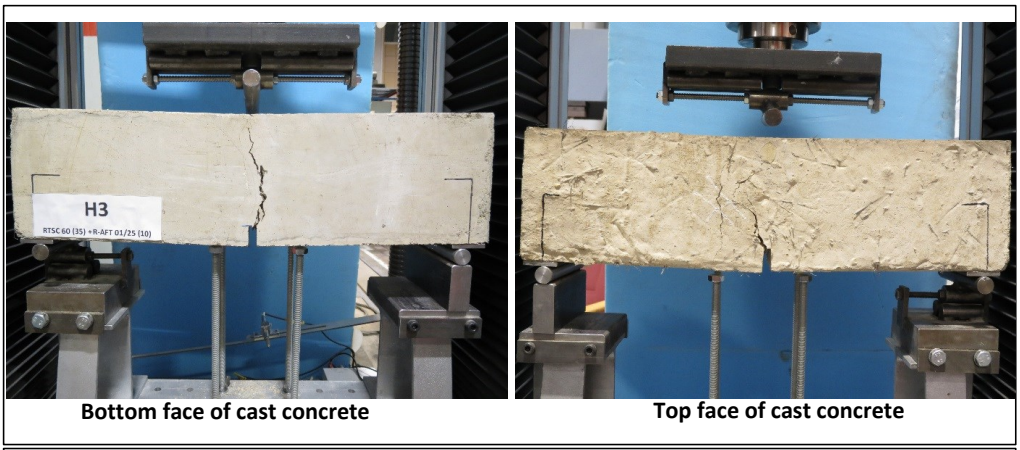

Bottom face of cast concrete

Top face of cast concrete

Crack zone of bottom face

Crack zone of top face

Stress-deformation graphs

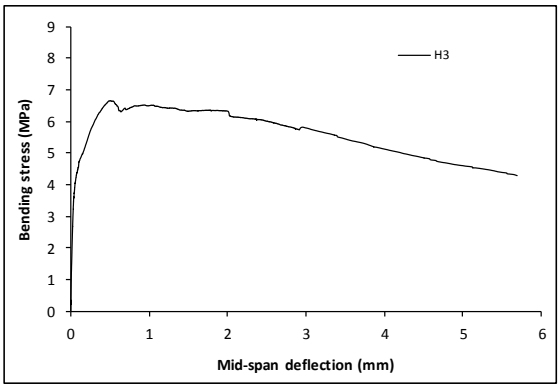

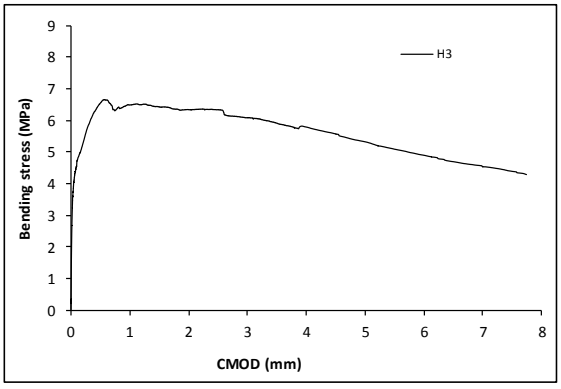

Specimen code name:		G4 (H4)	RTSC (35) + RTSF (10)		
Notched Depth dn	125	mm			
Depth, d	150	mm	Span, L	500	mm
Width, b	153.5	mm	Flexural strength	3.92	MPa

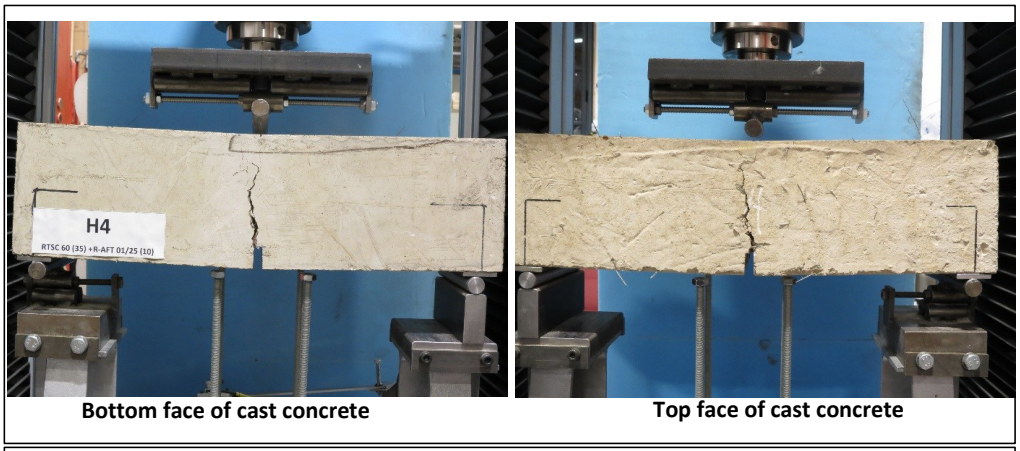

Bottom face of cast concrete | Top face of cast concrete

Crack zone of bottom face | Crack zone of top face

Stress-deformation graphs

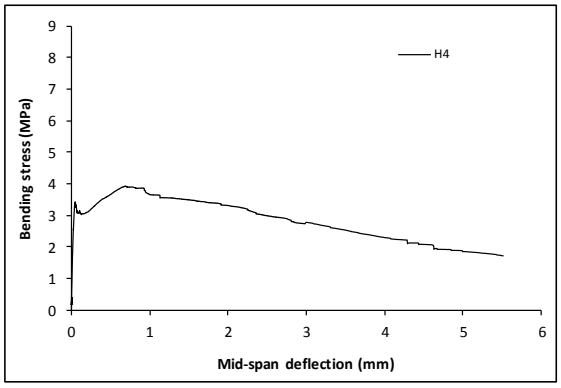

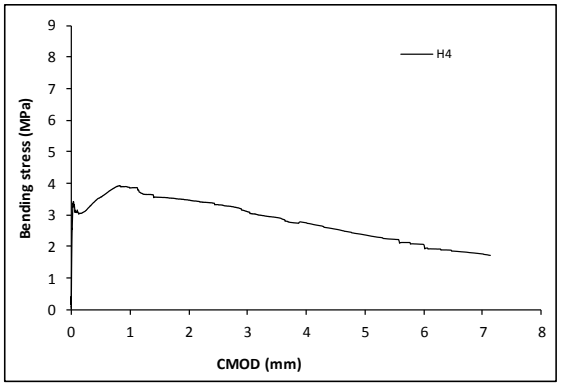

Specimen code name:		G5 (H5)	RTSC (35) + RTSF (10)		
Notched Depth dn	125	mm			
Depth, d	150.5	mm	Span, L	500	mm
Width, b	153.5	mm	Flexural strength	6.57	MPa

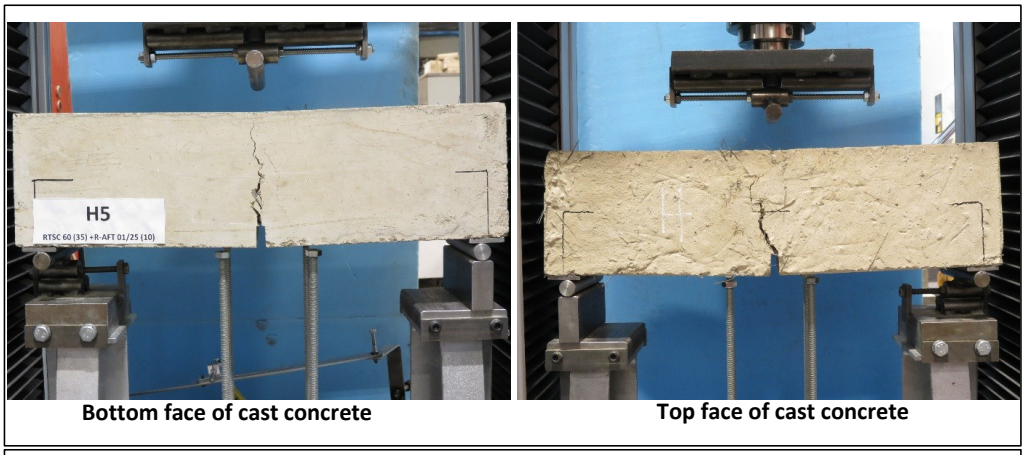

Bottom face of cast concrete | Top face of cast concrete

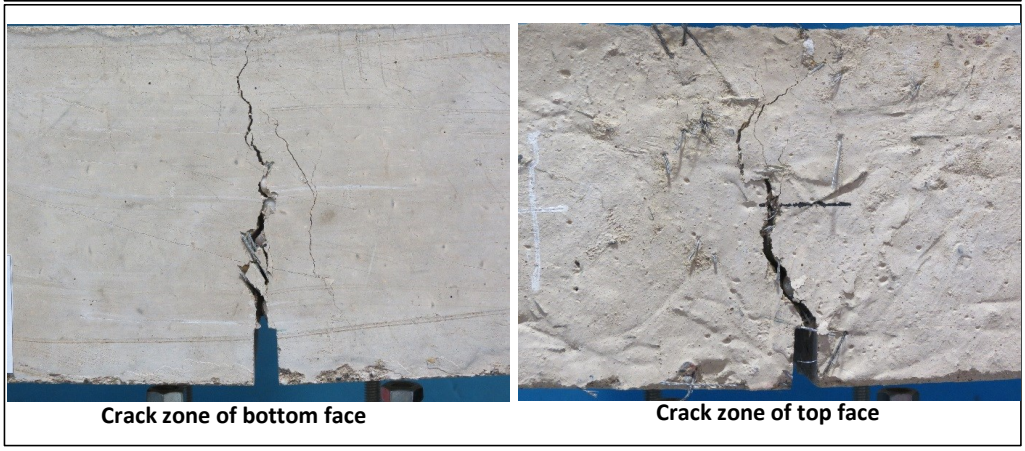

Crack zone of bottom face | Crack zone of top face

Stress-deformation graphs

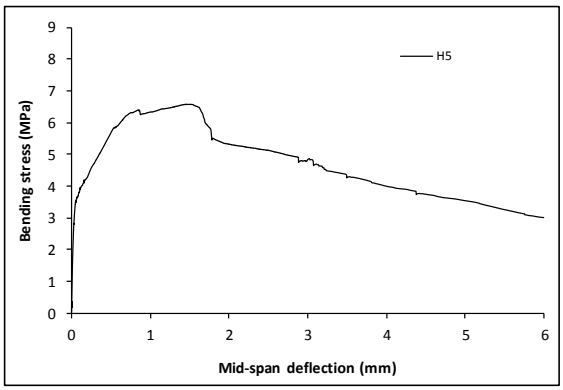

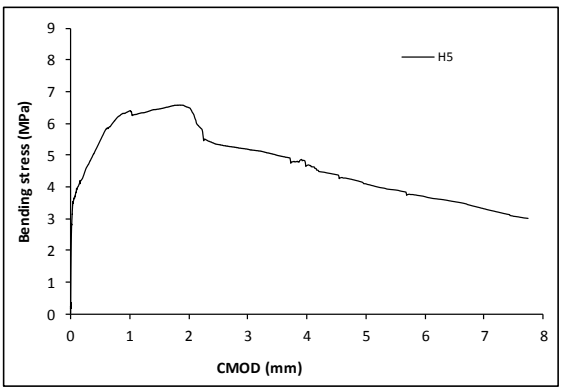

Specimen code name:		G6 (H6)	RTSC (35) + RTSF (10)		
Notched Depth dn	124.5	mm			
Depth, d	150.25	mm	Span, L	500	mm
Width, b	153.5	mm	Flexural strength	7.49	MPa

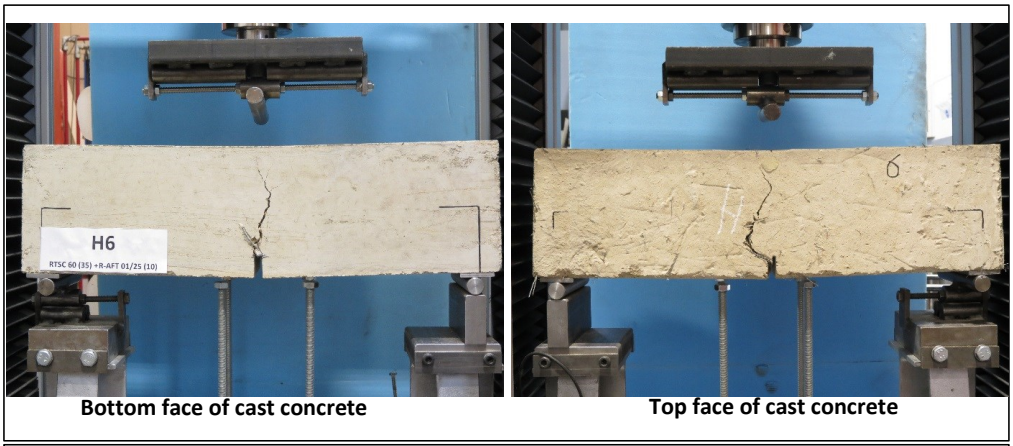

Bottom face of cast concrete | Top face of cast concrete

Crack zone of bottom face | Crack zone of top face

Stress-deformation graphs

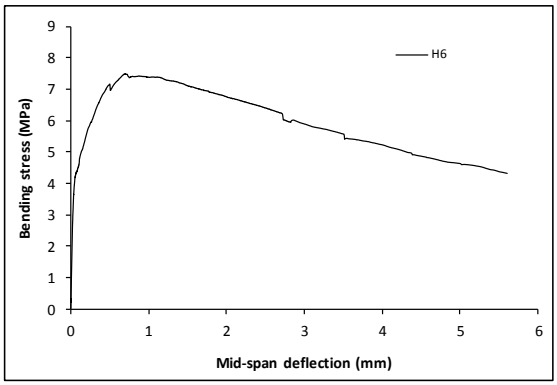

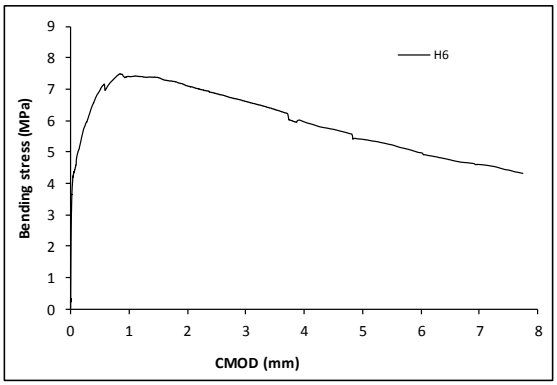

Specimen code name:		G7 (H7)	RTSC (35) + RTSF (10)		
Notched Depth dn	125.5	mm			
Depth, d	150	mm	Span, L	500	mm
Width, b	155	mm	Flexural strength	7.84	MPa

Bottom face of cast concrete

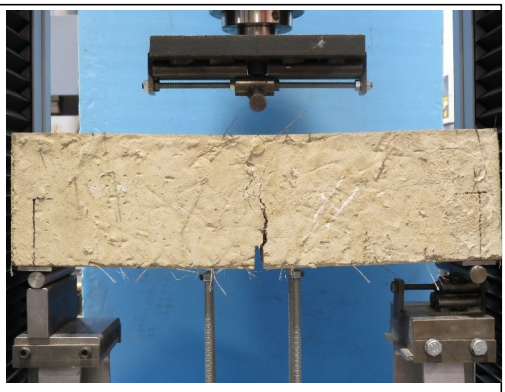

Top face of cast concrete

Crack zone of bottom face

Crack zone of top face

Stress-deformation graphs

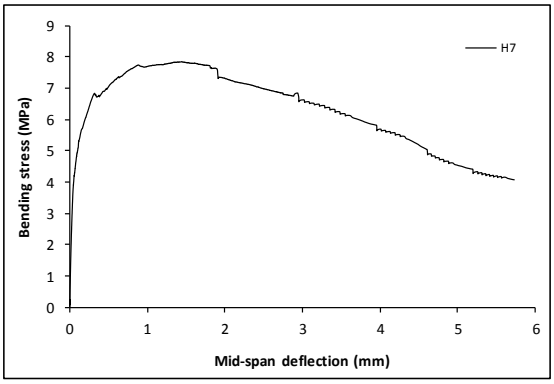

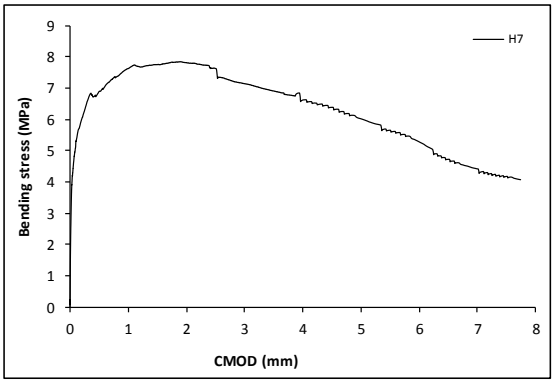

Specimen code name:		G8 (H8)	RTSC (35) + RTSF (10)		
Notched Depth dn	124.5	mm			
Depth, d	150	mm	Span, L	500	mm
Width, b	155.25	mm	Flexural strength	8.05	MPa

Bottom face of cast concrete

Top face of cast concrete

Crack zone of bottom face

Crack zone of top face

Stress-deformation graphs

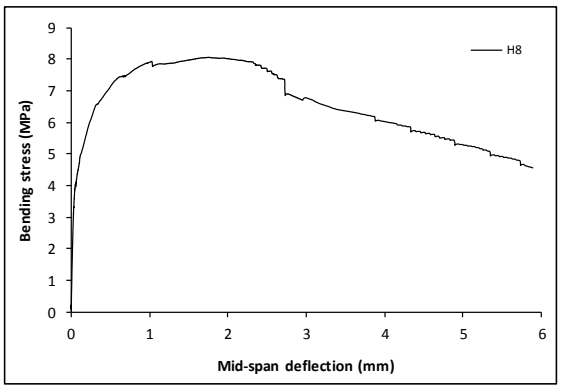

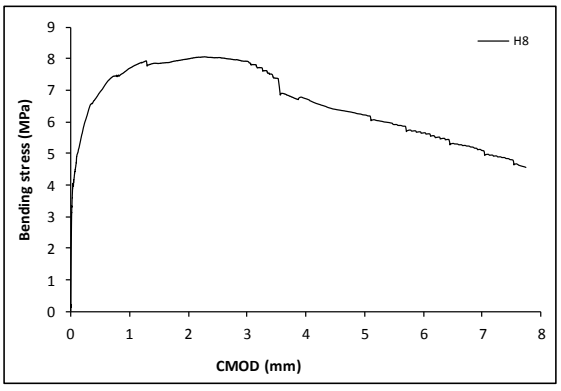

Specimen code name:		G9 (H9)	RTSC (35) + RTSF (10)		
Notched Depth dn	124	mm			
Depth, d	151	mm	Span, L	500	mm
Width, b	153	mm	Flexural strength	8.02	MPa

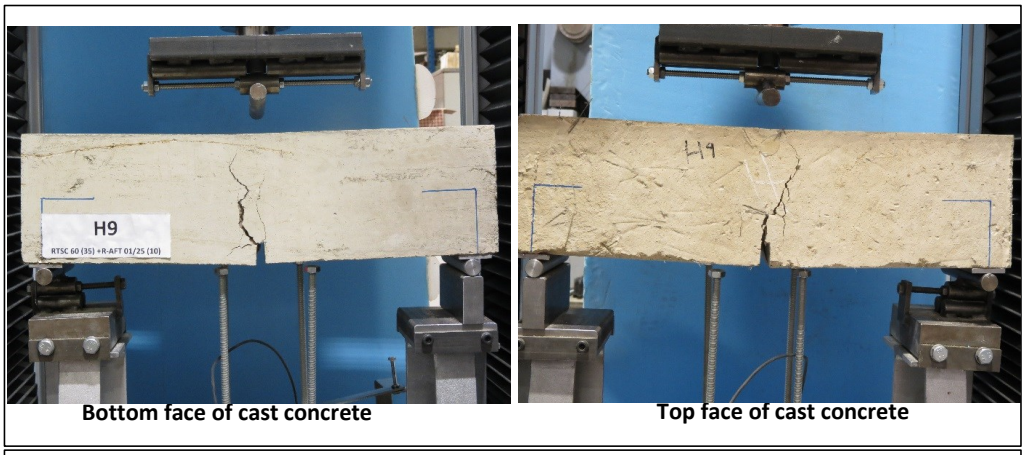

Bottom face of cast concrete

Top face of cast concrete

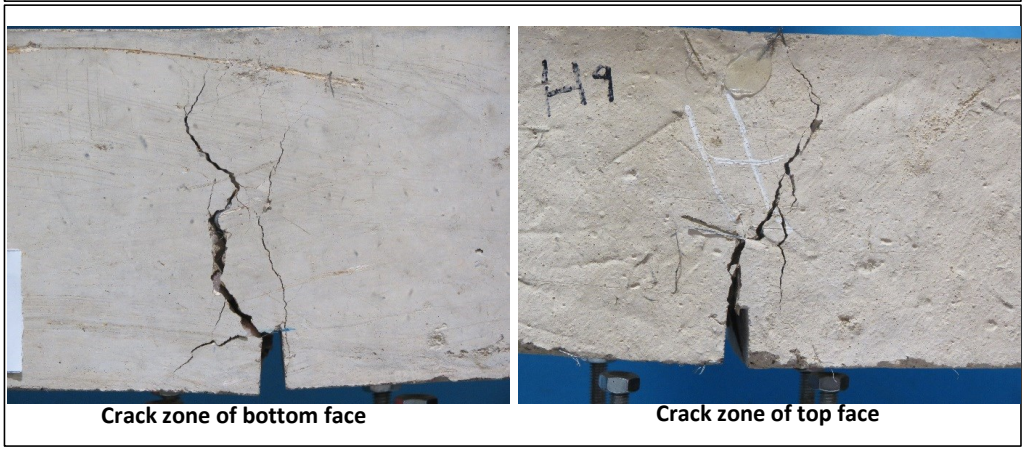

Crack zone of bottom face

Crack zone of top face

Stress-deformation graphs

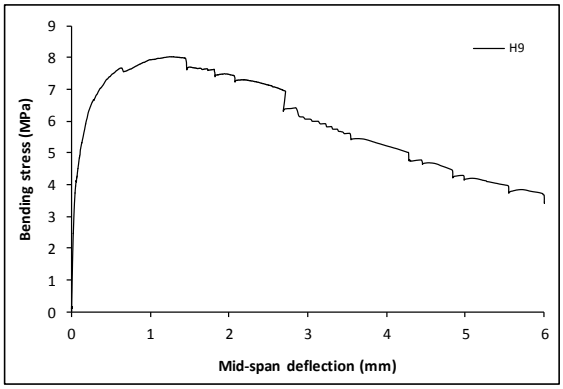

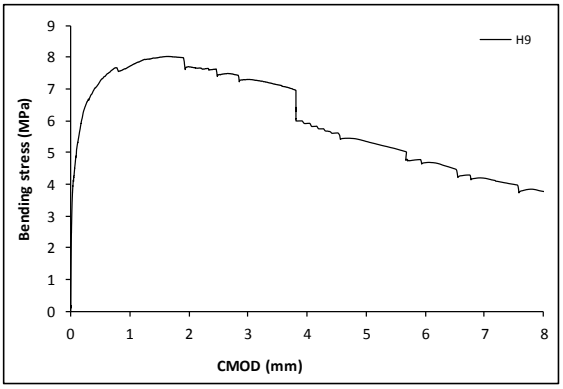

Specimen code name:		G10 (H10)	RTSC (35) + RTSF (10)		
Notched Depth dn	123.5	mm			
Depth, d	150	mm	Span, L	500	mm
Width, b	156	mm	Flexural strength	7.54	MPa

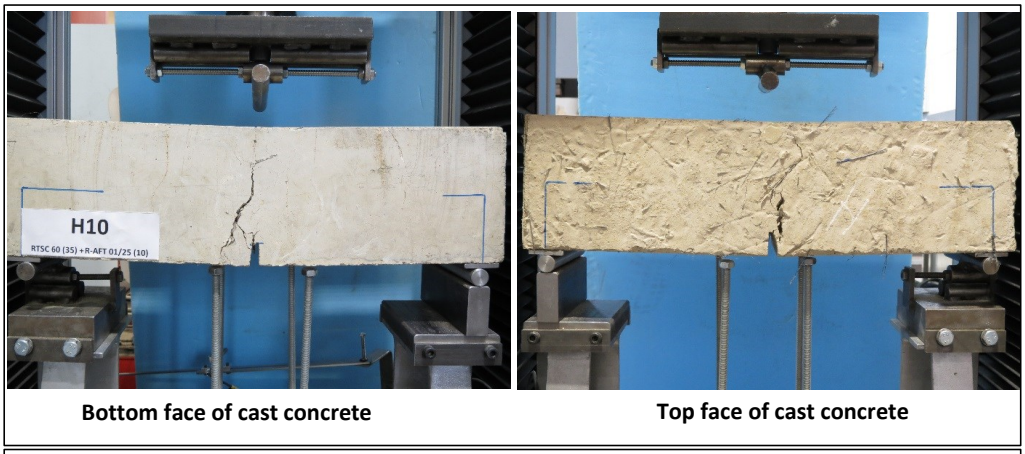

Bottom face of cast concrete | Top face of cast concrete

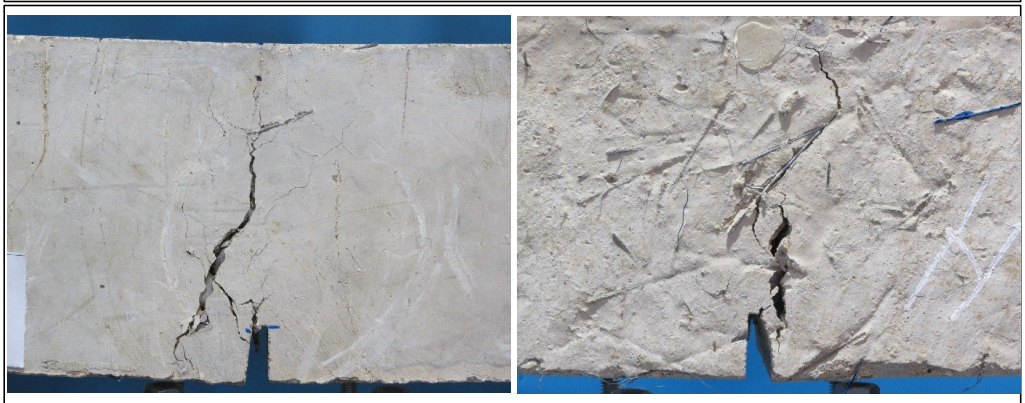

Crack zone of bottom face | Crack zone of top face

Stress-deformation graphs

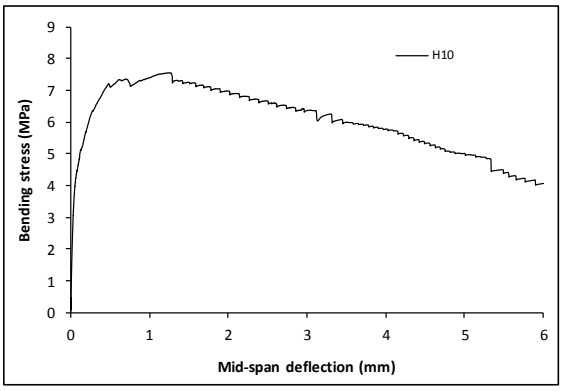

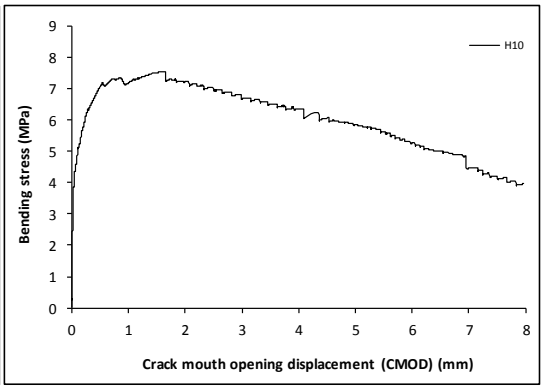

Specimen code name:		G11 (H11)	RTSC (35) + RTSF (10)		
Notched Depth dn	124.5	mm			
Depth, d	150	mm	Span, L	500	mm
Width, b	152	mm	Flexural strength	7.92	MPa

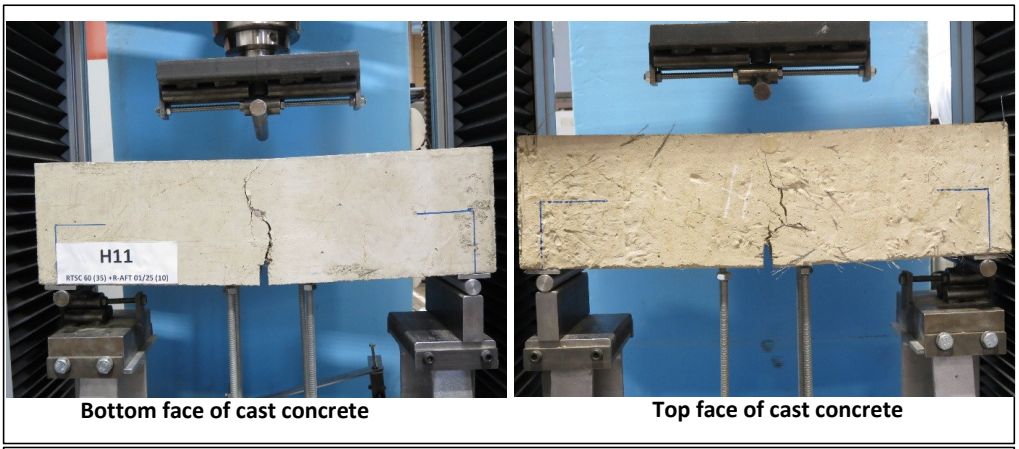

Bottom face of cast concrete | Top face of cast concrete

Crack zone of bottom face | Crack zone of top face

Stress-deformation graphs

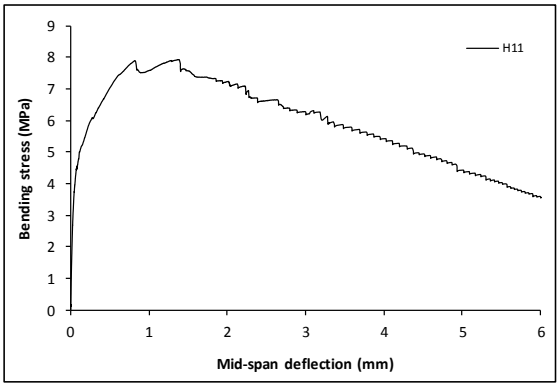

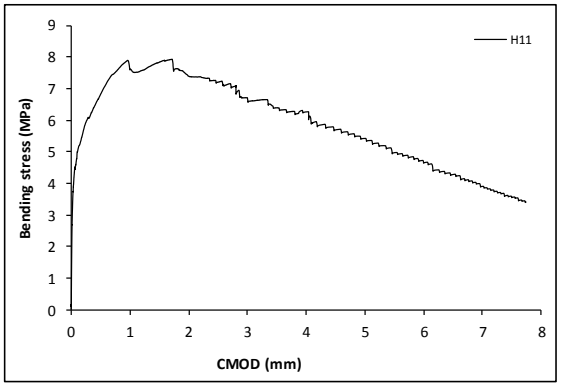

Specimen code name:		G12 (H12)	RTSC (35) + RTSF (10)		
Notched Depth dn	126	mm			
Depth, d	150	mm	Span, L	500	mm
Width, b	152.25	mm	Flexural strength	5.74	MPa

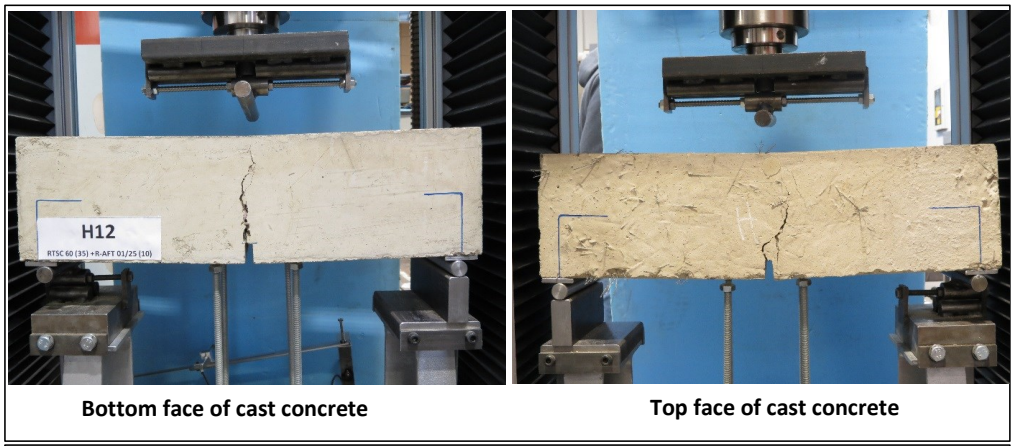

Bottom face of cast concrete | Top face of cast concrete

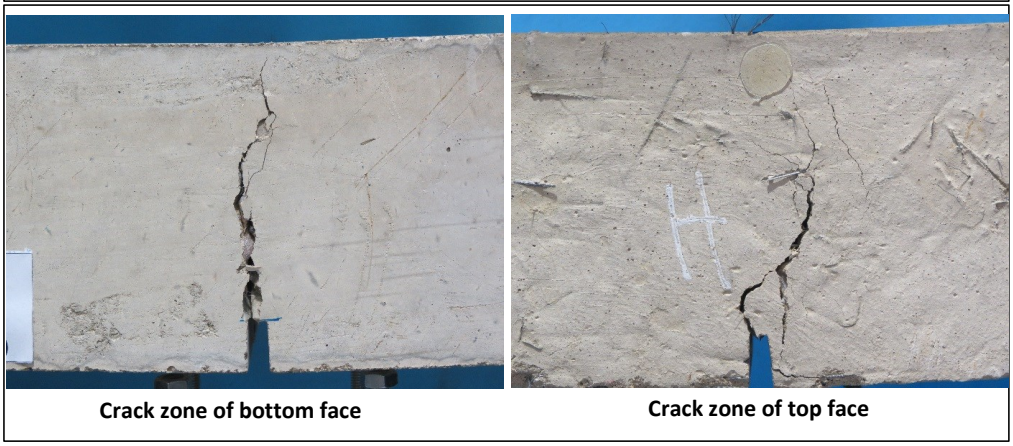

Crack zone of bottom face | Crack zone of top face

Stress-deformation graphs

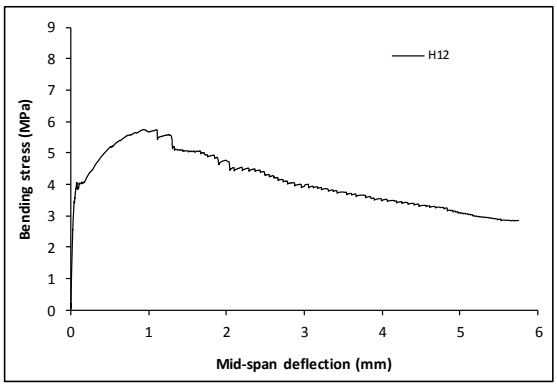

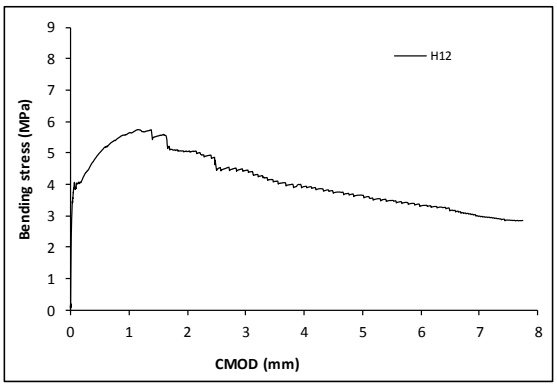

Mix:	G (H)	RTSC (35) + RTSF (10)	
Notched Depth dn	mm		
Depth, d	mm	Span, L	mm
Width, b	mm	Flexural strength	MPa

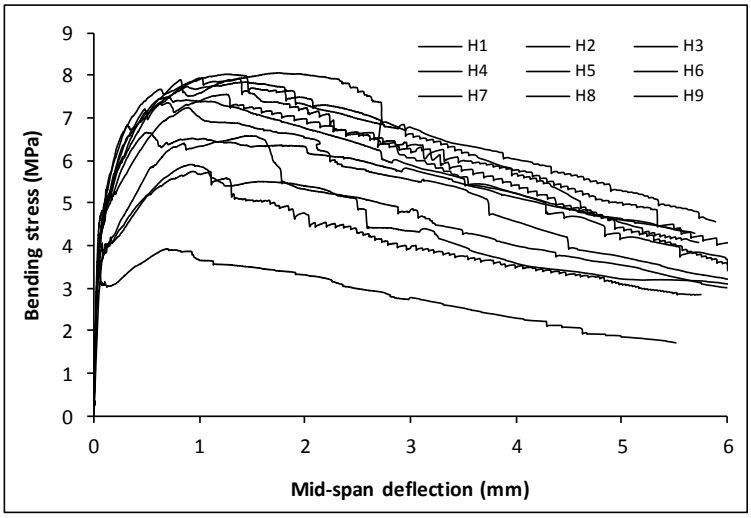

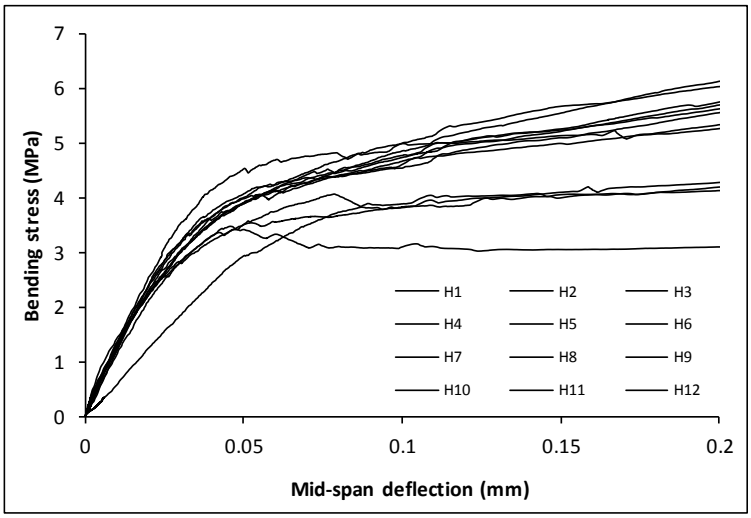

Specimen code name:		H1 (E1)	RTSC (45)		
Notched Depth dn	125.5	mm			
Depth, d	150	mm	Span, L	500	mm
Width, b	153.5	mm	Flexural strength	7.37	MPa

Bottom face of cast concrete

Top face of cast concrete

Crack zone of bottom face

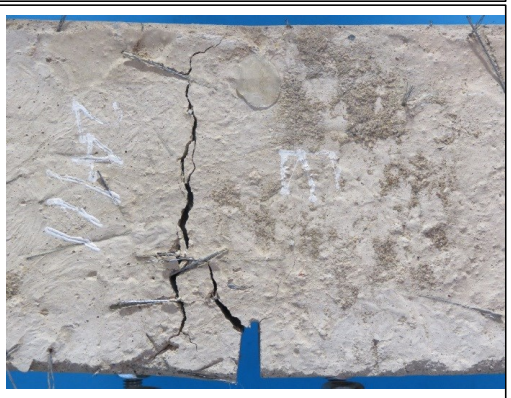

Crack zone of top face

Stress-deformation graphs

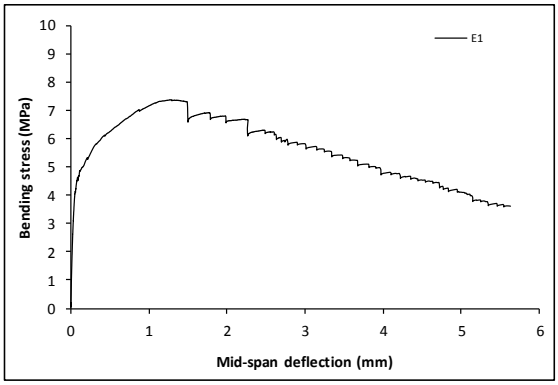

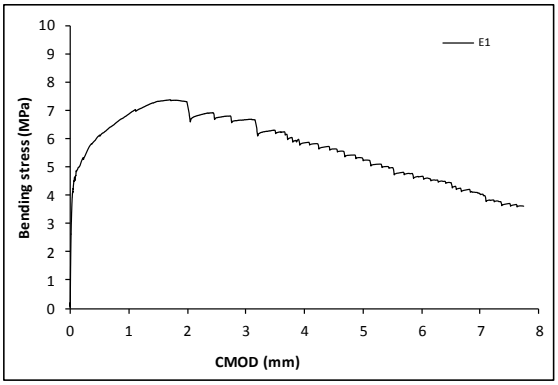

Specimen code name:		H2 (E2)	RTSC (45)		
Notched Depth dn	127.25	mm			
Depth, d	150.25	mm	Span, L	500	mm
Width, b	153.25	mm	Flexural strength	8.16	MPa

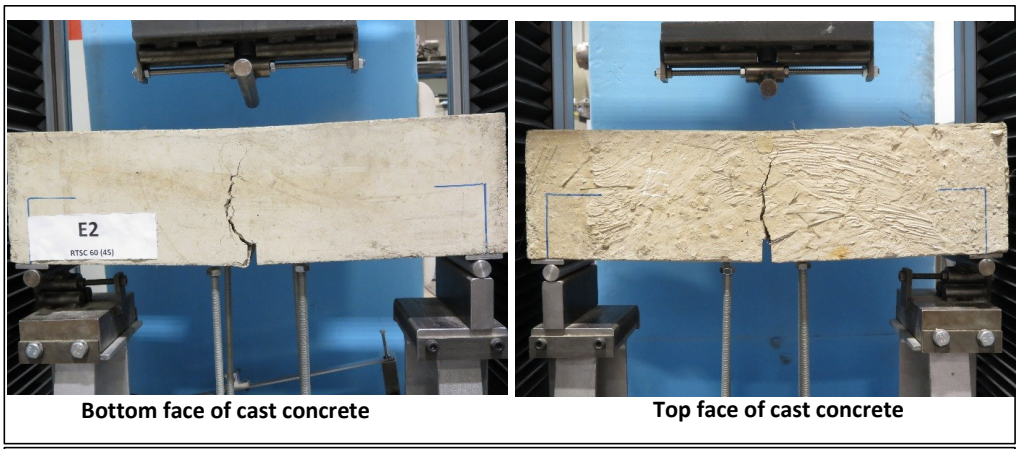

Bottom face of cast concrete | Top face of cast concrete

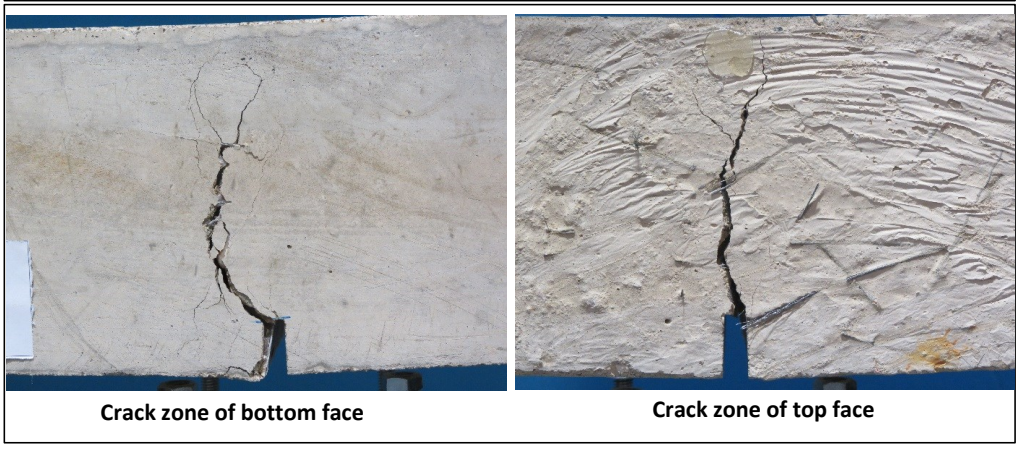

Crack zone of bottom face | Crack zone of top face

Stress-deformation graphs

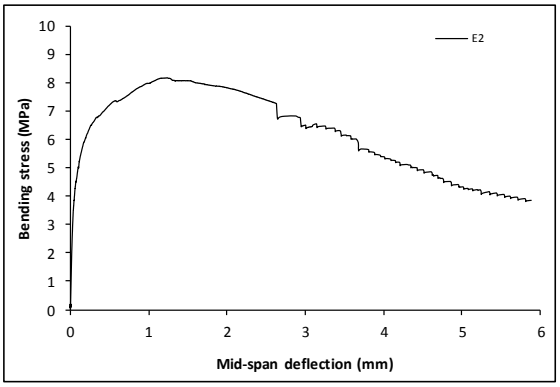

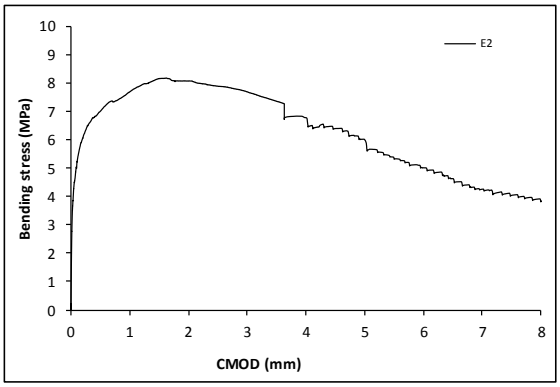

Specimen code name:		H3 (E3)	RTSC (45)		
Notched Depth dn	125	mm			
Depth, d	150	mm	Span, L	500	mm
Width, b	153.5	mm	Flexural strength	7.05	MPa

Bottom face of cast concrete

Top face of cast concrete

Crack zone of bottom face

Crack zone of top face

Stress-deformation graphs

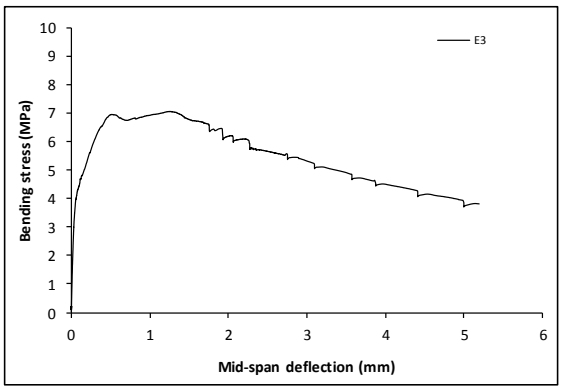

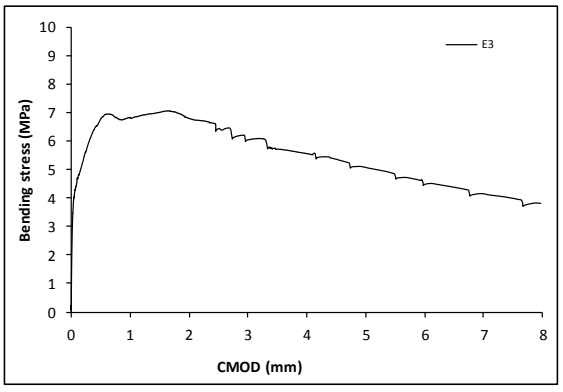

Specimen code name:		H4 (E4)	RTSC (45)		
Notched Depth dn	125	mm			
Depth, d	150	mm	Span, L	500	mm
Width, b	153	mm	Flexural strength	8.49	MPa

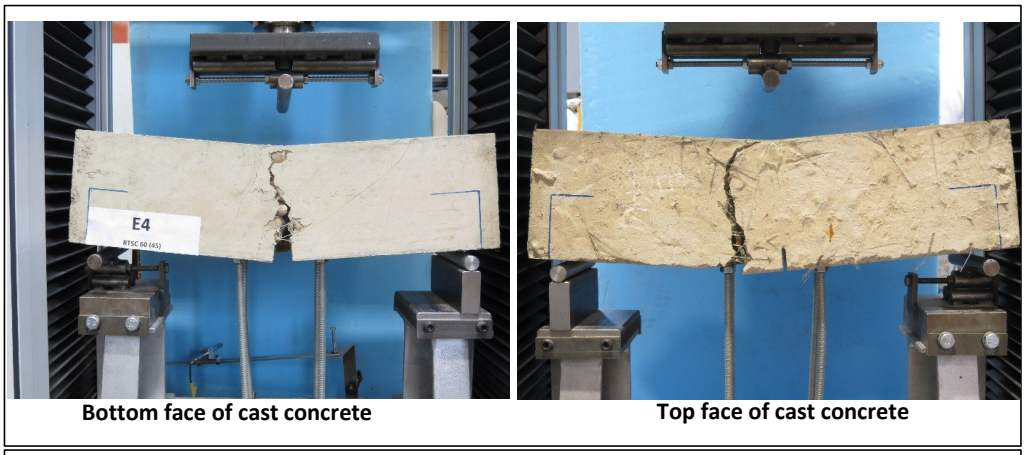

Bottom face of cast concrete | Top face of cast concrete

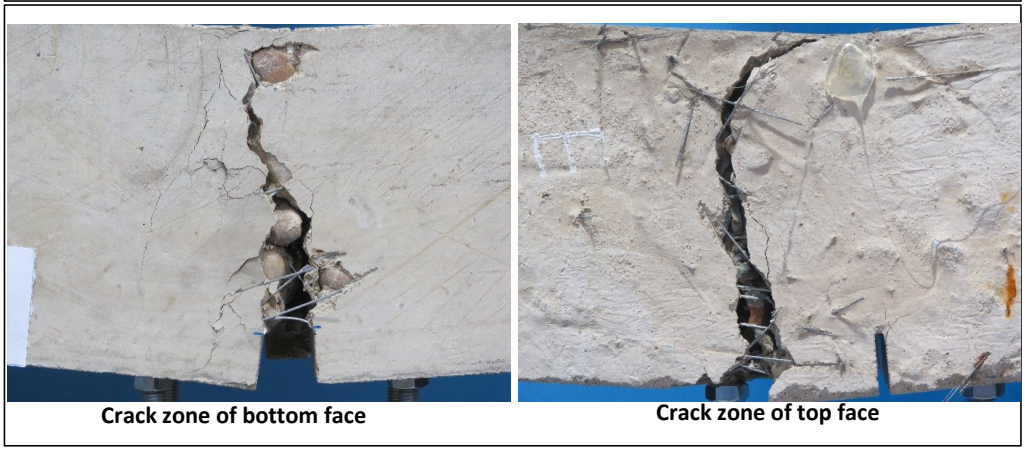

Crack zone of bottom face | Crack zone of top face

Stress-deformation graphs

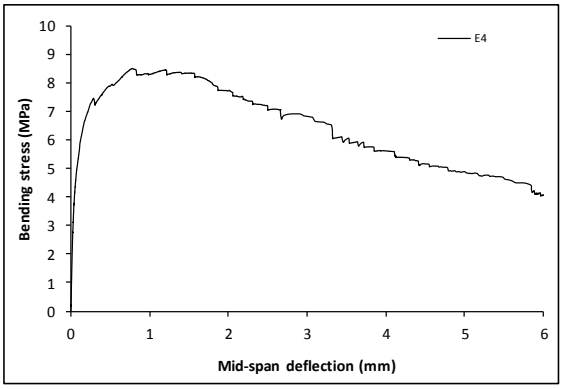

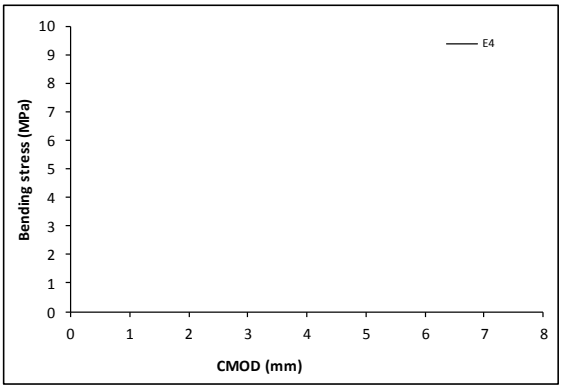

Specimen code name:		H5 (E5)	RTSC (45)		
Notched Depth dn	125.5	mm			
Depth, d	150	mm	Span, L	500	mm
Width, b	151.5	mm	Flexural strength	7.05	MPa

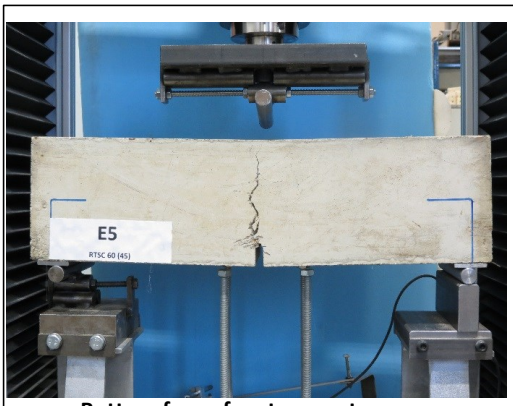

Bottom face of cast concrete

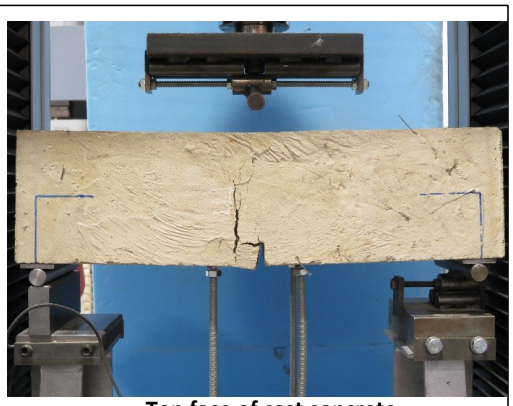

Top face of cast concrete

Crack zone of bottom face

Crack zone of top face

Stress-deformation graphs

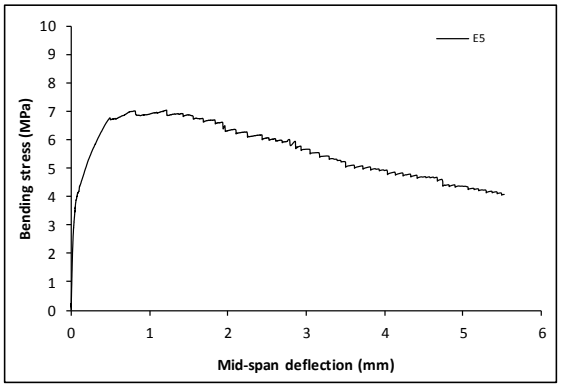

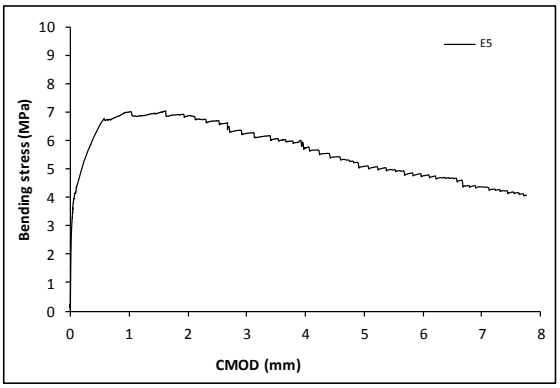

Specimen code name:		H6 (E6)	RTSC (45)		
Notched Depth dn	124.75	mm			
Depth, d	150	mm	Span, L	500	mm
Width, b	153.5	mm	Flexural strength	3.31	MPa

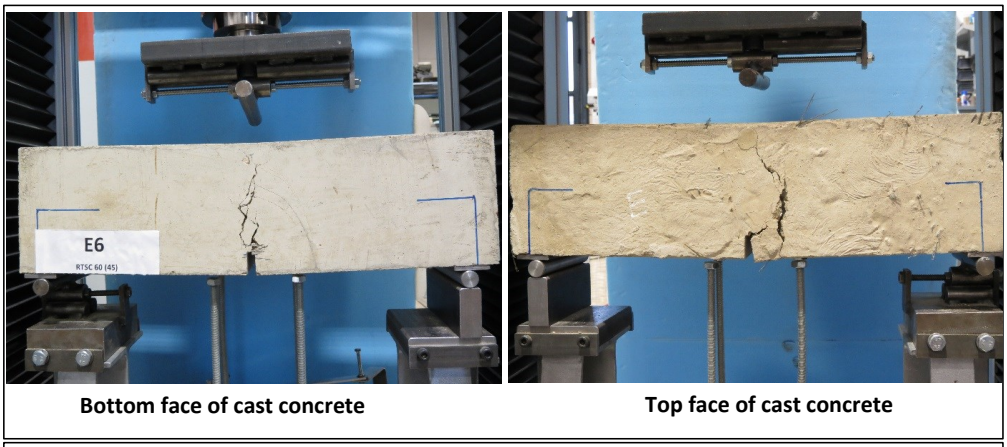

Bottom face of cast concrete | Top face of cast concrete

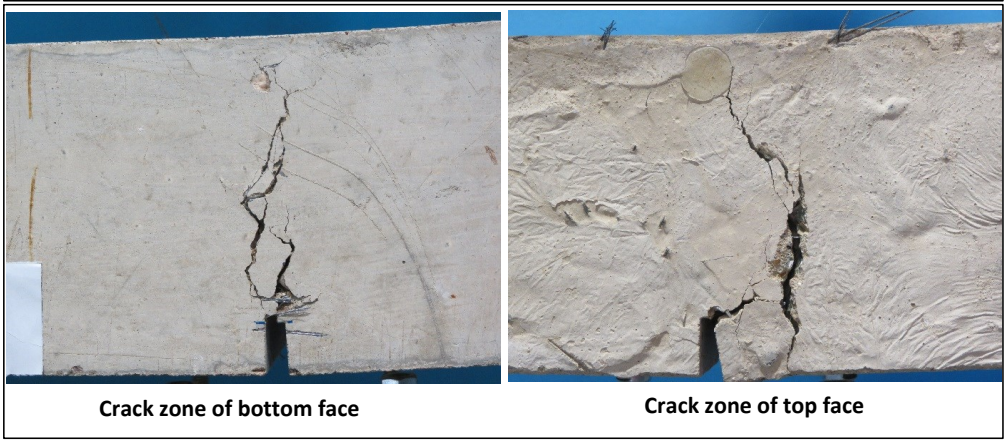

Crack zone of bottom face | Crack zone of top face

Stress-deformation graphs

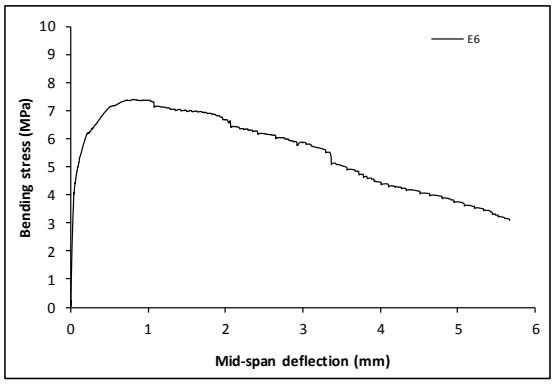

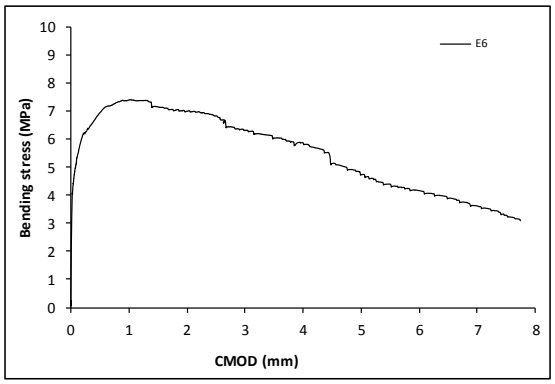

Specimen code name:		H7 (E7)	RTSC (45)		
Notched Depth dn	124.25	mm			
Depth, d	150	mm	Span, L	500	mm
Width, b	153.25	mm	Flexural strength	8.23	MPa

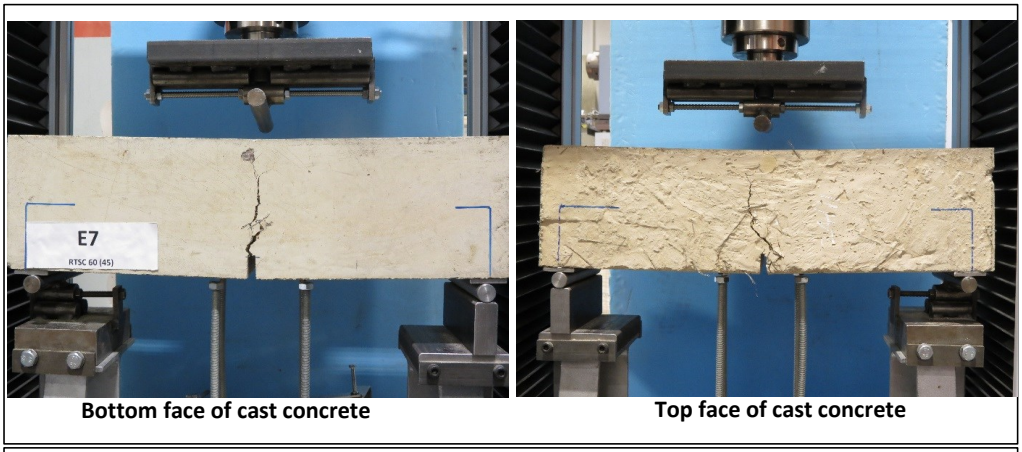

Bottom face of cast concrete | Top face of cast concrete

Crack zone of bottom face | Crack zone of top face

Stress-deformation graphs

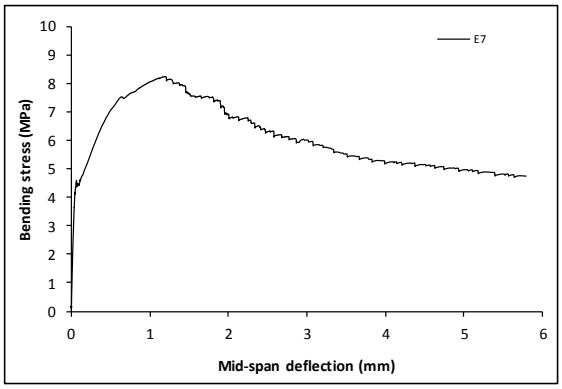

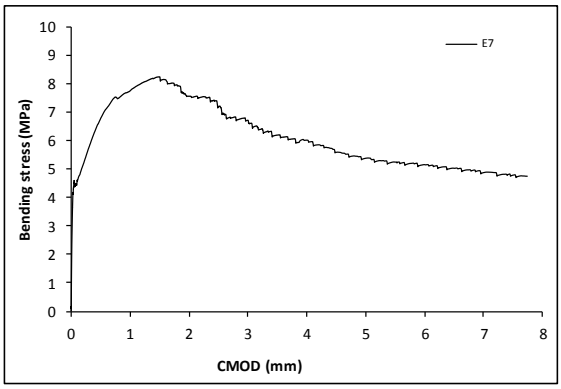

Specimen code name:		H8 (E8)	RTSC (45)		
Notched Depth dn	123	mm			
Depth, d	150.5	mm	Span, L	500	mm
Width, b	151.25	mm	Flexural strength	9.32	MPa

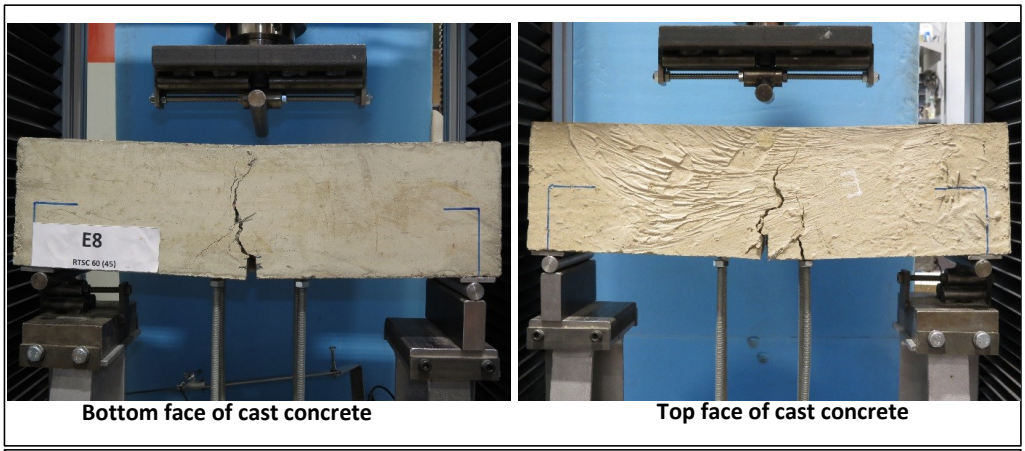

Bottom face of cast concrete | Top face of cast concrete

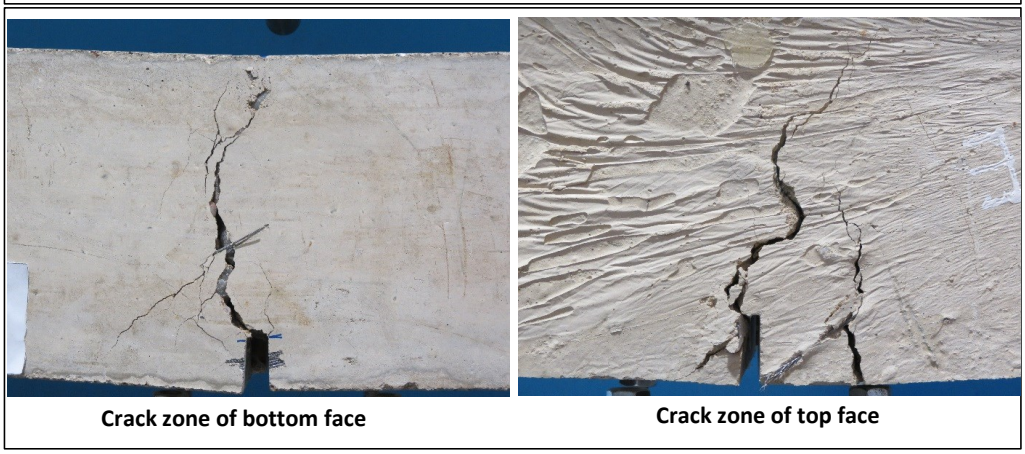

Crack zone of bottom face | Crack zone of top face

Stress-deformation graphs

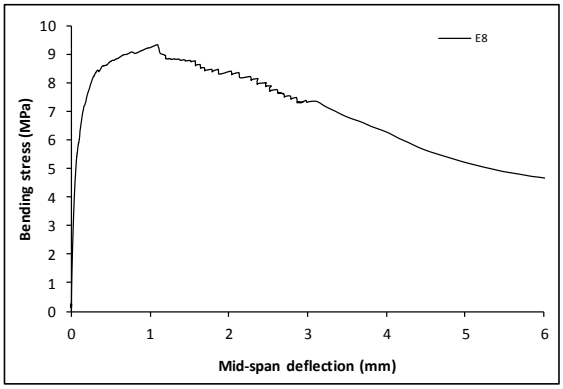

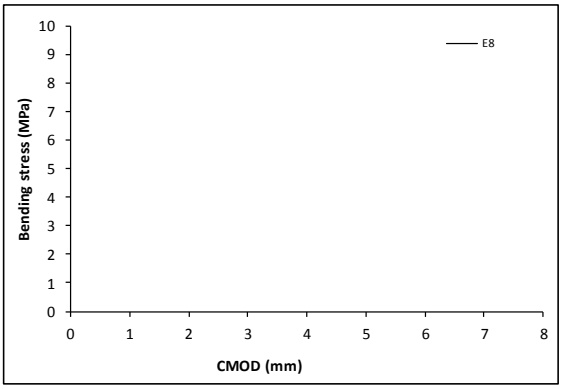

Specimen code name:		H9 (E9)	RTSC (45)		
Notched Depth dn	125	mm			
Depth, d	150	mm	Span, L	500	mm
Width, b	152.5	mm	Flexural strength	7.46	MPa

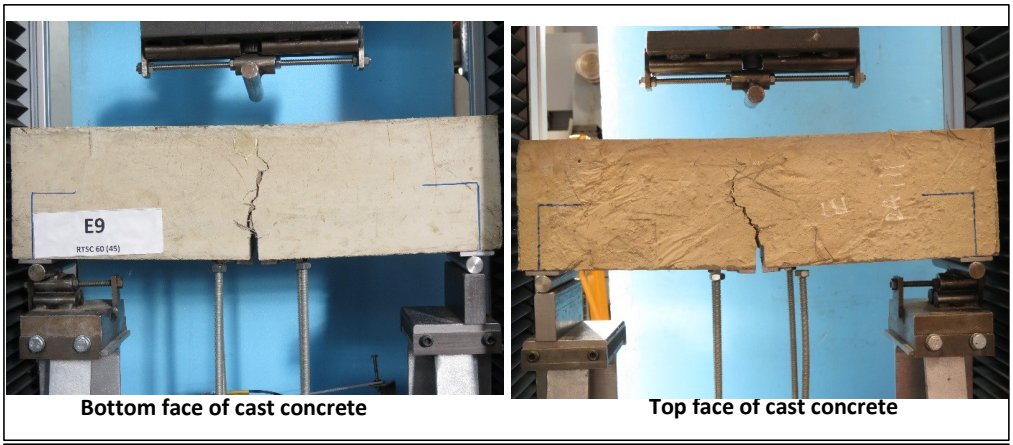

Bottom face of cast concrete

Top face of cast concrete

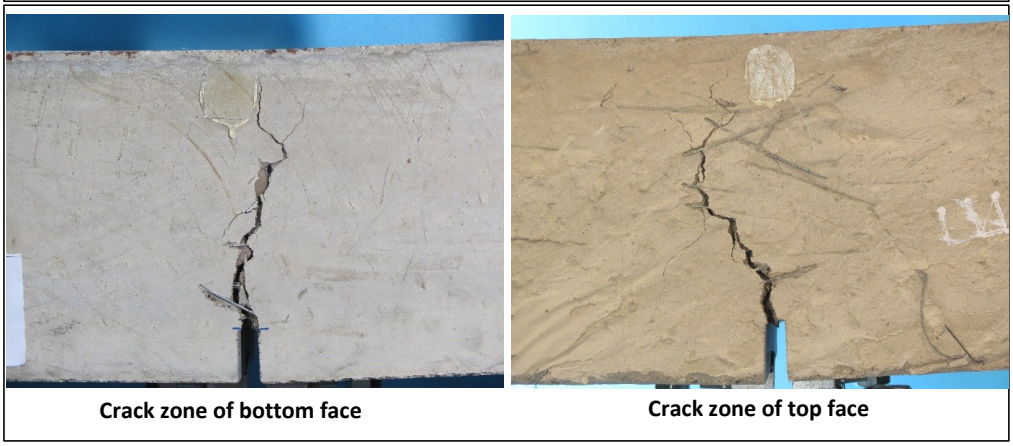

Crack zone of bottom face

Crack zone of top face

Stress-deformation graphs

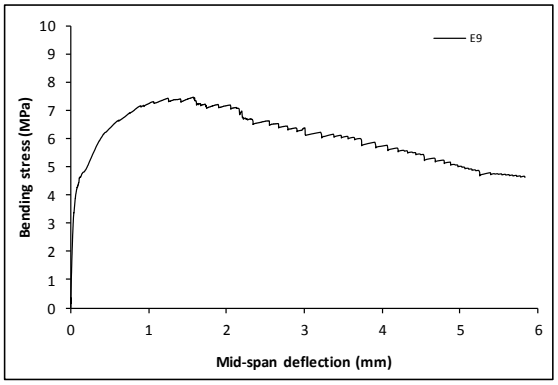

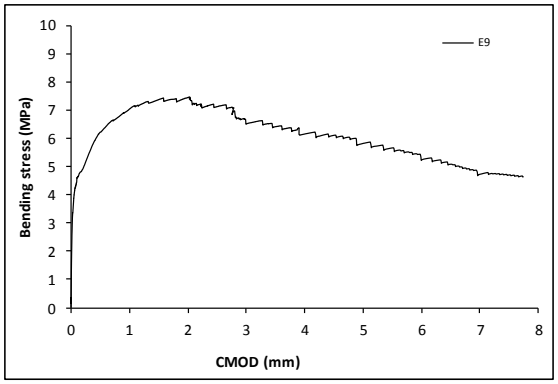

Specimen code name:		H10 (E10)	RTSC (45)		
Notched Depth dn	122.75	mm			
Depth, d	150	mm	Span, L	500	mm
Width, b	151.5	mm	Flexural strength	9.48	MPa

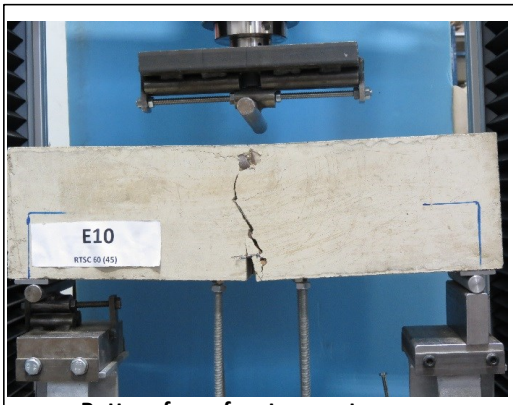

Bottom face of cast concrete

Top face of cast concrete

Crack zone of bottom face

Crack zone of top face

Stress-deformation graphs

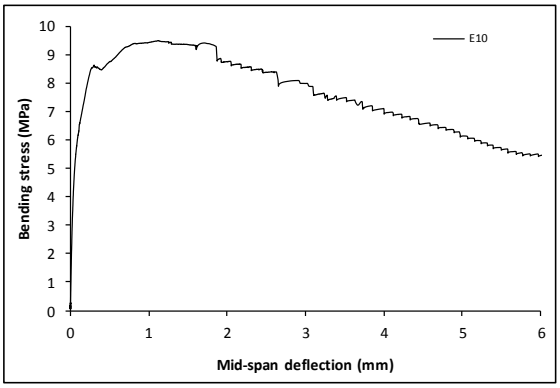

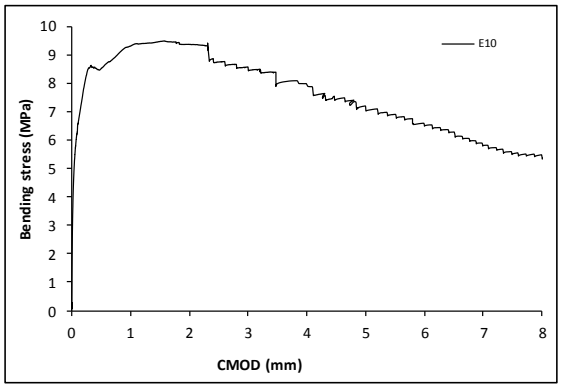

Specimen code name:		H11 (E11)	RTSC (45)		
Notched Depth dn	124.5	mm			
Depth, d	150	mm	Span, L	500	mm
Width, b	152.75	mm	Flexural strength	8.48	MPa

Bottom face of cast concrete

Top face of cast concrete

Crack zone of bottom face

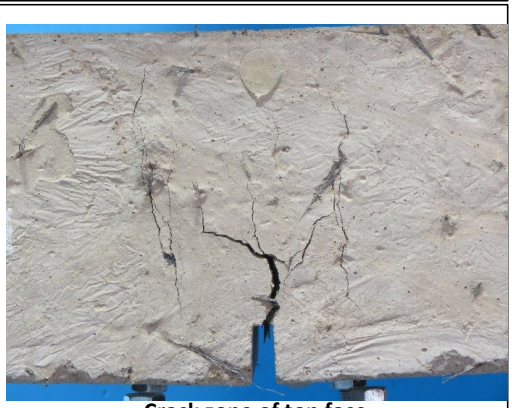

Crack zone of top face

Stress-deformation graphs

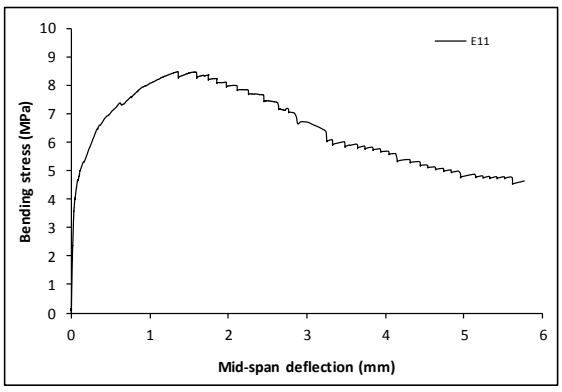

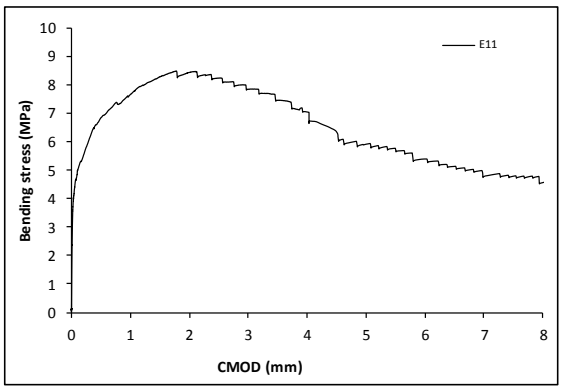

Specimen code name:		H12 (E12)	RTSC (45)		
Notched Depth dn	125.25	mm			
Depth, d	150.25	mm	Span, L	500	mm
Width, b	152.25	mm	Flexural strength	8.42	MPa

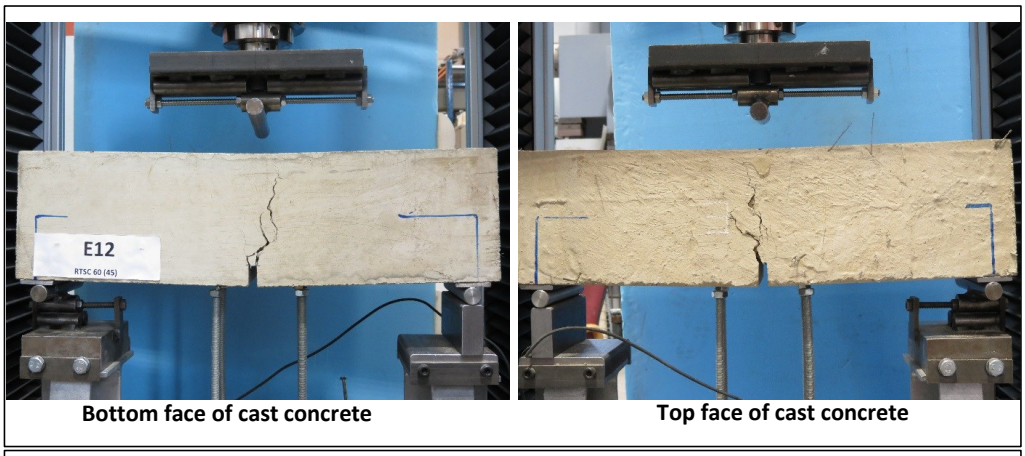

Bottom face of cast concrete | Top face of cast concrete

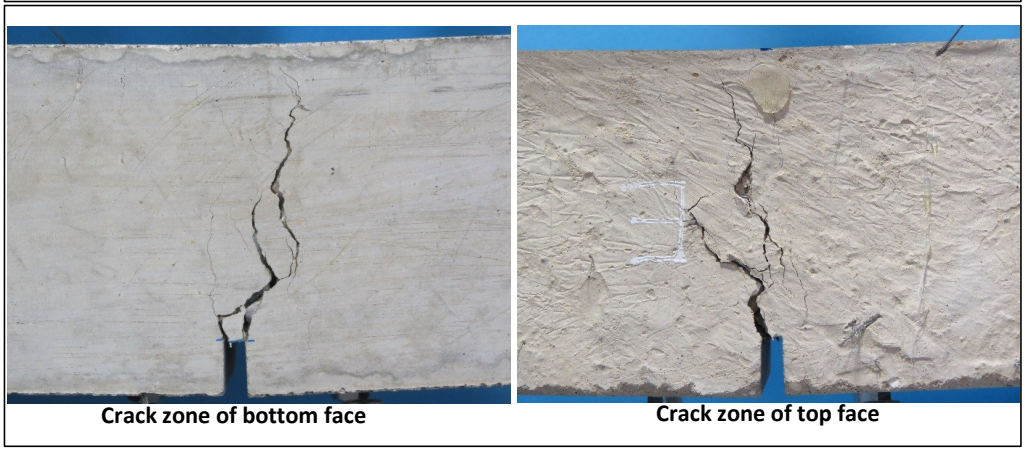

Crack zone of bottom face | Crack zone of top face

Stress-deformation graphs

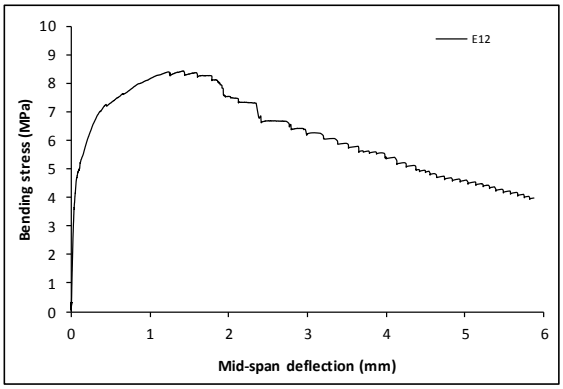

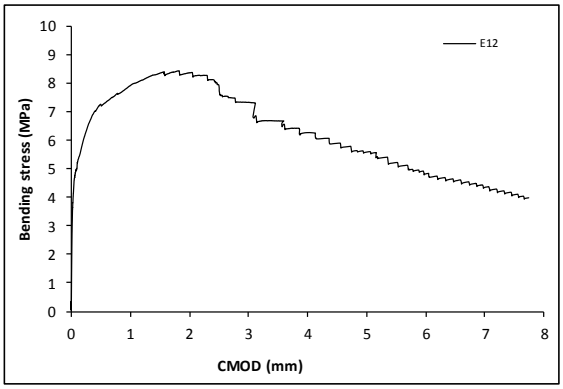

Mix:	**H (E)**	RTSC (45)	
Notched Depth dn	mm		
Depth, d	mm	Span, L	mm
Width, b	mm	Flexural strength	MPa

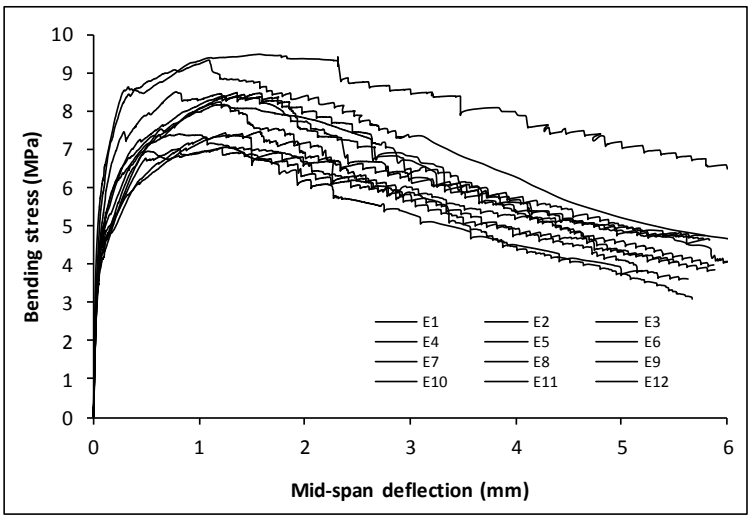

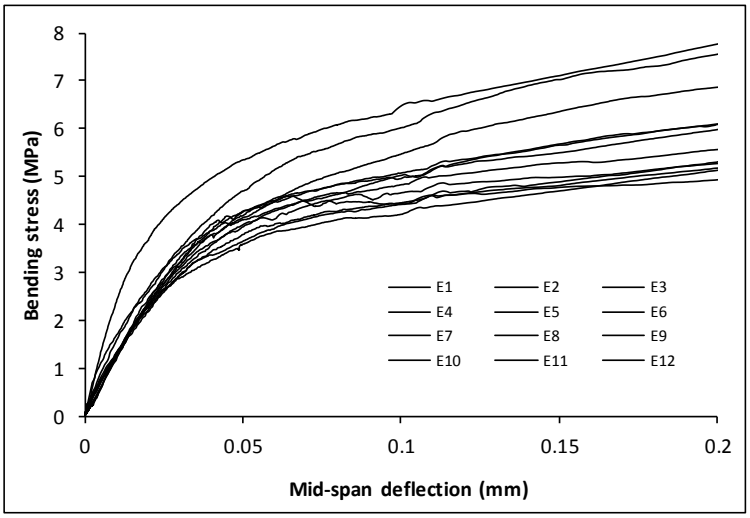

Specimen code name:		P2-1	Plain		
Notched Depth dn	125	mm			
Depth, d	151	mm	Span, L	500	mm
Width, b	149.75	mm	Flexural strength	3.64	MPa

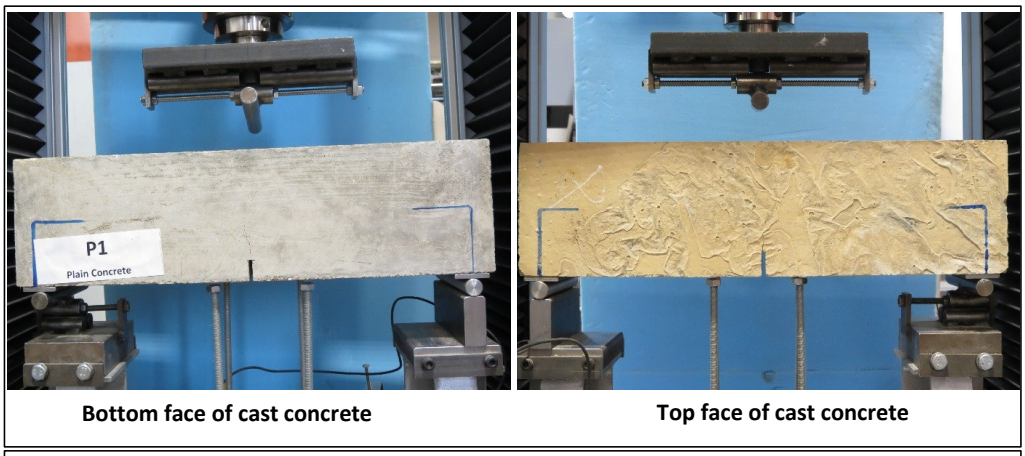

Bottom face of cast concrete | Top face of cast concrete

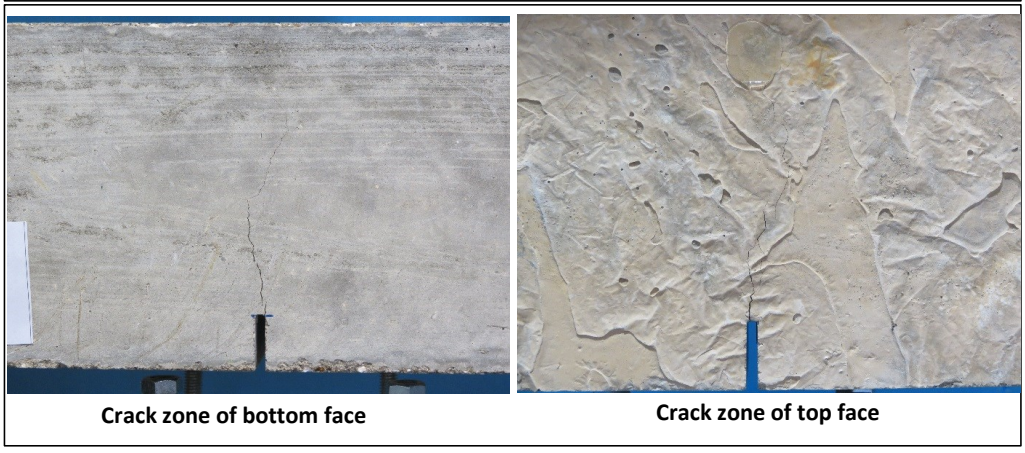

Crack zone of bottom face | Crack zone of top face

Stress-deformation graphs

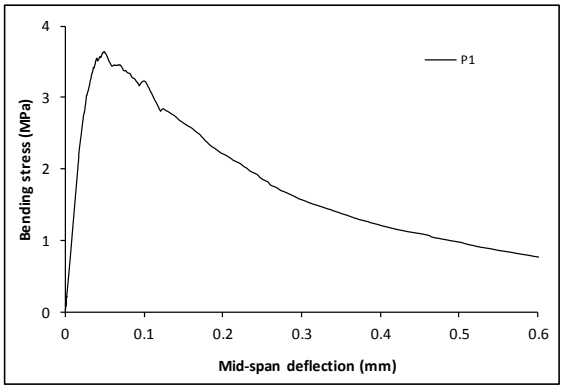

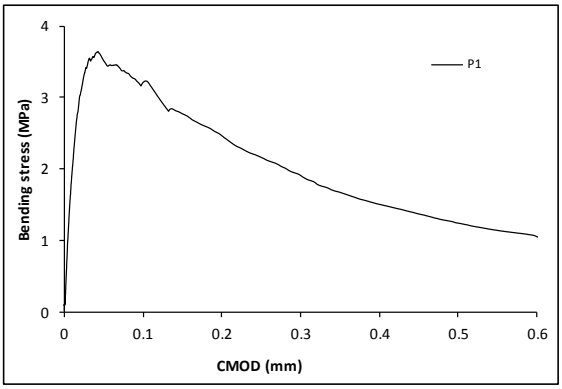

Specimen code name:		P2-2	Plain		
Notched Depth dn	124.5	mm			
Depth, d	150	mm	Span, L	500	mm
Width, b	150.25	mm	Flexural strength	3.48	MPa

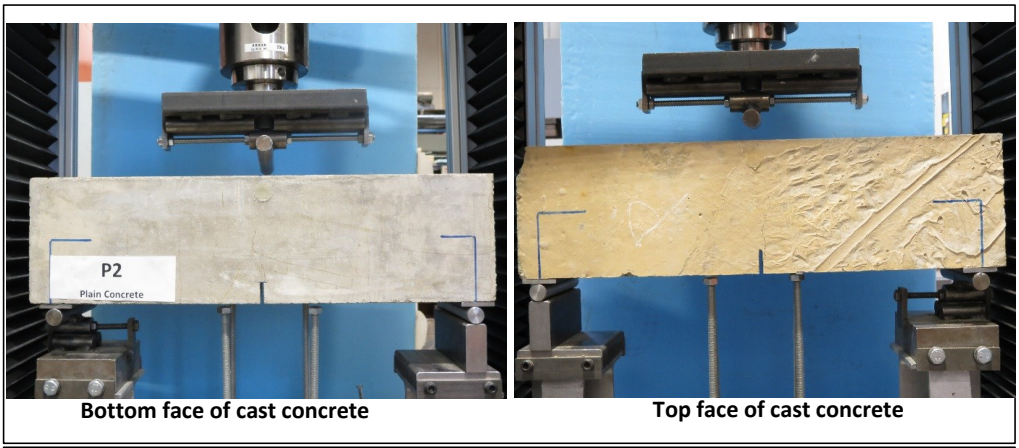

Bottom face of cast concrete | Top face of cast concrete

Crack zone of bottom face | Crack zone of top face

Stress-deformation graphs

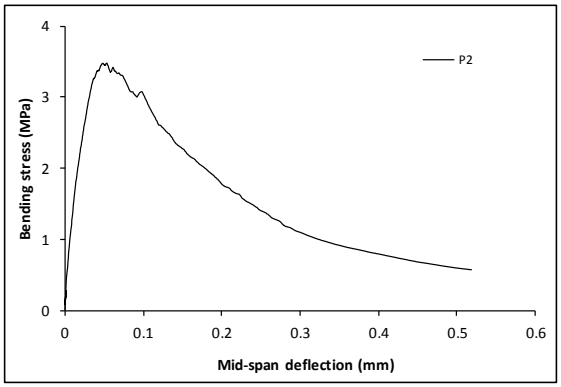

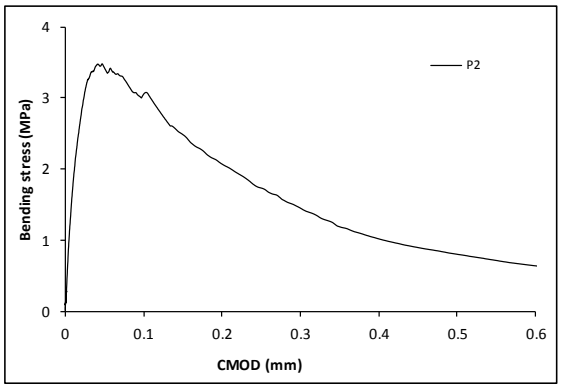

Specimen code name:		P2-3	Plain		
Notched Depth dn	123.25	mm			
Depth, d	150	mm	Span, L	500	mm
Width, b	150.5	mm	Flexural strength	3.53	MPa

Bottom face of cast concrete

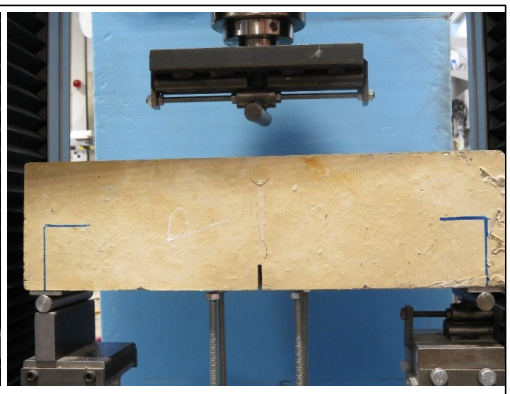

Top face of cast concrete

Crack zone of bottom face

Crack zone of top face

Stress-deformation graphs

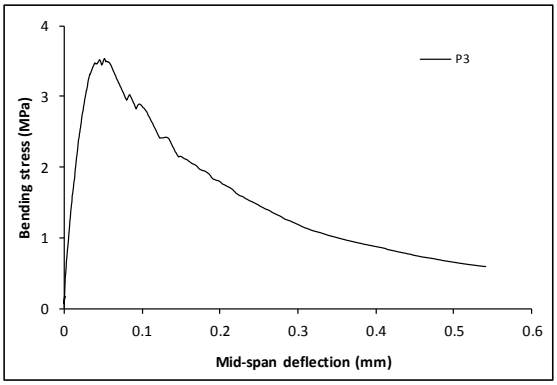

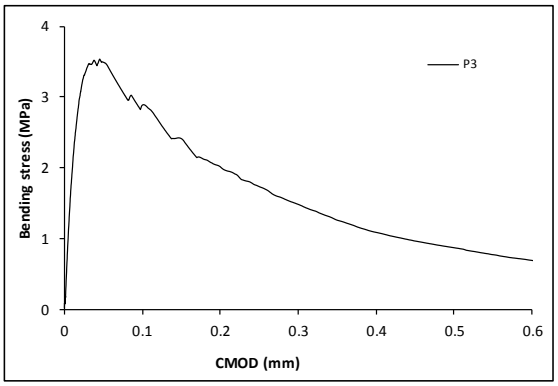

Specimen code name:		P2-4	Plain		
Notched Depth dn	124.5	mm			
Depth, d	150	mm	Span, L	500	mm
Width, b	150.75	mm	Flexural strength	3.78	MPa

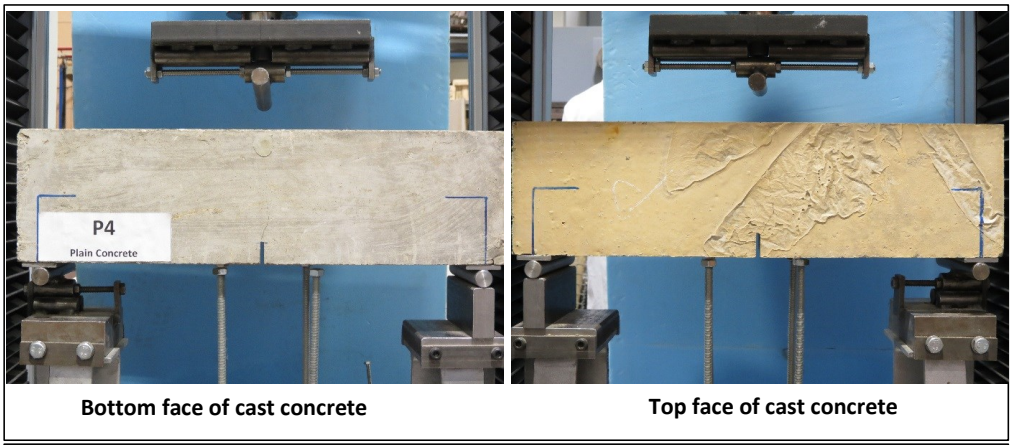

Bottom face of cast concrete | Top face of cast concrete

Crack zone of bottom face | Crack zone of top face

Stress-deformation graphs

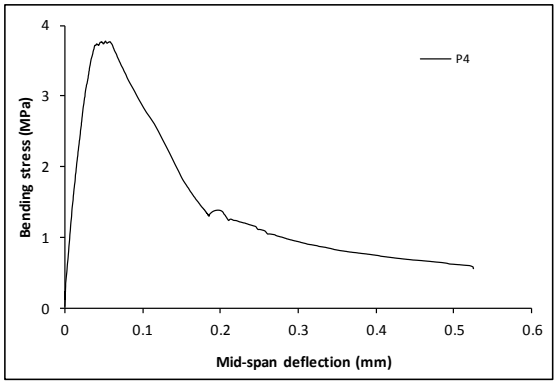

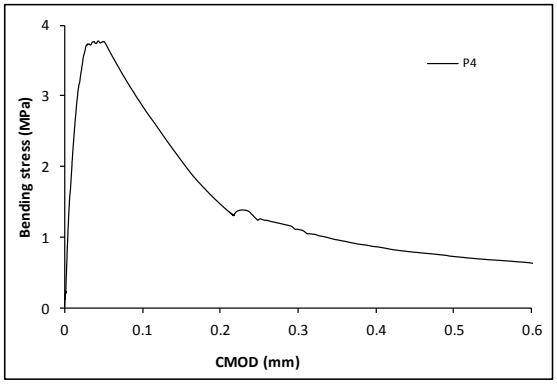

Specimen code name:		P2-5	Plain		
Notched Depth dn	123	mm			
Depth, d	150.5	mm	Span, L	500	mm
Width, b	150.25	mm	Flexural strength	3.98	MPa

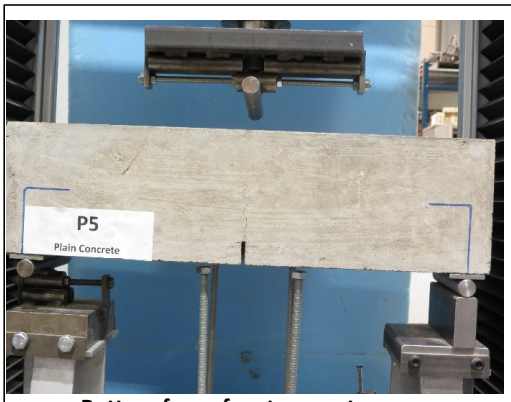

Bottom face of cast concrete

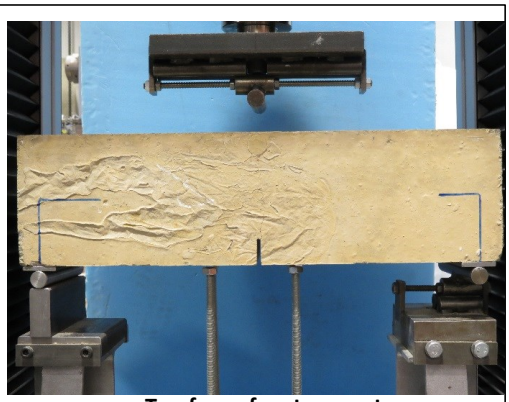

Top face of cast concrete

Crack zone of bottom face

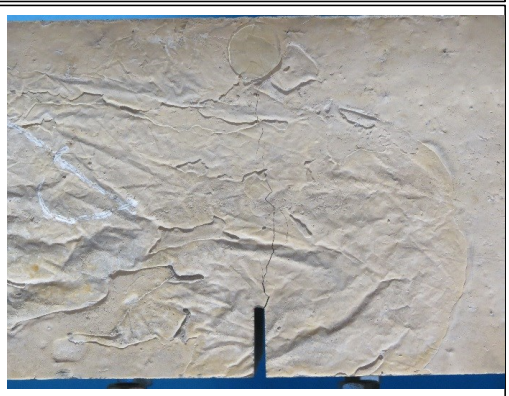

Crack zone of top face

Stress-deformation graphs

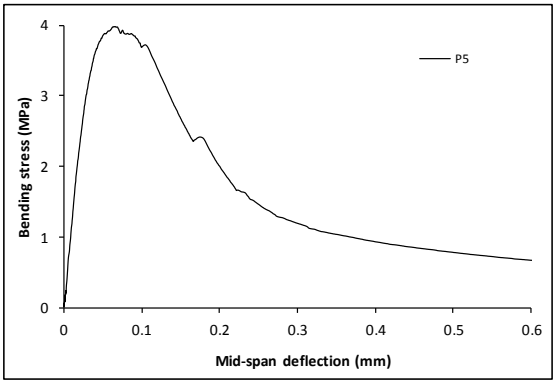

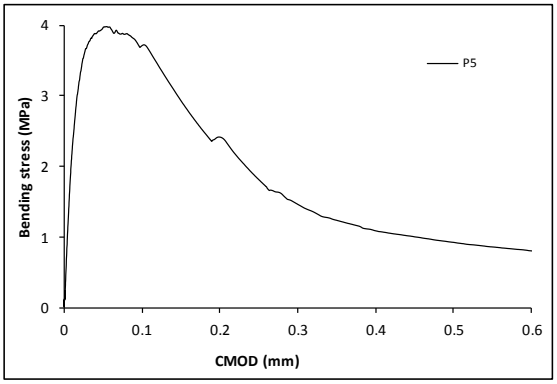

Specimen code name:		P2-6	Plain		
Notched Depth dn	125.25	mm			
Depth, d	150	mm	Span, L	500	mm
Width, b	150.5	mm	Flexural strength	3.30	MPa

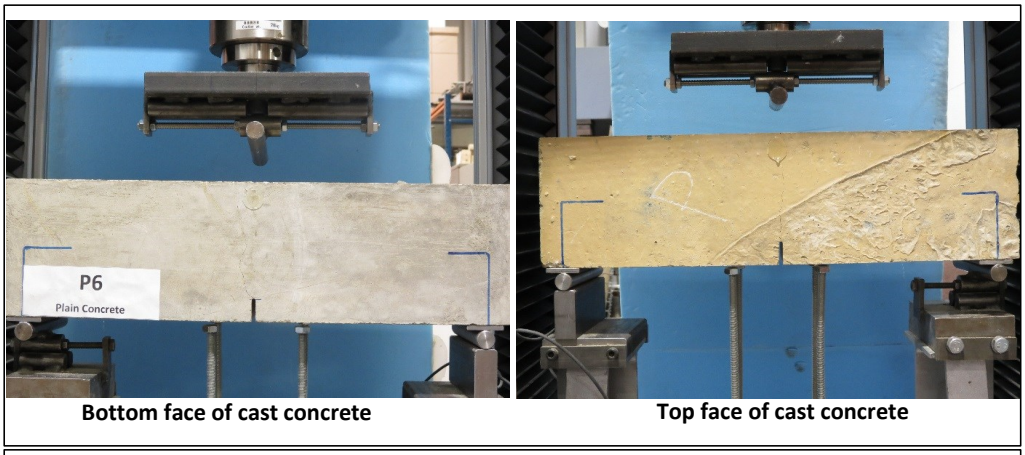

Bottom face of cast concrete | Top face of cast concrete

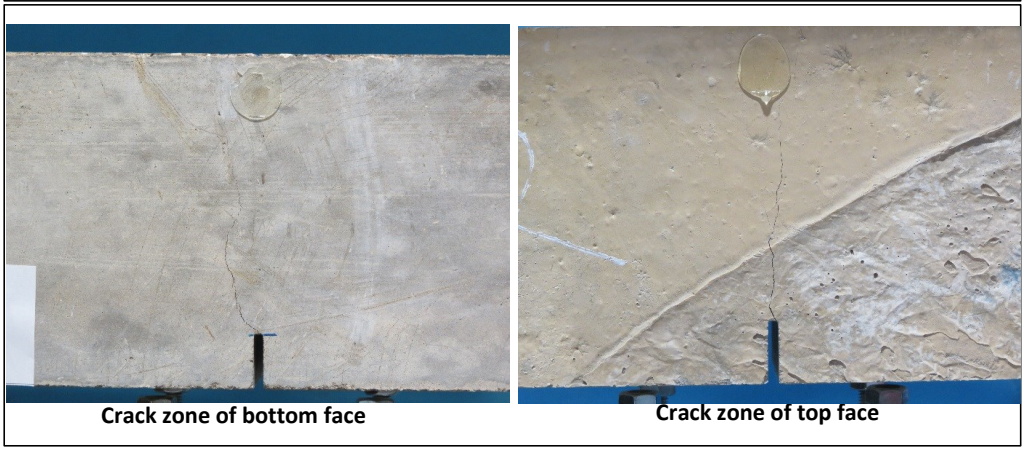

Crack zone of bottom face | Crack zone of top face

Stress-deformation graphs

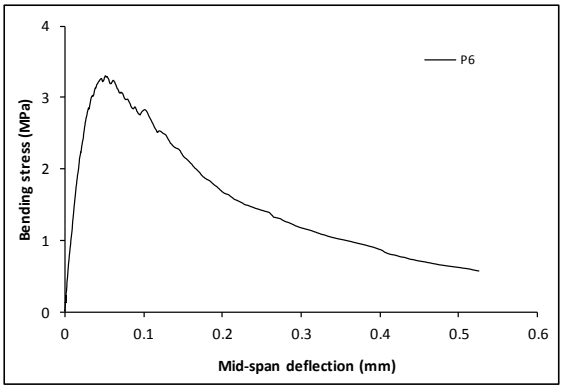

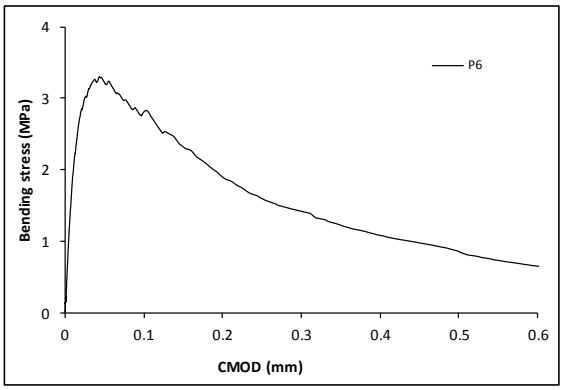

Mix:	**P2**	Plain	
Notched Depth dn	mm		
Depth, d	mm	Span, L	mm
Width, b	mm	Flexural strength	MPa

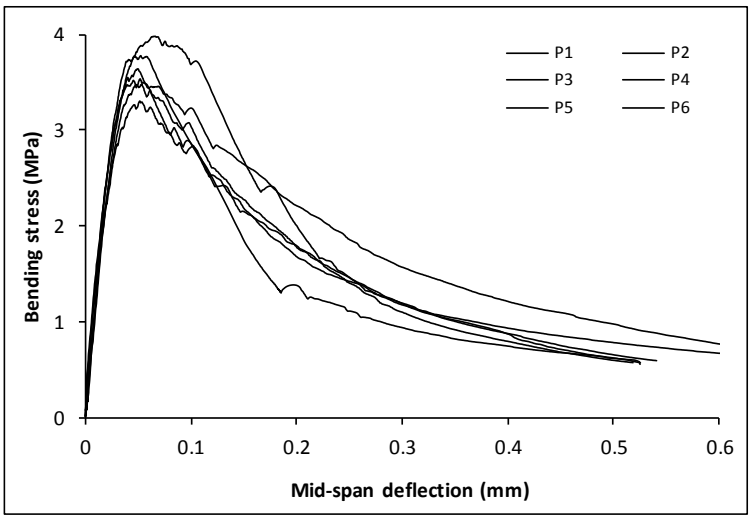

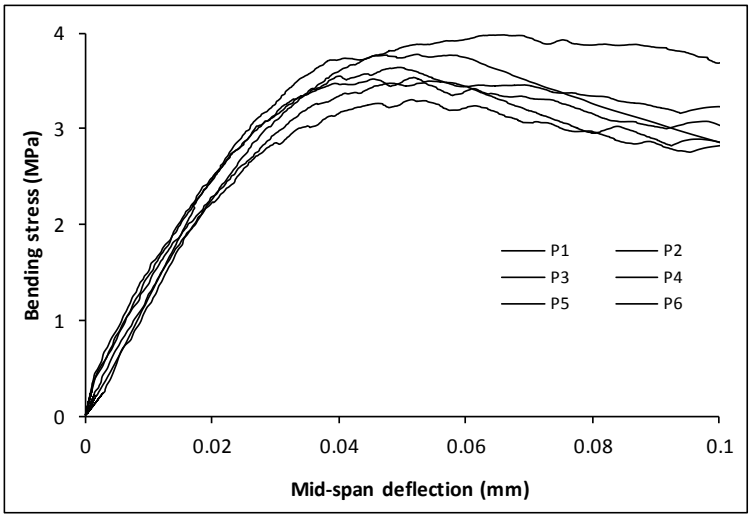

Appendix C:

FE Mesh sensitivity analysis –Chapter 4

Using three different meshes shown in Figure C-1, a mesh sensitivity study was performed for the blended SFRC mix 1M22.5R22.5. A two-dimensional plane stress solid element (CPS4) was chosen. The Concrete Damage Plasticity (CDP) model was adopted in the FE modelling, with the values of the parameters reported in Table 4-2. The input stress-strain relation for the mix was determined using three key (σ, ε) points, (2.22, 0.00006), (0.00206, 1.35) and (0.025, 1.35).

The load-deflection curves obtained from FE analysis and experiments are shown in Figure C-2. It is clear that the predicted load-deflection curves for mesh (b) and (c) match very well, whilst mesh (a) leads to an overestimate of the peak load and energy absorption capacity. Hence, mesh (b) with the minimum mesh size of 1 mm was adopted in the present study, since it could help to increase computational efficiency whilst maintaining accuracy.

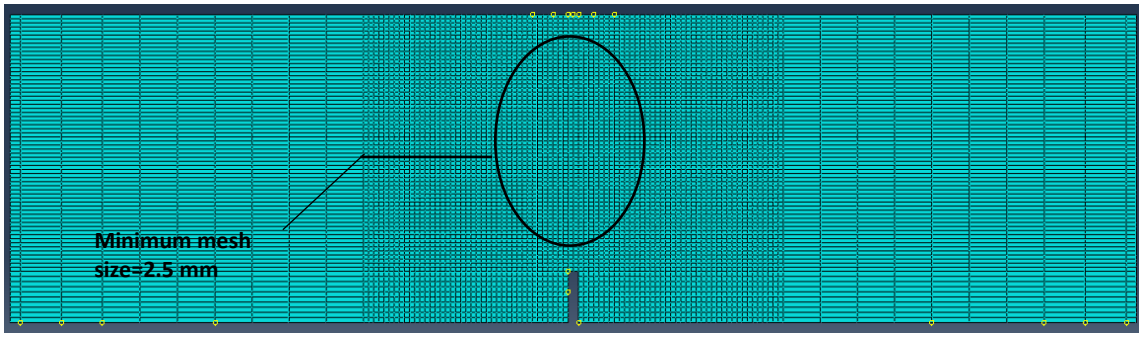

Mesh (a): Minimum mesh size=2.5 mm, about 3500 elements

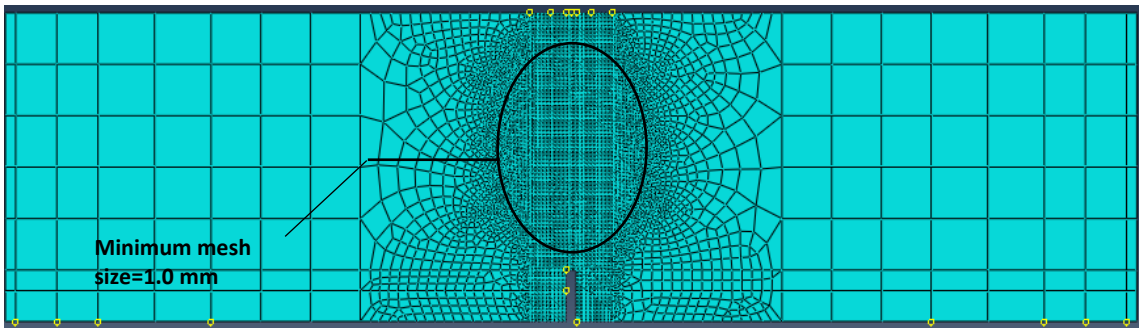

Mesh (b): Minimum mesh size=1.0 mm, about 9000 elements

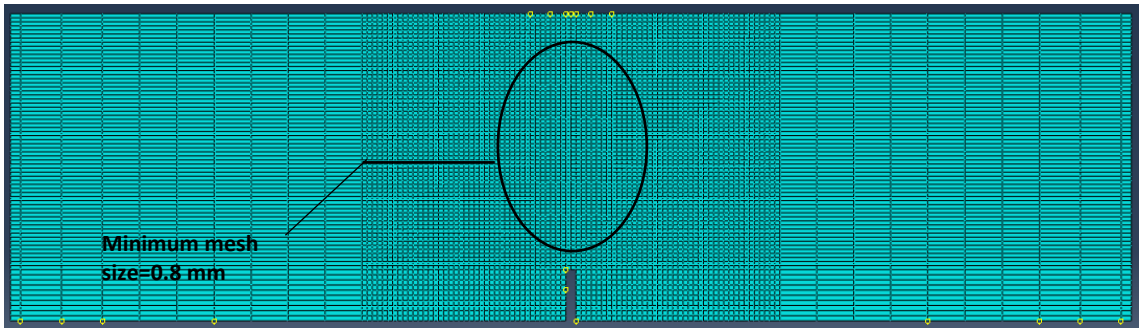

Mesh (c): Minimum mesh size=0.8 mm, about 34200 elements

Figure C-1: FE model with coarse, moderate and fine meshes

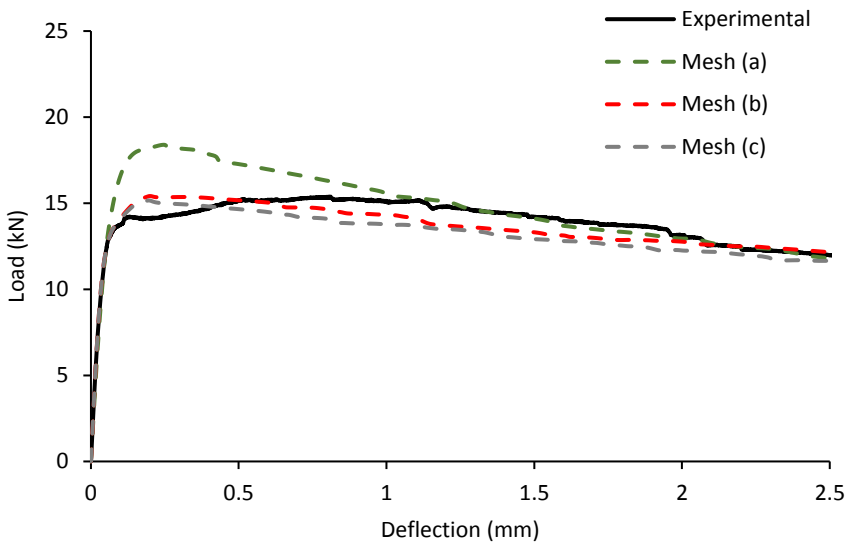

Figure C-2: Predicted load-displacement curves for mix 1M22.5R22.5